



Fourth International Oil Sands Tailings Conference

Lake Louise, Alberta, Canada: December 7-10, 2014

U of A Geotechnical Centre

IOSTC 2014, Lake Louise, AB - December 7-10, 2014

IOSTC

FOURTH INTERNATIONAL

OIL SANDS

TAILINGS CONFERENCE

Lake Louise, Alberta
Canada

December 2014

IOSTC 2014, Lake Louise, AB - December 7-10, 2014

Proceedings of the Fourth International Oil Sands Tailings Conference

7-10 December 2014, Lake Louise, Alberta, Canada

Fourth International Oil Sands Tailings Conference

Edited by

David Segó, G. Ward Wilson & Nicholas Beier

University of Alberta, Geotechnical Centre and
Oil Sands Tailings Research Facility

Copyright ©

All rights reserved. No part of this publication or the information contained herein may be reproduced, stored in a retrieval system or transmitted in any form or by any means, electronic, mechanical, by photocopying, recording or otherwise, without written prior permission from the publisher.

Although all care is taken to ensure the integrity and quality of this publication and the information herein, no responsibility is assumed by the publishers nor the author for any damage to property or persons as a result of operation or use of this publication and/or the information contained herein.

Published by: University of Alberta, Dept. of Civil & Environmental Engineering

ISBN 978-1-55195-326-7

Printed in Canada

FORWARD

It is with great pleasure that we present the **Fourth International Oil Sands Tailings Conference 2014 (IOSTC'14)**. There have been several sweeping changes in the management of oil sands tailings since the First International Oil Sands Tailings Conference held in 2008 (**IOSTC'08**), which offered an industrial and regulatory perspective on the needs for tailings research and management. In response to Directive 74 issued by the Energy Resources Conservation Board (ERCB, now Alberta Energy Regulator (AER)) in 2009, **IOSTC'10** focused on presenting technologies and approaches to meet the provincial regulator's tailings criteria and requirements for the oil sands industry. Two years later, **IOSTC'12** provided a venue to present the Oil Sands Tailings Technology Deployment Road Map prepared by the Consortium of Tailings Management Consultants (CMTc) on behalf of Alberta Innovates – Environment and Energy Solutions (AI-EES) and the Oil Sands Tailings Consortium (OSTC, now Canada's Oil Sands Innovation Alliance (COSIA)).

The aim of **IOSTC'14** is to provide a further exchange of information between the people responsible for managing the oil sands tailings: researchers and providers of tailings management services who have experience with this industry. This year's conference will have a special keynote address by Mr. Alan Fair, reflecting on over three decades' worth of experience he has acquired in the oil sand industry. **IOSTC'14** will also debut research from the Oil Sands Tailings Research Facility's (OSTRF) newest research initiative, the **NSERC/COSIA Senior Industrial Research Chair in Oil Sands Tailings Geotechnique** held by Dr. Ward Wilson, as well as an industry presentation session by member companies of Canada's Oil Sands Innovation Alliance Tailings Environment Priority Area (COSIA Tailings EPA).

We want to personally thank members of the OSTRF for their encouragement and support. The conference would not have been possible without the dedication of Nicholas Beier, Vivian Giang and especially Sally Petaske who provided so much assistance and leadership.

The technical challenges associated with mature fine tailings (MFT) require a holistic approach to ensure the sustainable development and environmental stewardship of Alberta's vast oil sands. It was with this in mind that the session themes and manuscripts were selected for presentation and inclusion in the proceedings. We want to thank our professional colleagues who willingly contributed their technical knowledge, experiences and especially their time to write the manuscripts that make the proceedings of this conference. May you find further insights to enhance your understanding of the current state-of-practice in oil sands tailings management through **IOSTC'14**.

David C. Segó and G. Ward Wilson

Co-Chairs, IOSTC 2014 Organizing Committee

IOSTC 2014, Lake Louise, AB - December 7-10, 2014

Thank you to the following sponsors for their support in making the 4th International Oil Sands Tailings Conference a huge success:



The UofA
Geotechnical Centre



UNIVERSITY OF
ALBERTA

PLATINUM SPONSORS:



WorleyParsons

resources & energy

 **BASF**

The Chemical Company



cosia[®]
CANADA'S OIL SANDS
INNOVATION ALLIANCE

DELIVERING
ENVIRONMENTAL
PERFORMANCE

GOLD SPONSORS:



SILVER SPONSORS:



**International Oil Sands
Tailings Conference 2014**



December 7-10
Lake Louise, AB

TABLE OF CONTENTS

KEYNOTE PRESENTATIONS

OIL SANDS TAILINGS: AN HISTORIAL PERSPECTIVE

A. Fair..... 3

BROAD SUITE OF PRACTICE AND TECHNOLOGY KEY TO SUCCESS IN TAILINGS MANAGEMENT

P. Read..... 9

SESSION 1 - TAILINGS DESICCATION

INFLUENCE OF AN UNDERLYING SAND BEACH ON THE DRAINAGE AND DESICCATION OF FINE TAILINGS

L. Kabwe, G.W. Wilson and J.D. Scott..... 19

SHRINKAGE AND SWELLING PROPERTIES OF FLOCCULATED MATURE FINE TAILINGS

Y. Yao, A. Frits van Tol, L. van Paassen and P. P.J. Vardon..... 27

DETERMINATION OF THE PERMEABILITY FUNCTION FOR DRYING OIL SANDS TAILINGS UNDERGOING VOLUME CHANGE AND DESATURATION

F. Zhang, D.G. Fredlund, G.W. Wislon and A. Sedgwick..... 37

PROBABILISTIC APPROACH TO EVALUATE TAILINGS DRYING

T. Fasking, C. Gantzer and P. Hinck..... 47

SESSION 2 - TAILINGS DESICCATION AND MODELLING

NUMERICAL SIMULATION OF FINE OIL SAND TAILINGS DRYING IN TEST CELLS

P.J. Vardon, T. Nijssen, Y. Yao and A. Frits van Tol..... 59

MULTILAYER DEPOSITION OF TWO BATCHES OF THICKENED OIL SANDS TAILINGS: EXPERIMENTS AND MODELING

P. Simms, T.I. Bernard, X. Yang and A. Segdwick..... 71

GEOMETRY OF POLYMER-AMENDED FINE TAILINGS DEPOSIT: YIELD STRESS MEASUREMENT AND NUMERICAL MODELLING

S. Mizani and P. Simms.....81

DESICCATION-CONSOLIDATION MODELING AND STRENGTH TESTING USING SIMPLE SHEAR OF POLYMER-AMENDED MFT

P. Simms, S. Soleimani and M. Gholami..... 91

SESSION 3 – MODELLING

MODELING BOTTOM SEEPAGE FROM OIL SANDS TAILINGS PONDS

S. Jeeravipoolvarn, W. Miller, J.D. Scott and L. Kawbe 101

ASSESSING A NOVEL TECHNOLOGY USING A TAILINGS MANAGEMENT SIMULATION MODEL

N. Beier, D. Segó and N.R. Morgenstern 113

MODELING DEWATERING OF OIL SANDS MATURE FINE TAILINGS USING FREEZE THAW

N.H. Pham and D.C. Segó 123

MODELLING OF HYDRAULIC SAND CAPPING ON CREEPING ULTRA-SOFT TAILINGS

L. Beuth, C. Dykstra and W. Jacobs..... 131

SESSION 4 – TAILINGS DEWATERING I

FEASIBILITY OF SAND FARMING TO DEWATER COARSE SAND TAILINGS

J. Stianson, R. Bashir, D. Fredlund, A. Nguyen, L. Sawatsky, W. Wilson and S. Martens 143

CENTRIFUGAL MODELLING OF OIL SANDS TAILINGS CONSOLIDATION

A.R. Sorta, D.C. Segó and G.W. Wilson 153

COLUMN CONSOLIDATION TESTING OF OIL SANDS TAILINGS

R. Sun, R. Spelay, J. Kan and A. Goldszal 163

SESSION 5 – COSIA SPECIAL SESSION I

PERFORMANCE MANAGEMENT OF FLUID FINE TAILINGS TO MEET CLOSURE COMMITMENTS

J. Sobkowicz, A. Hyndman, B. Watts and R. Dawson..... 175

MEASURING STRENGTH IN OIL SANDS TAILINGS DEPOSITS

H.A.W. Kaminsky..... 185

COSIA DESIGN OF EXPERIMENT STUDY IN SUPPORT OF DEVELOPMENT OF A STANDARD FOR FINES MEASUREMENT IN OIL SANDS

R. Currie, H. Mian, B. Zhao, B. Crickmore, L. Asplund, T. Malkova, B. Komishke, J. Clarke, T. White, & R. Mahmood.....195

SESSION 6 – COSIA SPECIAL SESSION II

DEMYSTIFYING THE METNYLENE BLUE INDEX

H. Kaminsky.....221

CONVENTIONAL OIL SANDS TAILINGS CAN ACHIEVE FINES CAPTURE OF 60% AND HIGHER

C. Fear, E. McRoberts, R.M. Nik, and G. Esposito231

FLOODING OF IN-LINE FLOCCULATED TAILINGS AFTER THIN LIFT DRYING

A. Najafi, H. Mian, R. Salehi, P. Lacoste-Bouchet, K. Friedrich, H. Keele, C. McWhan, R. Romero, F. Daliri, S. Jeeravipoolvarn, J. Boswell and T. Moore241

DRYING OF THICK LIFT OIL SAND TAILINGS USING SMOLDERING

B.A. Jajuee, S.R. Hickman and G. Rockwell.....251

FURTHERING TAILINGS R & D VIA THE COSIA TAILINGS EPA AND THE RESEARCH WORKING GROUP

A. Sedgwick and A. Fair257

SESSION 7 – TAILINGS MANAGEMENT I

THE INGENUITY GAP IN OIL SANDS TAILINGS TECHNOLOGY

J. Sobkowicz, J. Boswell and I. Gidley.....267

GEOTECHNICAL INSIGHTS INTO DEPOSITION, DEWATERING AND STRENGTH PERFORMANCE OF THICKENED AND PASTE TAILINGS DEPOSITS AT SHELL CANADA’S TAILINGS TEST FACILITY

S. Masala, R.M. Nik, G. Freeman and R. Mahood.....277

DEVELOPING AN APPROACH TO PREDICT DEWATERING AND MATERIAL PERFORMANCE OF POLYMER FLOCCULATED MATURE FINE TAILINGS

L. Boxill, D. Hockley, D. Van Zyl, J. Thompson and J. Olson.....289

SESSION 8 – TAILINGS MANAGEMENT II

MINING CUT-OFF GRADE POLICY AND TAILINGS PRODUCTION: COULD AN OUNCE OF PREVENTION BE WORTH A POUND OF CURE?

U. Thorley301

INTRODUCING A HOLISTIC APPROACH FOR THE OPTIMIZATION OF TAILINGS SYSTEM

H. Kheireddine and C. Mukherjee.....307

MINE CLOSURE PLANNING AND TAILINGS PLANNING TOOLS: SYNERGIES AND OPPORTUNITIES

M. Alostaz, J. McGreevy, D. Lee and C. Cooper315

SESSION 9 – TAILINGS DEWATERING II

ADVANCES IN THE ELECTROKINETIC TREATMENT OF OIL SANDS TAILINGS

L.R. Nelson, P. Garcia, B. Harris and D. Kimzey..... 323

CHEMICAL FREE MECHANICAL DEWATERING OF TAILINGS WHERE THE CAKE HAS SHEAR STRENGTH >>5KPA

H. Boele, M. Brocken and P. McEachern335

PERFORMANCE OF ELECTRICALLY CONDUCTIVE DRAIN-TUBE PLANAR GEOCOMPOSITES (eGCP) FOR DEWATERING OIL SANDS TAILINGS

P. Dolez, S. Bourges-Gastaud, E. Blond and P. Saunier.....341

SESSION 10 – WATER TREATMENT

IMPACT OF CO₂ ADDITION ON INITIAL BASE MINE LAKE WATER CLARITY

J. Brandon, W. Lu, V. Duong and A. Ulrich.....351

THE POTENTIAL IMPACT OF DIFFERENT TYPES OF TAILINGS ON WATER QUALITY AND QUANTITY REPORTING TO OIL SANDS END PIT LAKES: A PRELIMINARY MODELING EXERCISE

A. Holden, G. McKenna, X. Fan and K. Biggar359

BIOAMENDMENT OF OIL SANDS MATURE FINE TAILINGS ACCELERATED DEWATERING AND IMPROVED RELEASE WATER QUALITY

E. Cao, R. Sampaga, A. Olubodun, T. Burns and A. Ulrich.....369

DEGRADATION OF NAPHTHENIC ACIDS AT 20°C AND 10°C BY A PSEUDOMONAS SP. NATIVE TO AN OIL SANDS TAILINGS POND

S. Miles, D. Cologgi and A.C. Ulrich.....377

SESSION 11 – TAILINGS DEPOSITION AND MODELLING

A NEW APPROACH TO OPTIMIZE THE CAPTURE OF OIL SANDS FINES IN SAND BEACH R. Sun, J. Kan and A. Goldszal.....	387
MUDDY RIVER DELTAS AS ANALOGUES FOR OIL SANDS TAILINGS BEACHES: IMPROVING FINES CAPTURE AND OPERATIONAL EFFICIENCY WITH TAILINGS BEACH MODELING B. Sheets, T. Wagner, J. Swenson, J. Horton, J. Langseth, L. Sittoni, D-J. Walstra, H. Winterwerp R. Uittenbogaard, J. van Kestern and A. Talmon.....	397
SEDIMENT DEPOSITION – INTEGRATION OF PHYSICS AND ITS CONSEQUENCES FOR MODELLING D. Luger, R. Sisson, L. Sittoni and J. Pennekamp.....	407
SEMI-ANALYTICAL MODELING OF THICKENED TAILINGS FLOWS J.B. Swenson, B. Sheets, D. Kolstad and W. van Dkesteren.....	415

SESSION 12 – CHEMICAL APPLICATION

OIL SANDS TAILINGS POND RECLAMATION BY MFT POLYMERIZATION CAPPING AND CHARACTERIZATION OF THE MFT POLYMER J. Zhao and G. Gu.....	427
CLAY-FLOCCULANT INTERACTIONS IN DEVELOPING NEXT GENERATION FLOCCULANTS FOR OIL SANDS FLUID FINE TAILINGS MANAGEMENT C. Mohler, M. Poindexter, C. Acevedo, T. Sanders Jf., G. Meyers, C. Reinhardt, W. Chen, H. Sing and J. Atias.....	437
CONSOLIDATION RATES AND RESULTING PHYSICAL PROPERTIES OF PARTICULAR™ SILICA TREATED FLUID FINE TAILINGS R. Moffat and F.D. Godbille.....	447
FLOCCULATION OF ULTRA-FINE PARTICLES OF MATURE FINE TAILINGS R. Salehi, Z. Xu and J. Masilyah.....	457
OIL SANDS MATURE FINE TAILINGS SPIKING FOR THICKENER APPLICATION T. Dang-Vu, R. Salehi and S. Ramey.....	467

SESSION 13 – INSTRUMENTS AND PARAMETER MEASUREMENT TECHNIQUE

SOIL PARAMETER ESTIMATION AND SAMPLE COLLECTION USING AN UNMANNED GROUND VEHICLE

N. Olmedo and M. Lipsett..... 475

ROBOTIC SYSTEMS FOR MEASURING PROPERTIES OF TAILINGS DEPOSITS AND COLLECTING SAMPLES

M.G. Lipsett, N. Olmedo, B. Rivard and G.W. Wilson..... 483

DEPLOYMENT OF HYPERSPECTRAL IMAGING INSTRUMENTS FOR REMOTE MONITORING OF SOFT TAILINGS WATER CONTENT

I. Entezari, B. Rivard, M.G. Lipsett, J. Feng and G.W. Wilson..... 493

TIME DOMAIN REFLECTOMETRY (TDR) SENSORS-APPLICATION TO FLOCCULATED MATURE FINE TAILINGS PERFORMANCE MONITORING

J. Song, M. O’Kane, R. Mahood, C. Cote and D. Kolstad..... 499

SCALING INLINE STATIC MIXERS FOR OIL SAND MATURE FINE TAILINGS FLOCCULATION

A. Demoz..... 509

DEVELOPMENT OF STANDARD OPERATING PROCEDURES FOR STORAGE AND HANDLING OF WATER SAMPLES CONTAINING NAPHTHENIC ACIDS

H. Mahdavi, H. Mian, S. Hepperle and Z. Burkus..... 517

Keynote Presentations

OIL SAND TAILINGS: AN HISTORICAL PERSPECTIVE

Alan Fair

COSIA - Former Director of Tailings

INTRODUCTION

Tailings are an integral component of any mining operation. This is particularly true of the oil sands mining industry, which currently has some twelve active tailings ponds covering approximately 180 Km² of surface area in northern Alberta. Tailings ponds are essential to any water-based oil sands operation as they provide storage for the tailings generated as part of the extraction process. They also enable 85 – 95% of the water to be re-used in the extraction operations.

In addition to their large volume, oil sand tailings have one other unique attribute, the water-based extraction technology, in use by all of the existing operators (and planned to be used by all others considering the development of an oil sand mine), results in the generation of large volumes of what is referred to as Fluid Fine Tailings (FFT). These fluid fine tailings are mainly composed of clay particles that do not settle and remain in a “fluid form” (i.e. with the consistency of runny yogurt) for many, many decades. To date, across the industry, approximately one billion cubic meters of FFT has been accumulated. It is this large, and increasing, volume of FFT that poses the biggest challenge to the management of oil sand tailings.

This paper attempts to provide an historical perspective in relation to the understanding and management of oil sand tailings. The paper divides the history of oil sand tailings into 4 decades including the 1970s, 1980s, 1990s and 2000 up until present day. This represents over 40 years of oil sands mining history. It also represents the almost 40 years the author has spent working in the oil sand industry, much of it focussed on oil sand tailings. I recognize my effort to summarize the work to understand and manage oil sand tailings in terms of four decades is a gross simplification, but my efforts are not aimed at covering all of the detailed oil sand tailings work – they are intended to provide a high level understanding of why we are where we are today.

The 1970s

During the 1970s there were only two oil sands operations. Suncor (then Great Canadian Oil

Sands, GCOS) had begun operations in 1967. Syncrude started mining operations in 1977. I joined Syncrude in 1978. These were exciting times. Many of the things that both Suncor (GCOS) and Syncrude were attempting to do had never been done before – there were many unknowns and associated challenges. These unknowns and challenges included tailings operations. The initial tailings planning assumptions were based on oil sand tailings behaving much like other “conventional” tailings operations, albeit considerably larger volumes. The GCOS tailings plan assumed that only one tailings pond would be required over the proposed 25 year life of the mining operation, i.e. Pond 1 (also known as Tar Island Dyke). Tar Island Dyke was constructed along the Athabasca River escarpment adjacent to the mining operations. It was to be 10 meters in height and would be used (as is the case with most tailings ponds) to recycle the extraction water and provide initial storage for the coarse tailings sand, until the sand could be placed in the mined out pits. At the end of the day, Pond 1 grew to an eventual height of approximately 100 meters and is one of eight tailings ponds on the Suncor leases. Syncrude also assumed it would need only one tailings pond, referred to as the Mildred Lake Settling Basin (MLSB) over the planned 25 year life of the operation. It was recognized that it would need to be large – it covers approximately 17 Km² and remains one of the world’s largest tailings ponds. Although many things have changed over the years that led to the need for additional tailings facilities at Syncrude (and Suncor) there are now four tailings facilities at the two Syncrude mining operations mostly as a result of the protracted timeline for the FFT to settle/consolidate.

It was the ever-increasing volumes of FFT that resulted in the larger number of tailings ponds at both the Suncor and Syncrude sites. I would characterize the 1970s as a “decade of discovery” relative to oil sand tailings. The unknown was the fact that when the oil sands were processed using water-based extraction technology the resulting tailings fines created a “gel-like” structure that would not settle to any more than about a 30 – 35% solids (by weight). The most accepted reasoning for this seems to be that this is caused by the “zeta potential” or repulsive forces that are

generated between the clay platelets that cause them to not settle even over extended periods of time. The industry response at the time was to increase the size of the tailings ponds, hence the Tar Island Dyke elevation grew by 10 fold and the MLSB elevation was also increased as well. The assumption was that although oil sand tailings were slower to settle, they would eventually settle to a state that would allow them to be reclaimed. By increasing the size of the existing tailings ponds operators would gain the extra time they needed to allow the FFT to settle.

The 1980s

As the size of the Suncor and Syncrude tailings ponds grew so did the concerns about the stability of these very large tailings ponds. Tar Island Dyke was constructed along the Athabasca River and although the foundation material that it was built upon did not present any major concerns, the consequences of a failure (into the river) would have been disastrous. In addition, there were concerns about the leakage of process-affected water into the Athabasca River. The Mildred Lake Settling Basin had been constructed on an area of Syncrude's lease that was partially underlain by remoulded Clearwater clay, which resulted in less than ideal foundation conditions. In addition portions of the dyke had to be constructed over "ponded water" causing the foundation tailings dam materials to be very loose. Portions of the upstream beach were also placed sub-aqueously as well. These loosely placed tailings were, consequently, believed to be susceptible to liquefaction failures.

Considerable effort was expended to ensure the ongoing stability of these very large structures. The Observational Approach was adopted as a way to carry on with operations while maintaining the flexibility to make adjustments to the dams in the event that issues arose. Extensive instrumentation was used at both dams to ensure that any instability or seepage was detected early. Sophisticated drainage systems were incorporated into the design of the dams to help manage both the phreatic surface within the dams and any potential seepage of process-affected water. Over the years, various design changes were incorporated into the MLSB, including the inclusion of extensive toe berms along several kilometers of the perimeter of the dam and the use of "explosive densification" to densify the loose portions of the dam was carried out. The use of explosives to densify the loose tailings materials at Syncrude

was one of the first attempts (possibly the first at this large scale) to use this approach. It worked very well.

The Regulatory bodies responsible for the oil sands mining operations also got much more involved to help ensure the stability of the tailings dams. The Dam Safety Branch was very engaged and worked with the operators to ensure any issues were addressed. The Energy Resource Conservation Board (ERCB), now known as the Alberta Energy Regulator (AER), was also very involved. Extensive and ongoing analysis/reporting by the operators to the Regulators was required to ensure that all potential issues were being adequately addressed.

Both the operators and Regulators relied on external Review Boards, consisting of world class experts relative to the stability of large tailings dams, to help provide the assurance that the dams were safe.

The 1990s

As the oil sand mining industry moved into the 1990s, it became apparent that the timelines for the large volumes of FFT, that were continuing to accumulate, were going to take much longer than originally envisaged to settle/consolidate. Operators were finding it increasingly difficult to create enough storage capacity to manage the large volumes of FFT. New tailings ponds had to be created and/or facilities that were previously intended to be used solely for the storage of coarse tailings sand had to be "re-purposed" to also store FFT. Mined out in-pit storage areas that had previously been intended to store coarse tailings, now had to be used to store FFT.

Don Scott, at the University of Alberta, initiated an experiment utilizing 10 meter high columns filled with FFT to better understand the settling/consolidation behaviour of FFT. The experiment was recently terminated after more than 26 years. Over this time there was virtually no settlement/consolidation of the clay fines that make up FFT. In the mid-1990s there was a concerted effort to develop a better understanding of the fundamentals associated with FFT – it was referred to as the Fine Tailings Fundamentals Consortium (FTFC). A significant amount of research work was conducted by the Consortium, which resulted in the publication of a report that was known as the "Silber Bullet Report" at the time, or more accurately, "Advances in Oil Sands Tailings", published in 1995.

Consequently, it was determined that a process was needed to manage the inventory of FFT down over time. A process that was initiated by work conducted at the University of Alberta and subsequently developed and commercially implemented by both Suncor and Syncrude was viewed as the “Silver Bullet” that could be used to deal with the “FFT problem”. Depending on whether you worked at Suncor or Syncrude it was either referred to as Consolidated Tailings or Composite Tailings (in both cases it was known as CT). The concept was based on the notion that the clay fines, that made up the FFT originally, came from the oil sand so it should be possible to re-capture them within the pore space of the coarse sand particles. It was recognized that many of the clay fines were already being captured within the tailings pond beaches, both above and below the process-affected water/FFT. What was needed was a process that allowed the FFT to be “re-incorporated” into the coarse oil sand tailings. The CT process was developed and commercially implemented by Suncor in 1999 and Syncrude in 2000.

As the industry moved into the 2000s there was a degree of confidence that CT technology would finally allow the volume of FFT to be reduced to more manageable levels and that the resulting deposits, which needed some form of containment and, consequently, had to be placed in-pit would be reclamation- ready and could relatively easily be incorporated into the final mine landscape. However, as CT operations progressed, it became apparent that it had limitations. At Suncor, the CT deposit in-pit locations were largely inundated with process-affected water so the CT material had to be placed sub-aqueously. This made it difficult to create the non-segregating deposits needed to capture the clay fines. Syncrude experienced the same problem with the placement of their CT deposits and also struggled with being able to provide the optimum primary tailings slurry densities coming out of the extraction plant. In order to maximize fines capture, it is desirable to have a dense slurry, however, in order to maximize bitumen recovery in the extraction plant, it is important to be able to dilute the oil sand slurry in the separation vessels such that the bitumen can easily float. These competing objectives often resulted in much lower CT production than planned.

As the industry moved into the 2000s it became apparent that CT was not going to be the sole

answer to the management of the increasing volumes of FFT.

The 2000s to Present Day

With the recognition that CT technology was not going to solve industry’s FFT problems, it became apparent that there was not going to be one single solution, but that it was going to take a suite of technologies. The number of operating sites had now grown from two to five – each has their own unique features, i.e. the volume of existing FFT inventory; topography; amount of fines in the ore body; area available for tailings management; etc.

Much of the effort to develop this broader suite of tailings management technologies has come from the companies themselves, which have in turn been supported by numerous other individuals and organizations. Two basic approaches have been utilized relative to the management of oil sand tailings. They include:

- Recombined Tailings
 - Beach Fines Capture
 - Consolidated Tailings / Composite Tailings / Non-Segregating Tailings
- Separate Management of Coarse and Fine Tailings
 - Fines Drying (in thin lifts) – TRO, AFD
 - Thickened Tailings and Drying
 - MFT Centrifugation and Drying
 - CO₂ Coagulation (enhanced settling and fines capture)
 - Accelerated Dewatering
 - Water-Capped MFT

Industry’s efforts to develop tailings management technologies to deal with a common problem have led to a much more collaborative approach that helps to more effectively utilize the limited resources available. The Cooperative Oil Sand Tailings R & D Consortium was initiated in 2000 and initially centered its efforts around the development of thickener technology for application in the oil sands. The initial efforts to conduct collaborative tailings R & D tended to focus on specific projects, which limited the opportunity. In 2010 the Oil Sands Tailings Consortium (OSTC) was created. All of the existing operators and those who have plans to develop a surface mining oil sands operation, agreed to participate in the Consortium, which was based on four principles aimed at making the collaboration more effective. In 2012, the OSTC was integrated into an organization known as Canada’s Oil Sand

Innovation Alliance (COSIA) and is now referred to as the COSIA Tailings Environmental Priority Area or Tailings EPA. The membership of COSIA includes all of the surface mining oil sand companies and most of the in-situ oil sand companies, accounting for more than 90% of the total production in the oil sands. It has become the “hub” for most of the R & D environmental work done in the oil sands.

In addition to the increased level of effort on the part of industry, the Regulators have also been more active in terms of both the policy and regulations related to the management of oil sand tailings. The ERCB (now AER) issued a Directive (D074) in February of 2009 aimed at requiring specific amounts of “FFT forming fines” (defined as minus 44 microns) be captured in Designated Disposal Areas (DDAs). The Directive also requires that the resulting DDAs have a minimum shear strength of 5KPa within one year of placement. The Tailings Management Framework (TMF) is one of seven frameworks referenced within the Lower Athabasca River Plan (LARP). Work has been underway over the past several years to develop the TMF, which will provide the overall policy for management of oil sand tailings. Assuming things continue to progress, the TMF should be in place sometime early in 2015.

CONCLUSION

The history associated with learning how to manage oil sand tailings has been an “uphill battle” and has not been “won” as yet. The challenge is significant and getting bigger, now totaling almost one billion cubic meters of FFT. In order to successfully meet the challenge three things need to happen. We need to:

1. Dewater the fluid fine tailings,
2. Treat the residual process-affected water, and
3. Reclaim the resulting soft tailings deposits (both in terms of terrestrial and aquatic reclamation) so they can be integrated into the final mine landscape.

Industry has committed significant R & D resources over the past couple of decades – over the past 9 years alone, over \$630M has been spent across the industry on tailings research and development and the efforts continue through the COSIA Tailings EPA.

The Tailings Management Framework provides a solid “go forward” basis for the management of oil sand tailings, specifically the management of FFT. In order to successfully achieve the expectations associated with the TMF industry needs to make a number of things happen. They include:

- Meeting their FFT inventory targets,
- Meeting other environmental performance targets during active mining related to the total tailings footprint; water intensity; water quality; greenhouse gas emissions and energy intensity,
- Executing collaborative research and technology development programs that establish the capabilities of the treatment technologies and seek to push performance of these technologies by implementing a process of structured reviews and continuous improvement for all tailings technologies,
- Report transparently on annual progress of technology development programs,
- Conduct regular reviews of technology development programs,
- Design, build and operate the full-scale tailings management facilities,
- Meet the performance metrics for each deposit type for terrestrial and aquatic reclamation,
- Develop and implement industry best practice for wildlife safety (e.g. pond surface bitumen management, bird deterrent systems), and
- Evaluate opportunities for efficient, alternative use of process-affected water.

Over the past couple of years the COSIA Tailings EPA, working with the Canadian Association of Petroleum Producers (CAPP), has developed two “guideline documents” aimed at providing operators with the “tools” to successfully take on the “commercial” portion of the “things” that need to happen. They are available on the COSIA website and are referred to as:

- Technical Guide for Fluid Fine Tailings Management – 2012
- Guidelines for Performance Management of Oil Sands Fluid Fine Tailings Deposits to Meet Closure Commitments – 2014

A third document, entitled “A Guide to Audit and Assess Oil Sands Fluid Fine Tailings Performance Management” will also soon be published to complement the first two guides. The “Tailings

Technical Guides” provide a detailed and up-to-date technical review of current practices for managing the different types of tailings deposits using best available technology. Four different oil sand tailings deposits are included:

- Thin-layered Fines Dominated Deposits
- Deep Fines-Dominated (Cohesive) Deposits
- Fines-Enriched Sand Deposits
- Water-Capped Deposits

The Guides also include methodologies for the measurement, monitoring and reporting of Fluid Fine Tailings deposits. The Tailings Measurement Steering Committee, which is jointly chaired by a representative from COSIA and the AER, is also undertaking important work aimed at producing standards for the measurement of key tailings measures. This work will be another important part of what is needed to more effectively manage oil sand tailings.

Looking forward, there are a number of things that are important in order that we are successful in managing oil sand tailings. Firstly, in the longer term (i.e. before mine closure) a stable closure landscape must be established that directs surface water off the lease into established streams and supports the desired end land use objectives. When we say “stable” we mean resistant to natural processes, self-healing after natural erosion and there needs to be a self-sustaining, native vegetation cover. Secondly, in the shorter term (a limited timeframe after completing deposition) the ground surface needs to be reclaimed by placing a cover that is capable of supporting access and plant growth. We need to pursue solutions that make sense and fit the conditions and operating realities on each lease. We also need to use technically and environmentally effective and low-cost methods for the reclamation of oil sand tailings deposits. Lastly, oil sands operators need to be accountable to regulators for:

- Meeting the above objectives,

- Submitting plans that contain measureable performance goals,
- Measuring performance, reporting performance, and
- Taking action to improve performance when it doesn’t meet plans.

ACKNOWLEDGEMENTS

This paper, and associated key-note address at the 2014 IOSTC, has afforded me the opportunity to share my perspective on oil sand tailings, which has been a big part of my 35 year career in the oil sands. I very much appreciate the willingness of the conference organizers to give me the opportunity. Over my many years in the oil sand business I have had the opportunity to work with many great people – too many to mention, but I would like to take the opportunity to say thank you to all of them. Lastly, I would like to say thank you to my wife – she has supported me through all these years and I want her to know that I appreciate it very much!

REFERENCES

FTFC (Fine Tailings Fundamentals Consortium), 1995. In: *Advances in Oil Sands Tailings Research*, Alberta Department of Energy, Oil Sands and Research Division, Publisher.

Guidelines for Performance Management of Oil Sands Fluid Fine Tailings Deposits to Meet Closure Commitments, February 2014. Authors: John Sobkowicz, Alexander Hyndman, Richard Dawson and Bryan Watts.

Technical Guide for Fluid Fine Tailings Management, August 30, 2012, Authors: Nav Dhadli, Alan Fair, Alexander Hyndman, Adam Langer, Preston McEachern, Stuart Nadeau, Adrienne Nickerson, Fred Payne, Blair Penner, Bill Shaw and Rick Sisson.

BROAD SUITE OF PRACTICE AND TECHNOLOGY KEY TO SUCCESS IN TAILINGS MANAGEMENT

Peter Read
Syncrude Canada Ltd.

ABSTRACT

Tailings are a byproduct of the bitumen extraction process. Without intervention, the fluid fine tailings can remain suspended in slurry for decades, rendering timely terrestrial reclamation impossible. The challenge is amplified with rising tailings volumes that stem from the growth of the oil sands industry.

Oil sands operators are driven to solve the challenge in order to achieve their respective mine closure and reclamation objectives. Forgoing intellectual property conventions for common progress, stakeholders often come together in a variety of forums to share knowledge, results, resources, and best practices in the name of accelerated, industry-wide environmental progress.

Since conditions and circumstances vary from one location and time to another, there will very likely be no single solution to the tailings treatment challenge. A wiser and more prudent course entails a multi-pronged approach to research, development, and technology deployment—a program which produces a “silver suite” of technologies capable of addressing a host of technical and temporal problems. This paper summarizes some of the current and promising key elements in that suite.

INTRODUCTION

Background

Following the bitumen extraction process, tailings—a slurry consisting of oil sands process water, sand, silt, clay particles, and trace amounts of unrecovered bitumen—are placed into containment areas known as settling basins.

The tailings slurry, which initially ranges 45 percent to 55 percent solids, separates into three distinct parts in the settling basins: a sandy beach forms around the edges of the basin, a silt and clay layer

develops at the centre, and a water layer develops at the surface. Over time, the silt and clay layer consolidates.

As the settling of tailings occurs over time, water is released from the spaces between the silt and clay particles at the centre of the pond into the overlying water. This release of water causes the silt and clay to increase in density. This process is known as consolidation. Because this material is initially fluid-like, it is called fluid fine tailings. As it densifies, it will resemble a soft clay. Left to itself, fluid fine tailings can remain in a fluid state for decades, but this is not always the case.

The large volumes of tailings requiring containment need to be addressed in long-term mine and tailings plans and ultimately closure and reclamation landform planning.

Innovation is key to the reduction of environmental impact, the improvement of reliability, and to the reduction of cost. Syncrude’s “silver suite” of technologies to reduce and reclaim tailings currently comprises four components—centrifuged tails, composite tails, water capping, and accelerated dewatering. Research on these and other processes and technologies is systematic and ongoing.

Drivers of Performance

While the exact set of circumstances governing the pace and nature of tailings treatment from one operation to the next will vary, in the broad strokes there is a common context that will tend to guide or influence performance for all.

For example, the oil sands industry’s historical context envelops all operators, old and new—Syncrude was established in 1964 and began operations in 1978. As so-called legacy tailings are, to a degree, an inheritance from the past, the science and technologies in play or on the board today spring from a foundation of received sweat and intellect built in advance of the arrival of the current crop of young visionaries and geniuses. If

there are better ways, it is not too late to discover them. And no one starts from scratch.

Relatedly, leadership and continuous improvement in tailings treatment and reclamation technologies is typically a well-established mindset and long-standing value built into the mandates and driving the business plans of oil sands operators. The effective and responsible execution and achievement of closure and reclamation plans is a key goal and motivation of every environmental scientist, certainly a fundamental *raison d'être* of Syncrude's environmental research function, and a long-embedded principle underlying an ongoing commitment to corporate social responsibility, perhaps more commonly understood today as earning the social license to operate.

Oversight also frames leadership and commitment. There has been a long-standing requirement, for example, to contain all process-affected water on surface mined leases and tailings must be safely incorporated into reclaimed landscapes. Among guideposts are those contained in the Alberta Energy Regulator's Directive 074 (2009). It speaks to an undesirable increase in fluid tailings volumes, cites rising public concern, and "sets out new requirements for the regulation of tailings operations associated with mineable oil sands... [and] specifies performance criteria for the reduction of fluid tailings and the formation of trafficable deposits." Operators are required to "reduce fluid tailings through fines captured in dedicated disposal areas (DDAs)" and to submit DDA plans and annual compliance reports.

Tailings treatment will also typically take place within a business context comprising drivers such as affordability and technical feasibility (the Oil Sands Technology Deployment Roadmap project cited below, for example, found that the timelines for bringing potential tailings technologies to full commercial implementation ranged from five to more than ten years). This might be considered a limiting factor when viewed through a lens that focuses chiefly on economic variables like the timely allocation of scarce resources and opportunity cost-driven decisions. But, clearly, sufficient resources have been and remain in place—Syncrude, for example, is consistently one of Canada's top R&D spenders—to drive extensive and well-established science and research programs dedicated to a better understanding of the problems and of the best approaches to their resolution. Science is the foundation of the oil

sands industry and remains a key driver in almost all aspects of the modern-day business.

Partnerships in Innovation

While non-competitive collaboration in areas of strategic business operations is typically prohibited or frowned upon across most if not all industries, cooperation and the sharing of knowledge and information in oil sands science, research, and development in the name of improved environmental responsibility and preservation has in many ways become accepted, standard, innovative practice.

Some examples:

- Oil Sands Tailings Technology Deployment Roadmaps. In 2011, Alberta Innovates – Energy and Environment Solutions, in partnership with the Oil Sands Tailings Consortium, awarded a contract to the Consortium of Tailings Management Consultants to create a technology deployment roadmap and action plan to help achieve the goals spelled out in Alberta's Directive 074. The project produced five volumes of reports in 2012 that created a master list of technologies, documented the current state of practice and existing technology suites in the oil sands industry, captured the major constraints and influences on tailings management (every site at every point in time is unique), and formed feasible technology suites specific to each lease and mine. Nine technology deployment roadmaps were generated in a variety of tailings technology suites including centrifuging, thickening, and water-capped end pit lakes. It was concluded, among other things, that there is a "major opportunity to increase the performance and decrease the cost of existing tailings technologies."
- Canada's Oil Sands Innovation Alliance. COSIA brings together 13 oil sands producers—representing about 90 percent of Canadian oil sands production—to focus on accelerating environmental performance in oil sands through collaboration and innovation. Promoting transparency, sharing knowledge, collaborating on research and development, and eliminating monetary and intellectual property barriers, participating companies capture, develop, and share the most innovative approaches and best thinking to

improve environmental performance in the oil sands. There are four Environmental Priority Areas, or EPAs, including one for tailings which combines the experience and expertise of seven oil sands mining companies to find new technologies and solutions. Focus areas include the accumulation of fluid fine tailings within tailings ponds through the development of new and improved tailings management technologies, and accelerating the reclamation of tailings landforms so that they can be incorporated into the final reclaimed landscape. COSIA also builds on the experiences of the Canadian Oil Sands Network for Research and Development (CONRAD), which was established in 1994 as a network of companies, universities, and government agencies organized to facilitate collaborative research in science and technology for the oil sands. Its work has now been assumed by COSIA.

- The Oil Sands Tailings Research Facility. Owned by the University of Alberta and sponsored by COSIA, the OSTRF is dedicated to cross-disciplinary oil sands tailings research and development, and enables fundamental exploration of new concepts which can then be tested at a pilot scale. (Dr. Ward Wilson, NSERC Industrial Research Chair in Oil Sands Tailings Geotechnique at the University of Alberta, is also Principal Investigator at the OSTRF.) Conceived more than a decade ago in response to a growing industry awareness of a need for accelerated tailings reclamation, it is now the chief vehicle through which academia, industry, and government meet to discuss tailings issues in Alberta and disseminate research to the public. Locating the OSTRF adjacent to Natural Resources Canada's CanmetENERGY facility in Devon has allowed for closer collaboration and access to multi-million dollar state-of-the-art scientific research equipment and infrastructure.

A "SILVER SUITE" OF SOLUTIONS

While the fundamental challenge of tailings treatment can, in its expression, be reduced to simplicity—to create a trafficable surface for reclamation within a reasonable timeframe through dewatering—it has been understood for some time that there is no single antidote, no "silver bullet,"

for its resolution. There could well be, however, with the fitted puzzle pieces forming a somewhat altered final picture for each operator at any given time, a "silver suite" of solutions. In mine planning and operation, a solid slate of well-researched approaches imparts valuable flexibility and adaptability. It also helps reduce exposure to various risks: changing circumstances, new or amended regulation, ever-heightened stakeholder expectations, and growing knowledge bases, for example.

Accordingly, a number of tailings treatment technologies have been applied or are being tested, and some of the best proven or most promising are summarized below (respectfully noting that the probable bias in the selection towards technologies in play at the authors' employer is a function of familiarity and not deliberate favouritism).

Water Capping: Base Mine Lake

A key option for incorporating tailings into closure and reclamation plans is placing water over fluid fine tailings in an empty mine pit to create a relatively shallow lake.

Synchrude began investigating the feasibility of a lake concept in 1980 and initiated a rigorous research program that generated a large body of knowledge: 56 peer-reviewed scientific articles, for example, and 15 conference proceedings. There is more research behind this technology than any other tailings management technology in the oil sands.

A series of ten small test ponds and one larger pond were constructed in 1989. Findings show that the tailings at the bottom of the lake will continue to densify and become stronger over time. As this happens, the water layer on top will increase in depth, and biological changes (increasing populations of plants and aquatic life) are expected. Among some specific findings:

- An initial water cap depth of five metres is sufficient to prevent wind-induced mixing of tailings into the water cap.
- Over time, a layer of decayed organic material collects on the surface of the densifying tailings, further limiting the potential to re-suspend the tailings layer.
- Methanogens in the tailings can substantially increase the rate at which tailings densify.

- Movement of water from densifying tailings to groundwater would occur at rates that are negligible.
- Water quality will be influenced by the release of salts and bitumen from the densifying tailings. Water quality will improve over time as biodegradation and natural water inputs reduce concentrations of salt, bitumen, and organic compounds.

Toward proving the concept, Syncrude received Alberta government approval for the development of a commercial demonstration lake, called Base Mine Lake, in the former West Mine of the Mildred Lake site. The oil sands industry's first commercial-scale demonstration of water capping was commissioned in late 2012. A comprehensive research and monitoring program will study the performance of the lake as it develops into an aquatic ecosystem. The program will focus on issues of water quality, impacts of the underlying fluid fine tailings layer, performance of the littoral zone, interaction of biological communities, consolidation of the tailings, development of the shoreline, and establishment of plants and insects. Over a period of time, the lake is expected to develop characteristics similar to natural lakes in the region and be a healthy and sustainable aquatic environment.

Water capping is a safe method for long-term containment and densification of tailings, it does not require the addition of chemicals, and it allows time for natural processes to remediate water quality.

Centrifuging

Following more than 10 years of research including successful field pilots and an ongoing commercial demonstration project, centrifuge production capability will increase with when an additional tailings centrifuge plant now under construction at Syncrude is put in to service in 2015. With 18 centrifuges, the winterized \$1.9 billion plant will accelerate the reclamation process by centrifuging fluid fine tailings to create a clay soil material that can be used in post-mining landform construction.

In centrifuging, fluid fine tailings are withdrawn by a dredge situated in an existing fluid tailings pond. After initial screening of the FFT, gypsum and a polymer solution are added in the FFT stream and the mixture is fed into a centrifuge. Several centrifuges are utilized in parallel to handle the

desired volumes. The rotating speed and angle of the centrifuge control the amount of densification of the tailings. The resulting mud-like cake product is then fed onto a conveyor belt and dumped into a load-out facility for transfer into trucks for final cake deposition. The water phase in the centrifuges exits as centrate which is collected and then pumped back to the fluid tailings pond.

The cake will initially be used to reclaim portions of Syncrude's North Mine. Once the final deposit is sufficiently dense, reclamation soils are placed, and then planted with trees, shrubs, and other native vegetation.

The environmental benefit of centrifugation is immediate as it speeds the release of water from FFT and leaves behind a clay material that is dense enough and strong enough to meet the Alberta government regulations for tailings materials that can be used as a base for landform design and reclamation. Syncrude contributed the centrifuge technology to the COSIA Tailings EPA, which means it is available to all COSIA EPA members.

Composite Tailings

Composite Tailings, or CT, is another technology with a lengthy history of development that began in 1988-89 with a joint research effort between Natural Resources Canada and Syncrude. It quickly became known as the Fine Tails Fundamentals Consortium when others joined in the work. To produce CT, tailings are pipelined from the extraction plant to the CT plant, where they are cycloned to produce a densified coarse tailings stream. The stream (coarse sand) is combined with controlled amounts of fluid fine tailings and an amendment (gypsum) to create a non-segregating slurry. CT is transported hydraulically and discharged into a dedicated disposal area. Sub-aerial deposits consolidate relatively rapidly to form a soft, deposit that can be capped with sand and soil, enabling the development of landscapes that support forests and wetlands. Sub-aqueous deposits are expected to consolidate with continued loading and time to achieve a trafficable surface for reclamation. CT is being used in Syncrude's former East and West mines, as well as a portion of the North Mine which is still in operation.

CT placement in East Mine began in 2000 and was completed in 2011. Sand capping to establish closure drainage is ongoing. A 54-acre fen wetland

research project was constructed at the northwest end of this area. Permanent reclamation will begin in 2015.

In 2013, Syncrude completed the \$800-million Composite Tails plant at the Aurora Mine. Work is underway to improve CT deposition and increase fines captured through a technique which places CT under a layer of fluid fine tails in mined-out areas.

Accelerated Dewatering

A method called accelerated dewatering—also referred to as rim ditching and based on methods successfully used in the Florida phosphate industry—is being piloted to separate process water from large volumes of fluid fine tailings.

The technology mixes FFT with an organic flocculent—which binds the small clay particles suspended in water into larger flakes. Flocculent molecules wrap around the clay mineral particles in the FFT, forcing them to settle faster.

The flocculated FFT is then deposited in a containment area, and a rim ditch is dug around the deposit. As the sun dries this material, the surface begins to crack. Process water begins to drain out of the cracks, and is captured and drained off via the rim ditch and pumped back into the tailings pond. As the surface dries and becomes denser, it also becomes heavier which further weighs down on the rest of the wet materials inside the containment area accelerating the amount of water moving outward through the cracks. The process water is decanted down drainage ditches to a tailings pond, where it becomes available as recycled water for mine operations.

Initial tests have shown a reduction in FFT volume by 50 percent in three to five years. If field tests continue to be successful, accelerated dewatering could be an energy- and cost-efficient enhancement to tailings management activities.

The first Syncrude field study began in 2009 and a commercial-scale pilot project was conducted in 2013 to study how to more efficiently mix the FFT with flocculants. While helping to improve the accelerated dewatering process, the learnings will also help optimize flocculent mixing in other tailings treatment processes.

Overburden Mixing or Co-Mix

Over many years dating back to the mid-1980s, Syncrude has researched a method to co-dispose of overburden and FFT. Results suggest that the technology could be an innovative and efficient approach towards early reclamation.

Settling basin dredges are used to remove FFT which is pumped as slurry to a designated storage area. Overburden from regular mining activity is trucked to a location where it is mixed with the FFT using a controlled mass mixing ratio.

Overburden on the Syncrude leases commonly contains a clay shale material (Clearwater formation clays) with a very high plasticity range and is naturally very dry. FFT flows into this material and fills up void volume. Water is, thus, absorbed—FFT is “immobilized” in a block of soil—softening the clay shale, but leaving it with a strength of about 10 kPa. The deposit becomes strong enough to support a reclamation layer and will grow stronger with time as consolidation occurs.

Field pilots of the technology were being conducted at the time of writing to test variables such as deposit height and composition, slope stability, fluid retention, and other geotechnical properties, and mixing methods (e.g. wet crushing and conveyor).

The benefits of the technology are potentially several. For example, where other processes release some water, with Co-Mix the entire FFT volume is stored inside the existing void space of overburden stockpiles. There is no reliance on chemicals. Co-Mix is insensitive to FFT density, making it efficient for “mopping up” FFT that is not well suited for centrifugation. It is also cost efficient and a reclamation-ready surface can be produced without reliance on environmental drying.

Thickener Technology

Also known as paste technology, thickening involves rapid settling and sedimentation of tailings. Rather than being recovered from the settling basin, the tailings stream is sent from extraction through a cyclone separator, producing a coarse stream underflow and a fine stream overflow.

The underflow can be used as landform construction material. The fines-water overflow is directed to a thickener.

The Thickener induces gravity sedimentation with solids content being increased from a low of about 10 percent to high of about 55 percent (30-40 percent is typical). Thickening is aided by the addition of flocculants that bind the fines together into bigger particles and further accelerate gravity settling—what can take years to achieve in the settling basin can take just minutes or hours in the Thickener.

Once dried, the resulting clay material can be used directly in reclamation. Water, forced out of the fines as they are bound together and with little loss of process temperature, is recycled back to the plant.

Along with fellow researchers, Syncrude has conducted several large-scale thickened tailings field pilots starting in 2001.

Tailings Reduction Technology

Since 2003, Suncor has been researching, piloting, and commercializing an approach to tailings management called “Tailings Reduction Operations” (TRO™). Suncor is in the process of deploying this technology across its existing operations.

Shell Canada is also using a technology, called Atmospheric Fines Drying (AFD), to speed the treatment of tailings and create a dry material that will allow for faster reclamation. Through COSIA, Shell and Suncor, in conjunction with the other Tailings EPA members, are collaborating to improve these technologies.

In both the TRO and AFD processes, FFT is mixed with a chemical commonly used in municipal water treatment facilities to help settle out solids. This polymer flocculent sticks to the clay particles in the FFT and causes them to bundle together, allowing the clay to be separated from the water.

The thickened FFT is then deposited in thin layers on shallow slopes specifically constructed for dewatering. The water is returned to the tailings ponds where it can be reused in the bitumen

extraction process. The resulting material can be reclaimed in the same location where it was dried or transported to another location for final reclamation.

The use of TRO at Suncor’s oil sands mining operations is expected to result in a reclaimable surface ten years after initial disturbance, down from the 30 years it now takes.

Shell’s commercial-scale Atmospheric Fines Drying field demonstration has shown that AFD technology can make significant improvements to tailings drying time which can result in a fine tailings deposit which releases water and gains strength in weeks rather than decades.

Shell and Suncor have shared the work behind these technologies, in pursuit of working together to accelerate developments and improvements in the technology further and faster through COSIA.

CONCLUSION

While a great deal of progress has been made researching, developing, and deploying tailings treatment technologies over several decades, rising tailings volumes spurred by rising bitumen production present a serious and continuing business, social, environmental, and scientific challenge to oil sands operators.

Within the past decade or so, a variety of forces—rising social expectations and legislation established or amended to empower those expectations, key among them—have instilled a new, and not unwelcomed, sense of urgency throughout the industry—its multi-faceted, multi-disciplinary scientific component, in particular—to accelerate progress and the pace of reclamation.

Continued environmental leadership and steady adherence to the fundamental value of ensuring that the land is returned to the people of Alberta as according to closure and reclamation commitments are unwavering principles guiding practice in all circumstances. The future is, of course, unwritten and uncertain. But the foundation—a “silver suite” of treatment technologies—that will serve those who confront the challenges of tomorrow is a very strong and solid one.

REFERENCES

Oil Sands Tailings Technology Review, BGC Engineering Inc., July 2010.

Mining Methods and Mine Planning, T. Demorest, P. Read, K. Jonah, F. Payne, W. Kosik, R. Beers, Oilsands Handbook.

Oil Sands Tailings Technology Development Roadmaps, Project Report – Volume 1, Project Summary, J. Sobkowicz, June 2012.

Directive 074: Tailings Performance Criteria and Requirements for Oil Sands Mining Schemes February 3, 2009, Alberta Energy Regulator.

Directive 074 2013 Tailings Compliance and Pond Report, Syncrude Canada Ltd.

Syncrude Canada Ltd. 2013 Sustainability Report.

Also the websites of COSIA, Alberta Innovates – Energy and Environment Solutions, and the Oil Sands Tailings Research Facility.

Session 1

Tailings Dessication

INFLUENCE OF AN UNDERLYING SAND BEACH ON THE DRAINAGE AND DESICCATION OF FINE TAILINGS

Louis K. Kabwe, G. Ward Wilson, and J. Don Scott
University of Alberta, Edmonton, Alberta, Canada

ABSTRACT

Dedicated disposal areas for oil sands fluid fine tailings (FFT) are often constructed with underlying waste tailings sand. As drainage and drying of the fine tailings is an integral part of the disposal process, the influence of this more permeable foundation material is important in analyzing the performance of dedicated disposal areas. A laboratory research program was conducted to investigate the effect of such construction by conducting drying and soil water characteristic curve (SWCC) tests on flocculent amended oil sands FFT, on oil sands beach material and on a standard material (Devon silt fine soil). Geotechnical characterization tests on these three materials are first presented and reviewed, and then the drying and SWCC test results are presented and discussed. A comparison of the drying properties between the Devon silt standard material and oil sand FFT is made to investigate the unique properties and performance of FFT.

INTRODUCTION

Canada's oil sands operators produce large volumes of tailings from bitumen extraction processes. The fluid fine tailings (FFT) from the extraction plant are deposited in tailings ponds where sand is used to build dykes and beaches. Silts and clay fines with some residual bitumen flow into the tailings ponds and settle in about two years to a solids content of about 30%, and at this point the material is called mature fine tailings (MFT). Concern about the growing volume of stored FFT resulted in the Energy Resources and Conservation Board (ERCB, now Alberta Energy Regulator, AER) setting out new performance requirements for oil sands fine tailings (ERCB 2009). The objective was to reduce the amount of fluid tailings being produced through capturing 50% of the fines in the tailings feed in dedicated disposal areas. The criteria for acceptable disposal is that the FFT deposit must have a minimum undrained shear strength of 5 kPa after one year.

The objective of the research reported in this paper was to investigate the influence of the underlying sand beach on the drainage and desiccation of FFT. The performance of the FFT under various laboratory tests were compared to that of Devon silt standard material.

MATERIAL CHARACTERIZATION

Particle Size Distribution

The particle size distribution (PSD) properties of the FFT, Devon silt and beach sand samples are presented in Table 1 and Figure 1. Nondispersed and dispersed hydrometer tests were performed to determine PSDs and the degree of fines dispersion for the FFT and Devon silt samples (Scott and Jeeravipoolvarn 2004). The samples underwent hydrometer tests following the procedure outlined in ASTM D 4221-99R05 (ASTM 2005) to determine the dispersive characteristics of the clay soil by double hydrometer in conjunction with the ASTM D 0422-63R07 procedure for the standard particle size analysis of soils (ASTM 2007). The double hydrometer method compares the clay-sized fraction of a standard hydrometer test with a second hydrometer test that involves no mechanical agitation or addition of dispersing agent.

From previous testing experience, the nondispersive test better defines the particle sizes in flocculated oil sands tailings. These particles are composed of flocs and nondispersed clay aggregates while the dispersed test disperses these particles into their individual grain sizes. The nondispersed PSD is used in this paper to define the fines content ($< 45 \mu\text{m}$) and the clay size content ($< 2 \mu\text{m}$). Typically the dispersed measurements of the clay size content are larger than the nondispersed hydrometer measurements. The FFT had 93% fines while the Devon silt and beach sand had 100% and 11% fines, respectively. The clay-size content of the FFT was 10% while the clay-size contents of the Devon silt and beach sand were 30% and 5%, respectively.

The soil water characteristic curve (SWCC) properties of the FFT, Devon silt and beach sand are presented in Table 2 and Figure 2. The symbols represent measured data, and the solid lines represent the best fit lines generated using SoilCover software (2000). It should be noted that the SWCCs were measured using Tempe cells that have a maximum air entry of 500 kPa. Results of the tests presented in Figure 2 indicate that the air entry value (AEV) of the FFT could not be reached and is beyond 500 kPa. The first break in the FFT curve is due to sedimentation of the FFT in the cell and cannot be taken as the AEV curvature. The AEVs of the Devon silt and beach sand calculated using SoilCover are 6 kPa and 3 kPa, respectively. Figure 2 shows that all the specimens remained saturated at suctions below the AEV. As suction increases, the beach sand displays a sharp decrease (sharp slope) in water content past the AEV, while Devon silt displays a gradual decrease (smooth slope) in water content past its AEV. For example, as suction increases from 3 kPa to 10 kPa the water contents of the Devon silt and beach sand decrease from 21% to 4% and from 36% to 31%, respectively. Similarly, the water content of the FFT decreases from 45% to 37%. The residual water contents of the Devon silt and beach sand are 16% and 1%, respectively.

Drying Curves

Table 3 and Figure 3 present the drying test results for the FFT, Devon silt and beach sand. Figure 3 shows the ratio of actual evaporation to potential evaporation (AE/PE) versus time for each sample. All of the surfaces of the FFT, Devon silt and beach sand were initially wet or near saturation (i.e. AE/PE = 1) and were allowed to evaporate under atmospheric conditions. The AE/PE ratio for each sample began to decline as the availability of water decreased. In Figure 3, all of the drying plots show similar curvature at an AE/PE value of 0.8.

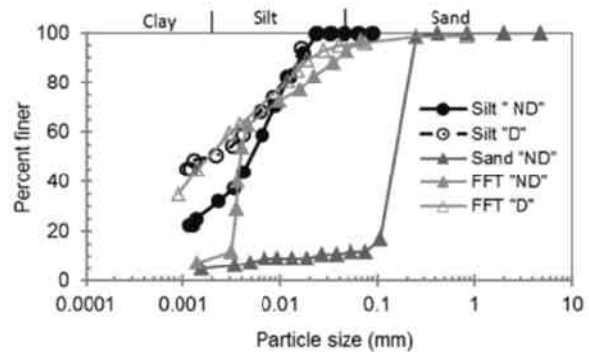


Figure 1. Particle size distributions of the FFT, Devon silt and beach sand

Table 1. Particle size distribution properties of the FFT, Devon silt and beach sand samples

Sample designation	Fines content (%) (D)	Fines content (%) (ND)	Clay size (%) (D)	Clay size (%) (ND)	Sand Content (%) (ND)
FFT	97	97	15	10	3
Devon silt	49	68	51	20	32
Beach sand	11	11	5	-	89

D= by dispersed hydrometer test; ND= by nondispersed

Table 2. Soil water characteristics curve (SWCC) properties of the FFT, Devon silt and beach sand

Sample designation	AEV (kPa)	Water content at 3 kPa (%)	Water content at 10 kPa (%)	Water content at 100 kPa (%)	Residual water content (%)
FFT	> 500	45	37	-	-
Devon silt	3	21	4	1	1
Beach sand	6	36	31	19	16

AEV = air entry value

Table 3. Properties of the FFT, Devon silt and beach sand during evaporation

Sample	AE/PE = 1 (Initial) Time (Day)	AE/PE ~0.8 (Boundary) Time (Day)	AE/PE ~0 (Residual) Time (Day)
FFT	0	11	28
Devon silt	0	7	16
Beach sand	0	7	10

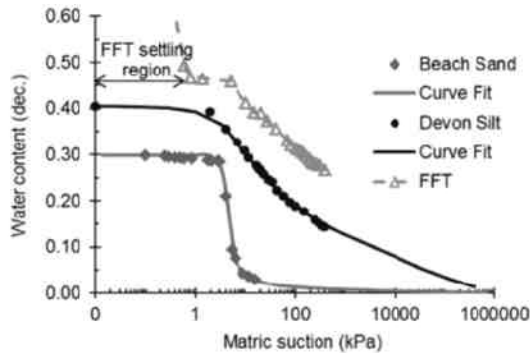


Figure 2. Soil water characteristics curves (SWCCs) of the FFT, Devon silt and beach sand

Soil Water Characteristic Curves

The AE/PE ratio for the FFT, Devon silt and beach sand initially decreased slowly with time, and each sample reached an AE/PE value of 0.8 at different times. The Devon silt and beach sand reached this value at the same time (i.e. Day 7), while the FFT reached this value at Day 11. As drying continued past the boundary, the beach sand displays a sharp drop in the AE/PE ratio, while the FFT and Devon silt display a gradual decrease in the AE/PE ratio to reach their lowest values of about zero. The AE/PE ratio of 0.8 represents the boundary between the saturated and unsaturated states of all the materials.

Table 4. Properties of the beach sand during direct shear

	Friction angle (°)
Peak	41.5
Residual	37.4

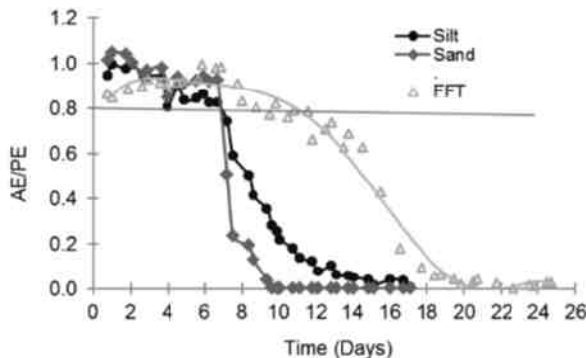


Figure 3. Drying curves of the FFT, Devon silt and beach sand samples

Direct Shear of Beach Sand

The drained, direct shear strength failure envelopes of the beach sand samples are presented in Figure 4. The friction angles are shown in Table 4 and are about 41° and 37° for the peak and residual strengths, respectively. These are characteristic of fairly dense fine/uniform sand.

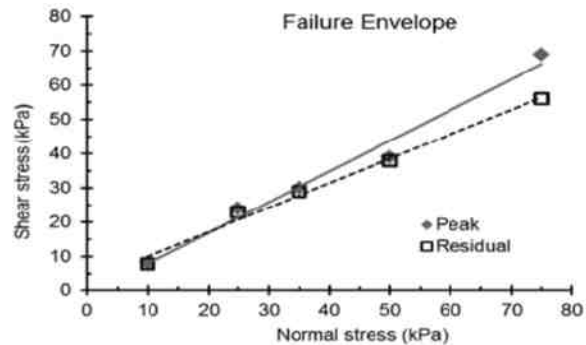


Figure 4. Direct shear test results for the beach sand

RESULTS AND DISCUSSION

Influence of an Underlying Sand Beach on the Drainage of FFT Material

Table 5 and Figure 5 present the results from the water drainage into the sandy underlying material, which were measured following the placement of FFT on the sand beach. The changes in suction were measured using two tensiometers installed in the sand beach at depths of 150 mm and 250 mm. The suction values at the near ground surface (150 mm deep) and 250 mm deep prior to placement of the FFT (i.e. Day 0) are 7 kPa and 5 kPa, respectively.

Following the FFT placement on Day 1, the suction at the near ground surface (150 mm deep) decreased rapidly from 7 kPa to 2 kPa, whereas the suction at a greater depth (250 mm deep) decreased slowly from 6 kPa to 5 kPa with time. The suctions for both tensiometers remained low for a period of about four days. The rapid decrease in suction at the near ground surface is attributed to rapid downward drainage of water released from the FFT placed on the sandy texture of the underlying material. It is also suggested that during downward drainage, water is simultaneously redistributing deeper into the sand profile due to capillary forces and gravity, thereby accelerating

drainage to greater depths. The time-variable rate of redistribution depends not only on the hydraulic properties of the sandy underlying material, but also on the initial wetting depth as well as on the relative dryness of the underlying layer (Capehart and Carlson 1997; Kabwe et al. 2005).

Figure 5 shows that the two drainage plots have similar curvatures following the placement of the second FFT layer (i.e. Day 17) on the previous dry FFT layer. The test data show a rapid decrease in suction from 10 kPa to 4 kPa and from 10 kPa to 6 kPa for the tensiometers at depths of 150 mm and 250 mm, respectively, and remain low for an extended period of time.

In summary, the downward drainage of water released from the FFT into the underlying sand material was initially rapid at the two depths due to

the free-draining texture and the dryness of the underlying material.

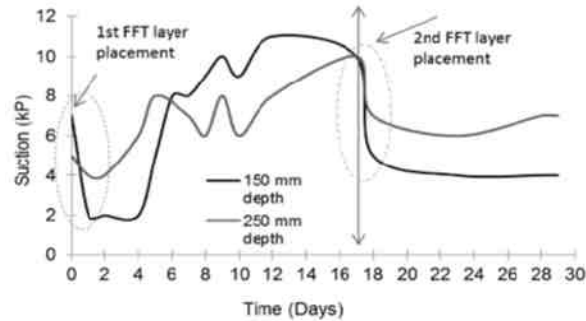


Figure 5. Drainage of the FFT into the underlying sand

Table 5. Properties of the beach sand during FFT placement

Depth of tensiometers in the sand (mm)	First layer of FFT placement suction (Initial 1)			Second layer of FFT placement suction (Initial 2)		
	Day 0 (kPa)	Day 1 (kPa)	Day 4 (kPa)	Day 17 (kPa)	Day 18 (kPa)	Day 24 (kPa)
150	7	2	2	10	4	4
250	5	4	31	10	5	5

Influence of an Underlying Sand Beach on the Desiccation of Silt Material

Table 6 and Figure 6 present the drying rates of the first layer of wet silt placed on the underlying dry and wet sand. Similarly, Table 7 and Figure 6 present the drying rates of the second layer of wet silt placed on the older dry silt layer. Figure 6 shows the AE/PE ratio versus time for each sample. All of the surfaces of the two samples were initially wet or near saturation (i.e. AE/PE = 1) and were allowed to evaporate under atmospheric conditions. The AE/PE ratio for each sample began to decline as the availability of water decreased.

The AE/PE ratios for both samples initially slowly decreased with time, and each sample reached an AE/PE value of 0.8 at different times. Results from Table 6 and Figure 6 indicate that it took about six days and 11 days for the silt on dry sand and on wet sand, respectively, to reach an AE/PE value of 0.8. As drying continued, the AE/PE ratios of the silt on dry sand and silt on wet sand then started to decline rapidly to reach their lowest values of about zero (i.e. residual). It can be concluded that

the AE/PE ratio of 0.8 represents the boundary between the saturated and unsaturated states of the two samples.

As the samples desaturate, their evaporation rates are the same. The silt on dry sand reaches its desaturation boundary faster because of the rapid downward drainage of water released from the wet silt to greater depths of the dry sandy texture. This is also due to capillary forces and gravity, thus hastening drainage to greater depths into the dry sand. This downward drainage of water was discussed in the previous section. The wet silt on wet sand with its higher initial water content dewatered much longer before it reached its desaturation boundary at an AE/PE of 0.8.

Table 6. Properties of the tested material after placement of the first FFT layer

Underlying material condition	First layer of wet silt placement		
	Initial AE/PE=1 (Day)	Boundary AE/PE=0.8 (Day)	Residual AE/PE=0.0 (Day)
Dry sand	0	6	13
Wet sand	0	11	18

Table 7. Properties of the tested material after placement of the second FFT layer

Underlying material condition	Second layer of wet silt placement		
	Initial AE/PE=1 (Day)	Boundary AE/PE=0.8 (Day)	Residual AE/PE=0.0 (Day)
Dry silt	25	28	48
Dry silt	25	28	48

Influence of an Underlying Sand Beach on the Desiccation of FFT Material

Table 8 and Figure 7 show the drying rates of the first layer of FFT alone and with FFT placed on dry and wet sand. All the surfaces of the three samples were initially wet or near saturation (i.e. AE/PE = 1; Day 1) and were allowed to evaporate under atmospheric conditions.

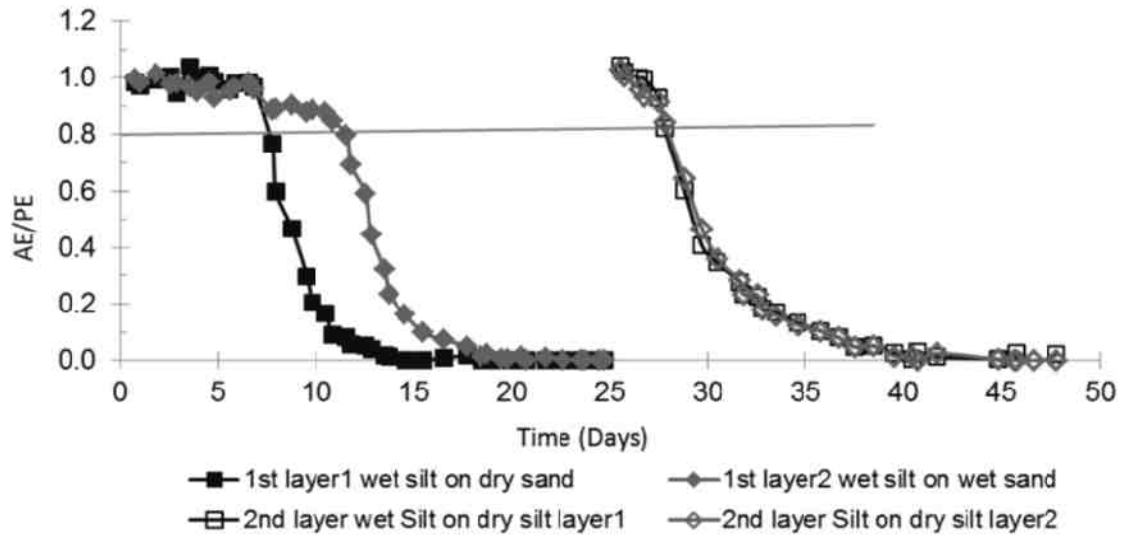


Figure 6. Drying curves of wet Devon silt placed on dry and wet underlying sand

The AE/PE ratios for all samples initially slowly decreased with time, and each sample reached an AE/PE value of 0.8 at different times. Results from Table 8 and Figure 7 indicate that it took about 10 days for the AE/PE ratios of the FFT alone and the FFT on dry sand to reach the value of 0.8. Similarly, it took 18 days for the AE/PE ratio of the FFT on wet sand to reach the value of 0.8. As drying continued, the AE/PE ratios declined rapidly at the same rate to reach their lowest values of about zero. For example, the AE/PE ratio of FFT on dry sand, FFT alone and FFT on wet sand reach their lowest values of 0.1 after 15, 17 and 21 days, respectively. It is interesting to note that the FFT alone desaturates faster than the FFT on wet sand. As noted previously in the silt drying tests, the wet FFT on wet sand with its higher initial water content will take much longer to reach its desaturation boundary at an AE/PE of 0.8.

Table 9 and Figure 7 also present the drying rates of the second layers of FFT placed on the older dry FFT layers. Results show that the second layers of all three FFT samples desaturate with the same

evaporation rate throughout the test period due to similar surface conditions.

In summary, during the drying tests, all of the drying plots for the three materials regardless of the underlying sand condition showed similar curvatures at an AE/PE ratio of 0.8. It was concluded that the AE/PE ratio of 0.8 represented the boundary between the saturated and unsaturated states of all the materials. The AE/PE rate is a function of soil texture, water availability and drying rate (Wilson et al. 1994 and 1997).

Table 8. Properties of the material during drying after placement of the first FFT layer

Underlying material condition	First layer of wet FFT placement		
	Initial AE/PE=1 (Day)	Boundary AE/PE=0.8 (Day)	Residual AE/PE=0.0 (Day)
Wet FFT	0	10	18
Dry sand	0	11	18
Wet sand	0	16	25

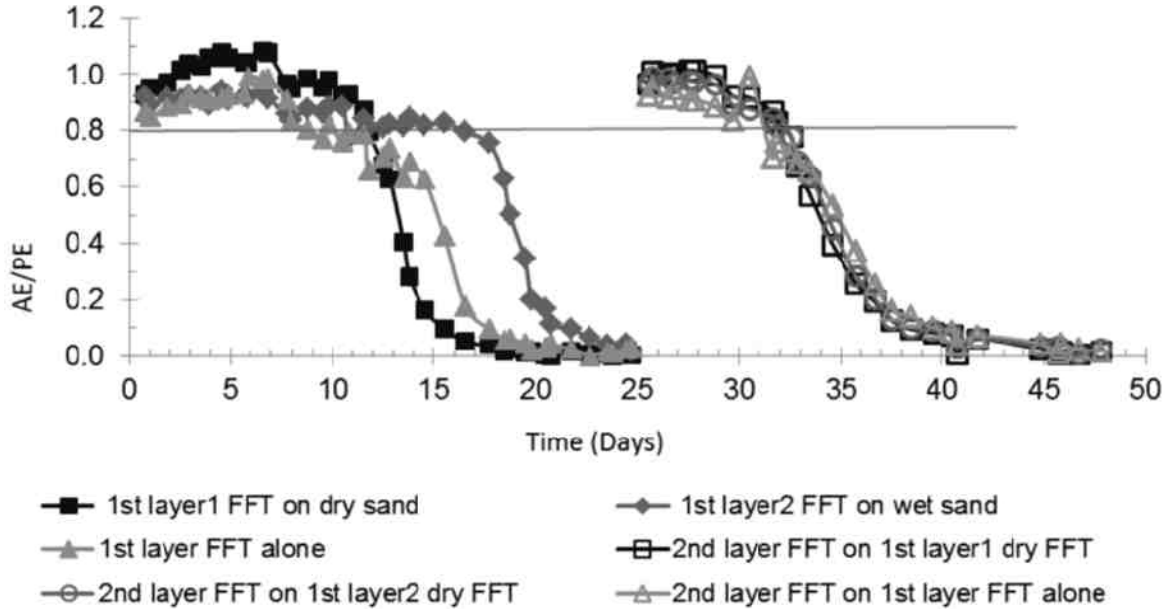


Figure 7. Drying curves of FFT placed on dry and wet underlying sand

Table 9. Properties of the material during drying after placement of the second FFT layer

Underlying material condition	Second layer of wet FFT placement		
	Initial AE/PE=1 (Day)	Boundary AE/PE=0.8 (Day)	Residual AE/PE=0.0 (Day)
Dry FFT	25	32	48
Dry FFT	25	33	48
Dry FFT	25	33	48

Comparison of the Influence of an Underlying Sand Beach on the Desiccation of Silt and FFT

Table 10 and Figure 8 compare the drying rates of the first and second layers of FFT and silt placed on dry underlying sand. Table 11 and Figure 9 compare the drying rates of the first and second layers of FFT and silt placed on wet underlying sand. Results from Table 10 and Figure 8 indicate

that it took about eight days and 12 days for the AE/PE ratio of the silt and FFT placed on dry underlying Devon silt, respectively, to reach the value of 0.8. Results also showed that it took three and eight days for the second layers of silt and FFT to reach the value of 0.8, respectively. Similarly, Table 11 and Figure 9 indicate that it took about 12 days and 18 days for the AE/PE ratio of the silt and FFT placed on wet underlying Devon silt, respectively, to reach the value of 0.8. Results also show that it took three and seven days for the second layers of silt and FFT to reach the value of 0.8, respectively. As all samples desaturate below the AE/PE ratio of 0.8, their evaporation rates are the same.

In summary, the Devon silt desaturates much faster (about 1.5 times) than the layer of FFT when placed either on dry or wet underlying sand.

Table 10. Properties of the material during drying after placement of the first layer on dry sand

Underlying material	First layer placement on dry sand			Second layer placement on dry first layer		
	Initial 1 AE/PE=1 (Day)	Boundary AE/PE=0.8 (Day)	Residual AE/PE=0 (Day)	Initial 2 AE/PE=1 (Day)	Boundary AE/PE=0.8 (Day)	Residual AE/PE=0 (Day)
Silt	0	8	14	25	28	41
FFT	0	12	19	25	33	46

Table 11. Properties of the material during drying after placement of the first layer on wet sand

Underlying material	First layer placement on wet sand			Second layer placement on dry first layer		
	Initial 1 AE/PE=1 (Day)	Boundary AE/PE=0.8 (Day)	Residual AE/PE=0 (Day)	Initial 2 AE/PE=1 (Day)	Boundary AE/PE=0.8 (Day)	Residual AE/PE=0 (Day)
Silt	0	12	18	25	28	40
FFT	0	18	23	25	32	46

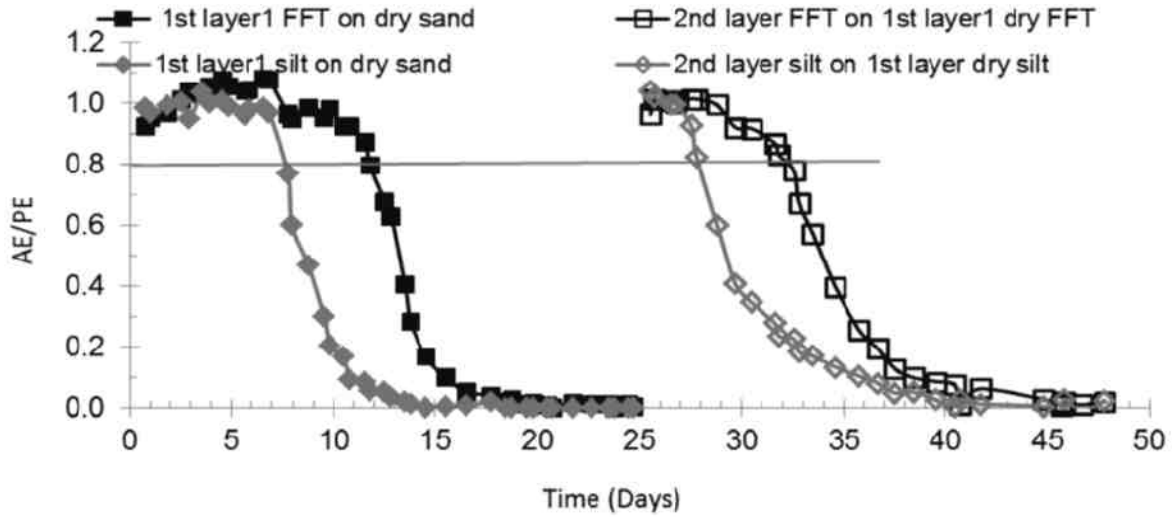


Figure 8. Drying curves of the Devon silt and FFT placed on dry underlying sand

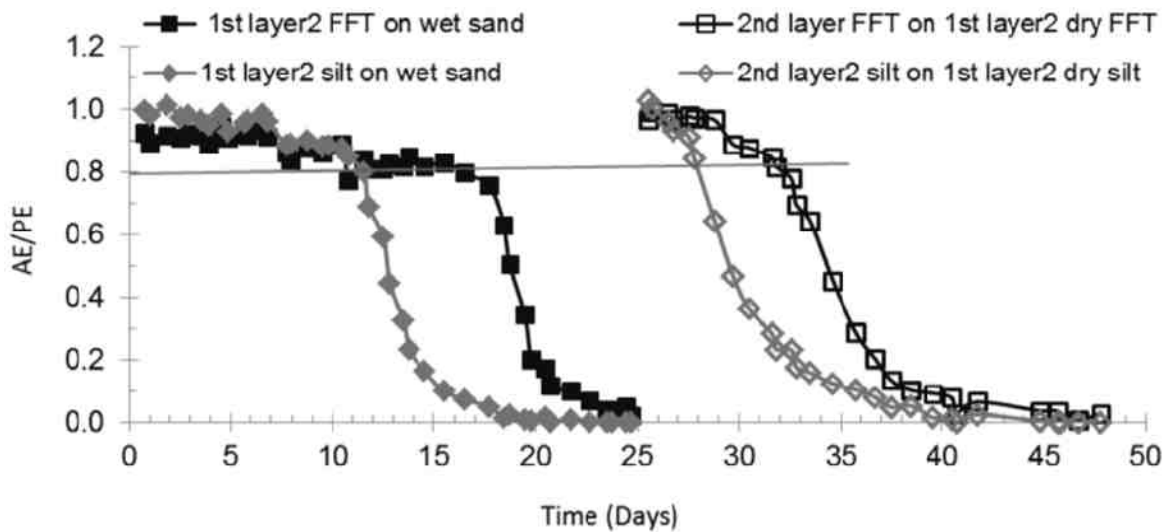


Figure 9. Drying curves of the Devon silt and FFT placed on wet underlying sand

OBSERVATIONS AND CONCLUSIONS

The AE/PE rate is a function of soil texture, water availability and drying rate. All of the drying plots

for the tested deposit layers regardless of the underlying material properties and conditions showed similar curvatures at an AE/PE ratio of 0.8. It was concluded that an AE/PE of 0.8 represented

the boundary between the saturated and unsaturated states of all the deposit materials. All of the samples' AE/PE ratios declined rapidly after an AE/PE of 0.8 and reached near zero within the same time. As the samples continued to desaturate below the ratio of 0.8, their evaporation rate is the same.

The AE/PE ratio of the first layer of silt/FFT placed on dry underlying sand results in lower initial water content and reached the boundary of AE/PE = 0.8 much faster than that placed on wet underlying sand. This is attributed to the drainage of water released from the silt/FFT deposit layer to the underlying sandy texture material. The silt/MFT layer placed on wet underlying sand with a higher initial water content initially dewatered much slower than that placed on dry sand.

There is no significant difference in drying time during the drying of the second silt/FFT layers placed on previous dry layers of the same material. A comparison between the drying rates of the first and second layers of Devon silt and FFT placed on either dry or wet underlying Devon silt shows that the Devon silt desaturates much faster (about 1.5 times) than FFT.

The oil sands industry is currently conducting a wide range of field tests as well as commercial-scale trials aimed at dewatering FFT deposits using atmospheric drying. The results of this study have demonstrated that the deposition of the first layer of FFT on a dry underlying porous sand material will result in rapid drainage of the water released upon deposition and therefore reduce the drying period of the FFT. The results of this study will help the oil sands operators in the construction and management of dedicated disposal areas for oil sands FFT.

ACKNOWLEDGEMENTS

This research was an internal project of the Geotechnical Centre at the University of Alberta and the graduate students who contributed to it are thanked. The authors also thank Vivian Giang from the University of Alberta Geotechnical Centre for her help in preparing the manuscript for publication.

REFERENCES

ASTM Standard D4221-99, 1999. 2005. Standard test method for dispersive characteristics of clay soil by double hydrometer. West Conshohocken, PA: ASTM International, doi: 10.1520/D4221-99R05.

ASTM Standard D422-63, 1963. 2007. Standard test method for particle-size analysis of soils. West Conshohocken, PA: ASTM International, doi: 10.1520/D0422-63R07.

ERCB. 2009. Directive 074: Tailings performance criteria and requirements for oil sand mining schemes. Calgary, AB: Energy Resources Conservation Board of Alberta.

Capehart, W.J. and Carson, T.N. 1997. Decoupling of surface and near-surface soil water content: A remote sensing perspective. *Water Resources Research*, **33**(6): 1383-1395.

Kabwe, L.K., Wilson, G.W. and Hendry, M.J. 2005. Effects of rainfall events on waste-rock surface-water conditions and CO₂ effluxes across the surface of two waste-rock piles. *Journal of Environmental Engineering and Science*, **4**: 469-480.

Scott, J.D. and Jeeravipoolvarn, S. 2004. Evaluation of particle size distribution test methods for Albian Sands Tailings. Technical report prepared for Alberta Energy Research Institute, Albian Sands Energy Inc. and Canadian Natural Resources Ltd.

Wilson, G.W., Fredlund, D.G. and Barbour, S.L. 1994. Coupled soil-atmosphere modeling for soil evaporation. *Canadian Geotechnical Journal*, **31**: 151-161.

Wilson, G.W., Fredlund, D.G. and Barbour, S.L. 1997. The effect of soil suction on evaporative fluxes from soil surfaces. *Canadian Geotechnical Journal*, **34**: 145-155.

SHRINKAGE AND SWELLING PROPERTIES OF FLOCCULATED MATURE FINE TAILINGS

Yutian Yao¹, A. Frits van Tol^{1,2}, Leon van Paassen¹, Philip J. Vardon¹
¹Delft University of Technology, Delft, the Netherlands
²Deltares, Delft, the Netherlands

ABSTRACT

In the atmospheric fines drying technique, mature fine tailings (MFT) are treated with polymers and deposited in thin layers on a sloped surface for sub-aerial drying. During the whole drying period, the tailings deposits can experience rewetting during periods of rainy weather or as result of the the placement of new layers. This paper addresses the shrinkage and swelling behavior of flocculated MFT (FMFT) under drying and rewetting cycles. The shrinkage and swelling paths of tailing samples were assessed by laboratory experiments. The results showed that the shrinkage-swelling process in a FMFT sample is reversible once the initial drying did not extend below the shrinkage limit of the soil or the soil reached an equilibrium stage which occurred after at least four shrink-swell cycles. The effects of the flocculation procedure on the shrinkage behavior were investigated.

INTRODUCTION

In Alberta, the atmospheric fines drying technique is currently being implemented on a commercial scale. In general, this technique involves the deposition of polymer treated mature fine tailings (MFT) of the oil sands mining process in a thin layer on a sloped surface. Upon deposition, the released water flows to the lower point and it is collected and recycled to the oil extraction process. The remaining clay sediments are subjected to atmospheric conditions for natural drying. Once a layer of mud is dried, another layer is placed on top of it and this process is repeated to build a soil deposit. Desiccation is the dominant process in the whole disposal period, meanwhile, the flocculated MFT experience rewetting due to environmental factors (i.e. precipitation) and the placement of new layers. As a result, the tailing deposits undergo cyclic shrinkage and swelling. In geotechnical engineering, the shrinkage and swelling behavior of soils is usually presented by the soil shrinkage or swelling characteristics curve,

SSCC, in which the volumetric water content is plotted versus void ratio. The shrinkage curve for a soil is one of the soil property functions, which is required when undertaking numerical modeling studies to predict the mechanical behavior of unsaturated soils (Fredlund 2000). The shrinkage behavior of clays with high water content has been extensively studied in recent years. Fredlund et al. (2011) assessed the SSCC of MFT sludge and used it to determine the primary reference point of the soil water retention curve (SWRC). The rewetting properties of MFT or flocculated MFT, however, are seldom reported.

This paper summarizes some results of the experimental program conducted at Delft University of Technology on oil sands fine tailings. In this research, the shrinkage and swelling paths of FMFT during several drying and rewetting cycles were determined. The data obtained from these experiments provide an insight into the properties of flocculated MFT and are necessary input for numerical modelling (e.g. Vardon et al., 2014).

SHRINKAGE AND SWELLING THEORY

The soil shrinkage is defined as the specific volume change of soil relative to its water content. It can be measured in most soils with more than 10% clay content (Boivin et al., 2006). The shrinkage property of a soil is characterized by its shrinkage curve which is a normally presented as a water content-void ratio plot. Figure 1 shows a typical shrinkage curve for a saturated soil. Several different stages of deformation can be identified from the curve. These stages are: (a) structural shrinkage, (b) normal shrinkage, (c) residual shrinkage and (d) zero shrinkage (Haines, 1923; Stirk, 1954). The structural shrinkage occurs only in well-structured soils. In the case of clay paste, this stage doesn't exist. In the normal shrinkage, decrease in total volume is equal to the volume of water lost. At the end of this stage, air enters the voids at a point that is regarded as the general air entry point and it is quite close to the plastic limit of

the soil. In the next stage, decrease in water upon drying exceeds the volume change of the bulk soil. Finally, the bulk volume of the soil remains constant as the water volume further decreases. During this stage, reorganization of clay particles does occur, leading to the formation of microscopic cracks. (Bruand and Prost, 1987, Cornelis et al., 2006). The shrinkage limit of a soil is defined as the water content corresponding to the minimum volume that a soil can attain upon drying to zero water content. It can be used to evaluate the shrinkage potential, crack development potential, and swell potential of cohesive soils. The shrinkage limit is determined experimentally, it can also be inferred from the SSCC which is shown in the graph.

Proposed by Fredlund et al. (2002), the shrinkage curve of an unsaturated specimen is similar to the one shown in Figure 2. There are also three stages during drying. In the first shrinkage stage, the shrinkage curve follows the line for the constant degree of saturation that the soil possessed before shrinkage. In the last stage, the void ratio remains constant as the water content further decreases.

microcracks close and the entrapped air further reduces. In the third phase, the soil reaches its maximum capacity of retaining water and no further volume changes take place.

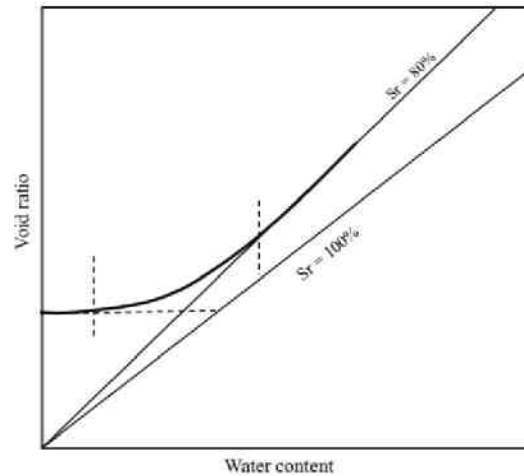


Figure 2. Schematic presentation of SSCC for a partially saturated clay after Fredlund et al. (2002)

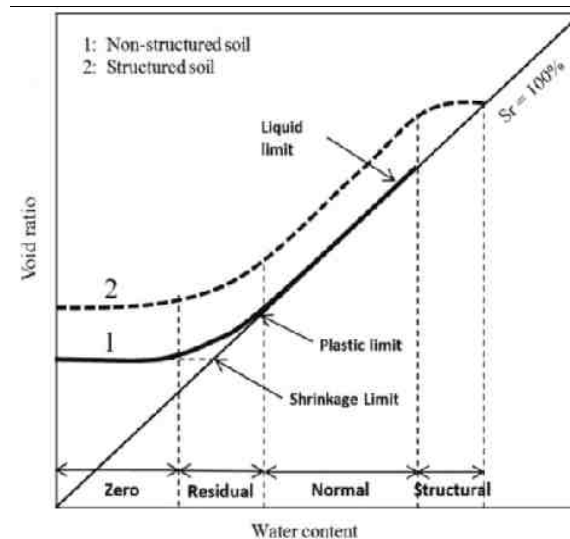


Figure 1. Typical SSCC for a nonstructured soil (solid line, 1) and a well-structured soil (dashed line, 2) after Cornelis et al. (2006)

Similar to the multistage shrinkage behavior of a soil, swelling of a desiccated soil also occurs in different stages that are, namely, (1) primary swelling, (2) secondary swelling and (3) zero swelling (Day, 1999). Most of the swelling completes in the primary swelling stage that occurs at a very rapid rate. In the second stage, some

MATERIALS AND METHODS

Materials and sampling method

MFT used in this program were obtained from Muskeg River Mine in Alberta, Canada. The MFT slurry contains 35% solids by weight and has a bulk density of 1200 kg/m³. Particle size analysis showed that approximately 90 % of solids are fines (<44 microns) and 60% of the material is classified as clay size particles (<2 microns). The specific gravity of the solids in MFT is 2.30. MFT sludge was flocculated by a high molecule weight polymer which was obtained from polymer company. Prior to flocculation, the MFT sludge was diluted to 21% in solids content suspension and about 500ml suspension was poured into a cylindrical mixing container which is 88 mm in diameter. A certain amount of polymer solution was injected into the tailings, then the MFT-polymer mixtures were agitated by a rotating paddle impeller which is 60 mm in diameter. The primary flocculation tests showed that the optimal dosage of polymer was 1000g dry polymers per ton of solids (1000g/t) and the optimal flocculation result was achieved when the mixtures were mixed at the speed of 200 rpm for 3 minutes. The optimum of flocculation result is defined as the fastest settling speed of flocs and the maximum amount of water released during 24

hours. After the mixing was completed, the sludge was allowed to settle for 24h and the released water was decanted. Next, the slurry was compressed in slurry consolidometer under air pressure (5-10 kPa) and oedometer (10-20 kPa) to remove excess water.

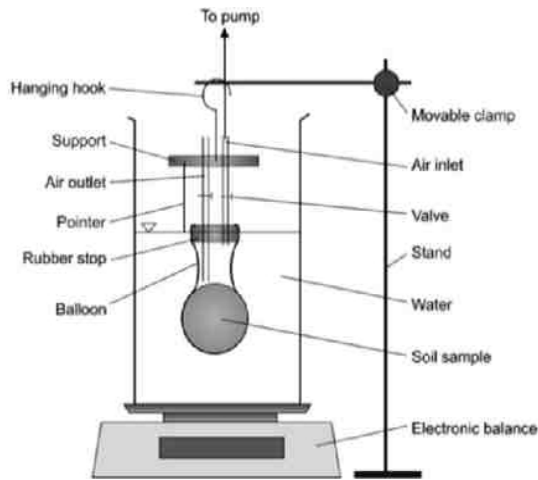


Figure 3. Setup for Tariq and Durnford balloon shrinkage test (Cornelis et al., 2006)

Soil shrinkage test

Determination of shrinkage curve requires continuous measurement of weight and bulk volume of a soil specimen during shrinkage. Two basic methods were employed to determine the SSCC. The first method (the geometry method) is to directly measure the dimension of the specimen at different stages of drying. The sample was confined in an oedometer ring and placed on a wax paper, and then the drying was commenced. At regular time intervals, the mass and dimension of soil were measured. The second method is called balloon shrinkage test developed by Tariq and Durnford (1993). The setup used in this test is shown in Figure 3. A soil clod (20-30 cm³) was inserted into a rubber balloon which was closed by a stopper with an air inlet and outlet. To allow drying, both valves were kept open and the air inlet was connected to an air pump which passed air at a low pressure (200 L/h) over the specimen. The mass of the specimen was measured by an electronic balance. The volume was determined by closing the air outlet and apply a small vacuum through the inlet to ensure a perfect fitting of the balloon around the soil sample, submerging the balloon under water and measuring the mass of

water replaced by the soil sample using the Archimedes principle. At the end of shrinkage, the soil sample was dried at 105 °C in the oven to calculate the water content at each measurement. The void ratio, e , and the degree of saturation, S_r , are calculated using the following formulas:

$$e = \frac{G_s(1+w)}{\rho_b} - 1 \quad (1)$$

$$S_r = \frac{G_s w}{e} \quad (2)$$

where G_s = specific gravity of solids, w = gravimetric water content, ρ_b = bulk density of soil.

Soil swelling test

Three different methods were used to investigate the swelling behavior. The first method is the volumetric swelling test performed with the oedometer device. The desiccated specimen was immersed under water in an oedometer cell and a surcharge pressure was applied on top of the specimen. The pressure applied was selected not to cause compression of the specimen during wetting process. The axial swelling of the specimen was monitored by a dial gauge that was connected to a computer. In the test two different boundary conditions were applied on the specimens. In the first condition, the only pressure applied on the specimen was the weight of the top loading cap. In this case, the soil was allowed to swell freely in both lateral and axial direction. In the second condition, the specimen was trimmed to be contained in an oedometer ring. During wetting, only axial swelling was allowed and measured.

In the second method, the tailing sample was wetted by applying a vacuum pressure (about 1 bar) in the vacuum saturation device. As shown in Figure 4, the soil specimen was contained in a steel ring between two pieces of porous stones and immersed under water in a vessel which is connected to the vacuum pump. During the saturation process, the lateral swelling is fully constrained while the axial swelling is partially constrained due to the elasticity of the rubber elastic. At different time, the total height (H) was measured using a caliper. Then the porous stones were removed and the weight of the soil and the ring) were determined. The third method is opposite to the shrinkage process, which aims to determine the rewetting paths of the SSCC. At the end of the shrinkage test, the soil sample (soil clod or cylindrical specimen) was immersed in water for

free swelling or confined swelling. The weight and volume of the sample were measured at different time by following the similar procedure to the shrinkage test. Prior to each measurement, free water left on the soil surface was removed by filter paper. To prevent collapse of the soil sample due to prolonged soaking, the cylindrical specimen was wound around by a plastic electrical tape (Figure 5). Since the electrical tape has some flexibility, the soil is in partially constrained condition in lateral direction.

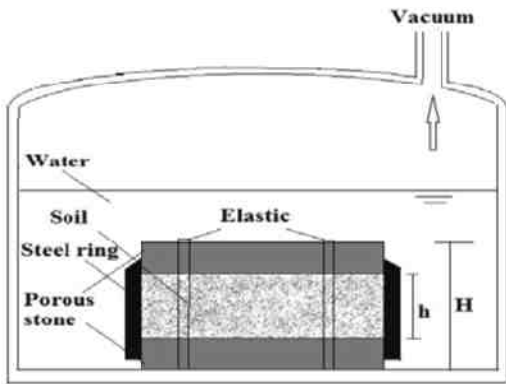


Figure 4. Vacuum saturation device used for rewetting of soil specimen



Figure 5. FMFT sample in the confinement of the electrical tape

RESULTS AND DISCUSSION

Shrinkage curve and shrinkage limit

Figure 6 provides the water content versus void ratio plots for saturated FMFT which were determined using the balloon method and the geometry method. The results obtained by the two methods were quite similar for the same material. However, the balloon method was capable of

generating a fluent curve which can be best fitted using the equation proposed by Fredlund et al. (1997, 2002, 2013). The equation has parameters with physical meaning, and is of the following form:

$$e(w) = a_{sh} \left(\frac{w^c}{b_{sh}c} + 1 \right)^{\left(\frac{1}{c}\right)} \quad (3)$$

where a_{sh} = the minimum void ratio, b_{sh} = slope of the line of tangency, c = curvature of the shrinkage, w = gravimetric water content, and $a_{sh}/b_{sh} = G_s/S_r =$ constant for a specific soil. In this case, the fitted parameters are: $a_{sh} = 0.705$, $b_{sh} = 0.303$, $c = 6.693$ and $a_{sh}/b_{sh} = G_s/S_r = 2.33$. Note that the experimental data did not coincide perfectly with 100% saturation line in the normal shrinkage stage, which is probably due to the accuracy of measurement. According to the SSCC determined, the plastic limit of FMFT was close to 40% (0.4) and the shrinkage limit was 31% (0.31). The minimum void ratio attained by the specimen was 0.70.

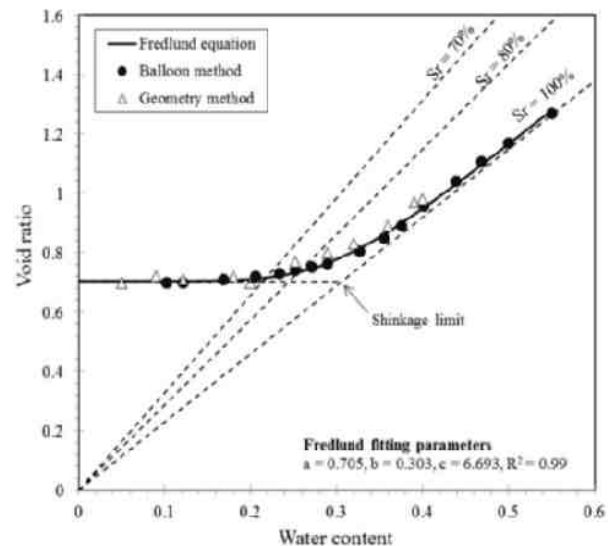


Figure 6. Observed SSCC for the flocculated MFT specimen (flocculated at the dosage of 1000g/t and mixed at 200 rpm for 2 min)

Swelling potential and swelling curves

Oedometer swelling tests provided information on the rate and magnitude of axial swelling for the tailings samples in different conditions. Figure 7 shows a time — vertical swell curve monitored for a desiccated FMFT (4% in water content) during free swelling. The three swelling stages (i.e.

primary, secondary and zero swelling) were identified from the curve. About 88% of total swelling completed in the first day upon wetting. The swelling speed then reduced significantly in the second stage and no swelling occurred in the third stage. Figure 8 shows the specimen at the end of swelling test, from which one can see a main horizontal crack and several minor vertical cracks on the side wall of the specimen. Occurrence of cracks could be attributed to the properties of FMFT and the method of experiment. In this case, microcracks may occur in the drying process due to reorganization of clay particles. Since there is no confinement on the soil during wetting, some of the cracks open up and grow bigger with increasing water content. The experimental results showed that this phenomenon was common for the FMFT samples when the specimen was not sufficiently confined during the long-term immersion in water. In this test, the total vertical swelling was 13% of the original height. The final void ratio and the saturation degree of the specimen were calculated using Eq. (2) and (3) and they were 1.17 and 90%, respectively. Note that in void ratio calculation the measured bulk volume of the soil contained the extra volume of cracks and it was larger than the real clay volume, thus the void ratio of the specimen was to some extent overestimated while the degree of saturation was underestimated.

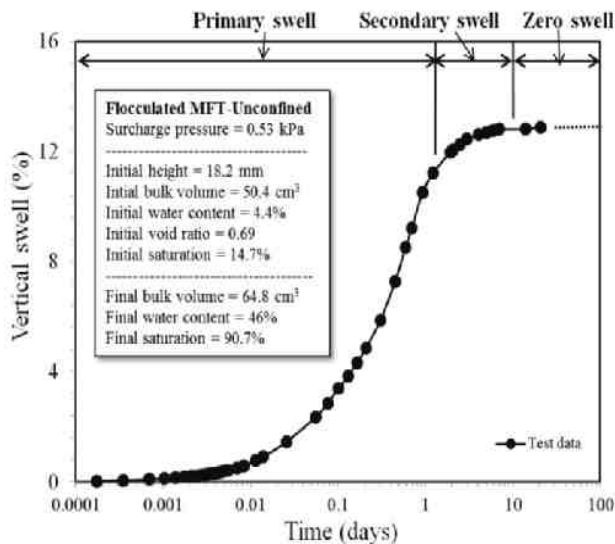


Figure 7. Vertical swell vs time curve determined for flocculated MFT in free swelling condition



Figure 8. FMFT specimen at the end of free swelling test

Table 1. Results of one-dimensional swelling tests for FMFT specimens

Sample ID	1	2	3	4
Surcharge (kPa)	1	1	1	20
Before swelling				
Height (mm)	16.6	19	19	15.2
Water content (%)	20	6	20	1.7
Void ratio	0.69	0.65	0.69	0.72
Saturation (%)	57	21	58	5.3
After swelling				
Height (mm)	20.6	22.9	23.0	15.8
Water content (%)	44	40	40	27
Void ratio	1.18	0.91	1.03	0.82
Saturation (%)	87	92	90	76
Swell potential	29	16	13	6

Table 1 offers the results of confined swelling tests. In this test, the FMFT samples were 50 mm in diameter and immersed in water under different surcharge pressures. The swell potential given in the table is calculated as:

$$Swell\ potential = \frac{\Delta e}{1+e_0} \times 100 \quad (4)$$

where Δe = increase in void ratio at the end of swelling, e_0 = void ratio of unsoaked sample. The results showed that the swelling potential of a specimen is related to its bulk volume, initial water content and surcharge pressure. In general, when the soil specimens are wetted in the same manner, the sample which initially has a smaller size, lower water content and lower surcharge pressure will have a larger swelling potential. Due to the lateral confinement of the ring, vertical cracks were not observed on the specimens, unlike for the free-swelling test (Figure 9). However, several very fine horizontal cracks occurred on the specimen,

except for Sample 4 which was under a significantly higher surcharge pressure. The final degree of saturation at the end of swelling was about 90% for samples 1, 2 and 3 and 73% for sample 4. As the free and confined swelling tests showed that the samples (provided they have an initial water content below 20%) did not reach full saturation upon rewetting under atmospheric conditions and apparently some entrapped air could not escape, the question was raised whether the desiccated tailings could reach a higher saturation value if they were saturated under vacuum conditions.

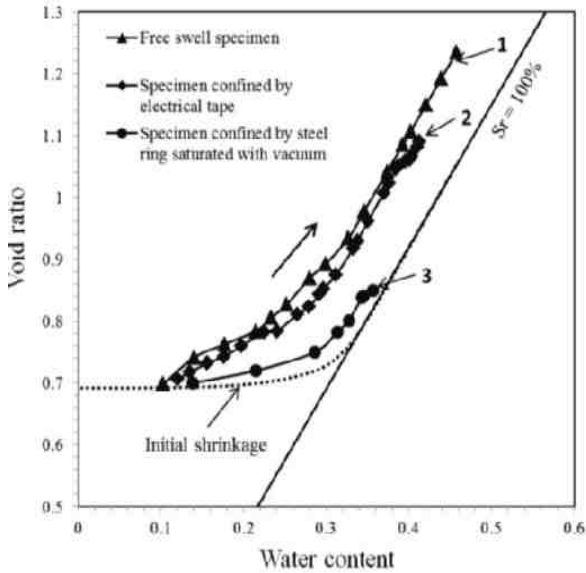


Figure 9. Rewetting curves for FMFT wetted in different conditions

Figure 9 shows the rewetting curves measured for different desiccated FMFT specimens. Specimen 1 and 2 were soaked with water in a container at atmospheric conditions. Specimen 1 was free swelling in all directions while specimen 2 was partially confined in lateral direction by an electrical tape (Figure 5). Specimen 3 was confined in a steel ring and saturated in a container under vacuum (Figure 4). It was seen that void ratios attained in the swelling path were higher than the corresponding values in the shrinkage path at the same water content, which is referred to as hysteresis. All of the swelling curves shared a similarity that two stages of swelling were identified. The first stage is a curvilinear portion with a higher tangent slope than the shrinkage curve in the same range of water content. In the second stage, the void ratio increases with the water content in a linear manner. The linear portion is parallel to the

100% saturation line. The results showed that the curve 1 and curve 2 were “parallel” to each other during the first and the early part of the second stage. At a water content of about 38%, the curve 2 bend off towards the 100% saturation line and formed a new line parallel to the 100% saturation line. Some fine cracks (0.1-0.2 mm) occurred on the specimen 1 and 2 during the second swelling phase. Reflected on the graph, the linear portion of the swelling path extended further since increase in bulk volume is equal to increase in crack volume. The curve 3 indicated that with the help of vacuum pressure (1 bar), most of the trapped air was discharged and thus a higher degree of saturation was obtained. Swelling cracks were successfully prevented due to the confinement of the steel ring and the porous stones. At the end of the second stage, the swelling curve approached the line of full saturation.

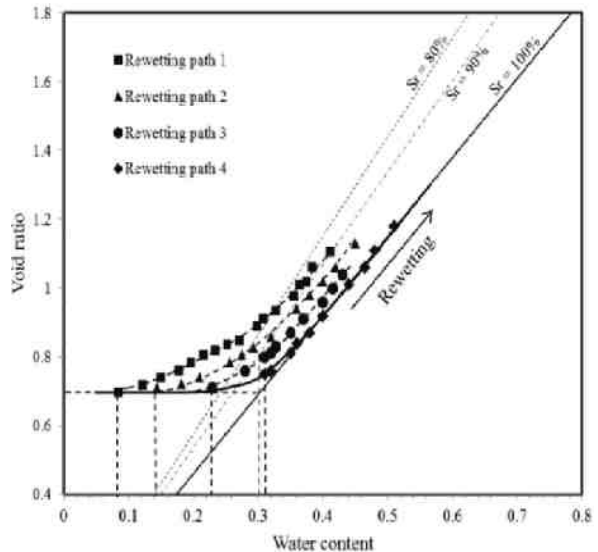


Figure 10. Effects of initial water content on the rewetting behaviors of FMFT

To evaluate the effect of the water content after drying on the swelling behavior of FMFT a couple of samples were dried to different water content. The specimens were then immersed under water without any confinement and the determined rewetting paths are shown in Figure 10. The graph shows that the rewetting paths are similar to each other in shape which consists of a curvilinear portion and a linear portion. As their initial water content decreases, length of the curvilinear portion increases and the residual saturation after rewetting. Note that for sample 4 which had the water content before swelling slightly higher than the shrinkage limit, the linear portion of the

swelling path coincided with the drying curve. We can conclude that once the soil drying does not extend below the shrinkage limit, the rewetting process is reversible. Otherwise, hysteresis occurs in the rewetting curves resulting a higher void ratio than the drying path.

Multiple shrinkage and swelling cycles

Figure 11 shows the shrink-swell paths of FMFT in the second drying and rewetting cycle. The soil specimen had the saturation degree of 86% at the end of the first shrinkage-swelling cycle. In the second cycle, the shrinkage path first followed the 86% saturation line before joining the initial shrinkage curve and ended at the same water content as the first drying process. The swelling path in the second cycle was above the drying path and it was almost the same as the swelling curve in the first cycle. Hysteresis in further drying and wetting paths reduced compared with the first cycle.

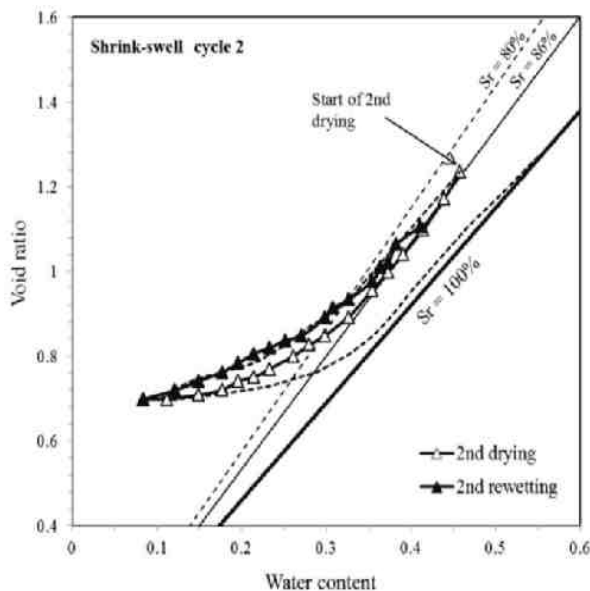


Figure 11. Shrinkage and swelling paths in the second drying and rewetting cycle

Based on the experimental results, a schematic presentation of the drying and rewetting paths is given in Figure 12. In this graph, point A is the minimum water content attained by the soil specimen during fist drying process. When the soil specimen is rewetted at this point, the difference in void ratio between the rewetting and drying path

(hysteresis) is maximized. The linear portion of the rewetting path AD is parallel to the 100% saturation line. Once the soil is dried for the second time at the point D, the drying path will follow the saturation line 1 and finally arrive at point B which has the same void ratio as point A. It indicates that the shrinkage curve for a partially saturated specimen will finally reach the initial shrinkage curve for the fully saturated specimen. The second rewetting path BE and the third drying path EC is similar to the curve AD and DB, respectively. The slope of the linear portion of the rewetting path is always less than that of the drying path.

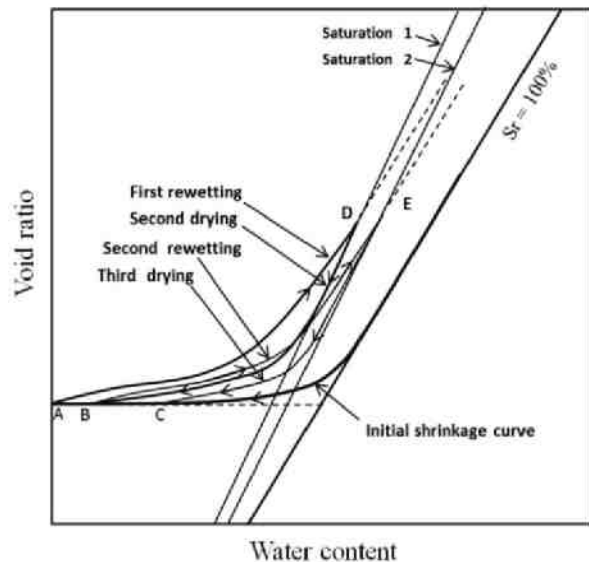


Figure 12. Schematic presentation of shrinkage and swelling curves for FMFT sample

Shrinkage and swelling behavior of a single desiccated FMFT specimen during five successive drying and rewetting cycles is illustrated in Figure 13. It was seen that hysteresis in drying and rewetting paths reduced with the increasing number of swell-shrink cycles. An equilibrium stage of soil occurred in the fourth cycle and the swell-shrink path was reversible. This phenomenon is quite similar to that observed by Tripathy et al. (2002) who performed drying and wetting tests on compacted expansive clay in four full swell-shrink cycles.

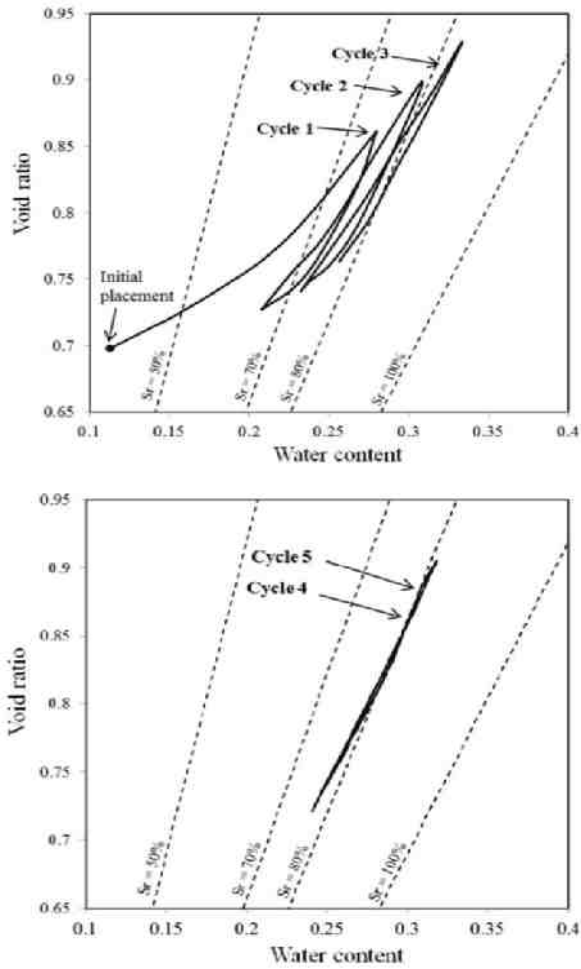


Figure 13. Shrinkage and swelling paths of the FMFT specimen in drying and wetting cycles

Effects of flocculation procedure

As indicated by Yao et al. (2012), the behavior of FMFT was affected by aspects of the flocculation procedure including type and dosage of polymer and mixing conditions. Figure 14 illustrates the effect of polymer dosage on the shrinkage characteristics of flocculated tailings. The curves showed that the minimum void ratio for the non-flocculated MFT was about 0.40 which increased to 0.57 and 0.7 after being treated with polymer at the dosage of 500g/t (0.5g/kg) and 1000g/t, respectively. The results indicate that, after being treated with polymer, the volume of the desiccated tailings increased by 12% and 25% for the FMFT specimens with 500g/t and 1000g/t, respectively.

Figure 15 shows the shrinkage results determined for FMFT samples that were mixed in different

conditions at a fixed dosage (1000g/t). In the residual and zero shrinkage stage, void ratios of the specimen varied with its mixing intensity and duration which is actually related to the mixing energy input. It indicates that when the specimen is over-mixed the final void ratio reduces relative to the specimen in optimal mixing condition. It is assumed that if the mixing is too intensive flocs are broken down and consequently leave an less open structure after settling and drying.

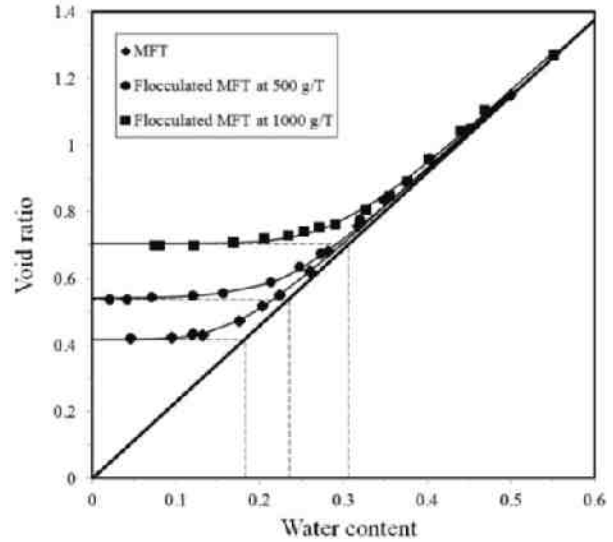


Figure 14. The shrinkage curves of tailings changing with polymer dosages

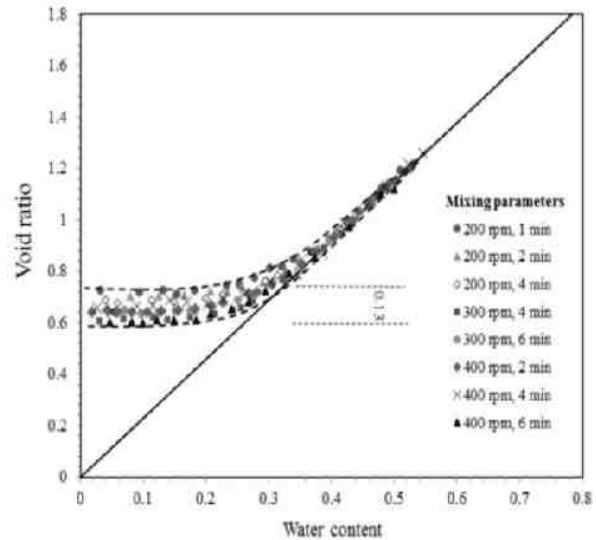


Figure 15. Effects of mixing conditions on the shrinkage curves of FMFT at 1000g/t

CONCLUSIONS

This paper explored the shrinkage/swelling behavior of flocculated MFT during drying and rewetting. The determined soil shrinkage characteristic curve (SSSC) showed that the shrinkage limit was 30% and the minimal void ratio was 0.7 for the tailing material that was treated by polymer at the dosage of 1000g/t and mixed at 200 rpm for 2 min.

Results of soil swelling tests showed that the rewetting properties of tailings were dependent on the initial water content, the confining pressure and the wetting method. Specimens with initial water contents below the shrinkage limit did not reach full saturation when allowed to soak up water under atmospheric conditions. When vacuum was used to rewet the soils full saturation was reached. In the free swelling condition, horizontal and vertical cracks occurred on the specimen which finally destructed the specimen. Therefore, the measured rewetting path of the specimen did not approach the fully saturation line. The determined rewetting curve consisted of a curvilinear portion and a linear portion that is parallel to the 100% saturation line.

Under the following conditions the shrink-swell process of the specimen is reversible: (1) when the initial drying process does not extend below the shrinkage limit of the soil and (2) when the soil is subjected to at least four shrink-swell cycles to reach an equilibrium stage. Otherwise, hysteresis occurs in the drying and rewetting paths showing larger void ratio in the wetting path than in the drying path.

Aspects of flocculation such as polymer dosage and mixing conditions can influence the properties of FMFT. Different polymer dosage results in different minimal void ratios of the specimen at the end of shrinkage, indicating a different volume of desiccated tailings.

REFERENCES

Bruand, A., Prost, R., 1987. Effect of water content on the fabric of a soil material: an experimental approach. *Journal of Soil Science*, **38**: 461–472.

Boivin, P., Garnier, P., and Vauclin, M., 2006. Modeling the soil shrinkage and water retention curves with the same equations. *Soil Science Society of America Journal*, **70**: 1082–1093.

Cornelis, W. M., Corluy, J., Medina, H., Diaz, J., Hartmann, R., Van Meirvenne, M., & Ruiz, M. E. 2006. Measuring and modelling the soil shrinkage characteristic curve. *Geoderma*, 137(1), 179-191.

Fredlund, M.D. 2000. Unsaturated soil property functions. Ph.D. dissertation. University of Saskatchewan, Saskatoon, 292 pp.

Fredlund, M., Wilson, G. and Fredlund, D. 2002. Representation and estimation of the shrinkage curve. Third international conference on unsaturated soils. UNSAT, 2002. March 10-13, 2002, Recife, Brazil. 145-149.

Fredlund D.G., Stone, J. and Stianson, J. 2011. Determination of water storage and permeability functions for oil sands tailings. *Proceedings tailings and mine waste 2011*. Vancouver, BC, Canada

Haines, W. B., 1923. The volume changes associated with variations of water content in soil. *Journal of Agricultural Science*, **13**: 296–311.

Stirk, G. B., 1954. Some aspects of soil shrinkage and the effect of cracking upon air entry into the soil. *Australian Journal of Soil Research*, **5**: 279–290.

Tripathy S, Rao K S S, Fredlund D G. 2002. Water content-void ratio swell-shrink paths of compacted expansive soils[J]. *Canadian Geotechnical Journal*, 2002, 39(4): 938-959.

Vardon, P. J., Nijssen, T., Yao, Y., van Tol, F. 2014. Numerical simulation of fine oil sand tailings drying in test cells. *Fourth International Oil Sands Tailing Conference (IOSTC'14)*.

Yao. Y., van Tol, F. Van Paassen, L. 2012. The effect of flocculant on the geotechnical properties of mature fine tailings: an experimental study. *Proceedings of 3rd international oil sands tailings conference*. Edmonton, Alberta, Canada, December 2-5, 2012.

DETERMINATION OF THE PERMEABILITY FUNCTION FOR DRYING OIL SANDS TAILINGS UNDERGOING VOLUME CHANGE AND DESATURATION

Feixia Zhang¹, Delwyn G. Fredlund², G. Ward Wilson¹ and Andrea Sedgwick³

¹University of Alberta, Edmonton, Alberta, Canada

²Golder Associates Ltd., Saskatoon, Saskatchewan, Canada

³Total E&P Canada Ltd., as Operator of the Joslyn Project, Calgary, Alberta, Canada

ABSTRACT

The coefficient of permeability function is one of the soil properties required for numerical modeling of transient seepage problems. Inaccuracies in the estimation of the coefficient of permeability can lead to erroneous numerical modeling results and can significantly affect subsequent engineering decisions. Both the degree of saturation and void ratio are factors that influence the coefficient of permeability. Methodologies presently available estimating the coefficient of permeability for an unsaturated soil are based on an assumption that no volume change occurs when soil suction is changed. In other words, consideration is only given to the influence of changes in degree of saturation. Conventional estimation techniques produce reasonable results when estimating the coefficient of permeability for unsaturated soils with low compressibility such as sands or silts, but the analysis protocols require changes when predicting the coefficient of permeability for materials that undergo volume change as soil suction changes, (e.g., Oil Sands tailings slurry). This means that the void ratio changes need to be considered as well as changes in degree of saturation. This paper presents a revised estimation procedure that considers the controlling factors of both volume change and desaturation.

INTRODUCTION

The oil sands bitumen extraction process in northern Alberta produces large volumes of high water content tailings composed of sand, silt, clay, and a small amount of unrecovered bitumen. When discharged into the tailings pond, the extraction tailings segregate with the sand plus about one-half of the fines dropping out to form dykes and beaches. The remaining water, bitumen, and fines flow into the tailings pond as Thin Fine Tailings (TFT) at approximately 8% solids content (BGC Engineering Inc., 2010). The fines settle to 20% solids content in a few months and to

30%-35% solids content in a few years. Upon reaching a solids content of 30%, the fine tailings are referred to as Mature Fine Tailings (MFT). MFT remains in a slurry state for decades and may take many years for self-weight consolidation because of its low water release rate (FTFC, 1995).

Significant portions of the fines remain in suspension after deposition resulting in a tailings management challenge for the industry. Different processes and technologies have been suggested to improve the water release characteristics of tailings. A more advanced disposal methodology named Fines-Sand Mixture Tailings (FSMT) has been developed and applied to improve the dewatering behavior of MFT. Composite/consolidated tailings (CT), thickened tailings, non-segregating tailings, and MFT-sand-overburden mixtures are four different FSMT disposal options that have been considered for treating Oil Sands Tailings (Sobkowicz & Morgenstern, 2009; BGC Engineering Inc., 2010). Sorta (2013) investigated the fundamental geotechnical behavior of FSMT at various SFRs including the relationships between Atterberg limits and clay content. The preliminary design of the tailings disposal often involves the numerical modeling of the dewatering behavior of FSMT at various SFRs. The correct numerical modeling of the dewatering behavior requires an appropriate coefficient of permeability function and a proper water storage function.

Both the void ratio and the degree of saturation are factors that influence the coefficient of permeability. Historically, the study of the coefficient of permeability for a soil has been categorized into two groups, namely, saturated coefficient of permeability and unsaturated coefficient of permeability. Saturated coefficient of permeability for most soils is a constant and thus measured experimentally. For a saturated soil that changes volume, the saturated coefficient of permeability becomes a function of the changing void ratio (Taylor, 1948; Chapuis, 2012). In unsaturated soil mechanics, the methods present in the existing

literature for estimating the coefficient of permeability for an unsaturated soil is based on an assumption that no volume change occurs as soil suction is changed, considering only the influence of the degree of saturation. Van Genuchten-Burdine equation (1980), van Genuchten-Mualem equation (1980) and Fredlund, Xing and Huang (1994) permeability function are three well-known unsaturated coefficient of permeability functions. These conventional methods produce reasonable estimations for the coefficient of permeability functions for either unsaturated soils with no volume changes or saturated soils with volume changes. FSMT has been found to be a typical soil that undergoes volume change as soil suction is increased during a drying process. In other words, neither a conventional unsaturated coefficient of permeability function nor a saturated coefficient of permeability function can mathematically describe the coefficient of permeability function of FSMT that undergoes a drying process featured by both desaturation and volume change. Both the void ratio and the degree of saturation must be considered when estimating the coefficient of permeability function for a drying FSMT.

This paper presents a revised methodology for the estimation of the coefficient of permeability function for soils that undergo volume change as soil suction is changed (e.g., Oil Sands tailings). Both the void ratio and the degree of saturation are taken into account as two influencing factors. Experimental data for Total tested thickened tailings are used to illustrate and explain the new estimation method.

CONCEPTUAL THEORY

Oil Sands tailings are a typical material that undergoes volume change as soil suction changes during a drying process. The drying process of such materials is complicated by the fact that both volume change and desaturation can occur during an increase in suction. The entire drying process can conceptually be divided into three stages. The first stage is within a suction range from zero suction up to the air-entry value (AEV) of the material. The AEV of the material (i.e., bubbling pressure) is the matric suction where air starts to enter the largest pores in the soil (Fredlund and Xing, 1994). The soil undergoes volume change with no desaturation during the first stage. During stage 1, the void ratio is the only factor controlling the coefficient of permeability of the material. In other words, the coefficient of permeability for a soil at the first stage is really the saturated coefficient of permeability changing with soil suction because of the changing void ratio that occurs with changing soil suction. The soil remains saturated as soil suction increases from zero to its AEV. Once the AEV is reached and exceeded, desaturation commences featuring the beginning of the second stage. The second stage of the drying process starts at the AEV and ends at a point where no further volume change occurs as desaturation continues with increasing soil suction. During the second stage, both volume change and desaturation impact the coefficient of permeability of the material.

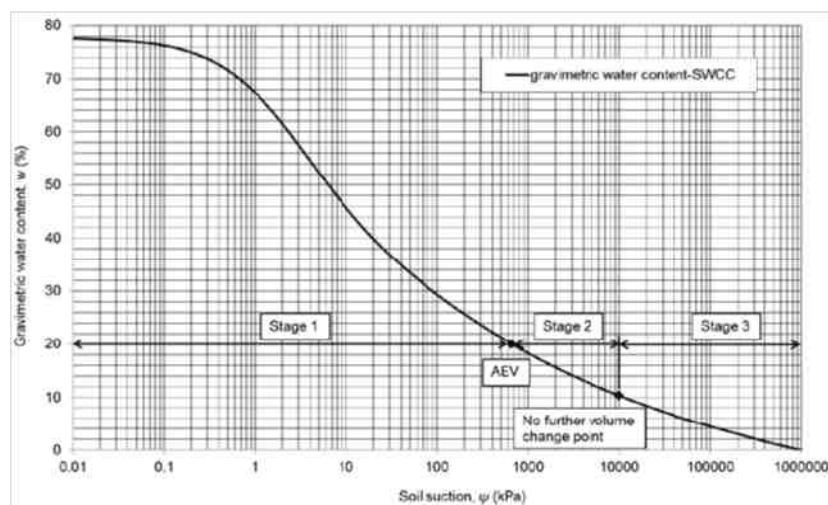


Figure 1. Conceptual plot showing three stages distinguished on the w -SWCC of a typical high volume change material.

At the end of the second stage, the third stage starts from the no-further-volume-change point and lasts until the zero water content point is approached. The coefficient of permeability for the soil at this stage is influenced by the degree of saturation.

The total suction corresponding to zero water content appears to be essentially the same for all types of materials. All materials become completely dry at a suction of approximately 10^6 kPa (Fredlund and Xing, 1994). Figure 1 is a conceptual plot showing the three stages distinguished for the w -SWCC (i.e., gravimetric water content SWCC) of a typical high volume change soil. The true air-entry value (AEV) should be determined from S -SWCC (i.e., degree of saturation SWCC).

ESTIMATION OF COEFFICIENT OF PERMEABILITY FUNCTION

Degree of saturation and void ratio are two controlling factors that influence the coefficient of permeability for a particular soil. Both degree of saturation and void ratio need to be considered in the estimation of the coefficient of permeability function over the entire suction range for a material that undergoes volume change during a drying process.

The coefficient of permeability at a particular soil suction during a drying process is the product of the relative coefficient of permeability and the saturated coefficient of permeability of the soil at the same state when it is undergoing single-phase water flow. A material at the same state means that it has the same skeleton with the same porous structure and void ratio without considering the degree of saturation.

$$k(\psi) = k_r(\psi) \times k_{ps}(\psi) \quad (1)$$

where,

$k(\psi)$ = coefficient of permeability at a particular suction ψ ,

$k_r(\psi)$ = relative coefficient of permeability at the suction of ψ ,

$k_{ps}(\psi)$ = potential saturated coefficient of permeability at a suction of ψ .

The potential saturated coefficient of permeability, $k_{ps}(\psi)$ does not mean that the material remains saturated at the suction of ψ with a saturated

coefficient of permeability of $k_{ps}(\psi)$. $k_{ps}(\psi)$ indicates the saturated coefficient of the permeability of a saturated material which has the same solid porous skeleton as the material at a suction of ψ during a drying process.

The relative coefficient of permeability must range between zero and one. In Phase 1, when soil suction ψ is less than the air-entry value (AEV), the soil remains saturated. The relative coefficient of permeability $k_r(\psi)$ for a saturated soil is 1.0. The coefficient of permeability $k(\psi)$ is the saturated coefficient of permeability equal to the relating potential saturated coefficient of permeability $k_{ps}(\psi)$ when the soil suction ψ is less than the AEV. In Phase 2 and Phase 3, when soil suction ψ exceeds the AEV, desaturation starts and the relative coefficient of permeability decreases from one down toward zero as the soil continues drying out. The coefficient of permeability $k(\psi)$ for a soil in the unsaturated state is smaller than the potential saturated coefficient of permeability $k_{ps}(\psi)$ due to the influence of desaturation.

Degree of saturation and void ratio are two main factors that control the coefficient of permeability of a particular material. Equation (1) reveals that degree of saturation influences the relative coefficient of permeability $k_r(\psi)$ while void ratio affects the potential saturated coefficient of permeability $k_{ps}(\psi)$. Changes in the degree of saturation change the tortuosity of the flow path within the porous media. The tortuosity controls the relative coefficient of permeability. In other words, the degree of saturation exerts an influence upon the relative coefficient of permeability by impacting the tortuosity of the flow path within the porous media. Theoretically, the saturated coefficient of permeability of a soil depends on pore sizes and the pore distribution or arrangement within the soil (Chapuis, 2012). A change in void ratio changes pore sizes, thus influencing the saturated coefficient of permeability of the soil. Degree of saturation and void ratio together govern the coefficient of permeability for a material that undergoes volume change as soil suction changes during a drying process, $k(\psi)$.

A number of research studies have been undertaken on changes in the saturated coefficient of permeability as a function of void ratio for saturated soils that undergo volume change (Chapuis, 2012). Equation (2) (Taylor, 1948) is found to be able to mathematically describe the relationship between the experimentally measured

saturated coefficient of permeability, k_{sat} and void ratio, e . This equation can be utilized in conjunction with a relative coefficient of permeability function to generate a coefficient of permeability function for a material that undergoes volume change as soil suction is changed during a drying process.

$$k_{sat}(e) = \frac{10^{-11} C e^x}{1+e} \quad (2)$$

where:

k_{sat} = saturated coefficient of permeability,
 e = void ratio,
 C, x = fitting parameters.

Void ratio is related to soil suction during a drying process where the material undergoes volume change as soil suction is increased (Fredlund et al., 2011). The relationship of void ratio to soil suction can be mathematically described by combining the shrinkage equation (Fredlund et al, 2002) and the mathematical equation for the gravimetric water content, w -SWCC (Fredlund and Xing, 1994). The potential saturated coefficient of permeability, $k_{ps}(\psi)$ can be mathematically described based on Equation (2) used in conjunction with the relationship of void ratio versus soil suction. The shrinkage curve equation (Fredlund et al, 2002) is shown as Equation (3).

$$e(w) = a_{sh} \left[\left(\frac{w}{b_{sh}} \right)^{c_{sh}} + 1 \right]^{\frac{1}{c_{sh}}} \quad (3)$$

where:

a_{sh} = the minimum void ratio, e_{min} ,
 a_{sh}/b_{sh} = slope of the line of tangency,
 c_{sh} = curvature of the shrinkage curve,
 w = gravimetric water content.

And the equation for the gravimetric water content, w -SWCC (Fredlund and Xing, 1994) can be written as shown in Equation (4).

$$w(\psi) = \frac{w_s \left(1 - \ln(1 + \psi/\psi_r) / \ln(1 + 10^6/\psi_r) \right)}{\left(\ln \left(\exp(1) + (\psi/a_f)^{n_f} \right) \right)^{m_f}} \quad (4)$$

Where:

ψ = soil suction;

a_f, n_f, m_f , and ψ_r = mathematical fitting parameters;

w_s = initial saturated gravimetric water content;

$w(\psi)$ = gravimetric water content at a designed soil suction of ψ .

The relative coefficient of permeability function $k_r(\psi)$ forms another important component composing the coefficient of permeability function $k(\psi)$ for a soil that undergoes volume change as soil suction changes. The relative coefficient of permeability of a material is a function of soil suction reflecting the influence of degree of saturation on the coefficient of permeability. Considerable research has been undertaken on the estimation of the relative coefficient of permeability in unsaturated soil mechanics. The relative coefficient of permeability is primarily determined by the pore-size distribution of the soil and its prediction is generally based on the soil-water characteristic curve. The Fredlund et al., (1994) permeability function is one of those commonly used unsaturated permeability functions. The Fredlund (1994) permeability function takes the following form:

$$k_r(\psi) = \frac{\int_{\ln(\psi)}^b \frac{\theta(e^y) - \theta(\psi)}{e^y} \theta'(e^y) dy}{\int_{\ln(\psi_{aev})}^b \frac{\theta(e^y) - \theta(\psi_{aev})}{e^y} \theta'(e^y) dy} \quad (5)$$

where:

$b = \ln(1000000)$,

y = a dummy variable of integration representing the logarithm of soil suction.

The soil-water characteristic, SWCC, presents the relationship between the amount of water in a soil and various applied soil suctions. There are four designations of water content commonly used to define the amount of water in a soil, namely, gravimetric water content, w , volumetric water content, θ (where the volume of water is referenced to the original total volume of the soil specimen), instantaneous volumetric water content, θ_i (where the volume of water is referenced to the instantaneous total volume of the soil specimen), and degree of saturation, S . With each designation of the water content, there is one form of the SWCC. As a result, there are four different forms of SWCC, namely, gravimetric water content-SWCC (w -SWCC), volumetric water content-

SWCC (θ -SWCC), instantaneous volumetric water content-SWCC (θ_r -SWCC), and degree of saturation-SWCC (S-SWCC).

For soils that do not undergo volume change as soil suction changes, all four SWCCs provide the same information to the geotechnical engineer when estimating other unsaturated soil property functions. However, for a soil that undergoes volume change as soil suction changes in a drying process, w -SWCC, θ_r -SWCC and S-SWCC are different from one another. It should be noted that S-SWCC must be used for the estimation of the relative coefficient of permeability function with Equation (5), while θ_r -SWCC should be used for the estimation of the water storage function in all cases.

PRESENTATION OF THE EXPERIMENTAL DATA

The thickened tailings, tested by Total E&P Canada (Total) are typical materials that undergo volume change as soil suction changes in a drying process. Box #11 and Box #2 (Fredlund et al., 2011) are two thickened tailings with different SFRs (sand fine ratios). Box #11 has a SFR of 0.8, and Box #2 has a SFR of 0.1. The experimental data of Box #11 and Box #2 are presented and interpreted using the proposed theory for the estimation of the coefficient of permeability function.

The thickened tailings in Box #11 had a liquid limit of 35% and a plastic limit of 15%. Box #2 had a

liquid limit of 55% and a plastic limit of 22%. Shrinkage curves and soil-water characteristic curves were measured. The shrinkage curve of the thickened tailings with SFR 0.8 (Box #11) is presented in Figure 2. The best-fitting parameters of the shrinkage curve for the thickened tailings with SFR 0.8 are $a_{sh} = 0.394$, $b_{sh} = 0.162$, and $c_{sh} = 3.208$. The average specific gravity of the tailings with SFR 0.8 was 2.43. The shrinkage curve of the thickened tailings with SFR 0.1 (Box #2) is presented in Figure 3. The best-fitting parameters of the shrinkage curve for the thickened tailings SFR 0.1 are $a_{sh} = 0.440$, $b_{sh} = 0.185$, and $c_{sh} = 7.277$. The average specific gravity of the thickened tailings with SFR 0.1 was 2.38.

Figure 4 shows the gravimetric water content, w , plotted versus soil suction for Total tested thickened tailings Box #11 and Box #2. The experimental data for the gravimetric water content soil-water characteristic curve, w -SWCC was best-fitted with Fredlund and Xing (1994) equation, Equation (4). The best-fitting parameters for Box #11 are $a_f = 0.457$ kPa, $n_f = 0.792$, $m_f = 0.907$ and $\psi_r = 52.84$ kPa. The initial gravimetric water content for Box #11 was 73.8%. The best-fitting parameters for Box #2 are $a_f = 1.250$ kPa, $n_f = 0.982$, $m_f = 0.612$ and $\psi_r = 107.4$ kPa. The initial gravimetric water content for Box #2 was 77.70%. w -SWCC is used in conjunction with the shrinkage curve to calculate other forms of SWCC and properly interpret the SWCC results to determine the true AEV and estimate the relative coefficient of permeability function.

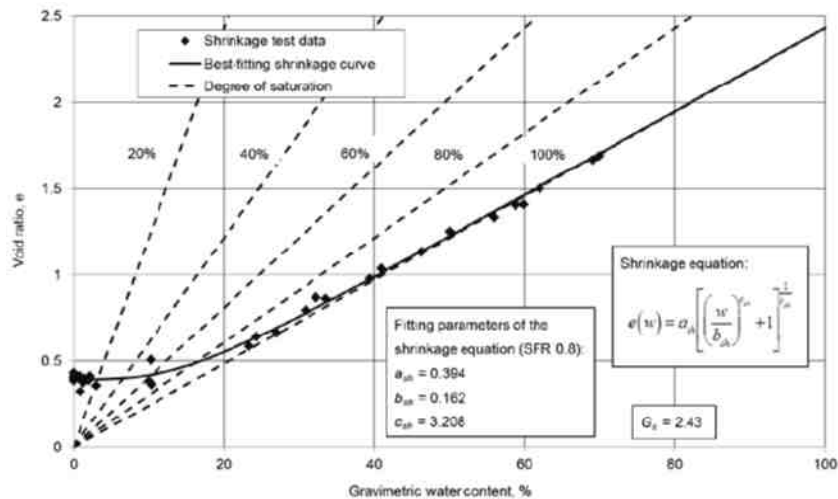


Figure 2. Shrinkage curve for Total tested thickened tailings of SFR 0.8 (Box #11).

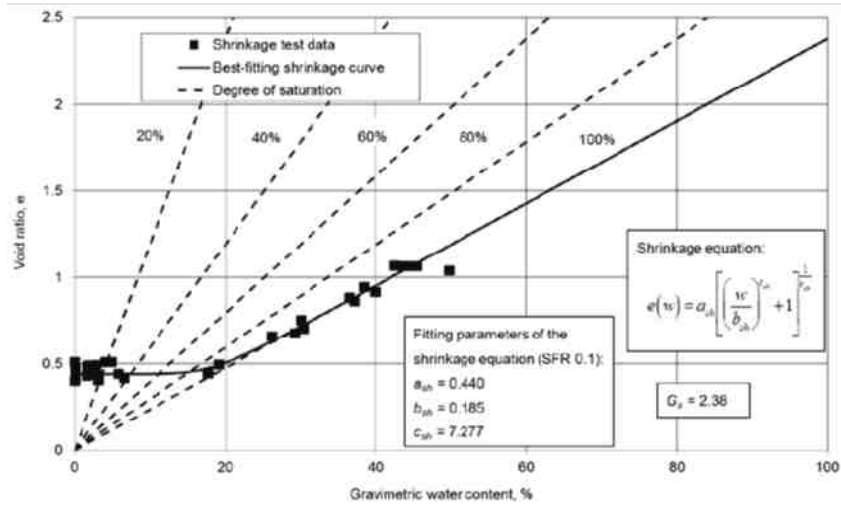


Figure 3. Shrinkage curve for Total tested thickened tailings SFR 0.1 (Box #2).

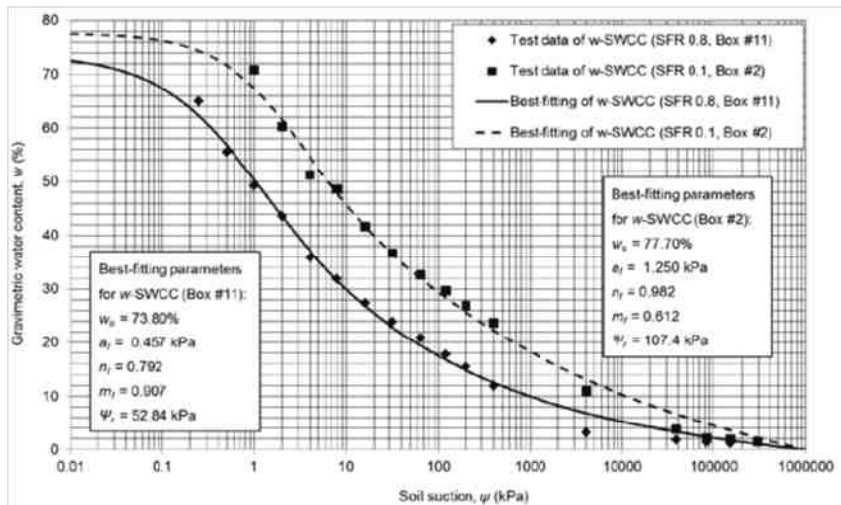


Figure 4. Gravimetric water content versus soil suction

The experimental data for the relationship of saturated coefficient of permeability versus void ratio were also obtained for Total tested thickened tailings. The experimental data were best-fitted by Equation (2). Figure 5 shows the measured data and the best-fitting curves for Box #11 and Box #2. The fitting parameters for Box #11 are $C = 226.47$ and $x = 3.277$. And the fitting parameters for Box #2 are $C = 8.073$ and $x = 3.042$.

These three curves obtained from the laboratory test, namely the shrinkage curve, the w -SWCC and the curve of saturated coefficient of permeability versus void ratio form the basis to further estimate the appropriate coefficient of

permeability function for a soil that undergoes high volume change as soil suction changes, such as thickened tailings tested by Total.

INTERPRETATION OF THE EXPERIMENTAL DATA

The gravimetric water content-SWCC, w -SWCC is combined with the shrinkage curve to obtain other forms of SWCC. The resulting plot of the S -SWCC is presented in Figure 6. The true air-entry value (AEV) for a material that undergoes volume change as soil suction is changed is obtained from

the S-SWCC of the soil. Using the graphical construction method suggested by Vanapalli et al., (1998), the true AEVs interpreted from the S-SWCCs in Figure 6 are 33.2 kPa for Box #11 and 658 kPa for Box #2. The plot of θ_r -SWCC is shown

in Figure 7. The θ_r -SWCC is the correct form of SWCC that should be used for the estimation of the water storage function in the case where soil undergoes volume change as soil suction is increased in a drying process.

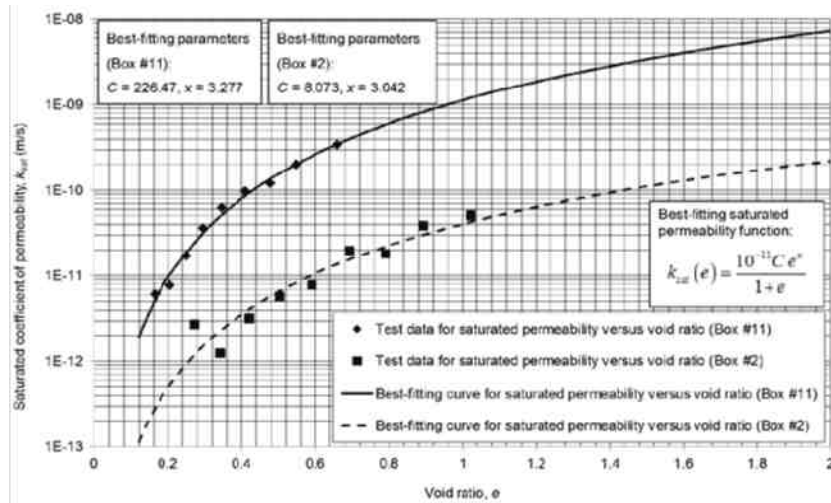


Figure 5. Measured data and its best-fitting of saturated coefficient of permeability versus void ratio for Total tested thickened tailings (Box #11 and Box #2).

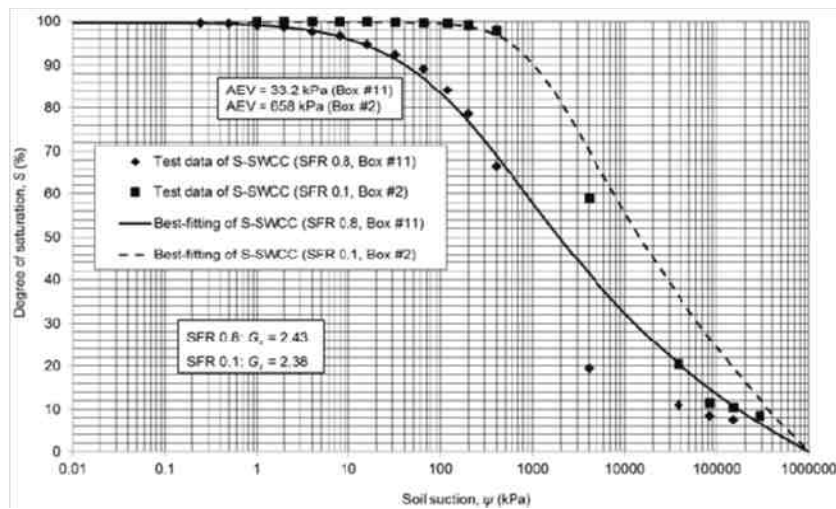


Figure 6. Measured data and its best-fitting of the S-SWCC for Total tested thickened tailings (Box #11 and Box #2).

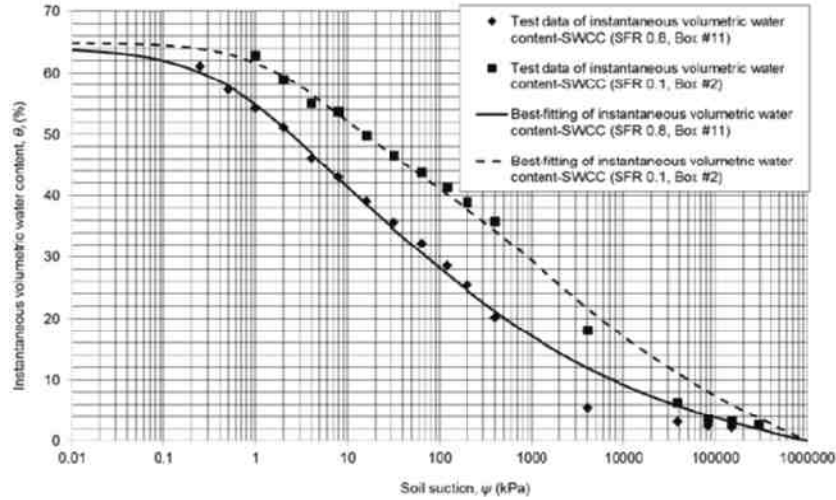


Figure 7. Measured data and its best-fitting of the θ_i -SWCC for Total tested thickened tailings (Box #11 and Box #2).

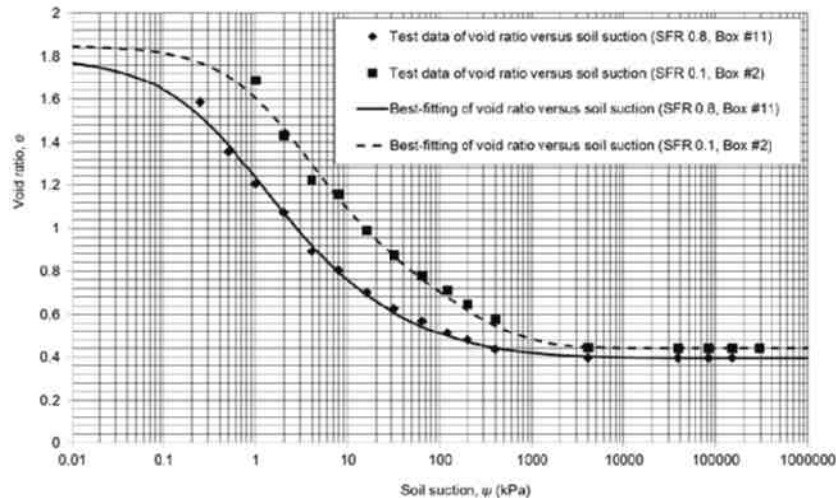


Figure 8. Measured data and its fitting for the relationship of void ratio versus soil suction for Total tested thickened tailings (Box #11 and Box #2).

The relationship between void ratio and soil suction is obtained by combining the w -SWCC and the shrinkage curve. The plot of void ratio versus soil suction is shown in Figure 8. For Box #11, the void ratio decreases from 1.798 to 0.603 when the soil suction increases from 0 to its AEV of 33.2 kPa. The void ratio at the AEV of 33.2 kPa is 0.603 for Box #11. For Box #2, the void ratio decreases from 1.849 to 0.507 when the soil suction increases from 0 to its AEV of 658 kPa. The void ratio at the AEV of 658 kPa is 0.507 for Box #2. For both Box #11 and Box #2, the soil specimen experiences significant volume change before the soil suction reaches the AEV during its drying process.

Comparing to the volume change at the early stage of the drying process before the AEV is approached, the volume change of the specimen is relatively small and insignificant after the soil suction exceeds the AEV.

The saturated coefficient of permeability is related to void ratio, while void ratio changes with soil suction during the drying process of Total tested thickened tailings. As a result, saturated coefficient of permeability can be written in terms of soil suction. When the saturated coefficient of permeability is related to soil suction, it is referred to as potential saturated coefficient of permeability

to make a distinction because there are both saturated and unsaturated conditions during the entire drying process. The curves of the potential saturated coefficient of permeability versus soil suction for both Box #11 and Box #2 are shown in Figure 9.

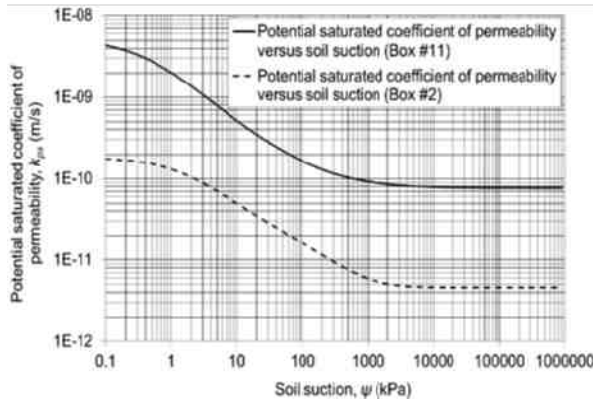


Figure 9. Potential saturated coefficient of permeability versus soil suction for Total tested thickened tailings (Box #11 and Box #2).

The curves of the relative coefficient of permeability versus soil suction for Total tested thickened tailings Box #11 and Box #2 are presented in Figure 10. Figure 10 shows that the relative coefficient of permeability remains 1.0 until the soil suction approaches the AEV of the soil. When the AEV is surpassed, the desaturation starts and the relative coefficient of permeability reduces from 1.0 towards zero. The correct curve for the relative coefficient of permeability versus soil suction is obtained from S-SWCC with the AEV as the lower limit of integration for the integral in the denominator of Equation (5). After having the relative coefficient of permeability function shown in Figure 10 and the potential saturated coefficient of permeability function shown in Figure 9, the coefficient of permeability function can be obtained by multiplying the relative coefficient of permeability function with the potential saturated coefficient of permeability function according to Equation (1). The curves of the coefficient of permeability versus soil suction for Total tested thickened tailings for Box #11 and Box #2 are presented in Figure 11.

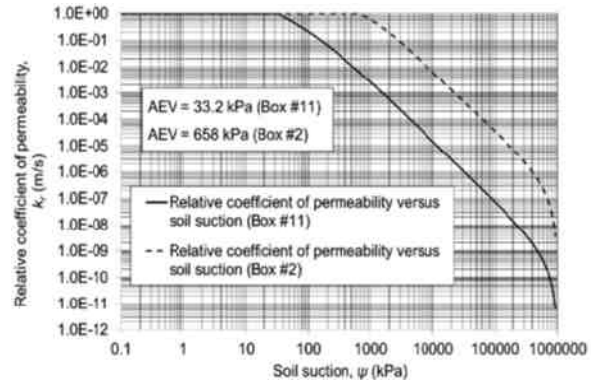


Figure 10. Relative coefficient of permeability versus soil suction for Total tested thickened tailings (Box #11 and Box #2).

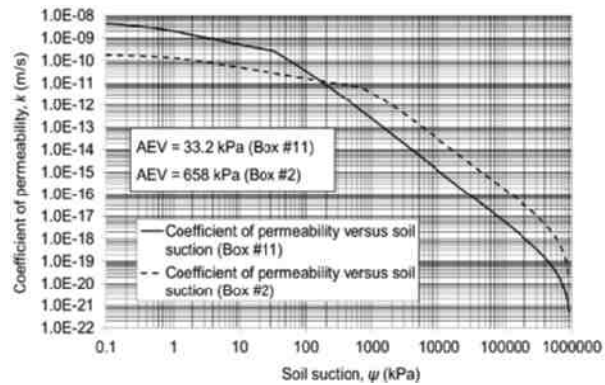


Figure 11. Coefficient of permeability versus soil suction for Total tested thickened tailings (Box #11 and Box #2).

CONCLUSIONS AND SUMMARY

This paper presents a revised theory for the reasonable estimation of the coefficient of permeability function for materials that undergo volume change as soil suction changes based on the Fredlund et al., (1994) permeability function. Both volume change and desaturation are taken into account in the revised theory. The coefficient of permeability function proposed in this paper consists of two main components, namely, the potential saturated coefficient of permeability function and the relative coefficient of permeability function. The coefficient of permeability function is the result of the multiplication between the potential coefficient of permeability function and the relative coefficient of permeability function. The

potential saturated coefficient of permeability function is controlled by the void ratio as soil suction changes and reflects the influence of volume change on the coefficient of permeability. The relative coefficient of permeability function must be estimated from S-SWCC using the AEV as the lower limit of integration. The influence of desaturation on the coefficient of permeability is reflected in the relative coefficient of permeability function. The experimental data for Total tested thickened tailings Box #11 and Box #2 are used to explain and illustrate the detailed procedure for the estimation of the coefficient of permeability function using the estimation method suggested in this paper.

REFERENCES

- BGC Engineering Inc. (2010). Oil sands tailings technology review (OSRIN Report No. TR-1). Retrieved from <http://hdl.handle.net/10402/era.17555>
- Chapuis, R.P. (2012). "Predicting the saturated hydraulic conductivity of soils: a review." *Bull.Eng.Geol.Env.*,71(3), 401-434.
- Fine Tailings Fundamentals Consortium (FTFC). (1995). Vol. I, Clark hot water extraction fine tailings. In *Advances in Oil Sands Tailings Research* (pp. 5–8), Edmonton, AB: Alberta Department of Energy, Oil Sands and Research Division.
- Fredlund, D.G., Stone, J., Stianson, J., and Sedgwick, A. (2011). "Determination of water storage and permeability functions for oil sands tailings." *Tailings and Mine Waste 2011* .
- Fredlund, D.G., and Xing, A. (1994). "Equations for the soil-water characteristic curve." *Canadian Geotechnical Journal*, 31(4), 521-532.
- Fredlund, D., Xing, A., and Huang, S. (1994). "Predicting the permeability function for unsaturated soils using the soil-water characteristic curve." *Canadian Geotechnical Journal*, 31(4), 533-546.
- Fredlund, M.D., Wilson, G.W., and Fredlund, D.G. (2002). "Representation and estimation of the shrinkage curve." *Proc., 3rd Int. Conf. on Unsaturated Soils, UNSAT 2002*, 145-149.
- Sobkowicz, J.C., & Morgenstern, N.R. (2009). A geotechnical perspective on oil sands tailings. Proceedings of the Thirteenth International Conference on Tailings and Mine Waste, xvii–xl.
- Sorta, A.R., Sego, D.C. and Wilson, G.W. (2013). "Behavior of oil sands fines-sand mixture tailings." *CIM Journal*, 4(4), 265-280.
- Taylor, D.W. (1948). *Fundamentals of soil mechanics*. J. Wiley & Sons; London: Chapman & Hall.
- Van Genuchten, M.T. (1980). "A closed-form equation for predicting the hydraulic conductivity of unsaturated soils." *Soil Sci.Soc.Am.J.*,44(5), 892-898.

PROBABILISTIC APPROACH TO EVALUATE TAILINGS DRYING

Todd Fasking, Charles Gantzer and Peter Hinck
Barr Engineering and Environmental Science Canada LTD, Calgary, Alberta, Canada

ABSTRACT

Evaporative drying of oil sands tailings is one approach operators continue to consider as a method for managing tailings inventory. Many of the key parameters that define actual evaporation rates are not controllable, such as potential evaporation (PE) rates and precipitation events. Tailings basin operators must consider the potential adverse impact of these uncontrollable parameters in combination with those that can be controlled when sizing drying. Because most of the uncontrollable, and some of the controllable, input parameters can be characterized by probability distributions, the evaporative drying of oil sands tailings can be characterized using Monte Carlo simulations.

In this study, we used Monte Carlo simulations to define the time requirements (as a probability distribution) to achieve a target outcome. Sample targets include water content or strength. Time to reach the target was a function of both constant and probabilistic inputs. Example inputs that did not vary included tailings type and the degree of tailings pretreatment. Probabilistic input parameters included climatic parameters (e.g., PE rate) and geotechnical properties of the tailings as a function of pretreatment (e.g., initial water content and yield stress of deposited tailings). We used GoldSim™ to perform the simulations. From the simulation results, the probability distribution of, for example, the minimum required time to reach a target strength was developed for sets of specified control parameters. These results and methods are suitable for use in economic trade-off evaluations balancing input controls with drying bed design and operations.

INTRODUCTION

Oil sands tailings management has been and continues to be a primary challenge for operators. How best to integrate tailings management with ongoing operational needs has been a topic of research for over two decades. The Alberta Energy Resources requirements for tailings management include two objectives: 1) reduce containment of

fluid tailings to facilitate progressive reclamation and 2) create a trafficable landscape at the earliest opportunity.

Thin lift drying has been identified as a promising option to manage tailings and operators have studied the various mechanisms of tailings drying and how to optimize the technology. As described by Song and O’Kane (2013):

“Evaporative drying technology takes advantage of the evaporation potential, following tailings deposition, to assist with dewatering tailings. The evaporative drying rate of fluid tailings is affected by environmental factors, characteristics of the tailings, and tailings depositional conditions/processes. The environmental factors include solar radiation, air temperature and relative humidity, wind speed, and precipitation intensity and duration. Characteristics of the tailings include salt concentration in the pore-fluid in the tailings and potential to form a crust (Simms et al., 2009) as well as tailings hydraulic characteristics. The factors associated with tailings deposition processes / conditions include tailings filling rates (i.e. deposition lift thickness and frequency), capillary barrier effects, and under-drainage conditions (Boswell and Sobkowicz, 2010). Both the foundation material in a tailings storage facility (TSF) and deposited tailings in the TSF can influence tailings dewatering through under-drainage.”

Research has defined most of the mechanisms at work in thin lift drying and operators have proven that the technology can work at larger scales. These activities have generated data and/or equations that can be used to help develop models to predict the performance and the design requirements of thin lift systems.

The goal of our work is not to necessarily advance the research of these mechanisms but rather to develop a tool that can help operators integrate the different mechanisms/results from studies to date and help model the relative impacts of the mechanisms relative to each other. The tool is

designed to present the results as a distribution so that operators can understand the level of design risk associated with outlying events and make operational choices as to how to address or mitigate these risks. The tool can then be used to evaluate the effect a selected mitigation strategy will have on reducing the range of outlying events.

To help do this, we have reviewed the literature and harvested available information in the form of relevant empirical datasets, including statistical distributions and equations, in an attempt to model and to provide a statistical representation of the expected behavior to help with design and planning efforts. A single point modeled outcome (deterministic simulation) is not helpful from a design standpoint because it does not quantify the effect of multiple uncertainties on the drying process. It also minimizes the impact of observed or expected process variation on performance. We used a probabilistic Monte Carlo approach to define the expected range and frequency of outcomes using the defined inputs. We used the GoldSim simulation software (GoldSim Technology Group, Version 11.0.7), which is designed as a flexible programming platform for performing time-dependent probabilistic simulations of complex natural and engineered systems.

Once the model is developed, it can be used a number of ways including to identify the expected design variability using a certain set of inputs (including exploring the impacts of using a different drying endpoint other than 5 kPa), perform culpability analyses to define which variables make the most sense to control (economic or operational considerations) and to evaluate impacts of adding or removing functions from the process.

APPROACH

Monte Carlo Simulations

Monte Carlo simulations seek to characterize the uncertainty in a modeled system by propagating the defined uncertainty in the input parameters through the model. Uncertainty in the input parameters is quantified in terms of probability distributions, which define mathematically how likely each parameter is to take on specific values (Thomopoulos, 2013). Probability distributions can be determined by fitting distributions to available data or by using subjective experience and/or professional judgment to define a distribution's bounds or shape.

Monte Carlo simulation is one method for translating uncertainties that rely on repeated simulation of uncertain systems rather than numerical solutions to determine output probability distributions. In a Monte Carlo simulation, the entire modeled system is simulated a large number of times (hundreds or thousands of realizations). Each individual realization represents one possible performance of the system in which all uncertain parameters are sampled from the defined probability distributions, and results in a single value for each model output. The results of these many realizations are then assembled into probability distributions of the possible model outcomes. The resulting distributions represent the cumulative uncertainty in the model output resulting from the uncertainty and variability in the model input parameters and their complex interactions with one another.

Estimating Time Requirements

An objective of these Monte Carlo simulations is to estimate the time requirements to dewater a poured lift of flocculated mature fine tailings (MFT) to a solids content of 60% by weight. This solids content was selected on the basis that it corresponds to an undrained shear strength of 5 kPa for flocculated MFT (Beier et al., 2013). The 5 kPa undrained shear strength target, while not necessarily the right target for reclamation, has been an important "target" since its adoption as the 1-year strength requirement for tailings in Directive 074, hence its use here. The simulations could readily be rerun with alternate "target" endpoints.

Following the conceptual dewatering model for flocculated MFT presented in Kolstad et al. (2012), three dewatering mechanisms were considered: the water release from the flocculated MFT during the initial 10 to 14 days following deposition, evaporation, and percolation to the drying bed's foundation. Total dewatering time was equal to the 10 to 14 days for water release plus the number of days required for evaporation and underdrain percolation to achieve a 60% solids content. A total of 500 realizations were performed for each calendar month. Simulated time requirements were expressed as cumulative distributions.

The situation considered by the Monte Carlo simulations was the pouring of flocculated MFT into a dedicated drying bed with a known slope. The initial lift thickness was assumed equal to the equilibrium flow depth for the poured MFT (shown below in Equation 1) (Liu and Mei, 1990):

$$h = \frac{\tau}{\rho g \sin(\theta)} \quad (1)$$

In Equation 1, h is the equilibrium flow depth [m], τ is the yield stress of the poured flocculated MFT [Pa], ρ is the bulk density of the MFT [kg/m³], g is the gravitational acceleration constant [9.8 m/sec²], and θ is the angle of the bed slope (degrees). Bulk density was calculated from the solids content assuming a solids specific gravity of 2.3 (Song and O’Kane, 2013). Water release from the flocculated MFT was a 10 to 14 day long process. Beyond 14 days, dewatering was only accomplished by evaporation and under-drainage flow. The effect of additional drying mechanisms such as freeze-thaw cycling was not included.

As indicated in Figure 1, the time-requirement simulations required several input parameters to estimate the mass of the water that must be removed to achieve a 60% solids content by weight and to estimate the rate at which water is

removed by evaporation [g/(m²•day)]. Probabilistic distributions were developed for several input parameters: daily actual evaporation rates, initial yield stress of the poured MFT lift, the initial solids content of the poured MFT lift, and the solids content of the MFT after water release.

The primary parameter not modeled with probabilistic distribution was hydraulic conductivity of the bed material. The daily under-drainage flow rates were estimated from a Darcy’s Law calculation that assumed a unit gradient at the base of the MFT deposit. The required unsaturated hydraulic conductivity was obtained from the simulated void ratio for flocculated MFT at the end of a simulated day and from a correlation provided in Song and O’Kane (2013). The slope of the drying bed was assumed to be a constant 2%, though this also later modeled with a distribution of values.

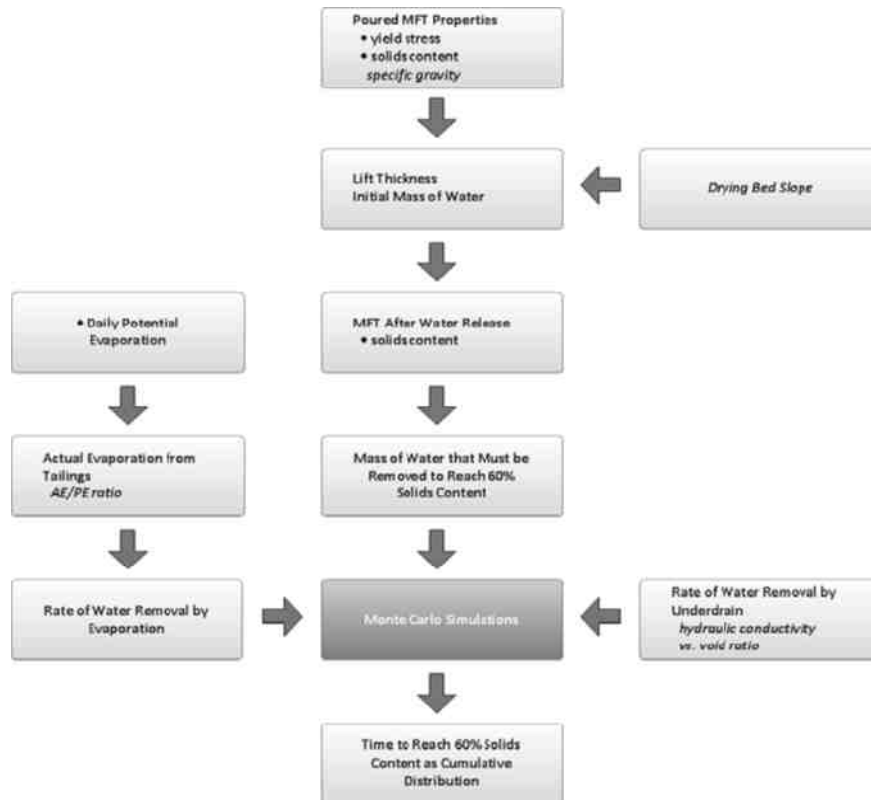


Figure 1. GoldSim algorithm for estimating time requirements for dewatering a poured lift of flocculated MFT. Bulleted input parameters were characterized by probabilistic distributions. Italicized input parameters were constants, but could be characterized by probabilistic distributions.

PROBABILISTIC INPUT PARAMETERS

Actual Evaporation Rates

Probabilistic distributions of daily actual evaporation (AE) rates on a semi-monthly basis were developed from 30 years of weather data and field-observed ratios of AE rates to potential evaporation (PE) rates.

Daily PE rates were calculated from hourly 1982-2011 Fort McMurray weather data obtained from the Integrated Surface Database maintained by the National Climatic Data Center (NCDC, 2014). The hourly PE rates were estimated using the ASCE hourly reference evapotranspiration equation (ASCE, 2005). The net radiation component of the ASCE approach was modified to consider the effects of cloud cover using the algorithms found in the EPA's PCRAMMET software (EPA, 1999). Also, the default albedo value and air-phase resistance factors in the ASCE approach were changed from values for cropland to values more representative of mud flats (Arya, 2001). The PE calculations assumed a flat tailings surface and assumed that the drying bed was not inclined toward the sun. The semimonthly daily PE rates are provided in Figure 2.

Daily AE rates were estimated by multiplying the calculated daily PE rate by 0.75, which assumes most precipitation reports as run off (Kolstad et al., 2012). Daily AE rates were compiled on a semi-monthly basis. The semi-monthly daily AE rates were assumed to follow a normal distribution and were expressed in terms of an average and standard deviation. The probabilistic AE distributions for the first-half of June (JUN) and the first-half of September (SEP) are provided in Figure 3. The plotted daily AE rate distribution for JUN has a greater average and standard deviation than the SEP distribution.

Yield Stress of Poured MFT

Equation (1) suggests that the process for flocculating MFT influences initial lift thickness via the yield stress and the initial solids content (bulk density) of the poured MFT. The probabilistic distribution of yield stress for flocculated MFT assumed in the Monte Carlo simulations is provided in Figure 4. The mean yield stress for the log-normal distribution is 225 Pa. The distribution spans from 125 to 364 Pa (90% confidence interval) which approximates the target design range reported in Wells et al. (2011).

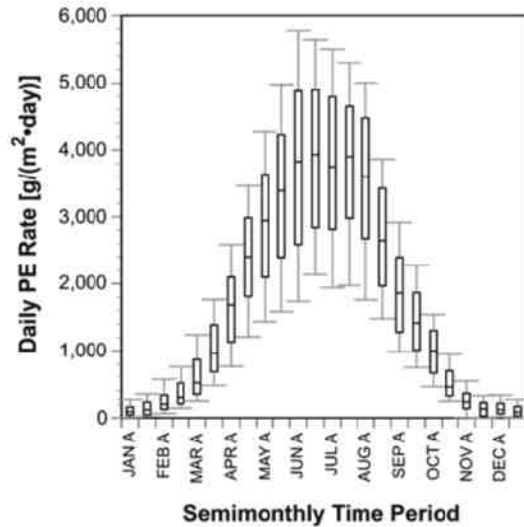


Figure 2. Daily PE rates for Fort McMurray from 1982 through 2011. “A” refers to the first half of the month. The PE values for the second half of a month are not labeled. The top, bottom, and line through the middle of the boxes correspond to the 75th percentile, 25th percentile, and 50th percentile (median), respectively. The bottom and top whiskers extend from the 10th percentile to the 90th percentile. Note: 1,000 g H₂O/(m²·day) is equal to 1 mm H₂O/day.

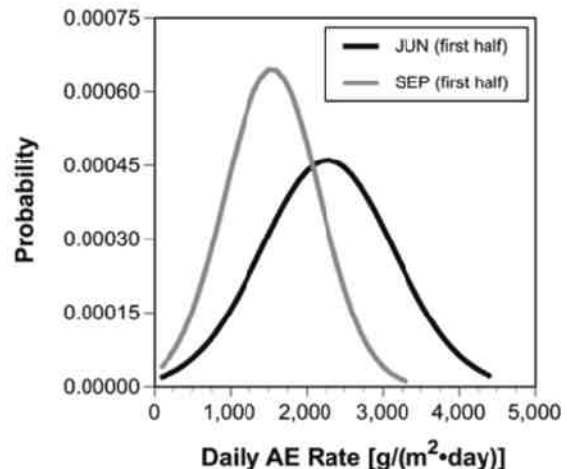


Figure 3. Probabilistic distributions of the daily AE rates for the first-half of JUN and the first-half of SEP based on hourly Fort McMurray weather for 1982 through 2011.

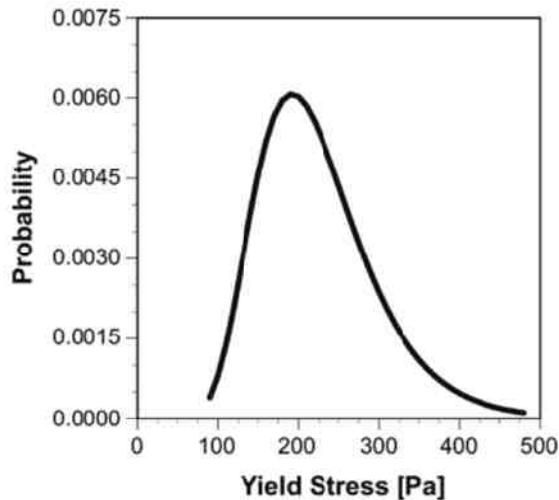


Figure 4. Probabilistic distribution of the yield stress for flocculated MFT poured onto a drying bed.

Solids Content of Poured MFT and of MFT after Water Release

The Monte Carlo simulations used two probabilistic distributions of solids content as input parameters. First, the solids content of the flocculated MFT as it is poured onto the drying bed is used to estimate the initial lift thickness via equation (1). The second is the solids content of the deposited MFT after 10 to 14 days of water release, which is associated with occurrence of most of the self-consolidation of the flocculated solids.

The probabilistic distributions for the solids contents of the poured MFT and of MFT after water release used in the simulations are provided in Figure 5. The normal distribution assumed for the poured MFT solids content has a mean of 30% by weight and spans from 22 to 38% (90% confidence interval), similar to the ranges documented by other authors (Kolstad et al. 2012, Wells et al. 2011, Song et al. 2011). The normal distribution assumed for the MFT solids content following water release has a mean of 48.5% by weight, representing an average removal of approximately 25% of the total water in the poured MFT. This is consistent with the results presented by other authors (Kolstad et al. 2012, Wells et al. 2011, Song et al. 2011).

The difference between the mean of poured MFT and MFT after water release in Figure 5 is about one-half of the water that must be removed to achieve a solids content of 60%. Thus, evaporation

and under-drainage flow must remove the remaining half of the required water to achieve an undrained shear stress of 5 kPa.

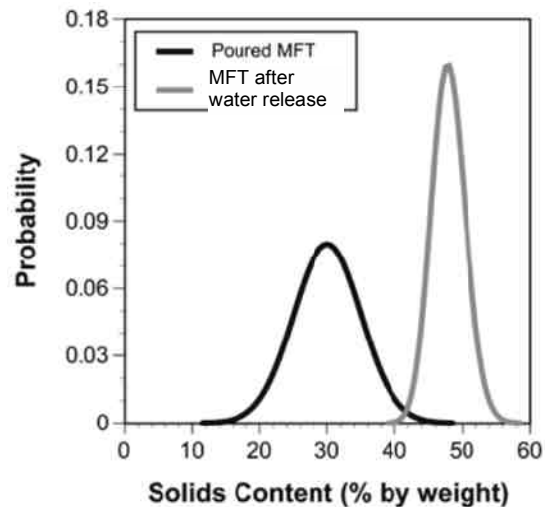


Figure 5. Probabilistic distribution of the solids contents (% by weight) for the poured MFT and for MFT after water release.

RESULTS

Time Requirements

The cumulative distribution of time required to achieve a 60% solids content for a 2% bed slope are plotted in Figure 6. The plotted time requirements are the sum of the 10 to 14 day water release period and of the time for evaporation and under-drainage flow to dry the MFT deposit to a 60% solids content.

The simulated drying times were shorter for MFT deposits placed in the drying bed during the beginning months of the drying season. Such lifts will be exposed to the highest AE rates of the season. AE rates are greatest from the second half of May through the first half of August. With an unfavorable combination of input parameters, there may be insufficient time remaining in the drying period for simulated MFT placement in the later months of the season to achieve a 60% solids content. For example, Figure 6 suggests that 80% of MFT lifts poured in May and June will require less than 55 days to achieve a 60% solids content – and thus be complete before the end of summer. MFT poured in August and September will require 113 and 147 days (i.e. to or beyond the end of the

calendar year) at the 80 percent return frequency, respectively. These results are similar to those from work previously performed (Kolstad et al. 2012) which provides a level of confidence that the model is representative.

Sensitivity to Initial Lift Thickness

The influence of selected parameters on the time to achieve 60% solids was evaluated during the Monte Carlo simulations. One observation was that the dewatering during water release had little correlation with overall time requirements, due to the relatively low variance of the solids content distribution after water release used for the simulation (Figure 5). The total drying time requirements were largely influenced by the rates of evaporation and under-drainage. This result would change if the effectiveness of water release were not controlled as demonstrated by the narrow distribution of the curve representing water content for MFT after water release.

Second, simulated time requirements were dependent on poured lift thickness, which incorporated both the yield stress and initial solids content (equation 1). This makes sense, because the initial lift thickness influences the initial mass of water that must be removed per unit evaporative area.

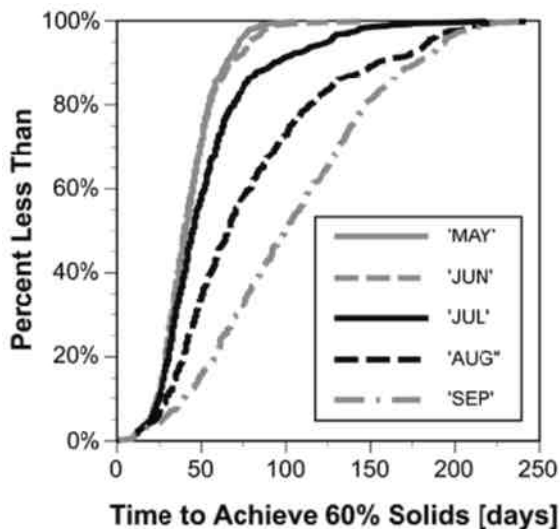


Figure 6. Cumulative distribution of time requirements to achieve a 60% solids content (by weight) as a function of the month the flocculated MFT was poured onto a drying bed. A constant bed slope of 2% is assumed.

As illustrated in Figure 7, the sensitivity of the simulated time requirements to lift thickness is important throughout the year but is even more pronounced as the lift placement occurs later in the drying season. Increased sensitivity in Figure 7 is indicated by the apparent increase in slope representing the distribution of results as placement changes from May to July to September.

The reduction in evaporation rates in the later portions of the drying season (Figure 2) means that thicker lifts or a slightly adverse combination of input parameters will prevent the lift from reaching 60% solids by the end of the drying season.

In Figure 7, the longest drying times for a given initial lift thickness were associated with low-end AE rates (representing adverse weather conditions) relative to the typical conditions for each month. In these situations, the primary means of water loss from the deposit is through the relatively consistent removal by under-drainage. In operational designs with multiple lifts, reduced under-drainage (not considered here) could further limit drying and increase the potential for long time requirements, especially for MFT placed late in the drying season. This suggests that operators consider the tradeoff in space requirements, handling requirements and other operational considerations between faster-drying single lift beds placed on free draining sand layers against placing multiple lifts on top of each other that will have lower under-drainage flow rates and associated limiting drying rates. This simulation tool can be used to help evaluate and optimize operation plans based on site-specific space and operational constraints.

Effect of Variation of Bed Slopes

Drying beds are designed with a target bed slope. Therefore we initially evaluated drying rates keeping the bed slope constant. However, we expect construction methods and non-uniform dispersal and accumulation of material over multiple lifts may result in slope variations. To address this operational consideration, we also evaluated the impact slope variability might have on drying rates.

After running the Monte Carlo simulation with a constant slope of 2%, the simulation was repeated with variable bed slope assuming a uniform probabilistic distribution of slopes between 0.5 and 3.5%. The resulting cumulative distributions of time are plotted in Figure 8.

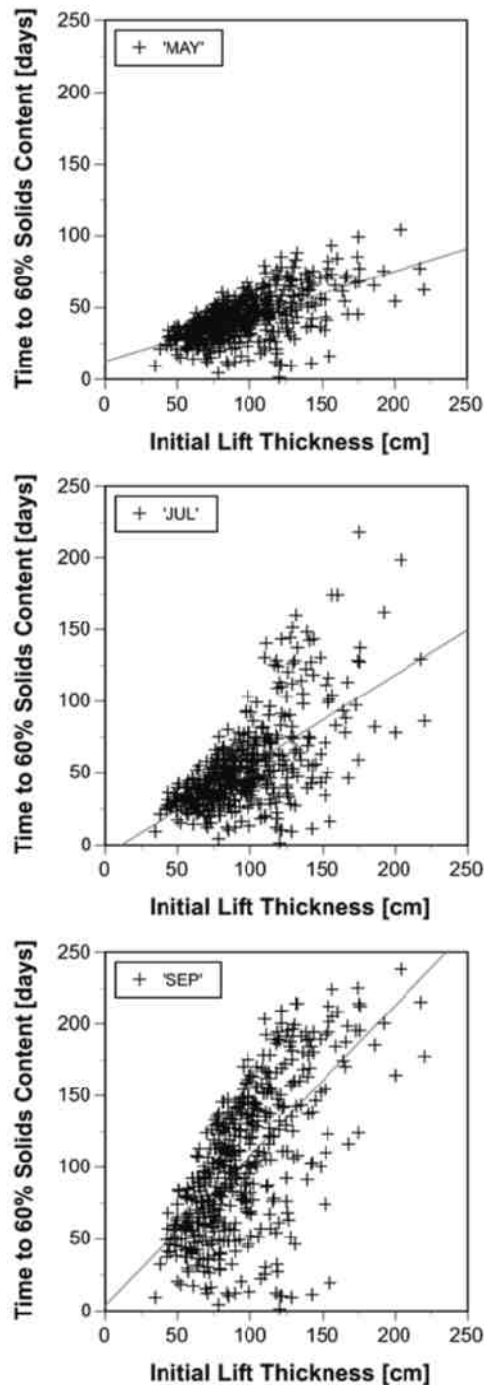


Figure 7. Sensitivity of simulated time requirements to initial lift thickness as a function of the month during which the flocculated MFT was applied to the drying bed. A constant bed slope of 2% was assumed. The graphs assumed application in May (top), July (middle), and September (bottom).

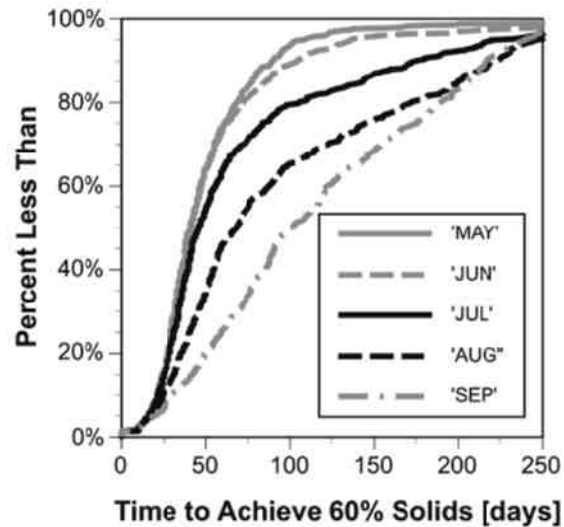


Figure 8. Cumulative distribution of time requirements to achieve a 60% solids content (by weight) as a function of the month the flocculated MFT was poured onto a drying bed with varying bed slopes. The uniform probabilistic distribution of bed slopes ranged from 0.5 to 3.5%.

Relative to the simulations with a constant drying bed slope (Figure 6), the simulations with a variable slope have little difference in the drying time on the low end of the result distributions (below the 50 percent return frequency). The possibility of a steeper-than-2% slope, therefore, does not appear to significantly increase the likelihood of a rapid drying time due to the environmental limitations on the drying rate.

On the high end of the result distributions (above the 50 percent return frequency), however, the simulations with a variable bed slope show increased drying times, especially for the second half of the drying season (e.g., July-September). At the 80 percent return frequency, MFT lifts poured in May, June, July, August, and September have simulated time requirements of 68, 72, 105, 172, and 189 days, respectively and appear to be related to shallower bed slopes and the corresponding increases in lift thickness. These values represent a 26% to 52% increase in the drying time that can be achieved with 80 percent probability. Therefore, controlling drying bed slope in the second half of the drying season should be considered by operators if attempting to achieve drying goals prior to freeze-up.

Suggested additional inquiries

The results and methodology suggest they could be further developed and lend themselves to other applications. While the impact of precipitation on AE is embedded into the PE vs AE ratio, additional detail on how and where the precipitation reports could be incorporated into this analysis. Also, the further definition of inputs that feed into the poured solids content and yield stress (such as admixture type or method) could be evaluated.

This methodology could be used to perform desktop optimization studies of tailings bed design including economic and space requirement evaluations. It could also be applied to other tailings disposal methods where variables controlling performance can be represented either mathematically or using empirically derived distributions or a combination of the two.

REFERENCES

- Arya, S. P. 2001. *Introduction to Micrometeorology Second Edition*, Academic Press, San Diego, CA.
- ASCE. 2005. *The ASCE Standardized Reference Evapotranspiration Equation*. American Society of Civil Engineers, Reston, VA.
- Beier, N., Wilson, W., Dunmola, A. and Segó, D. 2013. Impact of flocculation-based dewatering on the shear strength of oil sands fine tailings. *Can. Geotech. J.* 50(9): 1001-1007.
- Boswell, J.E.S. 2009. Strategies for dealing with fine fluid tailings and suspended fines: some international perspectives. In D.Segó, M. Alostaz and N. Beier (eds), *Proceedings of the Thirteenth International Conference on Tailings and Mine Waste '09*:171–184. Banff, 1–4 November 2009.
- Boswell, J.E.S. and Sobkowicz, J.C. 2010. Environmental assistance for tailings disposal. In *Proceedings of the 63rd Canadian Geotechnical Conference and 6th Canadian Permafrost Conference*: 665–669. Calgary, 12–16 September 2010. 166
- EPA. 1999. *PCRAMMET User's Guide*. U.S. Environmental Protection Agency, Office of Air Quality Planning and Standards, Research Triangle Park, NC. EPA-454-B-96-001.
- ERCB 2009. *Tailings performance criteria and requirements for oil sands mining schemes*. Directive 074, Energy Resources Conservation Board (ERCB), Edmonton, Canada, 14 p.
- Hyndman, A. and Sobkowicz, J. 2010. Oil sands tailings: reclamation goals & the state of technology. In *Proceedings of the 63rd Canadian Geotechnical Conference and 6th Canadian Permafrost Conference*: 642-655, Calgary, 12–16 September 2010.
- Kabwe, L.K., Kone, M., Sorta, A., Wilson, W.G., Scott, D., & Ulrich, A. 2013. Measurements of unsaturated soil properties of old and new mature fine tailings MFT. In *Proceedings of Mine Closure 2013*, Cornwall, 14-22 September 2013.
- Kolstad, D., Dunmola, A., Dhadli, N., O'Kane, M., Song, J., and Masala, S. 2012. Towards the improvement in geotechnical performance of atmospheric fines drying (AFD) deposits at Shell's Muskeg River Mine. In *Proceedings of the 3rd International Oil Sands Tailings Conference*, Edmonton, AB., 3–5 December 2012. pp. 411–420.
- Liu, K.F. and Mei, C.C. 1990. Approximate equations for the slow Spreading of a thin sheet of Bingham plastic fluid. *Physics of Fluids A* 2(1): 30-36.
- NCDC. 2014. National Climatic Data Center. <ftp.ncdc.noaa.gov/pub/data/noaa/isd-lite>
- Penman, H.L. 1948. Natural evapotranspiration from open water, bare soil and grass. *Proceedings of the Royal Society of London, Series A, Mathematical and Physical Sciences* 193: 120–146.
- Scott, J.D. and Ozum, B. 2010. Oil sands tailings: What needs to be done. *Mining.com Magazine*. September 2010.
- Seneviratne, N.H., Fahey, M., Newson, T.A. and Fujiyasu, Y. 1996. Numerical modelling of consolidation and evaporation of slurried mine tailings, *International Journal for Numerical and Analytical Methods in Geomechanics* 20: 647–671.
- Simms, P., Dunmola, A. and Fisseha, B. 2009. Generic predictions of drying time in surface deposited thickened tailings in a “wet” climate. In D.Segó, M. Alostaz and N. Beier (eds), *Proceedings of the Thirteenth International Conference on Tailings and Mine Waste '09*: 749-757. Banff, 1–4 November 2009.

Song, Q. and O’Kane, M. 2013. Evaluation of evaporation and under-drainage in dewatering oil sands tailings in northern Alberta. In G.W. Ward, D.C. Seago, and N.A. Beier (eds), *Proceedings of the Seventeenth International Conference on Tailings and Mine Waste*, 3-6 November 2013, Banff, Alberta, pp. 157-167.

Song, Q., O’Kane, M., Dhadli, N., and Matthews, J. 2011. Deposition thickness and evaporative drying for oils sands tailings in Northern Alberta. In A.B. Fourie, M. Tibbett and A. Beersing (eds.), *Proceedings of Mine Closure 2011*: 373-382. Lake Louise, 18-21 September 2011. Perth: Australian Centre for Geomechanics.

Thomopoulos, N.T. 2013. *Essentials of Monte Carlo Simulation*. Springer Science+Business Media, New York, NY. 171 pp.

Wells, P.S., Revington, A., Omotoso, O. 2011. Mature fine tailings drying—technology update. In R.J. Jewell and A.B. Fourie (eds.), *Proceedings of Paste 2011*, Perth: Australian Centre for Geomechanics. pp. 155-166.

Session 2

Tailings Desiccation and Modelling

NUMERICAL SIMULATION OF FINE OIL SAND TAILINGS DRYING IN TEST CELLS

Philip J. Vardon¹, Thomas Nijssen¹, Yutian Yao¹ and A. Frits van Tol^{1,2}
¹Delft University of Technology, Delft, the Netherlands
²Deltares, Delft, the Netherlands

ABSTRACT

As a promising technology in disposal of mature fine tailings (MFT), atmospheric fines drying (AFD) is currently being implemented on a commercial scale at Shell Canada's Muskeg River Mine near Fort McMurray, Alberta. AFD involves the use of a polymer flocculent to bind fine particles in MFT followed by thin lift sub-aerial drying. Upon deposition, the tailings-polymer mixtures are subjected to atmospheric conditions. The disposed layers undergo a cyclic drying and rewetting process due to precipitation and deposition of additional lifts on top of the dried layer. The current research aims to numerically simulate this process, including both periods of drying and wetting. An existing numerical drying model was extended with a realistic rewetting behavior, based on the shrinkage and water retention curves for drying as well as for rewetting. This improved model, that was validated with test results from laboratory columns, was used to simulate a large scale drying field test that is currently being performed by Shell Canada. The results of the simulation are published here without prior knowledge of the results by the authors, forming a Class A prediction.

INTRODUCTION

Mature fine tailings (MFT) or fluid fines can be a major challenge in the production of oil from oil sands. In general, MFT is a mixture of the clay and silt particles that remain in suspension in the tailings after the sand and other larger particles have settled. Naturally these particles may take decades to settle and can cause significant challenges in the amount of land that is required. One technology that has been developed to treat these tailings is atmospheric fines drying (AFD) (Shell, 2011). In this technology, MFT is mixed with a flocculent to help the particles settle and increase the speed of dewatering. The material is then laid in layers in a drying area which is open to the elements. The material layers have a slope to

actively drain water that has been driven out of the material or runoff from rain.

This work extends the development of the numerical model development reported by van der Meulen (2012), van der Meulen et al. (2012) and Nijssen (2013). In addition to this paper, a complementary paper is also presented in this conference on the wetting and drying characteristics of the material (Yao et al., 2014). The initial data of the field tests (initial lift size and climatic data) has been provided by Shell Canada (personal communication, 2014) from a field site, with the results of the deformation not yet provided for the authors – with this work thereby forming a Class A blind prediction.

THEORETICAL FORMULATION

The basis of the model has previously been reported (Kim et al., 1992, implemented by van der Meulen, 2012; van der Meulen et al., 2012; Nijssen, 2013) and therefore is only briefly reported here for clarity, alongside the details of several modifications.

For drying/wetting behaviour the processes can be reduced to a 1D scenario, with the assumption that lateral deformation does not take place. The soil undergoes large deformations therefore a material level coordinate system has been adopted:

$$dm = \frac{dz}{1+e} \quad (1)$$

where m is the 1D material coordinate, z is the Cartesian (real) coordinate and e is the void ratio.

Drying processes / Water transport

Water transport is governed by Darcy's Law with the water potential, ϕ , made up from a gravimetric component, $\gamma_w z$ (where γ_w is the volumetric weight of water), an overburden component, Ω , and a suction component, ψ . The suction is linked to the water content, $\theta = V_w/V_s$ (where V_w and V_s are the volumes of water and solids), via an

empirically determined Soil Water Retention Curve (SWRC). Both the well-known van Genuchten SWRC and the modified van Genuchten SWRC (Romero and Vanaut, 2000) have been implemented. The modified van Genuchten curve limits the maximum suction predicted by the SWRC. As this model is designed for virgin soils (sludges) subsequent re-wetting re-drying loop is likely to be significantly different from the first drying behaviour, with a lower water content yielded for the same suction value. Therefore, following the approach of Rijniersce (1983), a ten times stiffer relationship in a log-linear space has been utilized.

The hydraulic conductivity, K , used is a function of void ratio and degree of saturation.

The drying/wetting processes considered, i.e. the boundary conditions, are:

Base boundary:

1. Open (fixed zero potential), or
2. Closed (natural no flow boundary condition).

Top (atmospheric) boundary:

1. Flux boundary condition, calculated using the maximum of the average evaporation potential (including precipitation and the inverse) and the soil flux in the last element. Any free water is assumed to run-off.
2. The top boundary has been set up so that a time series of evaporation potentials / precipitation can be input.

Soil Deformation

The soil deformation is governed by a shrinkage curve – an empirical material curve linking the volumetric water content, $\theta = V_w/V_s$ (where V_w and V_s are the volumes of water and solids), and the void ratio. Hysteretic reswelling behaviour and non-linear compression due to additional overburden are also included. The shrinkage curve is defined as (Fredlund et al., 2002):

$$e = A_{sh} \left(\frac{\theta^{C_{sh}}}{B_{sh}^{C_{sh}} + 1} \right)^{\frac{1}{C_{sh}}} \quad (2)$$

where A_{sh} is the minimum void ratio, B_{sh} is a parameter defining the slope and C_{sh} is a parameter defining the transition between the linear portion and the minimum void ratio. The degree of saturation at which the sludge initially dries from is defined as B_{sh}/A_{sh} . Parameter A_{sh} is defined as a function of overburden stress as:

$$A_{sh} = A_{sh}^0 \left[1 - \frac{1}{C_{10}} \log \left(\frac{\sigma'}{\sigma'_0} \right) \right] \quad (3)$$

where A_{sh}^0 is defined as the minimum void ratio under zero overburden conditions, σ' is the current stress, σ'_0 is the initial stress and C_{10} is a material parameter.

Governing equation

The deformation behaviour is dominated by the shrinkage during drying, therefore the model has been implemented as a one directional coupling – with the water behaviour being the solved equation, with the mechanical (non-linear) constitutive behaviour being characterized by equations (2 and 3). The governing equation is therefore based upon the conservation of water mass. The equation solved is therefore (after Kim et al., 1992):

$$\frac{\partial \theta}{\partial t} = \frac{\partial}{\partial m} \left[K^* \left(\frac{\partial \psi}{\partial m} + SF1 + SF2 \cdot \frac{\partial \theta}{\partial m} \right) \right] \quad (3a)$$

$$SF1 = (1 + e) - (\theta + \gamma_s) \frac{\partial e}{\partial \theta} \quad (3b)$$

$$SF2 = \frac{\partial^2 e}{\partial \theta^2} \int_0^m (\theta + \gamma_s) dm \quad (3c)$$

where t is the time, K^* is the hydraulic conductivity transformed into the Lagrangian coordinate system ($K^* = K/(1 + e)$) and γ_s is the density of the solids.

Numerical implementation

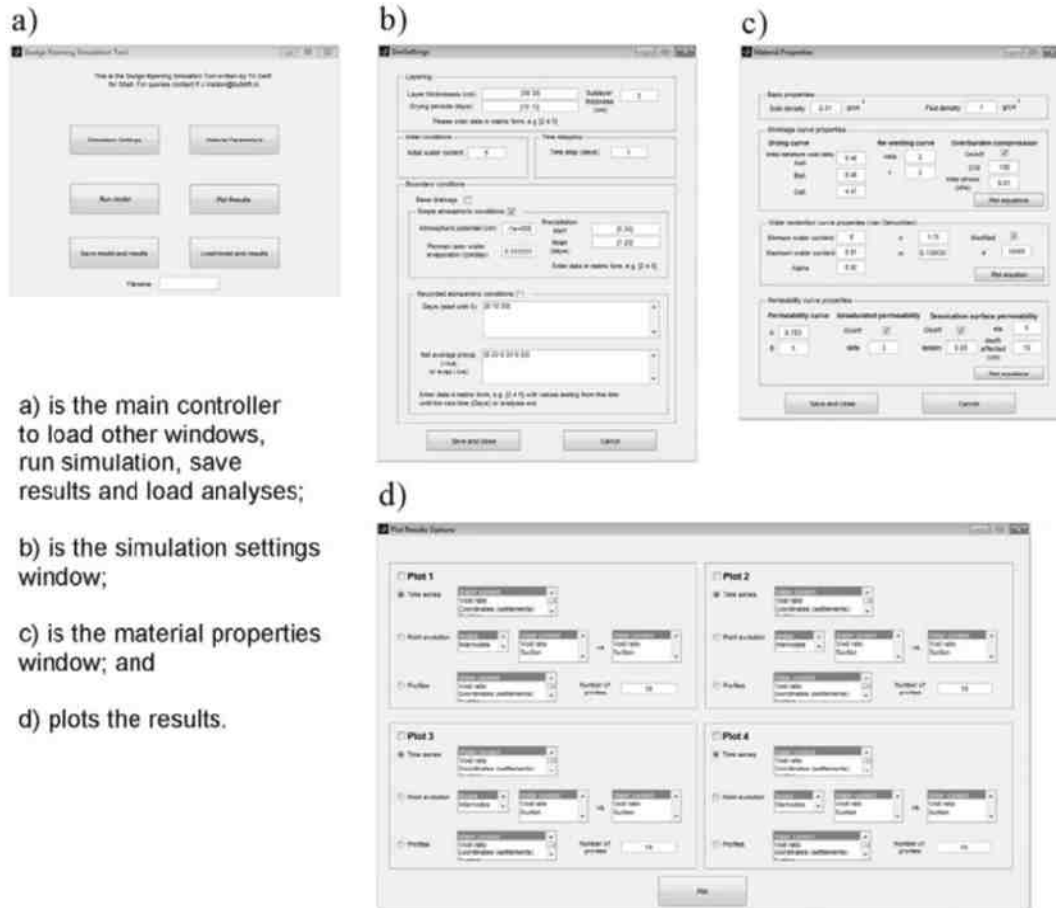
The theoretical formulation has been implemented in a discrete spatial domain via a finite difference formulation, and solved recognizing the highly non-linear behaviour utilizing an explicit Runge-Kutta method as implemented in Matlab. To account for hysteresis behaviour a constant time delay, i.e. not based upon the timestep, has been incorporated, via the selection of the dde23 solver (Shampine and Thompson, 2001).

Software implementation

A user interface has been developed utilizing the Matlab interface, so that the model can be easily operated. A main graphical window, controls the analysis, with separate windows for inputting (i) the material properties; (ii) the simulation settings (e.g. number of material layers, atmospheric conditions, etc..) and (iii) plotting the results.

The simulations are able to be saved, loaded or run from the main window. A suite of datafiles is used to contain the analysis data (geometry, precipitation conditions), the material data and the

results. Figure 1, shows an overview of the user interface.



a) is the main controller to load other windows, run simulation, save results and load analyses;

b) is the simulation settings window;

c) is the material properties window; and

d) plots the results.

Figure 1. Overview of user interface

EXPERIMENTAL DATA

Two sets of experimental tests have been undertaken and are available to test the simulation tool developed. First column tests have been undertaken and secondly field tests undertaken by Shell Canada. In the field tests the results have not been made available to the authors of this paper. Material properties of both the materials used in the laboratory and in the field test are summarized below. Column test were available on both flocculated MFT and non-flocculated. In this work only the columns with flocculated MFT have been simulated to match the material in the field tests.

Material properties

Soil Water Retention Curve

The modified van Genuchten SRWC is shown below:

$$S_e = C(s) \left(\frac{1}{(1 + (\alpha_{WRC} \cdot \varphi)^{n_{WRC}})^{m_{WRC}}} \right) \quad (4a)$$

$$C(s) = 1 - \left(\frac{\ln \left[1 + \frac{\varphi}{a_{WRC}} \right]}{\ln(2)} \right) \quad (4b)$$

$$S_e = \frac{\theta - WCR}{WCS - WCR} \quad (4c)$$

where S_e is the effective degree of saturation, WCR is the residual (volumetric) water content, WCS is the water content at full saturation and α_{WRC} , n_{WRC} , m_{WRC} and a_{WRC} are fitting parameters, where m_{WRC} is defined as $m_{WRC} = 1 - 1/n_{WRC}$.

Calibrated material parameters for the experimental data are: $WCR = 0.06$, $WCS = 2.2$, $a = 50000cm$, $\alpha_{WRC} = 0.11cm$ and $n_{WRC} = 1.23$. The resulting fit alongside experimental data for the Shell field tests (personal communication, 2014) is shown in Figure 2.

Shrinkage Curve

The shrinkage curve and associated experiments are reported in detail in Yao et al. (2014). The parameters for equation 2 and 3 were $A_{sh}^0 = B_{sh} = 0.5$, $C_{sh} = 3$ and $C_{10} = 2.5$. The experimental and numerical data are shown below in Figure 3.

Hydraulic Conductivity

The hydraulic conductivity, K , against void ratio in saturated conditions has been calibrated against oedometer tests shown in Figure 4. Material parameters are $A_{HC} = 1.7$ and $B_{HC} = 4.4$.

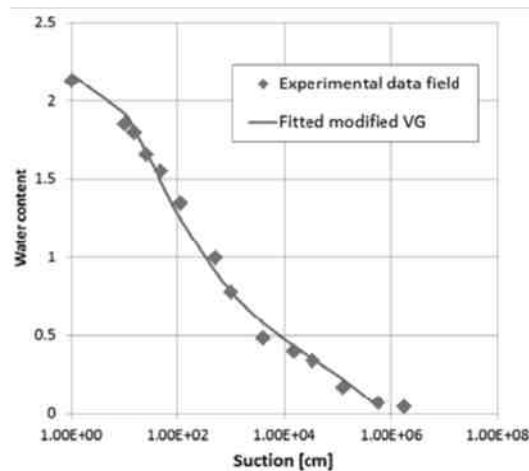


Figure 2. Soil Water Retention Curve

Column tests

The column settling tests are reported briefly here. The experimental procedure was that the column was filled to 20cm height with MFT with a water content of 4.27. After 16 days another 20cm height was added. An air pump has been used to provide dry air to the column surface. Six columns were

tested, 3 with flocculent and 3 without. Additionally a water filled column was tested to investigate the water evaporation potential. The water in this column was found to evaporate at 1.04cm/day.

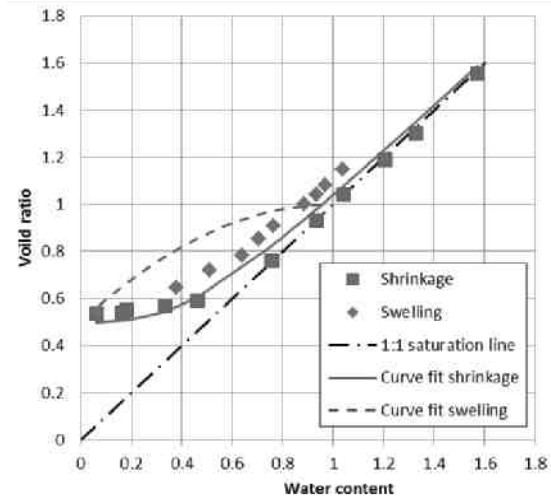


Figure 3. Shrinkage Curve

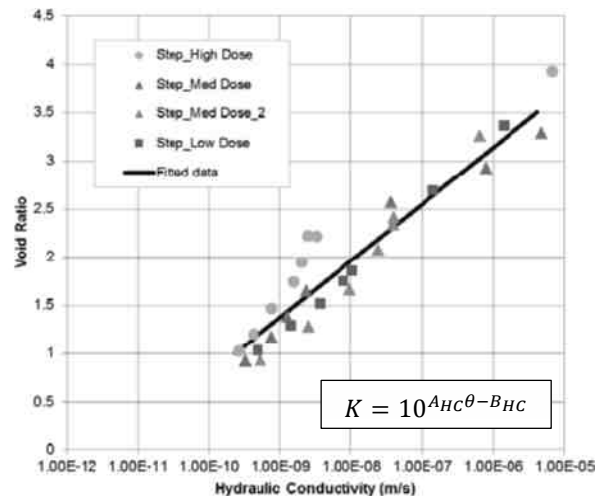


Figure 4. Saturated hydraulic conductivity

All columns were weighed throughout the experiment and additionally for a single column visual measurements of the height of tailings and water was noted. In contrast with the field tests, where water is able to run-off, the water that is removed from the sample through settling/overburden sat on top of the mud.

The results of a single multistage column test is shown in Figure 5 for both observed height and weight. The data is representative of all tests. It was noted that the evaporation rate from all the

experimental columns is significantly lower (~40% lower) even when free water is at the top of the column. This reduction is suggested to be due to oil residue at the top of the water (Figure 6). Due to run-off this reduction is unlikely to occur in the field tests. The weight reduction is observed to be linear at all times, suggesting that evaporation was not significantly limited by flow through the material.

Field tests

Three different field tests were undertaken by Shell with data briefly reproduced here (personal communication, 2014). The evaporation potential and precipitation has been measured daily. The monthly average values are shown in Figure 7. The experimental protocol for the three tests are shown below in Table 1.

The average initial water content was 3.5 with a standard deviation of 0.25, therefore a uniform initial water content has been used.

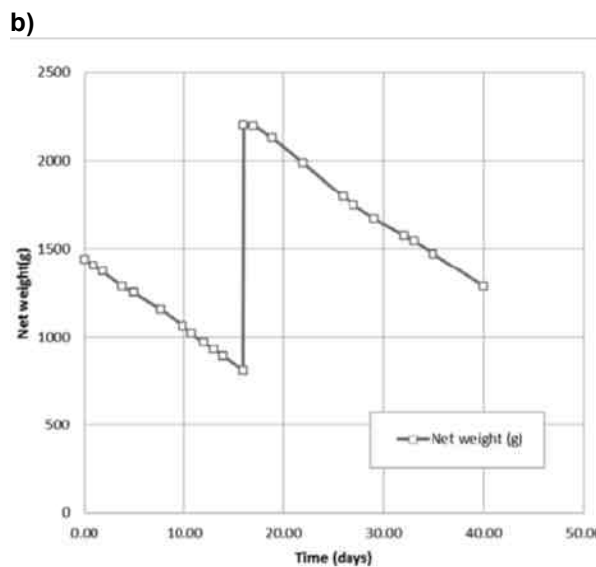
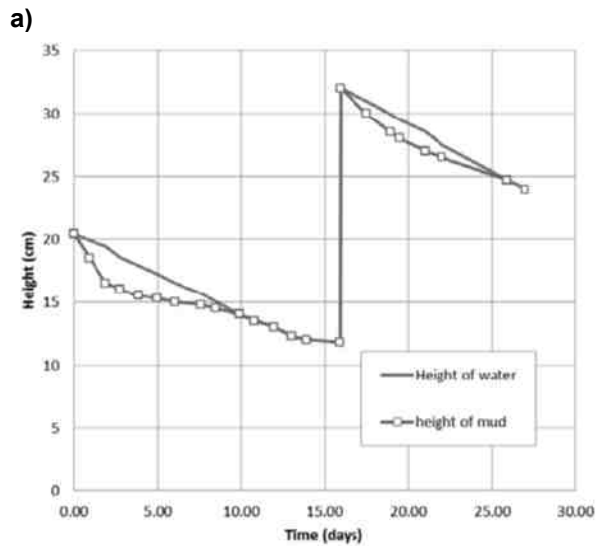


Figure 5. Experimental column test data a) for height and b) for weight.



Figure 6. Oil residue at the top of the experimental column

Table 1. Field test experimental protocol

Test	Lift	Days from start	Thickness (cm)
Thin multi-lift	1	0	90.0
	2	37	50.0
	3	257	50.0
	4	290	50.0
	5	317	60.0
	6	346	110.0
	7	365	40.0
Thick multi-lift	1	0	100.0
	2	257	180.0
	3	346	130.0
Deep stack	1	0	450.0

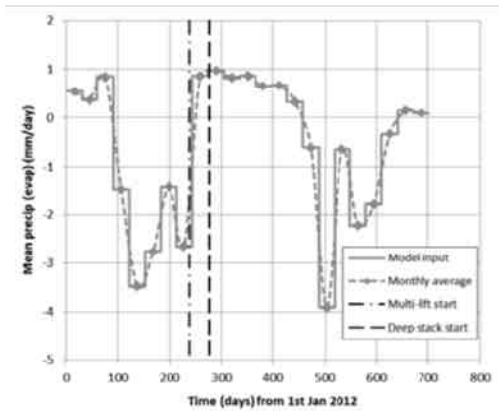


Figure 7. Field test climatic data, positive values are net precipitation and negative are mean evaporation.

SIMULATION RESULTS

Column tests

The experimental column, with results presented in Figure 5, has been simulated. The column has been discretized into 40 initially evenly spaced vertical divisions, i.e. 20 per layer. The material parameters described above were utilized. It was observed (see Figure 5a) that water had collected at the surface of the column initially for both layers. As the model presented does not have a facility to account for pooling, for the time periods where pooling was observed, no evaporation is applied to the boundary. Therefore in this time period, any consolidation is due to the overburden pressure.

The simulated height for select initially evenly spaced layers, with the observed result is presented in Figure 8, with the experimental results shown in red with data points and the layer surfaces shown in dotted bold lines.

The results show good qualitative agreement, although, in the early stages of the test for each layer, the simulated settlement rate is significantly higher than shown experimentally. It is hypothesized that this is due to the very high hydraulic conductivity predicted from the relationship illustrated in Figure 4.

The model is seen to be sensitive to hydraulic conductivity relationship. By calibrating the hydraulic conductivity parameter A_{HC} from 1.7 to 1.3 the results shown in Figure 9 are yielded. It is seen that the results match both qualitatively and quantitatively. Two major deviations are noted: the

first at the end of the first stage, where the model simulates a higher settlement, and the second at the start of the second stage of the test. The first is attributed to shrinkage away from the sides of the column experimentally – meaning that the assumption of 1D flow and deformation is not valid at this time. The second is an overestimation, which qualitatively is well represented. It is partly attributed to a degree of experimental error and partly to a combination of settlement of particles vs consolidation modelled here.

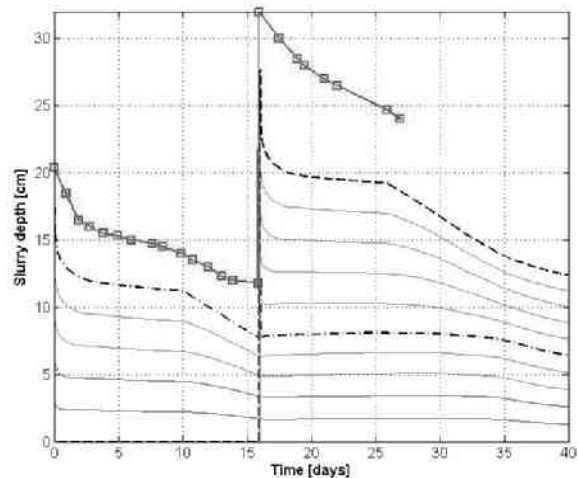


Figure 8. Numerical and experimental settlement results for the column test.

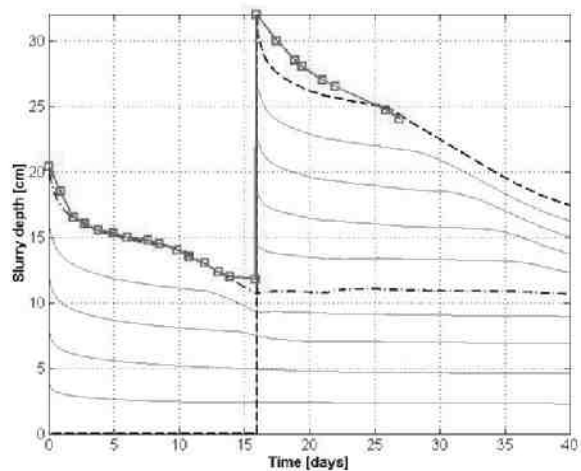


Figure 9. Numerical and experimental settlement results with calibrated hydraulic conductivity for the column test.

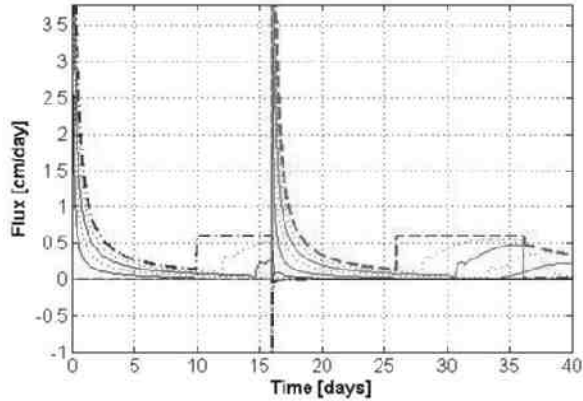


Figure 10. Simulated water fluxes for the column test.

In the simulations, the first layer is seen to show limited swelling after the deposition of the second layer and remain approximately constant. This highlights the potential advantage of depositing in layers.

The water fluxes at the same locations as the settlements are shown in Figure 10. The first layer is shown in blue and the second in red for clarity. The thicker lines for each layer are the layer surfaces. It can be seen that initially the fluxes due to the self-weight are high and reduce rapidly. These are responsible for the water pooling on the surface. The step in water flux observed in Figure 10 at day 10 and day 26 are due to evaporation starting (being switched on in the simulation) as the pooled water is no longer observed. This step in the fluxes are responsible for the gradient change in the deformation in Figures 8 and 9.

The void ratio over time is shown in Figure 11 with profiles through the length of the column shown in Figure 12, with the base of the figure coinciding with the base of the experimental column. It is clearly seen that in the early parts of each test, where the water is pooling on the surface, the consolidation behaviour yields a void ratio that is smoothly transitioning from top to bottom with the highest void ratio is at the surface. When the evaporation is driving the consolidation, the consolidation of the layers is more uneven, with the layers nearer the surface deforming significantly. The addition of a second layer, halts the rapid decrease in void ratio, but does not cause a rapid re-swelling.

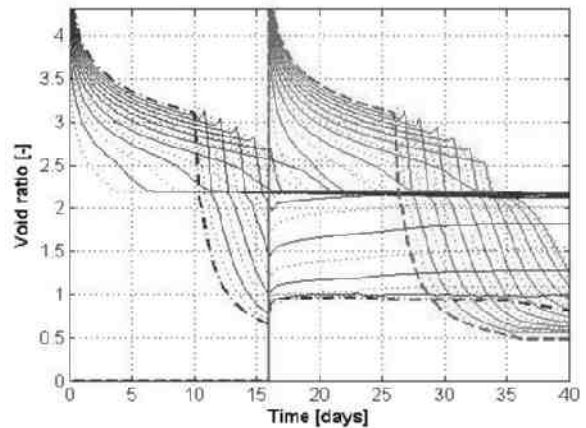


Figure 11. Void ratio against time for the column test.

Field tests

Each field test has been simulated with the layers as shown in Table 1. The original permeability parameters were used and in addition, as runoff was expected a reduction in the evaporation flux has not been applied. The evaporation potential and precipitation are averaged monthly and utilized from the start date shown in Figure 7. It is seen that for the multi-stack experiments a period of drying occurs at the start of each test, whereas for the deep stack test the initial period is one of wetting. The discretization is 10cm of the initial dimensions in each analysis.

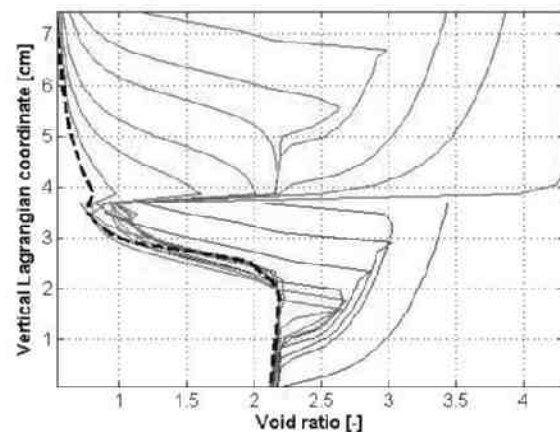


Figure 12. Profiles of void ratio.

Deep stack

The deformation of the deep stack analysis is shown in Figure 13. It is seen that the deformation mostly occurs at the start and decreases as time progresses. In addition there are some periods of

increased deformation around the 250 day and 300 day time, coinciding with the periods of greatest evaporation. It is worth noting that should the periods of evaporation have been earlier, then no benefit would have been gained as the flux due to overburden would have been greater and the evaporation would have been from the water runoff. This is seen clearly in Figure 16, where the fluxes are shown. The y-axis of the figure has been plotted on a logarithmic scale so that the full range of fluxes can be seen. Figure 14 shows the void ratio against time. It is clear that the surface is affected greatly by the periods of high evaporation, but that the desaturation effect is limited in depth.

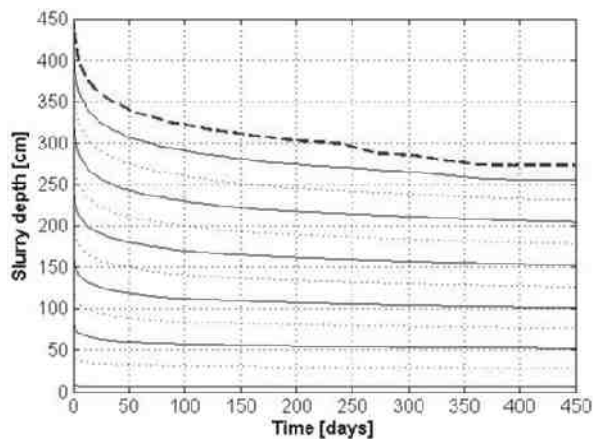


Figure 13. Settlement numerical results for the deep stack field test.

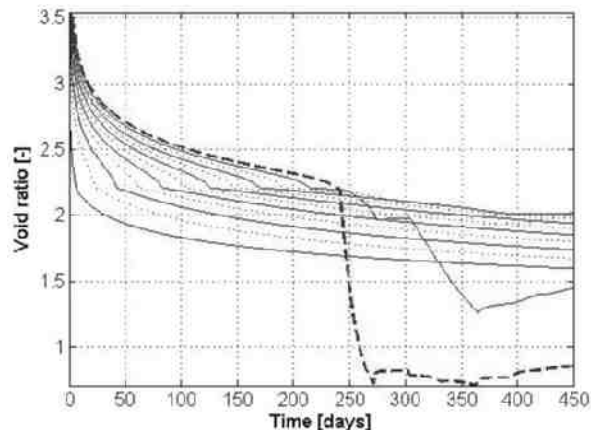


Figure 14. Void ratio against time for the deep stack field test.

In Figure 15, void ratio profiles are shown for various times, with the profiles moving from the right to the left over time. It shows that once the

surface is significantly dried then further drying is slow. This is due to the reduction of surface permeability.

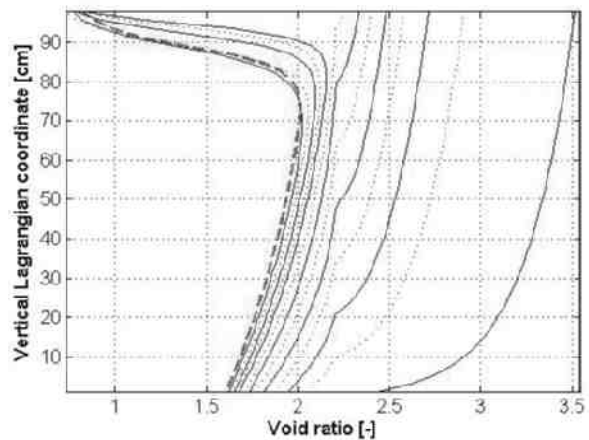


Figure 15. Void ratio profiles, spaced every 30 days, for the deep stack field test. The start position is in red on the right and the end with the red dashed line on the left. Coordinates are material level coordinates (see Equation 1).

Thick multi-stack

The settlement of the thick multi-stack is shown in Figure 17. The relatively uniform curves suggest mainly a single dominant water drying behaviour, which in this case is driven by the overburden. An increased gradient from approximately 300 to 325 days coincides with a period of increased drying due to evaporation – as can be seen from Figure 7. The water flux, shown in Figure 18, indicates this is where the evaporative flux is higher than the overburden driven flux (or self-weight consolidation), illustrated by the four black arrows.

It can be observed from Figure 18 that the two main periods of evaporative drying (between the 1st and 2nd arrows and 3rd and 4th arrows), are when the overburden flux is high as a new layer has been deposited.

Figure 19 shows void ratio profiles for the test. Denser layers due to evaporation at the end of the layers can be observed, however these are relatively shallow bands due to the limited evaporation time.

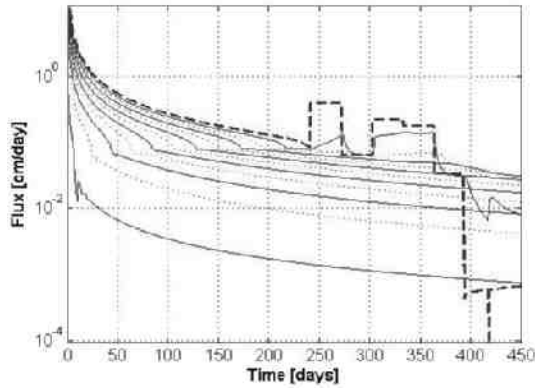


Figure 16. Water fluxes against time for the deep stack field test.

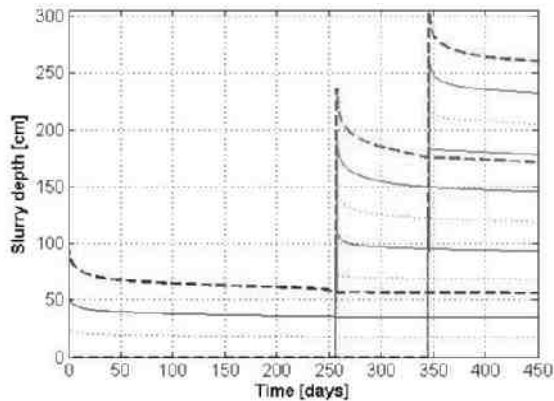


Figure 17. Settlement numerical results for the thick multi-stack field test.

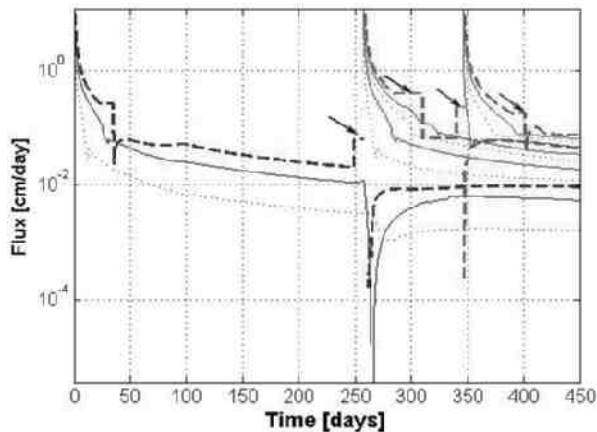


Figure 18. Water fluxes against time for the thick multi-stack field test.

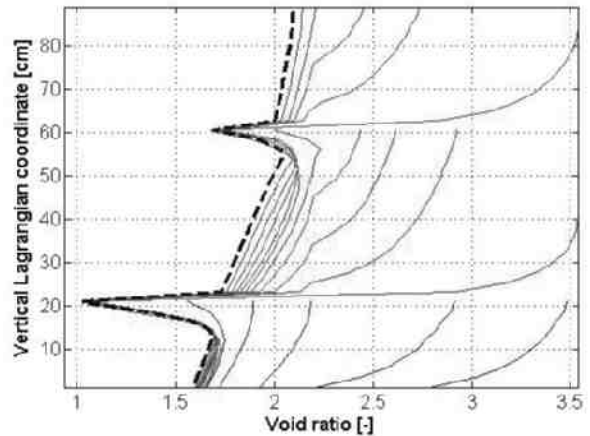


Figure 19. Void ratio profiles for the thick multi-stack field test.

Thin multi-stack

The final depth to surface of the thin multi-stack field test at 450 days is 285cm. The water fluxes are shown in Figure 20, with the final void ratio profile shown in Figure 21. Again, as with the thick multi-stack simulation, the main period of evaporative drying occurs when new layers are deposited, therefore the benefit of additional evaporation is neglected. The void ratio profiles show, as with the other simulations, that the overburden driven consolidation dominates for a considerable portion of the time and that the additional benefit of evaporation driven consolidation is limited to small depths in certain layers.

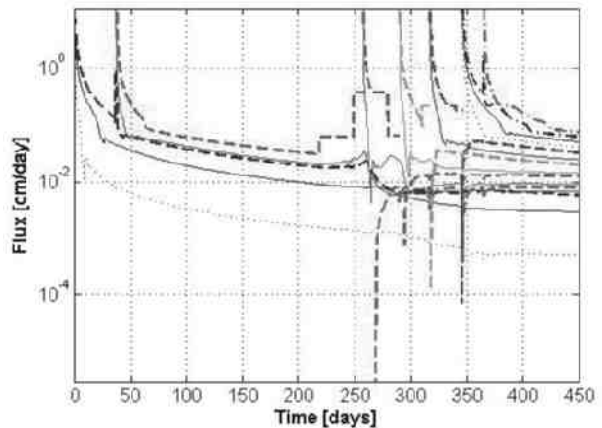


Figure 20. Water fluxes against time for the thin multi-stack field test.

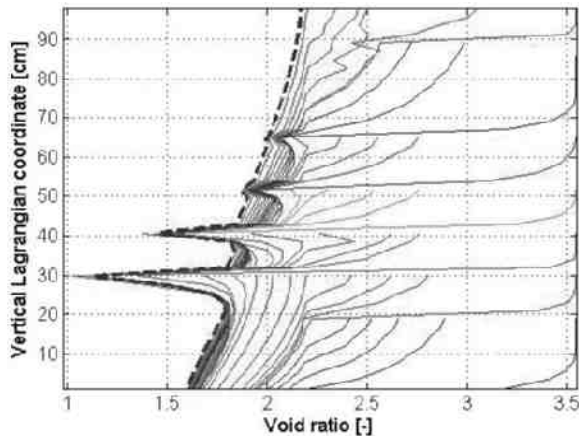


Figure 21. Void ratio profiles for the thin multi-stack field test.

The third layer deposited in the summer, while deposited at a time of evaporation, only has a limited period of time when overburden driven fluxes are dominant as the layer is thin.

DISCUSSION

An overall comparison of the field test simulations is given in Table 2. It is predicted that in this case the Deep stack test may have the minimum percentage of initial height remaining after 450 days, although there is only little difference in the final settlement of the tests.

Table 2. Summary of final heights of field test simulations.

Test	Total height deposited (cm)	Final height after 450 days (cm)	%height after 450 days
Thin multi-lift	450	285	63
Thick multi-lift	410	265	65
Deep stack	450	274	61

Overburden driven consolidation occurs with the densest layers occurring at the base, therefore the permeability reduction is smallest at the top. This aids ongoing overburden driven consolidation and means that the deepest slurry heaps may drain fastest, rather than in layers over time. In addition, in these tests the main evaporative times occur during layering for the multi-layer experiments and after considerable drying time for the deep stack test. However, lower void ratios, i.e. denser material, is produced when evaporation is

dominant, however the depth that these denser layers can be formed is limited by the reduction in permeability at the surface.

The deep stack is shown to have virtually stopped settling at the 450 day final simulation time. This is due to the denser low-permeability layer at the surface, caused by evaporation. The multi-stack experiments however, have not stopped settling and do not have such a dense low-permeability surface layer. Therefore it is likely that finally the multi-stack tests will have a higher final settlement.

Therefore, by planning layers that are deposited in periods of time when there is little evaporation initially, i.e. winter or autumn, then summer evaporation can be exploited to densify layers. Moreover, thinner layers could be used in the summer. Additionally if dense material is required, thin layers of e.g. 0.25m would be necessary.

As previously stated, the field tests are a Class A (i.e. blind) prediction, therefore differences between the simulations and the field cases may be expected. A number of possible causes and unknowns have been compiled and briefly discussed below:

- The model is a 1D model and the real behaviour may have 3D effects, e.g. lateral shrinkage and slopes. Water may also flow through the soil under the surface downslope.
- Surface desiccation may occur.
- Oil on water surface may affect evaporation.
- Surface run-off on rainy days has not been explicitly modelled, although is included as water pooling is not allowed.
- Snow and ice is not included, except for not having evaporation. Overburden driven fluxes are still allowed.
- Unsaturated hydraulic conductivity is unknown.
- The material is modelled as a uniform continuum, but some large voids (air or water filled) occur.

Comparison with measured field results will take place and will be published in a subsequent publication.

CONCLUSION

A model is presented to simulate atmospheric fines drying (AFD) of mature fine tailings (MFT). The model contains various features of drying, including overburden and evaporation driven pore pressure changes and changes due to swelling

and shrinkage cycles. The model is based upon the finite difference method and has been implemented via a graphical user interface for ease of use. The model has been utilized to simulate a column test undertaken in laboratory conditions, where the results compare favorably. Further, three field tests have been simulated, where the results are not known. A comparison with measured field results will take place and will be published in a subsequent publication.

ACKNOWLEDGEMENTS

The provision of data and funding via Shell Canada is gratefully acknowledged.

REFERENCES

Fredlund, M.D., Wilson, G.W. and Fredlund, D.G. 2002. Representation and estimation of the shrinkage curve. Third International Conference on Unsaturated Soils (UNSAT 2002), 145-149.

Kim, D. J., Diels, J. and Feyen, J. 1992. Water movement associated with overburden potential in a shrinkage marine clay soil. *Journal of Hydrology*, **133**: 179-200.

van der Meulen, J. 2012. Modelling of ripening behaviour of Albian oil sand tailings in Canada. MSc thesis, Delft University of Technology.

van der Meulen, J., van Tol, F., van Paassen, L. and Heimovaara, T. 2012. Numerical modeling of drying and consolidation of fine sediments and tailings. Third International Oil Sands Tailing Conference (IOSTC'12), 399-409.

Nijssen, T. 2013. Modelling of cyclic drying/re-wetting behaviour of Albian oil sand tailings. MSc thesis, Delft University of Technology.

Rijniersce, K. 1983. A simulation model for physical soil ripening in the IJsselmeerpolders, Rijksdienst IJsselmeerpolders.

Romero, E. and Vaunat, J. 2000. Retention curves of deformable clays. Experimental evidence and theoretical Approaches in Unsaturated soils, Tarantino & Mancuso (eds). Balkema, Rotterdam, 91-106.

Shampine L.F. and Thompson, S. 2001. Solving DDEs in Matlab. *Applied Numerical Mathematics*, **37**: 441-458.

Shell. 2012. Oil sands performance report 2011. <http://s07.static-shell.com/content/dam/shell-new/local/country/can/downloads/pdf/aboutshell/our-business/oil-sands/oil-sands-performancereport2011.pdf>

Yao, Y., van Tol, F. and van Paassen, L. 2014. Drying and Rewetting Characteristics of Fine Oil Sands Tailings. Fourth International Oil Sands Tailing Conference (IOSTC'14).

MULTILAYER DEPOSITION OF TWO BATCHES OF THICKENED OIL SANDS TAILINGS: EXPERIMENTS AND MODELING

Paul Simms¹, Tessa Innocent Bernard¹, Xiaoli Yang² and Andrea Sedgwick²

¹Carleton University, Ottawa, Canada

²Total E&P Canada, Calgary, Canada

ABSTRACT

Fine oil sand tailings prepared from two thickener pilots were tested in a multilayer deposition simulation employing a 0.7 m by 1 m in plan instrumented test cell. Each tailings type involved sequentially depositing three lifts of 0.20 m, with a drying time of about 1 month before placement of the next lift. The two tailings types varied in the amount of dissolved solids in the pore-water, and in some other physical properties such as hydraulic conductivity, though both types of tailings had similar Atterberg limits. Whereas accumulation of dissolved mass at the surface contributed to decreasing evaporation in the first few days, evaporation would subsequently increase in concert with the development of cracks. The influence of cracks is reflected in the evaporation data, where exposure of wetter material correlates with an increase in evaporation. Though the overall evaporation rate was similar for both types of tailings (about 4 mm / day), the lower salinity tailings exhibited much more uniform drying with depth. This is explained by the higher hydraulic conductivity measured for these tailings. This hypothesis is borne out by coupled unsaturated flow-consolidation modelling. The comparison between the model and the experiments also highlights the importance of cracking to the efficiency of evaporation as a dewatering mechanism.

INTRODUCTION

To address the problem of poor consolidation of fine tailings produced from the surface mining of oil sands, and to meet regulatory criteria for undrained shear strength post-deposition (ERCB, 2009), Total E&P Canada Ltd., as Operator of the Joslyn Project (referred as Total below), is exploring thickened tailings technology for dewatering the fine tailings. With the aid of flocculants in a thickener, tailings are produced with a solids concentration ranging from 50 to 55%. To allow for reclamation within a reasonable

time, Total is investigating tailings that will be deposited in thin lifts (<1m) where further dewatering and strength gain is expected through the processes of evaporation, freeze-thaw, and consolidation to allow for reclamation within a reasonable time.

This paper reports on a study investigating dewatering in relatively thin (~0.2 m) lifts by evaporation and consolidation. Multi-lift deposition is simulated in a 1 m by 0.7 m plan area experiments in the laboratory. Innocent-Bernard (2013) and Innocent-Bernard and Simms (2013) reported on a multilayer deposition test on one type of thickened tailings. This paper reports on two sets of drying box tests, using two different sets of tailings generated by the same pilot plant. The study investigates the influence of cracking and salinity on evaporation, and uses a coupled unsaturated flow- consolidation model to interpret the experiments.

Background

Water driven to the surface during evaporation in saline tailings (or soils) leaves behind dissolved mass. As the concentration near the surface approaches the solubility limit of constituent mineral phases, salts precipitate along the pores, cracks and on the surface. Several authors (Chen 1992, Fujiyasu & Fahey 2000, Fujimaki et al. 2006, and Shimojima et al.1996) have shown that this phenomenon can lower the evaporation rate by as much as 90%. The mechanisms by which this occurs may include an increase in albedo, the depression of water vapor pressure at the surface due to increased osmotic suction, and the physical obstruction by salt precipitates to moisture flow (Fujiyasu & Fahey 2000, Simms et al. 2007, Fisseha et al. 2010, Dunmola & Simms 2010). Simms et al. (2007) reported that salts at the surface shut down evaporation three (3) weeks after the start of a single layer field deposition trial at the Bulyanyulu Gold mine in Tanzania. Although the authors measured an increase in albedo, they concluded that it was not the sole contributor. Dunmola (2012) surprisingly found that for high

total suctions (> 1 MPa), osmotic suction was the dominant contributor (> 60%) to total suction in a gold tailings. Dunmola (2012) also found that total suction can be capped in some saline soils or tailings by the solubility limit of precipitating minerals phases, but further drying beyond this limit, correlated with mineral precipitation, reducing the evaporation rapidly to a low residual value. Fujiyasu and Fahey (2000) observed a significant decrease in evaporation in clayey tailings as a result of crust formation due to the rapid accumulation of salts at the tailings surface irrespective of the initial salt concentrations of the tailings under study.

It is well accepted that the presence of cracks increases evaporation from soil. Whereas there is some disagreement in the literature regarding whether the formation of cracks actually can increase evaporation above the potential rate, cracking definitely facilitates increased water loss, particularly in the case where surfaces become less permeable (Vogel et al., 2005). Fujiyasu et al (2000), in a field investigation of evaporation from highly clayey (60% kaolinite, Liquid Limit (LL) of 96%) fresh water tailings, reported an increase in evaporation rates with the appearance of cracks. The authors noted that when the top of the tailings had a very low water content, evaporation from cracks contributed significantly to total water loss. Simms et al (2010), however, reported no significant increases in the evaporation rate as a result of surface cracking in laboratory drying tests on gold thickened tailings (Plasticity Index (PI) of 1-3%). Obviously, the difference in size and frequency of cracks between these two studies was substantial.

It was anticipated that the behavior of thickened oil sand tailings might be somewhere between these two cases.

MATERIALS AND METHODS

Materials

The materials tested were two sets of fine grained oil sand thickened tailings of 55 % and 50% solids concentration (product of Total's 2010 Tailings Thickening Pilot), hereafter referred to as Tailings A and Tailings B. The tailings had settled during shipping, releasing pore water. Chemical analyses were performed on pore water to assess composition. Results on Type B indicate major concentrations of sodium (650-689 mg/L), chloride

(449-463 mg/L), bicarbonate (774-810) and sulphate (68-74) were present. The average electrical conductivity (EC) was 3.05 mS/cm. Both tailings batches were remixed to a solids concentration of 50% and tested for basic geotechnical properties.

The key differences between the two batches of tailings were the i) pre-shipment solids content, ii) the SFR as determined from standard hydrometer tests, iii) total dissolved solids and corresponding electrical conductivity of pore-water and pore-water composition, and iv) Hydraulic conductivity versus void ratio data from fixed wall hydraulic conductivity tests. No substantial differences were detected in mineralogy, rheology, or water-retention curves from re-mixed samples (Innocent-Bernard 2013). While there was some variability in terms of LL, this variability occurred in both Tailings bathes. The drums either had a LL near 25 or 35. PL (plastic limit) and SL (shrinkage limit) were 20 and 18 for both tailings types. Key differences in basic material properties are summarized in Table 1.

Table 1. Differences in basic properties, A and B tailings

Batch	Solids	SFR / Clay content from MBI	EC (microS/cm)	Na in pore-water (mg/L)
A	55%	1 / 0.33	2400	530
B	50%	0.75 / 0.38	3000	660

Saturated hydraulic conductivity values were determined using fixed-wall permeameters, and are presented in Figure 1, along with void ratio-hydraulic conductivity relationships from MFT and in-line flocculated cyclone overflow oil sands tailings (Jeervipoolvarn 2010). There is clearly a substantial difference in hydraulic conductivity. The Type A tailings exhibited at least an order of magnitude higher hydraulic conductivity than the Type B tailings at a given void ratio. The measured data is fitted with two power functions of the form Ae^{-7e} , e being the void ratio.

Methods - Experimental

The multilayer deposition tests were conducted in a 0.7 m (W) x 1 m (L) x 1m (adjustable height) box. A lift thickness of 0.2 m was employed. For each batch, three layers were subsequently deposited. Each layer was given about a month before

placement of the next layer. The box was mounted on load cells (Figure 2) to directly measure water loss through evaporation and drainage. Drainage was measured using a tipping bucket placed at the base of the drainage port. Geotextile material was placed at the base of the box to prevent soil particle loss.

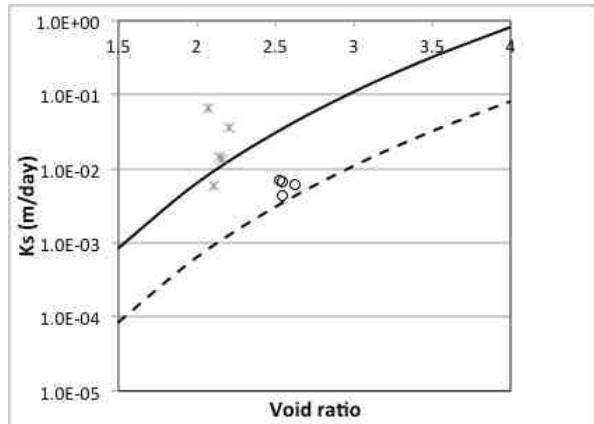


Figure 1. Measured and fitted hydraulic conductivity data for Tailings A and B



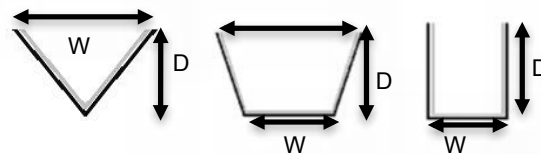
Figure 2. Multilayer Deposition Test

Above the box, four (4) ultrasonic non-contact distance sensors were placed to monitor the variation in height of the sample to estimate vertical volume change. T5 Tensiometers (UMS) were placed horizontally within 5 cm and 10 cm of the top of each layer to measure matric suction. Six (6) volumetric water content sensors (Decagon) were also placed at the same heights to measure volumetric water content (VWC), temperature and bulk electrical conductivity (EC).

Above the soil surface, a Relative Humidity (RH) Easy Log USB sensor was placed to observe RH and temperature change. Two electrical standing fans, set at the lowest speed, were used to simulate wind. The box was placed in an area of the laboratory bound by tarpaulins and with no sunlight reaching the setup thus minimizing the effect of radiation.

The top 1 cm of the tailings surface was sampled daily to measure total suction using a Dewpoint Potentiometer (WP4-T, Decagon Devices Inc.), as well as to obtain samples for gravimetric water content and electrical conductivity measurement. Additionally, surface crack development was monitored by the measurement of crack dimensions to estimate surface area and volume. Surface cracks were classified according to the shapes shown in Figure 3. Crack surface area (SA) and crack volume were then calculated based on these three geometries.

When the average water content of a given layer reached a GWC of 18% (corresponding to the shrinkage limit), sections of the tailings were removed and profiled for water content, total suction, and electrical conductivity with depth. The next layer was then deposited.



Perimeters are indicated in grey. W: Width; D: Depth

Figure 3. Crack Dimension and Measurement

The relative evaporation, RE, which is the ratio of Actual and Potential Evaporation rates, (AE/PE), was calculated using measured AE and PE rates. PE was calculated from the Penman-Monteith equation using relative humidity (RH) and temperature measurements, and back calculating the wind parameter assuming the evaporation during the first few hours was equal to the potential evaporation. The wind parameter was assumed to remain constant throughout the experiment. AE was determined directly from the load cell measurements, subtracting measured drainage.

Methods – Numerical

The experiments were modelled using a custom coupled consolidation-unsaturated flow software

developed by SoilVision, Saskatoon, Saskatchewan, obtained in January 2013. The software combines existing SVSolid (deformation analysis product of SoilVision) and SVFlux (unsaturated flow product of SoilVision) codes. Unsaturated behaviour is incorporated into consolidation by defining hydraulic conductivity, void ratio, and degree of saturation as three-dimensional functions of matric suction and vertical stress. These functions can be defined by measurements made using consolidation tests for data along the vertical stress axis, and measurements made during soil-water characteristic curve tests of water content and void ratio. A 3-D curve-fitting freeware (NLReg) was used to interpolate between the two sets of data. The SoilVision code uses a six parameter function to define each of these three material parameters.

The material property data used to generate the three functions are from the SWCC measurements of the tailings provided by Total, saturated hydraulic conductivity tests at different void ratios performed on those tailings, and void ratio-effective stress measured in the drying box tests themselves. It was assumed that the form of the saturated hydraulic conductivity-void ratio function was similar to other polymer-amended fine tailings streams, such as reported by Jeerivapoolvarn (2010) for sheared in-line flocculated cyclone overflow tailings, and by Dunmola et al. (2013) for in-line flocculated MFT.

The only difference between the material properties for modelling the drying boxes was the hydraulic conductivity function. The hydraulic conductivity value at a given void ratio was an order of magnitude higher for the drying box for Tailings A. The hydraulic conductivity relationships are shown with the measured data in Figure 1.

RESULTS

Where results from both tailings batches are not presented in the same figure, the plot for Tailings B follows the plot for Tailings A.

Evaporation

Evaporative behaviour was very similar between the two tests (Figure 4). For each layer deposited,

evaporation was characterized by an initial period of evaporation rates cycling between a low value and the potential evaporation, and a later period where the evaporation rate was relatively stable at about 2 or 3 mm/day. The overall evaporation rate across all 6 layers was 4 mm /day (within +/- 0.5 mm/day).

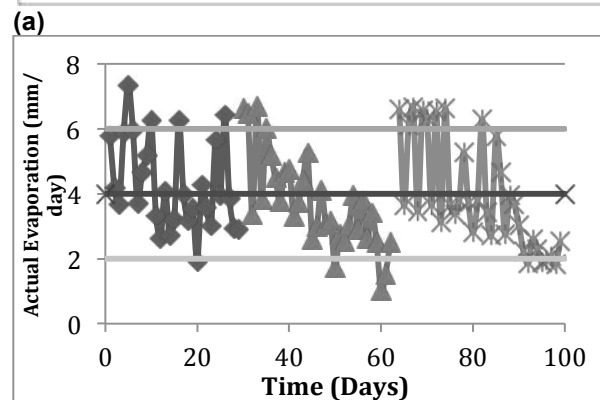
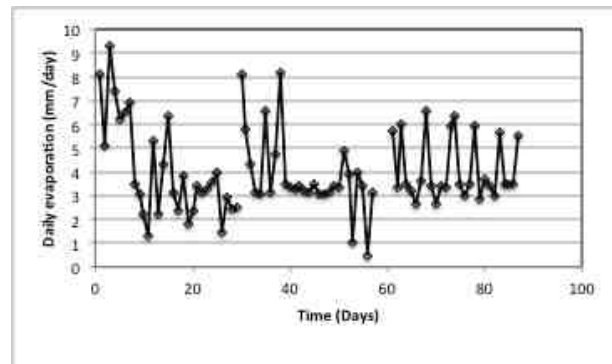


Figure 4. Actual evaporation in drying box tests

The initial fast decline in actual evaporation is due to rapid drying of the surface crust, accompanied by concentration of dissolved mass and mineral precipitation. Typically, water content in the top 1 m fell from 100% to less than 30% after the first 24 hours (Figure 5). This was accompanied by a rapid increase in total and osmotic suction, driven by mass transport of dissolved solids and decreasing water content at the surface. The values of total suction after 1 or 2 days were greater than 1 MPa, which is sufficient to substantially decrease AE (Innocent-Bernard et al. 2013).

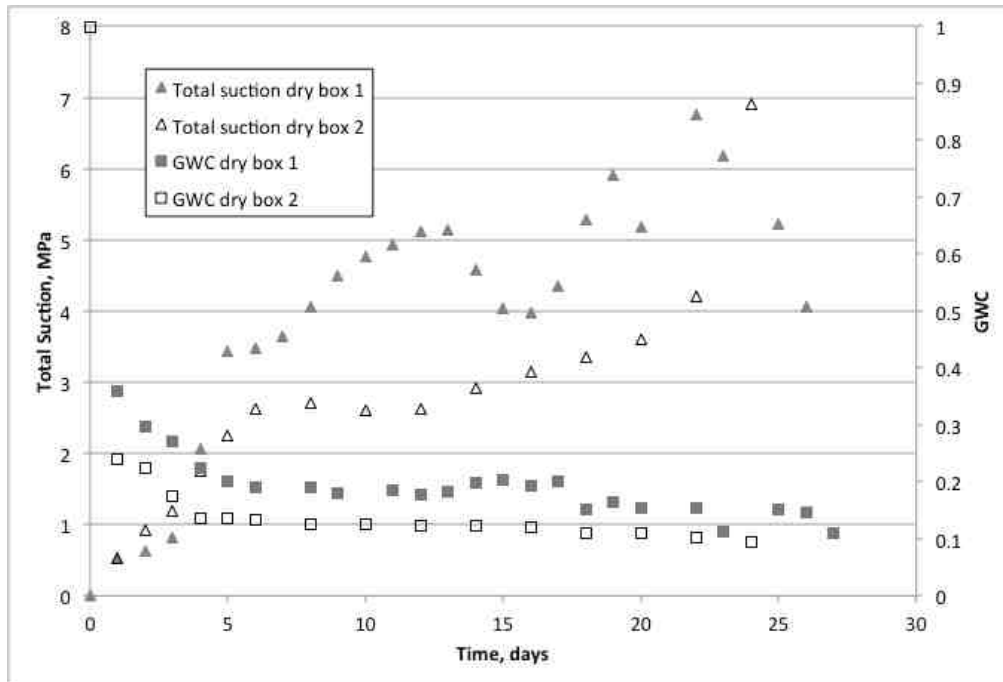


Figure 5. Surface GWC and total suction at the top 1 cm of tailings in both drying box tests

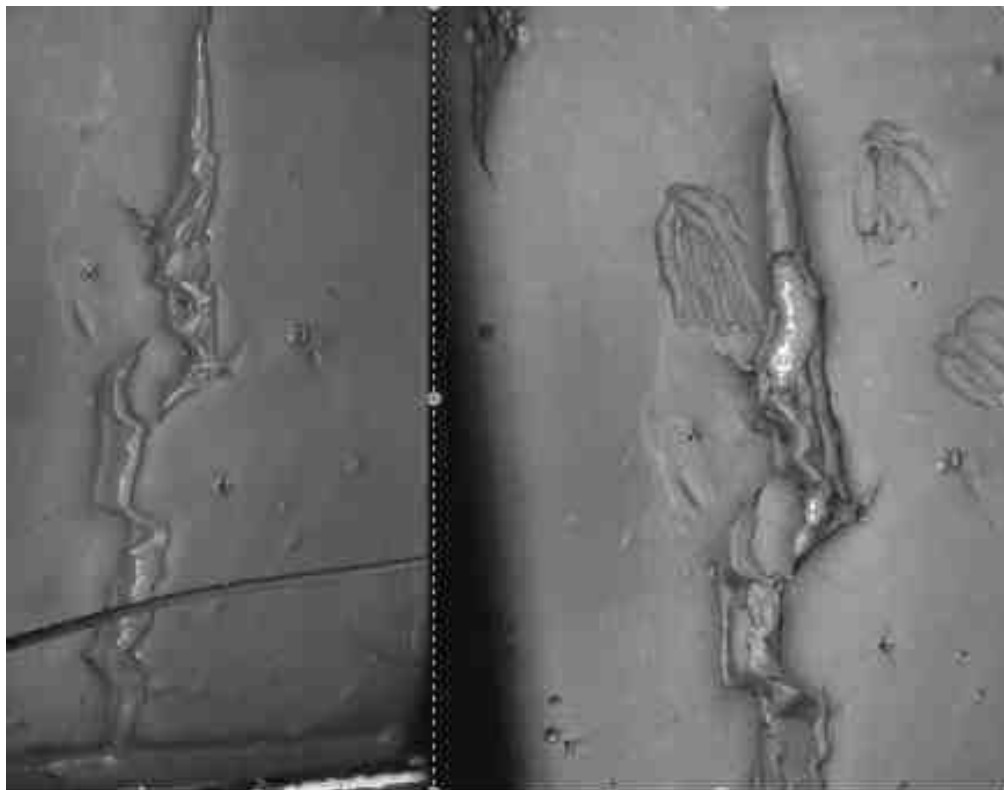
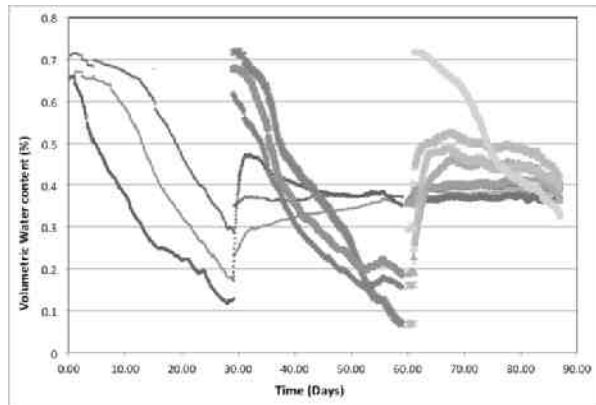
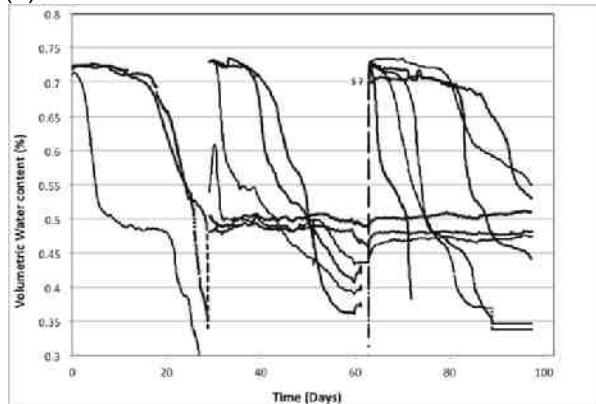


Figure 6. Crack initiation within 24 hours after placement of Layer 2, high saline tailings test, and the same crack 3 days later, showing exposure of fresh tailings.



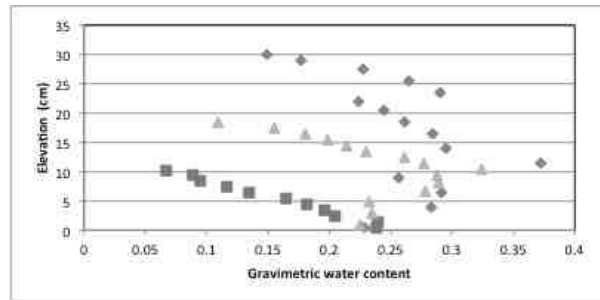
(a)



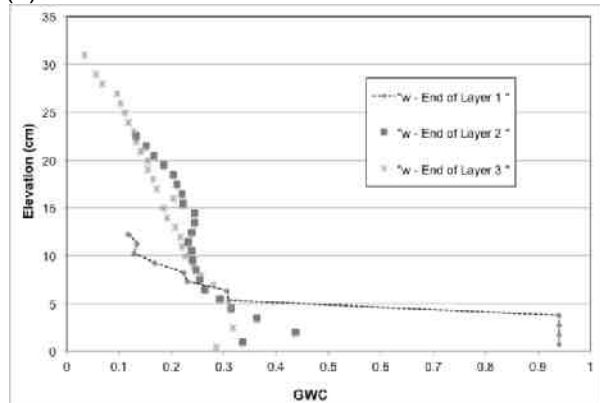
(b)

Figure 7. Volumetric water contents In drying box tests

The formation of a crust, was, however, co-incident with cracking, which facilitated exposure of fresh material. Wetter tailings would occasionally flow into the cracks, perhaps due to the “sinking” of the denser crust. The evolution of one crack is shown in Figure 6. This mechanism would continue for 15 days or greater, as old cracks dried out, and subsequently new cracks appeared. Measurements of water content and total suction in the cracks confirmed that crack surfaces were substantially wetter and would allow for more evaporation than at the surface. In most layers, however, this process eventually stopped, and evaporation assumed a constant residual value of about 2 or 3 mm /day. Overall, despite the complex drying behaviour, for each layer in the two tests, the average evaporation rate was 4 mm /day (+/- 0.5 mm /day). The average water content of each fresh layer took about a month to reach the shrinkage limit (18% GWC).



(a)



(b)

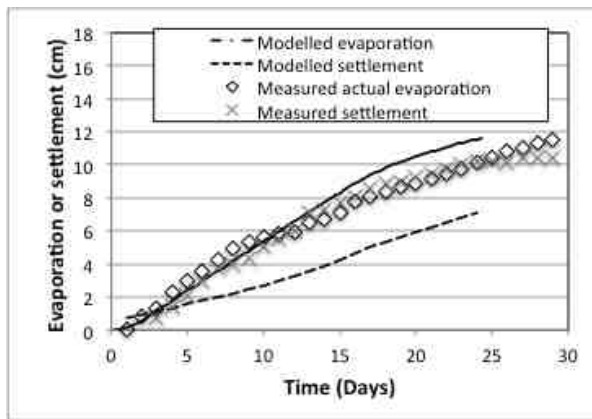
Figure 8. Depth profiles of GWC in each drying box test, 30 days after placement of each layer

Differences between the two types of tailings are evident in the uniformity of drying within a layer, shown in Figure 7 in terms of VWC sensor data, and profiles of GWC with depth taken at the end of the drying period for each layer. Drying occurs with more uniformity in Tailings A. This is most evident in the final GWC profile for layer 1 for both tests. In layer 1 for Tailings B, the bottom 5 cm was not much lower than the water content at deposition (100%). It then rapidly decreased to a value of 10% near the surface. In Tailings A, the distribution of GWC from top to bottom in Layer 1 was 7% to 24%.

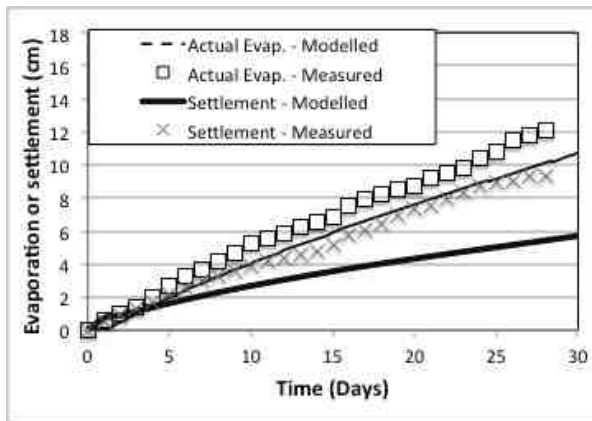
Modelling

The first layer of each box was modeled. As stated in the methods section, the only difference between the two simulations was to use hydraulic conductivity functions with one order of magnitude difference at any void ratio (Figure 1).

Modelled and measured results are compared in terms of evaporation and settlement in Figure 9. Final profiles of solids concentration at the end of layer 1 and volumetric water contents are found in Figures 10 and 11. Saving predictions of overall settlement, the model predictions provide reasonable fits to the measured data, and explains the differences between the two types of tailings. Therefore, our hypothesis as to the hydraulic conductivity difference being the key contributor to the different dewatering behavior of the two tailings types (more uniform dewatering in Type A), is borne out.



(a)



b)

Figure 9. Measured and modeled evaporation and settlement

The model under-predicts overall settlement for two reasons. The first reason is related to the reverse gradient in solids concentration (and density) predicted for the top 3 cm, as shown in Figure 10, which only develops in the last 10 days of the simulation. This appears to be due to the increase in total stress near the surface. In reality, however, the influence of salts is to cap the gravimetric water content immediately at the surface (Figure 5) near the shrinkage limit. Therefore at the surface, the model simulates more desaturation than occurs in reality.

The second reason for the discrepancy is the influence of cracks. Cracking, by providing a pathway for evaporation to occur from tailings at depth, will mean that evaporation will induce a greater volume change, as more of the evaporative demand is being consumed by volume change of wetter tailings, rather than by desaturation of tailings near the surface. This phenomenon is illustrated in Figure 12.

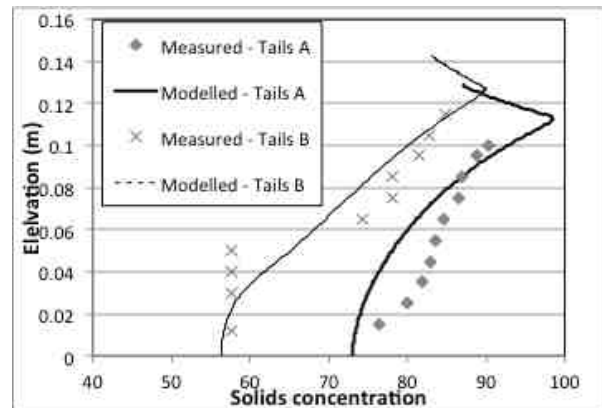
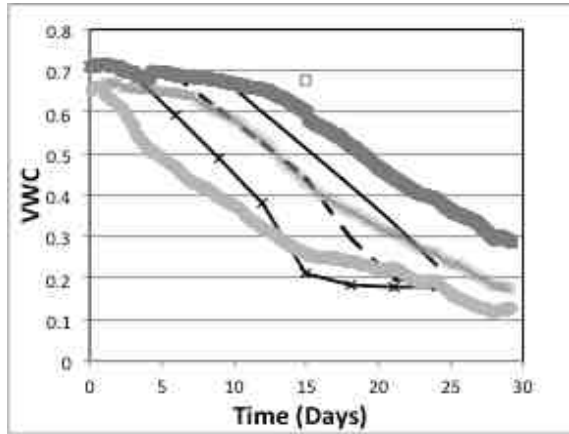
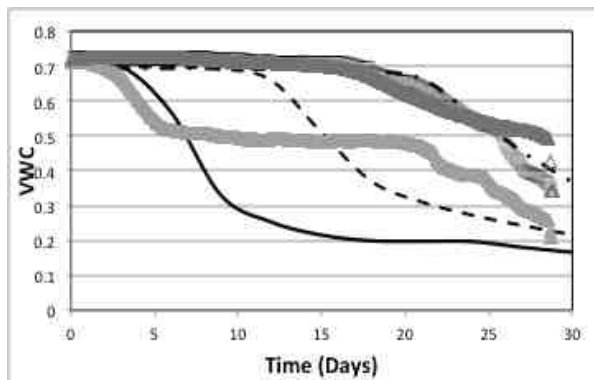


Figure 10. Measured and modeled solids concentrations at end of layer 1 drying



(a)



(b)

Figure 11. Measured and Modeled Volumetric Water Contents at different depths in Layer 1

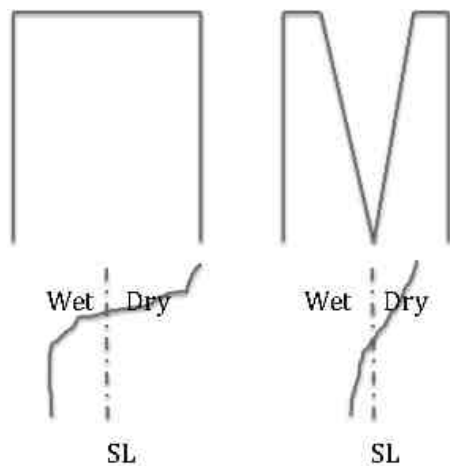


Figure 12. How cracks promote greater volume change in a drying layer of tailings

SUMMARY AND CONCLUSIONS

The key findings of the study are:

1. Both salinity and cracking had important effects on the evaporative behavior of the tailings, although they had somewhat compensating effects. The initial decrease in evaporation at the surface is strongly linked to the accumulation of osmotic suction at the surface, which is allayed by exposure of fresh material through cracking.
2. Despite the complexity of the drying behavior, the overall rate of evaporation from both sets of tailings over the 3 month tests was 4 mm/ day, where the potential rate average 6 mm /day.
3. The two batches of tailings were produced at the same pilot plant, with no documented variation in extraction or other processing parameters. This once again highlights the need for robust deposition designs that handle tailings variability.
4. The difference in the hydraulic conductivity function was proposed to be the reason to explain the differences in dewatering behavior, with Tailings A undergoing considerably more uniform drying with depth. This hypothesis was borne out by the modelling exercise.
5. The coupled unsaturated–consolidation model was able to replicate most of the experimental data with reasonable agreement, save underestimating the rate of settlement. It is argued that this is due to:
 - i)_ the shutdown of evaporation at the surface due to salts, and
 - ii) the presence of cracks causes greater volume change by allowing evaporation to proceed from deeper materials.

ACKNOWLEDGEMENTS

This work was primarily funded by Total E&P Canada.

REFERENCES

- Chen, X. (1992). Evaporation from a salt-encrusted sediment surface: Field and laboratory studies. *Aust. J. Soil Res*, 30, 429-442.
- Dunmola, A., Dhadli, N., Freeman, Kolstad, D., Fasking, T., Song, J., and Langseth, J. (2013) Geotechnical benefits of flocculation in dewatering oil sands mature fine tailings, in Proceedings 66th Canadian Geotechnical Conference (GeoMontreal 2013), 29 September – 3 October, Montreal, Canada.
- Dunmola, A. (2012). Predicting evaporative fluxes in saline soil and surface-deposited thickened mine tailings. PhD Thesis. Ottawa: Carleton University.
- Dunmola, A. S., & Simms, P. H. (2010). Coupled solute mass transport and evaporation in saline soil. In A. Gens (Ed.), *Unsaturated Soils* (pp. 1369-1374). CRC Press.
- ERCB, E. R. (2009, February 3). Tailings Performance Criteria and Requirements for Oil Sands Mining Schemes. Retrieved from <http://ercb.ca/directives/Directive074.pdf>.
- Fisseha, B., Bryan, R., & Simms, P. (2010). Evaporation, unsaturated flow, and salt accumulation in multilayer deposits of "paste" gold tailings. *Journal of Geotechnical Geoenvironmental Eng.*, 135(12), 1703-1712.
- Fujimaki, H., Shimano, T., Inoue, M., & Nakane, K. (2006). Effect of a Salt Crust on Evaporation from a Bare Saline Soil. *VadoseZone Journal*, 5, 1246-1256.
- Fujiyasu, Y., & Fahey, M. (2000a). Experimental study of evaporation from saline tailings. *Journal of Geotechnical and Geoenvironmental Engineering*, 18-27.
- Fujiyasu, Y., Fahey, M., & Newson, T. (2000b). Field investigation of evaporation from freshwater tailings engineering. *Journal of Geotechnical and Geoenvironmental Engineering*, 126(6), 556-567.
- Innocent-Bernard, T. (2013). Evaporation, cracking, and salinity in a thickened oil sands tailings. MSc Thesis. Carleton University., Ottawa, Canada.
- Innocent-Bernard, T., Simms, P., Sedgwick, A., Kaminsky, H. and Yang, X. (2013) Influence of surface cracking and salinity on evaporation in an oil sands thickened tailings, in Proceedings 17th International Conference on Tailings and Mine Waste, 3–6 November 2013, Banff, Canada.
- Jeeravipoolvarn, S. (2010) Geotechnical behaviour of in-line thickened oil sand tailings, PhD thesis, Department of Civil and Environmental Engineering, University of Alberta, Edmonton, Canada, 410 pp.
- Shimajima, E., Yoshioka, R., & Tamagawa, I. (1996). Salinization owing to evaporation from bare-soil surfaces and its influences on evaporation. *Journal of Hydrology*, 178, 109-136.
- Simms, P., Grabinsky, M., & Zhan, G. (2007). Modelling evaporation of paste tailings from the Bulyanhulu mine. *Canadian Geotechnical Journal*, 44, 1417-1432.
- Vogel, H..J, Hoffmann, H, Roff, K. (2005). Studies of crack dynamics in clay soil. *Experimental methods, results, and morphological quantification. Geoderma*, 125: 203-211.

GEOMETRY OF POLYMER-AMENDED FINE TAILINGS DEPOSITS: YIELD STRESS MEASUREMENT AND NUMERICAL MODELLING

Shabnam Mizani and Paul Simms
Carleton University, Ottawa, Ontario, Canada

ABSTRACT

Recent pilots on emerging oil sand tailings technologies have confirmed that deposit thickness is an important parameter controlling tailings dewatering, and a key parameter governing cost. Controlling or managing deposit thickness continues to be an important challenge for full-scale implementation of tailings technologies that exhibit a yield stress. From the perspective of deterministic modelling of such deposits, there are many challenges, including measurement of the relevant rheological parameters, and how to handle time-variant rheology when modelling. This paper investigates both these issues. The stress that best quantifies when the tailings stop, which we call the “arresting stress”, is examined for polymer amended fine oil sand tailings. It is shown that a controlled decreasing shear stress test appears to simulate the stress history likely to occur in the field. No amount of shearing completely eliminates the floc structure, and the floc structure recovers when the tailings are flowing at relatively low flow rates. The increase in yield stress post-deposition due to dewatering is also studied, as this may affect field scale geometry. Fortunately, the yield stress does not seem to appreciably increase for less than a day following deposition. Also presented are 3-D numerical simulations of bench scale tests, and 2-D simulations of bench and field scale tests using the commercial non-Newtonian flow model CFX.

INTRODUCTION

Several new fine tailings technologies in the oil sands generate polymer-amended materials that exhibit a yield stress upon deposition, and will therefore stack at a gentle slope. Anecdotally reported challenges with deposition geometry in oil sand pilots or commercial trials include i) poor spread-ability and associated lift thickness variation, underutilization of impoundment footprints, and overflowing of embankments, or ii) accumulation of low yield stress material at deposit topographical lows. While these challenges can

and have been dealt with by increasing the number of deposition points or otherwise increasing operational flexibility, or by rehandling the tailings, such solutions come at a cost. Improving understanding of the flow behaviour of new tailings products may reduce these potentially substantial costs. Consider an operation that deposits tailings at a volume of 500,000 m³/day, which dewateres to 300,000 m³/day, but requires rehandling: The cost of moving this material is likely to be well over a million dollars a day.

Prediction of tailings deposit geometry for hard rock tailings has been studied for many years, primarily in regards to beach slope prediction (Simms et al. 2011). The most commonly used beach slope prediction methods in practice are either those that assume the beach slope to be constrained by eroding behaviour of self-formed channels during tailings deposition (Fitton et al. 2014, and McPhail 1998) or those that involve predictions based on flow behaviour, usually involving simplifications of fluid mechanics (Li et al. 2011). Some of these methods have been used for oil sand tailings (Charlebois 2013). However, uncertainty in prediction of beach slope remains high, and pour geometry cannot be predicted using these methods.

The present paper contributes to improved understanding of flow behaviour of polymer amended tailings in two ways: i) Assessing what is the best way to measure the yield stress appropriate to model pour flow and deposition geometry, and ii) Attempting to model such flows at bench and pilot scales using either 3D or 2D numerical simulations. This is a continuation of work presented at the Paste 2014 conference in June (Mizani et al. 2014).

Determining the yield stress as the material flows down the beach and comes to a stop is not trivial, as the structure of the material is degraded by shear, but also may recover at lower shear rates. Mizani et al. (2014) used oscillatory tests to show that the structure indeed recovers, and proposed that a unique yield stress can still be used to model deposition. (Mizani et al. 2014) also noted, that for

field scale deposition, where deposition of a particular layer of tailings in may take days, that increase in yield stress of the tailings deposited early in the pour (due to dewatering) can influence the shape of the layer. This paper, therefore, continues to investigate shearing and recovery effects, but also studies the rate of yield stress increase for freshly deposited material.

Mizani et al. (2014) presented a 3-D numerical analysis of a flume experiment on polymer-amended MFT using the commercial CFX model. This paper presents another example of 3-D deposition, but also investigates the use of the simpler and faster 2D implementation of the same model.

MATERIAL

The MFT and reclaim water used in this study were obtained from Shell Canada’s Muskeg River Mine. With the raw MFT having an initial solids content of 35.5%. The procedures followed for preparing floc solution and flocculated MFT are as outlined in Mizani et al. (2013). Comparability of laboratory and field samples is shown in Mizani et al. (2013a). Tests were undertaken between 15 and 30 minutes following sample preparation. Basic properties of the MFT are reported in those references.

RHEOLOGY AND TEST PROCEDURE ON LABORATORY-PREPARED POLYMER AMENDED MFT

An Anton Paar Physica rheometer with a vane fixture was used to characterise the rheology of the tailings. The vane fixture has four thin blades, each measuring 4 cm in length and 2.2 cm in diameter. A number of rheometry techniques have been investigated, to examine which measure of yield stress is most appropriate for modelling deposition (what the author term the “arresting stress”). Rheometry techniques performed included measurements of dynamic oscillation and the following techniques:

Conventional flow curve – strain rate is increased in steps from zero or decreased from a high rate. In a given step, after an equilibrium value of stress is achieved, the strain rate is increased or decreased.

Stress growth –application of a low and constant shear rate. Yield stress is taken to be the peak or maximum stress measured.

Constant stress (Creep)– stress is increased in increments, strain is monitored. Yield stress is the stress at which strain increases indefinitely.

Stress relaxation - In this mode the material is first sheared at a constant shear rate. The speed is then reduced slowly or suddenly to zero. The yield stress is defined as the stress exerted by the material on the vane (Dzuy and Boger 1983).

Constant stress with stress decreasing in steps - The sample is initially sheared at high stress level. The stress is then decreased in steps. The yield stress is defined as the stress at which no significant movement of the vane is observed.

Several of these tests have been presented elsewhere (Mizani et la. 2014, Mizani et al. 2013). Select stress growth, controlled decreasing stress tests, and oscillatory measurements are presented for polymer-amened and raw MFT.

It should be noted that all rheometry tests were performed at about ½ hour following preparation of the polymer -mended samples.

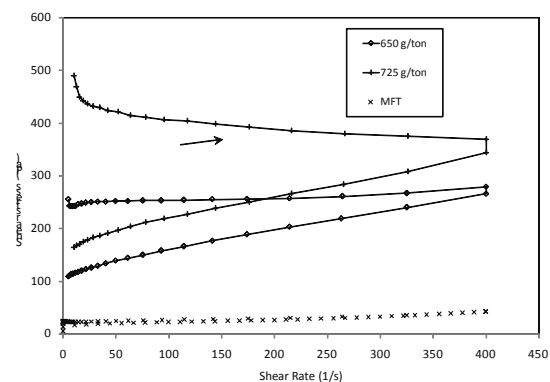


Figure 1. Flow curves on raw and flocculated MFT

Flow curve

Flow curves for raw and amended MFT are shown in Figure 1. Unlike typical flow curves, these show an initial spike in shear stresses at the start of the test, possibly due to errors arising from incomplete yielding of the sample or slip of the sample at the edge of the cylinder. Both ascending and descending curves are illustrated in this plot, which

shows a hysteresis loop that becomes more apparent as the floc dosage increases. Shearing of the flocs would explain the decreasing shear stress with increasing shear rate observed in the 725 g/t sample. Despite shearing, these samples retain a substantial yield stress (about 100– 150 Pa) on the descending loop.

Stress Growth

In stress growth technique a low and constant shear rate is applied to the vane and the torque is measured as a function of time. The torque is then converted to shear stress. The peak in the torque-time curve is related to the yield stress of the material.

Stress growth tests conducted on amended MFT in the range of 600 to 1200 g/t at shear rate of 0.1s^{-1} are illustrated in Figure 2. Polymer was added to raw MFT at an initial solid content of 35.5%. In the following figure the test results on raw MFT at different solid concentration (36%-61%) are presented.

Figures 2 and 3 illustrate that the addition of the polymer generates a substantial increase in yield stress when compared to the MFT at the same density (36% solids), but that the value of the stress growth yield stress is much higher than the yield stress on the descending branch of the flow curves in Figure 1.

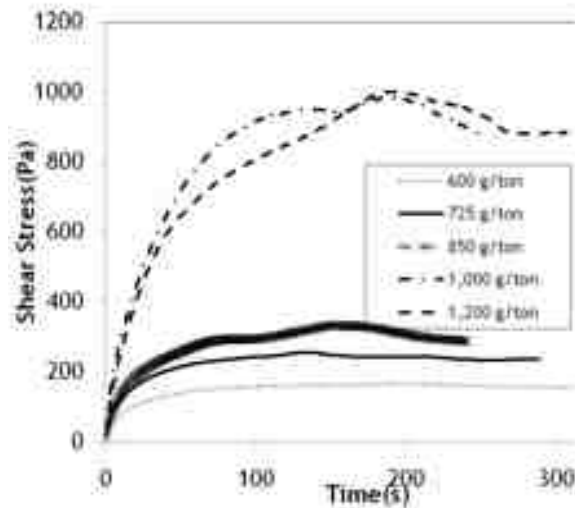


Figure 2. Stress growth diagrams of flocculated MFT at constant shear rate of 0.1s^{-1} .

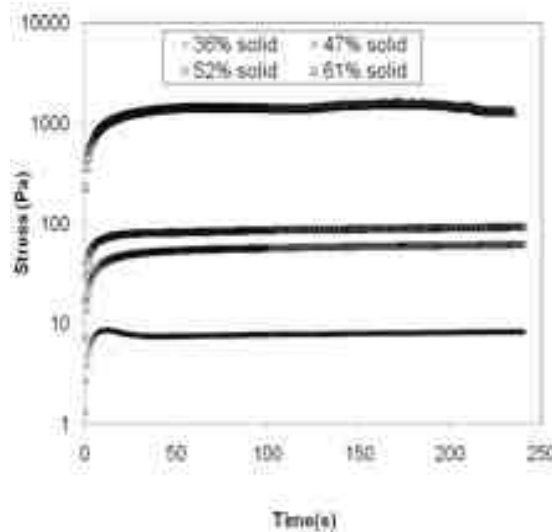


Figure 3. Stress growth diagrams of raw MFT at constant shear rate of 0.1s^{-1}

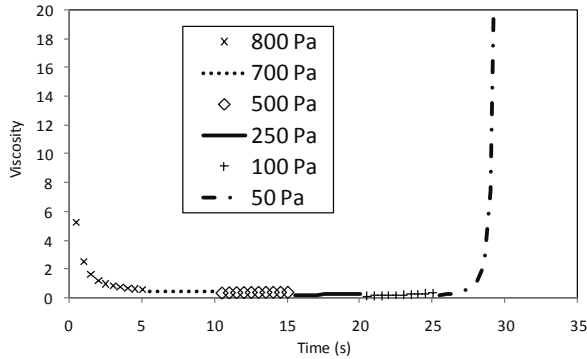


Figure 4. Viscosity plots for samples prepared at 850 g/t: stress was decreased in steps from 800 Pa to 5 Pa, and each step was held for five seconds

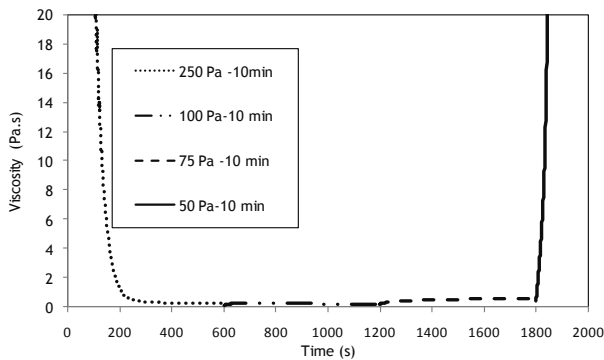


Figure 5. Viscosity plots for samples prepared at 850 g/t: stress was decreased in steps from 250 Pa to 30 Pa, and each step was held for 600 seconds

Controlled stress rheometry

Tailings experience different levels of shear stress as they flow down the beach. The highest level of shearing happens at the deposition point, and decreases with distance. Controlled stress tests were thus conducted to simulate the shear stress history of the material as experienced in the field. In these tests, a high stress was initially applied to the sample for a set time, and then the stress was gradually decreased in steps until the material stopped flowing. Figures 4 and 5 illustrate two of these tests conducted on MFT samples dosed at 850 g/t, where the stress was decreased from 800 Pa to 5 Pa in only 45 seconds (Figure 4) and from 250 Pa to 30 Pa in nearly 50 minutes (Figure 5). Each stress level was held for five seconds in the first test and 10 minutes in the second test. Due to overflowing of tailings from the rheometer at high stress levels, the 50-minute test

(pertaining to data in Figure 5) was started at lower stress levels. A dramatic increase in viscosity was observed when stress reached a level of 50 Pa in both cases. Therefore, the duration of shearing did not have a significant effect on the arresting behaviour.

EFFECT OF AGING AND SHEARING ON TAILINGS STRUCTURE

To further investigate the effect of shear history on rheology, the authors adopted the three interval thixotropy test, a method previously used by Watson et al. (2011) to evaluate floc breakage. This technique was used to study the effects of shearing and aging on the structure of the flocculated MFT. In this technique, the linear viscoelastic (LVE) region limit is first determined using the single frequency sweep test as explained in Nasser and James (2008). This sweep is performed by increasing the maximum stress applied to an oscillating vane, and measuring the materials responding strain over time. Very simply, this allows for the determination of the relative elastic (instantaneous response) and plastic component of strain, which are quantified in terms of the moduli G^I and G^{II} .

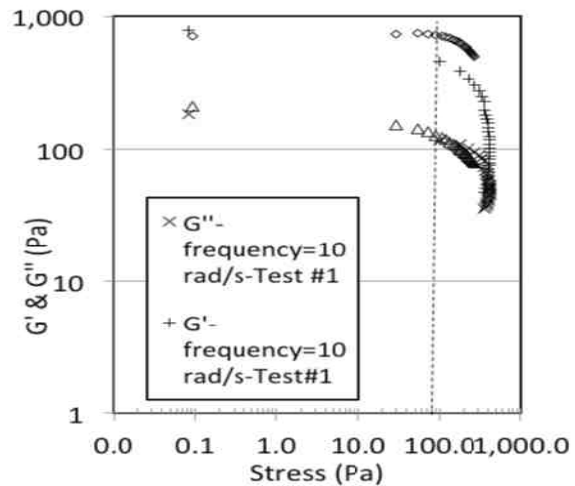


Figure 6. Effects of frequency on oscillatory test on G^I and G^{II} for different frequencies for Flocculated MFT at 850g/ton

Figure 6 and 7 illustrate the results of this test conducted on raw MFT and amended MFT dosed at 850 g/t. Two tests were done at different frequencies, 10 Hz and 10 rad/s, to show the independence of the behaviour to loading frequency. For the amended MFT, below 50 Pa, G' and G'' do not appreciably change, and G' is much larger than G'' . These data imply that, below 50 Pa, the structure of the material is not disturbed by the oscillations of the vane, and the behaviour of the material is largely elastic. Beyond that point, structure degrades, and eventually, beyond 300 Pa, G' drops below G'' , and the material is dominated by viscous behaviour. For raw MFT, the LVE range is determined to be around 7 Pa and G' dropping below G'' , at approximately 10 Pa.

After establishing the LVE range, the baseline rheology is then determined by applying an oscillating stress below the LVE range to ensure that the material is undergoing elastic deformation only. The material is then sheared at a high constant stress for a certain amount of time, after which an oscillating stress (the same as in the first step) is applied on the material. Recovery of the sample over time is then determined as the ratio of storage modulus at the end of the third interval to the storage modulus at the end of the first interval. Further details on this test can be found in Mizani et al. (2014) and Watson et al. (2011).

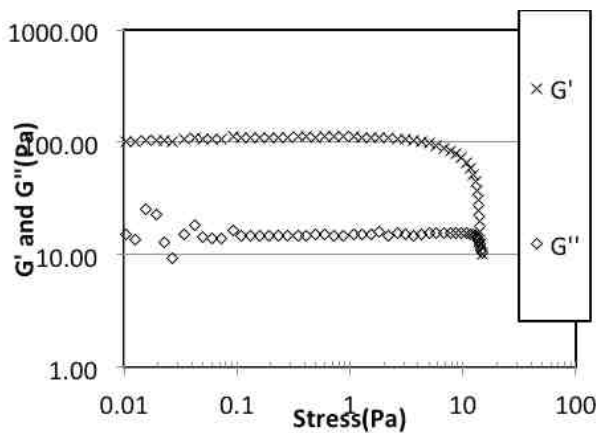


Figure 7. Oscillatory test on raw MFT at 36% solids

Figure 8, presents the G' values of raw MFT before and after shearing stage. Results indicated a 100% recovery after each loading for various solid

contents – there is fact there is no degradation of structure. However, this is not the case for flocculated MFT. Figure 9 illustrates percentage recovery of samples measured under shear loading similar to that experienced during deposition. After applying an oscillating shear stress of 10 Pa, the MFT material dosed at 850 g/t was sheared at 500 Pa for 10 seconds. The stress was then gradually decreased in steps (250 Pa, 100 Pa, 50 Pa, and 20 Pa), and each stress level was applied for only 10 seconds, giving a total time spent in Stage 2, of 50 seconds.

The test was then repeated on a newly prepared sample, but this time, each stress was held for one minute. A higher recovery rate was recorded in the latter case, which could be attributed to the longer time spent at low stress levels, despite the longer time at higher shear levels, thus giving the material more time to recover from the damage experienced. Therefore, the material recovers structure even as it flows.

Comparing the G' of the two materials, the elastic modulus (G') for the amended MFT is about twenty times that of the raw MFT at the same density. That is, the density of the polymer amended MFT at the time of testing (30 minutes after sample preparation) was not substantially different from that of the raw MFT, and the corresponding higher yield stress can be attributed to structure, not a density increase.

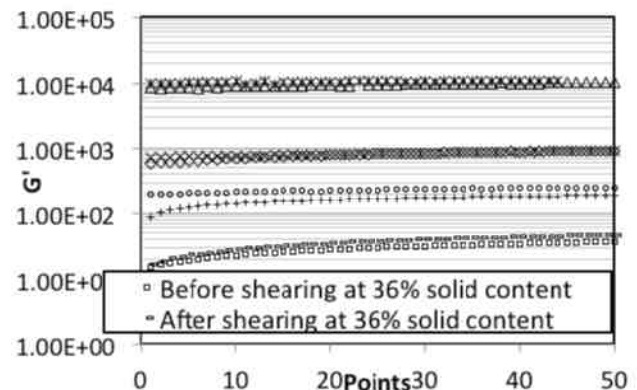


Figure 8. Post-shear recovery for raw MFT samples prepared at various solid contents after applying a shear stress of 50 Pa for 1 min

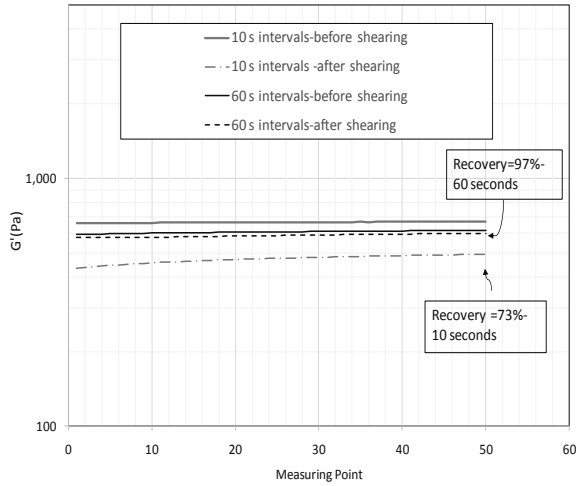


Figure 9. Post shear recovery for samples prepared at 850 g/t under constant decreasing shear stresses

CHANGE IN YIELD STRESS OF POLYMER AMENDED MFT POST-DEPOSITION

Rheology of the tailings increases as the material dewateres. Thus, if field deposition of a given layer takes long enough, the shape of the layer would be influenced by the gain in yield stress due to dewatering of the tailings deposited closer to the start of the pour. In order to measure the changes in the strength gain of amended MFT over time, stress growth tests were conducted on samples ranging in solid content and age. Amended MFT were placed in containers 10 cm in height after preparation and were tested at different times. A depth of ten (10) cm was chosen as it is the minimum height required for samples in the rheometer, and would minimize the role of self-weight consolidation. Thus, it is important to note that the degree of dewatering reported here is much less than occurs in actual lift thicknesses (0.5 m and higher).

Results are shown in Figure 10. While yield stress growth after 1 day appears to be correlated with dewatering (solids concentration), before Day 1 the yield stress of the material does not appreciably change, independent of dewatering. This is good news from a modelling perspective, in terms of simplicity of modelling deposition for less than 1 day, at least for this material.

NUMERICAL SIMULATION OF BENCH-SCALE FLOWS

Flows of pours at various floc dosages were simulated using the volume of fluid (VOF) method using the ANSYS CFX software. This is an established model used for simulating free surface flows of non-Newtonian material and to track the free surface of a fluid (Scardovelli and Zaleski, 1999; Minussi and Maciel, 2012).

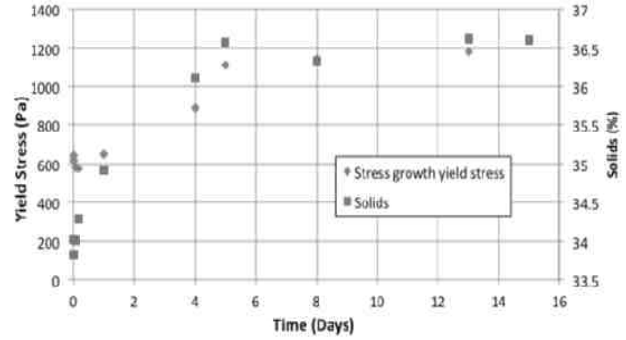


Figure 10. Yield stress increase due to dewatering in 10 cm thin samples of polymer amended MFT

The following mass and momentum equations for an incompressible fluid are solved:

$$\nabla \cdot V = 0 \quad (1)$$

$$\rho \frac{\partial V}{\partial t} + \rho \nabla \cdot (V \cdot V) = -\nabla P + \nabla \cdot \tau + \rho g \quad (2)$$

Where ρ is density, τ is stress tensor, P is pressure and g is gravitational force.

Volume fraction is defined as the ratio of the heavier phase (in this case tailings, the other phase is air) in each cell to the total volume. In case of two phase flow the interface will be located where volume fraction has a value between 0 and 1. Other cells will either have a volume fraction of 0 (filled with air) or 1 (filled with tailings). Viscosity and density in each cell can be then calculated through:

$$\rho = \sum_{i=1,n} (VF_i \rho_i) \text{ and } \eta = \sum_{i=1,n} (VF_i \eta_i) \quad (3)$$

Due to its simplicity, the Bingham model was used to describe the material rheological properties in these simulations. This model is commonly used for describing the rheological behaviour of

viscoplastic fluid. Bingham plastic model is formulated as

$$\tau = \tau_y + K \dot{\gamma} \quad (4)$$

Where:

τ_y = yield stress.

$\dot{\gamma}$ = shear rate.

K = viscosity.

Modelling of bench scale tests using 3D formulation

Initial modeling efforts were directed at 3D small scale simulations. Early results are presented in Mizani et al. (2014) Shown here is a simulations used of flow in a flume 2.00 m long, 0.15 m wide, and 0.30 m high. A total of 5.7 kg of tailings (viscosity = 0.5 Pa.s and yield stress = 60 Pa) were deposited through a circular inlet located 15 cm above the bottom of the flume. This yield stress value provides the best fit to the final geometry of the experiment (Figure 11). The numerical results show a somewhat longer horizontal distance compared to the experimental data. There is some error due to the plunge pool retaining its shape in the model, which does not happen in reality. Also, high shear stresses are only imposed on the sample for relatively short times (seconds), so the rheology may be in a less sheared state, and the actual arresting stress maybe somewhat higher. However, the best fit yield stress (60 Pa) is close to the value indicated by the controlled stress tests simulating shearing on the beach (50 Pa). Results of the numerical simulations at various times are illustrated in Figure 12. Stress plots at the bottom

of the flume illustrate the gradual decrease in shear stress away from the deposition point.

2D simulations of bench and field scale

Although the 3D simulations compare well with bench scale experiments, considerable computer resources are required to produce results in a timely manner. Therefore, a number of 2D simulations were conducted to investigate the utility of these simpler simulations. We employed the simplest way to implement flows in the model, by using dambreak type initial conditions, which are numerically easier to implement than flow boundary conditions. Figure 13 shows the initial condition of the simulations, where x and y define the arbitrary initial position of the tailings.

Figure 14 shows changes in free-surface profile of a material with a 100 Pa yield stress, which comes to rest at 0.6 s. While the shape of the flow near the toe (far from the deposition point) displays an increasing slope, the shape of the profile near the deposition point shows a decreasing slope from left to right. The former is the same as would be generated by predictions using lubrication theory (Mizani et al 2013b, Henriquez and Simms 2009), and is similar to what is seen in low-inertia flume tests. The latter conforms more closely to the shape of mature field deposits close to the deposition point. In reality, inertia would be generated by pour flow rate and not conversion from the potential energy of a high initial deposit. However the same backwater profile would be generated by sufficiently high flow rates.

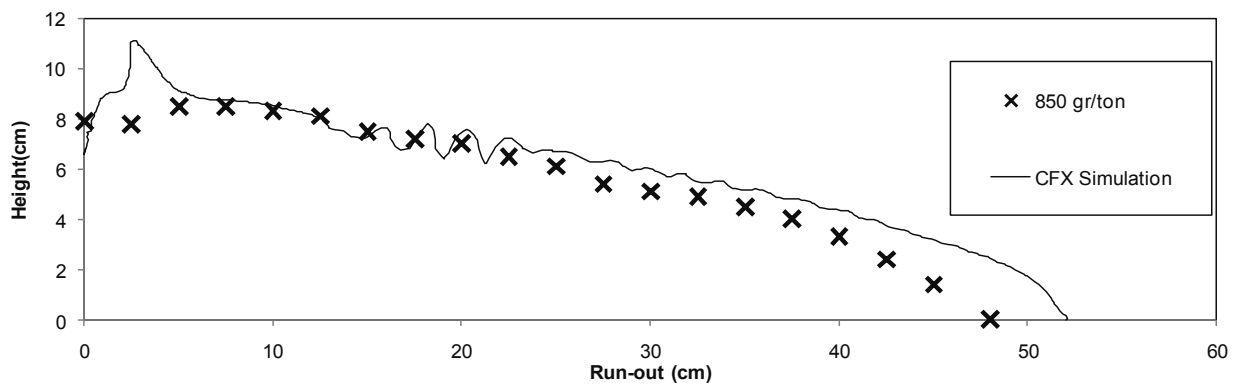
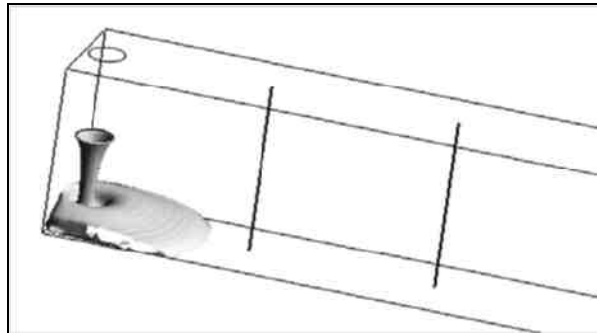
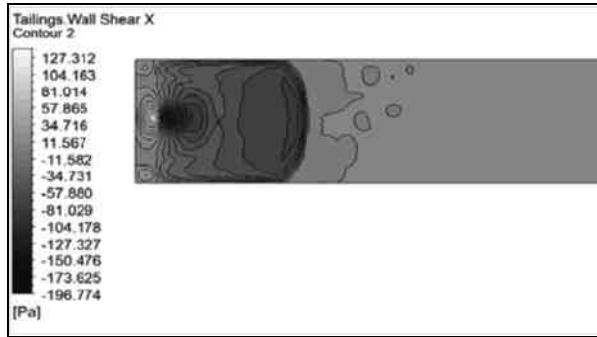
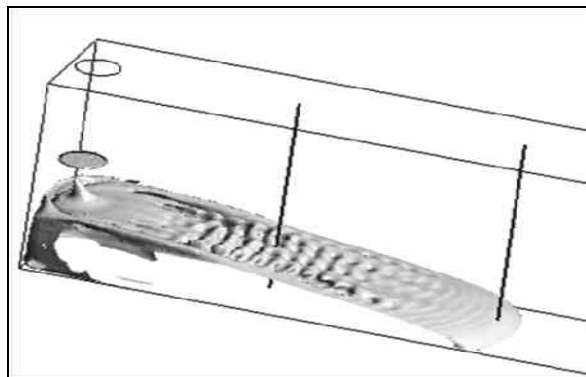
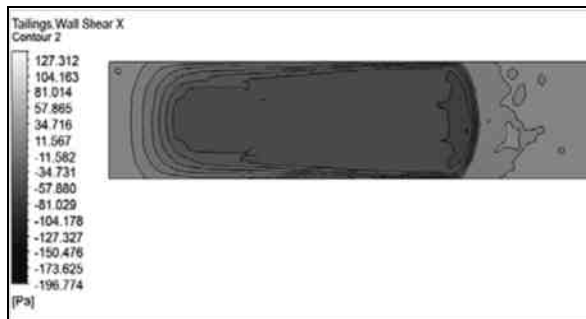


Figure 11. Numerical-experimental comparison of deposition of 5.7 kg of flocculated MFT into the flume



(a)



b)

Figure 12. Tailings deposition simulation at $t=2$ s and $t=10$ s, employing a yield stress of 60 Pa and viscosity of 0.5 Pa.s

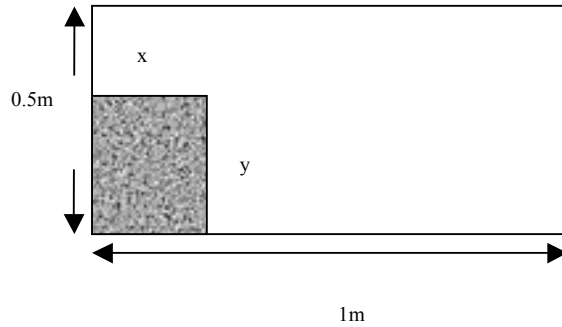


Figure 13. Schematic of initial position of tailings for 2D simulations.

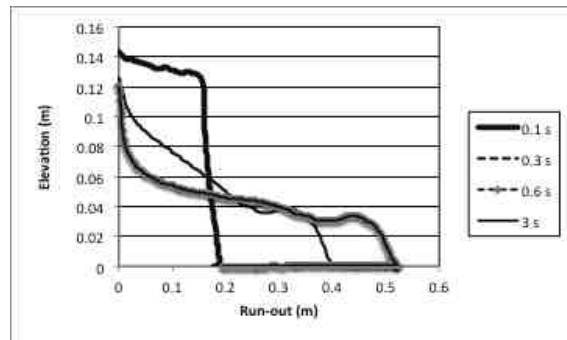


Figure 14. 2D simulation: Flow profiles of a 100 Pa yield stress fluid using an initial configuration of 0.15 m wide by 0.15 m high

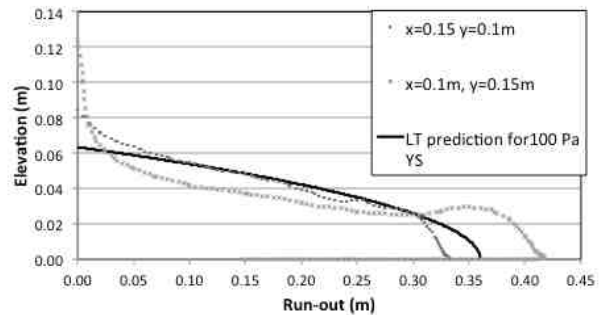


Figure 15. 2D simulation: Effect of height of initial configuration on shape of final profile for a 100 Pa yield stress material

Figure 15 shows the influence of height of the initial position of the tailings mass for a 100 Pa yield stress fluid. Increasing the height does increase the run-out, as well as the concavity in the

profile closer to the deposition point. The final profiles predicted by the numerical simulations are compared with the analytical solution for 100Pa yield stress fluid derived from lubrication theory, as per Henriquez and Simms (2009) and Mizani et al. (2013 b).

CONCLUSION

In this study, the rheological parameters of polymer-amended MFT and unamended MFT were examined using different rheometry techniques using a vane fixture characterizes when the tailings stop flowing – and hence the yield stress appropriate for deposition modelling. Additionally, the study presents numerical simulation of pour geometry. Specific conclusions are:

- Controlled shear tests were designed in order to simulate the stress history of the tailings as they flow down the beach. These tests showed that, despite considerable shearing, a residual yield stress of about 50 Pa was always retained by the material.
- Similar behaviour was also shown by oscillatory rheometry, which showed that though substantial degradation of the yield stress can occur by shearing. Recovery of the original structure of the polymer-amended tailings can occur, even while the tailings are still flowing.
- By comparison, the structure of raw MFT was not degraded under shear, but presented much lower moduli and lower yield stress than the polymer amended material
- Study the effect of dewatering on the rheology of already deposited tailings showed that the yield stress did not appreciably change for the first day following deposition. This will simplify modelling for field scale deposition.
- 3D numerical modelling of flume tests confirmed that using the yield stress measured by controlled decreasing shear tests was appropriate for deposition modelling
- 2D numerical modelling, which is computationally much less expensive than 3D, was able to capture some behaviour noticed at the field scale, such as concavity in the profile close to the deposition point. At

this time, modelling of real field profiles data is ongoing.

ACKNOWLEDGEMENTS

The authors would like to thank Robert Mahoud for his support, and acknowledge both Shell Canada and Barr Engineering for providing MFT and polymer samples and providing logistical support to the field sampling. Funding was provided by the Canadian Oil Sands Innovation Alliance (COSIA) and the Natural Science and Engineering Research Council of Canada (NSERC).

REFERENCES

- Chhabra, R.P. and Richardson, J.F. (2008) Non-Newtonian flow and applied rheology –engineering applications, 2nd edition, Oxford, Great Britain: Butterworth-Heinemann.
- Fitton, T., (2014) The accuracy of tailings beach slope predictions, in Proceedings 17th International Seminar on Paste and Thickened Tailings (Paste 2014), R.J. Jewell, A.B. Fourie, P. wells and D. Van Zyl(eds), 8–12 June 2014, Vancouver, Canada, Australian Centre for Geomechanics, Perth, pp. 47–58.
- Gandhi, K. and Salvoley, R. (1988) Dynamic mechanical behaviour of polymers containing carbon black, *Polymer Engineering and Science*, Vol. 28(14),pp. 877–887.
- Henriquez, J. and Simms, P. “Dynamic imaging and modeling of multilayer deposition of gold paste tailings”, *Minerals Engineering*, vol. 22, no. 2, pp 128-139, 2009.
- Li, A.L., (2011) Prediction of tailings beach slopes and tailings flow profiles , in Proceedings 14th International Seminar on Paste and Thickened Tailings (Paste 2011), R.J. Jewell, A.B. Fourie, (eds), 5–7 April 2011, Perth, Australia, Australian Centre for Geomechanics, Perth, pp. 307–322.
- McPhail, G. (1995) Prediction of the beaching characteristics of hydraulically placed tailings, PhD Dissertation, University of the Witwatersrand, Johannesburg, South Africa.
- Minussi, R.B. and Maciel, G.F. (2012) Numerical experimental comparison of dam break flows with

non-Newtonian fluids, *Journal of the Brazilian Society of Mechanical Sciences and Engineering*, Vol.34(2), pp. 167–178.

Mizani, S., He, X. and Simms, P. (2013a) Application of lubrication theory to modeling stack geometry of high density mine tailings, *Journal of Non-Newtonian Fluid Mechanics*, Vol.198, pp.59–70.

Mizani, S., Simms, P., Dunmola, A., Cote, C., Freeman, G(2014) Rheology for surface deposition of polymer-amended fine tailings, in *Proceedings 17th International Seminar on Paste and Thickened Tailings (Paste 2014)*, R.J. Jewell, A.B.

Fourie, P. wells and D. Van Zyl(eds), 8–12 June 2014, Vancouver, Canada, Australian Centre for Geomechanics, Perth, pp. 295–306.

Mizani, S., Soleimani, S. and Simms, P. (2013b) Effects of polymer dosage on dewaterability, rheology, and spreadability of polymer-amended MFT, in *Proceedings 16th International Seminar on Paste and Thickened Tailings (Paste 2013)*, R.J. Jewell, A.B. Fourie, J. Caldwell and J. Pimenta (eds), 17–20 June 2013, Belo Horizonte, Brazil, Australian Centre for Geomechanics, Perth,

Nasser, M.S., and James, A.E.(2007). Degree of flocculation and viscoelastic behaviour of kaolinite-sodium chloride dispersion, *Colloids and surfaces A:Physicoche Eng Aspects* 315 (208)165-175.

Nguyen, Q.D. and Boger, D.V. (1983) Yield stress measurement for concentrated suspensions, *Journal of Rheology*, Vol.27(4), pp.321–349.

Scardovelli, R. and Zaleski, S.(1999) Direct numerical simulation of free-surface and interfacial flow, *Annual Review of Fluid Mechanics*, Vol. 31, pp.567–603.

Simms, P., William, M.P.A, Fitton, T.G, Mcphail, G. “Beaching angles and evolution of stack geometry for thickened tailings — a review”. *Paste 2011 — R.J. Jewell and A.B. Fourie 2011 Australian Centre for Geomechanics, Perth, Australia.*

Watson, P., Fenderson, T., Mahmoudkhani, A., Nair, M., Patel, A. and Roberts, G. (2011) Breakage and reformation of flocs in oil sands tailings slurries, in *Proceedings Tailings and Mine Waste 2011, Vancouver, Canada, 6–9 November*, pp. 293–302.

DESICCATION-CONSOLIDATION MODELING AND STRENGTH TESTING USING SIMPLE SHEAR OF POLYMER-AMENDED MFT

Paul Simms, Sahar Soleimani, and Mahsa Gholami
Carleton University

ABSTRACT

Several technologies utilizing polymer to accelerate dewatering of oil sand fine tailings are under trial in the oil sands industry. Dewatering occurs through several mechanisms, including particle aggregation through application of the polymer, but also consolidation and desiccation through evaporation, drainage, or freeze-thaw. Understanding the relative contribution of each mechanism will assist in selecting optimal thickness, polymer dose, and rate of rise, to minimize and control impoundment footprints.

This paper reports on the role of desiccation on both dewatering and strength development in subsequently buried polymer amended MFT. Coupled unsaturated flow –consolidation modelling of field case is presented, and the role of cracks in promoting efficiency of evaporation is discussed. Experimental results include consolidation data, and simple shear element tests on samples of polymer-amended MFT that were self-weight consolidation with and without desiccation. A light amount of desiccation is shown to change the consolidation and the shear strength behavior of the tailings.

INTRODUCTION

Many dewatering technologies currently being trialed and developed in the oil sands use polymer to aid dewatering. Such technologies all also rely on post-deposition dewatering to meet regulations, improve geotechnical performance, and reduce tailings volumes. Post deposition dewatering includes consolidation, as well as surface processes (evaporation and freeze-thaw). Selection of optimal deposition design, or, how thick should a deposit be to take advantage of all these mechanisms at minimal cost, is improved by knowing the relative contributions of each mechanism to dewatering. Also, each mechanism may alter the strength behaviour: At the same density, tailings that have dewatered by evaporation may have a different strength that

tailings dewatered by consolidation. It has been recently shown that for hard rock tailings, desiccation substantially improves strength characteristics, even for tailings subsequently buried and consolidated after drying (Daliri et al. 2014.). Further, desiccation can also improve consolidation (hydraulic conductivity) characteristics, and therefore the rate of dewatering of subsequently buried tailings.

Of course MFT and various amended MFT products are quite different from hard rock tailings. The goal of this paper was to see how addition of polymer and desiccation by evaporation would modify the consolidation and strength behavior of MFT. These results are put in context using coupled unsaturated flow-consolidation modelling of field and laboratory data of in-line flocculated MFT. Specifically, the paper presents:

1. Review of desiccation-consolidation modelling originally presented by Soleimani et al. (2014).
2. Modelling of a new field case.
3. Presentation of consolidation and strength characteristics of polymer amended MFT, and polymer amended MFT that underwent a light degree desiccation

These results are then briefly discussed in the context of deposition planning.

UNSATURATED FLOW-CONSOLIDATION MODELLING

From a modelling perspective, a number of different phenomena have to be coupled, or at least accounted for, to describe dewatering during deposition. Soleimani et al. (2014) reviewed a number of different modelling approaches for coupling desiccation to consolidation (Simms et al. 2013, Abu-Hejleh and Znidarčić 1995, Seneviratne et al. 1996). Our group is working with a custom version of a coupled unsaturated flow finite strain consolidation model, developed by the software company SoilVision. The attraction of this model

over other methods lies in its relatively more realistic treatment of unsaturated flow. This is especially important in characterising the transfer of water between layers when a new layer is deposited on top of an older layer that may be partially unsaturated. The cost, however, is greater demand on computer resources, are more difficulty achieving convergence.

In saturated conditions, finite or large strain consolidation formulations require relations between void ratio (e) and effective stress (σ'), and between hydraulic conductivity (k_{sat}) and void ratio:

$$e = A\sigma'^B \quad (1)$$

$$k_{sat} = Ce^D \quad (2)$$

In unsaturated conditions, the relationship between water content and void ratio with matric suction is determined by measuring the soil-water characteristic curve (SWCC). These tests are usually performed on samples of about 20 – 90 centimetres in height, which therefore have low total vertical stress. For fine-grained soils, volume change must be measured during the SWCC test in order to accurately determine the degree of saturation and the relationship between void ratio and suction. Hydraulic conductivity as a function of the degree of saturation is usually determined theoretically from the measured SWCC (Leong and Rahardjo, 1997).

In the case of a fine-grained soil, where consolidation may be occurring simultaneously with desaturation, the material properties required (volume change, water content, and hydraulic conductivity) are now functions of both total stress and matric suction. Therefore, all these properties are now three-dimensional surfaces. For example, one surface for void ratio for a hypothetical soil is shown in Figure 1. In the SoilVision formulation, these surfaces are represented using a six-parameter fitting function developed by Vu (2002). We fit this function to data in the 0 suction plane (saturated consolidation data) and the 0 total

stress plane (data measured during the SWCC test), in order to define the six fitting parameters.

In Soleimani et al (2014), our group presented analysis of a 0.50m column of polymer-amended tailings using a dose of 650 ppm anionic polymer. A reasonable fit to height, pore-water pressure (and matric suction), and density depth profiles were obtained by adjusting only the measured hydraulic conductivity versus void ratio function in the saturated range (Equation 2), upwards by one order of magnitude.

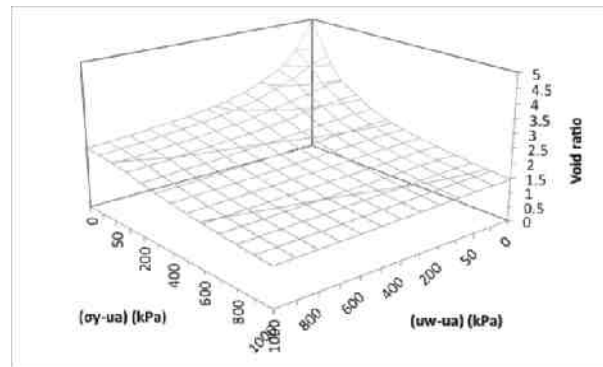


Figure 1. Example of a constitutive surface for void ratio.

The height of the measured and modeled tailings is plotted in Figure 2. The biggest discrepancy is for the first few days of dewatering, due to flocculation-induced sedimentation, which is not incorporated in the model. Thereafter, however, the simulation closely matched the experiment. The model was then applied to simulate one of test cells for AFD at Shell Muskeg River Mine. Figure 3 shows the prediction and measured solids concentration with depth 33 days after deposition of the first lift in one of the test cells. This prediction was without additional calibration, and the fit is quite reasonable. More details on these modelling results are available in Soleimani et al. (2014). The Shell AFD test cells are described in Dunmola et al. (2013).

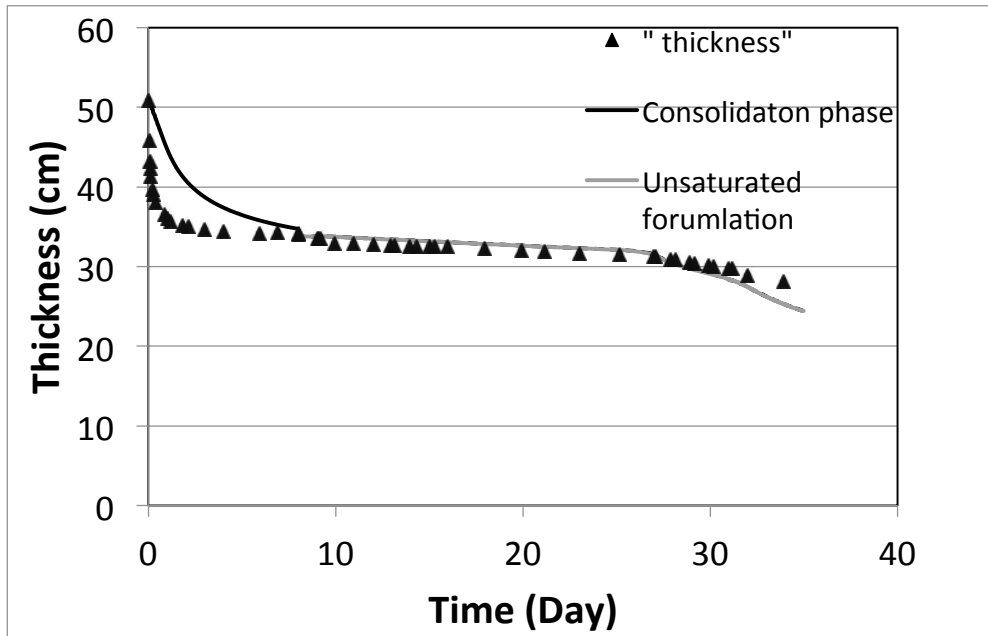


Figure 2. Measured and modelled depth of MFT placed in column within a few minutes of mixing with 650 ppm anionic polymer (Modified from Soleimani et al 2014).

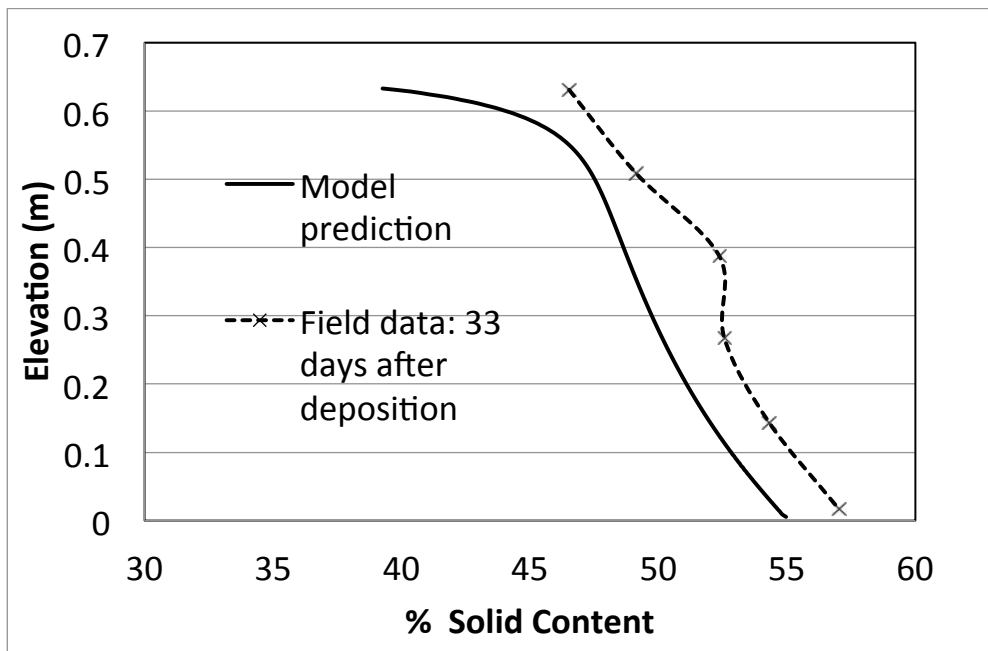


Figure 3. Modelling solids concentration in first thin lift of Shell AFD test site, deposited September 2012 (Modified from Soleimani et al. 2014).

The field case in Soleimani et al. (2014), did not test the unsaturated component of the model, as this lift was placed in late summer, and dewatered during relatively wet weather. Another field case is presented here from Shell AFD, deposition of a

2.26 m layer on top of 0.7 m of previously deposited tailings in May 2013 and left 89 days . The average PE was about 3.8 mm/day. The bottom boundary, at the interface between two lifts, was assumed to be no flow. The materials

parameters were the same as used for modelling the laboratory test and the field case in Soleimani et al. (2014).

Modelled and measured solids content profiles are shown in Figure 4. The model successfully simulates the change in gradient of density, from increasing with depth to decreasing with depth at the surface, which is due to evaporation. However, dewatering is more uniform with depth in the measured data.

This is likely due the presence of significant cracking (Figure 5). Field measurements of total suction and water content at the surface taken from this lift a few days before deposition of the next lift, show very high suctions at the surface of the tailings, but much lower values within the exposed crack surfaces. The total suction measurements are made on small (< 100 g) samples of about 1 cm depth, which are waxed, and later measured for Total suction using a WP4 Dewpoint Hygrometer. Figure 6 compares field measurements with laboratory derived SWCC.

From our group's experience using "drying box" tests, the values of total suction at the surface correlate with very low evaporation rates (e.g Innocent-Bernard et al. 2013). Cracking not only maintains overall evaporation from the deposit near the potential evaporation, but facilitates more uniform drying with depth. Put another way, cracking improves the efficiency of drying, as more water loss will come from volume change, as opposed to only de-saturating a thin layer near the surface.

Work is ongoing between various parties working at the Shell AFD site to better quantify the role of cracking. Layer thickness in clays influences crack morphology, deeper layer having less frequent but wider cracks. However, what this means is the modeling described in this paper is conservative with respect to quantifying the contribution of evaporation to dewatering.

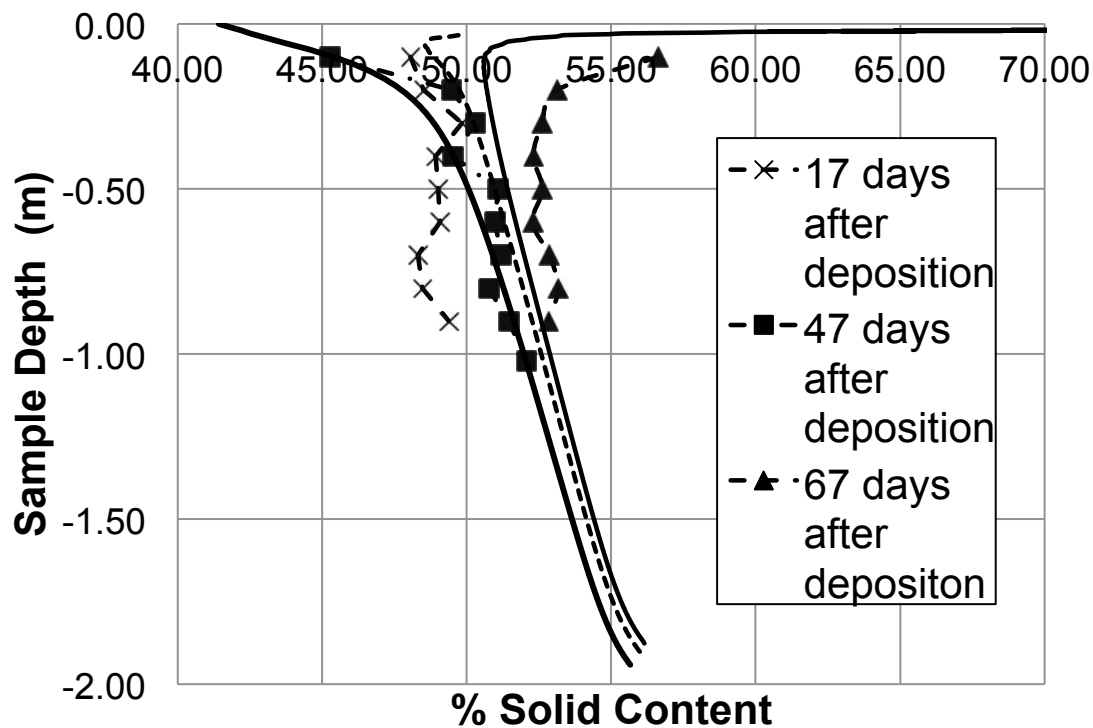


Figure 4. Measured and modelled solids concentrations in Shell AFD thick multilift cell for lift deposited May 2013.

Shear strength of polymer-amended tailings

The coupled unsaturated flow consolidation modeling appears to be relatively robust and conservative, and therefore we expect it to be a useful tool to help engineers evaluate potential deposition schemes in terms of dewatering. The flip side of the question is what is the strength associated with a certain degree of dewatering, and what is the role of stress history (desiccation versus consolidation), if any?

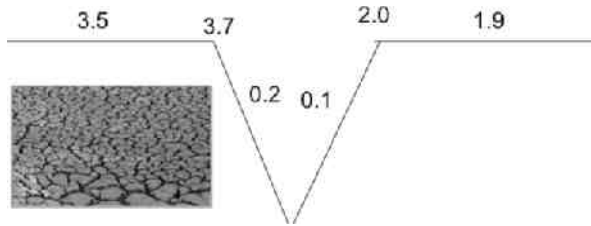


Figure 5. Transect of total suctions (MPa) across crack in thick multi-lift cell early August.

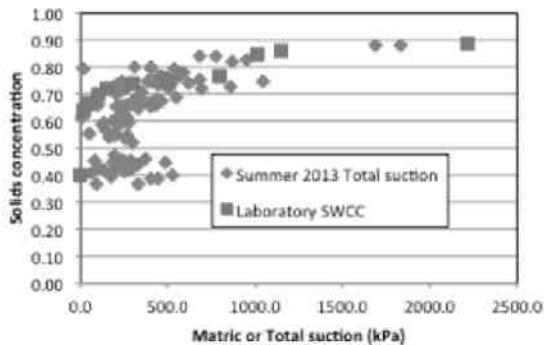


Figure 6. Laboratory and field derived SWCC for polymer amended MFT.

We attempted to analyze strength by performing simple shear element tests on polymer-amended MFT after self-weight consolidation, and polymer amended MFT after self-weight consolidation and some desiccation. Polymer amended samples were prepared at 650 ppm according to mixing protocols documented in Mizani et al. (2013). Samples were then deposited into 0.10 m diameter 0.25 m tall PVC split columns. After about three months, the columns were removed, and the bottom 3.5 cm of the material was trimmed and placed in a specialized oedometer that had the same diameter as the simple shear device (70 mm). The samples at the start of the oedometer ranges in solid concentration between

60 and 62%, with void ratios of an average of 1.25. Separate samples were loaded to 25, 50, and 75 kPa.

Desiccated samples were prepared by allowing evaporation to take place at the surface of the split mold columns under ambient conditions of the laboratory (~1.5 mm / day potential evaporation). The time was varied until relatively uniform samples could be trimmed from the top of the sample, at about 60-64% solids. This corresponds to a low degree of desiccation (Less than 20 kPa suction).

The oedometer results are compared in Figures 7 and 8. For samples with no desiccation, we modelled consolidation in the oedometer using the consolidation model described in the previous section, and using the same consolidation functions used in the unsaturated flow-consolidation analysis. We assumed double drainage (pore-water pressure = 0 boundaries), and, for purpose of numerical stability, ramped up loading of the samples over 1 hour (as opposed to instantaneous loading). Measured and modeled results, shown in Figure 7, were in relatively close agreement, though better for the 75 kPa simulation than the 25 kPa simulation. Simulation of oedometer tests may serve as a means to verify other tests used to obtain large strain consolidation parameters. Both the test itself and the modelling can be done over two days.

The desiccated samples had somewhat initially higher void ratios (1.4 compared to 1.25) for about the same initial solids content, due to a small amount of desaturation of the desiccated samples. Desiccated samples, as shown in Figure 8, were somewhat stiffer than non-desiccated ones. Desiccation increasing the stiffness of subsequently consolidated materials has been documented for hard rock tailings (Daliri et al. 2014).

What is the effect on strength? Samples were transferred to the simple shear device, reloaded to the same stress level, and then sheared at a rate of 20% shear strain per hour. Both desiccated and non-desiccated showed relatively similar behavior: shear stress increasing and leveling off (Figure 9), while exhibiting contractive behavior in the stress path (Figure 10). No strain softening, however, was detected. The behavior is similar to other soft clays, in that the ultimate strength is not reached until relatively high shear strains.

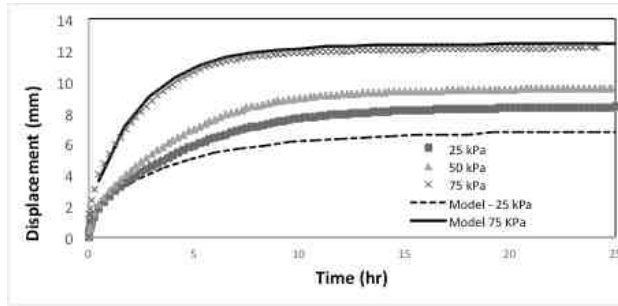


Figure 7. Measured and modelled displacement of polymer-amended tailings in oedometer.

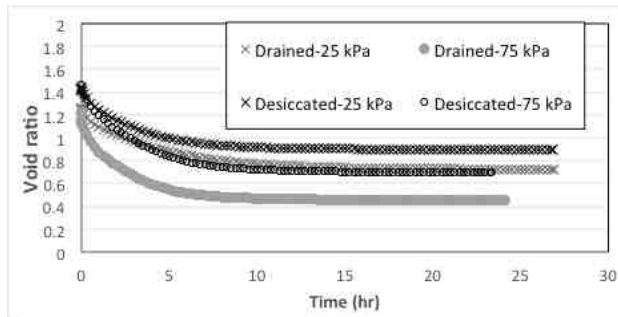


Figure 8. Void ratio in oedometer of polymer amended MFT, with and without desiccation.

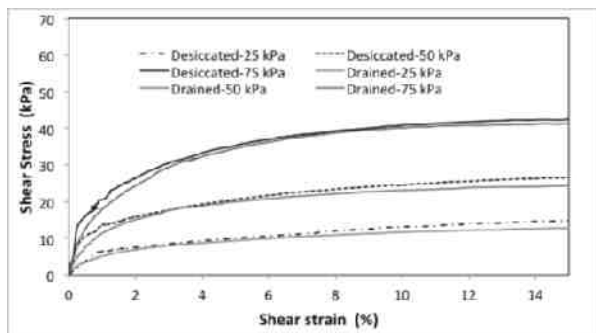


Figure 9. Shear stress versus shear strain from simple shear tests on polymer amended MFT.

On an effective stress basis, there is some but no substantial difference between the desiccated and non-desiccated samples at a given consolidation pressure. The desiccated samples are perhaps somewhat stiffer at early strain response, but if one overlays the shear stress plots normalized with consolidation pressure (Figure 11), the differences are difficult to distinguish.

There is a significant difference, however, in terms of shear strength versus void ratio. Figure 12 shows that the desiccated samples give similar strengths to the non-desiccated samples, but at higher void ratio (lower densities).

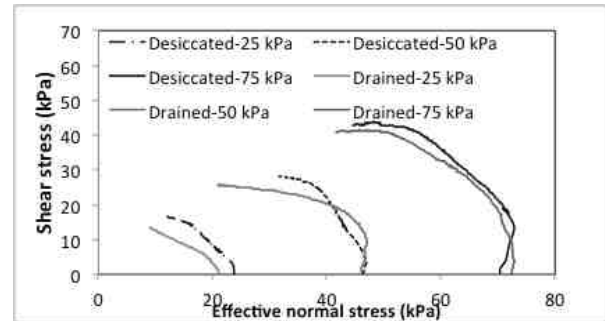


Figure 10. Stress paths for simple shear tests on polymer amended MFT.

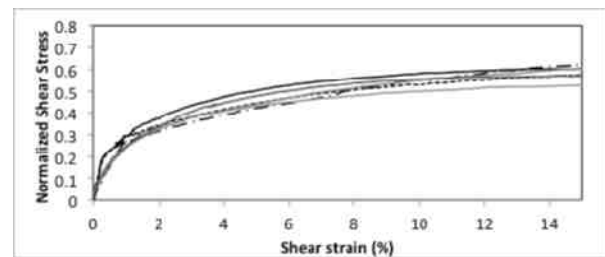


Figure 11. Shear stress normalized with effective normal consolidation pressure in simple shear tests.

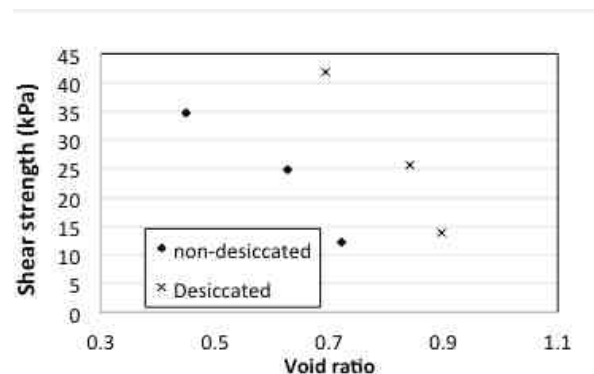


Figure 12. Ultimate shear strength versus void ratio for desiccated and non-desiccated polymer amended tailings.

DISCUSSION

Cracks appear to be an important aspect for near-surface dewatering. The presence of cracks means that dewatering due to evaporation will be greater than what 1-D models predict. Cracking may also assist greater consolidation due to freeze/ thaw effects, by allowing cool air deeper access into the deposit, at least before snowfall.

Many in industry would prefer to minimize cycling of tailings deposition and rehandling by maximizing layer depth. The role of surface processes and cracks in strengthening the tailings at the surface remains important in such scenarios, to create a thick crust that has sufficient bearing capacity despite softer soil at depth.

We see some evidence that stress history due to desiccation has positive effect on strength (greater strength at lower density) compared to tailings that only underwent consolidation. This needs to be balanced against differences in compressibility (and possibly hydraulic conductivity) of the desiccated tailings, to see if this phenomenon can be usefully applied in deposition design.

Though the tailings are soft, no catastrophic strain softening behavior was observed. This may somewhat alleviate the concerns raised by Beier et al. (2013) on the potential sensitivity of polymer-amended MFT. We plan to conduct cyclic shear tests to investigate possible strain softening behavior.

CONCLUSIONS

1. Coupled unsaturated flow consolidation modeling shows reasonable but somewhat conservative comparisons to field cases presented in this paper and in Soleimani et al. (2014). Cracking appears to be an important mechanism promoting more efficient dewatering with depth due to evaporation.
2. A small degree of desiccation (< 20 kPa suction) was sufficient to increase the stiffness of the tailings under subsequent loading in an oedometer
3. The oedometer measurements could be modeled using a large strain consolidation code. This may be a means to verify compressibility and hydraulic conductivity measurements obtained by other kinds of tests.

4. Shear strength behavior in terms of effective stress was very similar between the lightly desiccated and non-desiccated tailings, the desiccated tailings perhaps showing slightly greater stiffness at low shear strains. No peak and therefore no post-peak softening were observed in the simple shear tests.
5. The lightly desiccated tailings do show greater strength at a given density. Whether this is favourable phenomenon from the perspective of deposition design, needs to be investigated further in light of the different dewatering characteristics of the desiccated tailings (for example, lower compressibility).

ACKNOWLEDGEMENTS

Project is financed by a NSERC Collaborative Research and Development Grant, which is jointly funded by COSIA and NSERC. Essential In-kind support by Shell Canada in terms of tailings, field work, and regular co-ordination and feedback on the research project, is gratefully acknowledged. Support by Barr Engineering personnel with the field work is also acknowledged. The simple shear device at Carleton is funded by a CFI grant to Professor Siva Sivathayalan.

REFERENCES

- Abu-Hejleh, A.N. and Znidarcic, D. (1995) Desiccation theory for soft cohesive soils, *Journal of Geotechnical Engineering*, American Society of Civil Engineers, Vol. 121(6), pp. 493–502.
- Al-Tarhouni, M. , Simms, P. , and Sivathayalan, S. (2011). "Cyclic behaviour of reconstituted and desiccated–rewet thickened gold tailings in simple shear." *Can. Geotech. J.* , 48(7), 1044–1060.
- Beier, N., Wilson, W. Dunmola, A., Sego, D. 2013. Impact of flocculation-based dewatering on the shear strength of oil sands fine tailings. *Canadian Geotechnical Journal*, 50(9): 1001-1007
- Daliri, F., Kim, H., Simms, P., and Sivathayalan, S. (2014). "Impact of Desiccation on Monotonic and Cyclic Shear Strength of Thickened Gold Tailings." *J. Geotech. Geoenviron. Eng.*, 140(9), 04014048.

Dunmola, A., Cote, C., Freeman, G., Kolstad D., Song, J., and Masala S. (2013) Dewatering and shear strength performance of in-line flocculated mature fine tailings under different depositional schemes, in Proceedings 17th International Conference on Tailings and Mine Waste, G.W. Wilson, D.C. Segó and N.A. Beier (eds), 3–6 November 2013, Banff, Canada, pp. 5–14.

Innocent-Bernard, T., Simms, P., Sedgwick, A., Kaminsky, H. and Yang, X. (2013) Influence of surface cracking and salinity on evaporation in an oil sands thickened tailings, in Proceedings 17th International Conference on Tailings and Mine Waste, 3–6 November 2013, Banff, Canada.

Leong, E.C. and Rahardjo, H. (1997) Permeability functions for unsaturated soils, *ASCE Journal of Geotechnical and Geoenvironmental Engineering*, Vol. 123(12), pp. 1118–1126.

Mizani, S., Soleimani, S., Simms, P. (2013) Effects of polymer dosage on dewaterability, rheology, and spreadability of polymer-amended mature fine tailings, in Proceedings 16th International Seminar on Paste and Thickened Tailings (Paste13), R.J. Jewell, A.B. Fourie, J. Caldwell and J. Pimenta (eds), 17–20 June 2013, Belo Horizonte, Brazil, Australian Centre for Geomechanics, Perth, pp. 117–131.

Seneviratne, N.H., Fahey, M., Newson T.A. and Fujiyasu, Y. (1996) Numerical modelling of consolidation and evaporation of slurried mine tailings, *International Journal for Numerical and Analytical Methods in Geomechanics*, Vol. 20(9), pp. 647–671.

Soleimani, S., Simms, P. Dunmola A., Freeman, G., Wilson, W. (2014). Desiccation and consolidation in thin-lift deposition of polymer amended MFT. In Proceedings 17th International Seminar on Paste and Thickened Tailings (Paste 2013), R.J. Jewell, A.B. Fourie, J. Caldwell (eds), 3-9 June 2014, Vancouver, Canada, Australian Centre for Geomechanics, pp. 75–86.

Simms, P., Daliri, F. and Sivathayalan, S. (2013) Desiccation in dewatering and strength development of high-density hard rock tailings, in Proceedings 16th International Seminar on Paste and Thickened Tailings (Paste 2013), R.J. Jewell, A.B. Fourie, J. Caldwell and J. Pimenta (eds), 17–19 June 2013, Belo Horizonte, Brazil, Australian Centre for Geomechanics, pp. 75–86.

Session 3

Modelling

MODELING BOTTOM SEEPAGE FROM OIL SANDS TAILINGS PONDS

Silawat Jeeravipoolvarn¹, Warren Miller², Don Scott³ and Louis Kabwe³

¹Thurber Engineering Ltd., Calgary, Alberta, Canada

²WorleyParsons Ltd., Perth, Australia

³University of Alberta, Edmonton, Alberta, Canada

ABSTRACT

Bottom seepage from oil sands tailings ponds into underlying strata may result in long term environmental impact. Generally it is assumed that the tailings will consolidate at the bottom of a pond and seal against possible leakage. However, little research has been performed to evaluate this phenomenon. To simulate a tailings pond underlain by a permeable stratum, 2 m high standpipe tests with bottom drainage layers were performed on i) typical oil sands fine tailings, ii) higher hydraulic conductivity fine tailings, and iii) coagulant modified fine tailings. The results from the three standpipe tests which were conducted for up to 2 years were used to validate a finite strain consolidation model. The model used compressibility and hydraulic conductivity relationships obtained from large strain consolidation tests on the three materials. It was found that the model was capable to qualitatively capture these behaviours in the standpipes. The model was then used to investigate the potential seepages through the bottom of tailings deposits in a commercial scale. The downward seepage rates and the downward seepage volumes for commercial scale tailings ponds containing these three types of tailings were compared. The rate and amount of bottom leakage from a commercial tailings pond depended on the consolidation properties of the tailings but was not significantly greater for the higher hydraulic conductivity tailings. Such analyses can also be used to preliminary model the long term downward seepage from end pit lakes.

INTRODUCTION

Recent research published by Environment Canada has provided a strong indication that oil sands tailings water is seeping into the Athabasca River (Frank et al. 2014). Potential seepage paths from a tailings pond are sketched in Figure 1.

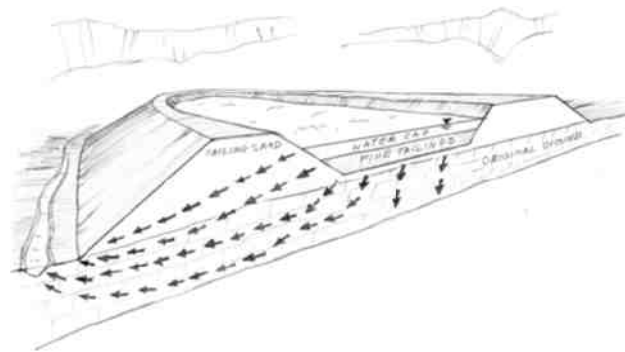


Figure 1. Potential seepage paths from a tailings pond (not to scale) (modified from CEMA 2012)

In this figure the vertical scale is exaggerated to show details better. While the height of the tailings dam may be from 50 m to 100 m, the width of the pond can be up to several kilometers. The bottom area of the pond therefore is much greater than the area adjacent to the surrounding dyke. The oil sand companies attempt to keep tailings seepage rates low with monitoring systems and collection wells and ditches built into tailings containment structures as shown in Figure 2.

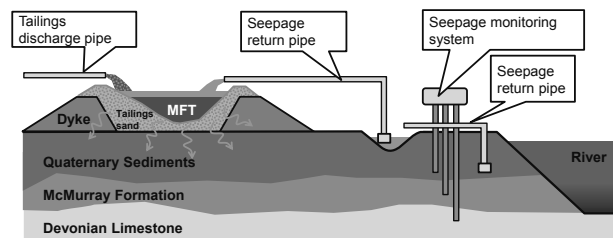


Figure 2. Oil sands tailings pond seepage control (not to scale) (modified from Alberta Government 2014)

This figure is also not to scale and the downward seepage through the bottom area of the pond may be much greater than the seepage through and under the dykes. Because of the large bottom area of the ponds, the monitoring and collection systems in the dykes may not monitor the downward seepage and the collection systems may have little effect on the amount of bottom

seepage. The rate and amount of bottom seepage depends on how well the consolidating tailings at the bottom of the pond seal the bottom, the hydraulic conductivity of the underlying strata and the hydraulic head in the underlying strata.

Figure 3 shows the regional subsurface structure underlying the McMurray Formation oil sands in the Athabasca oil sands area. Strata immediately underlying oil sand tailings ponds vary greatly from permeable outwash sand and gravel to low hydraulic conductivity shale. The most important stratum is the thick Prairie Formation composed of halite (salt) which is the originator of solution channels and sink holes which contribute greatly to downward and horizontal flow beneath the oil sands deposits.

The Alberta Energy Regulator has made it a priority that each operator must employ a tailings technology and management plan in a manner that allows the tailings to dewater and form a solid deposit within the life of the mine (ERCB 2009). Several tailings dewatering technologies and deposition plans have been introduced in order to reach the reclamation goals. Many rely on self-weight consolidation in a deep deposit scheme where tailings are deposited in a containment area or a mined-out pit underlain by the original ground or the bottom of the mine. Typical design basis assumes that a tailings deposit will seal itself at the bottom due to self-weight consolidation and that bottom seepage is practically small and negligible. A few articles have described a technique to seal a tailings pond bottom by using fine tailings material

(Clark and Moer 1974, Soderberg and Busch 1977); however, little research has been performed to evaluate this bottom seal assumption. Seepage of tailings water into an underlying stratum can result in a long term detrimental environmental impact. The rate and amount of bottom seepage therefore should be evaluated as part of the design process.

In this paper, a consolidation model based on finite strain consolidation theory was utilized to study seepage into the bottom of tailings deposit for three tailings types – one is caustic oil sands tailings representing a typical tailings material; another is a non-caustic oil sands tailings with a greater hydraulic conductivity; and the third is a coagulant modified caustic fine tailings. Large strain consolidation tests on all three materials developed the compressibility and hydraulic conductivity relationships required in the model; void ratio as a function of effective stress and hydraulic conductivity as a function of void ratio. Validation of the large strain consolidation test results and the finite strain consolidation model was performed by modelling test results on the three tailings in 2 m high standpipe tests with a bottom drainage layer which ran for about two years. The validation analyses showed that the developed material relationships and the numerical model can qualitatively model the long term performance of the bottom drainage standpipe tests. The model and material relationships were then used to assess the potential seepage through the bottom of commercial scale tailings deposits.

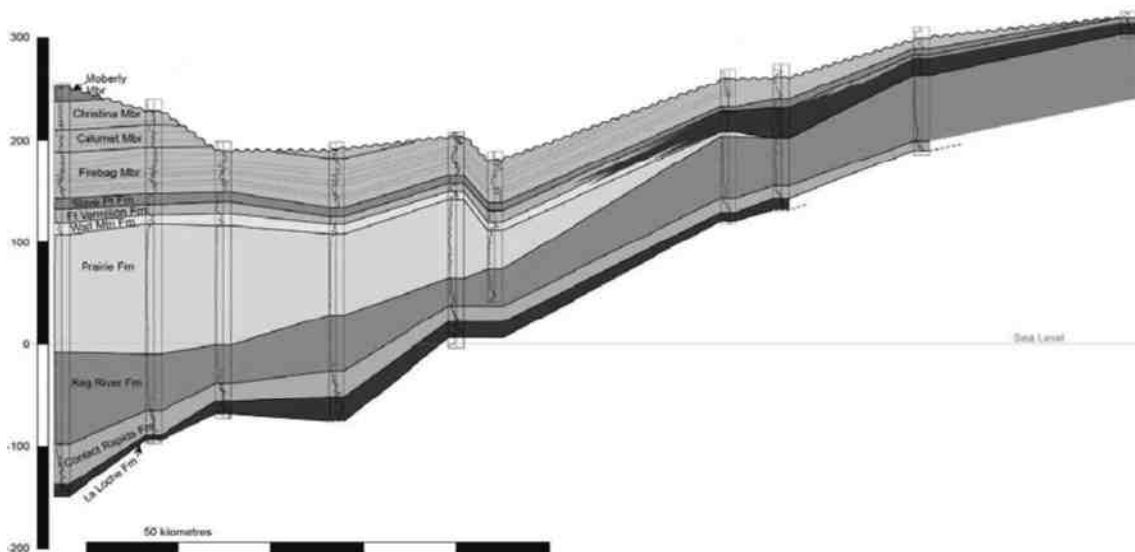


Figure 3. Regional subsurface structure (Schneider et al. 2012, OSRIN 2012)

PROPERTIES OF THE THREE OIL SANDS FINE TAILINGS

The index properties and the consolidation properties of the three fine tailings are discussed in this section. The fine tailings were generated from samples of typical Suncor Energy Inc. ore that were processed using both a caustic and a non-caustic extraction method (Miller et al. 2010a). An additional fine tailings material was created by the addition of 600 ppm of CaSO₄ (in solution) to the caustic fine tailings. The calcium sulphate was proposed as a coagulant to improve the settling behaviour of the fine tailings due to the aggregation of clay particles. Therefore, aside from changes in salinity caused by the coagulant addition, this fine tailings will not differ significantly from the caustic fine tailings in the index properties but will substantially differ in the consolidation properties.

The index properties are shown in Table 1. All three tailings have similar relative densities of the solids, Atterberg limits and fines (<45 µm) contents. The bitumen content of the tailings was approximately 6% by dry mass and the bitumen has been considered as part of the solids in all definitions and calculations.

The major difference of the three tailings in Table 1 is in the clay size content (<2 µm). Caustic oil sands tailings are those tailings formed by the Clark hot water extraction process. This process uses caustic soda to disperse clay particles. Caustic oil sands tailings typically exhibit a low consolidation rate and low shear strength. Non-caustic processes have been developed to improve bitumen recovery, improve the process

water chemistry and reduce the dispersion of clays during bitumen extraction (Miller et al. 2009). Producing tailings with reduced clay dispersion improves the consolidation properties of the fine tailings (Miller et al. 2010b). Generally less clay size particles are reflected in higher hydraulic conductivity tailings which can consolidate faster.

Compressibility and hydraulic conductivity relationships with void ratio are engineering properties that will influence the long-term disposal of the fine tailings. They are used in large strain consolidation analyses of a storage pond to predict water release rates, long term surface elevations and long term seepage. A step loading large strain consolidation test was developed and used to determine consolidation characteristics of these highly compressible tailings. These tests allow large deformations during consolidation and direct measurement of hydraulic conductivity. Between each load step, a hydraulic conductivity test is conducted to determine the hydraulic conductivity at a specific void ratio that is then used to develop the hydraulic conductivity-void ratio relationship. The compressibility of the three tailings is shown in Figure 4. The caustic and non-caustic tailings have similar compressibilities but the CaSO₄ added tailings is less compressible. It has been found that adding coagulants or flocculants to the tailings causes bonding in the tailings and under a load the tailings will not compress as much (Jeeravipoolvarn 2010). The hydraulic conductivity relationships for the three tailings are shown in Figure 5. As expected the non-caustic tailings has the highest hydraulic conductivity followed by the coagulated caustic tailings and the caustic tailings, respectively.

Table 1. Fine tailings index properties (Miller et al. 2010a)

Tailings	Relative density	Liquid limit (%)	Plastic limit (%)	Plasticity Index (%)	Bitumen Content (% by dry mass)	Non-dispersed Fines content (% <45 µm) ¹	Non-dispersed Clay content (% <2 µm) ²
Caustic	2.48	52.1	26.9	25.2	5.9	97	41
Non-caustic	2.45	58.3	28.2	30.1	6.7	97	30
Caustic+CaSO ₄	2.48	58.3	29.1	29.2	5.9	-	28

1 – by non-dispersed wet sieve method, 2 – by non-dispersed methylene blue testing

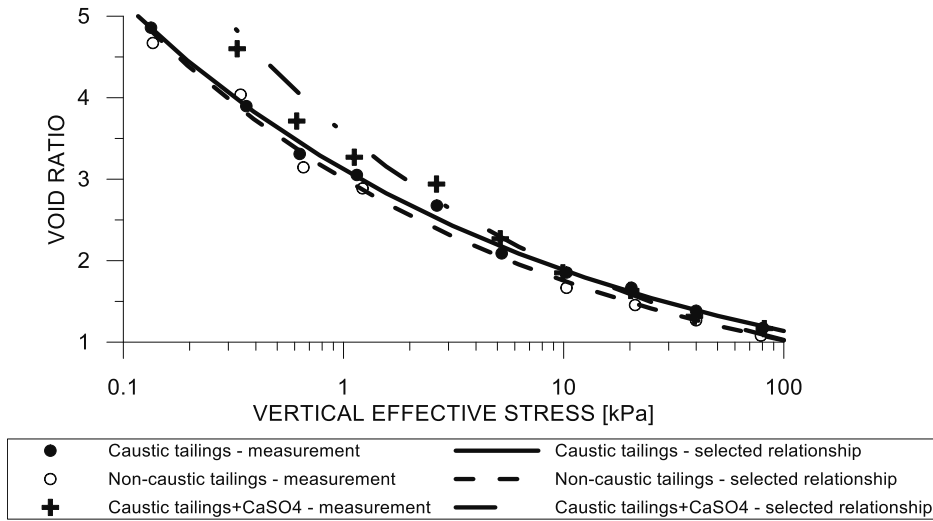


Figure 4. Compressibility of the oil sands fine tailings

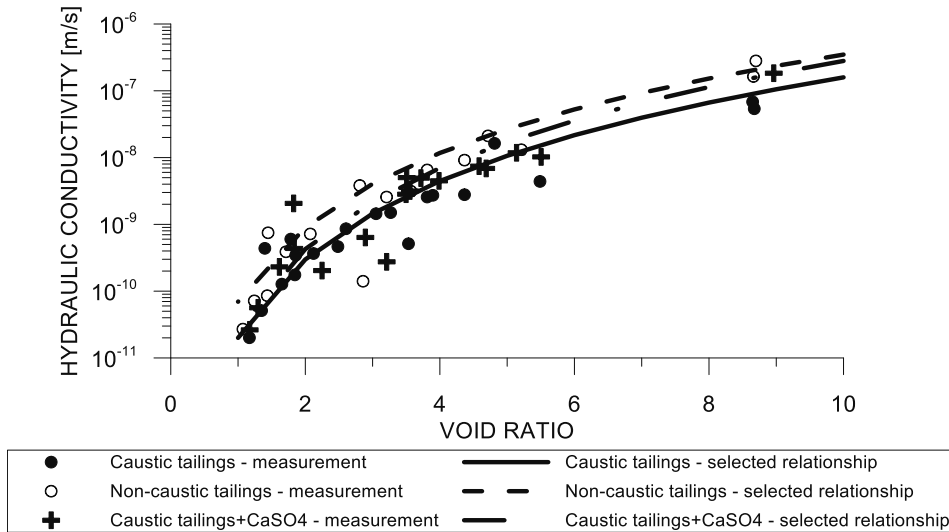


Figure 5. Hydraulic conductivity of the oil sands fine tailings

STANDPIPE TEST WITH BOTTOM DRAINAGE

To validate a finite strain consolidation model with bottom drainage, two meter high standpipe tests with a bottom drainage layer were performed (Figure 6). The standpipe was made of a Plexiglas cylinder with an inside diameter of 13.3 cm and a wall thickness 0.65 cm. Each standpipe has 10 manometers spread at 20 cm intervals to measure pore water pressures. The standpipe also had sampling ports at 20 cm intervals to monitor changes in void ratio. The standpipes were designed for double drainage to simulate the

drainage conditions if a porous layer underlaid the fine tailings in a tailings pond. In this setup, a drainage channel covered by a filter was opened at the base of the standpipe and both downward and upward consolidation flow was allowed. The bottom drainage head and the water surface in the standpipe were set to 2 m. These water levels were kept constant during the tests so no seepage hydraulic gradient was imposed on the fine tailings samples. The bottom of the standpipe was a compound filter separating the tailings and a base drainage channel. These self-weight tests were stopped when the fine tailings had reached close to 100% consolidation based on pore pressure

readings or at a predetermined time limit of roughly two years.

The initial properties of the fine tailings in each standpipe are shown in Table 2. The initial solids contents of the three tailings were approximately 22% which is a void ratio of about 9. The caustic tailings had not completed self-weight consolidation by two years but sufficient consolidation had occurred to allow a validation of the consolidation model. The non-caustic and the coagulated caustic tailings were close to full consolidation in less than a year and a half.

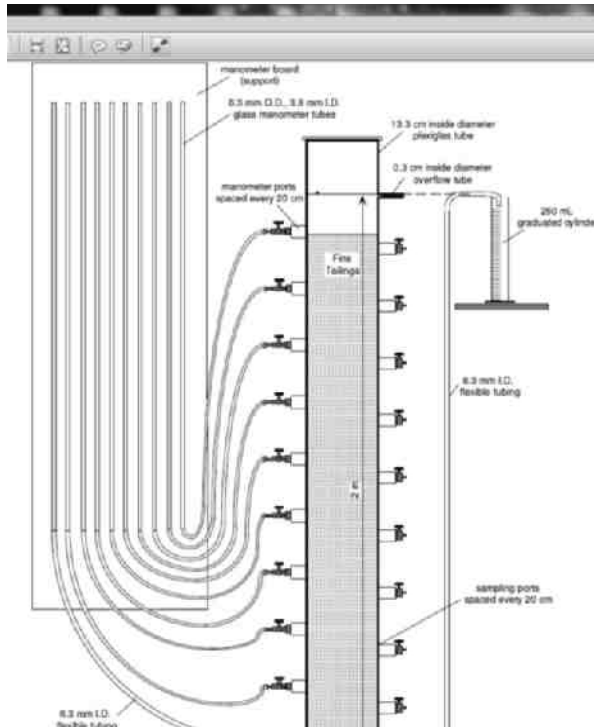


Figure 6. Two meter standpipe test

Table 2. Initial conditions of the fine tailings (Miller et al. 2010a)

Tailings	Solids Content (%)	Void Ratio	Initial Height (m)
Caustic	22	8.8	2
Non-caustic	22	8.7	2
Caustic+CaSO ₄	22	8.8	2

VALIDATION OF THE FINITE STRAIN CONSOLIDATION MODEL WITH BOTTOM DRAINAGE

Standpipe tests were conducted for all three oil sands fine tailings. The measurements in the standpipe tests with time included elevation of interface, downward drainage volumes and pore water pressures. These measurements and the calculated void ratios were used to validate the large strain consolidation test results and the finite strain consolidation model. One dimensional finite strain consolidation theory by Gibson et al. (1967) was used to model the consolidation process of these soft fine grained soils or slurries. The theory unlocks the restrictions of the conventional model (Terzaghi 1923) from small strain and linearity therefore allowing more complex problems to be analyzed. In geotechnical engineering, the theory is often used to simulate slurry consolidation behaviour specifically self-weight consolidation problems which give answers to containment size, seepage, strength implications and excess pore pressure dissipation in the slurry. The model validations for the three tailings are presented in the following subsections.

Caustic oil sands tailings

The comparison between the standpipe measurements of top and bottom seepage volumes and the model prediction is shown in Figure 7. The excess pore water measurements and the model predictions are given for four elapsed times in Figure 8. Measured void ratio profiles at two times and the predictions are shown in Figure 9.

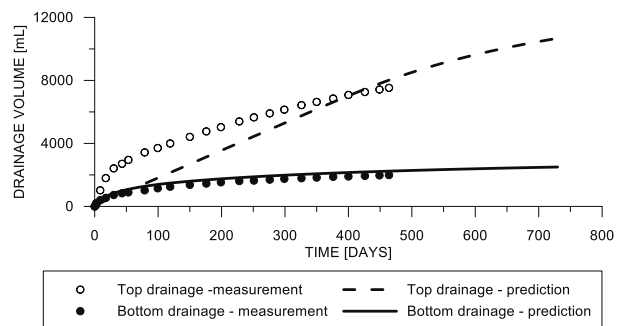


Figure 7. Drainage volume comparison – caustic oil sands tailings

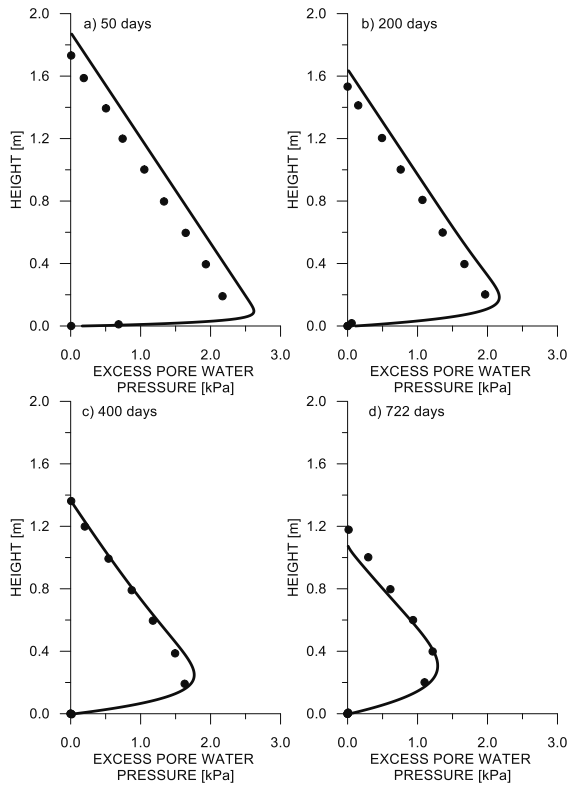


Figure 8. Excess pore water pressure comparison – caustic oil sands tailings

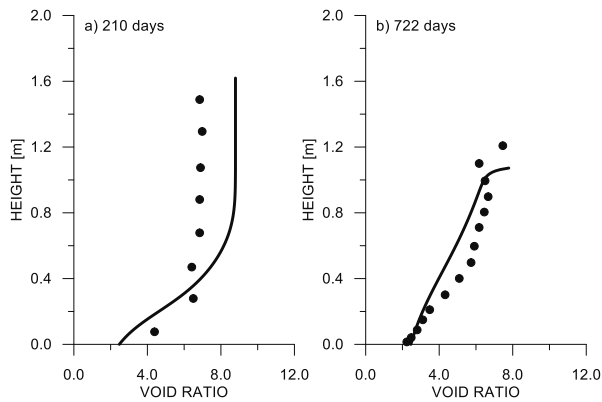


Figure 9. Void ratio comparison – caustic oil sands tailings

Non-caustic oil sands tailings

Figures 10, 11, and 12 show drainage volumes, excess pore water pressures and void ratio comparisons between the model and the laboratory measurements for the non-caustic oil sands tailings.

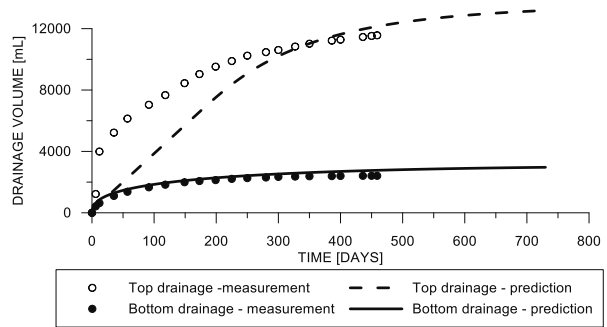


Figure 10. Drainage volume comparison – non-caustic oil sands tailings

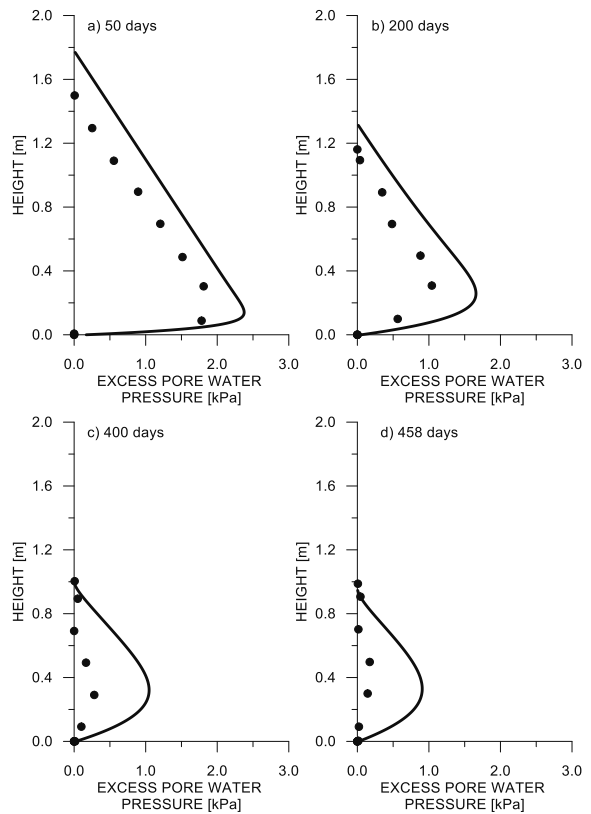


Figure 11. Excess pore water pressure comparison – non-caustic oil sands tailings

Caustic Oil Sands Tailings with CaSO₄

Figures 13, 14, and 15 show drainage volumes, excess pore water pressures and void ratio comparisons between the model and the laboratory measurements for the coagulant amended caustic oil sands tailings.

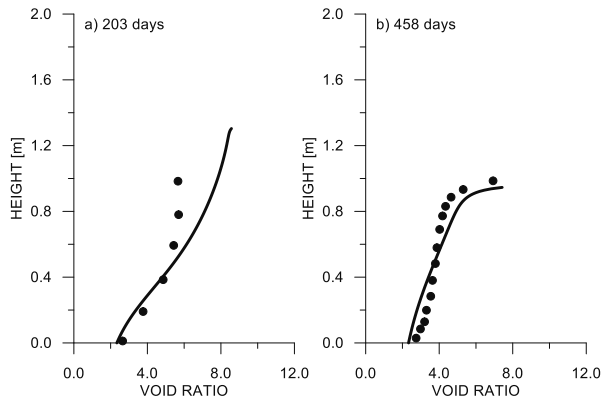


Figure 12. Void ratio comparison – non-caustic oil sands tailings

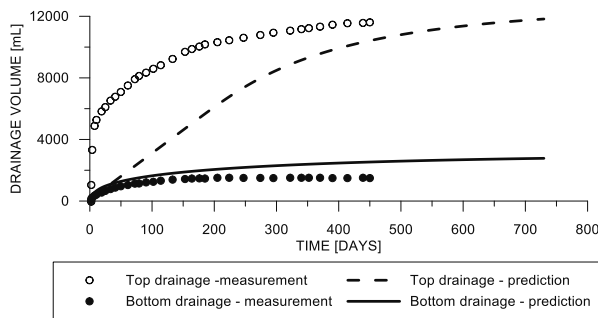


Figure 13. Drainage volume comparison – caustic oil sands tailings with CaSO_4

Figures 7, 10 and 13 show that the bottom seepage can be accurately predicted by the model. The top drainage comparisons, however, show underestimation of the upward flux by the model during the early stage of the process. The discrepancy is caused by the reduction of void ratio near the top of the standpipe early on during the consolidation process (Figures 9 and 12). This type of behaviour has been described by several researchers to be related to time-dependent compressibility and/or hydraulic conductivity (Bolger 1960, Been 1980, Pane 1985, Edil and Fox 2000, Jeeravipoolvarn et al. 2008, Miller 2010, Scott et al. 2013).

The excess pore water pressure predictions show a good agreement with the experimental data for the caustic fine tailings (Figure 8).

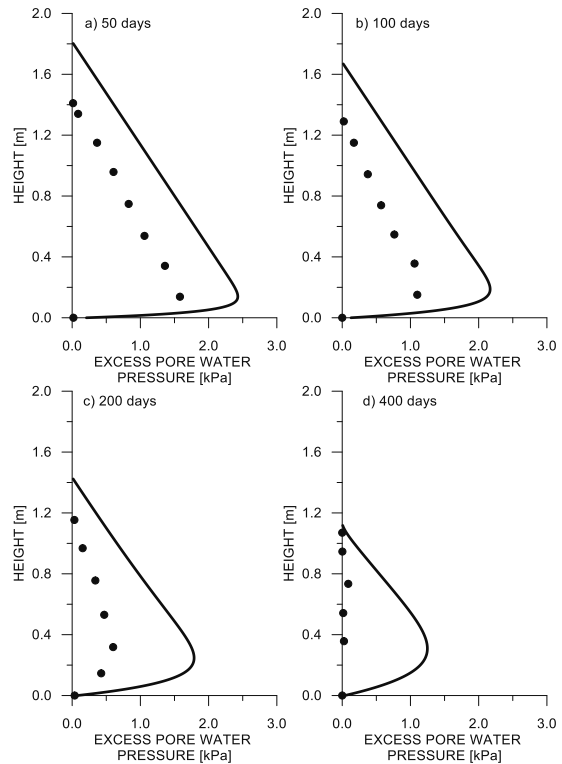


Figure 14. Excess pore water pressure comparison – caustic oil sands tailings with CaSO_4

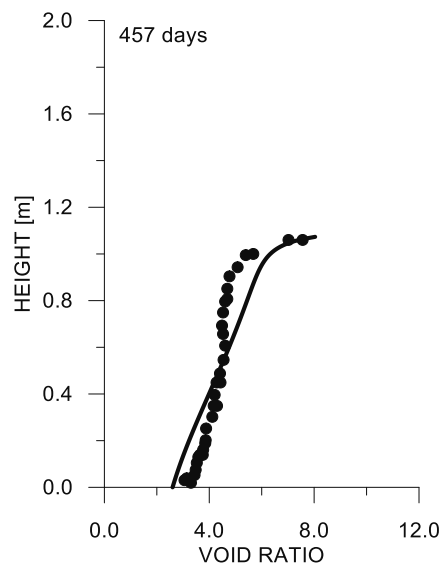


Figure 15. Void ratio comparison – caustic oil sands tailings with CaSO_4

Under estimation of the excess pore water pressure dissipation however is found for the non-caustic case (Figure 11) and the coagulated caustic tailings (Figure 14) – both tailings dissipated faster than the prediction. In other words the model with the input parameters from the large strain consolidation appears to provide a conservative prediction for the rates of compression of these materials.

Figures 9 and 12 show that the materials were compressed quickly at the bottom resulting in a large void ratio reduction at the bottom – from the initial void ratio of about 9 to about 2.5. This cake formation at the bottom of the standpipe causes a rapid reduction in hydraulic conductivity in the order of 2 magnitudes for these particular standpipe tests (Figure 5).

Regardless of the observed discrepancies, in a practical sense, the material consolidation properties and the model are considered qualitatively consistent with the validation standpipes for all three tailings materials. In real application, a model calibration shall be considered to match the standpipe performance – this calibration is beyond the scope of this study. The consolidation properties and the model presented in this paper will be further used to assess potential seepage in commercial scale tailings ponds in the next section.

DOWNWARD SEEPAGE IN COMMERCIAL SCALE TAILINGS PONDS

Hypothetical commercial scale tailings ponds with depths of 25 m, 50 m and 100 m were selected to assess for potential downward seepage for the three tailings. It is assumed that the ponds are filled instantaneously and that the bottom drainage is a free draining boundary into underlying strata with ultimate bottom pore water pressure equal to the pond water surface hydrostatic pressure. Figure 16 shows the predicted bottom seepage flux in terms of cubic meters of tailings water per square meter of pond bottom per year for the caustic oil sand tailings during 50 years. Similar plots for the non-caustic and coagulant amended oil sand tailings are presented in Figures 17 and 18 respectively.

It is found that the bottom seepage flux is approximately less than 10% of the top seepage flux; and the bottom seepage volume is less than 10% of the total seepage volume. The results also suggest that there is a very small bottom seepage volume difference of less than 2% between these tailings with the slightly higher seepage from the non-caustic oil sands tailings.

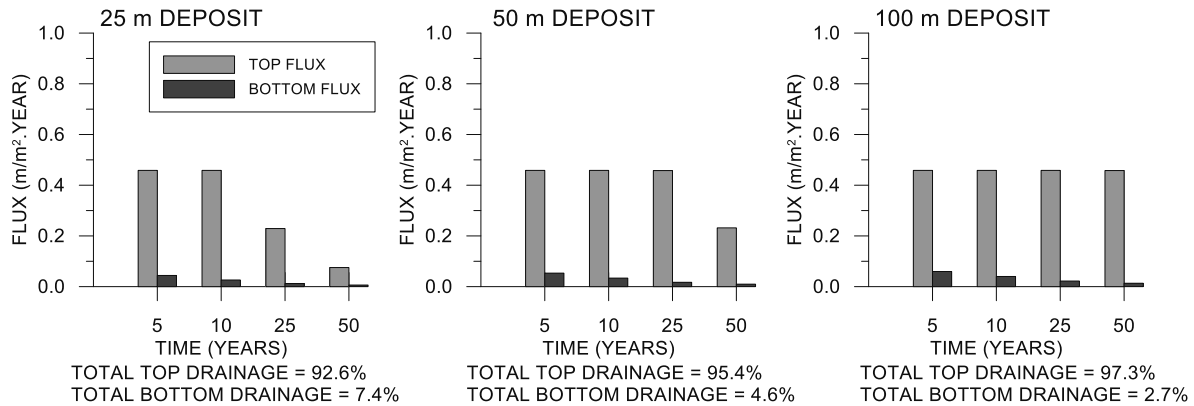


Figure 16. Drainage flux prediction – caustic oil sands tailings

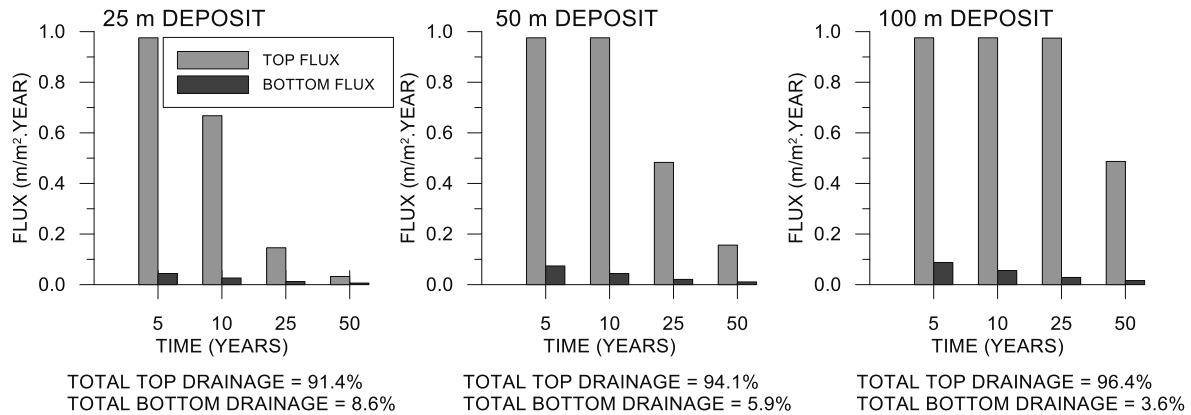


Figure 17. Drainage flux prediction – non-caustic oil sands tailings

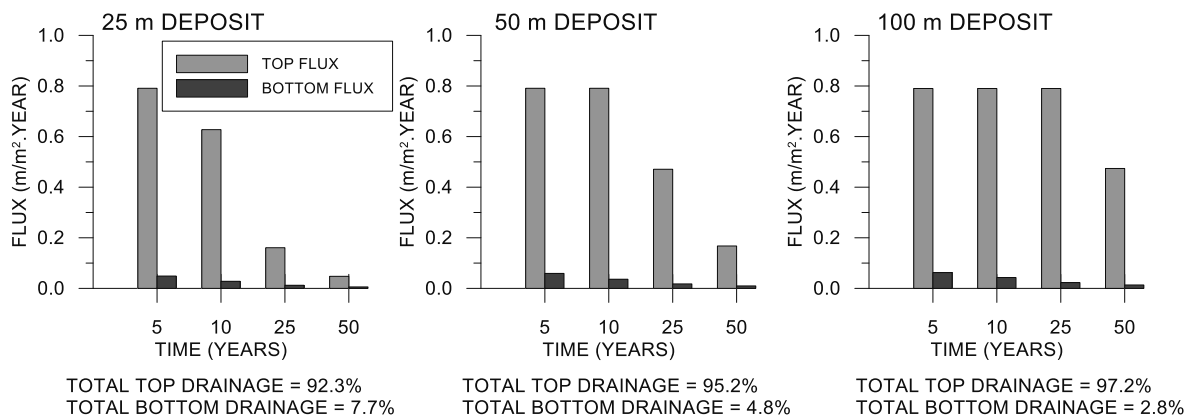


Figure 18. Drainage flux prediction – caustic oil sands tailings with CaSO₄

Figures 19, 20 and 21 shows bottom seepage flux and percent consolidation near the bottom for the three tailings. The bottom seepage rate is directly related to the percent consolidation near the bottom of the deposit, both exponentially changing with time. The consolidation causes reductions in void ratio and hydraulic conductivity. The hydraulic conductivity of the material at this location is reduced rapidly from the initial value of about 10^{-7} m/s to the final value of about 10^{-10} m/s; lower than the value required for clay liners for landfills (Alberta Environment 2010).

It must be noted that, unlike in this hypothetical numerical example, in an actual operation tailings is deposited continuously, a foundation material will have variable hydraulic conductivity, as well as a generally lower hydrostatic water level (Hackbarth and Nastasa 1979). In an effort to reduce downward seepage, an initial operation with a high fines tailings deposition could introduce a formation of low hydraulic conductivity cake early on which will decrease the long term seepage into

the ground. Use of geosynthetic liners could also be considered but because of the great area of oil sands tailings ponds even these will have some leakage. While these initial preparation techniques will reduce the rate and amount of seepage in the long run, it is inevitable that some amounts of seepage will occur without considering other drainage control options. Design engineers of particular facilities must ensure that local regulations are followed and that the design and operations of the tailings facility are executed in a way that the environmental impact is under control and minimized. To this end, it is required during the design process that the ground water regime, foundation material properties, tailings consolidation behaviour as well as mining and tailings deposition planning be integrated and analyzed together for effective assessment of overall environmental implications of the downward seepage.

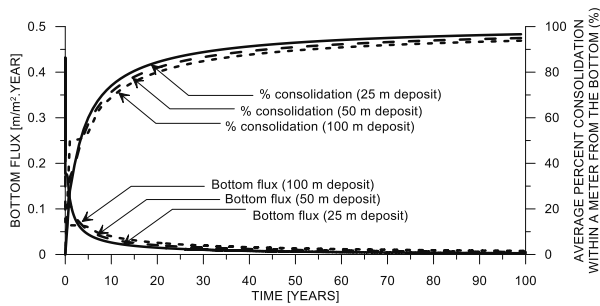


Figure 19. Drainage flux prediction – caustic oil sands tailings

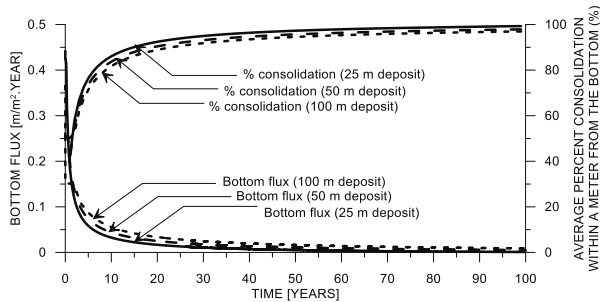


Figure 20. Drainage flux prediction – non-caustic oil sands tailings

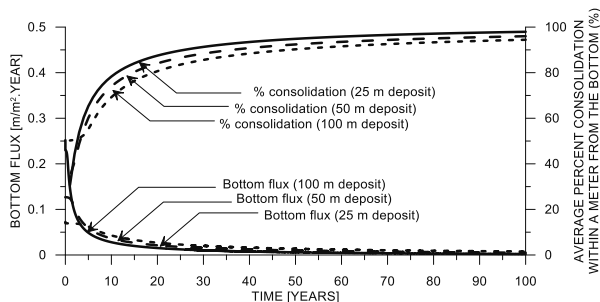


Figure 21. Drainage flux prediction – caustic oil sands tailings with CaSO₄

As well, deep monitoring wells need to be implemented before tailings facilities are constructed to assess the initial long term regional ground water flow and ground water chemistry. At the present time, monitoring wells are only installed around the perimeter of the tailings pond and to fairly shallow depths. Deep directionally drilled monitoring wells may be required to measure ground water flow and ground water chemistry below the tailings pond.

SUMMARY

It has been demonstrated in this paper that the finite strain consolidation theory is a useful tool for assessment of rate and amount of the bottom seepage. The model based on this theory was verified with large scale laboratory bottom drainage standpipe tests for caustic, non-caustic and coagulant amended caustic oil sands tailings in which reasonably good agreements are obtained. The assessment of bottom seepage in commercial scale deposits was also performed for all three tailings. The increased hydraulic conductivity of the non-caustic oil sands tailings and the coagulant amended caustic oil sands tailings does not appear to substantially increase the bottom seepage as compared to that of the caustic oil sands tailings. Finally it is important that the assessment of the bottom seepage integrates the ground water regime, foundation material properties, tailings consolidation behaviour, mine plan and tailings deposition strategy for effective and responsible tailings storage facility design and operation. As well, shallow and deep monitoring wells need to be implemented before tailings facilities are constructed to assess the initial long term regional ground water flow and ground water chemistry and their change with time.

ACKNOWLEDGEMENTS

The authors would like to acknowledge the support from the University of Alberta, WorleyParsons Ltd. and Thurber Engineering Ltd.

REFERENCES

- Alberta Environment 2010. Standards for landfills in Alberta, Government of Alberta, p. 13.
- Alberta Government 2014. Altera's Clean Energy Future – Tailings: Tailings Seepage recapturing and Monitoring Systems.
- Been, K. 1980. Stress strain behaviour of cohesive soil deposited under water. Ph.D. thesis, Oxford University, UK.
- Boger, J.C. 1960. Rheology of kaolin suspensions, PhD thesis, department of chemical engineering, Massachusetts Institute of Technology, Cambridge, Massachusetts.

- CEMA 2012. End Pit Lakes guidance document.
- Clark, D.A. and Moyer, J.E. 1974. An evaluation of tailings ponds sealants. National Environmental Research Center. U.S. Environmental Protection Agency, Corvallis, Oregon.
- Edil, T. B. and Fox, P.J. 2000. Geotechnics of High Water Content Materials, ASTM Publisher.
- ERCB 2009. Directive 074, Tailings performance criteria and requirements for oil sands mining schemes, 14 p.
- Frank, R.A., Roy, J.W., Bickerton, G., Rowland, S.J., Headley, J.V., Scarlett, A.G., West, C.E., Peru, K.M., Parrott, J.L., Conly, F.M. and Hewitt, L.M. 2014. Profiling oil sands mixtures from industrial developments and natural ground waters from source identification. *Environ. Sci. Technol.*, 2014, 48 (5), pp 2660–2670.
- Gibson, R.E., England, G.L. and Hussey M.J.L. 1967. The Theory of One-dimensional Consolidation of Saturated Clays I Finite Non-linear Consolidation of Thin Homogeneous Layers, *Géotechnique*, 17(3), pp. 261–273.
- Hackbarth, D.A. and Nastasa, N. 1979. The hydrogeology of the Athabasca Oil sands Area, Alberta. Bul 038. Alberta Geological Survey.
- Jeeravipoolvarn, S., Chalaturnyk, R.J. and Scott, J.D. 2008. Consolidation modeling of oil sands fine tailings: History matching. *Canadian Geotechnical Conference 2008*, pp. 190-197.
- Jeeravipoolvarn, S. 2010. Geotechnical behaviour of inline thickened oil sands fine tailings. PhD thesis, University of Alberta.
- Miller, W.G., Scott, J.D. and Segó, D.C., 2009. Flume Deposition Modeling of Caustic and Noncaustic Oil Sand Tailings, *Canadian Geotechnical Journal*, June, v 46, n 6, pp 679-693
- Miller, W.G., Scott, J.D. and Segó, D.C., 2010a. Influence of the Extraction Process on the Characteristics of Oil Sands Fine Tailings, *Canadian Institute of Mining, Metallurgy and Petroleum Journal*, v 1, n 2, pp 93-112.
- Miller, W.G., Scott, J.D. and Segó, D.C., 2010b. Effect of Extraction Water Chemistry on the Consolidation of Oil Sands Fine Tailings”, *Canadian Institute of Mining, Metallurgy and Petroleum Journal*, v 1, n 2, pp 113-129.
- OSRIN, 2012. Summary of the oil sands ground water – surface water interactions workshop.
- Pane, V. 1985. Sedimentation and consolidation of clays. . PhD thesis, University of Colorado, Boulder.
- Schneider, C.L., Mei, S., Grobe, M. and Huah, K. 2012. Beneath the oil sands: stratigraphy and structural features of the Devonian of Northeast Alberta. *GeoConvention 2012:Vision*: 5p.
- Scott, J.D., Kabwe L.K., Wilson, G.W., Sorta, A. and Jeeravipoolvarn, S. 2013. Properties which affect the consolidation behaviour of mature fine tailings. *Tailings and Mine Waste 2013*, November 3-6, Banff, AB, Canada, pp. 69-90.
- Soderberh, R.L. and Busch, R.A. 1977. Design guide for metal and non-metal tailings disposal. Bureau of Mines Information Circular. U.S. Depart of Interior.
- Terzaghi, K. 1923. Die Berechnung der Durchla ßsigkeitsziffer des Tones aus dem Verlauf der hydrodynamischen Spannungserscheinungen. *Akad. Wiss. Wien. Math-naturw. Klasse 132*, No. 3/4, 125-128.

ASSESSING A NOVEL TECHNOLOGY USING A TAILINGS MANAGEMENT SIMULATION MODEL

Nicholas Beier, David Segó and Norbert Morgenstern
University of Alberta, Edmonton, Alberta, Canada

ABSTRACT

The following paper demonstrates the application of a dynamic simulation model, TMSim, developed to assess oil sand tailings dewatering technologies. A tailings plan was compiled using a potential new dewatering technology, cross flow filtration, as the core tailings technology. The TMSim model was then used to evaluate the tailings plan. The modeling process and a sample of the simulation results will be presented. The cross flow filtration process provides a potential opportunity to immediately recycle process water back to extraction. Additionally, through spiking of MFT into whole tailings prior to dewatering, existing inventories of MFT could be consumed and stored within the pore space of the resulting deposit.

INTRODUCTION

Tailings management is an inherent component of any water based mining process. In the oil sands mining industry, tailings management has evolved from simple fluid storage in single external impoundments to multistage, mechanical and chemical dewatering processes and storage in several in-pit and external impoundments. The industry is currently focusing on transforming their fluid tailings and waste materials into deposits that can be incorporated into closure landforms and subsequently reclaimed. As discussed in Sobkowicz and Morgenstern (2009), there are numerous technologies that may potentially transform the fluid tailings streams into geotechnically stable deposits. A joint industry-government study (Tailings Roadmap) was undertaken in 2012 to screen and evaluate the hundreds of tailings dewatering and reclamation technologies (Sobkowicz 2012). The Tailings Roadmap project ranked and sorted the technologies based on professional, qualitative opinions and developed nine “technology roadmaps” with potential to improve oil sands tailings management practices. Since the evaluations did not include site specific considerations, each technology requires

assessment of applicability to the individual mine sites. Additionally, new technologies, processes and applications are constantly brought forward to the industry. Several of the technologies and vendors lack detailed understanding of oil sands operations (i.e. technology exploited from another industry) or the technologies are conceptual or bench scale and require further research and development.

There are three stages of dewatering tailings may go through before they meet their end reclamation targets (Boswell and Sobkowicz 2010). The first stage involves mechanical or natural classification of the tailings stream. Mechanical separators such as hydrocyclones may be used to separate a tailings slurry stream into a low density, fine grained overflow and coarse, dense underflow. Tailings may also undergo natural segregation/dewatering when they are discharged sub-aerially. In this case, a coarse beach deposit and a low density, fine grained slurry run off are formed. The beach run off collects within the impoundment and may settle with time. The second stage of dewatering includes the various mechanical, chemical and electrical methods described in Sobkowicz and Morgenstern (2009). These technologies will typically dewater the tailings streams to near, but still wet of their liquid limit. Upon deposition, the tailings deposits will typically have strengths of a few hundred pascals (Boswell and Sobkowicz 2010). The final stage of dewatering following deposition (Stage 3) includes time dependent and environmental dewatering processes. Stage 3 dewatering includes sedimentation/consolidation processes, and environmental dewatering processes such as freeze/thaw dewatering, desiccation and evapotranspiration. With an appropriate deposition and management strategy, Stage 3 dewatering can be maximized in order to dewater the tailings and achieve the strength required to meet reclamation targets.

Management of tailings also includes the construction and operation of tailings storage facilities (i.e impoundments). Impoundments may be constructed from the tailings (hydrocyclone underflow, or sub-aerial beach deposits) or from

other mine waste. The construction of the impoundments must be coordinated with the deposition and storage requirements of the tailings and associated process water to ensure sufficient storage capacity and freeboard is available. The required capacity of the impoundment is a function of the tailings dewatering processes (described above), the interaction with the environment (i.e. seepage, precipitation, evaporation), and process water demands from the extraction process. Mine operators manage their tailings through the implementation of a tailings management system (TMS) that incorporates all aspects of the tailings dewatering and their associated storage facilities.

To address the ongoing need to evaluate tailings management technologies and processes, a dynamic systems model, TMSim was developed (Beier et al. 2012). The TMSim model provides a quantitative tool that can aide in the evaluation of technologies and provide guidance to the developers on strengths and limits of the technology. TMSim was developed to incorporate mine plan data, various stages of dewatering including classification, pre- and post- deposition dewatering, and an impoundment material balance including tailings, process water, construction material and capping materials.

The objective of this paper is to demonstrate the application of the TMSim simulation tool to evaluate a potential new dewatering technology. The modeling process and a sample of the simulation results will be presented.

A TMS plan utilizing cross flow filtration dewatering (new technology), as presented by Beier and Segó (2008) and Zhang (2010) was developed. The Syncrude Canada Ltd. (Syncrude) Aurora North (Aurora) mine was chosen as the model site (Syncrude 2012). All data utilized in the following simulation were collected from publically available sources.

TMSIM MODEL

The TMSim model tracks the stocks (accumulation in a containment facility) and flows of mass (solids [mineral including both fine and coarse], water, and chemicals) throughout the TMS. A suite of sub-models were used to represent individual components such as the extraction plant, tailings dewatering Stage 1, 2 or 3, impoundment and the environment (Figure 1). Critical processes (such as consolidation, Stage 2 dewatering, seepage, etc) within each component will dictate mass transfer between the sub-models.

The TMSim model process contains three components. The first component is the data input requirements. A spreadsheet will be used as the data entry/interface for all model inputs such as site properties, tailings properties, mining and extraction rates, environmental data and pertinent management decision variables (i.e. constraints on the system).

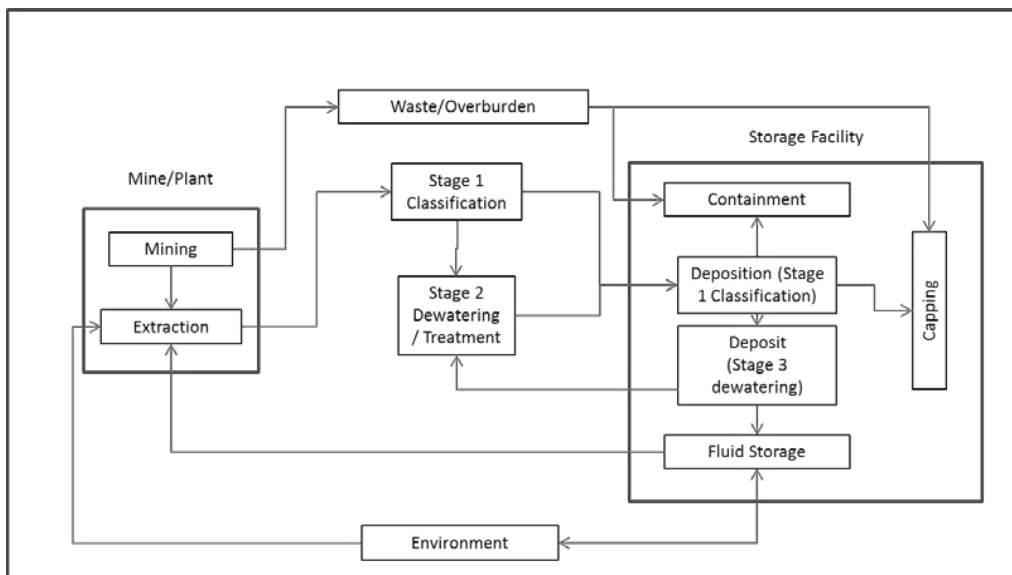


Figure 1. TMSim conceptual model.

The user will have the option to utilize built in functions and sub-models or implement their own models (user defined models, UDF). The UDFs can be simple or complex numerical models, depending on the level of detail available and objective of the modelling. Implementation of user

specific models/data would be completed either in the data input spreadsheet or the Goldsim model directly (Beier et al., 2012). A summary of the input requirements from each of the sub-models is provided in Figure 2.

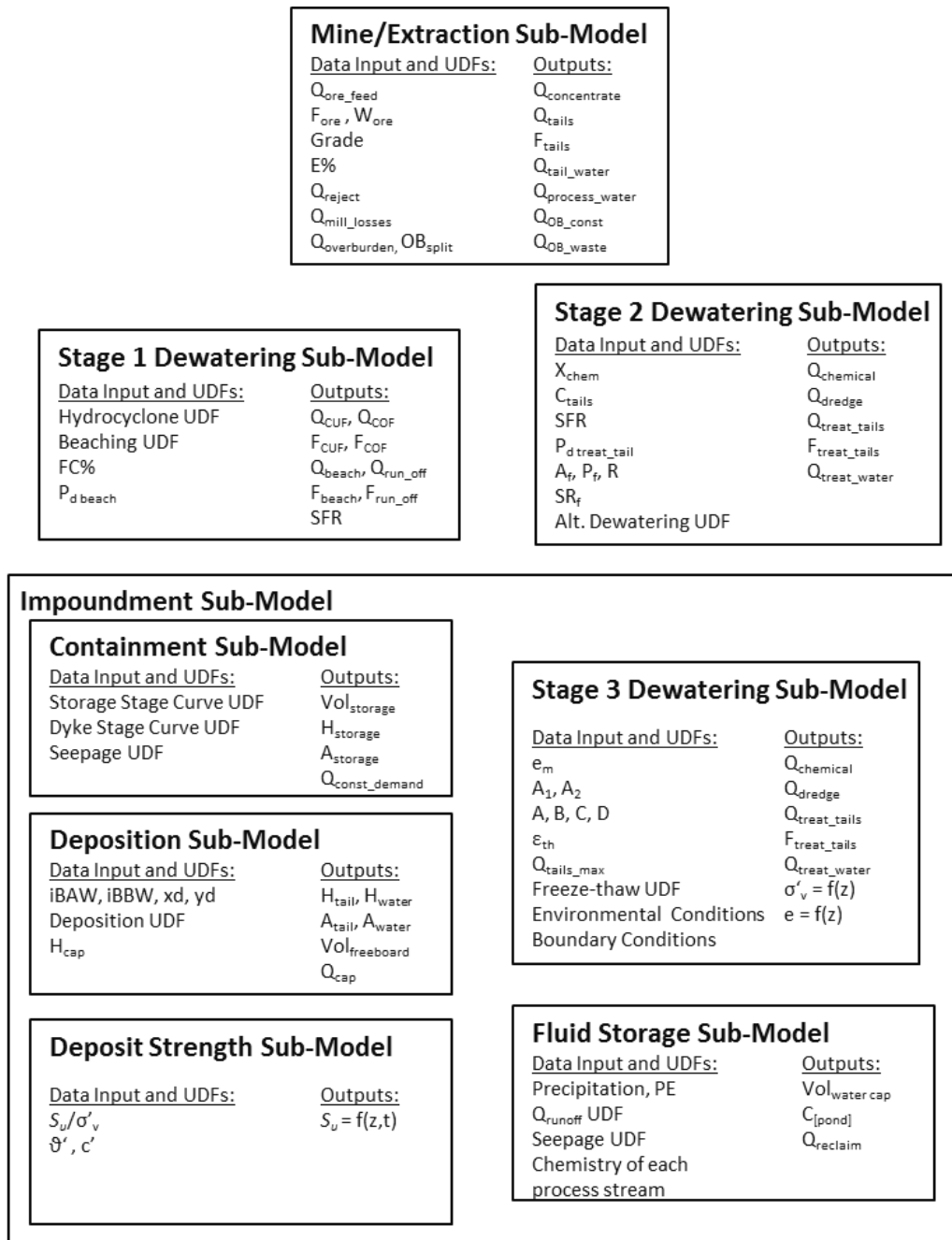


Figure 2. Data inputs, UDFs and outputs for each TMSim sub-model.

In addition to the variables and UDFs for each of the sub-models, the decision logic required to allow for the switching between dewatering technologies and deposition points must also be provided by the user. It is obvious that a TMS is multifaceted, interrelated and complex. Therefore, the TMSim will be a simplification of the real mining system and include only the important user defined processes. The accuracy of the model will depend on the level of detail and parameters available to the user.

The Aurora oil sands mine (started in 2000) uses truck and shovel surface mining technology. A warm water extraction process is utilized to separate bitumen from the ore. Bitumen froth produced at Aurora is pipelined to another Syncrude mine site, Mildred Lake, for further processing and upgrading. The Aurora mine excavates approximately 100 Mm³ of ore and mine waste overburden per year resulting in approximately 200,000 bbl/day of bitumen production.

OIL SAND MODEL DATA SET

The following information for the Syncrude Aurora mine and tailings management data were obtained from the Aurora North Environmental Impact Assessment report (Reeves 1996), the 2012 Annual Tailings Plan report (Syncrude 2012), or from publically available literature.

The average Aurora ore contains 11.1 % bitumen, 3.5 % water, 15.1 % fine mineral solids (<45 µm) and 70.3 % coarse mineral solids. Stripped overburden (mine waste) consists of high, medium and low spec materials, classified for applicability as construction material and plant rejects. The average ratio of excavated ore to overburden and mine waste is approximately 1.59. A summary of the annual ore and waste production schedule is included as Figure 3.

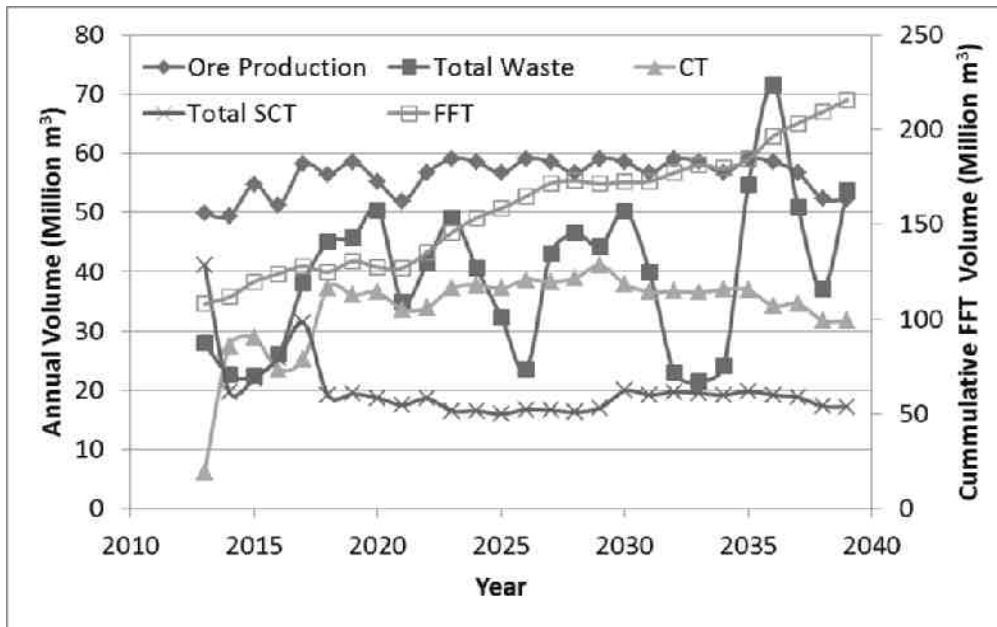


Figure 3. Annual ore, waste and tailings production at Syncrude Aurora North mine.

Based on a digitized plan, the Aurora pit covers approximately 52.5 km². Using an average mining rate of 100 Mm³ over the expected 37 year mine life (2000 to 2037), an average pit depth was calculated as 70.5 m. Based on the average ore to overburden ratio of 1.59, the overburden thickness is approximately 26 m and the ore is 44.5 m thick. These estimated values agree with Reeves (1996) report, with an overburden thickness (including

intraburden) of 23 to 28 m and ore depths from 41.7 to 53.7 m on average.

The primary extraction process at Aurora produces a tailings stream consisting of sand, silts, clay, residual bitumen and water referred by Synrude as straight coarse tails (SCT) otherwise known as whole tailings. A small volume stream of floatation tailings are also produced during the extraction

process. The floatation tailings are incorporated and managed with fluid fine tailings (FFT) deposits. Historically, the SCT stream was deposited into an external tailings facility (Aurora settling basin, ASB). The coarse fraction of the tailings stream settled to form beaches and structural components of the ASB while the fine grained fraction settled in the pond to form FFT which settle to form mature fine tailings (MFT). The ASB was used to store tailings (SCT and FFT) until sufficient pit space was available in mid-2010. The ASB was constructed with overburden materials and straight coarse tailings (SCT) using beaching and cell construction techniques. The ASB currently contains 79.9 Mm³ of FFT and 46.5 Mm³ of process water (Syncrude 2012) and is at its maximum construction elevation. The maximum planned storage volume of the ASB is 129.8 Mm³ (based on maximum volume calculated from Syncrude 2012).

The Aurora mine pit will eventually be used as in-pit storage areas or dedicated disposal areas (DDAs) for the tailings. In-pit dykes will be used to segregate each of the DDAs and allow safe deposition of tailings and fluid storage while mining progresses within the pit. An existing DDA currently contains 18.6 Mm³ of FFT, 0.7 Mm³ of water and 47.3 Mm³ of SCT.

CROSS FLOW FILTRATION DEWATERING

A potential alternative tailings management technology for an oil sands mining operation is crossflow filtration (Beier and Segó 2008). Crossflow filtration (CFF) is a pressure driven filtration process that can be used for dewatering slurries of fine particles and can offer improvements over conventional filtration. In CFF, the slurry flows parallel to the filtration membrane developing a cake on the filtration surface (i.e. a porous pipe). However, due to shear of the flowing slurry, the build up of cake will reach an equilibrium thus maintaining a relatively constant filtration rate. CFF offers an opportunity to deposit tailings without inducing segregation of the fines from sand, therefore preventing further accumulation of FFT. Early testing also indicates, no chemical additives were needed to achieve filtration, therefore, release water from the CFF tailings will be similar to the process water from extraction. It also provides immediate recycle of process water to the extraction plant. This will reduce the energy costs required for heating process water resulting

in Green House Gas reduction associated with the extraction process.

CFF was evaluated in the Tailings Roadmap project and was prioritized as a medium level technology, on par with CT and NST technologies (Boswell et al 2012). CFF has only been applied at the laboratory and bench scale (Beier et al. 2008) for oil sand tailings applications. Therefore it will serve as a sufficient candidate to demonstrate the TMSim modeling capability of a new, developing technology.

The CFF process can be implemented in an oil sands mine to dewater extraction tailings or SCT prior to deposition, thus negating the formation and subsequent build up of FFT. Sufficient water must be removed from the extraction tailings during CFF so upon deposition, the tailings do not segregate. For typical extraction tailings at ~55% solids content by mass (C_w), approximately 50% of the water must be removed to bring the C_w to at least 70-75% to prevent segregation (Beier and Segó 2008). Upon dewatering to 70% or greater C_w , the CFF-tailings could then be deposited as stacks within the mined out pit. Sufficient overburden material should be available to provide in pit containment dykes for the CFF-tailings.

CFF Dewatering Model

The following CFF dewatering model is based on the preliminary CFF studies by Beier and Segó (2008). They used a mixture of kaolinite and coarse oil sand beach sand to develop a surrogate whole tailings with a C_w of 55% and a 15% fines content ($f\%$). For reference, the average fines content of the whole tailings stream at Aurora is calculated to be 18.9 % +/- 5%. The resulting tailings stream was then pumped through a 3 m section of porous filter pipe. At an in-pipe slurry velocity of 1.7 m/s, Beier and Segó (2008) achieved an average filtration rate of 0.008 L/s/m² of filter surface. Zhang (2010) achieved a similar filtration rate (0.005 L/s/m²) with a mixture of oil sand fine tailings and beach sand under the same operating conditions. Therefore, results from the surrogate oil sand tailings stream are considered suitable for the CFF design. Both Beier and Segó (2008) and Zhang (2010) also found that the filtration rate did not diminish as the solids content of the slurry was increased. Therefore, the CFF design can assume a constant filtration rate, regardless of the slurry C_w . The CFF will however, depend on the cake properties, specifically the resistance to filtration or permeability.

Filtration experiments on oil sand tailings were also conducted by Xu et al. (2008) to assess the impact of fines content and flocculation on the filtration rate for a vacuum filtration process. Tailings slurries with fines contents ranging from 4.3% to 83.3% were filtered in a bench scale filtration apparatus. They determined the specific resistance to filtration, r (m/kg), as a function of fines content and flocculation condition (Figure 4). The specific resistance from Beier et al (2008) and Zhang (2010) were also plotted on Figure 4 for comparison. Beier et al (2008) and the Zhang (2010) data fit within the range of unflocculated tailings Xu et al (2008) data. Therefore, the unflocculated filtration data from Xu et al (2008) may be suitable to represent the CFF filtration conditions at different $f\%$.

Using the Xu et al (2008) relationship between r and $f\%$ of the slurry, the volume of filtrate for a unit area (1 m^2) and unit time (1 hr) can be determined. The filtrate volumes were calculated assuming a constant pressure (150 kPa), using the method presented in Xu et al (2008). Using the filtrate volume and time, filter surface area and applied pressure, an equivalent permeability, k_{cake} (m/s), of the filter cake can be calculated using the D'Arcy equation (Equation 1).

$$Q = k_{\text{cake}} * \Delta h / \Delta L * A \quad [1]$$

Where Δh is the applied pressure in m of water and ΔL is the thickness of the filter cake. Assuming the in pipe slurry velocity is similar to the Beier et al (2008) experiments the estimated cake thickness should be 0.005 m. The calculated equivalent cake permeability versus $f\%$ is presented on Figure 5. A power function (Equation 2) representing the unflocculated tailings and Equation 3 for flocculated tailings data can be used to estimate the equivalent permeability of the CFF cake as a function of $f\%$.

$$k_{\text{cake}} = 5E^{(-7)} * f\%^{(-1.42)} \quad [2]$$

$$k_{\text{cake}} = 2E^{(-6)} * \exp^{(-0.13 * f\%)} \quad [3]$$

According to Devenney (2009), an average of 0.8 m^3 of process water is required per tonne ore processed. Based on the average mining rate of 118 Million tonnes/year, 97 million tonnes of mineral solids will report to the tailings stream (Syncrude 2012). Assuming a nominal process water loss of 2.5% (Reeves 1996), the average C_w of extraction tailings stream is calculated as 51% at a flow rate of $14,700 \text{ m}^3/\text{hr}$. To achieve the

desired CFF dewatered C_w of 75%, approximately 46 % of the flow needs to be removed as clear water filtrate or approximately $6,800 \text{ m}^3/\text{hr}$.

Using the k_{cake} relationship for the unflocculated tailings at a $f\%$ of 15% and an applied filter pressure of 150 kPa, approximately $58,000 \text{ m}^2$ of filter surface area (FSA) would be required to achieve the desired dewatering. This FSA is not practical. However, the flocculated tailings would only require an average of 2500 m^2 of filter area, a more realistic surface area. Based on unpublished work on the CFF system with unflocculated tailings, the dewatering performance was improved at least an order of magnitude by optimizing the velocity and using alternative filter media. Therefore, untreated tailings have the potential to be dewatered with a CFF system. However, given the lack of publically available data, the flocculated tailings filtration data will be used to demonstrate the design of the CFF system.

Using the flocculated tailings filtration data, the required FSA per year based on actual yearly tailings flow rate and $f\%$ is presented on Figure 5. Due to the variability in ore fines content and tailings flow rates, the FSA varies considerably from 1500 to 4000 m^2 . An actual CFF system would require a static FSA. Using the average FSA, the CFF tailings would meet the target C_w of 75% (+/- 5%) only 40-50 % of operating time. Therefore, there could be years where the system is underutilized and years where the CFF is unable to meet the dewatering demand. A potential opportunity exists to balance the FSA requirements and consume accumulated MFT. The sand to fines ratio (SFR) of the whole tailings stream ranges from $\sim 4:1 - 7.2:1$. The whole tailings stream could be spiked with MFT to stabilize the SFR ratio, thus reducing the fluctuations in the FSA requirements. Specifying a target SFR of 4.75:1, the calculated FSA and total flow of whole tailings and MFT is presented on Figure 5. There is a significant reduction in fluctuations and are attributed only to the tailings flow rates with an average FSA of 3275 m^2 . By spiking the whole tailings, a potential of over 167 Mm^3 of MFT can be consumed by the CFF process. For comparison, an SFR of 5:1 would require an FSA of 3000 m^2 , but only consume $\sim 120 \text{ Mm}^3$ of MFT.

To ensure sufficient FSA is available and provide a contingency, a design FSA of 3500 m^2 will be used to dewater the MFT spiked extraction tailings at an SFR of 4.75:1. The total average flow rate with

MFT spiking is 15,100 m³/hr. Based on CFF laboratory work, an in pipe velocity of greater than 3 m/s will provide optimum filtration. Assuming a diameter of 60 cm, five sections of filter pipe, each 366 m long are required to meet the dewatering requirements.

CFF Deposit Behaviour

Although detailed studies on the depositional behavior of the CFF tailings have not been completed to date, they are expected to behave in a similar manner to CT deposits.

Following deposition, consolidation dewatering will be the dominant dewatering process, therefore compressibility and permeability functions are required. Since the compressibility has limited influence on the rate of settlement (influences the magnitude), estimates from similar tailings materials may be sufficient for modeling purposes. The large strain dewatering compressibility behavior of CT materials for Syncrude CT at various SFRs was extracted from Matthews et al. (2002) and can be expressed in the form of Equation 4,

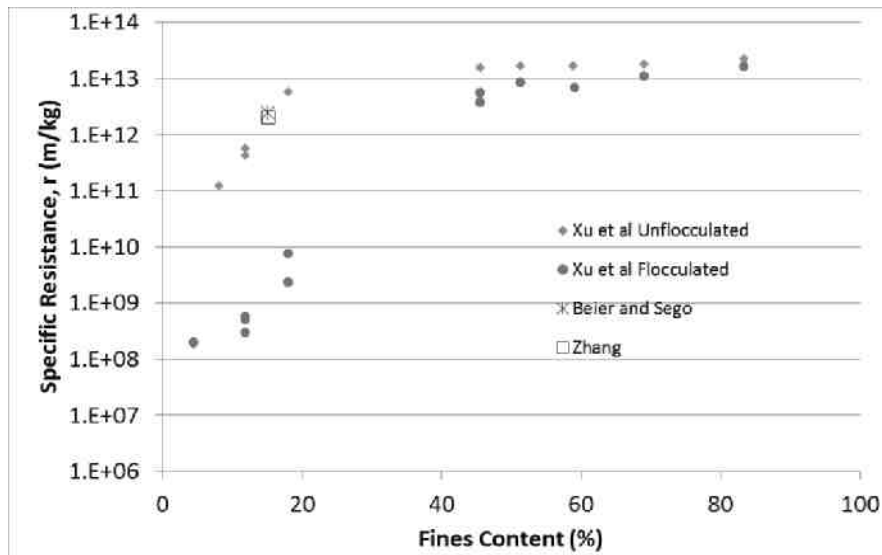


Figure 4. Specific resistance to filtration for various tailings streams and fines contents.

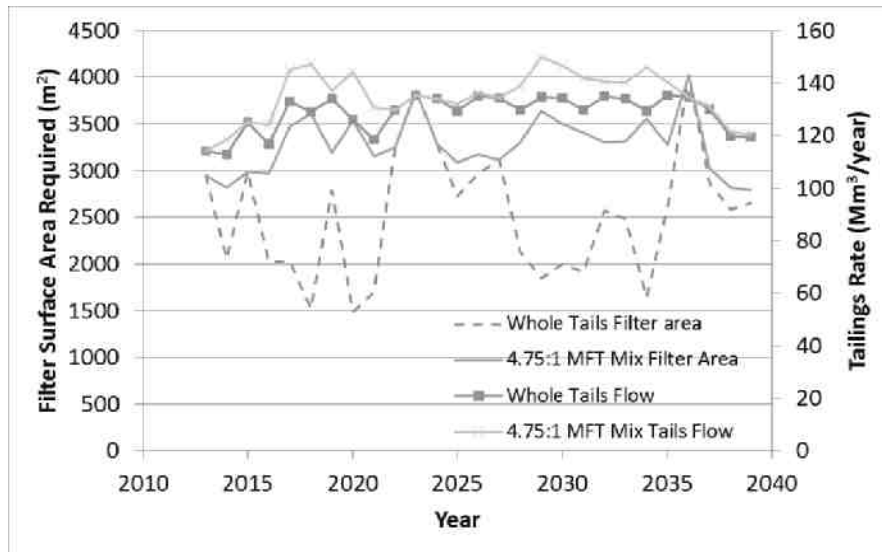


Figure 5. Filter surface area and tailings flow rates.

$$e = A\sigma^{-B} \quad [4]$$

where the 'A' and 'B' parameters can be calculated based on the varying f% as expressed in Equations 5 and 6.

$$A = 0.304 \ln(f\%/100) + 1.404 \quad [5]$$

$$B = -0.156 \ln(f\%/100) - 0.374 \quad [6]$$

The permeability (k) as a function of void ratio (e) is also required (Equation 7) where e_{fines} is the fines void ratio calculated from Equation 8.

$$k = C * e_{\text{fines}}^D \quad [7]$$

$$e_{\text{fines}} = e(1 + \text{SFR})/1 \quad [8]$$

Based on several Syncrude fine tailings samples, the parameter C was determined to be a function of f% (Equation 9) and D is 3.774.

$$C = 0.0002(-1.583 * f\% + 71.66)^{-2.871} \quad [9]$$

The expected slope of the CFF tailings upon deposition has not been studied. However, due to the high solids content upon deposition, the CFF tailings are expected to behave similar to beached tailings and attain a slope of at least 2%.

CFF Deposition

Based on the current status of mining operations at Aurora, if a CFF dewatering technology were implemented in year 2013, a dedicated disposal area (DDA) is available in pit. This DDA 1, is estimated to be 7.5 km² and 70.5 m deep. It is bounded by pit walls on three sides and an overburden dyke constructed to full height and at 5:1 side slopes. CFF tailings will be deposited into the DDA from the pit walls and in-filled to above grade level to account for settlement after deposition has ceased. DDA 1 will reach capacity after 9 years of filling.

A second DDA 2, will be bounded by two pit walls, the dyke from DDA 1 and a small toe dyke (Figure 6). CFF tailings will be deposited from a central riser within the DDA 2 forming a conical tailings stack with a nominal slope of 2%. CFF tailings will be deposited to an elevation above grade to account for future settlement. The third DDA 3 is adjacent to DDA 2 and bounded by a second small toe berm and the tailings stack in DDA 2. A second central riser will be used to

deposit CFF tailings within DDA 3 forming a stack and in-filling DDA 3 and 2 (Figure 6).

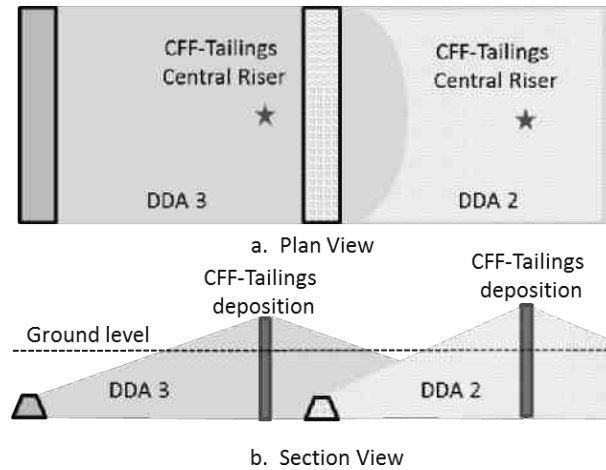


Figure 6. Deposition plan for DDA 2 and 3.

CFF MODEL RESULTS

The TMSim model was utilized to assess the CFF dewatering model developed based on the Aurora mine and tailings plan. The following summarizes some of the key simulation results.

Deposition into DDA 1 will provide storage for 9 years. The tailings deposit will reach a maximum height of 80 m (Figure 7). The deposit will attain a C_w of nearly 77 % at end of filling. At the end of mining (year 27), the deposit will have consolidated to an average C_w of 81.2%, an approximately 10% volume change and will have settled to the existing ground level. Prior to year 9, a small (20 m high) containment dyke is required to provide containment for DDA 2 and separation of mining activities from active tailings deposition. Approximately 10 Mm³ of overburden can be used to construct this berm. Starting in Year 8, a large overburden containment berm is required to provide containment for the in-pit overburden deposition area (Figure 8). The berm will be constructed to full elevation of 70.5 m and require 100 Mm³ of overburden. The in-pit overburden storage area will provide a total of 350 Mm³ of storage. Residual overburden will require storage in piles out of the pit, or used as a surcharge/cap for tailings deposits. Before year 18, a second toe berm will be required to an elevation of 30 m (35 Mm³) to provide containment for DDA 3. After year 9, deposition of CFF tailings will move to DDA 2. A central riser (or several risers) is

proposed as the deposition method to develop a conical tailings stack. Tailings in DDA 2 will reach an elevation of 84.6 m after 9 years (Year 18) with an average C_w of 77%. Sufficient tailings will have been deposited to allow for re-grading and settlement so the surface of the deposit will be at ground level. After a further 18 years of settlement, the deposit surface will be approximately 76 m at its highest point.

Tailings deposition will then move to DDA 3 (Year 19), which partially in-fills DDA 2 (Figure 6). At the end of mining (Year 27), the tailings deposit will reach an elevation of 85.8 m at the central riser. Again, the average C_w of the tailings deposit is 77%. Sufficient tailings will have been deposited to allow for re-grading and settlement so the surface of the deposit will be at ground level. After a further 18 years of settlement, the deposit surface will be approximately 76.5 m at its highest point.

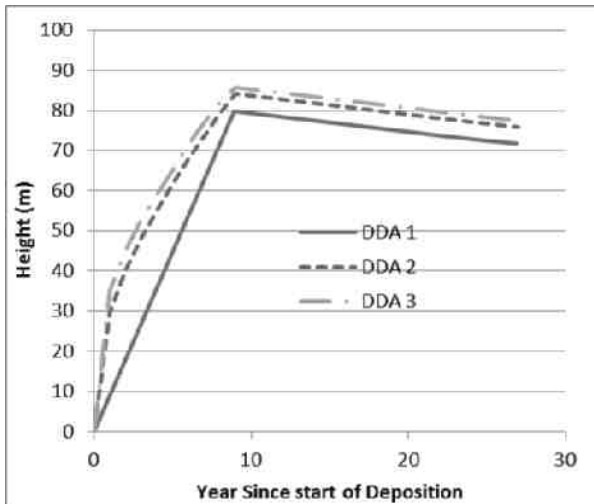


Figure 7. CFF tailings elevations with time.

After 27 years of deposition, the total required storage volume required in pit for CFF deposit, including spiked MFT is 1955 Mm^3 (Figure 8). The total volume of CFF tailings at the end of mining is nearly identical to the total in pit CT tailings volume estimated in the Aurora mine plan (Syncrude 2012). This is expected since SFR and final C_w of the CT and SFR are similar and are based on the same mass of sand in the deposit. However, in a CFF process, all of the MFT inventory could be consumed after 19 years of operation. This allows for 8 years of contingency to consume any FFT that has developed during capping activities, froth

tailings and potential segregation of CFF tailings during deposition.

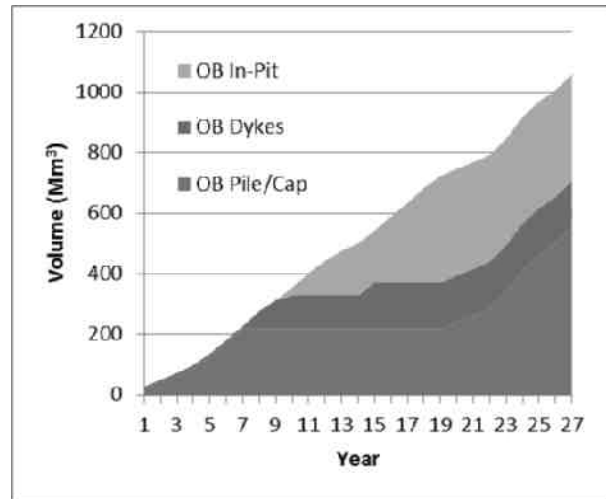


Figure 8. Overburden deposition volumes

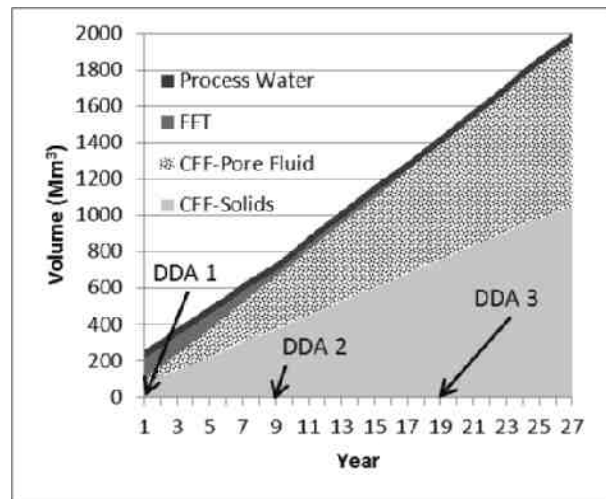


Figure 9. Tailings deposition volumes.

At the end of deposition, the CFF tailings in each DDA will reach an average C_w of 77% (void ratio of 0.79). Based on a CT deposit design by Canadian Natural Resources Limited (CNRL) with a similar SFR, a surcharge cap of 2 to 5 meters may be required to achieve the desired 5 kPa to 10 kPa strengths (CNRL 2010).

An average of 92 Mm^3 /year of water is required for the extraction process. The CFF dewatering process provides an immediate 62 Mm^3 /year of water available as direct recycle. The CFF tailings contain 30 Mm^3 /year as pore water that is lost to the deposit. Accounting for runoff and mine

depressurization an annual make up volume of 25.5 Mm³ is therefore required to meet the extraction demand. According to the Aurora mine plan, this is satisfied through water transfers from the Mildred lake site.

CONCLUSIONS

The CFF dewatering process described above provides an opportunity to deposit high density tailings stacks requiring minimal containment. Two thirds of the yearly process water demand can be satisfied by immediate recycle from the CFF process. Additionally, if MFT spiking is incorporated, the existing inventory can be consumed and stored in the pore space of the CFF tailings.

The process of compiling the necessary input data required by the TMSim model provided significant insight into the CFF process. For example, further bench scale and pilot testing is required to confirm the fines content-specific resistance relationship is valid for tailings with or without flocculation. The dewatering rates presented above provide a minimum target that should be achieved to ensure a satisfactory tailings plan. The influence of bitumen content on filtration rates and potential filter membrane fouling should also be investigated. Additionally, the tailings behavior such as deposit slope and consolidation parameters need to be determined from actual CFF tailings generated from laboratory and pilot testing. The TMSim simulations presented above provide a baseline for further refinement and sensitivity analyses of the technology and depositional scenarios. As research and development progresses on the CFF process, the model can be refined, providing an improved understanding of the impact of the CFF technology to a mine and tailings plan.

REFERENCES

Beier, N. and Segó, D. 2008. Dewatering of Oil Sands Tailings Using Cross Flow Filtration. 61st Canadian Geotechnical Conference and 9th joint IAH-CNC Groundwater Specialty Conference, Edmonton, Alberta, 22-24 September 2008. 8 pp.

Beier, N., Segó, D., and Morgenstern, N. 2012. Simulation of Tailings Management Options. 3rd International Oil Sands Tailings Conference, Edmonton, Ab. Dec 5-8, 2012. 9 pp.

Boswell, J.E.C. and Sobkowicz, J.C. 2010. Environmental assistance for tailings disposal. 63rd Canadian Geotechnical Conference, Calgary, Alberta, 12-16 September 2010, pp. 665-669.

CNRL, 2010. Horizon Tailings Management Plan. Revision 2. November 2010. 90 pages.

Matthews, J.G., Shaw, W.H., MacKinnon, M.D., and Cuddy, R.G. 2002. Development of composite tailings technology at Syncrude. International Journal of Surface Mining, Reclamation, and Environment, 16(1): 24-39.

Reeves, B. 1996. Environmental Impact Assessment for the Syncrude Canada Limited Aurora Mine. BOVAR Environmental, 1996.

Sobkowicz, J.C. The oil sands tailings technology roadmap and action plan: Introduction and key recommendations. Third International Oil Sands Tailings Conference. Edmonton, Alberta. December 2-5, 2012. Pp. 13-23.

Sobkowicz, J.C. and Morgenstern, N.R. 2009. A geotechnical perspective on oil sands tailings. 13th International Conference on Tailings and Mine Waste, Banff, Alberta, 1-4 November 2009. University of Alberta, pp. xvii-xli.

Syncrude Canada Ltd. (Syncrude). 2012. 2012 Annual tailings plan submission Syncrude Aurora North (Leases 10, 12 and 34). 30 September 2012.

Xu, Y., Dabros, T., and Kan, J. 2008. Filterability of oil sands tailings, Process Safety and Environmental Protection, 86(4): 268-276.

Zhang, C. 2010. Cross Flow Filtration of Oil Sand Total Tailings. MSc Thesis submitted to the Department of Civil and Environmental Engineering, University of Alberta. 182 pp.

MODELING DEWATERING OF OIL SANDS MATURE FINE TAILINGS USING FREEZE THAW

Nam H. Pham, David C. Segó
University of Alberta, Edmonton, Alberta, Canada

ABSTRACT

During freezing, ice lens surround frozen peds of mature fine tailings and therefore, the grain to grain contacts between the soil particles changes, from a card house to face to face structure. Upon thawing, water is released increasing solids content (reduce moisture content). Thawed tailings have higher hydraulic conductivity and lower compressibility than never-frozen and thawed tailings.

The amount that is frozen and thawed is determined by the local climate and thermal properties of the deposited tailings. At Fort McMurray, under a thin layer deposition scheme, the frozen thickness varies significantly depending on initial placement temperatures and layer thickness. The total frozen thickness varies between 4.0 m and 8.4 m for deposition layers of 0.2 m. However, during summer the maximum thickness thawed is 3.7m, under a thaw strain of 58% and average summer temperatures. However, under a warm tailings cap of 50 °C, a 5 m frozen thickness can be thawed in a summer. Numerical results were used to compare with the freezing and thawing depth measured in the field at the Suncor site (Fort McMurray).

INTRODUCTION

Oil Sands mine wastes are overburden and tailings consisting of coarse tailings sand and fluid fine tailings (a high moisture content fine grained slurry with small fractions of bitumen and solvents). Environmental issues develop without proper management of these waste products. Financial and technical challenges associated with the management of tailings and overburden have been important factors for closure planning of these mines. Specifically for tailings, the main concerns associate with any dewatering technology are reduction of volume to achieve the required-strength while being financially feasible. There are various methods used to decrease tailings volume (by dewatering via physical/mechanical, chemical

and natural processes). The natural processes include freeze/thaw, desiccation, biological and consolidation.

As tailings undergo freeze/thaw, the micro-structure of tailings changes significantly as a result of ice lens formation. This ice lens growth over-consolidates the tailings through the enhancement of the contacts between the grains. As a result, when the tailings thaw, they have increase in solid content and permeability along with a decrease in compressibility. By placing thin layer to maximize the volume of tailings frozen during a typical winter in Fort McMurray, the solid content of mature fine tailings increased from 30 % to 43%) (Johnson et al., 1993) while Proskin (1998) reported an increase from 35% to 62%. Segó and Dawson (1992a) initiated research on the freeze-thaw dewatering and post-thaw consolidation of MFT (Mature Fine Tailings) with initial solid contents between 28% and 30%. They conducted both single layer and multiple layer freezing tests to investigate the solid content increase. By using various temperatures at boundaries resulting in different freezing rates, they concluded that lower freezing rates resulted in higher solid content in post-thaw material. In addition, freeze-thaw becomes less effective as the initial solid content increases. Segó and Dawson (1992b) by using large strain oedometer demonstrated an increase of 2 orders of magnitude in hydraulic conductivity and lower compressibility compared to never-frozen MFT at a given void ratio.

Figure 1 shows the relation between initial and post thaw solids content and the initial solids content varies between 16 % and 66 % (Segó and Dawson, 1992a; Segó and Dawson, 1992b; Johnson et al., 1993; Proskin, 1998; Bale, 2008; Beier and Segó, 2009 and Yang, 2012). The figure indicates that at solids content approaching 70 %, the change associated with freeze thaw is insignificant. For MFT (Mature Fine Tailings) with solids content around 30 %, the thawed solids content ranges between 34 % to 50 % with an average of 45 %. This is because the thawed solids content depends not only on

physical/chemical properties of the MFT, such as grain size distribution and chemical signature, but also the freeze/thaw process, such as freezing rate and number of freeze/thaw cycles. However, for a given MFT the freeze/thaw process gives the most benefit following the first cycle and the latter freeze/thaw cycles shows much less effect (Proskin, 1998). The black solid line in the figure is the fitting curve to the data.

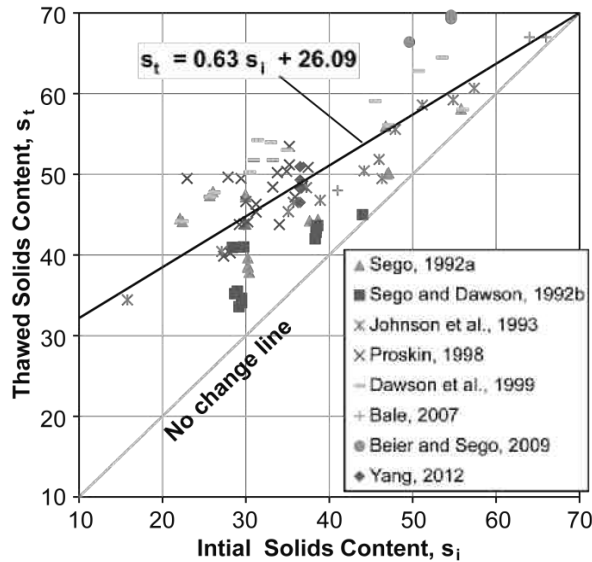


Figure 1. Initial and thawed solids content under freeze/thaw cycles.

Based on data from Figure 1, bulk density and thaw strain can be determined using the specific gravity through Eqs. (1) and (2).

Bulk density:

$$\rho = \frac{G_s}{s + G_s(1-s)} \quad (1)$$

Thaw strain

$$\delta = \frac{e_i - e_t}{1 + e_i} \quad (2)$$

which, G_s , s , e_i and e_t are specific gravity, solids content, initial and thawed void ratio with an assumption of fully saturated tailings.

Figure 2 shows the relation between bulk density of tailings and thaw strain undergoing freeze/thaw cycles. The fitting curve of tailings can be written as:

$$\delta = 1.07\rho^{-5.17} \quad (3)$$

The Eq. (3) indicates that at a bulk density close to 1 g/cm³ (basically water) thaw strain is 1 and at a bulk density is close to 2 g/cm³ thaw strain is negligible. In addition, Figure 2 also shows the curve for permafrost soils reported (Speer et al., 1973) which can be expressed as:

$$\delta = 0.736 - 1.018 \ln \rho \quad (4)$$

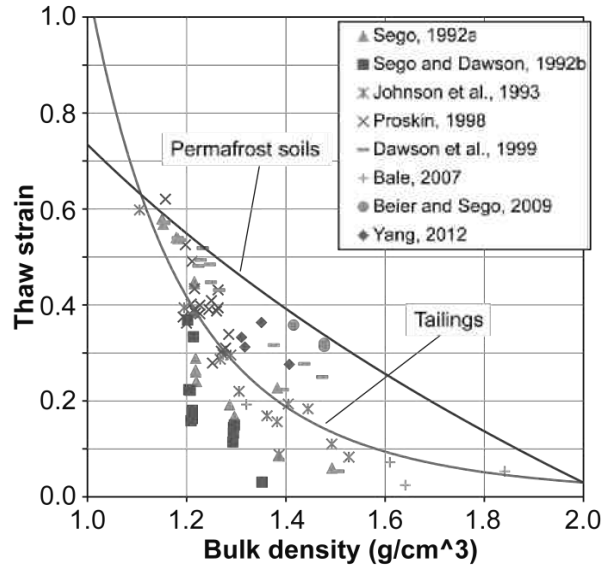


Figure 2. Initial bulk density and thaw strain relation.

Eq. (4) is applicable for a bulk density range between 1.09 g/cm³ and 2.05 g/cm³ and above this range the thaw strain is insignificant. The study to develop Eq. (4) was a result of intensive research on thaw settlement associated with an oil pipeline planned from Prudhoe Bay, Alaska to Edmonton during 1971 and 1972. Figure 2 indicates that over most density the thaw strain of tailings is less than reported for permafrost soils and the difference is associated with the amount of excess ground ice typically found in permafrost soils.

Freeze/thaw is effective a increasing the solids content of MFT. However, the freeze/thaw process is only suitable in cold climate regions. Furthermore, at some sites, a multi-layer thin layered deposit can result in more frozen tailings thickness than can be frozen as a single thick deposit. However, these frozen layers needs to be thawed during summer to eliminate of frozen tailings that can impeded drainage within the deposit.

The basic idea of the freeze/thaw technique is that DDA (dedicated disposal area) is divided into cells in which tailings are deposited continuously from a loop as thin layers so that when at the end of the cycle the first layer in the cycle is completely frozen. The process is repeated until the design frozen thickness is achieved. During spring/summer months, water is released as the deposit undergoes thaw settlement and post thaw consolidation. To maximize the thaw depth, the released water is removed as quickly as possible. Drainage layers can be placed in the tailings deposit to enhance post thaw consolidation.

This paper presents an analytical and numerical solution to model thin layer freeze/thaw tailings deposits in the Fort McMurray regions of Alberta.

RESULTS AND DISCUSSION

Freezing thin layers analysis

A solution to a freezing problem in which fluid tailings initially is at a uniform temperature T_i that is higher than the phase change temperature T_o and for time $t > 0$ has its tailings surface maintained at T_s (below 0°C). The advancement of the freezing front is determined as (Hahn and Ozisik, 2012):

$$X(t) = 2\lambda(\kappa_f t)^{1/2} = \alpha_f t^{1/2} \quad (5)$$

where, $X(t)$ is the location of the freezing front relative to the surface at a time t , κ_f is the thermal diffusivity of frozen tailings, $\alpha_f = 2\lambda\kappa_f^{1/2}$ is the freezing rate parameter and λ is the solution of below equation:

$$f_1(\lambda) + f_2(\lambda) = f_3(\lambda) \quad (6)$$

where:

$$f_1(\lambda) = \frac{e^{-\lambda^2}}{\text{erf}(\lambda)}$$

$$f_2(\lambda) = \frac{k_u}{k_f} \left(\frac{\kappa_f}{\kappa_u} \right)^{1/2} \frac{T_o - T_i}{T_o - T_s} \frac{e^{-\lambda^2 \left(\frac{\kappa_f}{\kappa_u} \right)}}{\text{erfc} \left(\lambda \left(\frac{\kappa_f}{\kappa_u} \right)^{1/2} \right)}$$

$$f_3(\lambda) = \frac{\lambda L \sqrt{\pi}}{C_f (T_o - T_s)}$$

where: k_u and k_f are the thermal conductivity of thawed and frozen tailings respectively, a_u is the thermal diffusivity of thawed tailings, L and C_f are the contained latent heat of tailings and heat capacity of frozen tailings. Eqn. (6) can be solved numerically for λ . Table 1 shows the thermal properties used in below analyses.

Table 1. Thermal Properties Of Tailings

Parameter *	Value
Frozen thermal conductivity (W/(m K))	2.18
Thawed thermal conductivity (W/(m K))	1.05
Heat capacity of frozen tailings (MJ/(m ³ K))	2.10
Heat capacity of thawed tailings (MJ/(m ³ K))	3.80
Latent heat of water in frozen tailings (MJ/m ³)	268
Latent heat of water in thawed tailings (MJ/m ³)	235

* Frozen properties calculated based on 33 % solids content and 68 % solids content for thawed properties (Proskin, 1998).

Figure 3 shows that at a given surface temperature, the warmer T_i will result in smaller λ . As a result, smaller frozen thickness are achieved. At $T_s = -18^\circ\text{C}$ and $T_i = 50^\circ\text{C}$, the frozen thickness per day is 10 cm, whereas at $T_i = 10^\circ\text{C}$, the thickness increases to 14 cm, which is a 40 % increase. In addition, at a given T_i , the amount that can be frozen per day depends on the surface temperature. At $T_s = -18^\circ\text{C}$, the frozen thickness is 14 cm and it reduces to less than 8 cm at $T_s = -6^\circ\text{C}$ with $T_i = 10^\circ\text{C}$. This indicates that during the freezing period, the amount that can be frozen per day changes according with the current weather.

In the Figure 3, T_s varies between 0°C and -18°C . This surface temperature range corresponds to the average air temperature at Fort

McMurray between 1980 and 2010 with $n_t = 2.0$ and $n_f = 0.9$ (Figure 4). As shown in Figure 4, STI (Surface Thawing Index) at Fort McMurray is 2.4 x SFI (Surface Freezing Index) means that the weather at the site can thaw more than it can freeze under a single thick layer deposit. Therefore, to increase the frozen thickness placed during winter, the thin layer deposition should be utilized.

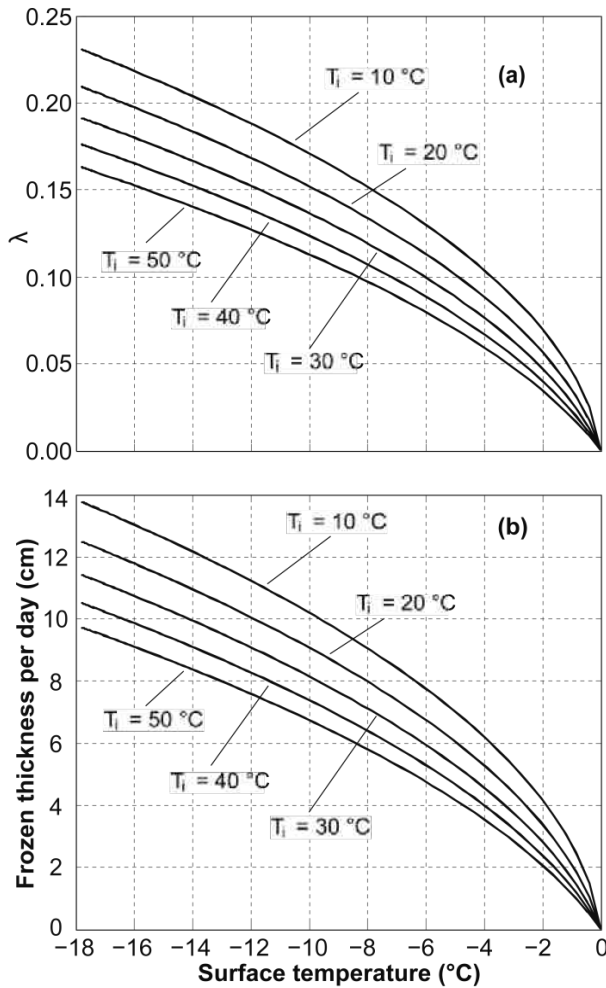


Figure 3. The evaluation of the values of λ and frozen thickness per day at various T_i and T_s .

Figure 5 shows the total tailings thickness can be frozen per year for different layer thicknesses and initial tailing placement temperatures. At $T_i = 10^\circ\text{C}$ and deposit layer thickness of 0.2 m, the total frozen thickness per year is 8.3 m, whereas at 1 m layer deposit the total frozen thickness is 1.8 m. The relation between the deposit layer thickness and the total frozen thickness is nonlinear.

However, at $T_i = 50^\circ\text{C}$ the total frozen thickness is 4.0 m at 0.2 deposit thickness and decreases to 0.9 m under a 1 m thick deposit.

Thawing analysis

Under thin layer deposition, more tailings can be frozen than can be thawed the following summer. Therefore, in order to achieve more thawed tailings, the surface water released during thawing needs to be removed immediately. Because without removing it, the surface water will become an insulation layer reducing the depth thawed. Upon thawing the previously frozen tailings undergoes thaw strain, δ . To integrate the thaw strain into the thawing analysis, δ is added into the equation determining λ or α_u , thawing rate parameter (Carslaw and Jaeger, 1959).

$$\lambda = \sqrt{\frac{C_u(T_s - T_o)}{2L(1 - \delta)}} \quad (7)$$

$$X(t) = 2\lambda(\kappa_u t)^{1/2} = \alpha_u t^{1/2}$$

where, C_u is the unfrozen specific heat capacity.

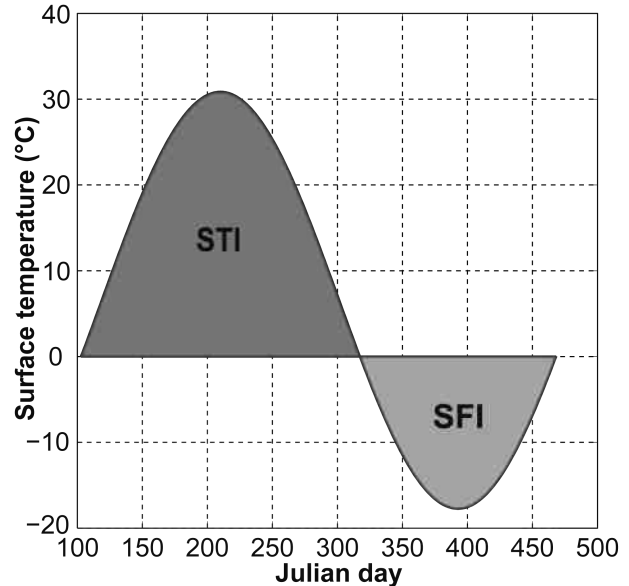


Figure 4. Calculated surface temperature at Fort McMurray, STI (surface thawing index) = $\Sigma(T_s t)$, $T_s > 0 = 4124.0^\circ\text{C-days}$ and SFI (surface freezing index) = $\Sigma(T_s t)$, $T_s < 0 = 1744.1^\circ\text{C-days}$.

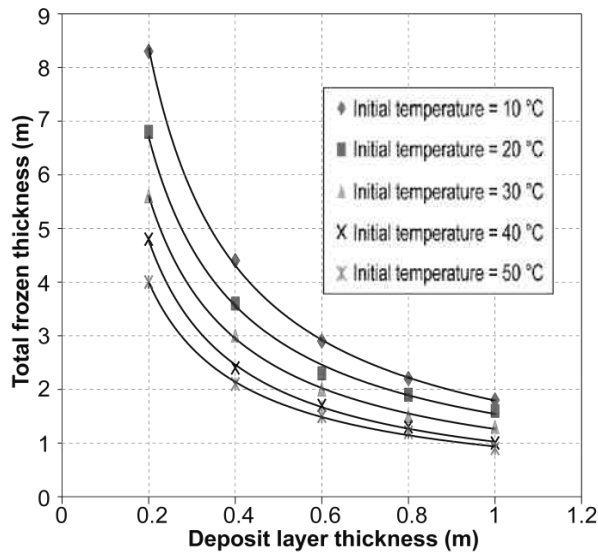


Figure 5. Total frozen thickness per year at various deposit layer thickness and initial tailings temperatures.

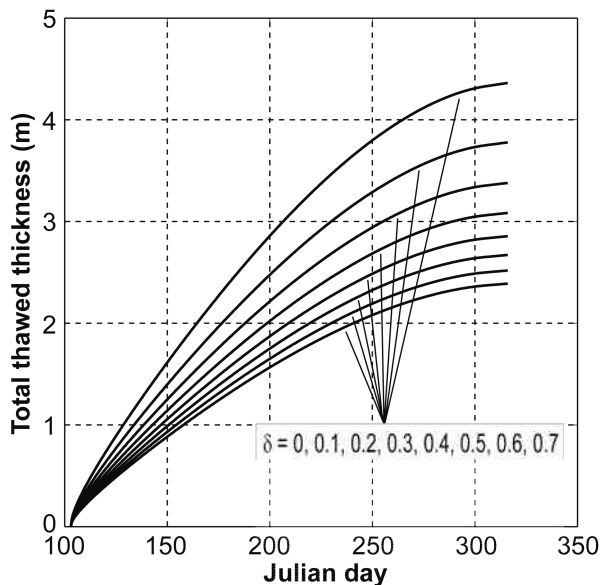


Figure 6. The total thawed thickness versus time at various thaw strains. The thawing period is from 103 to 316 days. Ground temperature at the base is 3 °C.

Thawing analysis in this section includes thawing from the top surface due to warm weather during summer and thawing from the base due to warm ground temperatures. Figure 6 shows that without thaw strain the total thawed depth is 2.4 m during the thawing period. However, at a thaw strain of 70 %, the thawed thickness increases to 4.4 m.

The actual total thawed thickness can be greater because consolidation during the thawing period is not taken into account in this calculation. For MFT with the initial solids content of 30 %, the thaw strain is about 43 % (Figure 2) therefore the thawed thickness is around 3.2 m.

To achieve greater thawing warm tailings can be deposited over the current frozen tailings thus increasing the thaw depth. If the warm tailings is 20 °C, the thawed thickness is 3.5 ($\delta = 0.5$). When the temperature of warm tailings is 50 °C, the thawed thickness is 5 m (Figure 7).

From the Figures 5, 6 and 7, it is easy to obtain larger frozen thickness using thin layers deposit (≤ 0.2 m) than the amount of tailings that will thaw during the summer when accounting for the thaw strain and even by placing warm tailings on the surface. Therefore, the amount of tailings deposited in thin layers is determined by the depth that can be thawed in summer.

Numerical analysis compared to analytical results

In this section, numerical solution of heat conduction was used with the parameters summarized in Table 1. As shown in Figure 5, the maximum frozen thickness of tailings placed at 50 °C is 4 m and this result is comparable to the numerical results shown in Figure 8. Tailings placed at a rate of 0.15 m/5 days with initial temperature of 50 °C and over the freezing period is 150 days are shown in Figure 8. The boundary condition at the base is insulated (no heat flux) and at the surface is subjected to the surface temperature of Figure 4. Figure 8 shows that at the end of the freezing period (Day 150) the ground temperature at base is around -10 °C. This cold ground temperature will cool the underlying soil foundation.

When the temperature of the tailings being placed reduces, the total frozen thickness increases (Figure 5). As indicated in Figure 9, the numerical result of frozen thickness is around 8 m for an placement tailings temperature of 10 °C. The ground temperature at the base is close 0 °C and colder near the middle with the ground temperature of -6 °C (Figure 9). Compared to temperatures within tailings as in Figure 8, the temperatures near the end of winter in this case is warmer.

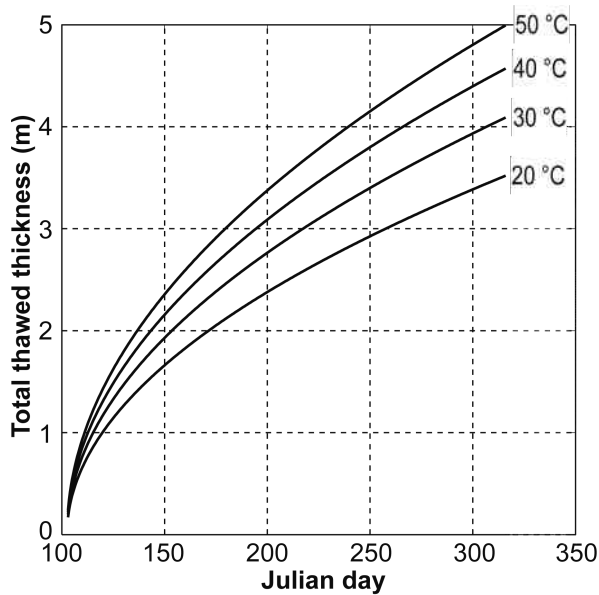


Figure 7. The total thawed thickness versus time at various warm temperatures and $\delta = 0.5$ and Ground temperature at the base of 3 °C.

Numerical analysis of a field test

Proskin (1998) conducted a comprehensive study of freeze/thaw technology, both under laboratory and field conditions with treated and untreated MFT. The field data in this section were reported by Proskin (1998). In the field tests, MFT from Suncor's tailings Pond 2 were chemically treated prior to, being deposited into three Ponds called Ponds 2A, 2B and 2C in which Ponds 2A and 2B were placed using thin layers. The total tailings placed in Pond 2B during the winter 1992/1993 was 1.73 m. There was a layer of 1 m sand at the base of the test Ponds to serve as a drainage system during the thawing period. During the winter 1992/1993, temperature at the bottom of the sand was around 3 °C and this was used as a boundary condition in the thermal modeling. The surface temperature used during the numerical runs was obtained by fitting a sinusoidal function fitted to the measured field surface temperature.

Figures 10 and 11 show that there is a discrepancy of ground temperatures between numerical and field results. However, the numerical results capture accurately the advance of the freezing and thawing fronts. The Figures also indicate the placed tailings completely frozen during the this period but the underlying sand remained above freezing.

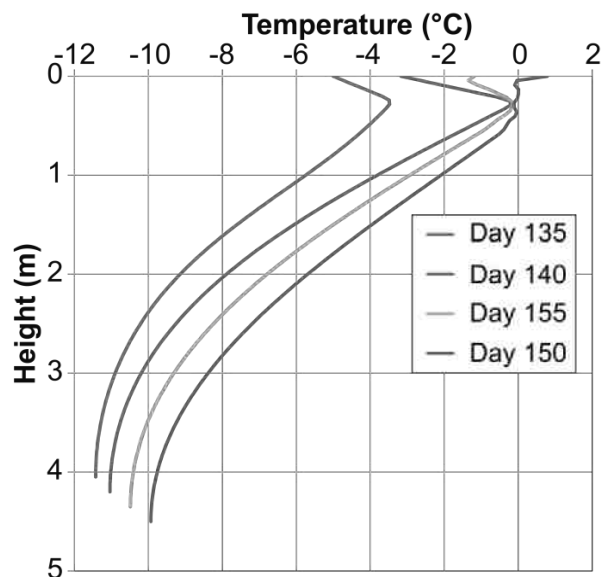


Figure 8. Numerical temperatures at an initial temperature of 50 °C.

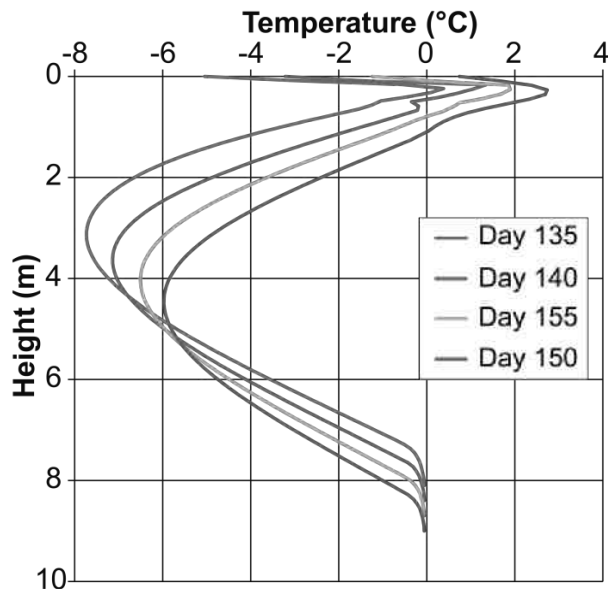


Figure 9. Numerical temperatures at an initial temperature of 10 °C.

Based on the field measured temperatures, Proskin (1998) determined the freezing rate parameter $\alpha_f = 3.9 \times 10^{-4} \text{ m/s}^{0.5}$. With $T_s = -9.4 \text{ °C}$ and $T_i = 15 \text{ °C}$, these values were interpolated from field data (Proskin, 1998), an analytical value of α_f , based on Figure 3a, is $3.3 \times 10^{-4} \text{ m/s}^{0.5}$. The thawing rate parameter of field data is $\alpha_u = 4.2 \times 10^{-4} \text{ m/s}^{0.5}$ (Proskin, 1998) meanwhile

based on Eqn. (7) with $\delta = 0$ and an average T_s of $4.7\text{ }^\circ\text{C}$, the value of $\alpha_u = 2.1 \times 10^{-4}\text{ m/s}^{0.5}$. Even at a high thaw strain of 0.7, the value of α_u is $3.7 \times 10^{-4}\text{ m/s}^{0.5}$ and it is still smaller than the field result, $4.2 \times 10^{-4}\text{ m/s}^{0.5}$.

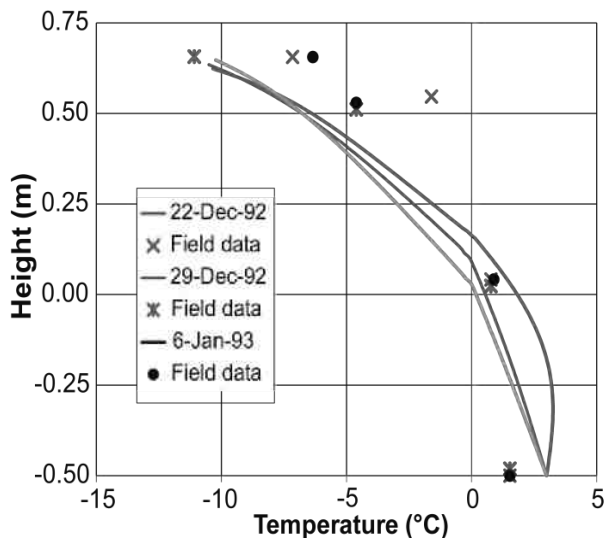


Figure 10. Numerical and field temperatures between Dec 22, 1992 and Jan 6, 1993 of Pond 2B

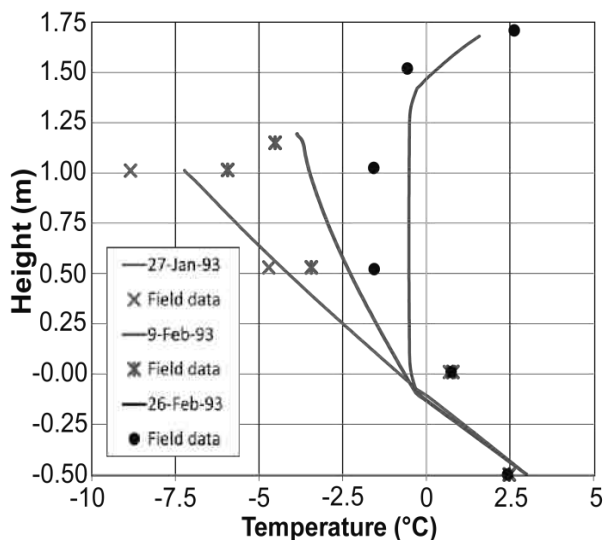


Figure 11. Numerical and field temperatures between Jan 27, 1993 and Feb 26, 1993 of Pond 2B

The field calculated freezingeing/thawing rate parameters are slightly larger than those

determined using tailings properties therefore, frozen/thawed depths in the field would be slightly larger. According to Proskin (1998), when the tailings was completely thawed, the thaw strain in the field deposit was 58 %. Using this thaw strain and surface temperature of Figure 4, the tailings thawed is 3.7 m.

In the field, by the end of July 1993, the ponds had thawed completely and an additional two months of warm weather was available for post-thaw consolidation and desiccation of the thawed tailings. The field solids content increased to 67.6 from the initial solids content of 35 %, which is a 93 % increase (Proskin, 1998). According to Figure 1, with the initial solids content of 35 %, the thawed solids content is 48.1 %, which is 38 % gain or 33 % by Proskin (1998). Therefore, there is about 55 % increase in solids content due to both post-thaw self-weight consolidation and desiccation (Proskin, 1998).

CONCLUSIONS

Managing of tailings is technically challenged and also constrained by the financial aspect. Among other techniques of dewatering tailings, freeze/thaw cycles can be a major tool in a region where the weather permits freeze and thaw of tailings as part of its management.

For a region like Fort McMurray, under thin layers ($\leq 0.2\text{ m}$) deposit the tailings thickness that can be frozen is greater than the amount that can be thawed within a year. Therefore, the amount that can be thawed is a controlled factor of the deposit thickness per year. To accelerate and increase the amount of tailings thawed, a warm tailings cap should be used.

Post thaw consolidation and desiccation are also an important factor to increase the solids content of thawed tailings.

ACKNOWLEDGEMENTS

The first author would like to thank NSERC for its financial support. The financial and technical support of Suncor during construction and operation of the 1992-93 field test utilizing thin layered freeze thaw is also recognized. Mr Bob Burns then of Suncor is thanked for his vision and support concerning "What freeze thaw could contribute to dewatering mature fine tailings".

REFERENCES

- Bale, B. R. (2007). *Freeze-Thaw Dewatering of Oil Sands Tailings As Part of a Natural Remediation Strategy*. Master thesis, University of Alberta.
- Beier, N. A. and Segó, D. C. (2009). Cyclic freeze-thaw to enhance the stability of coal tailings. *Cold Regions Science and Technology*, Volume 55, Issue 3, March 2009, Pages 278-285.
- Carslaw, H. S. and Jaeger J. C. (1959). *Conduction of heat in solids*. Oxford University Press, Oxford.
- Hahn, D. W. and Ozisik, M. N. (2012). *Heat Conduction*. John Wiley & Sons, Inc, New Jersey.
- Johnson, R., P., B., Allen, E., James, W., and Koverny, L. (1993). *Oil sands sludge dewatering by freeze-thaw and evapotranspiration*. Alberta Conservation and Reclamation Council, Reclamation Research Technical Advisory Committee.
- Proskin S. (1998). *A Geotechnical Investigation of Freeze-Thaw Dewatering of Oil Sands Fine Tailings*. PhD thesis, University of Alberta.
- Segó, D. C., and Dawson, R. F. (1992a). *Freeze-thaw dewatering of OSLO cold water process fine tails*. Submitted to Imperial Oil Resources Canada Ltd., 76p.
- Segó, D. C., and Dawson, R. F. (1992b). *Influence of freeze-thaw on behaviour of oil sand fine tails*. Submitted to Alberta Oil Sands Technology and Research Authority, 77p.
- Zhang, Y. (2012). *Laboratory Study of Freeze-Thaw Dewatering of Albian Mature Fine Tailings (MFT)*. Master thesis, University of Alberta.

MODELLING OF HYDRAULIC SAND CAPPING ON CREEPING ULTRA-SOFT TAILINGS

Lars Beuth¹, Chris Dykstra² and Walter Jacobs²

¹Deltares, the Netherlands

²Royal Boskalis Westminster NV, the Netherlands

ABSTRACT

Worldwide, large inventories of ultra-soft tailings are accumulating in hundreds of active ponds. Reclaiming these ponds is difficult due to their large scale and the low strength of their filling.

State-of-the-art floating dredging equipment allows to carefully install subsequent thin sand layers on top of soft sediment. It provides a practical and proven technology for the subaqueous construction of a sand cap of several meters which renders a stable platform for further reclamation and reforestation. Such sand capping may be a promising, safe and cost-efficient technology for reclaiming tailings ponds.

However, the bearing capacity of ultra-soft tailings remains even after decades of consolidation lower than typically encountered in geotechnical engineering. Assessing the potential of sand capping is therefore not straightforward.

The deposition of sand layers renders a gradual increase of tailings strength due to near-surface consolidation. In view of the low strength of tailings, this increase requires special attention when assessing the feasibility of sand capping.

In this paper, the authors put forward a novel approach for assessing the feasibility of sand capping taking into account this strength increase. A numerical study on near-surface consolidation due to sand cap installation is presented. Here, the modeling of creep is taken into account. The significance of creep to the consolidation process of the tailings considered in this paper has been shown in experimental work. Strength profiles are derived from numerical results for installation phases of the sand cap. These can be used as input for comprehensive stability analyses of the entire sand cap installation process to assess its feasibility.

INTRODUCTION

With hydraulic sand capping sand is rained onto submerged mud from a floating device in a controlled and adaptive manner to gradually form a thick layer of sand on top. Figure 1 shows such a floating device in operation. This procedure proved in numerous projects worldwide to be a practical, efficient and safe technique to cover and isolate contaminated material and for large-scale land reclamation (Jacobs et al, 2012). Application to oil sands tailings seems self-evident were it not for the extremely low strength of this almost liquid material of less than 1 [kN/m²].

The first and second author recently presented a numerical study on the deposition of a thin sand layer onto tailings using the Material Point Method (Vermeer et al. 2013). The gradual deposition of a submerged sand ridge and of a circular heap of sand onto tailings, as it may occur during hydraulic sand capping, has been simulated. An elastic-plastic material model using the Tresca yield criterion has been used to model tailings under undrained conditions. An estimated constant undrained shear strength profile s_u increasing linearly with depth by 500 [N/m²] per meter from a value of 100 [N/m²] at the mud line has been specified for the tailings. These analyses allow estimating for the considered strength profile the slope inclination and layer thickness at which failure occurs. They also provide estimates of the spatial extend of the failure.

Figure 2 shows the predicted failure mechanisms for the two problems. Only a slice of the plane-strain symmetrical problem, axisymmetric problem respectively, has been discretized. The heightening of the thin sloping sand layer has been modeled by the application of an increasing distributed load. Shallow failure mechanisms reaching not deeper than 50 [cm] are obtained. For the sand ridge, failure occurs at a slope inclination of 1:8 and a sand layer thickness of 18 [cm], for the heap at a maximum inclination of 1:7 and a sand layer thickness of 22 [cm].



Figure 1. Computer-controlled spreader pontoon in shallow water. A sand-water mixture is distributed by a chute to form a sand cap for land reclamation.

Such stability analyses can be extended to the installation process of successive sand layers for a comprehensive feasibility study of sand capping. This requires taking into account the increase of undrained shear strength due to near-surface consolidation. Once a sand cap is partially in place, it creates excess pore pressures and subsequent consolidation of the tailings. This implies an increase of effective stresses and subsequently of the tailings strength.

Such a strength increase can be taken into account in the proposed stability analyses by updating strength profiles for the respective installation stages from analyses of near-surface consolidation.

Consolidation of tailings is a complex process as observed at the Canadian University of Alberta during an outstanding long-term consolidation test (Pollock 1988, Suthaker 1995, Jeeravipoolvarn 2009, Scott et al. 2013). In this experimental study, self-weight consolidation of Mature Fine Tailings (MFT) taken from the Athabasca oil sands region was monitored in a 10 meters standpipe over a period of 30 years. Due to its low permeability, consolidation under self-weight or under an applied sand cap happens very slowly rendering only a slow increase of effective stresses with time. Creep-induced excess pore pressures were found to have a significant impact on this process (Jeeravipoolvarn, 2005) and thus the generation of strength.

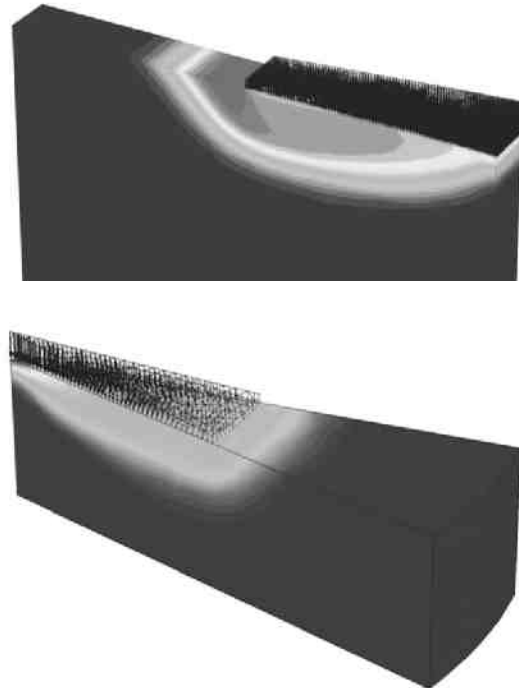


Figure 2. Relative magnitude of velocities at failure of a sand ridge (top) and a sand heap (bottom) on top of ultra-soft tailings material.

Predicting the development of tailings strength with numerical methods therefore requires advanced modeling of the tailings material. Recent work by the authors proved that the Soft-Soil-Creep model (SSC model) developed by the second author and published amongst others in Leoni et al. (2008) is able to capture the complex mechanical behavior of MFT extremely well. Its application to MFT has been successfully validated by back-calculating the long-term settlements observed in the standpipe test at University of Alberta (Vermeer et al., 2015).

Now, the SSC model has been applied by the authors to the simulation of creep-consolidation due to hydraulic sand capping on MFT for an exemplary staged cap installation. The one-dimensional case of placing layers of sand onto tailings has been considered. The Finite Element Method (FEM) has been used for this analysis. Strength profiles were derived from results. Their application in stability analyses still remains to be done.

In the following Section 2, the modeling of creep with the SSC model will be briefly described. The performed analysis of creep-consolidation due to

sand capping is presented in Section 3. The increase of strength beneath the sand cap is treated in Section 4. The paper ends with conclusions on the performed work and an outlook on future work.

MODELLING OF CREEP

The considered analysis involves only small one-dimensional deformations of tailings. The following brief description is therefore constricted to this simple instance. The reader is referred to Leoni et al. (2008) for further information on the modelling of creep including its formulation for large-deformation and 3D analyses with the SSC model. The total strain rate is decomposed into an elastic component and an irreversible, time-dependent strain rate component to take into account creep, expressed in the following in terms of void ratio e

$$\dot{e} = \dot{e}^e + \dot{e}^c \quad (1)$$

A dot over a symbol implies differentiation with respect to time. The first term, the elastic change of void ratio \dot{e}^e , is formulated as

$$\dot{e}^e = -\frac{C_s}{\ln 10} \frac{\dot{\sigma}'}{\sigma'} \quad (2)$$

where σ' denotes effective stress. C_s is the swelling index which describes the response of soil to recompression. The second term \dot{e}^c represents the time-dependent plastic deformation of soil. It can be written as

$$\dot{e}^c = \frac{\dot{e}_{nc}^c}{OCR^\beta} \quad \text{with} \quad \beta = \frac{C_c - C_s}{C_\alpha} \quad (3)$$

and

$$\dot{e}_{nc}^c = -\frac{C_\alpha}{\ln 10} \frac{1}{\tau} \quad (4)$$

Here, OCR denotes the overconsolidation ratio defined as

$$OCR = \frac{\sigma_p}{\sigma'} \quad (5)$$

where σ_p is the preconsolidation stress, the highest effective stress under which a soil probe has previously consolidated. \dot{e}_{nc}^c denotes the rate of creep observed in oedometer tests for normally consolidated soil, i.e. soil with a stress state of $OCR = 1$. C_c and C_α are the well-known compression index, secondary compression index

(creep index) respectively. τ denotes a reference time.

Figure 3 shows the response of soft soil to a change of effective stress as applied in oedometer tests, illustrating the terms mentioned above. It includes depiction of a soil state above the normal consolidation line (NC-line) with $OCR < 1$ which occurs if a normally consolidated soil is further loaded and then left to consolidate and creep.

The red line exemplifies creep deformation from a state of $OCR < 1$ to an overconsolidated state of $OCR > 1$.

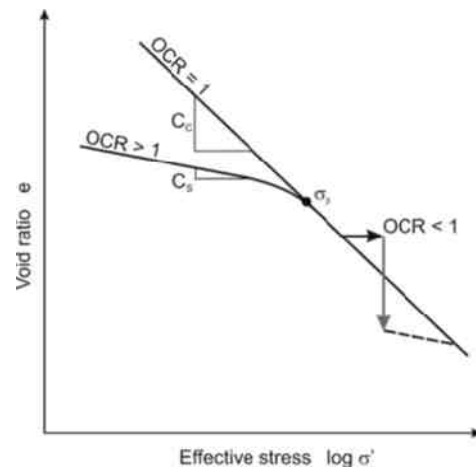


Figure 3. Response of soft soil to compression as measured in oedometer tests, plotted on a semilogarithmic basis.

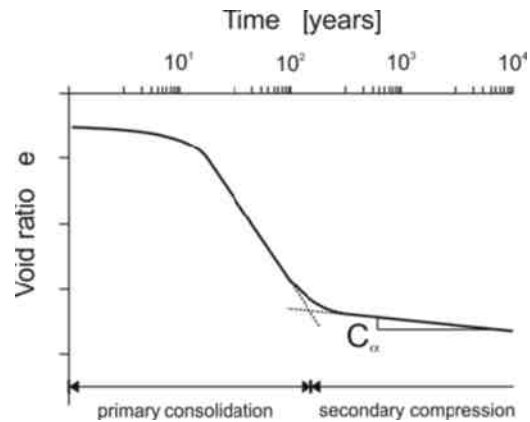


Figure 4. Time-dependent compaction of soft soil, plotted on a semilogarithmic basis.

The dashed line indicates the increase of σ_p due to creep deformation as observed in experiments and predicted by the SSC model. With increasing preconsolidation stress, OCR increases which leads according to Equation 3 to a significant decrease of the creep rate. In contrast, for the case of $OCR < 1$ Equation 3 renders a very high creep rate.

Figure 4 shows the change of void ratio with time typical for a soil subjected to normal compression. Once excess pore pressures dissipated largely out of the soil sample (primary consolidation phase), creep described by C_α dominates the soil deformation (secondary compression).

Typical values for C_c , C_s and C_α for clay are $C_c \approx 0.15$ with $C_s = C_c/10$ and $C_\alpha = C_c/30$. This renders for β a typical value of 27.

With the performed analysis values of $C_c = 2.3$, $C_s = 0.288$ and $C_\alpha = 0.115$ are used. These have been determined on the basis of published laboratory test results on MFT taken from the Athabasca oil sands region, specifically the material used in the Alberta standpipe test, as reported in Vermeer et al. (2015). With these values $\beta = 17.5$ is obtained.

The reference time τ depends on the determination of the NC-line. When based on an oedometer test with daily doubling of the load, it takes a value of 1 day. This value has been used with the performed analysis, though this choice might require further consideration for the case of MFT (Vermeer et al., 2015).

CREEP-CONSOLIDATION DURING SAND CAP INSTALLATION

In order to illustrate the increase of effective stresses and thus strength in time beneath deposited sand layers, the authors considered the staged installation of a particular sand cap. The following deposition scheme was assumed. The submerged unit weight of the sand was assumed to be $10 \text{ [kN/m}^3\text{]}$, so that a meter of sand yields additional stresses of $10 \text{ [kN/m}^2\text{]}$.

- 1a instantaneous deposition of 0.1 [m] of sand, i.e. extra stress of $1 \text{ [kN/m}^2\text{]}$ at mud line
- 1b consolidation period of 2 months

- 2a instantaneous deposition of another 0.2 [m] of sand, i.e. in total $3 \text{ [kN/m}^2\text{]}$
- 2b another consolidation period of 2 months
- 3a instantaneous deposition of another 0.3 [m] of sand, i.e. in total $6 \text{ [kN/m}^2\text{]}$
- 3b another consolidation period of 2 months
- 4a instantaneous deposition of another 0.4 [m] of sand, i.e. in total $10 \text{ [kN/m}^2\text{]}$
- 4b consolidation period of 6 months

This implies that 1 [m] of sand is deposited in an operational season of 6 months followed by a relatively long (winter) period of 6 months of consolidation.

With the used FE software (Plaxis 2D Version 2012) loads were applied instantaneously at the beginning of a capping phase in a first undrained analysis. For each capping phase, a consolidation analysis was performed subsequently with the respective above mentioned periods of time using the SSC model. With the used consolidation formulation, displacements of the solid phase and the pore fluid pressures are used as basic variables (Shiomi and Zienkiewicz, 1984).

Depositions of the considered MFT are young and creep densification has hardly occurred. As a consequence, the bulk density is low with values in the range between $1,250$ and $1,350 \text{ [kg/m}^3\text{]}$. Effective initial stresses in such a light-weight material are obviously low and as a consequence it features low strength. In this study it is assumed that initial excess pore pressures are zero. For the initial state of the tailings, a unit saturated weight and unit water weight of

$$\gamma_{\text{sat}}^0 = 12.31 \text{ [kN/m}^3\text{]} \text{ and } \gamma_w = 9.81 \text{ [kN/m}^3\text{]}$$

has been adopted so that the initial vertical stress is found to be

$$\sigma'_0 = (\gamma_{\text{sat}}^0 - \gamma_w) \cdot z = 2.5 \text{ [kN/m}^3\text{]} \cdot z \quad (6)$$

at least for the assumed initial hydrostatic pore pressures.

Considering a grain density of $2,220 \text{ [kg/m}^3\text{]}$ of the tailings material based on data provided by Scott et al. (2013), an initial void ratio e_0 of 4 is obtained. In this preliminary simplified analysis this initial void ratio is used as constant with depth.

As a consequence of sand capping, the void ratio will decrease and so will the permeability k . This is taken into account according to the equation

$$\log\left(\frac{k}{k_0}\right) = \frac{e-e_0}{c_k} \quad (7)$$

with a permeability variation coefficient c_k of 1.5 and an initial permeability of $k_0 = 5 \cdot 10^{-3}$ [m/day] for $e_0 = 4$. These values render a good fit with published data on the change of permeability of MFT by amongst others Pollock (1988) and Jeeravipoolvarn (2005).

The initial overconsolidation ratio OCR_0 is also assumed to be constant with depth. A relatively large value of 1.5 has been chosen. It has been obtained from a preliminary check analysis of the filling process of a typical tailings pond. The assumption of a constant OCR_0 is felt to be more appropriate than the one on the void ratio.

The assumption of fully saturated tailings with incompressible pore water implies that the load of an applied sand layer is instantaneously fully carried by the pore water. This implies an undrained Poisson's ratio ν_u of 0.5. With the used FE software $\nu_u = 0.499$ has been inputted for numerical reasons. In combination with a chosen effective one of $\nu' = 0.35$ this implies that 97 % of the load is initially taken by the pore water, see Vermeer et al. (2015) for further details.

All parameters of the analysis are listed in Table 1. The considered initial state and material parameters of the MFT represent estimates and the performed analysis is a preliminary study. In order to assess the feasibility of sand capping for a particular pond, numerical analyses would have to be complemented by field measurements.

Being interested in the effect of a short period of consolidation due to sand capping (in total 1 year), there is no need to model the MFT over the full depth of a pond. Indeed, a short period of consolidation will only affect tailings just underneath the sand cap. In the present analysis, a depth of 2 m is considered.

Figure 5 shows the applied mesh and its dimensions. High gradients of excess pore pressure and effective stress are expected at the top draining mesh boundary and this requires a rather fine mesh just below the mud line. 15-noded triangular elements were used. Mesh refinement analyses confirmed that the chosen mesh is

sufficiently fine to reproduce stresses near the top surface with appropriate accuracy.

Table 1. Model and state parameters.

Density		
Initial saturated unit weight	γ_{sat}^0	12.31 [kN/m ³]
Unit weight of water	γ_w	9.81 [kN/m ³]
Initial void ratio	e_0	4
Permeability		
Initial Darcy permeability	k_0	$5 \cdot 10^{-3}$ [m/day]
Permeability variation coefficient	c_k	1.5
Deformability		
Compression index	C_c	2.3
Swelling index	C_s	0.288
Creep index	C_ϵ	0.115
Effective Poisson's ratio ν'	ν'	0.35
Undrained Poisson's ratio	ν_u	0.499
Stress initialisation		
Initial OCR	OCR^0	1.5

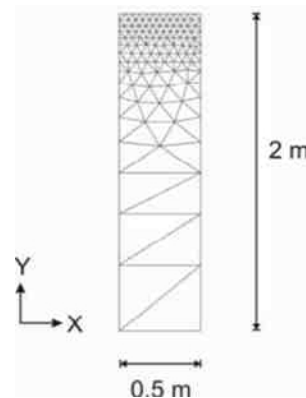


Figure 5. Discretization of 1D hydraulic sand capping analysis.

Figure 6 shows the change of effective stress for the upper 50 cm of the tailings column as pore water dissipates out of the tailings. After capping phase 1 an effective stress of 0.83 [kPa] is obtained at the mud line and after capping phase 2 an effective stress of 2.4 [kPa]. This computational output is reasonable, as the theoretical values are 1 and 3 [kPa] respectively.

Figure 7 shows the volume change in the upper 1 [m] of the tailings in the course of the considered 12 months period. The total settlement of the mud line is 7.6 [cm], being largely due to compaction of the top 30 [cm]. In this zone the final average strain is about 20 per cent. The thickness of this zone is thus reduced from 30 to 24 [cm]. The top 10 [cm] undergoes a total average compaction of about 30 per cent. The thickness of this zone thus reduces from 10 to 7 [cm]. This implies that the void ratio reduces to about 2.7. Equation 7 renders that the permeability reduces to 10^{-4} [m/day]. This is only 2 per cent of the initial permeability.

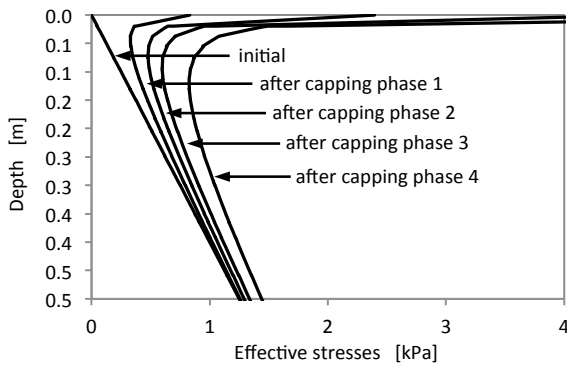


Figure 6. Computed effective stresses for deposition stages.

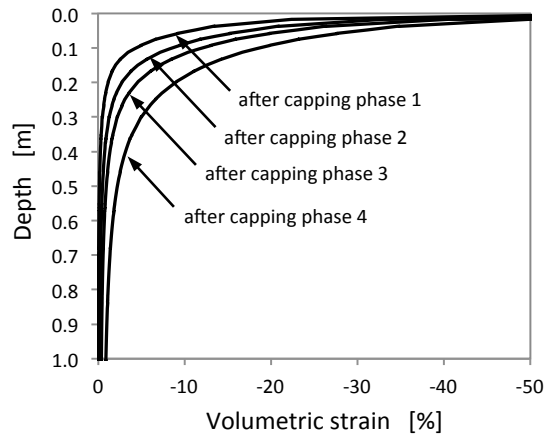


Figure 7. Volumetric strain at the end of the respective consolidation phases of the installed 4 lifts, close-up on the upper half of the considered tailings column.

Figure 8 shows the development of OCR for the four capping phases. A red line indicates OCR at the very beginning, i.e. at the end of the previous phase. Blue lines indicate values a week later and black lines values at the end of a capping phase.

In order to understand Figure 8, we will consider the state of the tailings directly at the mud line of phase 2, being easier to illustrate than for the initial situation. At the mud line, the effective stress is initially 0.83 [kPa] and with OCR^0 equal to 1.27, σ_{p0} is 1.06 [kPa].

The more or less instantaneous deposition of the first sand causes an abrupt increase of the effective stress from 0.83 [kPa] to 2.4 [kPa]. In contrast, σ_p is not changing abruptly as it is linked to the void ratio which can only change gradually with time. The abrupt increase of the effective stress causes an abrupt decrease of OCR, a sudden change from 1.27 to a value of 0.44.

This extremely low value will cause a high creep rate at and directly below the mud line, being associated with densification and a gradual increase of both the pre-consolidation stress and OCR. The latter is also observed in the computational results for OCR, as can be seen in Figure 8. Indeed, after 1 week of consolidation OCR exceeds again 1.0 and after 2 months it is again beyond 1.3. This is observed for all four stages of capping.

INCREASE OF MFT STRENGTH

According to Jamiolkowski et al. (1985), the undrained shear strength s_u of soft soil relates to the effective stress by

$$s_u \approx 0.23 \sigma' \quad (8)$$

Figure 9 shows the effective stresses at the beginning of the respective cap installation phases considered in the previous section. For stability analyses of sand capping it is proposed to take into consideration a simplified increase of strength due to near-surface consolidation by assuming a constant shear strength in an upper layer whose s_u -value and thickness are adjusted for each cap installation phase. The red lines in Figure 9 indicate such alternative stress profiles. The black solid lines indicate effective stress profiles for the respective phases without near-surface consolidation.

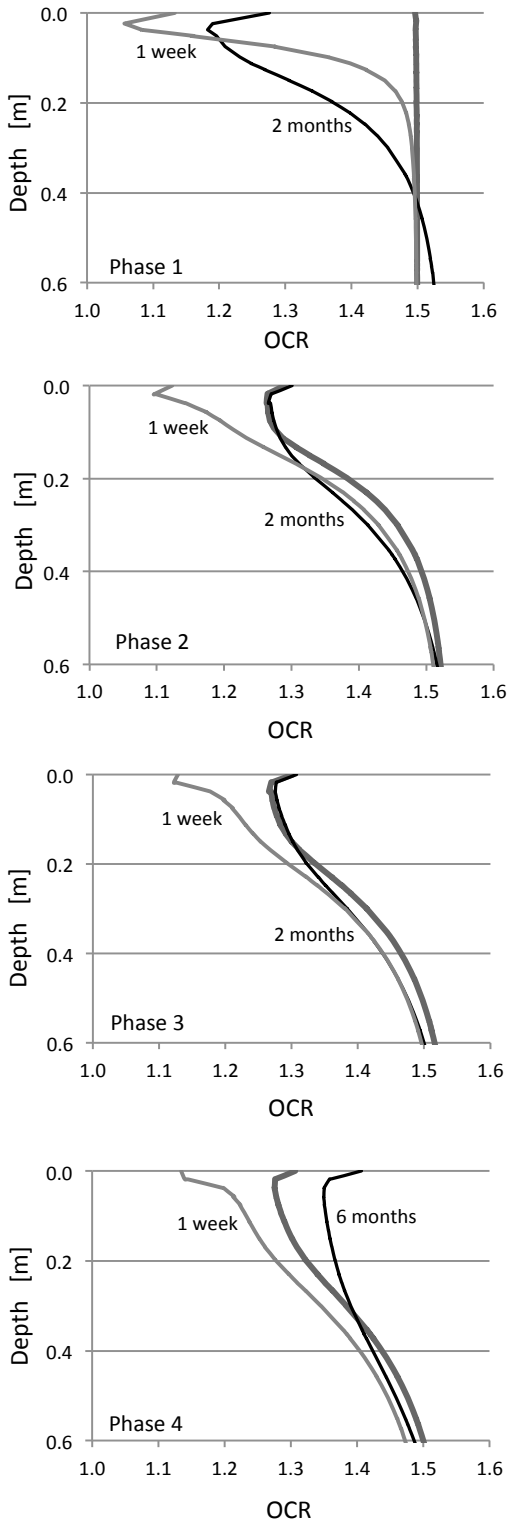


Figure 8. Development of OCR for capping phases 1 to 4 from top to bottom.

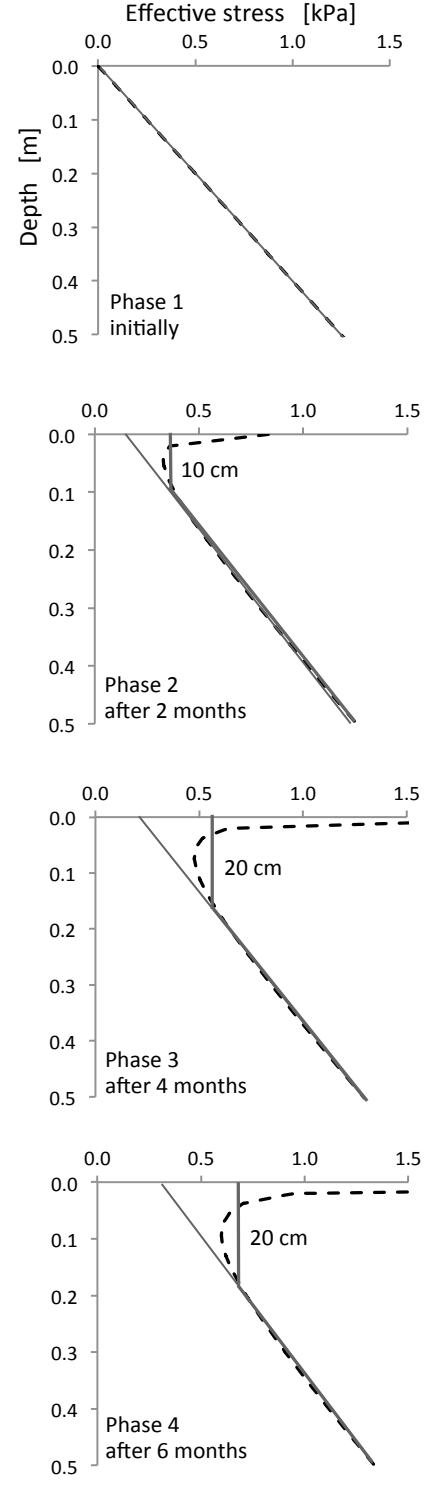


Figure 9. Computed effective stresses at the beginning of the first four deposition stages; proposed stress distributions for determination of strength profiles.

Equation 8 implies zero initial strength at the mud line. However, measurements show that some initial shear strength is often available at the tailings surface. Therefore, the more general equation

$$s_u \approx s_{u,top} + 0.23 \sigma' \quad (9)$$

is proposed for estimating the initial tailings strength profile from effective stresses.

CONCLUSIONS

A Finite Element consolidation analysis has been performed of Mature Fine Tailings subjected to the layered installation of a sand cap. The Soft-Soil-Creep model has been used for the modelling of the MFT. This analysis was done to derive strength profiles for cap installation stages. Results show a considerable increase of the undrained shear strength within a thin layer beneath the sand cap for the considered material properties, initial conditions and cap installation scheme.

Previously, the uneven deposition of a thin sand layer on tailings has been studied numerically (Vermeer et al. 2013). This study allowed quantifying the maximum slope of a sand ridge and sand heap before failure occurs for the considered strength profile.

This contribution allows the extension of these previous analyses to the deposition of sand onto an installed sand layer taking into account a strength profile adjusted for near-surface consolidation.

The presented methodology allows a comprehensive assessment of the feasibility of sand capping for a typical oil sands tailings pond. This remains yet to be done. The performed analyses can be relatively easily adapted to specific ponds. In order to apply this methodology, a good data basis on tailings material properties has to be available. This includes density and strength profiles as well as the over-consolidation state of the tailings. Cone penetration testing could provide such information. However, special attention must be paid on the accuracy of this test in order to derive from it typical low tailings strength profiles.

Analyses might be refined through consideration of large deformations to take into account the

stabilising effect of tailings deformations during sand deposition.

Current research at Deltares aims at modelling state transitions in assemblies of solid particles with the Material Point Method. This will enable the investigation of erosion-type transitions of a soil into a sediment suspension and inversely sedimentation-type transitions followed by consolidation. It would allow for an even more comprehensive study of sand cap installation.

Furthermore, laboratory experiments for quantification of the sand penetration along the mud line as well as of the thixotropic strength gain of tailings would be of great benefit to further studies. The employment of vertical drains in advance of sand capping would be another interesting subject of study.

ACKNOWLEDGEMENTS

The authors would like to thank Paul Bonnier from Plaxis B.V. for kindly contributing with his expert advice to the research efforts leading to this publication.

REFERENCES

- Garlanger, J.E. 1972. The consolidation of soils exhibiting creep under constant effective stress. *Géotechnique*, **22(1)**: 71-78.
- Jacobs, W., Dykstra, C., Van Kesteren, W. 2012. In Situ Hydraulic Capping of Soft Tailings. Proceedings of the International Oil Sands Tailings Conference, Edmonton.
- Jeeravipoolvarn, S. 2005. Compression Behaviour of Thixotropic Oil Sands Tailings. PhD thesis, Department of Civil Engineering, University of Alberta.
- Jeeravipoolvarn, S., Scott, J.D., Chalaturnyk, R.J. 2009. 10 m standpipe tests on oil sands tailings: long-term experimental results and prediction. *Canadian Geotechnical Journal*, **46**: 875-888.
- Leoni, M., Karstunen, M., Vermeer, P.A. 2008. Anisotropic creep model for soft soils. *Géotechnique*, **58(3)**: 215-226.

Pollock, G.W. 1988. Large strain consolidation of oil sand tailings sludge. PhD thesis, Department of Civil Engineering, University of Alberta.

Scott, J.D., Kabwe, L.K., Wilson, G.W., Sorta, A. 2013. Properties which affect the consolidation behavior of mature fine tailings. Proceedings of the Seventeenth International Conference on Tailings and Mine Waste, University of Alberta.

Shiomi, T., Zienkiewicz, O.C. 1984. Dynamic behavior of saturated porous media; the generalized Biot formulation and its numerical solution. *International Journal for Numerical and Analytical Methods in Geomechanics*, **8**, 71-96.

Suthaker, N.N. 1995. Geotechnics of oil sand fine tailings. PhD thesis, Department of Civil Engineering, University of Alberta.

Vermeer, P.A., Więckowski, Z., Sittoni, L., Beuth, L. 2013. Modeling soil-fluid and fluid-soil transitions with applications to tailings. Proceedings of the Seventeenth International Conference on Tailing and Mine Waste, University of Alberta.

Vermeer, P.A., Dykstra, C., Jacobs, W., Beuth, L. 2015. Creep-Consolidation Analyses of Alberta Mature Fine Tailings. Prepared for publication.

Session 4

Tailings Dewatering I

FEASIBILITY OF SAND FARMING TO DEWATER COARSE SAND TAILINGS

Jason Stianson¹, Rashid Bashir¹, Delwyn Fredlund¹, Andy Nguyen², Les Sawatsky², Ward Wilson³ and Scott Martens⁴

¹Golder Associates Ltd., Saskatoon, SK., Canada.

²Golder Associates Ltd., Calgary, AB., Canada.

³University of Alberta, Edmonton, AB., Canada,

⁴Shell Canada Energy, Calgary, AB, Canada

ABSTRACT

The paper describes a project conducted to determine the effectiveness of sand farming planned at the Shell Canada Muskeg River Mine (MRM) site to dewater coarse tailings sand (CST) for use as a backfill material. Work included laboratory testing and a numerical modelling program to assess the feasibility of sand farming as well as detailed design of a test cell for proving the analysis at field scale. The sand farming concept considered the construction of a dedicated sand farming area, cycles of hydraulic placement of CST layers, periods of gravity drainage and evaporative drying, followed by excavation and transport of the CST after adequate dewatering. The feasibility of the sand farming operation was evaluated based on a need to dewater a 4 metre vertical thickness of CST each month during non-freezing conditions to a geotechnical water content of 9% or less.

The saturated hydraulic conductivity and water storage characteristics of the CST was measured through a program of grain size analysis, Soil-water characteristic curves (SWCC), and saturated hydraulic conductivity testing. A series of one metre column and evaporative tray tests were conducted to provide direct measurements of CST drainage, evaporation, and test instrumentation. Numerical modelling was conducted to assess the feasibility of sand farming at a field scale. The numerical analyses considered a number of variables that influence the water balance of CST deposits including hydraulic properties, gravity drainage, evaporation, precipitation, and deposit thickness. A field-scale test area comprising two test cells was designed to verify the analytical predictions.

INTRODUCTION

A study was conducted to determine the feasibility of farming Coarse Sand Tailings, CST, planned for the Shell Canada Muskeg River Mine (MRM) site.

Bench scale column and tray tests were used to evaluate a number of variables considered to be influential with respect to the feasibility of sand farming activities.

Column and Tray Testing was used to:

- Identify the primary CST dewatering mechanism between gravity drainage and evaporation;
- Determine the effect of CST particle size distribution (PSD) variability, coarse or fine, on gravity drainage and evaporation;
- Determine the effect of CST density variability on gravity drainage and evaporation;
- Recommend whether compacting the material would enhance dewatering; and,
- Recommend whether ploughing the CST would be expected to significantly increase the removal of water through evaporation.

A modelling program was used to assess the feasibility of sand farming at a field scale including CST deposits in the order of 4 m thick, exposed to site atmospheric conditions (i.e., evaporation and precipitation). The modelling provided a means of linking the dewatering behaviour measured in the column and tray testing to the anticipated performance in the field.

TAILINGS PROPERTIES

A total of 56 CST samples were collected from various locations around the perimeter of Cell 10 of

the External Tailings Facility to capture the potential variability of the CST material to be farmed.

The first sampling campaign was conducted on May 11, 2013 and consisted of 36 pails of CST, each 2.5 gallons, collected from a conventional beach discharge point within Cell 10. Eighteen pails were collected from a location approximately 20 m downstream of a discharge point, while another eighteen pails were collected from a location about 70 m downstream of the discharge point. The field crew noted that the samples were taken directly from the stream bed, and based on visual inspection were judged to be representative of the CST.

A second sampling program was conducted on June 19, 2013 to collect twenty additional 2.5 gallon pails of sample. The samples were collected from two different locations approximately 15 to 20 m from the edge of the pond. Ten pails were taken from each of two locations.

Index Properties

Figure 1 shows a range of particle size distribution (PSD) measurements on samples from the CST beach. The data includes a wide range of historical measurements, coarse and fine column testing sample groups, and representative Sample A, Sample B, and Sample C used for modelling purposes.

The historical PSD measurements show the variation of the CST material over several years of deposition. By visual inspection of the historical PSD data, three representative samples were selected for initial modelling purpose including Sample A (average CST), Sample B (fine CST), and Sample C (Finest CST). Statistical data provided later showed that the PSD for Sample A was similar to the mean of the historical PSD measurements, that Sample B was a conservative estimate of fine CST that could be encountered during farming, and that Sample C was

unrealistically fine and could be assigned a lower priority for modelling purposes. The presented field scale modelling results are based on Sample B properties. Sample B is finer than the material used in the column study and provides a level of the conservatism in the field predictions of dewatering performance.

The 56 pail samples were divided into two main groups and mixed to produce larger samples of coarse and fine CST for column testing. Sieve and hydrometer tests were performed on the mixed samples and the results are shown in Figure 1 including a group of coarser samples used for columns 1 and 2 and a group of finer samples used for columns 3, 4, and 5. Material from the coarse and fine column samples were used to further characterize the hydraulic properties of the CST including saturated permeability and soil water characteristic curve measurements.

The column testing program considered the potential variation in the CST by using coarse and fine samples deposited under different conditions to achieve either a low or a high density sample. The low density range was selected to be in the order of 1,500 kg/m³ and the high density range was selected to be in the order of 1,800 kg/m³.

Saturated-Unsaturated Flow Properties

Saturated hydraulic conductivity measurements were made for the selected samples using the falling head method. The samples were compacted near the low and high density targets. The saturated hydraulic conductivity for the coarse sample was 4.0x10⁻⁴ m/s for the low density sample and 1.5x10⁻⁴ m/s for the high density sample. The saturated hydraulic conductivity for the fine sample was 7.3x10⁻⁵ m/s for the low density sample and 4.3x10⁻⁵ m/s for the high density sample. The saturated hydraulic conductivity of Sample B was measured to be 4.0x10⁻⁵ m/s and was lower than all of the other CST used for column testing.

Table 1. Summary of Saturated Hydraulic Conductivity Measurements

Type	Low Density	High Density
Coarse CST	4.0x10 ⁻⁴ m/s	1.5x10 ⁻⁴ m/s
Fine CST	7.3x10 ⁻⁵ m/s	4.3x10 ⁻⁵ m/s
Sample B	4.0x10 ⁻⁵ m/s	-

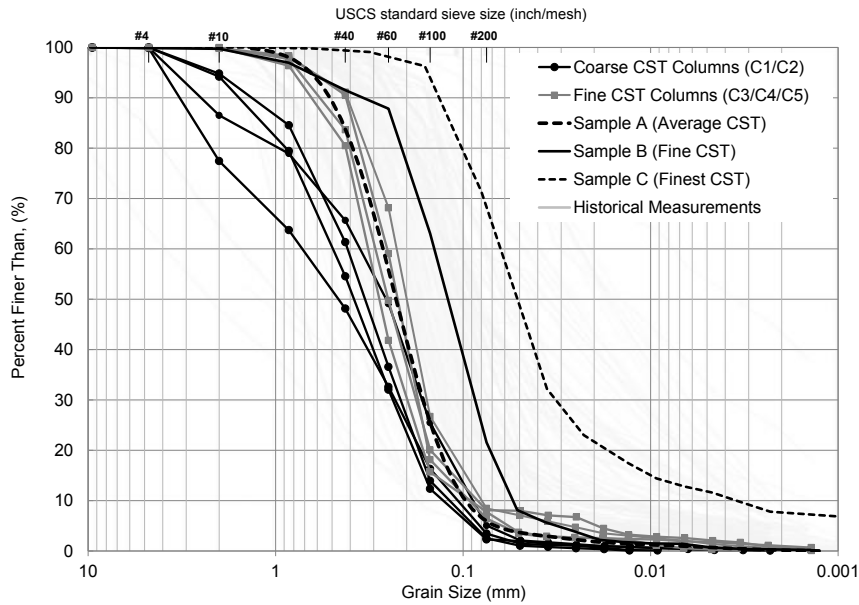


Figure 1. PSD of coarse and fine column testing sample groups, Sample A, Sample B and Sample C modelling curves, and the range of historical PSD measurements on samples from the CST beach.

Soil-water characteristic curves were measured on CST samples compacted to similar low and high densities ranges as described for the saturated hydraulic conductivity testing. The results are shown in Figure 2. The Fredlund and Xing (1994) fit to the experimental data is also shown. The following observations can be made from the test results; i) the effect of density on water storage and retention properties was minimal for the coarse samples, ii) the high density resulted in less saturated storage and higher retention at higher suction values for the fine samples.

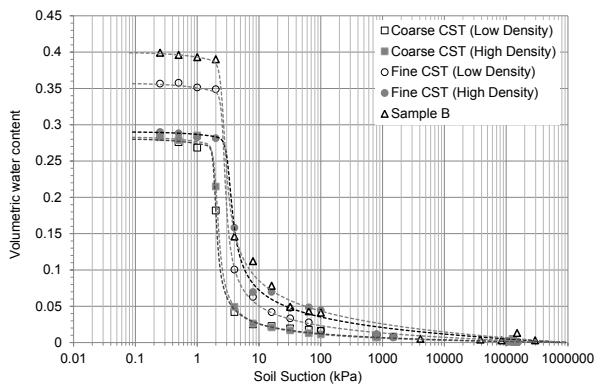


Figure 2. SWCC measurements for the coarse and fine samples placed at low and high densities.

The Fredlund et al., (1994) procedure was used to estimate the unsaturated permeability functions using the saturated coefficients of permeability and the SWCC. This allowed for the calculation of five permeability functions corresponding to the low and high densities of the samples as shown in Figure 3.

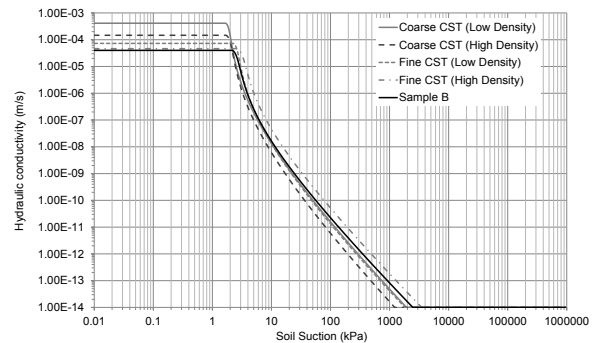


Figure 3. Permeability functions for coarse and fine samples compacted at low and high densities.

COLUMN AND TRAY TESTING

Initial estimates by Shell suggested that the sand farming operation may be feasible if a 4 m profile

of CST could be dewatered to 9% gravimetric water content within a one month time frame. A column and tray testing program was initiated as a method to test the feasibility of dewatering the CST at a bench scale, through measurements made on a series of 1 m columns and larger surface area trays.

Column Testing

Figure 4 shows an example of one of the columns used in the testing program. The test columns were approximately 1 m tall with a diameter of 15.2 cm (6"). The columns had ports at regular vertical spacing to facilitate taking tensiometer readings at the end of the test. The PSDs for samples used in testing are shown in Figure along with the PSDs used for later modelling scenarios.

The column testing program considered the variability of the CST by using coarse and fine samples deposited as low or a high density material. Different placement procedures were adopted to achieve sample densities. In some cases, CST was deposited under saturated conditions and allowed to settle through a column of process water (i.e., process water was maintained 5 cm to 10 cm deep as the CST was placed). In other cases, the material was deposited essentially dry and loose or at a nominal water content and compacted. The CST was saturated from the bottom to the top with process water and dewatered by gravity drainage and evaporation. The top of the columns remained uncovered to allow evaporation and ports near the bottom of the column were used to collect drainage (Figure 4)

Mass Balance Measurements

A mass balance was maintained by recording the water content of CST samples prior to placement, the weight of moist CST added to the column, and the weight of process water added to the column. The mass balance and known volume of the CST layer were used to calculate the initial conditions of the as-placed CST.

In some cases, a process water pond approximately 1 cm deep was added above the final surface of the CST at the end of deposition. The process water pond allowed the rate of potential evaporation to be measured by recording the change in weight of the column as the pond evaporated. The rate of potential evaporation was subsequently compared to the measured rate of actual evaporation as the CST was dewatered.



Figure 4. Column test apparatus

Gravity drainage was initiated after the pond of water evaporated and the process water was at the surface of the CST. Drainage and evaporation continued until the system reached pseudo steady-state conditions where drainage stopped and the change in the column weight was negligible.

The water loss due to drainage and evaporation from Column 1 (i.e., the coarse high density sample) were monitored over a period of 14 days until the readings indicated that dewatering had essentially stopped (Figure 7). The dewatering records indicated that 43% of the initial process water was removed from the column; 41% as a result drainage and 2% as a result of actual evaporation. The majority of the drainage, (i.e., approximately 86%), occurred in the first two days of the test.

A comparison of the water balance records from the column tests is presented in Table 2. The dewatering records were similar for all the tests in that the majority of water was removed by gravity drainage and that most of the drainage was collected over the first two days of the test.

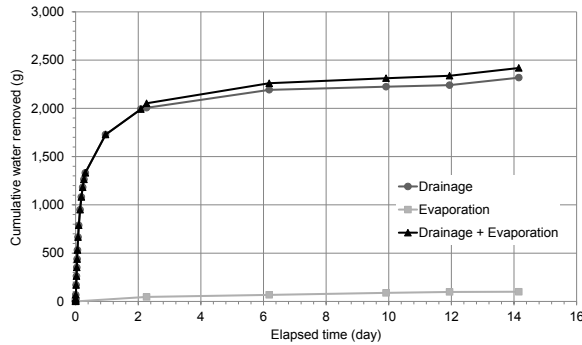


Figure 5. Column water balance in Column 1 for the coarse high density Oil Sands tailings

Suction Profile Measurements

After drainage was complete, matric suction measurements were taken along the profile of the sample by inserting a tensiometer through ports spaced vertically at 5 cm increments along the column. The matric suction measurements were later paired with the gravimetric water content measurements taken at the same elevation. The combined pairs of matric suction and gravimetric water content measurements represent the Soil-water characteristic curve, SWCC, for the CST placed in the column. The SWCCs measured from the columns were compared with the SWCC measurements made using a Pressure Plate apparatus. The final water content profiles were measured on sub-samples of CST as the material was excavated from the column at the end of the test.

The suction profile measured at the end of the Column 1 test is presented in Figure 6. The matric suction measurements lie close to the hydrostatic line, which increases from a suction of 0 kPa at the level of the water table to approximately 9.81 kPa at an elevation of 1 m above the water table. The matric suctions are slightly less than the hydrostatic line between elevations 50 cm and 80 cm indicating that additional water would likely be released if the column was left to drain for

a longer period of time. The matric suction measurements are higher than the hydrostatic conditions over a depth of approximately 5 cm at the top of the column due to evaporation. The matric suction measured at a depth 4.5 cm was approximately 12 kPa and increased above 100 kPa at a depth near 1.5 cm.

The final water content profiles measured at the end of the column tests are presented in Figure 7. The water content of the CST remained near saturated levels to an elevation near 30 cm above the water table. The sharp reduction in water content at an elevation of 30 cm indicates that the air-entry value, AEV, of the CST is approximately 3 kPa. The water content was reduced below 9% over a depth ranging from of 40 cm to 80 cm.

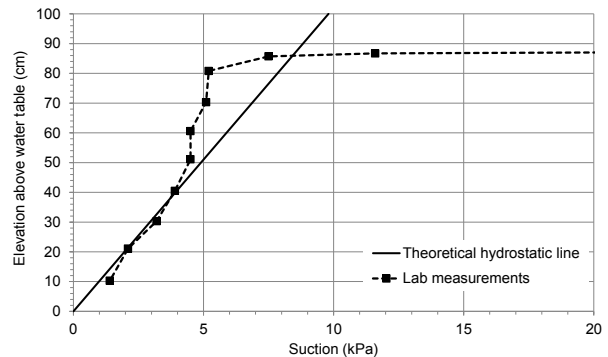


Figure 6. Column 1 matric suction measurements

The thickness of the zone with a water content greater than 9% at the base of the column (i.e., above the water table) is related to the AEV value of the material and will be similar for any thickness of CST deposit. In other words, a thicker field deposit of CST would be expected to drain to a water content less than 9% over the majority of the profile with a saturated (or sacrificial) zone about 0.5 m thick remaining at the base of the deposit.

Table 2. Water Balance Comparison from the column tests.

Test	Density (kg/m ³)	Gravity Drainage (%)	Evaporation (%)	Total (%)
C1 (Coarse)	1,777	41%	2%	43%
C2 (Coarse)	1,514	59%	2%	61%
C3 (Fine)	1,613	36%	4%	40%
C5 (Fine)	1,726	30%	5%	35%

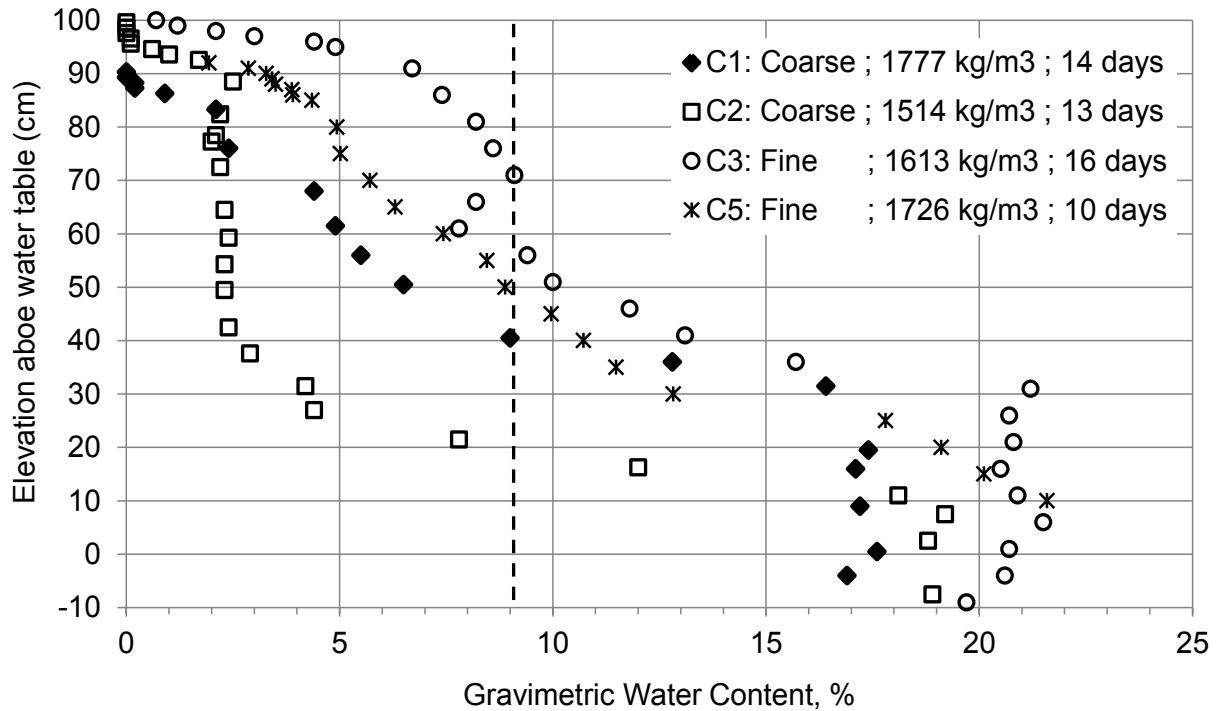


Figure 7. Water content profiles measured at the end of the column tests

Comparison of SWCC from Pressure Plate and Column Tests

The SWCC measured from the column test (i.e., matric suction and water content measurements) can be compared to the SWCC independently measured in the Pressure Plate apparatus. A reasonable comparison between the two SWCCs provides evidence that tensiometers can be used as a tool to determine when a field deposit has achieved a sufficient amount of drainage and could be excavated. The results for the coarse low density column 2 are shown in Figure 8.

There was close agreement between the two sets of results confirming that the handheld tensiometer provided reasonable matric suction measurements. The AEV of the CST is below 2 kPa in both cases. The slope of the SWCCs are steep indicating that the material desaturates with a relatively small increases in matric suction. Residual water content conditions are reached near a matric suction of 3 kPa. The comparison shows that tensiometer measurements greater

than 2 kPa could be used to confirm that the CST had drained to a gravimetric water content less than 9%. A similar approach could be developed to monitor CST deposits in the field.

Tray Evaporation Tests

Tray testing was used to observe evaporation performance over a larger surface area as opposed to the column test surface area. The trays were about 33 cm long by 26 cm wide and 20 cm deep providing a CST surface area equal to approximately 870 cm² compared to the 180 cm² for the columns.

Evaporation was expected to proceed at a faster rate near the beginning of the test when the surface of the CST was saturated. The evaporation rate was then anticipated to slow at some point when the surface of the CST became unsaturated. Similar to the column testing program, different CST placement procedures were used to produce different density materials for the coarse and fine samples of CST.

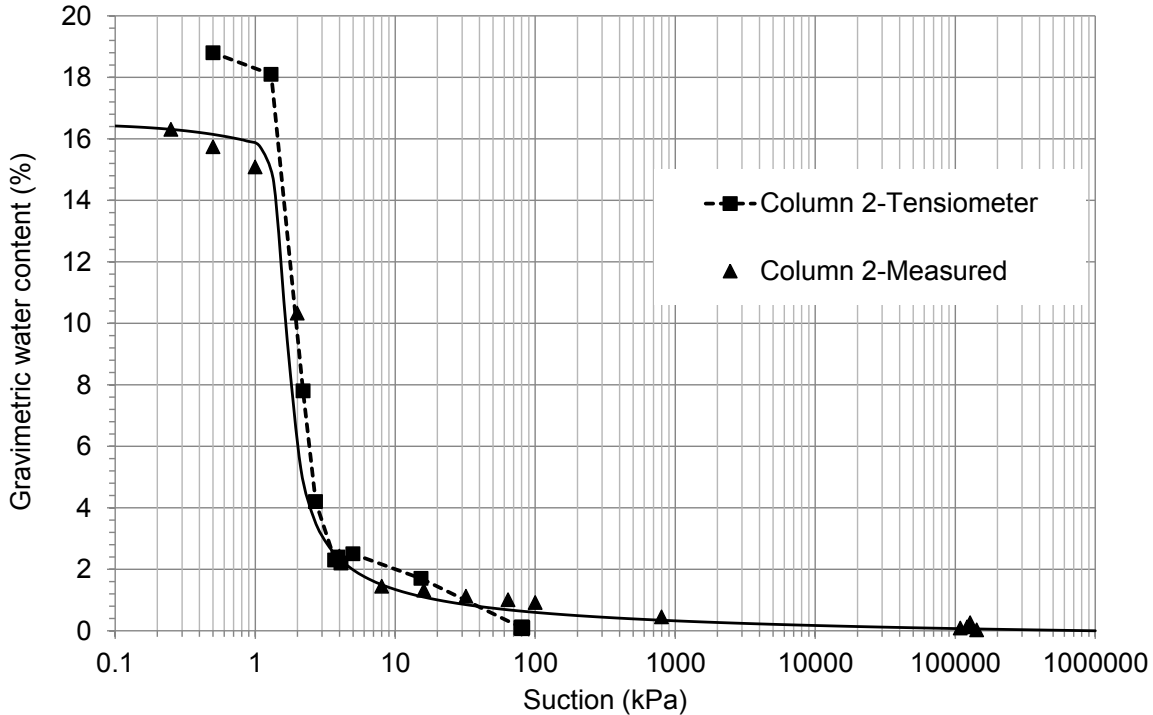


Figure 8. SWCC Comparison of SWCC measured in Pressure Plate and Column 2 test.

A pond of process water, approximately 1 cm deep, was added above the CST surface to observe the relationship between the time when water was no longer visible at the surface and any change in the evaporation rate. The evaporation performance was determined by measuring the change in weight of each tray at regular time increments. The cumulative amount of process water evaporated from each tray over the duration of the testing of all trays is presented in Figure 9.

The evaporation rate for the trays began to decrease after a period of 30 and 40 days. As an example, the evaporation rate reduced from 1.6 mm/day to 0.3 mm/day for Tray 1. In comparison, the average evaporation rate from a process water surface was measured to be 2.6 mm/day from the column tests.

The process water pond on top of the tailings was no longer visible after 14 days for Tray 1 and 8 days for Tray 2. The high initial rates of evaporation continued even after the process water ponds evaporated from sight. The evaporation rate would likely be higher in the field due to wind and solar radiation. While the rate of evaporation in the field would initially be higher, the rate of evaporation should quickly be reduced to

below 1 mm/day. The tray and column testing both showed that relatively small amounts of process water would be removed from the CST by evaporation.

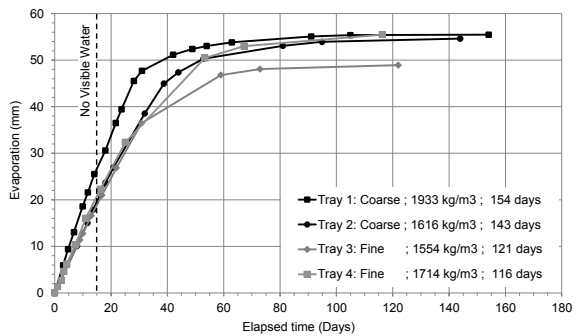


Figure 9. Tray Evaporation Measurements

Column and Tray Testing Summary

The observations from the column and tray testing can be divided into sections related to the primary objectives of the program; namely, observing the drainage performance between coarse and fine CST, low density and high density CST, and the relative roles of evaporation and drainage.

The following results pertain to coarse and fine CST:

- A comparison of the water content profiles from the column tests shows that the coarse material dewatered to lower water contents than that observed for the finer CST. However, both coarse and fine CST were dewatered below the target water content of 9%.
- The AEV CST, (i.e., 2 kPa to 3 kPa), were similar. for the coarse CST, (i.e., 1 kPa to 3 kPa), and finer
- Most dewatering appeared to be complete within two days for the coarse and fine CST.

The following results pertain to low and high density CST:

- The coarse low density column dewatered to a lower water content than the coarse high density column. The effect of density seemed less distinguishable when comparing the columns with finer CST.
- Most drainage appeared to occur within two days, and this result was independent of the amount of water that needed to be drained. In other words, it did not matter that more water needed to be drained from the lower density material, and less water needed to be drained from the higher density material.
- The amount of gravity drainage seems to indicate that there would be little benefit achieved in compacting the material during the sand farming operation.

The following results pertain to the evaporation and drainage process:

- Drainage was shown to be the primary dewatering mechanism with evaporation contributing less than 5% of the overall amount of water removed from the columns.
- The increase in matric suction near the top of the column results in a similar decrease in the coefficient of permeability of the CST. The reduced permeability explains why water loss due to evaporation is of little significance in the field.
- The nominal amount of water removed through evaporation and the mechanism contributing to the shutdown of evaporation vitiates the use of ploughing to increase the rate of evaporation, and overall dewatering of the CST.

MODELLING FIELD CONDITIONS

The primary objective of the modelling program was to assess the feasibility of sand farming at a field scale including CST deposits in the order of 4 m thick, exposed to site atmospheric conditions (i.e., evaporation and precipitation). The modelling provides a means of linking the dewatering behaviour measured in the column and tray testing to the anticipated performance in the field. Similar to the column testing, modelling scenarios were selected to evaluate a set of variables considered to be the most influential with respect to the feasibility of sand farming activities. The specific variables considered in the analysis are listed below.

- Dewatering performance of CST layers in the order of 4 m thick;
- Confirm the primary CST dewatering mechanism associated with gravity drainage and evaporation;
- The effect of site specific climatic boundary conditions on infiltration, evaporation and drainage characteristic of the CST materials; and
- Conservative CST hydraulic properties based on Sample B material (i.e., finer CST with lower hydraulic conductivity than the material used in the column tests.).

The simulated water loss from 4 m and 10 m thick CST profiles is presented in Figure 10. Both profiles drained below the desired void space thresholds in less than 5 days and reached a near steady-state condition after approximately 20 days. In other words, the fluctuations in the amount of stored water as a result of precipitation or further drainage were minimal after a period of 20 days. The results suggest that the favourable drainage conditions observed in the column tests are not diminished by the longer drainage path in a 4 m or 10 m thick CST profile.

Figure 11 shows the water balance results for the 4 m thick CST profile exposed to average climatic conditions over an extended period of time (i.e., longer than 30 days to show the environmental effects). Deep percolation (DP) represents the amount of water drained from the base of the profile, Actual Evaporation (AE) is the total amount of water evaporated from the surface of the CST, and net infiltration (NI) is the net amount of water entering or leaving the surface of the profile

considering both precipitation (P) and AE (i.e., $NI = P - AE$, where a positive NI value indicates that more water is entering the surface from precipitation that is being removed by AE.).

removed from AE in all cases. For “Average Drying” conditions, it appeared that AE was enough to counter the effects of precipitation resulting in near zero net infiltration. The results demonstrate the primary role of gravity drainage versus evaporative drying.

The amount of water removed by drainage significantly exceeded the amount of water

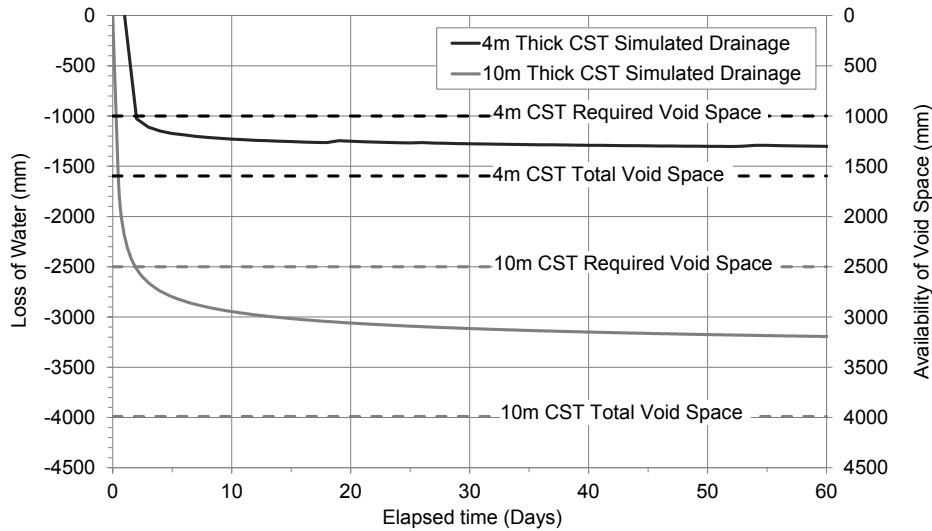


Figure 10. Simulated Dewatering Performance for 4 m and 10 m thick CST Profiles With Sample B Properties.

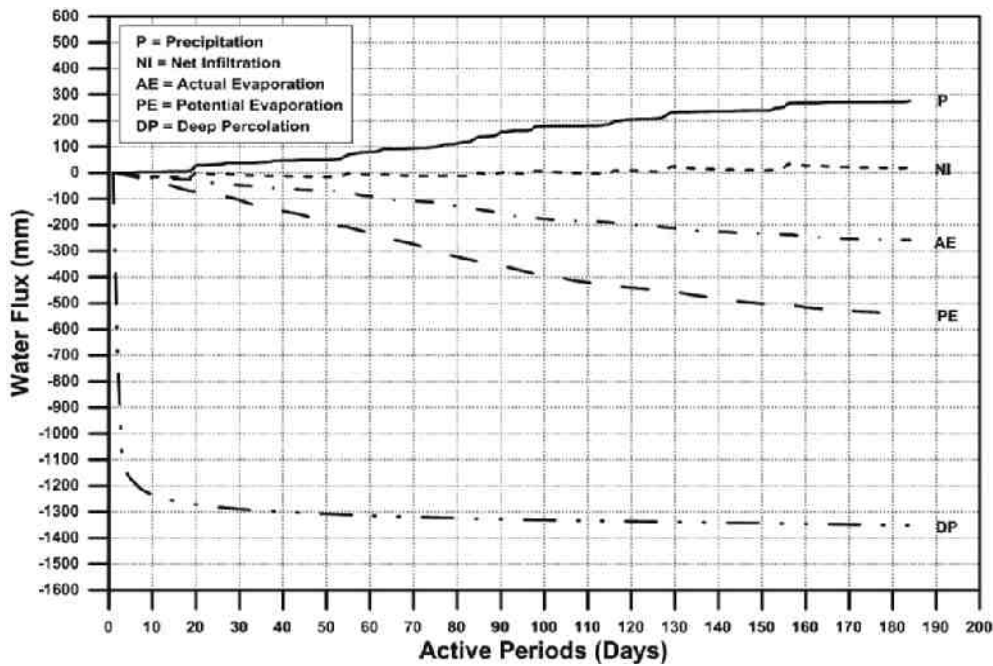


Figure 11. Water balance for a 4m CST profile with three different climate boundaries.

CONCLUSIONS

The study showed that the CST can be dewatered at a sufficient rate to result in a feasible sand farming operation. The observations are based on direct measurements conducted on a set of bench scale column and tray tests, and scale up modelling results for 4 m and 10 m thick profiles of CST. The following conclusions provide a summary of the main outcomes of the study.

- The water content along the majority of the CST profile was reduced below 9% based on measurements on CST columns excavated after 10 to 16 days. Drainage records showed that most of the water drained from the columns in as little as 2 days.
- The elevation of saturated CST above the water table is related to the AEV of the CST and does not change as the thickness of the CST is increased. The thickness of the saturated fringe is expected to remain at approximately 50 cm for full scale CST deposits near 4 m thick (or thicker).
- The similarities between Column and Pressure Plate apparatus SWCCs suggest that field instrumentation should provide a reasonable indication of the SWCC for the as-placed sand farming deposit and can be used to indicate when drainage of the deposit is complete.

- The modelling results demonstrated the feasibility of sand farming using a conservative set of soil properties representative of the finest sand farming material. Sensitivity simulations showed that the dewatering performance was maintained for CST deposits between 1 m and 10 m thick and for the range of climatic conditions at the site.
- Column tests and modelling scenarios showed that gravity drainage is the primary dewatering mechanism.
- Ploughing, densification of the upper CST surface, or other means to enhance actual evaporation is expected not to have a significant effect on the dewatering process.

REFERENCES

- Fredlund, D.G., and Xing, A. 1994. Equations for the soil-water characteristic curve. *Canadian Geotechnical Journal*, 31: 533-546.
- Fredlund, D.G., Xing, A., and Huang, S. 1994. Predicting the permeability function for unsaturated soils using the soil-water characteristic curve. *Geotechnical Journal*, 31(3): 521-532.

CENTRIFUGAL MODELLING OF OIL SANDS TAILINGS CONSOLIDATION

Amarebh R. Sorta, David C. Seago and G. Ward Wilson
Department of Civil and Environmental Engineering, University of Alberta, Edmonton, Canada

ABSTRACT

The self-weight consolidation of oil sands tailings are modelled using a new geotechnical beam centrifuge located at the University of Alberta (GeoREF centrifuge). The centrifuge is used to create prototype effective stress regime in the model and to reduce the consolidation time. Large strain consolidation parameters are derived from centrifuge tests and the centrifuge scaling laws and repeatability of centrifuge tests are evaluated. Interface settlement, void ratio profiles and excess pore pressure dissipation are monitored in-flight during the centrifuge tests. The paper describes the modelling aspect, the instrumentation and monitoring of the centrifuge tests. The centrifuge results are presented, discussed and compared with large strain numerical model and large strain consolidation tests.

INTRODUCTION

Millions of cubic meters of extraction tailings are produced annually as a by-product of bitumen extraction from oil sands ore in northern Alberta. Upon deposition of the tailings, the coarse portion (sand) of the extraction tailings segregates and forms beaches and is used to construct containment dykes. The fines particles are highly dispersed during the extraction process, and during the tailings deposition, flow to a large fluid containment to form fluid fine tailings (FFT). FFT have generally a very slow rate of consolidation and create numerous environmental and geotechnical challenges.

The long-term behaviour of untreated and treated tailings needs to be determined to evaluate the performance of different tailings treatments and disposal options. Large- and small-scale settling column tests, field pilot tests, and mathematical models based on laboratory-derived soil parameters are commonly used to study the sedimentation/consolidation behavior of FFT or fines-sand mixture tailings. However, the use of these conventional testing methods is inadequate

not only because of stress dissimilarities between laboratory tests and field conditions, but also because of the extended testing time required to complete the tests, owing to the slow dewatering behavior of FFT. The use of pilot field tests is limited by the cost and the length of time required obtaining long-term experimental results. The numerical approaches depend on a consolidation test that requires many weeks/months to produce inputs for the numerical model. Furthermore, the models are highly sensitive to the consolidation parameters and need long-term prototype scale experimental results for modelling verification.

In this paper, the self-weight consolidation of oil sands tailings is investigated using centrifuge modelling. A centrifuge is used in order to reproduce prototype (field) stress conditions in model tests and to simulate consolidation phenomena that may take many years under field conditions but only a few hours in a centrifuge run. The centrifuge testing technique is also used here to derive material constitutive relations in a shorter time than is needed for conventional testing method. The study also aims to verify the centrifuge modelling application for high water content materials.

CENTRIFUGE AND CENTRIFUGE MODELLING PRINCIPLE

Geotechnical centrifuge testing involves the study of gravity-dependent geotechnical events using small-scale models subjected to acceleration fields that are many times Earth's gravitational acceleration (g). Centrifuge testing is most suitable for geotechnical structures in which gravity is a primary driving force, such as natural and man-made slopes, retaining structures, buried structures, underground excavation, self-weight consolidation, and groundwater contaminant migration.

Soil has nonlinear mechanical properties that are dependent on effective stress and stress history, and thus it is important to maintain the same stress in model tests as in the prototype. Centrifuge

testing is carried out to maintain the same self-weight stress in soil and its modelling principle is based on stress similarity between prototype and model. In the centrifuge test, the model of size (1/N) of the prototype and with the same material as a prototype is used. Prototype self-weight stress is achieved by the application of a centrifugal acceleration N times Earth's gravitational acceleration on the model placed at the end of a centrifuge arm, thereby achieving stress similarity between prototype and model. Figure 1 illustrates the centrifuge modelling principle.

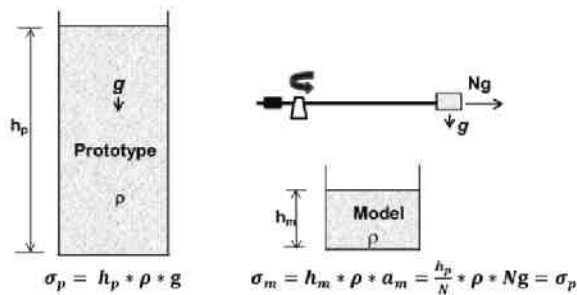


Figure 1. Schematic representation of centrifuge modelling principle, modified from Taylor (1995)

CENTRIFUGE SCALING LAW

The centrifuge modelling technique has theoretically derived and some experimentally proved scaling laws that can be used to relate model and prototype. Table 1 summarizes the scaling law between a prototype and a model in centrifuge modelling.

Equation 1 shows the time-scaling relationships between a model and a prototype during the consolidation process. The time-scaling relation was derived without using any specific consolidation theory (Cargill & Ko, 1983; Croce et al., 1985) and is based on a theory that accounts for large deformation (Eckert et al., 1996; Bloomquist, 1982).

$$t_m = \frac{t_p}{N^2} \quad [1]$$

where t_m is elapsed time in the model, t_p is elapsed time in the prototype for an equal degree of consolidation as in the model, and N is the ratio of centrifugal acceleration to Earth's gravitational acceleration or the ratio height of the prototype to the height of model.

Equation 1 implies that the consolidation process that may take many years in a prototype can be simulated in a few hours using a centrifuge. For example, consolidation that may take 55 years in a prototype can be modeled in 2-days continuous centrifuge flight, if the centrifuge is set to run at 100g. This reduction in testing time is one of the main advantages of using centrifuge to study the consolidation behaviour of oil sands tailings.

Table 1. Scaling relations between model and prototype

Quantity	Prototype	Model
Length	N	1
Area	N ²	1
Acceleration	1	N
Weight force	N ²	1
Mass	N ³	1
Stress	1	1
Strain	1	1
Mass density	1	1
Darcy flow rate	1	N
Hydraulic conductivity	1	N
Time (consolidation)	N ²	1
Time (creep)	1	1

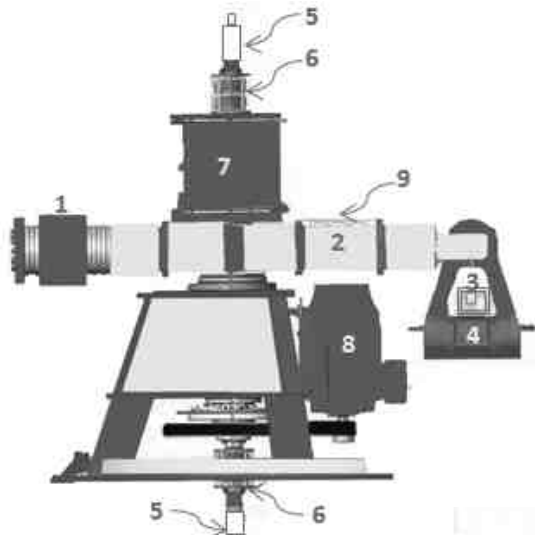
Like other soil testing techniques, centrifugal model testing has limitations. It is important to take these into consideration when modelling and interpreting the test data. Some of the limitations includes: (1) the actual vertical stress distribution in the model is not a linear, (2) in a prototype, self-weight stress acts in a vertical direction only, while in a model there is also a horizontal stress component, (3) the influence of long-term chemical effects, thixotropy, and creep are not appropriately modelled in the model test, and (4) the testing technique may enhance the segregation of particles, the formation of dewatering structures, and lateral drainage.

CENTRIFUGE TESTS

Description of centrifuge

Most of the centrifuge tests were conducted using the GeoREF geotechnical beam centrifuge that is installed in the Natural Resources Engineering Facility (basement floor), University of Alberta,

Canada. The centrifuge is a one-beam, 50 G-Tonne centrifuge of 2 m radius to the base of a swinging platform. The maximum payload capacity of the centrifuge is 935 kg-m, the maximum payload volume is 0.6 m wide x 0.8m length x 0.9 m height, and the maximum speed is 281 rpm. Figure 2 shows the general arrangement of the GeoREF centrifuge at rest (hanging position). Details of the centrifuge can be found in Zambrano-Narvaez and Chalaturnyk (2014).



1- counter weight, 2- metal tube (beam), 3- test package, 4- swinging platform, 5- rotary unions, 6- slipping rings, 7- center cabinet, 8- drive motor, 9- data acquisition system (DAS)

Figure 2. General arrangement of GeoREF geotechnical beam centrifuge, modified from Zambrano-Narvaez and Chalaturnyk (2014)

Description of materials and centrifuge tests

The materials used for this study are oil sands tailings and Edgar Plastic Kaolin (EPK) clay. The oil sands tailings are from Albian Sands Energy Inc.: FFT (AL-15), thickened tailings of 50 and 60% fines (TT-50 and TT-60). The geotechnical properties of the materials are summarized in Table 1. The initial solids content of the materials are chosen to be higher than the solids content of the materials on the centrifuge segregation boundary based on a previous study (Sorta et al., 2012) conducted using these materials.

Table 2. Descriptions and geotechnical properties of materials used in the study

Material Designation	Material Description	Bitumen (%)	LL (%)	PL (%)	Fines (%)	Clay (%)
Kaolinite	EPK Kaolin clay	0.0	52	31	98	61
AL-15	Albian FFT	7.0	40	22	91	38
TT-50	Thickened tailings, 50% fines	3.1	26	16	50	26
TT-60	Thickened tailings, 60% fines	3.3	30	17	60	31

LL = Liquid limit; PL=Plastic limit; bitumen content is defined as the mass of bitumen in the tailings relative to total solids mass; fines content is defined as particles less than 45 micrometers; and clay is particles less than 2 micrometers.

Table 3 summarizes the types of centrifuge tests conducted, the test designation, as well as the initial compositions of tested materials. The centrifuge tests CT001-CT007 tests were conducted for modelling verification, modelling self-weight consolidation, and deriving consolidation parameters. All tests were carried out under one-way drainage conditions, with drainage towards the top of the model. CT001 and CT002 were run for nearly 8 hours, and the remaining centrifuge tests were run continuously until excess pore pressure fully dissipated. CT001 was conducted at the C-CORE center whereas CT002-CT007 tests were conducted at GeoREF.

Table 3. Initial materials properties, acceleration level and flight hours of centrifuge tests

Centrifuge Test code	Material Designation	Initial Solids (%)	Relative Acceleration	Initial Height (cm)	Flight Duration (hrs)
CT001	AL-15	46.5	80	10.0	8
CT002	AL-15	46.5	80	10.0	8
CT003	Kaolinite	43.9	100	10.0	6.4
CT004	Kaolinite	43.9	80	12.5	10.3
CT005	Kaolinite	43.9	60	16.7	16.3
CT006	TT-50	61.3	100	12.0	46.1
CT007	TT-60	61.6	90	13.5	41.3

The interface settlements of the tailings were monitored using in-flight cameras during the test flight of CT001 and CT002. Interface settlement, pore-pressure profile and solids content profile of consolidating materials were monitored during the centrifuge flight of CT003-CT007. Five miniature pore pressure transducers (MPPT) and one general purpose pore pressure transducer (SPPT) were utilized to measure pore pressure profiles during the centrifuge flight. Laser displacement sensors (LDS) and/or in-flight cameras were used for interface settlement monitoring. The solids content profiles of the centrifuge models tests were monitored using TDR probes installed through the wall of a centrifuge consolidation cell at a spacing of 2 cm, starting from 1.6 cm above the base. Centrifuge technology does not yet have a reliable solids content profile measuring apparatus. Thus, several different solids content measuring methods were evaluated and time domain reflectometry (TDR) was used for in-flight solid contents profile measurements. The detail of this investigation can be found in Sorta et al. (2013a), with results indicating that the TDR can be used to measure the solids content of tailings over a wide range of solids content with acceptable measuring accuracy. Figure 3a-c shows schematic drawings and pictures of consolidation, transducers, and camera set-up positions in the swinging platform for CT003-CT007 runs.

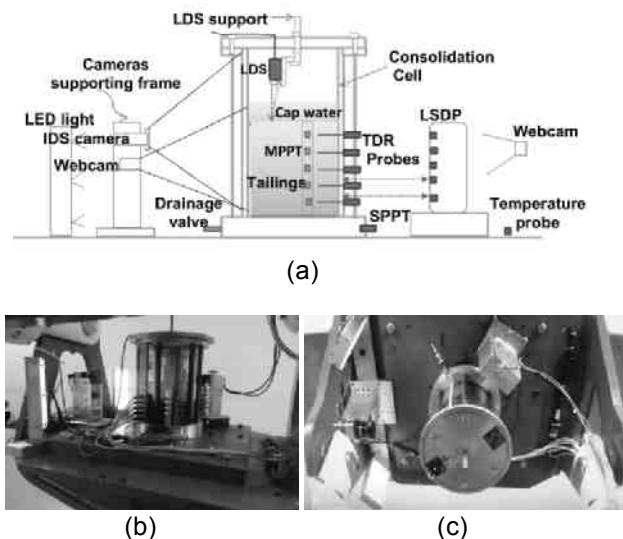


Figure 3. (a) Schematic of the test setup, (b) Centrifuge test package setup, at rest position, (c) Centrifuge test package, in-flight position

REPEATABILITY OF CENTRIFUGE TEST AND VERIFICATION OF SCALING LAWS

Centrifuge tests CT001-CT007 are used to check centrifuge test repeatability and to verify centrifuge scaling law. These centrifuge runs are necessary because the GeoREF centrifuge is new and so there is a need to verify that correct modelling procedure is followed. Three types of verification tests were carried out: repeating tests conducted at C-CORE center, modelling of models tests, and running centrifuge tests on TT samples to compare with the trend of results obtained at Earth gravitational acceleration.

Self-weight consolidation of Albion FFT (AL-15) was conducted at Memorial University of Newfoundland and Labrador using a 5.5 m radius C-CORE centrifuge. Details of the centrifuge and the centrifuge facility can be found in Phillips et al. (1994). The test was conducted at 80g for close to 8 hours. The initial height and solids content of the tailings were 10 cm and 46.5%, respectively. The self-weight consolidation test was then repeated using the GeoREF centrifuge at the University of Alberta (test CT002). The material type, initial solids content, initial height, relative acceleration and the consolidation cell in both facilities were kept the same. The interface settlement was monitored using in-flight cameras in both facilities. The interface settlement-time plots of CT001 and CT002 runs are shown in Figure 4. As Figure 4 demonstrates, the interface settlements from the two models are close, indicating that the test is repeatable and the correct modelling procedure was followed.

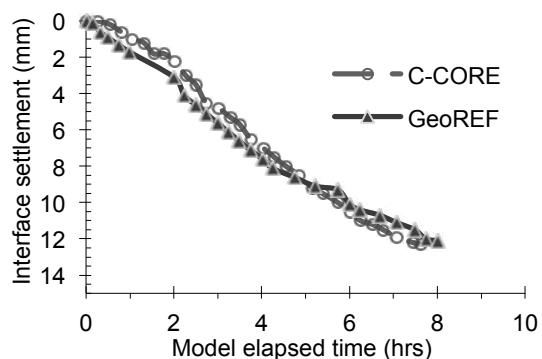


Figure 4. Interface settlement of AL-15 at 80-g centrifuge test at C-CORE and GeoREF

As part of centrifuge modelling verification, two centrifuge tests were conducted on thickened tailings of 60 and 50% fine (TT-60 and TT-50) at an acceleration of 90 and 100g (tests CT006 and CT007). The initial void ratio of the tailings and the prototype height were kept the same. Tests using fine-sand mixture tailings at Earth gravitational acceleration indicate that the behaviour of fine-sand mixture tailings (such as shear strength, plasticity, rate of settling, and segregation) depend more on fines void ratio (volume of voids/volume of fines) than on void ratio (volume voids/volume of solids) (Sorta et al., 2013b). The magnitude of ultimate settlement, however, depends more on the thickness of the deposits and the initial void ratio than on the fines void ratio. Centrifuge tests CT006 and CT007 conducted on thickened tailings started at the same initial void ratio and were subjected to the same self-weight stress. They were thus expected to give the same ultimate settlement if the scaling relation was valid and the correct modelling procedure followed. The centrifuge tests on the two materials were run until the end of consolidation while monitoring the interface settlement, solids and pore pressure profiles.

Figure 5 shows the average void ratio as a function of time for the two thickened tailings. The average void ratio is computed from the height of the interface, which was measured at different elapsed times. The settling rates of the two tailings are different but the ultimate settlements are close, indicating that the modelling procedure is acceptable and the deformation scaling relation in Table 1 is valid.

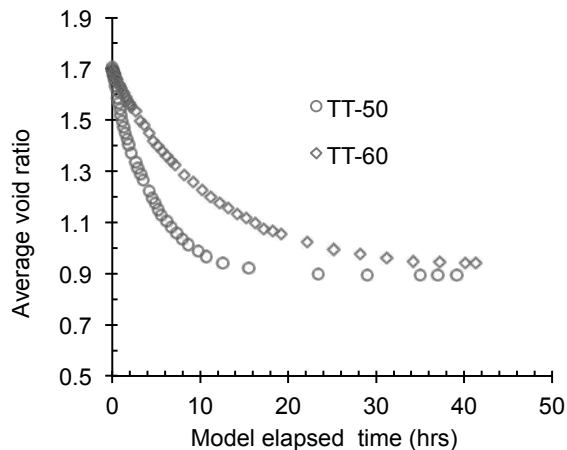


Figure 5. Interface settlement of TT-50 and TT-60, CT008 and CT012 tests

Three centrifuge tests (CT003-CT005) were conducted on kaolinite clay slurry to verify the similitude between different experiments and/or to verify the scaling relation between the model and the prototype. The three tests were conducted at accelerations of 60, 80 and 100g. The initial solids content of the slurry was kept close to 44% for the three tests. The initial height of the slurry was chosen to represent the same 10 m-high pseudo prototype. The three tests represent the same prototype but are modeled using different accelerations. They are thus expected to give the same prototype response, if correct modelling procedure was followed and centrifuge scaling factors are valid. This model verification technique is known as “modelling of models”, after Ko (1988). The interface settlement, pore pressure and density profiles were monitored in-flight in the three tests. The centrifuge tests were run until the interface settlements ceased and excess pore pressure fully dissipated. At the end of the tests, the solids content profiles were determined by slicing the sediments.

Figure 6 shows the compressibility (void ratio-effective stress relationship) of the kaolinite models after the centrifuge tests. The compressibility curves at 100% consolidation of the three tests are close, indicating that the same prototype response can be found for the end of the consolidation. The same magnitude of ultimate settlement were obtained from the three tests that indicate the height or deformation scaling relation between the model and prototype as being the same as the theoretical value in Table 1.

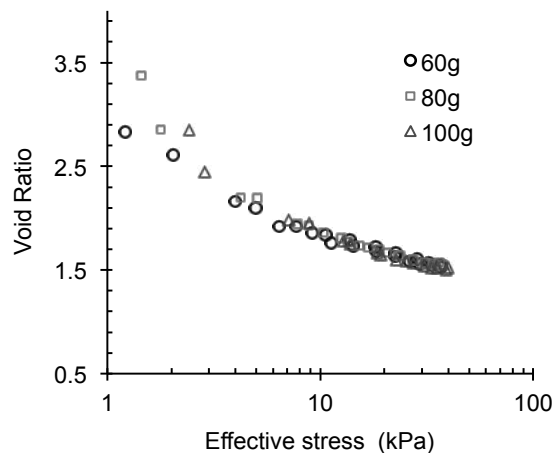


Figure 6. Compressibility of kaolinite from the modelling model test

Equation 1 can be expressed as $t_p = t_m N^x$. The exponent x is called the time scaling exponent. The theoretical time scaling exponent is 2 for consolidation and 0 for creep type of settlement (Table 1). Figure 7 shows the degree of consolidation versus prototype elapsed time for the centrifuge tests CT003-CT005, using the time-scaling exponent of 2. The prototype responses from the three tests (CT003-CT005) are very close for consolidation less than 60%; however, they vary with the gravity level used in the centrifuge for consolidation greater than 60%. The results in Figure 7 indicate that the rate of consolidation may depend on the relative acceleration used in the centrifuge for modelling a given prototype.

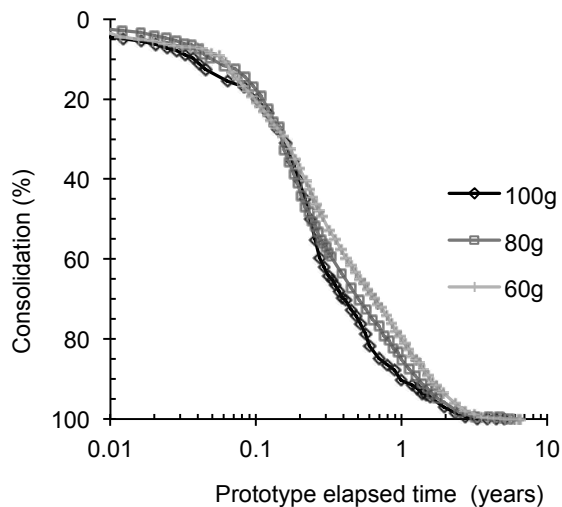


Figure 7. Degree of consolidation as function of prototype elapsed time; model extrapolated using time scaling exponent of 2

The results in this section demonstrate that the centrifuge testing procedure is acceptable and that the deformation scaling relation between the model and prototype is similar to the theoretical values. The analyses of modeling of model experiments indicate that the theoretical time-scaling exponent falls short of satisfying the scaling relation between the model and the prototype at certain stages during consolidation. Similar to the results of this study, previous modelling of model experiments by Scully et al. (1984) and Bloomquist and Townsend (1984) using Phosphatic clay also reveal that time-scaling is not constant and shows a trend towards increasing relative to the degree of consolidation.

CONSOLIDATION PARAMETERS FROM CENTRIFUGE TESTING

Centrifuge has been used for evaluating the consolidation parameters of soft soils (e.g. by Mikasa & Takada, 1984; Takada & Mikasa, 1986). The water content profile at the end of a centrifuge test are commonly used to derive the void ratio-effective stress relationship, and the initial settlement rates of models prepared at various initial void ratios are used to derive the hydraulic conductivity versus void ratio relationship (e.g., Takada & Mikasa, 1986). However, this approach requires a number of centrifuge model tests to be conducted at various initial void ratios for evaluating the hydraulic conductivity versus void ratio relationship (Mcvay et al., 1987).

In this study, the large strain consolidation parameters of oil sands tailings and kaolinite slurry are determined from a centrifuge test instrumented with density and pore pressure transducers, without the need for running a number of centrifuge tests on the same material at different initial solids contents. The advantages of this approach are that the consolidation parameters can be evaluated from a single model test and the relationship can be determined from a number of data points. The method does, however, require in-flight solids content, pore pressure profile measuring probes as well as monitoring the interface settlement during the test flight. The large strain consolidation test (LSCT) method requires many days or months to complete, depending on the permeability and initial solids content of the tailings. The objective of the centrifuge test is to examine the derivation of the large strain consolidation parameters of tailings from the centrifuge in a shorter time than that required for LSCT.

Centrifuge tests CT003-CT007 were conducted by monitoring the interface settlement, solids and pore pressure profiles. Based on the measured interface settlement, solids content and pore pressure profiles at various elapsed times, and using a generalized Darcy's law, principle of continuity and use of material coordinate system, the large strain consolidation parameters of tailings and kaolinite were derived from the centrifuge tests.

Figures 8-9 presents the compressibility and permeability of the materials from the centrifuge tests for TT-60 material. For comparison, the large strain consolidation test results are included in the

figures. The compressibility curves are found by connecting the void ratio-effective stress of soil elements along the model profile at particular elapsed times.

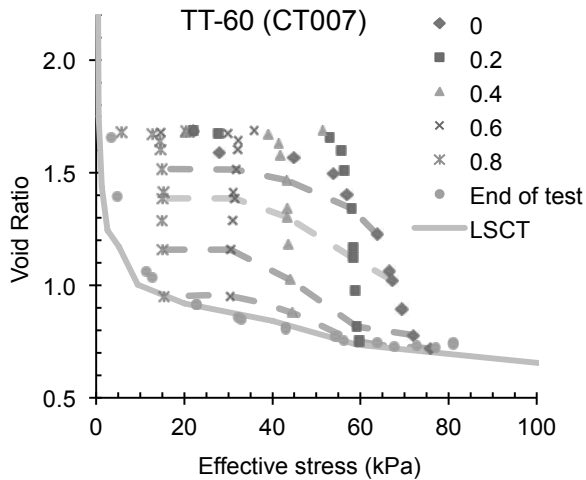


Figure 8. Compressibility of TT-60 from centrifuge and LSCT

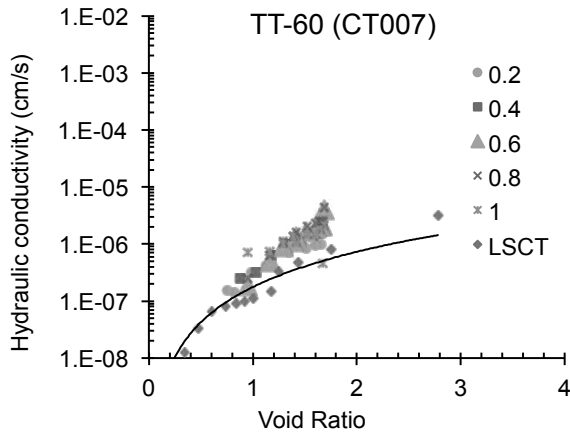


Figure 9. Permeability of TT-60 from centrifuge and LSCT

The test results indicate that the permeability of the centrifuge is generally higher than that of the LSCT results, and that the compressibility at the end of the tests is similar to the LSCT test results. In contrast, compressibility during the test flights is above that of LSCT. As the settling progresses, the compressibility measured during the centrifuge flight tends to move towards compressibility at the end of the test or LSCT compressibility. Depending on the stage of consolidation, the compressibility variation indicates that the compressibility of a given material is not a unique function of void ratio.

The non-unique compressibility during the test flights may be related the strain rate effect. In centrifuge tests, the strain rate is higher than conventional tests and is not constant during the test. Because of the viscous fluid behaviour, higher strain rates mobilize higher effective stresses, and thus compressibility is well above the compressibility from the LSCT at the initial stages of settling. Furthermore, as the consolidation progresses, the strain rate decreases and the compressibility is correspondingly lowered.

CENTRIFUGE RESULTS VERSUS NUMERICAL MODEL PREDICTION

The suitability of large strain numerical models in predicting changes in the volume behavior of tailings is examined in this section by comparing numerical model prediction with centrifuge test results extrapolated to prototype. Input parameters for numerical models were derived from the LSCT apparatus. The FSConsol slurry consolidation program was used for the numerical modelling prediction.

Figures 9 and 10 compare numerical model predictions and centrifuge test results for TT-60 material. The marked points represent the centrifuge results and the solid lines represent (FSConsol-1) the results from the numerical model using LSCT consolidation parameters. The ultimate settlements of the numerical model are comparable but the settlement rates are slower than the measured centrifuge results.

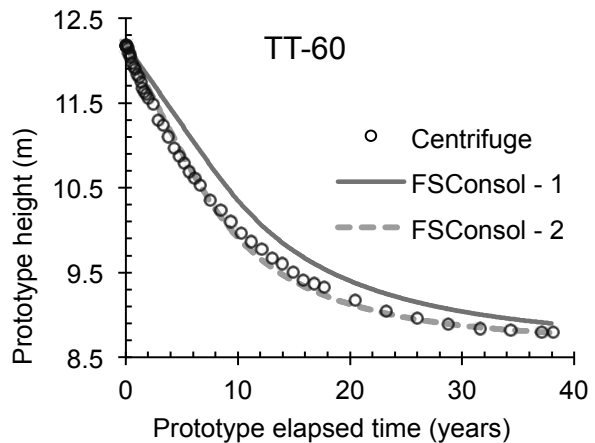


Figure 10. Comparison of centrifuge results and FSConsol prediction - TT-60

The numerical method and the centrifuge tests do not consider the time-dependent effects, and thus the differences in settlement rates may not be related to time-dependent effects. The centrifuge result is not affected by the segregation of particles, as non-segregating materials were selected for the test program. Moreover, the void-ratio profile at the end of the centrifuge does not indicate sorting of particles based on particle size. Images taken during the tests and observations made at the end of the tests do not indicate the formation of internal dewatering pathways (structures). The reasons for this discrepancy are somewhat uncertain, but the strain-rate effect is not considered in the numerical model and the hydraulic gradient used in the LSCT may result in lower hydraulic conductivity. Generally, the permeability from the centrifuge tests was found to be higher than the LSCT permeability, as shown in permeability plots in Figure 9. The centrifuge results were extrapolated using theoretical time relation between the model and prototype, but the modeling of the model results in this study indicates that the time-scaling relation between the model and the prototype may differ from the theoretical value at certain stages of consolidation thus may be the reason for discrepancy between centrifuge and numerical model prediction

In order to fit the centrifuge results, a series of numerical analyses were run with different sets of large strain consolidation parameters. The numerical model prediction and centrifuge results were found to be close when using the measured compressibility data but higher than the measured permeability data of the LSCT (the dotted line in Figures 10). The permeability was increased by less than one order of magnitude.

CONCLUSIONS

The following conclusions can be made from the investigation of the repeatability of centrifuge tests, the verification of scaling laws, the modelling of oil sands tailings consolidation, the deriving of consolidation parameters, and the comparison of centrifuge result with numerical model.

- Centrifuge tests conducted at the C-CORE center and GeoREF with the same material type, initial solids content, initial height, relative acceleration and consolidation cell indicate that the centrifuge test is repeatable.

- Centrifuge tests conducted on two types of thickened tailings that were started at the same initial void ratio and subjected to the same self-weight stress indicate that the centrifuge modelling procedure is acceptable and the theoretical deformation scaling relation between model and prototype is valid.
- The modelling of the model test conducted on kaolinite clay slurry indicates that the same prototype response can be found at the end of the consolidation, but the theoretical time-scaling exponent falls short of satisfying the scaling relation between the model and the prototype at certain stages of consolidation.
- The permeability of oils sands tailings and kaolinite slurry derived from centrifuge tests is generally higher than those derived from LSCT. The compressibility at the end of the centrifuge tests is similar to LSCT test results. However, compressibility during the test flights is above that of LSCT and may be associated with high strain rates in centrifuge testing.
- The settlement rates of tailings or kaolinite from the numerical model prediction are slower than centrifuge results, but the ultimate settlement predictions are comparable to centrifuge results. The numerical model prediction and centrifuge results are close when using the measured compressibility and higher than the measured permeability data of LSCT.

ACKNOWLEDGEMENTS

The authors greatly acknowledge Dr. Rick Chalaturnyk (GeoREF principal investigator) for the unlimited access to the GeoREF centrifuge facility and Dr. Gonzalo Zambrano (centrifuge manager) for facilitating the tests conducted in the facility. The technical support of Steve Gamble, Sander Osinga and Christine Hereygers is highly appreciated. The authors would like to thank Dr. Ryan Phillips, Gerald Piercy and Derry Nicholl for facilitating of the test conducted in the C-CORE centrifuge center. The research and the first author are funded by the Oil Sands Tailings Research Facility (OSTRF).

REFERENCES

- Bloomquist D (1982) Centrifuge Modelling of Large Strain Consolidation Phenomena in Phosphatic Clay Retention Ponds, *PhD dissertation*, University of Florida, Gainesville, USA.
- Bloomquist DG and Townsend FC (1984) Centrifuge modelling of phosphatic clay consolidation. In *Sedimentation Consolidation Models—Predictions and Validation* (Yong RN and Townsend FC (eds)). ASCE, New York, NY, USA, pp. 565–580.
- Cargill KW and Ko H-Y (1983) Centrifugal modeling of transient water flow, *Journal Geotechnical Engineering*, ASCE, **109(4)**: 536-555.
- Croce P, Pane V, Znidarcic D, Ko H-Y, Olsen HW and Schiffman RL (1985) Evaluation of consolidation theories by centrifuge modeling. In *Proceedings of the International Conference on Applications of Centrifuge Modelling to Geotechnical Design*. Balkema, Rotterdam, the Netherlands, pp. 380–401.
- Eckert WF, Masliyah JH, Gray MR and Fedorak PM (1996) Prediction of sedimentation and consolidation of fine tails. *AIChE Journal* **42(4)**: 960–972.
- Ko H-Y (1988) Summary of the State-of-the-Art in Centrifuge Model Testing. In *Centrifuge in Soil mechanics* (Craig WH, James RG and Schofield AN (ed.)), Balkema, Rotterdam, Netherlands, pp. 11-18.
- McVay MC, Townsend FC, Bloomquist DG and Martinez RE (1987) Reclamation of Phosphatic Clay Waste Ponds by Capping. Volume 6: Consolidation Properties of Phosphatic Clays from Automated Slurry Consolidometer and Centrifugal Model Tests. Florida Institute of Phosphate Research, Bartow, FL, USA, FIPR publication no. 02-030-073.
- Mikasa M and Takada N (1984) Self-weight consolidation of very soft clay by centrifuge. In *Sedimentation Consolidation Models—Predictions and Validation* (Yong RN and Townsend FC (eds)). ASCE, New York, NY, USA, pp. 121–140.
- Phillips R, Clark JI, Paulin MJ, Meaney R, Millan DEL and Tuff K (1994) Canadian National Centrifuge Center with Cold Regions Capabilities, In: *Centrifuge 94: Proceedings of the International Conference, Singapore '94* (Lee FH, Leung CF and Tan, TS (eds)). Balkema, Rotterdam, Netherlands, pp. 57-62.
- Scully RW, Schiffman RL, Olsen HW and Ko HY (1984) Validation of consolidation properties of phosphatic clays at very high void ratios, predictions and validation. In *Sedimentation Consolidation Models—Predictions and Validation* (Yong RN and Townsend FC (eds)). ASCE, New York, NY, USA, pp. 158–181
- Sorta AR, Segó DC and Wilson W (2012) Effect of thixotropy and segregation on centrifuge modelling. *International Journal of Physical Modelling in Geotechnics*, **12(4)**: 143–161.
- Sorta AR, Segó DC and Wilson W (2013a) Time Domain Reflectometry measurements of Oil Sands Tailings Water Content: A Study of Influencing Parameters. *Canadian Institute of Mining, Metallurgy and Petroleum (CIM) Journal*, **4(2)**: 109-119.
- Sorta AR, Segó DC and Wilson W (2013b) Behaviour of Oil Sands Fines-Sand mixture Tailings. *Canadian Institute of Mining, Metallurgy and Petroleum (CIM) Journal*, **4(4)**: 265-280.
- Takada N and Mikasa M (1986) Determination of consolidation parameters by self-weight consolidation test in centrifuge. In *Consolidation of Soils: Testing and Evaluation* (Yong RN and Townsend FC (eds)). ASTM, West Conshohocken, PA, USA, ASTM STP 892, pp. 548–566.
- Taylor RN (1995) Centrifuges in modeling: principles and scale effects. In *Geotechnical Centrifuge Technology* (Taylor RN (ed.)). Blackie Academic & Professional, London, UK, pp. 19–33.
- Zambrano-Narvaez G and Chalaturnyk R (2014) The New GeoREF Geotechnical Beam Centrifuge at the University of Alberta, Canada, *Proceeding of the 8th International conference in Physical Modelling in Geotechnics*, Perth, Australia, pp. 163-167.

COLUMN CONSOLIDATION TESTING OF OIL SANDS TAILINGS

Ruijun Sun¹ and Ryan Spelay¹, Jianmin Kan² and Alexandre Goldszal²

¹Saskatchewan Research Council, Saskatoon, Canada

²Total E&P Canada Ltd, as Operator of the Joslyn Joint Venture, Calgary, Canada

ABSTRACT

The objective of this study was to evaluate the impact of process conditions on oil sands tailings consolidation behavior. Those conditions included tailing compositions, flocculent dosage, process water salinity and tailings rheology. Weather effects such as freeze and thaw, as well as natural evaporation were also studied.

Fresh oil sands tailings were tested in thirteen vertical steel columns with dimensions of 2.7 m (H) x 0.6 m (ID). Tailings consolidation in the columns was monitored for 12 months or longer, during which the column vertical solids concentration distributions and pore pressure profiles were measured periodically. The combination of vertical solids concentration distributions with lateral pore pressure measurements provided accurate consolidation profiles.

Among the thirteen columns, seven were tested indoors and six tested outdoors, the latter of which experienced at least one cycle of freeze and thaw. At the end of testing period, samples were taken and tailings peak shear strengths were measured at 10 different depths of a 2.5 m deep deposit. The percentage of water freed, tailings volume reduced and vertical consolidation profiles were also examined and used to analyze the tailings consolidation behavior.

It was found 1-3% w/w flyash addition increased deposit undrained shear strength but under indoor conditions it failed to reach 5 kPa after 1 year consolidation in column due to slow water release. Under outdoor freeze and thaw, 3% w/w flyash addition achieved the same degree of consolidation as tailings without flyash.

It was also found change of process conditions such as feed concentration, SFR, sodium concentration and yield stress affected tailings consolidation behavior.

INTRODUCTION

In surface mining of oil sands, hot water is used to separate and extract valuable bitumen from the ore. After secondary and tertiary recovery of bitumen, the remaining solids (sand, silt, clay), water and residual bitumen from the extraction process is disposed as tailings. The large scale of oil sand extraction processes results in a significant quantity of tailings which create unique challenges.

Historically, the tailings have been transported by pipeline to a disposal facility where the tailings are discharged and stored in a tailings pond or settling basin existing as Fluid Fine Tailings (FFT). Following discharge, the coarse sand settles immediately while the fines remain suspended in the dilute fine particle slurry. The fines (-44 µm) in FFT consolidate extremely slowly. The result is a dense sludge-like material referred to as Mature Fine Tailings (MFT) which takes decades to fully settle. To accommodate the large volumes of FFT that are continuously being produced, settling basins are very large, holding up a significant volume of water. Currently the volume of MFT requiring long term containment is estimated to be 720 million m³ [1].

Since 2009, the Energy Resources Conservation Board (ERCB) has set up a series of strict regulations for oil sands mining operators regarding the disposal of their tailings material. The ultimate goal is to minimize FFT and their long-term storage. In particular, ERCB Directive 074 [2] states that a tailings disposal strategy must be able to reduce FFT stored in ponds by increasing the fines capture in the Designated Disposal Area (DDA), and improve on the rate at which land is being reclaimed and made trafficable. Even though the directives are managed on a project-by-project basis, the same objectives must be met by all operators, specifically:

1. 50% of the fines in the total feed to be captured in the DDA (by 2013 annually and every year thereafter)
2. Minimum undrained shear strength of 5 kPa for the material deposited in the previous year, and a deposit which is ready for reclamation within 5 years after active deposition has ceased (with shear strength of 10 kPa).

To date, there is a wide range in predicted consolidation rates and shear strengths for a particular deposit, depending on the selection of compressibility and permeability properties, as well as field test locations. This study will provide some information regarding the consolidation behavior of oil sands tailings.

EXPERIMENTAL METHODS

Thickener Operation and Column Feed

Using the optimum flocculent dosage and thickening conditions (feed concentration, flowrate and residence time) developed in the same project, a 0.6 m diameter pilot thickener provided by FLSmidth was utilized to generate fresh thickener underflow for column consolidation tests (Figure 1).

Table 1 which is presented in the Illustration section shows the test matrix and properties of feed used in the consolidation tests. Flotation underflow tailings supplied by CNRL were used as feed for the thickener operation. The average flotation underflow concentration to the thickener was between 15-23% w/w and Sand to Fines Ratios (SFR₄₄, with a 44 micron cut off for fines) at 0.6-0.8. Fresh thickener underflow tailings were used as feed to the consolidation columns and had a base case solids concentration of ~50% w/w and SFR₄₄ value of 0.8 (these conditions were used for column Tests C#1 as indoor base case and C#5 as outdoor base case; also used for Test C#10 as confirmation test to C#1).

Adjustments were made to the feed properties for some of the column tests to evaluate the impact of variation in the feed properties (see Table 1 for specific details). Feed for Tests C#2 and C#6 had low solids concentration of 40%-45% w/w. Sodium ion concentration (Na⁺) for feed of Test C#12 had been increased to 1200 ppm to mimic high salinity of thickener feed.



Figure 1. 0.6 m ID FLS Deep Cone Thickener

Flocculent dosage was based on gram of flocculent per tonnes of total solids (gpTs), dry basis. AF 309 (supplied by SNF) was used as flocculent and the dosage for the majority of thickener operations was at 150 gpTs, except Test C#5 which was generated with 200 gpTs. Feed for C#11 was generated from two stage flocculation (100 gpTs for the 1st stage and 50 gpTs for the 2nd stage).

To mimic tailings being transported from thickener operation to the DDA, fresh thickener underflow tailings were pre-sheared to 20-30 Pa before loaded into column, or before added with flyash. The feed mixed with flyash had higher yield stresses. The feed for Test C#7 and C#10 were pre-sheared to below 10 Pa, to mimic a well sheared thickener underflow to be deposited in the DDA.

For selected tests, flyash was added to thickener underflow tailings just before being loaded into consolidation columns. Feed for Tests C#3, C#4, C#8, C#2-II and C#4-II had various percentage of flyash addition. Coanda Research and Development Corp. provided the mixing apparatus and operations for mixing dry flyash powder with tailings slurry.

Consolidation Column Tests

Thirteen steel columns were constructed and used for consolidation tests for both indoor and outdoor

conditions (Figures 2 and 3) for 12 months or longer. Deposits in the outdoor columns experienced at least one cycle of freeze and thaw, some also experienced summer drying. Figure 3 shows wooden hats on top of some columns, which were constructed for drying columns to prevent rainwater or snow entering the column.



Figure 2. Indoor Consolidation Columns

Each column has dimensions of 0.6 m (ID) x 2.7 m (H), and is equipped with lateral pore pressure ports (20 cm apart) on the side of column. A gamma traversing densitometer was designed and used to measure the vertical solids concentration profile in a space of 10 cm apart.



Figure 3. Outdoor Consolidation Columns

At the end of test period, hand-held vane tester and piston sampler were used to measure the deposit peak shear strength and to take sample from column for determining deposit concentration and solids particle size distributions.

RESULTS AND DISCUSSION

Thirteen column consolidation tests were conducted between 2012 and 2014. The tests covered a broad range of conditions such as flyash addition, winter freeze and thaw, low feed concentration and SFR, as well as high sodium (Na⁺) ion concentration etc.

A large amount of data was generated from the consolidation columns, only partial data from thirteen columns are presented for a high level discussion in this paper. The test results are presented in Table 2 (Illustration section).

Case Study of Consolidation Column Test

Traversing gamma density and lateral pore pressure measurements provided good instruments to analyze the deposit consolidation pattern.

In this section, Column #2-II is selected as a case study to illustrate the analysis. The feed for column C#2-II was slightly oxidized after the flotation underflow tailing had been stored in a tank for more than 6 months before been used for thickener operation. The objective of Test C#2-II was to determine if long term storage and oxidization of thickener feed had any impact on thickener flocculation and thickener underflow tailings consolidation behavior.

Figure 4 shows the column deposit solids concentration profiles as a function of consolidation time for Column C#2-II. The biggest gain in solids concentration was between day 1 and day 11, which indicated the deposit's fast settling and water release. The deposit consolidated progressively until it reached equilibrium at day 120.

Figure 5 provides the total pore pressure profiles versus consolidation time and shows that, as consolidation progressing, total pore pressure decreased steadily at each height level of the column. This indicates that more weight of the solids was transmitted to the bottom of column rather than contributing to the fluid surround it at each level, a clear sign of consolidation. In addition, the reduction in pore pressure at layers near the bottom were greater than layers near the top, indicating more consolidation occurred near the bottom.

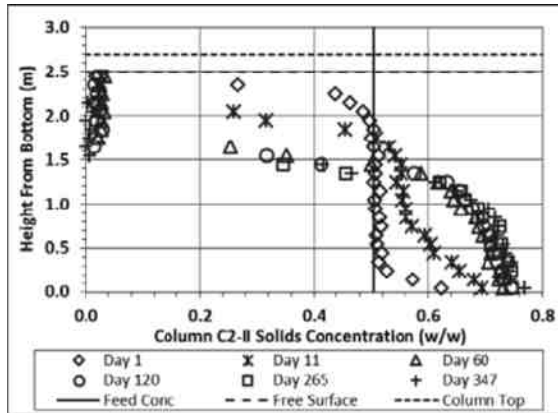


Figure 4. C#2-II Gamma Solids Concentration Profiles

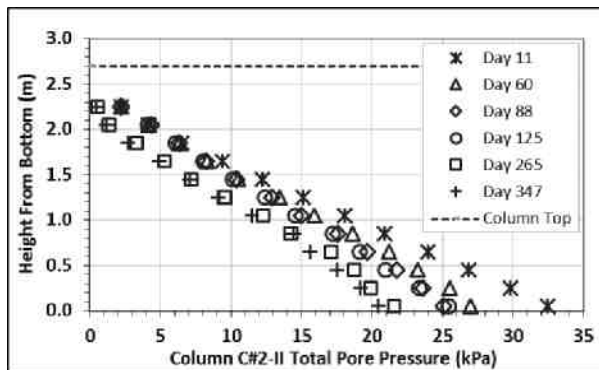


Figure 5. C#2-II Total Pore Pressure Profiles

Figure 6 shows the column excess pore pressure versus consolidation time. As the deposit consolidated, the excess pore pressure decreased and moved progressively towards y-axis at zero excess pore pressure (fully consolidated state). It was also observed that the consolidation was from bottom up as the “protrude” was moved upward after each measurement.

Figure 7 shows the deposit effective stress increased with consolidation time, especially for the three layers near the bottom of the column (0.051 m, 0.251 m and 0.451 m above bottom respectively), a clear indication of consolidation in that region. The increase seen in the lower layers not only resulted from the decrease of pore pressure as discussed above, but also from the total stress increase at each height level due to more solids entering the lower layers from the layers above, and consolidating in these layers.

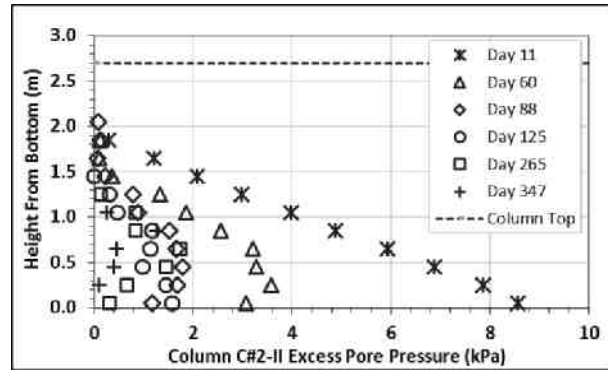


Figure 6. C#2-II Excess Pore Pressure Profiles

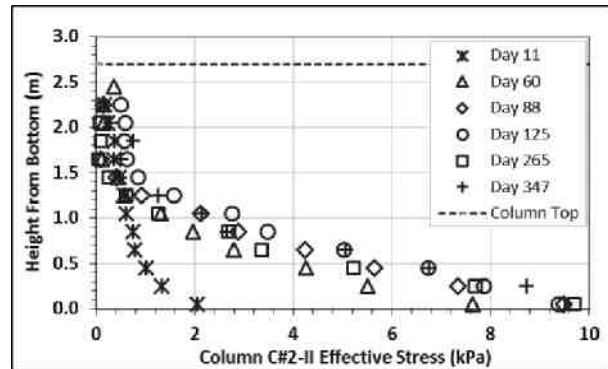


Figure 7. C#2-II Effective Stress Profiles

Figure 8 shows compressibility of deposit progressed with consolidation time. The biggest compressibility gain was during the first 60 days. The compressibility progressed slowly but steadily until reached equilibrium at 88 days.

The case study for C#2-II shows the value of combination of gamma concentration profile and lateral pore pressure profile can provide in the examination of tailings consolidation behavior. The impact of feed oxidization will be discussed in the following sections.

Flyash Addition

Flyash was added to the base case thickener underflow tailings at concentrations of 1, 2 and 3% w/w (for column Tests C#3, C#4-II, C#4 for indoor, and column Test C#8 for outdoor). In this section, base case feed of 0% w/w flyash addition (column Test C#1 for indoor and C#5 for outdoor) were also examined.

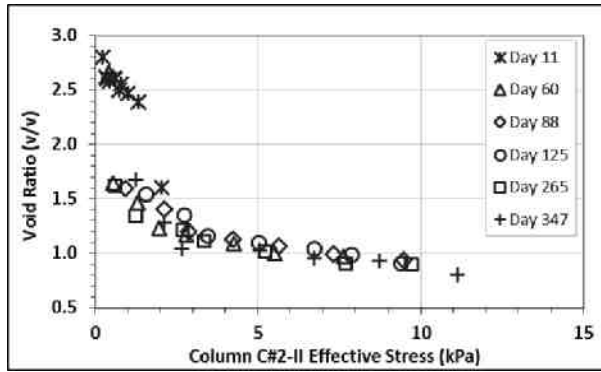


Figure 8. C#2-II Deposit Compressibility Profiles

The major objective of flyash addition was to increase the shear strength of the tailings deposit in a very short time, such that it can reach 5 kPa within a specific consolidation time limit. Figure 9 shows the impact of flyash addition on tailings shear strength after settled for 7 months. For columns tested indoors, flyash addition slightly increased the deposit's shear strength over the base case, however none of the additions (1%, 2%, and 3% w/w) increased the deposit shear strength to over 5 kPa in 7 months under conditions of no evaporation and no drainage of runoff water.

For outdoor columns and after one cycle of freeze and thaw, shear strength of deposit with 3% w/w flyash addition (C#8) exceeded 5 kPa for all layers 1.25 m above the bottom. 3% w/w flyash addition also represents an increase of 3-5 kPa of shear strength compared with deposit without flyash addition (outdoor base case column C#5) at the same depth level and exposed to the same freeze and thaw conditions and time period.

As consolidation progresses, water is separated and can be removed as runoff. Deposit volume reduction is a measure of the consolidation process. Figure 10 shows that for indoor columns after one year consolidation, column with 0% flyash addition experienced 30% reduction in the feed volume (C#1). Columns C#3 and C#4-II which had the addition of 1-2% w/w flyash saw 20-23% reduction in the feed volume, while Column C#4 with 3% w/w flyash addition had only an 8% reduction in the feed volume after the same 7 months consolidation period. These results demonstrate that the flyash addition prevented fast water release and volume reduction.

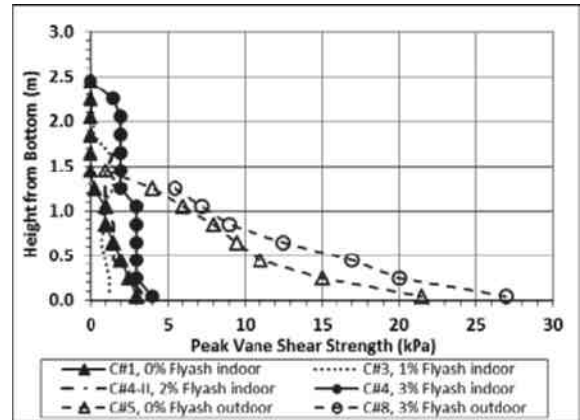


Figure 9. Peak Vane Shear Strength of Tailings With and Without Flyash Additive

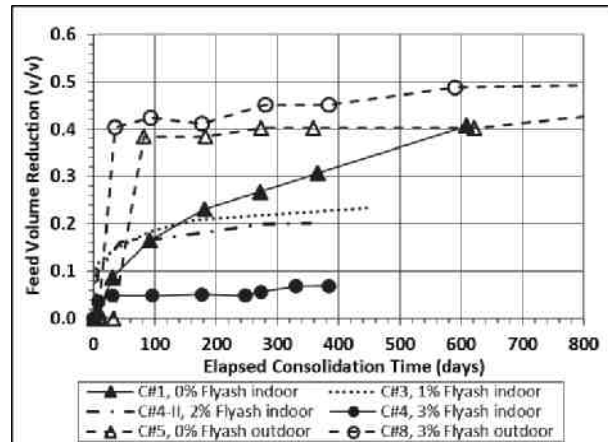


Figure 10. Feed Volume Reduction for Tailings With and Without Flyash Addition

Under freeze and thaw conditions, a big fraction of water in tailings can be released quickly in a shorter period of time. Figure 10 shows that for outdoor columns, freeze and thaw can reduce about 40% of feed volume in 90 days for both the tailings with 3% w/w flyash addition (C#8) and 0% flyash addition (base case C#5). Column C#8 reduced more volume than C#5 after one year consolidation, this was due to column C#8 had an open column drying season so the deposit dried quicker than C#5 which had its column covered (but not sealed) all the time.

Figure 11 shows the deposit concentration change as a function of consolidation time for tailings with and without flyash addition. The initial deposit concentrations were all started at about 50% w/w.

For indoor columns, since flyash prevented fast water release, the deposit concentration of 1-2% w/w flyash addition (C#3 and C#4-II) increased to about 57-58% w/w one year after consolidation, while the deposit of 3% w/w flyash addition (C#4) had increase to 55% w/w. As comparison, the deposit without flyash addition (C#1) reached 66% w/w after the same consolidation period.

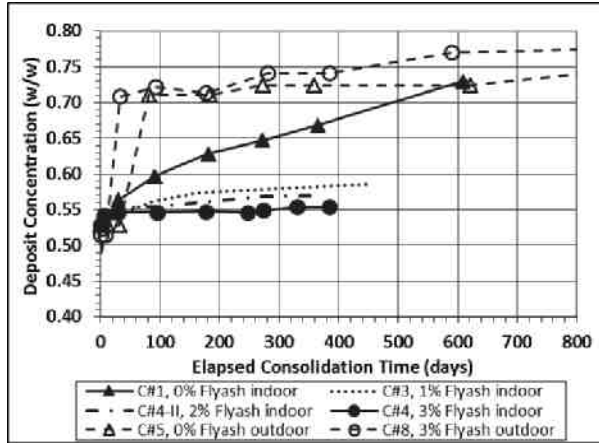


Figure 11. Deposit Concentration for Tailings With and Without Flyash Addition

For outdoor columns, both concentrations of deposits with and without flyash addition increased to over 70% w/w in 90 days under freeze and thaw. However the gain from 3% flyash addition (C#8) was only slightly more than the base case of 0% flyash (C#5).

Freeze and Thaw

The impact of freeze and thaw on deposit properties was further examined with several other tailings mixtures during the winters of 2012 and 2013. After the 1st freeze and thaw, the tailings were kept in each respective column through the summer of 2013.

Figure 12 shows that tailings generated from high salinity (Na+) feed material (C#12), two stage flocculation process (C#11) and low SFR feed (C#6) achieved 15-20% volume reduction. This was much less than the base case tailings (C#5) which reached up to 39% after the 1st freeze and thaw season. Only after a summer drying, did the volume reduction of the other tailings mixtures approach that of the base case tailings.

For well sheared tailing (C#7), there was a quick volume reduction right after deposition and even

before the 1st freeze started, which indicated that lower tailings yield stress promoted fast settling.

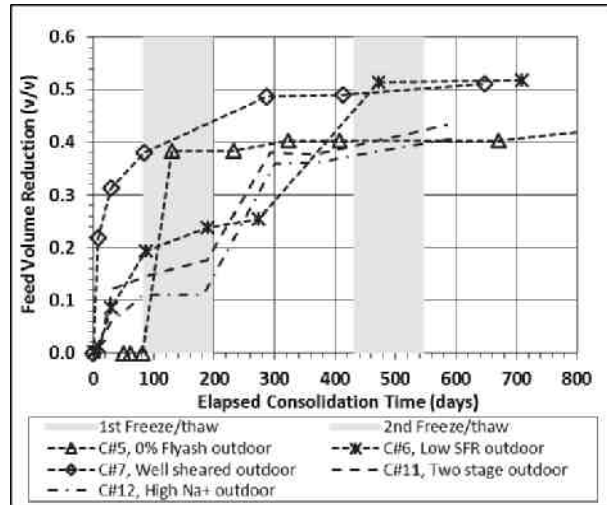


Figure 12. Feed Volume Reduction for Tailings Experienced Freeze and Thaw

The 1st freeze and thaw further enhanced its volume reduction, and this mixture achieved about 50% volume reduction after the 1st freeze and thaw cycle. This indicated lower tailings rheology has a positive impact on consolidation behavior, however the magnitude of rheology impact has to be evaluated for the specific feed and deposition such that to prevent fast settling and separation of coarse particles and leave fines behind to form MFT.

The 2nd freeze and thaw cycle had less impact on the feed volume reduction than the 1st cycle. This was because after the 1st cycle of freeze/thaw and summer drying, there were not many water filled voids left in the deposit for the 2nd cycle of freeze and thaw. Only the tailings with low SFR (C#6) achieved 6-8% volume reduction during the 2nd freeze and thaw cycle, which was probably because this material started with lower concentration (~40% w/w) and it still had unseparated water after the 1st freeze/thaw and summer drying.

Figure 13 shows the impact of freeze and thaw on the change of tailings solids concentration. The pattern is similar to the impact on feed volume reduction. All tailings average solids concentration were increased to 72-74% w/w after the 1st freeze/thaw and summer drying, except tailings

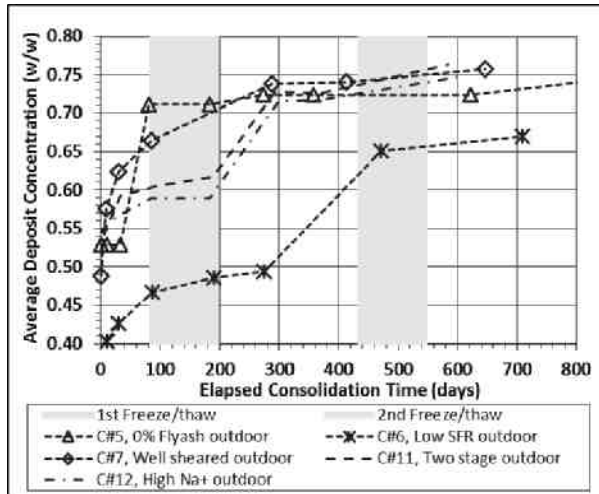


Figure 13. Deposit Concentration for Tailings Experienced Freeze and Thaw

with low SFR (C#6) which reached about 62% after the same consolidation period. Low SFR samples are known to have difficult consolidation due to its poor permeability. However C#6's magnitude of concentration increase was similar as the other tests.

Indoor Consolidation

Besides the flyash addition tests, additional column tests were conducted under indoor conditions for comparison purposes.

Figure 14 shows columns C#1 and C#10 which had the same feed conditions and achieved very similar results. The reproducible results indicated the validity of the test method. The feed for column C#2 had low solids concentration and the feed for C#2-II was oxidized, both experienced fast water release and volume reduction. This was because both low solids concentration and oxidized feed contributed to a low feed yield stress, which resulted a fast settling.

Figure 15 shows only the oxidized feed (C#2-II) achieved higher volume reduction and deposit concentration than other indoor tests in the 12 month consolidation period under the same conditions. C#2 had fast volume reduction but the consolidated concentration was similar as the other column because its start concentration was low at 45% w/w. The effect of feed oxidization on tailings consolidation behavior needs to be investigated further.

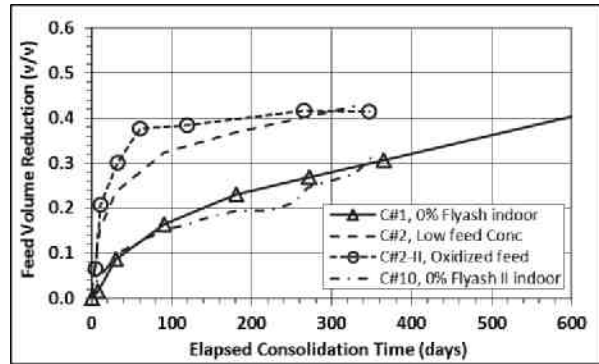


Figure 14. Feed Volume Reduction for Tailings Experienced Indoor Consolidation

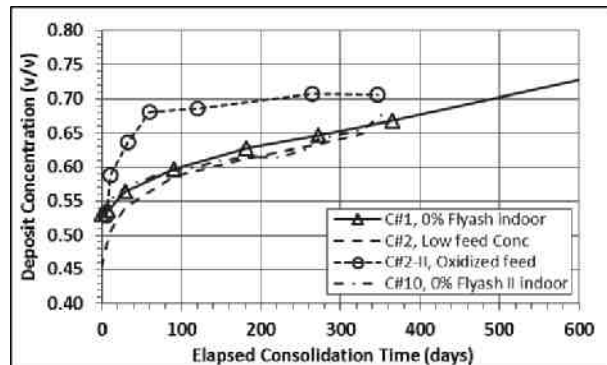


Figure 15. Deposit Concentration for Tailings Experienced Indoor Consolidation

KEY LEARNINGS

1. Traversing gamma density scan provided accurate solids concentration results for column consolidation tests. The gamma data can be combined with lateral pore pressure at the same layer and enable the construction of profiles for deposit total pore pressure, effective stress, excess pore pressure and compressibility; it also provided a good instrument to study the tailings consolidation behavior.
2. For tailings with flyash addition, water release was provided by another mechanism such as freeze and thaw, as flyash prohibits water release. However flyash addition increases deposit shear strength.
3. Under freeze and thaw conditions, the deposit shear strength was well above 5 kPa after only 1 cycle of freeze and thaw. 3% w/w flyash

addition showed shear strength 3-5 kPa higher than the base case material.

4. Freeze and thaw sped up the consolidation process by promoting fast water release and volume reduction for the tailings deposit. On average, one cycle of freeze and thaw can reduce up to 40% v/v feed volume and increase the deposit solids concentration by almost 40% w/w. The impact of 2nd cycle freeze and thaw on the same deposit is limited if the 1st freeze/thaw and summer drying is efficient.
5. Changes in the feed conditions, such as high Na⁺, low SFR and two stage flocculation, impacted the deposit consolidation performance. On average these changes resulted in less than 50% of volume reduction and concentration increase which were achievable by base case feed tailings.
6. Well sheared feed had fast settling and quick water release even before the freeze and thaw started, which indicated lower tailing yield stress had an impact on consolidation behavior. The magnitude of impact has to be evaluated for the specific feed and deposition.
7. The oxidized feed tested here achieved 10% more feed volume reduction and 5% more deposit concentration increase, compared to base case tailings. One possible reason is the

lower feed yield stress. However, the mechanism of this improvement needs to be investigated further.

FUTURE WORK

1. Large scale oil sands tailings consolidation tests using bigger columns (e.g., 1.0-1.5 m ID x 6 m H) are required to better understand tailings consolidation behavior under controlled conditions such as freeze and thaw.
2. The combination of traversing gamma density scan and lateral pore pressure measurement has proved to be a powerful tool to examine the tailings consolidation behavior. This technique can be applied to larger scale tailings consolidation tests.

REFERENCES

1. Energy Resource Conservation Board, "News Release – ERCB Releases Major Directive on Oil Sands Tailings management and Enforcement Criteria", Feb. 23, 2009.
2. Energy Resources Conservation Board. 2009, "Tailings Performance Criteria and Requirement for Oil Sands Mining Schemes, Directive 074".

Table 1. Column Test Matrix and Feed Conditions

Column Test ID	Test Start Date	Column Location	Description	Column Feed			Floculent Dosage (gpTs)	Flyash Additive (% w/w)
				Conc. (w/w)	SFR ₄₄ (w/w)	Yield Stress (Pa)		
C#1	18-Jan-12	Indoor	Indoor base case	0.531	0.77	27.4	150	None
C#2	17-Apr-12	Indoor	Low feed concentration	0.449	0.70	6.5	150	None
C#3	28-Jun-12	Indoor	TT0.8 + 1% flyash	0.490	0.73	18.3	150	1%
C#4	22-Feb-12	Indoor	TT0.8 + 3% flyash	0.529	0.83	281.3	150	3%
C#2-II	13-Jun-13	Indoor	Oxidized Feed	0.505	0.66	N/A	150	None
C#4-II	6-Jun-13	Indoor	TT0.8 + 2% flyash	0.490	0.59	24.5	150	2%
C#10	21-Mar-13	Indoor	Indoor base case II	0.535	0.82	6.5	150	None
C#5	12-Jan-12	Outdoor	Outdoor base case	0.528	0.90	18.3	200	None
C#6	12-Jun-12	Outdoor	Low feed SFR	0.399	0.47	29.9	150/200/300	None
C#7	13-Aug-12	Outdoor	Well sheared feed	0.488	0.96	4.3	150	None
C#8	22-Feb-12	Outdoor	TT0.8 + 3% flyash	0.514	0.81	265.7	150	3%
C#11	3-Oct-12	Outdoor	Two stage Flocculation	0.545	N/A	32.0	100+50	None
C#12	27-Sep-12	Outdoor	1200 ppm Na+ feed	0.546	0.92	36.7	150	None

Table 2. Column Test Results

Column Test ID	Test Start Date	Column Location	Elapsed Time (days)	Supernatant Available or Removed (L)	Water Freed From Feed (w/w)	Volume Reduced From Feed (v/v)	Average Deposit Conc. Cm (w/w)
C#1	18-Jan-12	Indoor	365	219.69	0.440	0.307	0.668
C#2	17-Apr-12	Indoor	328	304.91	0.560	0.427	0.649
C#3	28-Jun-12	Indoor	447	171.37	0.321	0.235	0.585
C#4	22-Feb-12	Indoor	330	49.14	0.098	0.068	0.554
C#2-II	13-Jun-13	Indoor	347	296.34	0.577	0.415	0.706
C#4-II	6-Jun-13	Indoor	354	144.26	0.275	0.201	0.570
C#10	21-Mar-13	Indoor	355	231.03	0.460	0.320	0.680
C#5	12-Jan-12	Outdoor	358	290.25	0.575	0.403	0.724
C#6	12-Jun-12	Outdoor	274	181.46	0.319	0.254	0.493
C#7	13-Aug-12	Outdoor	287	351.70	0.664	0.487	0.738
C#8	22-Feb-12	Outdoor	384	325.84	0.633	0.451	0.741
C#11	3-Oct-12	Outdoor	369	272.88	0.550	0.378	0.726
C#12	27-Sep-12	Outdoor	370	261.60	0.528	0.362	0.717

Session 5

COSIA Special Session I

PERFORMANCE MANAGEMENT OF FLUID FINE TAILINGS TO MEET CLOSURE COMMITMENTS

John Sobkowicz¹, Alexander Hyndman², Bryan Watts³ and Richard Dawson⁴

¹Thurber Engineering Ltd.

²Consultant, Magnus Limited

³Klohn Crippen Berger Ltd.

⁴NorWest Corporation

ABSTRACT

Alberta's oil sands mines operate the largest tailings facilities in the world. Tailings are deposited in above-ground and in-pit tailings impoundments. Sound engineering and management principles are used to design and operate these facilities to meet engineering and safety standards and to minimize environmental impacts. The reclamation process must contend with a unique feature of oil sands tailings – the slow sedimentation and consolidation of fine tailings initially deposited in tailings ponds. These fluid fine tailings (FFT) require intervention with accelerated dewatering technologies, to support progressive reclamation during the active mine life and mine closure within a reasonable time after the cessation of mining.

In February of 2014, COSIA issued Guidelines for Performance Management of Oil Sands Fluid Fine Tailings Deposits to Meet Closure Commitments. This paper is a summary of that document, which provides oil sands mining operators with guidelines for creating FFT management plans, consistent with Alberta policy and regulatory goals for progressive reclamation. The management plan is based on the concept of limiting the volume of FFT over the life of the mine using best available, currently deployed tailings treatment technologies, and technologies under development that are considered practical and workable. The plan includes the predicted volume of FFT and projections on the performance of FFT treatment processes, and the behaviour of resulting deposits. Every five years, a report is made on conformance to plan of FFT volume, deposit formation and deposit behaviour. The report also updates the plan and includes a discussion of adaptive management and implementation of any needed contingency actions.

INTRODUCTION

Background

The Alberta government has taken several actions to address public concerns over the oil sands fluid tailings issue: 1) the predecessor to the Alberta Energy Regulator (AER) enacted Directive 074 in 2009 to focus industry attention on disposal of FFT within set time frames, b) in August 2012, the Lower Athabasca Regional Development Plan was released, which encouraged “timely and progressive reclamation” of industrial sites, and c) earlier this year (June) AESRD released a draft of its “Tailings Management Framework for Mineable Athabasca Oil Sands”, which “provides direction to manage fluid tailings volumes during and after mine operation in order to manage and decrease environmental risk and financial liability resulting from the accumulation of fluid tailings on the landscape”.

At the same time, the oil sands industry has been active in developing a comprehensive set of practices for tailings management. The first of these was the “Technical Guide for Fluid Fine Tailings Management” (COSIA, 2012); others are listed on Figure 1. This paper presents a summary of the information contained in one of these documents (outlined in red on Figure 1): “Performance Management of Oil Sands Fluid Fine Tailings Deposits to Meet Closure Requirements” (COSIA, 2014c), which will herein be referred to as the PMFFT.

The PMFFT provides oil sands mining operators with guidelines for creating fluid fine tailings (FFT) management plans, consistent with the intent of evolving government policy and regulations. The purpose of FFT management plans is to facilitate closure of oil sands mines by accelerating FFT conversion into stable closure landscapes.

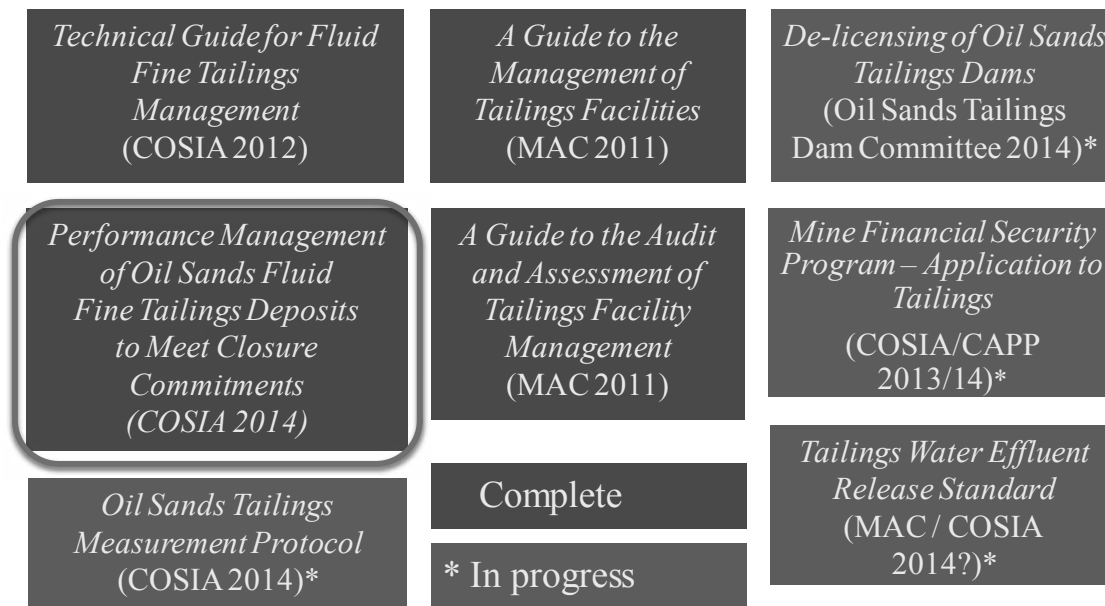


Figure 1. Oil Sands Industry Practices for Tailings Management

The FFT management plan must be achievable and progressively verifiable. The oil sands operator makes a commitment to:

- Manage FFT over the life of the mine to a volume profile consistent with the approved tailings management plan.
- Place FFT in permanent deposits, where they will progress, at an approved rate, to a reclaimable state and where their behaviour will be monitored.

These commitments must align with a large spectrum of operational and planning objectives, including the following typical mine closure objectives:

1. To eliminate long-term storage of FFT behind dams in the closure landscape.
2. To establish a stable closure landscape, with sustainable and diverse ecosystems, within a reasonable time after cessation of mining activities.
3. To develop a sustainable surface drainage including a functional lake system.
4. To facilitate progressive reclamation.
5. To optimize full lifecycle costs without compromising reclamation objectives.

FFT Progress Towards Closure

A distinction is made in this paper between two states or “conditions” of FFT as they progress toward closure:

- Condition 1 – FFT that are in their final position in the closure landscape, on a trajectory to being reclaimed (simply needing time, as defined by the closure plan), and needing no further processing. Eventually this material will dewater further, gain more strength and progress to a stable deposit.
- Condition 2 – FFT that need processing, re-processing, or other treatment measures, and may not be in their final position in the closure landscape or are not on a trajectory to being reclaimed. This is either material generated from normal tailings operations or “off-spec” material produced from some other secondary treatment process.

TAILINGS PERFORMANCE MANAGEMENT

Management of tailings performance is a part of responsible stewardship of FFT. The process is shown in Figure 2.

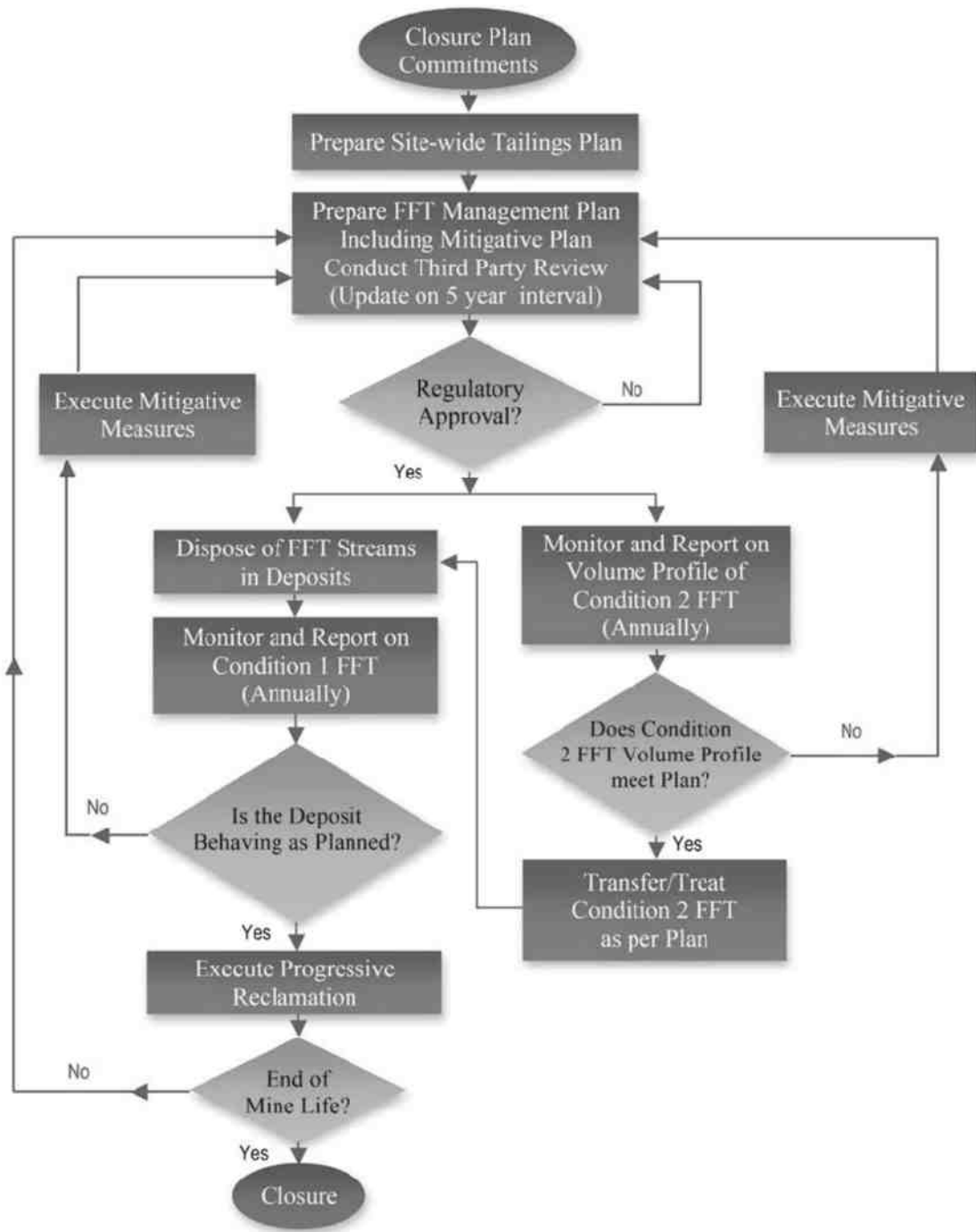


Figure 2. Tailings Performance Management Process

The tailings management process has the following steps:

1. The desired closure landscape is defined in the mine closure plan. This includes landforms that contain all mine waste products: overburden, tailings (generally), and FFT (in particular), as well as a sustainable drainage system that will facilitate the return of process-affected water of acceptable quality to the environment.
2. Long- and short-term tailings plans are developed that define the tailings streams produced from the extraction plant and where they will be disposed.
3. A FFT management plan is produced that contains the specific details of the commitments outlined previously, and details how and when the mine operator will achieve those commitments. This plan includes a discussion of the treatment technologies used to dewater the FFT and new treatment technologies in development.
4. The FFT management plan is executed, FFT behaviour is measured and FFT performance is assessed and reported to company senior management and regulatory authorities. Performance is also independently assessed (third-party review) on a five-year interval.
5. If the FFT behaviour is not consistent with the management plan, treatment technologies are improved or updated. In some cases, new treatment technologies might be developed and implemented. In either case, the objective is to bring the FFT behaviour into compliance with the mine operator's commitments. As a natural consequence, the operator might update the FFT management plan but the operator's closure commitments remain.

The PMFFT deals with Step 3 to Step 5 of the tailings performance management process.

CLASSIFICATION OF OIL SANDS TAILINGS

Oil sand tailings are classified according to the information given in: "The Oil Sands Tailings Measurement Protocol" (COSIA 2014a).

Oil sand tailings deposits are classified according to the information given in: "The Technical Guide

for Fluid Fine Tailings Management" (OSTC/COSIA 2012).

ELEMENTS OF A FLUID FINE TAILINGS MANAGEMENT PLAN

The FFT management plan contains the following elements:

- A general description of the amount of ore being mined and the FFT streams produced by the plant site.
- A discussion of the predicted behaviour of the Condition 1 FFT.
- A discussion of the volume profile of the Condition 2 FFT.
- A comparison of predicted Condition 1 FFT behaviour with actual behaviour, i.e., FFT performance.

Condition 1 FFT Predicted Behaviour

The operator will predict the behaviour over time of Condition 1 FFT in each DDA or other tailings deposit. This will include its progress toward reclamation and closure, and the end state that is consistent with the design of the closure landscape.

Table 1 shows the unique behaviour of each tailings deposit type and the corresponding primary performance factors for measuring behaviour.

Condition 2 FFT Predicted Volume Profile

The FFT management report will provide a predicted total volume profile for all Condition 2 FFT on the lease (Figure 3). FFT volumes are measured regularly to provide the basis for revised FFT volume projections and containment needs, and adjustments to the tailings plan.

The FFT predicted volume will be given in terms of its absolute amount with time, as well as volume per tonne of ore processed. The intent is to demonstrate that the volume trajectory is consistent with the progressive reclamation commitments underlying submitted plans, particularly closure plans, and to ensure that there are no trends in the trajectory that would trigger the need for additional containment.

Table 1. Deposit Performance Factors

Deposit Type	Primary Performance Measures	Purpose
Thin-layered, fines-dominated	Strength	Indicate readiness for removal or next lift (if stacking).
Deep fines-dominated	Solids content, excess pore pressure dissipation and settlement of final surface.	Progress of consolidation and readiness for capping.
Fines-enriched sand and sandy fines	Sand/Fines Ratio (SFR) distribution, solids content, excess pore pressure dissipation and settlement of final surface.	Degree of segregation, liquefaction susceptibility and readiness for capping.
Water-capped end-pit deposits	Water quality in water cap and elevation of top of FFT zone.	Suitability of water cap to meet reclamation objectives; consolidation of FFT.
FFT contained in overburden dumps	Strength change with time and settlement of dump.	Demonstrate FFT meets dump design requirements; consolidation of FFT.
Deep, low-SFR FFT deposits	Solids content, excess pore pressure dissipation and settlement of final surface.	Progress of consolidation and readiness for capping.

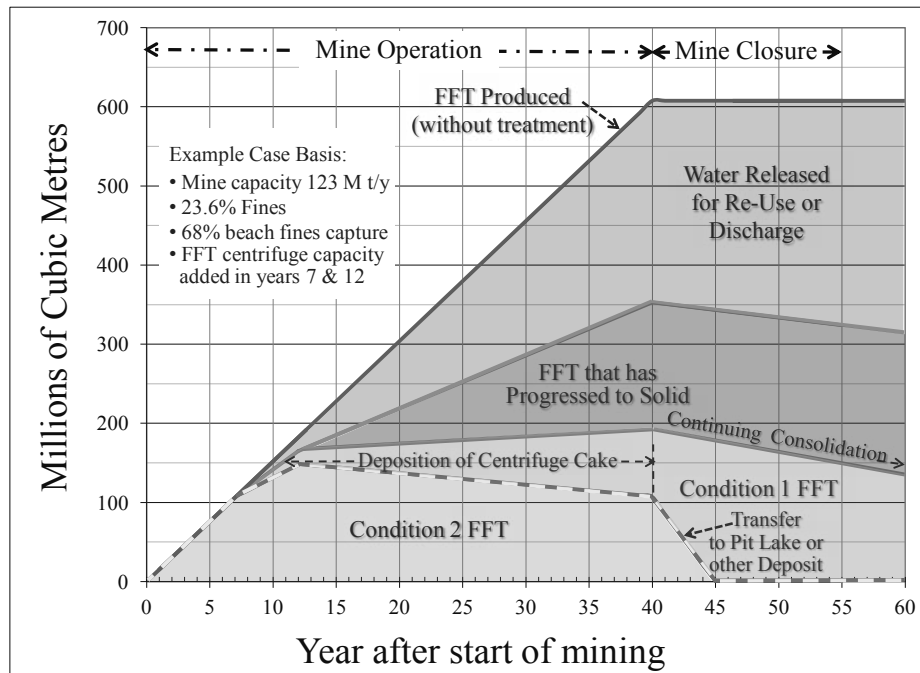


Figure 3. Schematic FFT Volume Profiles – An example of the production of Condition 2 FFT and its transition to Condition 1 FFT. The lower curve (yellow/red dashed line) on this figure would be used as the basis of a mine operator’s commitment to manage Condition 2 FFT to a maximum volume profile.

The example shown on Figure 3 is based on the parameters in the figure and applies only to that specific case. The upper line shows the volume of FFT that would accumulate if there were no additional dewatering; the lower two lines show the volumes of Condition 1 and Condition 2 FFT that would accumulate if centrifugation was introduced in two stages in the life of the mine – Year 7 and Year 12.

Report on FFT Behaviour and Performance

A mine operator will measure the volume of all FFT on its lease and the behaviour of treated deposits, in all areas described in the previous two sections. Reference will be made to the Oil Sands Tailings Measurement Protocol (COSIA 2014a) for information on measurement methods for FFT deposits. The operator will report FFT volumes and treated deposit behaviour annually.

The operator will compare the behaviour of each FFT deposit to that predicted in the FFT management plan, to establish its performance (acceptable or not). If tailings deposition proceeds according to approved plans, the tailings management report should be updated/resubmitted every five years. If there is an out-of-compliance performance or significant changes to the basic FFT management plan, the plan should be updated and resubmitted more frequently, as needed. The oil sands industry is committed to maintaining alignment of its mine, water, tailings and closure plans; revisions in any of these plans that result in a revision of the FFT management plan should trigger submission of a revised tailings management report.

Independent Performance Assessment

The operator will arrange for an independent (third-party) assessment of Condition 1 FFT and Condition 2 FFT performance ([actual–predicted] behaviour; Table 1 and Figure 3) against the FFT management plan, at least every five years, using the procedures outlined in “A Guide to the Audit and Assessment of Tailings Facility Management” (MAC 2011b) and in the newly released “A Guide to Audit and Assess Oil Sands Fluid Fine Tailings Performance Management” (COSIA 2014d). In particular, the qualifications of the assessment team, as outlined in this Guide, are critical in assessing the key performance aspects related to these unique FFT deposits. It is also vital that the audit/assessment process confirm company senior management commitment.

STEWARDSHIP TO THE FFT MANAGEMENT PLAN

Compliance

The Condition 2 FFT volume accumulation or the Condition 1 FFT deposit behaviour could be in or out of compliance with the FFT management plan. Compliance is defined as:

- A volume of Condition 2 FFT that is less than or within the range of the committed maximum volume profile (see Figure 4 for an example).
- In each tailings deposit, the actual behaviour of Condition 1 FFT that is within the range or is better than the predicted behaviour.
- Important in the assessment of FFT volume compliance are both the absolute value and the trend of the FFT behaviour. As indicated in Figure 4, actual accumulation of Condition 2 FFT could remain less than the committed volume profile, in which case it is in compliance, or it could be trending outside the committed volume profile, in which case it is, or might in the future be, out of compliance. The slope of the trend line is important as it conveys the urgency with which mitigation measures need to be implemented.

In Figure 4, the first 25 years of the volume commitment profile from Figure 3 are expanded to illustrate the situation where the accumulating FFT volume could become non-compliant with the committed FFT volume profile. In the initial years, the measured volumes remain within the commitment maximum profile, but with a small margin.

After Year 8, it becomes clear that without additional action, the committed maximum volume will be exceeded. This triggers the need for contingency action and highlights several important facets of FFT management:

- The maximum volume profile commitment should be set with a high probability of attainment, taking into account what can practically be accomplished if available contingency measures are implemented, as required.
- When measured FFT volumes are close to the commitment maximum profile, increased diligence is warranted.

- Contingency implementation needs to occur based on the trend toward exceedance, so that exceedance is avoided.

as required and/or as new technologies become available.

Adaptive Management and Contingency Actions

The approach recommended in this paper anticipates that undesirable changes can occur in FFT behaviour and adopts an adaptive management process to deal with these changes. Five-year progress reports will reflect all changes in production, resource assessment and evaluation of FFT behaviour and process performance.

As part of the adaptive management process, the operator will define contingency actions to deal with possible out-of-compliance FFT behaviour in its initial FFT management plan, will implement these actions, if necessary, and will update them

Contingency actions available to an operator in the event of non-compliance include:

- Increase the capacity of technologies or actions that perform well.
- Implement concrete and practical measures to improve the efficiency and effectiveness of current operations.
- Adopt alternative current technology that improves performance.
- Develop and implement new technology to improve performance (which has a lead time and so might not in all cases be a practical contingency action).

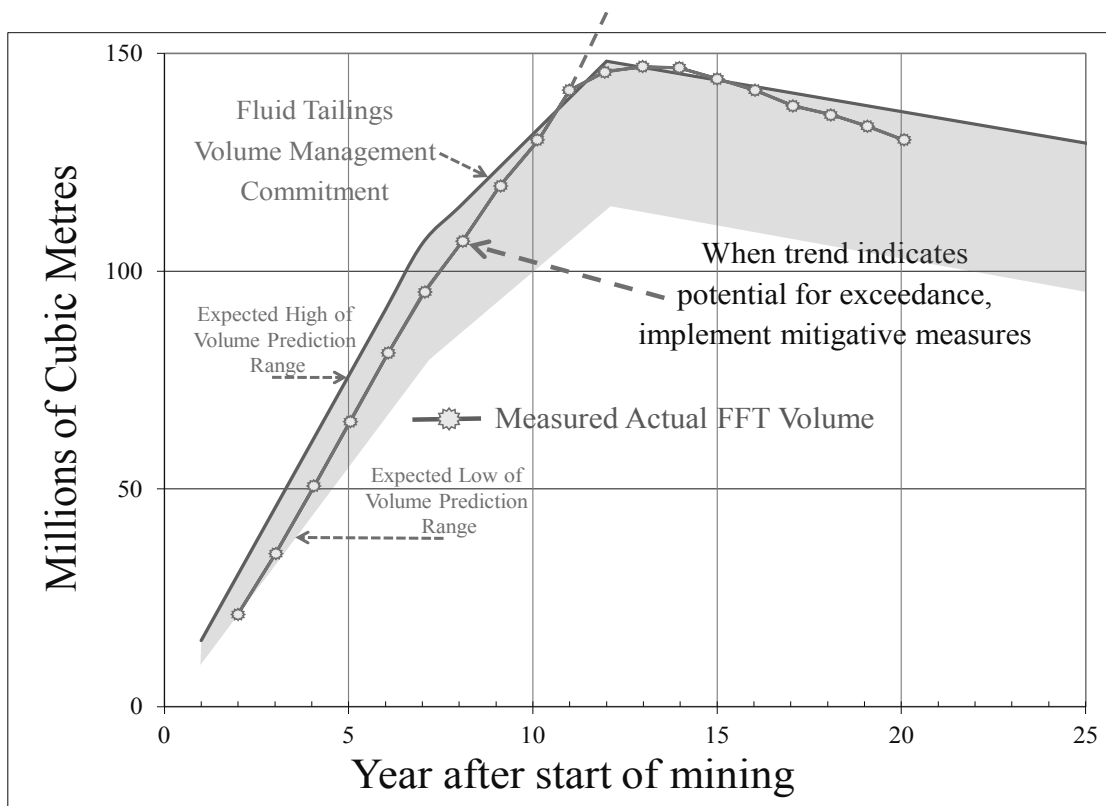


Figure 4. FFT Volume Compliance – Mitigation Measures (Illustrative)

Contingency plans need to be practical and economically viable. They also need to be identified and pre-engineered, so that they can be

implemented in time to meet FFT management and closure plan commitments (keeping in mind that where capital implementation is involved, it

could take two years or more to complete a pre engineered solution). Operators must identify how the Condition 2 material will be changed to Condition 1 material, on a deposit-by-deposit basis.

The mitigation plan should contain:

- Technology to be used, and a description of its robustness and practicality.
- Time required to implement that technology, which must be consistent with the closure plan and schedule.
- Assessment of the likelihood of success of the contingency plan.
- Impacts on the Condition 2 volume profile.

In some cases, the operator could elect to have contingency plans audited to establish robustness and likelihood of success, (see COSIA 2014d).

AUDIT AND ASSESSMENT OF FFT MANAGEMENT PLANS

COSIA has recently published “A Guide to Audit and Assess Oil Sands Fluid Fine Tailings Performance Management” (COSIA 2014d). A preview of what is in this document follows.

The Audit and Assessment Guide complements the previous COSIA documents (Figure 1) as well as the PMFFT. It describes the independent third-party audit and assessment of FFT plans and performance of operations against those plans, as called for in the PMFFT. Every five years, well-trained, third-party experts will carry out this audit and assessment process. They will verify that plan versus actual performance comparisons are correct, that the performance commitments outlined in the FFT Management Plan have been met and that plans are realistic. An important outcome of this evaluation will be an independent opinion specifying whether or not mitigation measures need to be considered.

Progressive reclamation and mine closure design require the effective integration of several engineering and other applied science disciplines. Ineffective management of FFT can necessitate building additional containment volume, may delay reclamation timing and require a greater amount of FFT treatment at mine completion than was foreseen. The scale of mining, large volumes of

FFT accumulation and the technical complexities involved in FFT treatment and measuring deposit performance justify the need for audit and assessment methods focused on these matters within an overall tailings management framework.

The audit of the management and organizational framework will determine if the key results are built into the organization from the most senior executive responsible for the mine operation through the technical and operations leaders, and the personnel responsible for planning, executing and reporting of FFT management activities.

The technical assessment will determine whether:

- Tailings plans are aligned with the production plan and forecast of fines in ore feed.
- FFT treatment processes are being operated in accordance with the production rates and specifications required to accomplish plans.
- FFT deposit behaviours are within the range of projections included in plans.
- Measurement, monitoring and reporting accurately reflect process performance and deposit behaviour.
- Plans have a reasonable probability of attainment.
- Contingency actions are necessary to achieve plan goals.

There will be a need to ensure the availability of a pool of multi-disciplined technical experts familiar with both oil sands operations and the audit and assessment process, to carry out this work. This is also addressed in the audit and assessment document.

ACKNOWLEDGEMENTS

The PMFFT document described in this paper was prepared by a committee of independent industry experts under the sponsorship of the COSIA Tailings Environmental Priority Area. The authors of the PMFFT are the same as the authors of this paper.

The authors would like to recognize and thank the following people, who reviewed the original PMFFT document:

1. Representatives from the COSIA Tailings Environmental Priority Area.

2. Technical Reviewers:

- a. Norbert Morgenstern, P.Eng., Ph.D., University of Alberta.
- b. Ross Eccles, B.Sc., M.Sc., Senior Principal, Environmental Management, Stantec.
- c. John Errington, Ph.D., John C Errington and Associates Ltd.
- d. Barry Hurdall P.Eng., C.Eng., MICE, Managing Director, BJH Engineering Ltd.
- e. Eddy Isaacs, Ph.D., FCAE, CEO, Alberta Innovates – Energy and Environmental Solutions.
- f. Bernard J. Roth BA (Hons), LLB, LLM, Partner, Dentons Canada LLP.

3. Regulatory reviewers:

- a. Jim Dilay, P.Eng., former AER (ERCB) Board member, reviewed this document for its practicality with regard to regulatory matters.
- b. Wayne Clifton, P.Eng., D.Sc., consultant to Saskatchewan Environment, Chair of the SK Environmental Code Development Committee and author of a report¹ on results-based environmental regulation of the resource industry in Saskatchewan, reviewed this document for consistency with Canadian practice and recent regulatory reform trends.

The most recent version of the PMFFT document and associated references are available through COSIA.

www.cosia.ca

¹ *Towards a Results-Based Regulatory System*. 2009. Report to the Saskatchewan Ministry of Environment. February 2009.

REFERENCES

Alberta Energy Regulator (previously Energy Resources Conservation Board). 2009. Directive 074: Tailings Performance Criteria and Requirements for Oil Sands Mining Schemes.

COSIA (Canada's Oil Sands Innovation Alliance). 2014a. Oil Sands Tailings Measurement Protocol. Report to COSIA by Thurber Engineering Ltd. and Barr Engineering.

COSIA. 2014b. Predicting FFT Volumes from Oil Sands Ore Production. (In Preparation.)

COSIA. 2014c. Performance Management of Oil Sands Fluid Fine Tailings Deposits to Meet Closure Requirements.

COSIA. 2014d. A Guide to Audit and Assess Oil Sands Fluid Fine Tailings Performance Management.

COSIA/CAPP. 2014. Mine Financial Security Program – Application to Tailings.

Oil Sands Tailings Dam Committee. 2014. De-Licensing of Oil Sands Tailings Dams, (available on the OSRIN web site).

MAC (Mining Association of Canada)–COSIA. 2014. Tailings Water Effluent Release Standard. (In Preparation.)

MAC. 2011a. A Guide to the Management of Tailings Facilities.

MAC. 2011b. A Guide to the Audit and Assessment of Tailings Facility Management.

OSTC/COSIA (Oil Sands Tailings Consortium). 2012. Technical Guide for Fluid Fine Tailings Management.

MEASURING STRENGTH IN OIL SANDS TAILINGS DEPOSITS

Heather A.W. Kaminsky

On Behalf of the COSIA Deposit Characterization Committee

ABSTRACT

Directive 074 has specified that undrained shear strength must be measured annually in a company's Dedicated Disposal Area (DDA) to ensure progress towards a reclaimable deposit. This specification implies that the DDA's would be fines dominated deposits and therefore cohesive deposits exhibiting undrained conditions during testing. In reality many different types of DDA's are envisioned with a wide range of expected fines contents and drainage behaviour. The COSIA deposit characterization committee was tasked with selecting appropriate measurement techniques for determining performance equivalent to Directive 074 requirements in all deposit types. Furthermore the committee was tasked with producing a recommended standard method for measurement to ensure consistent data and consistent data interpretation between operators. The committee has determined that Cone Penetration Testing (CPT) can be used to characterize all deposits greater than ~1m thick. However the committee has also concluded that there is no equivalent to Directive 074 for drained or partially drained deposits. For drained deposits CPT/BallCPT testing is recommended with calibration to Field Vane Shear tests. This paper documents the rationale of the committee, the limitations of the techniques and the key features of the recommended standard practices.

INTRODUCTION

In 2009 the Alberta Energy Regulatory (AER) implemented Directive 074 aimed at reducing the inventory of fluid fine tailings stored in the oil sands region. This directive specifies that 50% of material equal to or less than 44 micron in diameter be captured in dedicated disposal areas and reach an undrained shear strength of 5kPa within one year. Oil sands operators have implemented a variety of site specific tailings strategies in an effort to meet this directive and internal business needs. The operators have also adopted a variety of methods to measure and report on the performance criteria outlined in Directive 074. It has been realized by

the industry that the variety of methods creates confusion in reporting, communicating and efficiently regulating tailings performance. To this end, Canada's Oil Sands Innovation Alliance (COSIA) was asked by the AER to evaluate the technical merits of the different reporting methods and propose standard methods that would be appropriate across the industry.

In January 2013, a concerted effort by COSIA towards standard measurement techniques resulted in the "Oil Sands Tailings Measurement Protocol Workshop". The Protocol identified that the measurement of undrained shear strength may be an appropriate tool for monitoring regulatory compliance in fines-dominated deposits, but noted that there may be issues in applying the technique to non-fines dominated deposits and therefore recommended further studies. In response, the Deposit Characterization Committee, referred hereafter as the committee, was formed in July 2013. The committee was comprised of representatives from COSIA member companies and AER and was given the following tasks:

1. To select in situ strength measurement technique(s) for each oil sand deposit type to measure deposit performance equivalent to Directive 074 requirements (5kPa undrained shear strength in fines dominated deposits within one year); and
2. To review current ASTM standards, and/or industry developed procedures of the selected technique(s) and develop documentation to provide the industry with guidance towards standardizing the recommended measurement method(s).

This paper provides a summary of the work completed by the committee and the thought process involved.

Background

Prior to the work of the deposit characterization committee, COSIA had commissioned Thurber Engineering Ltd. to prepare the "COSIA Tailings Measurement Protocol" which proposed a Universal Oil Sands Tailings Classification System

(UOSTCS) and reviewed appropriate measurement techniques including those for measuring strength. The Protocol identified that the measurement of the undrained shear strength may be an appropriate tool for monitoring regulatory compliance in fines-dominated deposits, and noted that current methods used for in situ strength testing in deposits with a fines content <50% may not be meaningful.

The COSIA Tailings Measurement Protocol proposed that solids content or pore pressure dissipation may be used as an alternative tailings performance indicator to assess fluid tailings progress towards reclamation. This proposal was based on the knowledge that the consolidation of fluid tailings is associated with dissipation of excess pore water pressure and decrease in void ratio. Since void ratio and solids content are interchangeable parameters for saturated materials such as oil sands tailings, measuring either pore pressure dissipation or solids content would provide an indication of consolidation and hence an indication of the progress towards reclamation. The protocol indicated that current methods of solids content measurement do not have the resolution required for year over year compliance reporting. The protocol did not evaluate the resolution of current pore pressure measurements.

The committee decided to accept the recommendations in the measurement protocol that Field Vane Shear Testing (FVST) was an appropriate method for measuring undrained shear strength in undrained, cohesive deposits, but felt that there were outstanding issues around defining what was an undrained cohesive deposit and further issues around the repeatability of current FVST standards. The committee also recognized that FVST is an expensive technique and therefore there is a need for more practical options. Furthermore the committee recognized the need to explore methods of measuring compliance in drained deposits.

To address these questions the committee decided to:

- Conduct a literature review to assess in situ monitoring methods used to characterize loose sandy deposits in other parts of the world;
- Conduct a literature review to assess geophysical methods of measuring solids and fines contents in oil sands tailings;

- Review the use of pore pressure measurements to monitor consolidation progress;
- Review of standard test methods for FVST and electrical Cone Penetration Test (CPT) in cohesive soils;
- Survey experts and providers of FVST and CPT regarding the use of CPT/Ball-CPT and FVST for measurement of undrained shear strength as required by Directive 074; and
- Evaluate CPT-Sample data pairs from 118 logs.

KEY FINDINGS

Literature Survey of Monitoring Methods Used in Loose, Sandy Deposits

Sand dominated natural alluvial deposits have similar compositions to oil sands composite tailings (CT) and non-segregated tailings (NST). Based on the literature search of monitoring methods in other deposits and considering the overall performance of each technique, CPT with either pore pressure or seismic sensors has been recommended as the in situ test method for “characterizing” sandy tailings deposits.

Literature Review to Assess Geophysical Methods of Measuring Solids and Fines

It was determined from this literature review that there are currently no commercially available techniques that can be relied upon for in situ solids or fines content measurement in oil sands tailings. The literature review identified that; based on accuracy, applicability and deficiency of each technique, Frequency Domain Reflectometry and Gamma Ray Logging/Gamma CPT appear to be the two most suitable geophysical methods of determining solids content within the oil sands fluid tailings.

Report For Evaluating Applicability of Pore Pressure As A Method For Measuring Deposit Performance Per Directive 074

The report concluded that pore water pressure measurements cannot be used as a performance indicator relative to the strength criteria outlined in Directive 074 since pore water pressure measurement cannot be directly related to the strength of a material.

As part of the report, instrument accuracies and resolutions for various pore water pressure measurement techniques were collected and compared with simulated consolidation behaviour of typical oil sands tailings deposits. It was further concluded from the work that:

- For long term consolidation tracking, the commercially available piezometers can be used to track the cumulative change in pore water pressure for all types of oil sands tailings deposits;
- For yearly consolidation tracking, the commercially available piezometers are primarily suitable for sandy fine deposits (SF);
- Not all available pore pressure instruments are suitable for monitoring deep oil sands tailings deposits. The most suitable instruments for monitoring pore pressure in deep tailings deposits are either vibrating wire or electrical resistance piezometers; and
- Conventional standpipe piezometer and the CPT_u are not considered suitable for monitoring cumulative or yearly pore pressure changes in deep tailings deposits.

Review of Standard Test Methods for FVST and CPT in Cohesive Soils

The committee reviewed ASTM D 2573-08 (FVST) and accepted it as a standard method for measuring undrained shear strength in oil sands fine tailings. The committee recognized that, while the method was not as repeatable as desired, the process of replacing the standard would be beyond the capacity of the committee. To improve the repeatability of the measurement Dr. Peter Robertson and Dr. John Howie were contracted to write an addendum to the standard outlining the additional procedural requirements specific to the measurement of fine-grained oil sand tailings with very low shear strength. The addendum recommends the use of CPT to identify undrained areas in a specific deposit that are suitable for FVST. Undrained conditions are identified when a CPT_u pore pressure dissipation test carried out using a standard 10cm² cone with pore pressure measurement at the cone shoulder (u₂ position; ASTM D5778-12) gives the time to 50% pore pressure dissipation, t_{50} , of greater than 100 seconds (DeJong et al., 2013).

The committee also reviewed ASTM D 5778-12 and accepted the procedure as the standard method for CPT testing. The Dejong modification

(Dejong 2010) proposed for adapting the ASTM standard to Ball-CPT testing was also accepted.

Evaluation of CPT-Sample Data Pairs from 118 Logs

Peter Robertson provided a range of CPT tip resistances expected for the range of unit weights and cone/ball factors experienced in oil sands. Figure 1 shows how the pore pressure corrected tip resistance of a cone is expected to vary as a function of depth in a normally consolidated, uniform material exhibiting an undrained shear strength of 5kPa. Using this plot one could assume that any measured tip resistance greater than the maximum line would certainly be greater than 5kPa regardless of site specific factors. Similarly any measured resistance that plotted below the minimum line would certainly not meet 5kPa regardless of site specific factors. He also recommended that since CPT tip resistance could be generated in any type of deposit a simple regulatory compliance tool may be to: *“Measure the CPT Cone Tip Resistance profile in a particular deposit, and compare such a profile to an expected theoretical profile for tip resistance in a deposit with 5kPa undrained shear strength.”*

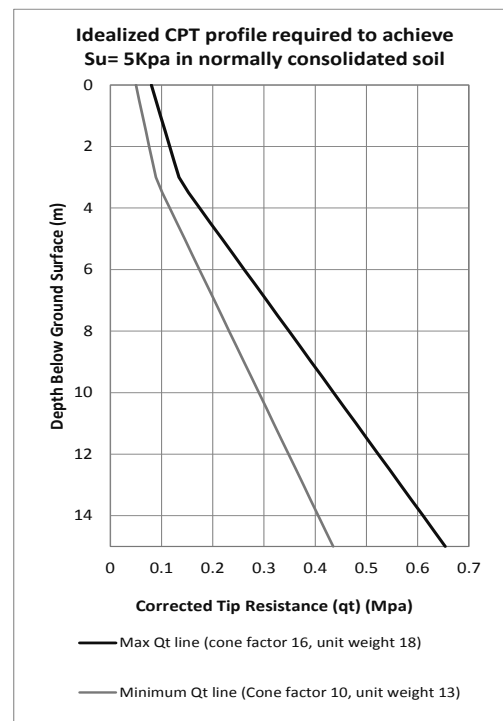


Figure 1. Expected theoretical CPT profile for a deposit with 5kPa undrained shear strength.

Based on this proposal; analysis of CPT data from various oil sands operators was undertaken to assess the applicability of CPT tip resistance to characterize deposit types as identified in the UOSTCS and to be used as an alternative measure to the 5kPa undrained shear strength requirement. Figure 2 shows CPT data from various operators plotted on the ternary diagram. It should be noted that pairing CPT and solids content data is not a trivial exercise as the samples are not taken in exactly the same location or time and the solids content measurements are at discrete locations rather than in a continuous profile. The following can be observed from Figure 2.

- The data sets evaluated were concentrated in the loose sand region (border of S/SF and T regions). The rest of the data were either in the region of fluid fines dominated tailings (T2 and F2) or sands above water (S) with less than 10% fines.
- Minimal data was found in the band of fines dominated semi solid tailings (along the liquid limit boundary) and fines dominated solid tailings deposit (F3).
- There is an area where low, moderate, and high cone tip resistance values overlap. This area is around the boundary between S and SF/T regions. It is anticipated that tip resistance should increase rapidly with increasing solids content in this area and therefore slight differences (i.e. ± 2 to 5%) could change the expected behaviour significantly. Furthermore, the presence of high strength layers will influence the tip resistance up to 25 tip diameters ahead of the tip which complicates the interpretation. Additional work is needed to fully understand these issues.

In addition to the data presented in Figure 2, statistics of average of median tip resistance of three tailings phases (as classified by the laboratory paired data): fluid (top portion of ternary diagram), semi-solids (see Figure 2), and solids (bottom portion of Figure 2) are provided in Table 1. As expected, fluid tailings produce a tip resistance that is on average far less than that of solid tailings, however there is a wide degree of scatter making analysis solely based on tip resistance difficult.

DISCUSSION

During the committee's deliberations it was evident that the measurement of undrained shear strength was not possible in drained or partially drained deposits. Therefore much of the committee's deliberations focused on determining the equivalence to the Directive 074 measurement of 5kPa undrained shear strength for these drained deposits.

Table 1. Summary of CPT Tip Resistance by Soil Type as Defined by Lab Testing

	Sand Dominated (SFR>1.5:1)			Fines Dominated (SFR<1.5:1)		
	Fluid	Semi-Solid	Solid	Fluid	Semi-Solid	Solid
Average qt (MPa)	2	2	5	0.1	1	2
Standard Deviation (MPa)	2	3	6	0.2	1	2
Count of Data (#)	36	945	249	281	73	35

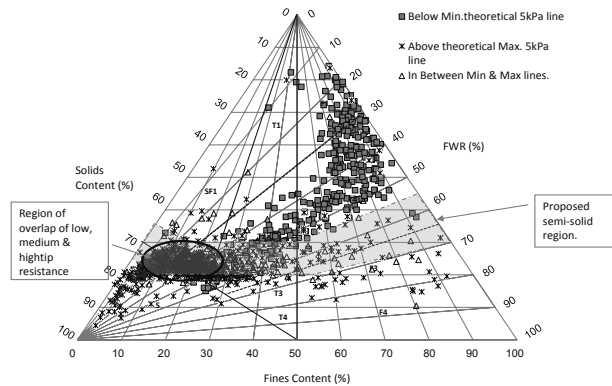


Figure 2. Plot of CPT data provided representing all operators plotted by solids and fines content on UOSTCS chart.

In these oil sands tailings types, the committee explored three proposals for equivalency to the 5kPa requirement in drained and partially drained deposits:

- Detecting liquefaction potential;
- Detecting semi-solid/fluid boundary; or
- Numerical equivalence of CPT tip resistance.

Use of Liquefaction Potential

The committee considered using liquefaction potential of a deposit as an equivalent to the Directive 074 strength requirements. Soil liquefaction potential describes a phenomenon whereby a saturated or partially saturated soil substantially loses strength and stiffness in response to an applied stress. The committee decided that where such a parameter may be suitable for long term stability of the deposits, it may not be appropriate for reporting year by year improvements within the tailings deposits. Similarly, it was recognized that the liquefaction potential of a deposit is influenced in part by the containment design and thus is extremely site specific. It was agreed upon that a criterion based on liquefaction potential was quite complex and was not appropriate as a regulatory tool for Directive 074 compliance.

Detecting Solid/Fluid Boundary

During the committee's discussions it was understood that the AER's undrained shear strength requirement of 5kPa was essentially a way of classifying fines dominated material as a soil. Fines dominated material is not expected to behave as a fluid if the material is above the liquid limit. The liquid limit of a fine grained soil typically has an undrained shear strength exceeding ~2kPa, (Terzaghi and Peck, 1996). The committee understands that the 5kPa peak undrained shear strength was considered in Directive 074 to ensure when the moisture content of the material was lower than the liquid limit and therefore no longer a fluid.

It was also postulated that since the CPT tip resistance could be used to provide an "indirect measure" of both undrained shear strength and soil density, one could perhaps use the CPT tip resistance to identify the solid/fluid boundary in oil sands fluid tailings. Having postulated this, the committee analyzed 108 CPT logs, from three (3) oil sands operators, paired with solids and fines content data. The data was analyzed extensively to observe if there was a particular "CPT Tip Resistance Value" which would differentiate between fluid and solid material. Accurate solids and fines content profiles are essential to evaluate quality of the CPT data. It was observed through the work that solids content determination of samples collected using a sonic sampler may not have sufficient spatial resolution to capture the changes occurring within the deposit. It was

recommended that it is worth looking into a better solids content measurement method in the future (e.g. geophysical methods of measuring volumetric water content that could then be converted to solids content). Based on these results, the committee further concluded that there wasn't a sufficient quantity and quality of data to identify and make a recommendation for the CPT tip resistance to be used to detect solids/fluid boundary as defined by theoretical solids/fines composition within the oil sands tailings.

Use of CPT Tip Resistance

It was recognized that both CPT and Ball-CPT have the ability to "characterize" all types of tailings deposits across UOSTCS and therefore generate a tip resistance value in all deposit types. Robertson's approach of comparing a measured CPT plot to a theoretical plot at 5kPa was considered to greatly simplify the complexity of the challenge. While such a simplification was viewed as acceptable to some committee members, it was not universally accepted by all committee members.

In conclusion, although there were several alternatives proposed and evaluated, the committee did not find an option that was an appropriate equivalent performance measure of Directive 074 compliance within drained or partially drained deposits.

MEASURING UNDRAINED SHEAR STRENGTH

Applicability of Measurement

The measurement committee agreed with the conclusions of the tailings measurement protocol that any oil sands deposit with a sand to fine ratio (SFR) <1.5 can be considered to be undrained under most loading conditions.

DeJong et al. (2013) suggest that materials in which a CPT_u dissipation test gives the time to 50% pore pressure dissipation, t_{50} , greater than 100 seconds will behave in an undrained fashion when penetrated by a 10 cm² cone penetrometer at the standard rate of 2cm/s. Similarly, material which has a t_{50} pore pressure dissipation time exceeding 100s as measured by a CPT pore pressure dissipation test may be considered undrained regardless of their SFR.

The committee concluded that undrained shear strength is typically appropriate for use in materials with a SFR ≤ 1.5 or in materials having a t_{50} pore pressure dissipation time greater than 100s.

Directive 074 is not specific as to whether peak or residual strength is required for compliance. For regulatory compliance the subcommittee understood the 5kPa requirement to be the “peak shear strength of the deposit under undrained conditions”.

Two methods of measuring undrained shear strength were recognized as most appropriate by the committee CPT/Ball-CPT and FVST.

- The committee concluded that FVST is a direct measure of undrained strength and is an appropriate technique when performed according to appropriate ASTM standards.
- CPT/Ball-CPT is an indirect measurement of undrained shear strength. The reliability, repeatability and productivity of these tests far exceed that of FVST. As such, these are the preferred undrained shear strength test methods recommended by the committee. The CPT/Ball-CPT measures an intermediate between peak and residual undrained shear strength (this has not been verified with lab data). The correlation between tip resistance and undrained shear strength is site specific, depending on the unit weight and the specific correction factor of the tailings.
- Hand-held vane testing is recognized as a less reliable version of FVST or CPT but the test is acceptable for testing deposits where FVST or CPT/Ball-CPT are deemed impractical or uneconomical.
- CPT-Ball CPT testing should be calibrated/verified on a site specific basis using FVST on a limited number of holes when used for oil sands tailings deposit measurements.

FVST

FVST is performed by inserting a four-bladed vane into the intact soil at discrete depths and rotating the vane at a constant rate by applying a measured torque to create a cylindrical failure surface in the material. Both peak and remolded undrained shear strength can be obtained without further strength corrections. FVST has the advantage that it measures undrained shear strength (S_u) directly, but is slow, expensive, discontinuous and is limited to only soft fines-dominated soil. FVST is generally limited to, S_u

$<200\text{kPa}$ and in that regards is well suited to soft fines dominated oil sands tailings. FVST can be significantly operator dependent when measuring undrained shear strength.

During consultation with technical experts it was agreed upon that the COSIA Tailings EPA should not continue to develop a COSIA standard for FVST, but should instead write an addendum to the existing ASTM Standard D2573-08 with requirements specific to the very low shear strengths of the oil sand tailings. It is recommended that for oil sands tailings the test be conducted using ASTM D 2573-08 along with the addendum provided by Robertson & Howie as provided in the Appendix.

Limitations of FVST

To achieve good FVST results it is important to ensure that the material being tested is in fact undrained. It is recommended that initial testing be carried out using CPT (in accordance with D5778-12) to define stratigraphy and determine zones of fine-grained tailings in which FVST may be appropriate.

A CPT_u pore pressure dissipation test carried out using a standard 10cm² cone with pore pressure measurement at the cone shoulder (u₂ position; ASTM D5778-12) gives the time to 50% pore pressure dissipation, t_{50} , greater than 100s (DeJong et al., 2013) to ensure that undrained conditions exist. In such soils, it is conventionally assumed that a FVST carried out in general accordance with the ASTM D2573-08 will provide a measurement of undrained shear strength. It is assumed that a precision of $\pm 0.5\text{kPa}$ is required in order to measure compliance with Directive 074. In order to achieve such precision, the torque load cell must be calibrated to account for all factors affecting the measured torque. The recommended minimum thickness of the deposit to be tested should be 6H, where H is the height of the vane.

It is thus recommended that CPT testing be done to confirm the stratigraphy of the deposit and select appropriate sampling locations.

CPT/Ball-CPT

CPT consists of inserting a penetrometer with a conical point and friction sleeve into the soil at a constant penetration rate while electronically measuring cone resistance, sleeve resistance, and pore water pressure to produce a continuous data

profile with depth. The tip resistance can be corrected for necessary design data (undrained shear strength, friction angle and state parameters etc.) through the use of well-established correlations after a determination of the appropriate site specific correction factors. For example, undrained shear strength (S_u) of fines dominated deposit ($SFR < 1$) can be interpreted from cone tip resistance by a theoretical relationship with a site specific correction factor (N_{kt}).

Based on field work performed by oil sands operators, undrained shear strength derived from CPT tip resistance in fines dominated deposits correlates well with those from FVST. The test procedures should follow ASTM D 5778-12. For Ball-CPT, modification suggested by Dejong (2010) should be followed along with ASTM D5778-12 (i.e. locating the pore pressure measurement at the equator of the ball, penetration rate of 0.2 to 0.3 diameters/second, appropriate calibration and recording measurements on both extraction and penetration of the ball).

Quality Assurance

CPT is an indirect measurement technique which requires empirically and theoretically derived relationships to convert the cone tip resistance to various soil parameters. CPT experts John Howie and Peter Robertson have indicated that conventional limit of accuracy for cone is 25kPa and 10kPa for ball (Deposit characterization committee final report, Appendix E).

Care should be taken to ensure the cone capacity and tip size is in the appropriate range to provide the desired accuracy. In addition, extra attention must be paid to the load cell calibration to ensure repeatability. Most cones have an accuracy/repeatability of about 0.2% of full-scale output (FSO), although it is possible to be better than 0.1% under ideal conditions. If a cone has a measurement accuracy/repeatability of 0.2% of FSO, the FSO for the tip resistance (q_c) should not exceed about 5MPa for accuracy of 10kPa and 15MPa for an accuracy of 30kPa.

Limitations of CPT

CPT measurement is influenced by the material properties - not only the soil layer the cone is in, but by the soil layers ahead of and behind the penetrating cone. The transition from one soil layer

to another will not necessarily be registered as a sharp change in tip resistance at the interlayer boundary. In soft material, the cone tip is typically reading information 5 cone diameters ahead of the tip, while in harder materials it is influenced by material 20 to 25 cone diameters ahead of the tip (Ahmadi and Robertson, 2005). This effect must be well understood when analyzing CPT data. It is for this reason that CPT is not recommended for deposits less than 1m in thickness, though with appropriate care an interpretation is feasible. Low capacity small diameter cones may be suitable in the less than 1m range as the smaller tip diameter means a smaller sphere of influence ahead of the cone. Smaller tips may, however, lead to a reduced sensitivity which may be inappropriate in very soft deposits.

CONCLUSIONS

In summary based on the committee deliberations, expert reviews, the workshops, and inputs from technical experts the following main conclusions are drawn:

- Undrained shear strength as specified in Directive 074 can only be measured in undrained deposits. Undrained deposits are defined as having an $SFR \leq 1.5$ or a time to 50% pore pressure dissipation (t_{50}) greater than 100 seconds as measured by a standard 10cm^2 cone with pore pressure measurement at the cone shoulder (u_2 position ; ASTM D5778-12).
- CPT is appropriate to “characterize” all deposits types and could be used to provide the stratigraphy of deep or mixed deposits.
- CPT done in accordance with ASTM D5778-12 calibrated to FVST measured in accordance with ASTM D2573, and the Howie addendum is the recommended method for measuring undrained shear strength in fines dominated deposits.
- Hand held vane testing is considered an appropriate technique where the use of CPT/Ball-CPT or FVST is impractical or uneconomical. Other tests which can demonstrate a correlation to CPT or FVST are also considered acceptable by the committee.
- The threshold of $S_u = 5\text{kPa}$ is at the very low end of the shear strengths typically measured in land-based geotechnical characterization.
- The committee could not agree on a definition of equivalent performance measure to

Directive 074 in drained or partially drained deposits (SFR>1.5, with t_{50} <100s).

Trempe Moore, Bill Shaw, Jamie Sharp, John Howie, Peter Roberston, and Tom Posey for your contributions to the committee.

RECOMMENDATIONS

To truly assess the repeatability, reliability and physical meaning of CPT measurements in oil sands tailings more CPT data should be collected and analyzed. The committee recommends that the following questions be answered in such an analysis:

- How precisely can CPT identify the semi-solid/liquid transition in fines dominated deposits?
- How repeatable is the use of CPT in sandy oil sands deposits?
- Is the field chart proposed by Dejong et al (2013) applicable for oil sands and therefore can CPT testing be conducted at faster velocities to maintain undrained conditions?

Accurate solids and fines content profiles are essential to evaluate quality of the CPT data. It has become evident through the work that solids content determination of samples collected using a sonic sampler may not be accurate. A field testing program should be developed and carried out to gain confidence in solids content data. It will be worth looking into a better solids content measurement method in the future (i.e. geophysical methods of measuring volumetric water content that could then be converted to solids content).

Further analysis is also recommended for the FVST to:

- Determine if and by how much the use of the addendum vs. the ASTM method alone improves the repeatability of FVST in fines dominated oil sands tailings.
- Determine whether FVST can be carried out at a faster torque rate than is currently allowed within ASTM D2573 to push partially drained materials into the undrained sphere.

ACKNOWLEDGEMENTS

Thank you to the members of the Committee: Mohammad Al-Mamun, Paul Cavanagh, Africa Geremew, Michael Graham, Ted Lord, Haneef Mian, Wayne Mimura, Reza Salehi, and Vivian Zhang. Thanks also to Arif Abu, John Sobkowicz,

REFERENCES

Ahmadi, M. M., & Robertson, P. K. (2005). Thin-layer effects on the CPT qc measurement. *Canadian Geotechnical Journal*, 42(5), 1302–1317.

Alberta Energy Regulator (formerly ERCB) (2009) Directive 074: Tailings Performance Criteria and Requirements for Oil Sands Mining Schemes.

ASTM Standard D2573-08, 2008. Standard Test Method for Field Vane Shear Test in Cohesive Soil. ASTM International, DOI: 10.1520/D2573-08.

ASTM Standard D5778-12, 2012. Standard Test Method for Electronic Friction Cone and Piezocone Penetration Testing of Soils. ASTM International, DOI:10.1520/D5778-12

COSIA (Canada's Oil Sands Innovation Alliance). 2014. *Oil sands tailings measurement protocol*. Report to COSIA by Thurber Engineering Ltd., Barr Engineering and WHS Engineering.

COSIA (Canada's Oil Sands Innovation Alliance). 2014. *Performance Management of Oil Sand Tailings Deposits to Meet Closure Commitments*.

COSIA (Canada's Oil Sands Innovation Alliance). 2014. *Deposit Characterization Committee Final Report*.

DeJong, J.T., Yafrate, N.J., DeGroot, D.J., Low, H.E., Randolph, M.F.(2010). Recommended Practice for Full-Flow Penetrometer Testing and Analysis. *Geotechnical Testing Journal*, 33(2): 1-13

DeJong, J.T., Jaeger, R.A., Boulanger, R.W., Randolph, M.F., and Wahl, D.A.J. (2013). Variable penetration rate cone testing for characterization of intermediate soils, *Geotechnical and Geophysical Site Characterization 4*, Coutinho & Mayne (eds) Taylor & Francis Group, London, ISBN 978-0-415-62136-6

Terzaghi, K. And Ralph B. Peck. (1996) *Soil Mechanics in Engineering Practice* 3rd. Edition, Wiley-Interscience, New. York, 549 pp.

APPENDIX

Proposed Addendum to D2573-08, (Standard Test Method for Field Vane Shear Test in Cohesive Soil) for Application to Assessing Compliance with Directive 74.

It is anticipated that initial testing will be carried out using the piezocone penetration test (CPTu carried out in accordance with D5778-12) to define stratigraphy and determine zones of fine-grained tailings in which Field Vane Shear Testing (FVST) is appropriate. The method set out in this addendum is applicable in fine-grained tailings in which a CPTu pore pressure dissipation test carried out using a standard 10cm² cone with pore pressure measurement at the cone shoulder (u_2 position - ASTM D5778-12) gives the time to 50% pore pressure dissipation, t_{50} , greater than 100 seconds (DeJong et al., 2013). In such soils, it is conventionally assumed that the vane shear test carried out in general accordance with the ASTM D2573-08 will provide a measurement of undrained shear strength. The minimum thickness of layer to be tested should be 6H, where H is the height of the vane.

Vane Size

D2573-08 allows for vane sizes of 35 to 100mm. For the Oil Sand Tailings (OST), the vane size should be at least 65mm in diameter and vanes up to 150mm in diameter are allowed.

In order to keep the level of disturbance consistent with past experience, the dimensions of the vane, the blade thickness and the shaft to which the vanes are attached should have a vane area ratio (defined in D2573-08) less than 12%. In addition, Lunne et al. (2011) recommend that the vane blade thickness should be kept as low as possible with a perimeter ratio ($=4e/d_{vane}$, where e is the vane blade thickness and d_{vane} is the vane diameter) no more than 3%. The ratio of vane diameter to push shaft diameter should be at least 3. These additional constraints should be considered in the sizing of the vane.

Procedure

The procedure should follow D2573-08 but with some adjustments when measuring very low strengths.

The vane should be pushed or lowered into position and testing should begin within about 1 minute and certainly less than 5 minutes. This will limit the potential for dissipation of excess pore pressure created by vane insertion.

The vane should be rotated by a geared torque motor capable of the required rates of rotation. If a measurement of remoulded strength is required, then the torque motor should also be capable of rotating the rods at a faster rate (say 1 degree/s) for the required 5 to 10 turns before recording the remoulded strength.

For measurement of shear strength, the vane should be rotated at a rate between 0.05 to 0.2 degrees/s as specified in D2573-08.

Torque should be measured with a torque load cell mounted just above the vane. Location of the load cell should conform to the requirements of Section 6.1.5 of D2573-08. The capacity of the torque load cell will depend on the vane size but should be sufficient to achieve a calculated shear strength with a target accuracy of ± 0.5 kPa.

Calibration

The torque measurement device must be calibrated before and after project deployment to demonstrate that the required accuracy can be achieved. To ensure the required accuracy, the torque load cell should be capable of measuring a calculated shear strength of the larger of 0.5kPa or 10% of the measured value. Check calibrations according to Section 7 of D2573-08 should be carried out periodically during the project.

As torque is to be plotted against angular rotation in degrees, it will be necessary to calibrate the rods for twist between the point of application and the vane as per Section 6.3.2 of D2573-08.

Reporting

In addition to the requirements of D2573-08, Section 10, the results of the FVST should be plotted in terms of uncorrected and corrected torque vs. rotation (degrees) and also in terms of Vane Shear Stress vs. Rotation (degrees). The rates of rotation applicable to each portion of the curve should be noted on the curve.

REFERENCES

- Ahnberg, H., Larsson, R. and Berglund, C. (2004). Influence of vane size and equipment on the results of field vane tests. In *Richards, A.F. (ed.). Geotechnical and Geophysical Site Characterization*, Rotterdam, Millpress, Vol.1:271-277.
- Biscontin, G. and Pestana, J.M. (2001). Influence of peripheral velocity on vane shear strength if an artificial clay. *Geotechnical Testing Journal*, 24(4), 423-429.
- Chandler, R.J. (1988). The in-situ measurement of the undrained shear strength of clays using the field vane. *Vane Shear Strength Testing of Soils: Field and Laboratory Studies*, ASTM STP 1014:13-45.
- DeJong, J.T., Jaeger, R.A., Boulanger, R.W., Randolph, M.F., and Wahl, D.A.J. (2013). Variable penetration rate cone testing for characterization of intermediate soils, *Geotechnical and Geophysical Site Characterization 4*, Coutinho & Mayne (eds) Taylor & Francis Group, London, ISBN 978-0-415-62136-6.
- Lunne, T., Andersen, K.H., Low, H.E., Randolph, M.F. and Sjørsen, M. (2011) Guidelines for offshore in situ testing and interpretation in deepwater soft clays, *Can. Geotech. J.* 48: 543–556.
- Perlow, M., Jr. and Richards, A.F.(1977), *Geotechnical Division, Proc. of the ASCE*, Vol. 103, 19-32.
- Peuchen, J., and Mayne, P.W. (2007). Rate effects in vane shear testing. In *Proceedings of the 6th International Offshore Site Investigation and Geotechnics Conference: Confronting New Challenges and Sharing Knowledge*, Society for Underwater Technology, London. pp. 187–194.
- Randolph, M.F. (2004). Characterisation of soft sediments for offshore applications. *Proc. 2nd Int. Conf. on Site Characterization, Porto*, Vol. 1, 209-231.

COSIA DESIGN OF EXPERIMENT STUDY IN SUPPORT OF DEVELOPMENT OF A STANDARD FOR FINES MEASUREMENT IN OIL SANDS

*Ron Currie, *Haneef Mian, *Bei Zhao, Brenda Crickmore¹, Lauren Asplund², Tea Malkova³, Brad Komishke⁴, John Clarke⁵ and Robert Mahood²

¹Syncrude Canada Ltd.

²Shell Canada Energy

³Canadian Natural Resources Limited

⁴TECK Resources Ltd.

⁵TOTAL E & P Canada Ltd.

On behalf of the COSIA Fines Measurement Working Group *NAIT Applied Research Centre in Oil Sands Sustainability (NARCOSS)

ABSTRACT

Canada's Oil Sands Innovation Alliance (COSIA) Tailings Environmental Priority Area (EPA) and its Fines Measurement Working Group (FMWG) is working to develop a standardized method for the measurement of % fines at 44 micron in support of an initiative by the Alberta Energy Regulator to standardize key tests supporting D-74 reporting requirements.

This method will enable Operators and their internal and contract laboratories analyzing samples, ranging from oil sands cores to fluid tailings, to generate data with an acceptable level of precision. There are five major steps in the fines measurement method: sample cleaning, disaggregation, subsampling, dispersion and measurement. Several different procedures are currently being practiced for each of these major steps in the test method, depending on the Operator requirements and the laboratory conducting the tests. The FMWG has proposed a standard method with several options available to conduct each of the 5 major steps. ASTM E1169 suggests that ruggedness testing be performed as part of a validation phase of a standard test method before conducting an inter-laboratory study, and this paper will present the results of a full-factorial design of experiment (DOE) study with a focus on two disaggregation, three dispersion, and three measurement procedures. The data will reveal whether these different procedures can generate fines measurement data without any relevant statistical differences. It is expected that the result will be of value to ensure the success of the subsequent COSIA inter-laboratory fines measurement study. Preliminary results of the COSIA inter-laboratory study (ILS) will be shared if available at this time, as these results will be used

to establish the analytical precision using the procedures established by the FMWG.

INTRODUCTION

Background

COSIA (Canada's Oil Sands Innovation Alliance) is currently working with the AER (Alberta Energy Regulator) and oil sand Operators to develop an oil sand industry standardized Unified Fines Measurement method for measurement of the fines fraction (% fines at 44 micron) to fulfill the reporting requirements of Directive 74.

The intent is that this method will be able to be used by all laboratories reporting on samples ranging from oil sands cores to fluid tailings. The Fines Measurement Working Group (FMWG) within COSIA Tailings EPA (Environmental Priority Area) has been tasked with leading this initiative. The FMWG contracted NARCOSS to conduct a Design of Experiment (DOE) in support of this task and to confirm and refine assumptions about the suitability of the proposed standard method. This report presents the interim results for the work in progress in developing the Unified Fines Measurement method.

Once an agreement on standard operating procedures (SOPs) for fines measurement has been achieved within COSIA, an inter-laboratory study (ILS) will be conducted by COSIA with support from Alberta Innovates Technology Futures (AITF). This will assess the ability of individual laboratories, based on their confidential reports, to generate consistent fines measurement data using the established SOPs. Any of the procedures adopted must generate fines

measurement results that have an acceptable level of precision for all sample types.

Early discussions resulted in a plan that involved five fundamental steps for fines measurement. These are: sample cleaning, disaggregation, subsampling, dispersion and measurement. Although the mandate was to focus on % fines at 44 micron, it was also deemed incidentally valuable to assess the effects of procedural variations on the entire particle size distribution (PSD) including the sub 44 micron particles.

Existing particle size distribution methods commonly in use by the oil sand industry, as well as established institutional methods used in other industries, were evaluated with laboratory data as part of this method development. The unique nature of the sample materials requires more sample preparation in terms of cleaning and dispersion than standards already established for soils provide.

Significant challenges remain that impact this method, and include obtaining representative sampling within an operating oil sands processing facility that is outside the scope of this study. Specific challenges to the method include obtaining consistent measurement of particles with organic attachment, variation in fine tails constituents affecting particle density assumptions, laboratory occupational health and safety concerns, and scope and cost increases that may be incurred compared to the various laboratory methods presently in use.

Method Discussion

Sample cleaning is the first step in the method since bitumen is not to be reported as part of the fines measurement. Several of the optional procedures in the method would be adversely affected by the presence of bitumen including some of the actual measurement options. The two sample cleaning procedures proposed were Dean Stark (D&S) and Cold Wash. Studies conducted by members of FMWG suggested that either of these methods generate data for % fines at 44 micron that is equivalent.

The second step in the method requires disaggregation. Unfortunately during the cleaning and drying steps the samples become severely aggregated. To ensure aggregated fines particles are not removed during a 2000 micron sieving step, and ultimately missed in the measurement

step, it is essential that disaggregation procedures be performed. Disaggregation must not crush materials that are not aggregated fines since this would increase the fines content of the measured sample. The two disaggregation procedural options proposed were mortar and pestle (M&P) and hammer mill (HM). The pestle used in the M&P procedure as well as the jaws on the hammer mill must not disintegrate during the crushing of the aggregates and add to the fines being measured.

The amount of sample used in the measurement step of the method must meet the sample loading requirements for the procedure whether sieving (S), hydrometer (H) or laser diffraction (LD). Two options for subsampling the disaggregated materials are chute or rotary riffing. Although the literature indicates rotary riffing is capable of the greatest precision in subsampling; studies conducted by FMWG members have suggested that, with experience, acceptable precision can be obtained with chute riffing. Slurry subsampling can also be used following complete dispersion of the sample. Unfortunately, the particle size distribution must be narrow to effectively subsample in this manner. Efficient agitation of the sample such that particles are moving both vertically and horizontal is also needed to ensure the aliquot is representative.

The importance of complete dispersion of the riffled samples is shown in Figure 1 - 3. In Figure 1 a comparison of undispersed, partially dispersed and fully dispersed fines is illustrated. The data indicates only the fully dispersed fines would depict the true % of fines and particle size of the fines. The issue in achieving mass balance with incomplete dispersion is illustrated in Figure 2 where an imbalance in the dispersion between feed and the distribution of fines following extraction is illustrated. Although the extraction feed is considered to be a 100% due to incomplete dispersion of the feed stock, the effects of partial dispersion at the various sites of partially and fully dispersed fines, leads to a total fine calculation of 117% showing a mass balance cannot be achieved. However, when complete dispersion is achieved for both the feed and the sites where the fines are distributed (Figure 3) a complete mass balance is possible.

Factors affecting dispersion of particles is very complex, especially for the clays. The negative charge on the surface of clays is imparted by cation deficiency in the imbalance of positive and

negative charge in the structure of the clay. Isomorphous substitution is a factor contributing to this imbalance of charge. Since like charges repel this contributes to dispersion. Dissociation of the lattice hydroxyl groups at high pH enhances the negative charge and can also contribute to dispersion. Another factor affecting the negative charge is when the sites of anion exchange on the broken edges of clay particles is used to bind polyphosphates. Sodium hexametaphosphate (SHMP), for example, is a large polyphosphate polymer capable of enhancing the negative charge on the clay particle. SHMP also sequesters divalent cations which when bound to the clay hinder dispersion. The sodium displaced from SHMP when the calcium is sequestered permits the sodium to ion exchange with the clay and improve dispersion.

Another factor affecting the dispersion of clays is the nature of the cation shell or cloud surrounding the clay particle. Hydrated multivalent cations will be more strongly attracted to the negative charge associated with the clay than monovalent cations. A more diffuse layer of positively charged monovalent cations will help keep the clay particles apart contributing to greater dispersion. However, if the concentration of cations in solution becomes too high the diameter of the cation cloud about the clay can be reduced and impede dispersion. Thus a fine balance needs to be struck between these opposing forces to achieve and maintain the dispersed state so essential to achieving mass balance.

FULL FACTORIAL DOE

Before engaging laboratories in the ILS it was considered essential that the proposed method be tested using a full factorial design of experiment (DOE). This is needed to ensure the various procedures proposed for each of the steps in the fines measurement method will generate % fines at 44 micron with an acceptable level of precision. The need for ruggedness testing before conducting an ILS is supported by ASTM E1169.

The NAIT Applied Research Centre in Oil Sands Sustainability (NARCOSS) is an independent non-commercial laboratory and was considered to be ideally positioned to conduct this investigation. A full factorial DOE was considered essential to not only enable a statistical assessment of each of the main factors in the test method but also

interactions between factors which could bias conclusions regarding main factor effects.

A decision was made to initiate the DOE even before SOPs were finalized by FMWG. This meant that both FMWG labs and NARCOSS had to engage in several mini-studies to ensure procedures being implemented in the method were generating data with an acceptable level of precision. The initial DOE was implemented with a single sample cleaning procedure, D&S; and a single subsampling procedure for the disaggregated solids, spin riffing. The main factors where procedural variations were being tested were: disaggregation (2 options), M&P and HM; dispersion (3 options), soaking/boiling and a D422 high speed mixer using as the dispersing solution 40 g/L SHMP with the pH between 9.6 - 9.9 through sodium carbonate addition and sonication using a sonication probe in filtered tap water; measurement (3 options), wet sieving (WS) (< 74 micron according to ASTM D422) followed by H, WS (.44 micron) followed by LD and dry sieve (DS) (< 2000 micron) by LD. The full factorial DOE required 18 experiments for a single block and thus a total of 54 experiments to acquire a total of 3 blocks or replicates for each sample type.

ANOVA data from the DOE on a high fines sample showed no statistical differences between the disaggregation procedures, M&P and HM (P value = 0.111 and blocks (P value = 0.402). The fact there was no statistical differences between blocks shows good agreement between the triplicate readings. However, there were significant differences for both the dispersion (soaking/boiling, D422 mixer, sonication, P value = 0.001) and measurement procedures of Wet Sieve/Hydrometer, Wet Sieve/Laser Diffraction, Dry Sieve/Laser Diffraction (WSH, WSLD, DSLD; P value = 0.000).

The DOE results show that the procedures for dispersion and measurement were not equivalent and required revision. A clue to the problem is highlighted in the statistic for the interaction between dispersion and measurement where a very significant effect was being observed (P value = 0.000). An interaction plot showed that the source of the problem was primarily due to variations in the dispersion procedure when using WSH as the measurement method and an abnormally high fines for the <45 micron values measured by H.

DISPERSION AND MEASUREMENT STUDY

In order to assess the source of the variation several dispersing reagents were prepared to determine their effects on % fines at 44 micron using WSH and WSLD measurement options.

One of the concerns associated with the WSH measurement data was the large range between the WS 74 micron % fines and the H % fines value for the largest particle size measured by strictly following the ASTM D422 procedure. The largest particle determined by the H method was usually in the range of 30 micron. In order to assess the % fines at 44 micron, interpolation between these two divergent readings had to be made contributing to concerns regarding the effect on the precision of the % fines at 44 micron. For this reason the 74 micron wet sieve recommended by ASTM D422 was replaced by WS using a #325 mesh sieve for both H and LD.

Additionally, it was observed that although sonication and soaking/boiling gave similar data for the high fines sample, the high speed mixer consistently generated % fine values that were lower than the other two dispersion methods. It should be emphasized that the dispersion with the mixer involved strict adherence to the ASTM D422 method without any modifications. As a result of both the interpolation and high speed mixer dispersion concerns, the ASTM D422 procedure was abandoned and not included in the dispersion study.

In order to expedite the study, HM was used for disaggregation and soaking/boiling was the only dispersion procedure used. The following dispersion solutions were tested: 20 g SHMP/L without pH adjustment, 20 g SHMP/L pH 9.6, 40 g SHMP/L without pH adjustment, 40 g SHMP/L pH 9.6 and 0.015 M NaHCO₃ adjusted to pH 9.6 using 10% by weight NaOH (buffer solution).

The choice of reagents were based on current practice by several FMWG members, ASTM D422, the bicarbonate buffer commonly in use for methylene blue index (MBI) determinations and conditions used in the original DOE.

Figure 4 shows the results for the various dispersing solutions using WS (45 micron) and H measurements. The most notable effect is the use of SHMP particularly at high pH. Adjusting the pH

to 9.6 is desired to enhance the negative charge on particularly the clay particles and thus promote dispersion. The use of SHMP under conditions of no pH adjustment (pH range 6.8 – 7.1) for 20 and 40 g SHMP/L respectively and smaller quantities of SHMP (20 g/L) at pH 9.6 showed less of variation in the % fines data. However, it is most noteworthy that in all cases SHMP increased the % fines at 44 micron compared to the bicarbonate buffer.

Table 1 contains the % fines at 44 micron following interpolation using the Forecast function of Excel between adjacent % fines for WS (45 micron) and the largest particle size read using the hydrometer.

This supports the chart data where elevated % fines readings were found in the presence of high SHMP concentrations and high pH (% fines at 44 micron = 52.9). The bicarbonate buffer has proven to be very effective in dispersing clays for the MBI procedure but yet indicates a much lower % fines at 44 micron value (48.3%).

Figure 5 reveals a similar profile for the various dispersing solutions when using WS (45 micron) and LD measurements. The effects are not as pronounced as when using the hydrometer but the SHMP dispersed fines are still elevated.

Table 2 shows the interpolated % fines at 44 micron. The LD % fines at both 44 and 31 micron were included with the WS (45 micron) % fines in the Forecast function. The greatest contrast in values is shown for SHMP at high pH and concentration (50.1%) and bicarbonate buffer (48.9%).

This data is difficult to interpret on the basis of dispersion theory alone. The % passing the 45 micron wet sieve using the dispersing solution consisting of 40 g SHMP/L adjusted to pH 9.6 was 50.2 % of the total solids. The hydrometer indicated a % fines of 63.7 for a particle size of 40.1 micron. This is an impossibility for the % fines to be that much higher than the fines passing the sieve even if fines passing the sieve had a high aspect ratio. Although several properties of SHMP may explain these effects, it was decided that the bicarbonate buffer would be used for dispersion procedures in the revised DOE. The well know success of this buffer in dispersing clays for MBI determinations and the ability to reproducibly control pH made it a logical choice.

REVISED FULL FACTORIAL DOE

The main factors in the revised DOE where procedural variations were being tested were: disaggregation (2 options), M&P and HM; dispersion (2 options), soaking/boiling and sonication in a 15 mM NaHCO₃ solution that has had the pH adjusted to 9.6 using NaOH; measurement (4 options), wet sieving (WS) (< 45 micron) followed by either H or LD and dry sieve (DS) (< 2000 micron) by a small (0.8 L) and large volume (4 L) reservoir LD. A feature associated with the small reservoir LD was a 45 second pre-measurement sonication that was not used in the large volume LD. The full factorial DOE required 16 experiments for a single block and thus a total of 48 experiments to acquire a total of 3 blocks or replicates for each sample type.

The DSLD in the first DOE used a large volume (4L) reservoir recirculator allowing the sample mass to be large ensuring reliable data for samples with a wide particle size range. Since most labs do not have a large reservoir LD it was considered essential to include a small reservoir LD in the revised DOE. The mass of sample needed to obtain an acceptable obscuration or % transmittance value for a small reservoir LD is much lower. Measurement errors were considered possible due to inadequate particle numbers, especially for larger particles in the PSD range.

Quality control investigation of procedures

In order to ensure confidence in the conclusions of the DOE study it is essential that each of the steps in the Unified Fines Measurement method show the capability to generate quality data.

Sample cleaning

Table 3 shows the bitumen, solids and water content of the various sample types and the %RSD associated with each of the measurements. The % bitumen is low for the high fines and MFT sample types, 3.82 and 2.94 respectively, compared to the low fines sample, 12.7%. The % solids is the lowest in MFT due to the high water content of MFT.

Table 4 reveals the results following the Fisher Method to group the means for mass balance following Analysis of Variance (ANOVA). MFT at 100.1% is statistically different from the low and high fines values, 99.8% and 99.6% respectively, but the statistic is evident due to the excellent

precision achieved and is not practically different. The data on the low fines sample shows the poorest precision (1.24%) and is likely due to the large %RSD associated with the measurement of water content (Table 3).

The fact that the %RSD for the solids is less than 1% for all sample types (Table 4) suggests that the precision is acceptable for the DOE

Disaggregation

Disaggregation was performed using M&P and HM. M&P is a very subjective method of disaggregation and it is very difficult to achieve the same level of uniformity in the size of the disaggregated solids as with HM.

An additional concern when following disaggregation procedures is the possible loss of fines. The data from a two-factor ANOVA for the percentage of solids lost during disaggregation indicated significant differences for both sample type (*P value* = 5.13E-06) and disaggregation procedures (*P value* = 6.56E-07).

The significant effect of sample type on solid loss is supported in Figure 6 where MFT, high fines and low fines samples are plotted from left to right on the chart. MFT (markers with circles and dots) have a very high fines content and show the greatest loss of solids during disaggregation (~1.6%, HM). As the fines content drops from high fines (~1.1%, HM) to low fines (~0.2%, HM) the amount of solids lost decrease. Although the scatter in the data is much greater for M&P (borders only for markers) the same trends are noted. These observations suggest that the major source of the solids loss are small particles.

M&P disaggregation shows considerably more scatter but generally reveal a smaller solids loss than with HM. However, this procedure is also most likely to be associated with a gain in solids as shown by the negative datum points on the chart. Several rubber pestles were tested to reduce the likelihood of pestle disintegration during the disaggregation procedure but the negative values show that this could still be an issue. Another possibility is that thimble fibres are being incorporated into the sample during solids removal from the thimble but this source would be considered to be common to both HM and M&P procedures.

Subsampling

A rotary riffler was used to subsample for wet sieving procedures for both H and LD measurements. Due to the much smaller sample sizes needed for DSLD, multiple riffing steps were required. This was also necessary for the low fines sample where both large (16 tubes) and micro riffers (8 tubes) were used.

In order to assess the precision in the riffing steps the mass of the solids within each of the tubes was determined following riffing. A %RSD was calculated for each riffing procedure. The %RSD for all riffing steps were then subjected to an F-test to compare whether disaggregation procedures influenced the subsampling precision for all sample types.

Table 5 shows the average %RSD value for both M&P and HM disaggregation procedures, the number of tubes weighed and the resulting F-test *P value* for each sample type.

Although the mean %RSD is greater for M&P than HM for the majority of the riffing comparisons, the large riffler showed the poorest precision and also deviated from this trend. Although the mean %RSD for M&P tended to be larger than HM it didn't confirm a significant statistical difference. The *P value* for the high fines samples was 0.134 indicating no statistical difference in the riffing precision. However, both the MFT and low fines micro riffler revealed a significant difference in the precision of riffing for M&P versus HM disaggregation procedures (*P values* = 0.0013 and 0.037 respectively).

The tendency for M&P to show poorer precision in the riffing step than HM, is likely due to the reduced uniformity in the size of particles following the more subjective M&P disaggregation procedure. MFT is most difficult to disaggregate and may be part of the reason the *P value* is so small.

Dispersion

The effectiveness of both dispersion procedures, soaking/boiling and probe sonication, are expected to be revealed using ANOVA analysis during the revised DOE.

An alternative method of assessing dispersion, particularly for clays, is by conducting methylene blue (MB) titrations. A greater methylene blue

index (MBI, meq MB/100 g clay) is considered to be evidence of greater dispersion for a given sample type. Although the MBI is expected to vary with sample type, a significant difference in the MBI for a given sample type would suggest the dispersion procedures are not equivalent.

A two-factor ANOVA was used so that the effect of disaggregation could be distinguished from dispersion especially when there is not statistical evidence of interaction between these factors.

The high fines sample showed no statistical differences in the dispersion and disaggregation procedures (*P values* = 0.095 and 0.113 respectively). This suggests that no differences in these steps of the fines measurement method would be expected in the DOE.

For MFT, MBI values showed a significant effect with dispersion procedures (*P value* = 0.009). The soaking/boiling procedure had a higher MBI value than sonication. However, an anomaly was noted in the MBI titration.

The endpoint for the MB titration is evident when the MB halo is permanent for greater than 60 s. During the titration a halo that is seen at 20 s but disappears when tested at 40s is evidence that the endpoint is nearing and enables smaller MB volume additions. It was noteworthy that during the MFT titration the 20 s halo began to be seen and then disappear at about 70% of the total volume needed to reach the endpoint. This occurrence was not found in the MB titration when sonication was used. This difference in the titration may give evidence of some issues with MB being able to freely interact with the clays. It may also suggest some issues with dispersion may be expected when using soaking/boiling for MFT dispersion.

The low fines sample showed statistical differences between both disaggregation and dispersion procedures (*P value* = 0.046 for both). However, the differences in MBI values are very small with overall average values of 0.22 and 0.24 meq MB/100 g clay for sonication and soaking/boiling, respectively. This would suggest that differences in disaggregation and dispersion procedures are unlikely for low fines samples in the DOE.

Measurement

Wet sieving (WS) was required for both the WSH and WSLD measurement procedures. Riffing

procedures were used to ensure overloading of the #325 mesh sieve was not occurring but yet sufficient fines were available to generate acceptable H and LD data.

Dry sieving is necessary to generate PSD data between 2000 and 45 micron. However, it is common to see fines <45 micron passing the dry sieve. An obvious question is why are fines of this size passing the dry sieve when they should have all been passing the #325 mesh sieve during WS.

Possible explanations could be inefficiencies in the wet sieving procedure where simply some of the fines of this size had not passed through the #325 sieve. The point at which the wet sieving is considered complete is when the wash appeared clear. However, this is very subjective assessment depending on the operator.

Another explanation for the < 45 micron DS solids is that fines with a high aspect ratio have a probability that they can be oriented to pass the #325 sieve due to the prolonged dry sieving step.

Table 6 shows the distribution of solids observed for a high fines sample using WS and DS procedures. Details of the determination are found under the parameter heading.

The DS <45 micron material was found to be 1.5 wt% based on the material passing the #325 mesh sieve and retained in the receiving pan. The source of the DS solids was the material retained following WS on the #325 mesh sieve. The DS PSD came from the retained material for 2000, 1000, 850, 500, 425, 355, 250, 180, 125, 106, 75, 45 sieves.

Based on the total solids applied to the #325 mesh for WS, the < 45 micron fines was determined to be 63.1 wt%. However, when the total solids applied to the WS is used to calculate material passing the #325 mesh for both WS and DS, the <45 micron fines are 65.1 wt%.

The <45 micron % fines used to generate the % fines at 44 micron for WSH data in the DOE study chose the total %fines based on material passing both the WS and DS procedures in the ensuing calculations. An interpolation between the <45 micron sieve data and the % fines for the largest particle measured using the H was the method used to calculate % fines at 44 micron for the WSH DOE values.

An additional complication when analyzing the WSLD data is the effect of measuring the material passing the WS #325 mesh sieve by LD. Table 7 shows that although only <45 micron would be expected to be passing, there are particle sizes greater than 44 micron. For some samples particles sizes as large as 250 micron were being measured by LD. An explanation for these results may relate to the difference in the particle sizing procedures. Materials with a high aspect ratio could theoretically orient to pass through the sieve even though the particle size is much larger. It is generally accepted that with LD the measured volume of the particle is influenced by the rotational diameter of the particle. This is influenced by the turbulence created by the circulation pump needed to keep all particle sizes suspended allowing all particles to have an equal probability of measurement.

In all cases, the Vol% measured for the % fines at 44 micron material is less than 100%. As seen in Table 7 this is usually about 96% of the fines being measured. In the DOE the value used for WSLD reflected this discrepancy. The %fines <45 micron based on both WS and DS data was multiplied by the Vol% fraction determined by LD. Even though the larger <45 micron % fines was used, the value reported was consistently less than the <45 micron material obtained by WS data alone ($65.1 \text{ DS+WS} * 0.96 = 62.5$ compared to 63.1 for WS). However, the discrepancy between WS and WSLD was smaller using this approach.

DS for DSLD reflects material passing the 2000 micron HM screen or a 2000 micron dry sieving of material undergoing disaggregation using M&P. A suitable mass to obtain an acceptable obscuration or % transmittance for this wide range of particle sizes was used. The % fines at 44 micron reported for both the small and large reservoir LDs were used in the DOE.

PROCEDURAL EFFECTS ON % FINES AT 44 MICRON

Although the DOE has included < 2000 micron PSD data for the three sample types, the current regulation requires reliable reporting of % fines at 44 micron. Table 8 summarizes the % fines at 44 micron for the various procedural options in the DOE study measured by LD and WS.

Although the agreement between the percent fines at 44 micron is quite good for the three different sample types, there is some notable exceptions. Boiling as a dispersion technique for MFT severely affects the % fines measurement for WS (M&P, 35.1 and HM, 49.3) and large volume LD (M&P, 65.3 and HM 61.8). It should be noted that the small volume LD subjected all samples prepared for measurement to a 45 second pre-measurement sonication. The effects on the LD measurement with sonication is dramatic with the % fines at 44 micron reading M&P, 86.1 and HM, 82.8. The data suggest that boiling for some samples is an inadequate dispersing procedure while sonication is effective.

A more thorough discussion around the procedural effects on measurement of fines will be provided in the discussion of the DOE data.

HIGH FINES FULL FACTORIAL DOE

Table 9 summarizes the raw data for a high fines sample obtained during the DOE study. This is based on the 16 experiments conducted in triplicate involving each of the procedural options. Although the LD data is the same as that in Table 8, the sieve hydrometer and sieve laser diffraction values are influenced by the H and LD sub-44 micron measurements and thus differ from the WS data alone presented in Table 8

The analysis of variance (ANOVA) for the full factorial DOE on this sample showed no statistical difference between blocks (P value = 0.968) confirming the replicate data was acceptable. There was no statistical difference between the M&P and hammer mill when disaggregating the samples (P value = 0.951) nor between dispersion procedures (P value = 0.066).

However, there are statistical differences between measurement (P value = 0.000) and the interaction between dispersion and measurement (P value = 0.001). The significant interaction statistic may suggest that the manner of interaction between dispersion and measurement procedures are affecting the % fines at 44 micron.

An approach to observe the performance of each of the main factors is to examine least squares means values. The orthogonal design of the DOE permits a comparison of the least squares means for individual procedures. However, it must be understood that the means being calculated for

each of the main factors reflect the influence of other factors. Thus the least squares means for soaking/boiling dispersion would be a result of all the % fines at 44 micron experiments where this dispersion procedure was used and not sonication.

This could be particularly confusing when comparing measurement values, for example. The % fines at 44 micron being reported reflects the influence of both dispersion and disaggregation procedures. If any of these procedures are performing poorly the least squares means for any of the measurement procedures will be reporting low. However, due to the balanced design, all measurements are being influenced by the other factors in the same manner allowing for measurement effects between dispersion, disaggregation and measurement to be compared.

Table 10 contains the least squares means for the main factors and dispersion*measurement interaction values. The smallest value for measurement was for WSH (60.7) and the largest was DSLD (large reservoir, 68.9). This large difference due to measurement procedures contributes to the significant P value in the DOE.

The least squares means for dispersion*measurement interactions are interesting since it allows insight into how dispersion procedures affect each measurement option. The data for both DSLD measurement options show small differences due to the effect of dispersion procedures. DSLD (large reservoir) and DSLD (small reservoir) show differences in the least squares means between dispersion procedures of 0.7 and 0.8 respectively. However, both WSH and WSLD measurements show much greater variation. The difference between soaking/boiling and sonication for WSH is 5.9 and WSLD is -2.6.

Figure 7 indicates that sonication resulted in lower % fines values for sub-45 micron particles using H. Thus the interpolated value for % fines at 44 micron was lower. The WSH data in Table 9 confirm this where the sonication values for both disaggregation procedures are smaller.

A contrast is seen with WSLD data plotted in Figure 8 where the sonication % fines are now larger than soaking/boiling. The WSLD data in Table 9 confirm these observations.

This apparent contradiction related to dispersion procedures may in part be due to the contrast in

the fundamental nature of H and LD measurements.

Figures 7 through 9 show the effects on the particle size distribution (PSD) for different dispersion and disaggregation procedures for WSH, WSLD and DSLD measurements, respectively. Since the retained materials on the #325 sieve are dried and then stack sieved, the % fines reported above 45 micron is based on dry sieve data for the WSH and WSLD charts.

Figure 10 compares the discrepancy between the small and large reservoir recirculator LD. Especially for small particles, the large reservoir LD is reporting higher fines values and corroborates the differences reported in Tables 8 and 9.

The small differences in the charts between M&P and HM disaggregation steps support the very large *P values* found in the ANOVA DOE. However, the data confirms the benefits of moving away from SHMP in dispersing the samples. The troublesome shoulder observed in the Figure 4 and 5 charts is no longer evident.

MATURE FINE TAILINGS FULL FACTORIAL DOE

Table 11 summarizes the DOE data for the MFT sample. DOE ANOVA showed acceptable agreement between replicates (Block *P value* = 0.342). However, significant differences between procedures are indicated for disaggregation (*P value* = 0.006), dispersion (*P value* = 0.000) and measurement (*P value* = 0.000). Additionally, the interaction between disaggregation and measurement (*P value* = 0.022) dispersion and measurement (*P value* = 0.000) is once again expected to affect the interpretation of the major factors affecting the fines measurement. This is complicated further by a significant interaction between all 3 major factors of the fines measurement method being studied (*P value* = 0.002).

The least squares means shown in Table 12 help identify the problem. The means are very far apart for each of the procedural options but is most evident for the dispersion procedures; soaking/boiling = 59.3 and sonication = 87.9. It is likely that it is this factor that is dominating the significant interactions observed in the ANOVA table. The lack of precision is also evident by the

much larger standard error of the mean associated with this data.

The charts shown in Figures 11 to 13 highlight the issues in measuring fines of this sample type. The effects of cleaning and then oven drying the high fines MFT is contributing to issues with both disaggregation and dispersion procedures. Figure 11 where WSH is being used accentuates the problem. The larger particle size range in M&P disaggregated solids give evidence of severe problems with dispersion through soaking/boiling. Sonication for this sample type is better in achieving dispersion. The M&P procedure for disaggregation tend to show higher % fines values than HM. This gives evidence that an effective dispersion technique is more important than the disaggregation procedure.

Figure 12 confirms the issue with soaking/boiling to achieve dispersion. The fact that WSH tends to accentuate differences for poorly dispersed samples is evident by comparing Figures 11 and 12. The step in the data around 45 micron in Figure 11 is not so obvious. The issues with the PSD is not confined to the <45 micron measurements by H and LD. It is obvious that the dry sieve data (PSD >45 micron) has also been biased by disaggregation and dispersion issues.

Figures 13 and 14 supports the importance of sonication since DSLD data for the small reservoir recirculator showed significant improvements in the agreement between the large and small reservoir LD data when used. However, the issues with disaggregation of MFT and its effects on dispersion and measurement is evident.

LOW FINES FULL FACTORIAL DOE

The DOE data for the low fines sample is in Table 13. The DOE ANOVA showed good agreement between replicates (Block *P value* = 0.524). Dispersion shows no significant difference between procedures (*P value* = 0.925 but disaggregation (*P value* = 0.000), measurement (*P value* = 0.000) show significant differences. Once again, interactions between factors cloud the interpretation of the major factors with dispersion*measurement (*P value* = 0.000) and all three major factors (*P value* = 0.002) showing significant differences.

However, when the least squares means are examined (Table 14), the values show very little difference. The standard error of the mean is also

very small showing high precision. Once again, it is unreasonable to expect the fines measurement method to differentiate such subtle differences. Although the procedures are statistically different it is unreasonable to expect this level of precision in the ILS.

Figure 15 to 17 all show little difference between procedural options. Figure 18 reveals the greatest discrepancies between the small and large reservoir LD data with larger particles but the trends are not consistent. Particles larger than 500 micron are shown to have a larger percentage than the small reservoir since the difference has a negative sign.

CONCLUSIONS

The conclusions reached in this paper are confined to the conditions outlined in the section entitled: “quality control investigation of procedures”. The paper is intended to assess procedural implications of these options during the development of a Unified Fines Measurement method. The investigation has examined effects of procedures on the complete PSD rather than just the % fines at 44 micron. This has been done to ensure procedural options do not adversely affect the determination of solids of other particle sizes. The most variable factor affecting the % fines at 44 micron was dispersion using soaking/boiling under the conditions used in this study. The procedure was found acceptable for oil sand samples but severely impacted dispersion of MFT. Sonication was found to improve dispersion for all sample types studied.

A comparison of the WS <45 micron data in Table 8 with WSH and WSLD data in Tables 9, 11 and 13 show reasonably good agreement between the % fines at 44 micron for oil sands samples. This agreement between WS only and the interpolated value for WSH and WSLD is believed to be due to combining both the WS and DS <45 micron fines before interpolation with the H and LD data.

FUTURE WORK

The information presented may need to be evaluated to determine if the precision or accuracy of the data reported matters relative to Regulatory and Industry objectives and if and what future work may be required.

The effects of reagents such as SHMP so commonly used in fines measurement may require further study to understand the reasons for the observations reported. Fully understanding the impact of aspect ratios on methods of measurement of the particles at 44 micron will also be of value.

ACKNOWLEDGEMENTS

FMWG would like to recognize the important contribution of its members in developing the SOPs and conducting the numerous mini-studies needed to resolve questions during method development. A thank you for the contributions of the members of the COSIA FMWG Committee: Brenda Crickmore, Brad Komishke, Lauren Asplund, Tea Malkova, Robert Mahood, Tara Wang, Todd White, Oladipo Omotoso, James Walker and support from Sean Wells and Jim Lorentz.

NARCOSS would like to acknowledge the technical support of Irfan Khan, MSc and currently Co-op student from the NAIT Chemical Technology Program; Adeeb Mohammed Co-op student in Chemical Engineering from U of Waterloo. Sohaib Roy, a graduate of the NAIT Chemical Engineering program provided assistance with dry sieving near the conclusion of the DOE study.

FMWG and NARCOSS appreciate the support from research and development staff at Syncrude in providing technical and equipment support for the DOE study. Particularly the contributions of Willis Sherstabetoff and Drew Ziegler are to be recognized.

TABLES

Table 1. Effect of dispersing solutions on % fines at 44 micron as measured by WSH

Dispersing solution	20g SHMP/L (pH 7.1)	20g SHMP/L (pH 9.6)	40g SHMP/L (pH 6.8)	40g SHMP/L (pH 9.6)	Bicarbon-ate buffer (pH 9.6)
% fines at 44 micron	50.4	51.0	50.7	52.9	48.3

Table 2. Effect of dispersing solutions on % fines at 44 micron as measured by WSLD

Dispersing solution	20g SHMP/L (pH 7.1)	20g SHMP/L (pH 9.6)	40g SHMP/L (pH 6.8)	40g SHMP/L (pH 9.6)	Bicarbon-ate buffer (pH 9.6)
% fines at 44 micron	49.1	49.8	49.3	50.1	48.9

Table 3. Bitumen, solids and water content for different sample types

Sample type	Parameter	Bitumen, wt%	Solids, wt%	Water, wt%
High fines	Average	3.82	88.8	6.91
	%RSD (n=56)	4.72	0.22	5.63
MFT	Average	2.94	32.2	64.9
	%RSD (n=56)	5.01	0.75	2.01
Low fines	Average	12.7	85.6	1.48
	%RSD (n=56)	2.57	0.57	31.23

Table 4. Grouping information using the Fisher Method to compare mass balance means for different sample types following ANOVA

Sample type	N	Mean	%RSD	Grouping
High fines	56	99.6	0.693	B
MFT	56	100.1	0.326	A
Low fines	56	99.8	1.24	B

Table 5. Effects of disaggregation procedures on subsampling precision

Sample type	M&P Average %RSD	Number of tubes measured (M&P)	HM Average %RSD	Number of tubes measured (HM)	F-test <i>P</i> value (one-tail)
High fines	2.06	240	1.47	208	0.134
MFT	2.73	280	2.05	224	0.0013
Low fines (large, 16 tubes)	10.2	96	14.1	96	0.150
Low fines (micro, 8 tubes) (small riffler, 8 tubes)	1.33	48	1.10	48	0.037

Table 6. Wet sieve and dry sieve distribution of solids from a high fines sample

Wet sieve (WS) and dry sieve (DS) parameters	Wt %	%RSD (n = 8)
1. Total solids applied to WS	100	N/A
2. Total solids (+45) after WS, (value from #325 retained mass)	36.9	3.6
3. Total (+45 & -45) solids from DS of WS (+45) retained solids, (value from measured total of DS & receiving pan masses)	36.5	6.5
Discrepancy in WS retained and total DS solids (Difference between 2 & 3)	0.4	184.5
4. Total solids (+45) after dry sieving, (value from total of +45 DS masses)	34.9	5.8
Total solids (-45) after dry sieving, (difference between 3 & 4)	1.5	38.7
5. Total solids (-45) after wet sieving, % (difference between 1 & 2)	63.1	2.2
6. Total solids (-45) dry sieving, (difference between 1 & 4)	65.1	2.0
Discrepancy between DS and WS (-45) solids, (difference between 5 & 6)	1.9	38.0

Table 7. Partial PSD of < 45 micron material passing wet sieve using laser diffraction measurement

Particle diameter (micron)	Vol %	%RSD (n = 12)
250	100.00	0.01
180	99.98	0.04
125	99.88	0.08
88	99.69	0.17
62	98.84	0.23
44	96.21	0.97

Table 8. Summary of % fines at 44 micron based on laser diffraction and wet sieve

Sample Type	Disaggregation and dispersion pre-treatment options	% Fines at 44 micron					
		Small Volume LD		Large Volume LD		Wet sieve (45 micron sieve)	
		Mean	% RSD (n = 3)	Mean	% RSD (n = 3)	Mean	% RSD (n = 6)
High Fines	M&P; sonication	63.2	5.2	68.5	1.2	65.0	1.0
	M&P; boiling	64.7	4.1	69.6	1.7	62.2	1.2
	HM; sonication	63.6	3.3	68.8	0.1	64.1	1.1
	HM; boiling	63.7	1.2	69.0	1.3	61.8	1.0
MFT	M&P; sonication	89.3	1.5	84.9	10.9	91.2	0.6
	M&P; boiling	86.1	0.7	65.3	1.4	35.1	8.4
	HM; sonication	87.9	3.4	93.8	5.6	90.9	0.8
	HM; boiling	82.8	1.8	61.8	3.5	49.3	5.1
Low Fines	M&P; sonication	3.0	8.3	3.4	3.9	3.1	6.8
	M&P; boiling	3.0	1.5	3.0	7.0	2.6	8.2
	HM; sonication	3.2	10.0	3.3	7.3	3.4	4.7
	HM; boiling	3.4	6.1	3.1	7.0	2.8	4.1

Table 9. Summary of DOE data for a high fines sample reporting % fines at 44 micron

Preparation Steps	MEASUREMENTS			
	SIEVE/Laser Diffraction	SIEVE/ Hydrometer	LASER DIFFRACTION (Large Recirculator)	LASER DIFFRACTION (Small Recirculator)
	MEAN (STDEV)	MEAN (STDEV)	MEAN (STDEV)	MEAN (STDEV)
D&S; HM; B	61.0 (1.1)	63.0 (0.2)	69.0 (0.9)	63.7 (0.8)
D&S; HM; S	63.4 (0.5)	58.8 (1.4)	68.8 (0.1)	63.6 (2.1)
D&S; M&P; B	60.8 (0.3)	64.3 (4.5)	69.6 (1.2)	64.7 (2.7)
D&S; M&P; S	63.7 (1.4)	56.8 (4.6)	68.4 (0.8)	63.2 (3.3)

Table 10. Least squares means from DOE on the high fines sample

Procedural options	Least square means	SE Mean
Disaggregation		
HM	63.9	0.448
M&P	64.0	0.448
Dispersion		
Soaking/boiling	64.5	0.448
Sonication	63.3	0.448
Measurement		
WSLD	62.2	0.634
WSH	60.7	0.634
DSLDD (large reservoir)	68.9	0.634
DSLDD (small reservoir)	63.8	0.634
Dispersion*Measurement		
Boiling*WSH	63.7	0.896
Sonication*WSH	57.8	0.896
Boiling*WSLD	60.9	0.896
Sonication*WSLD	63.5	0.896
Boiling*DSLDD (large reservoir)	69.3	0.896
Sonication*DSLDD (large reservoir)	68.6	0.896
Boiling*DSLDD (small reservoir)	64.2	0.896
Sonication*DSLDD (small reservoir)	63.4	0.896

Table 11. Summary of DOE data for a mature fine tailings sample reporting % fines at 44 micron

Preparation Steps	MEASUREMENTS			
	SIEVE/Laser Diffraction	SIEVE/ Hydrometer	LASER DIFFRACTION/ Large Recirculator	LASER DIFFRACTION /Small Recirculator
	MEAN (STDEV)	MEAN (STDEV)	MEAN (STDEV)	MEAN (STDEV)
D&S; HM; B	49.6 (0.5)	52.4 (7.8)	61.8 (2.2)	82.8 (1.5)
D&S; HM; S	88.4 (0.6)	86.4 (6.8)	93.8 (5.2)	87.9 (3.0)
D&S; M&P; B	37.0 (5.6)	39.8 (0.6)	65.3 (0.9)	86.1 (0.6)
D&S; M&P; S	90.1 (0.8)	82.4 (1.2)	84.9 (9.2)	89.3 (1.3)

Table 12. Least squares means from DOE on mature fine tailings sample

Procedural options	Mean (% fines at 44 micron)	SE Mean
Disaggregation		
HM	75.4	0.949
M&P	71.9	0.949
Dispersion		
Soaking/boiling	59.3	0.949
Sonication	87.9	0.949
Measurement		
WSDL	66.3	1.343
WSH	65.2	1.343
DSL D (large reservoir)	76.5	1.343
DSL D (small reservoir)	86.5	1.343

Table 13. Summary of DOE data for a low fines sample reporting % fines at 44 micron

PREPARATION STEPS	MEASUREMENTS			
	SIEVE/Laser Diffraction	SIEVE/ Hydrometer	LASER DIFFRACTION/Large Recirculator	LASER DIFFRACTION /Small Recirculator
	MEAN (STDEV)	MEAN (STDEV)	MEAN (STDEV)	MEAN (STDEV)
D&S; HM; B	2.9 (0.1)	3.2 (0.3)	3.1 (0.2)	3.4 (0.2)
D&S; HM; S	3.3 (0.1)	2.8 (0.4)	3.4 (0.2)	3.3 (0.3)
D&S; M&P; B	2.5 (0.1)	3.2 (0.4)	3.0 (0.2)	3.0 (0.1)
D&S; M&P; S	3.2 (0.6)	1.8 (0.2)	3.4 (0.1)	3.0 (0.2)

Table 14. Least squares means from DOE on a low fines sample

Procedural options	Mean (% fines at 44 micron)	SE Mean
Disaggregation		
HM	3.2	0.0485
M&P	2.9	0.0485
Dispersion		
Soaking/boiling	3.0	0.0485
Sonication	3.0	0.0485
Measurement		
WSDL	3.0	0.0686
WSH	2.7	0.0686
DSL D (large reservoir)	3.2	0.0686
DSL D (small reservoir)	3.2	0.0686

FIGURES

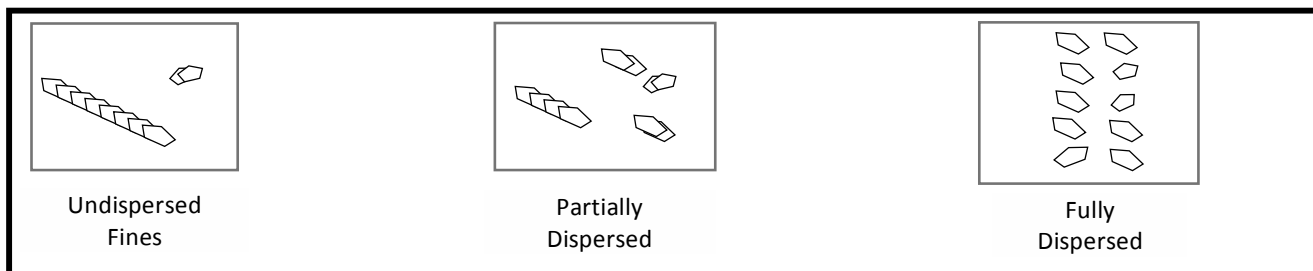


Figure 1. Comparison of dispersion states

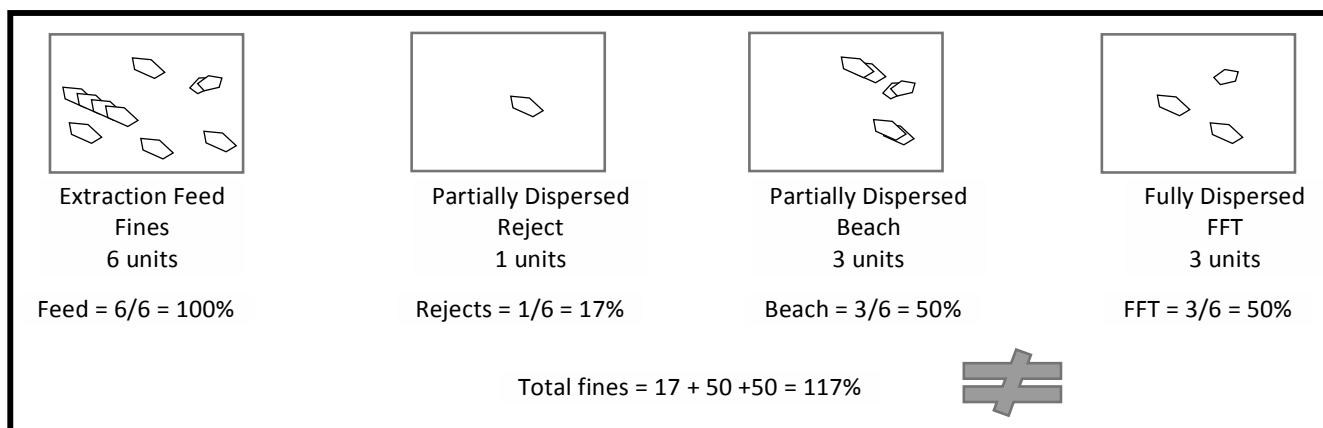


Figure 2. Incomplete dispersion does not permit a proper fines balance

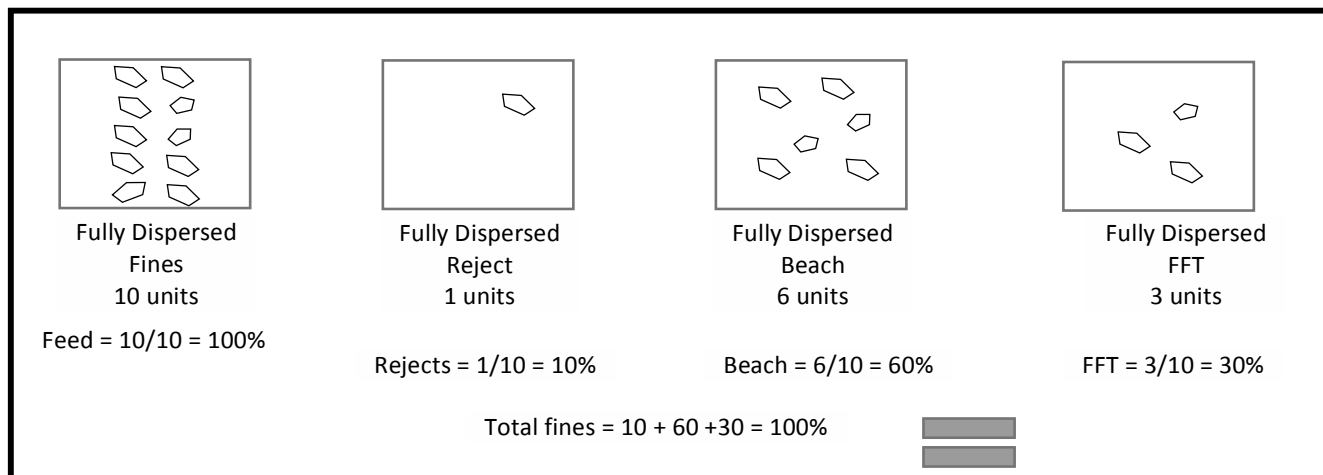


Figure 3. Complete dispersion ensures a fines balance is possible

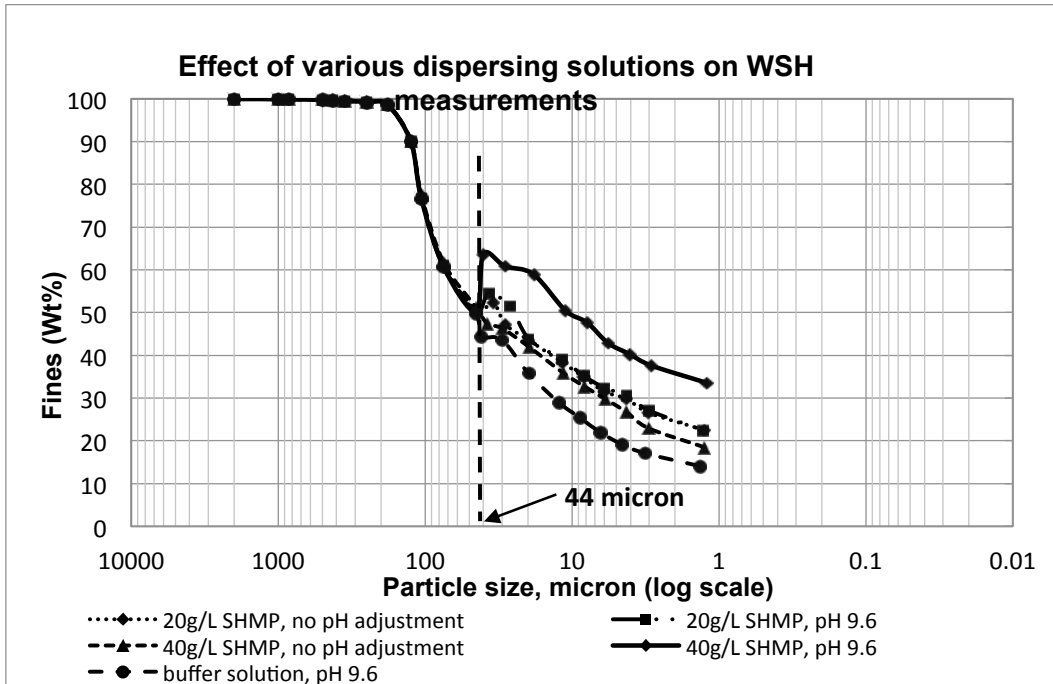


Figure 4. Effect of different dispersing solutions on wet sieve - hydrometer measurements

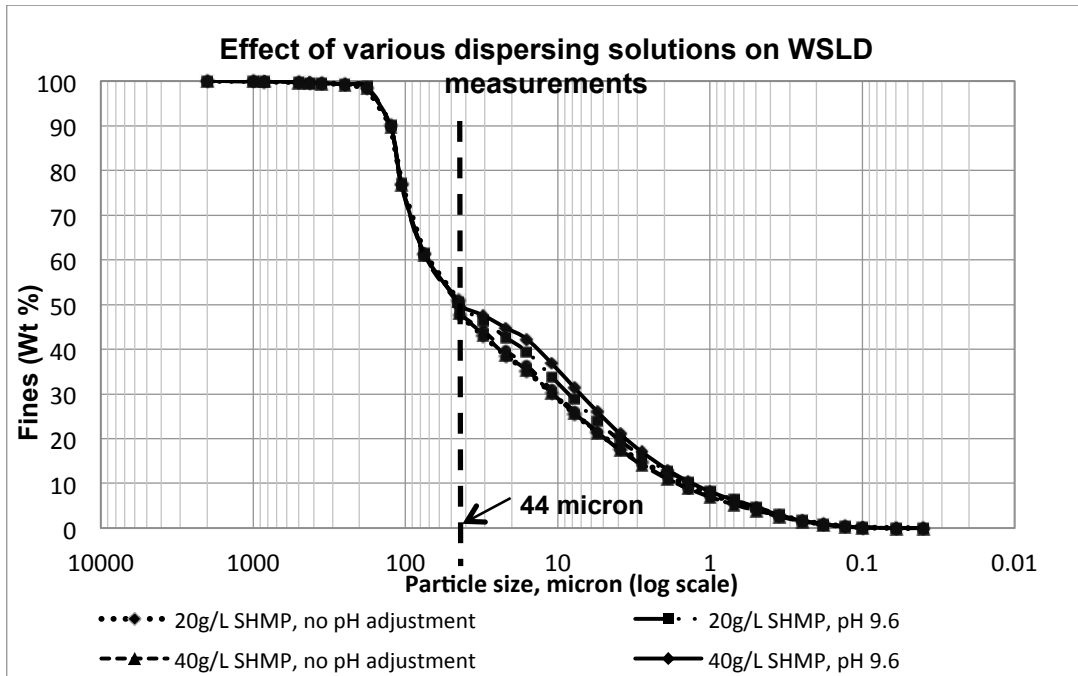


Figure 5. Effect of different dispersing solutions on wet sieve – laser diffraction measurements

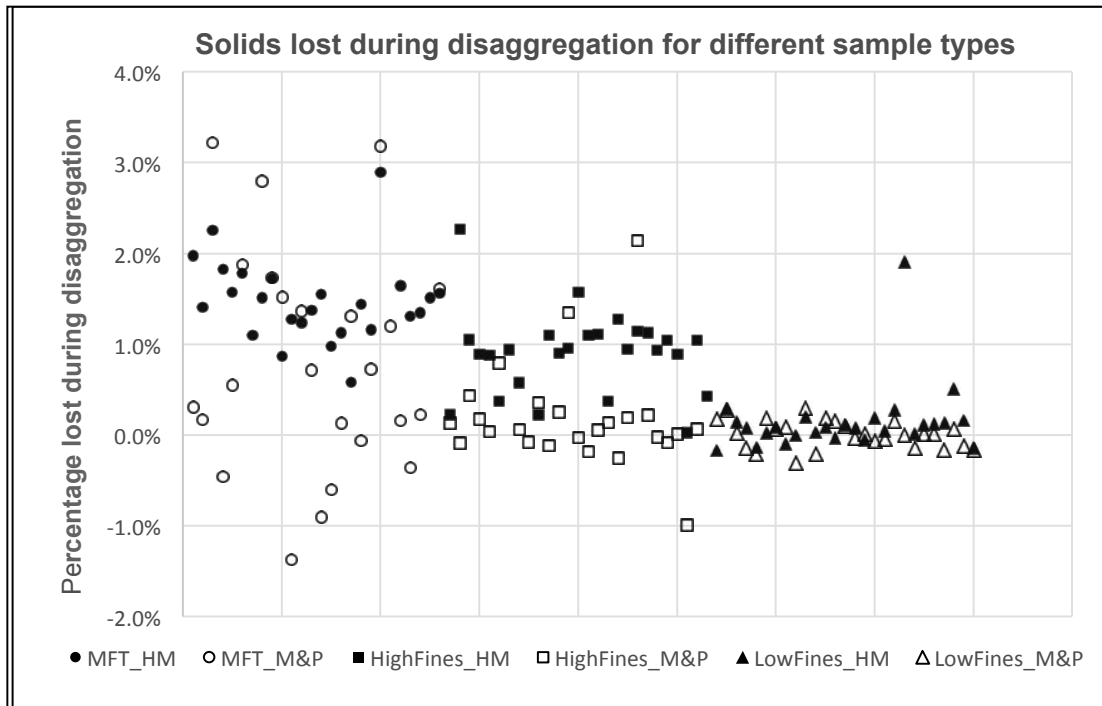


Figure 6. Comparison of sample type and disaggregation procedures on solids lost

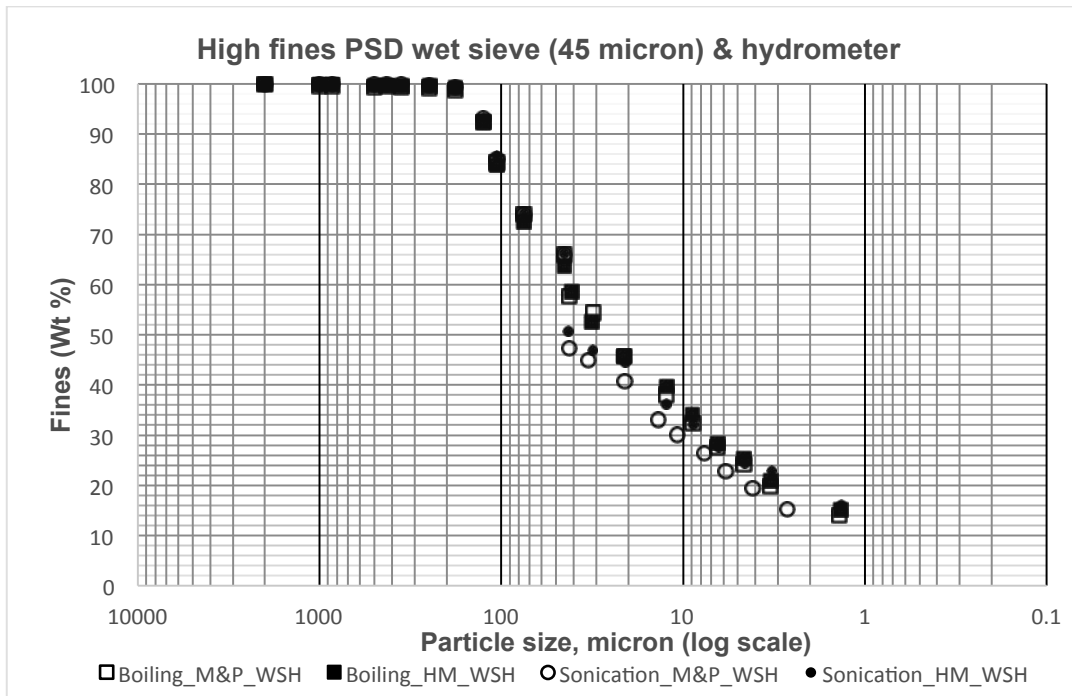


Figure 7. %Fines measured (high fines) using wet sieve and hydrometer for different procedures

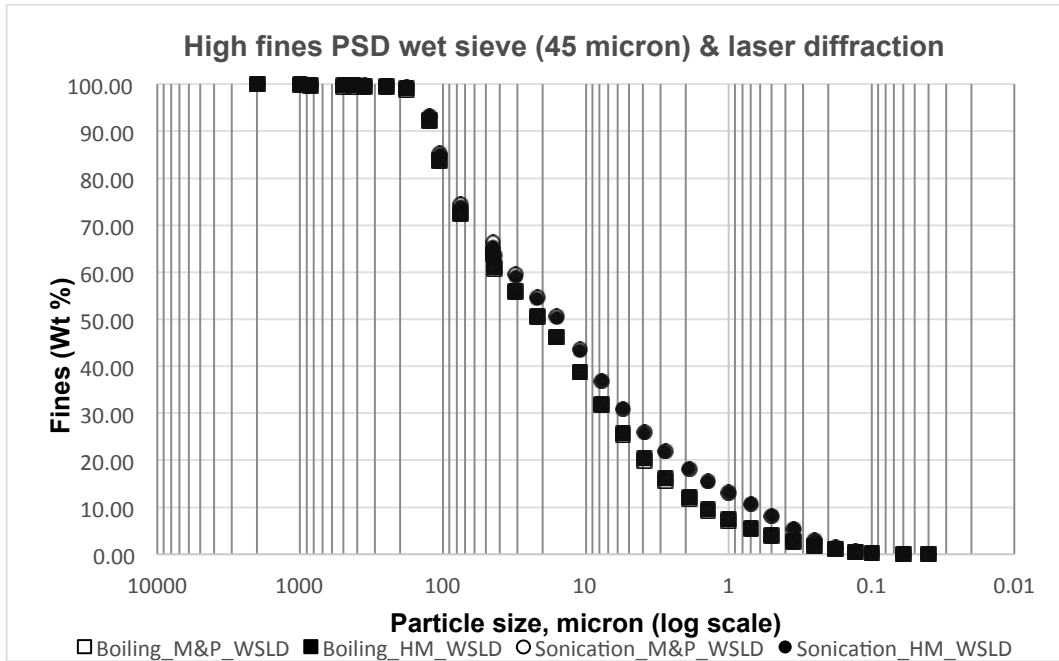


Figure 8. %Fines measured (high fines) using wet sieve and laser diffraction for different procedures

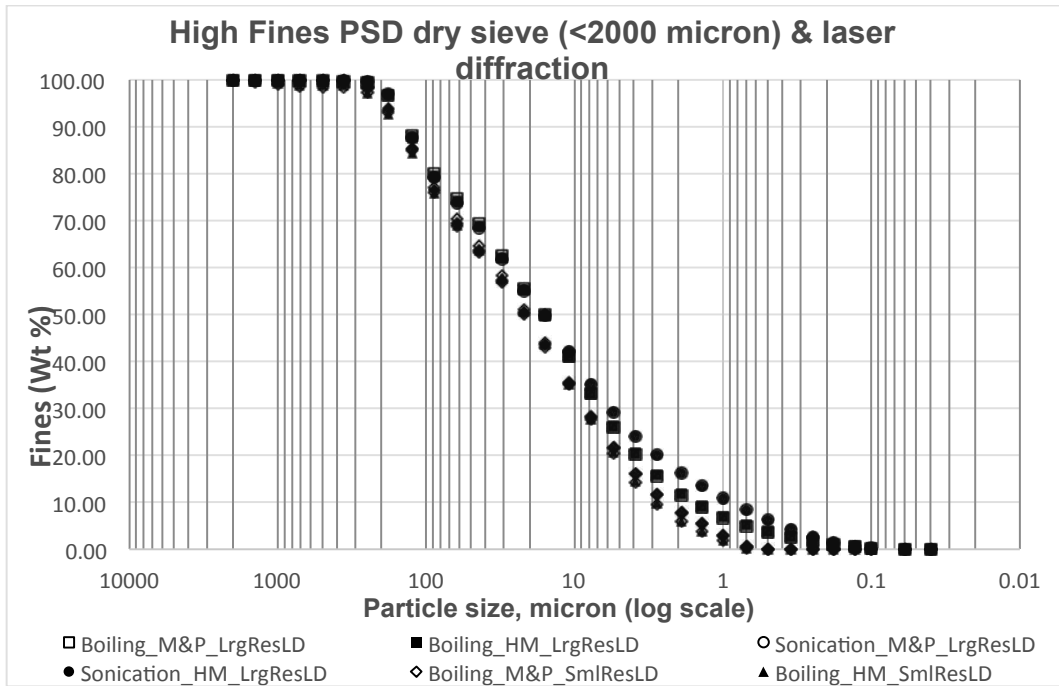


Figure 9. %Fines measured (high fines) using dry sieve and laser diffraction for different procedures

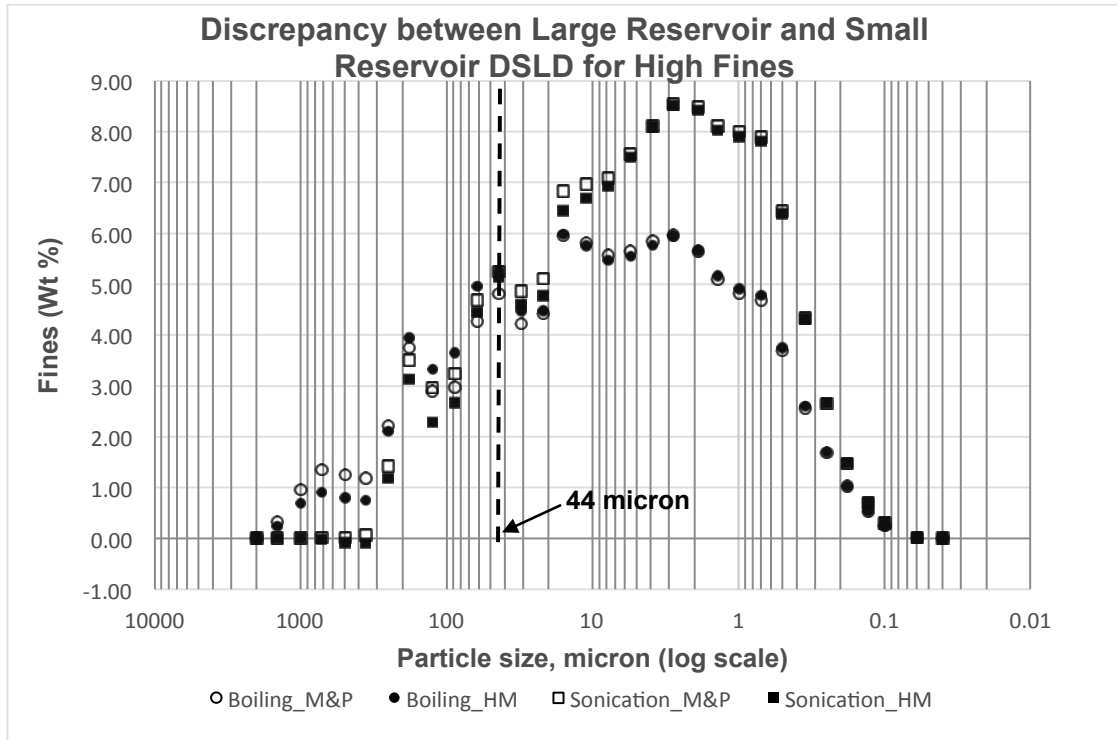


Figure 10. PSD variation (high fines) between small and large reservoir recirculators using laser diffraction

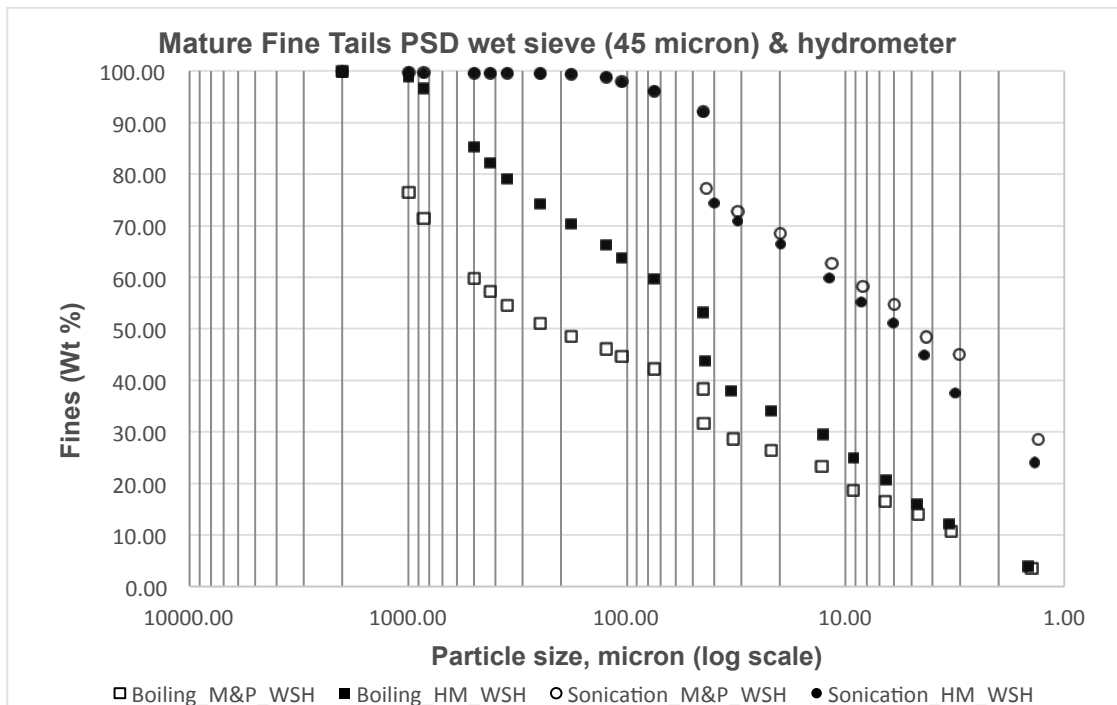


Figure 11. %Fines measured (MFT) using wet sieve and hydrometer for different procedures

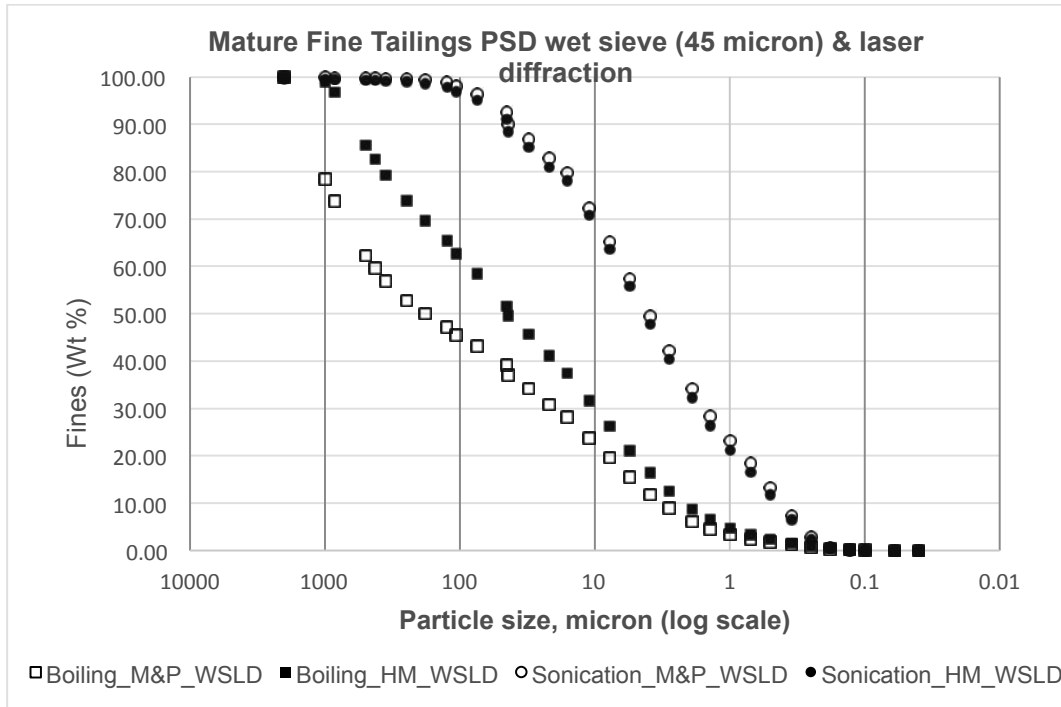


Figure 12. % Fines measured (MFT) using wet sieve and laser diffraction for different procedures

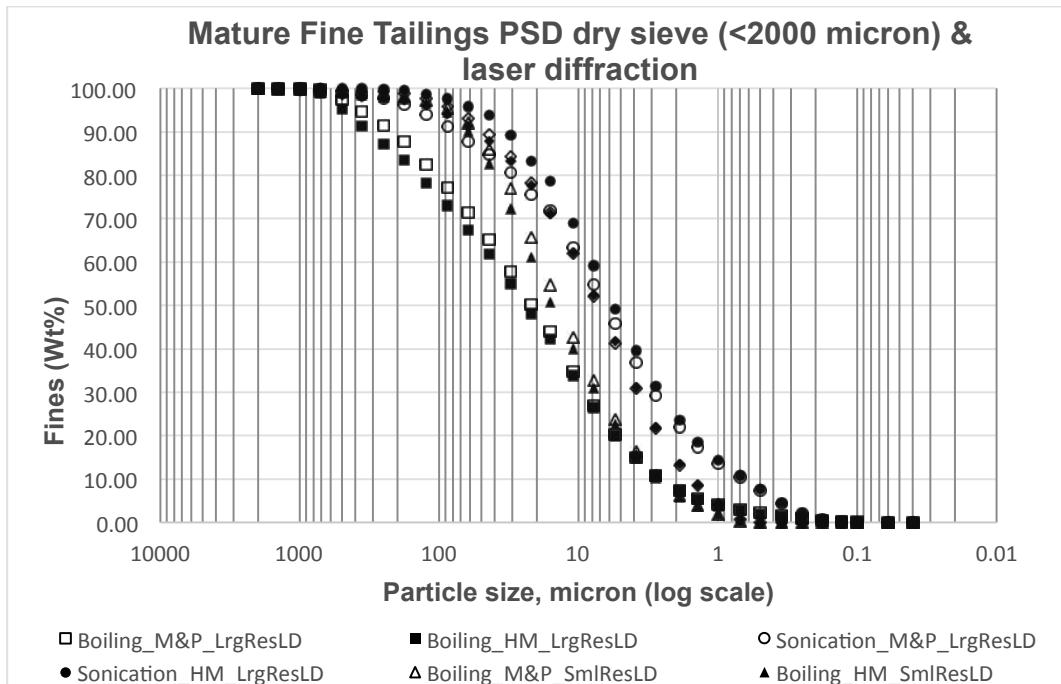


Figure 13. %Fines measured (MFT) using dry sieve and laser diffraction for different procedures

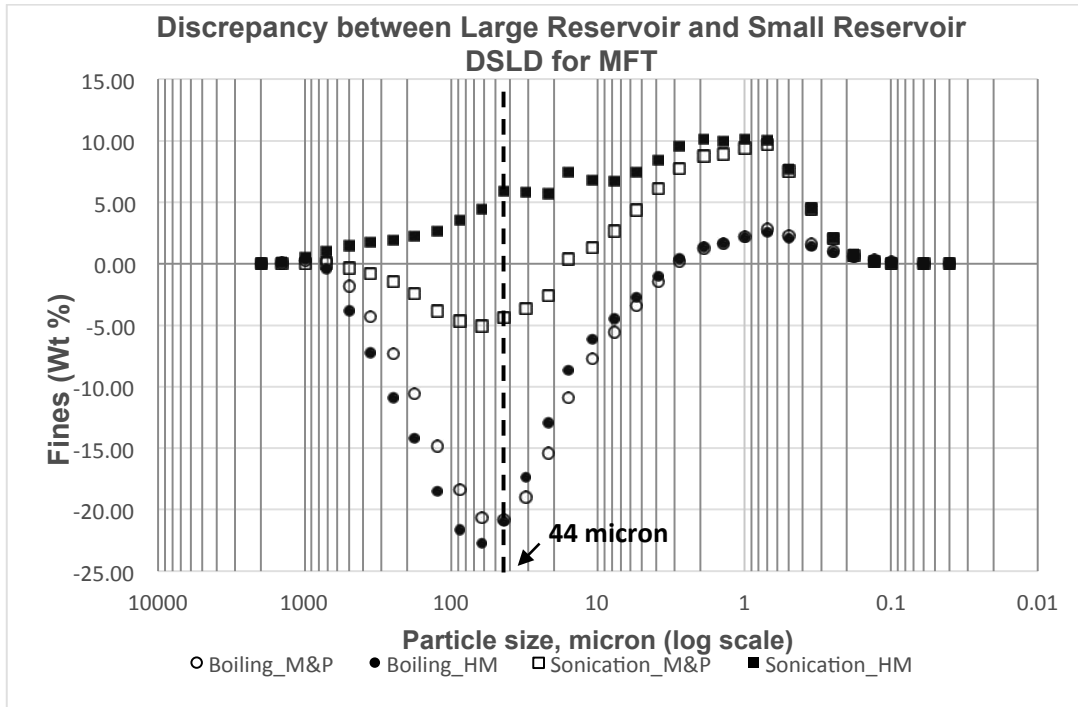


Figure 14. PSD variation (MFT) between small and large reservoir recirculators using laser diffraction

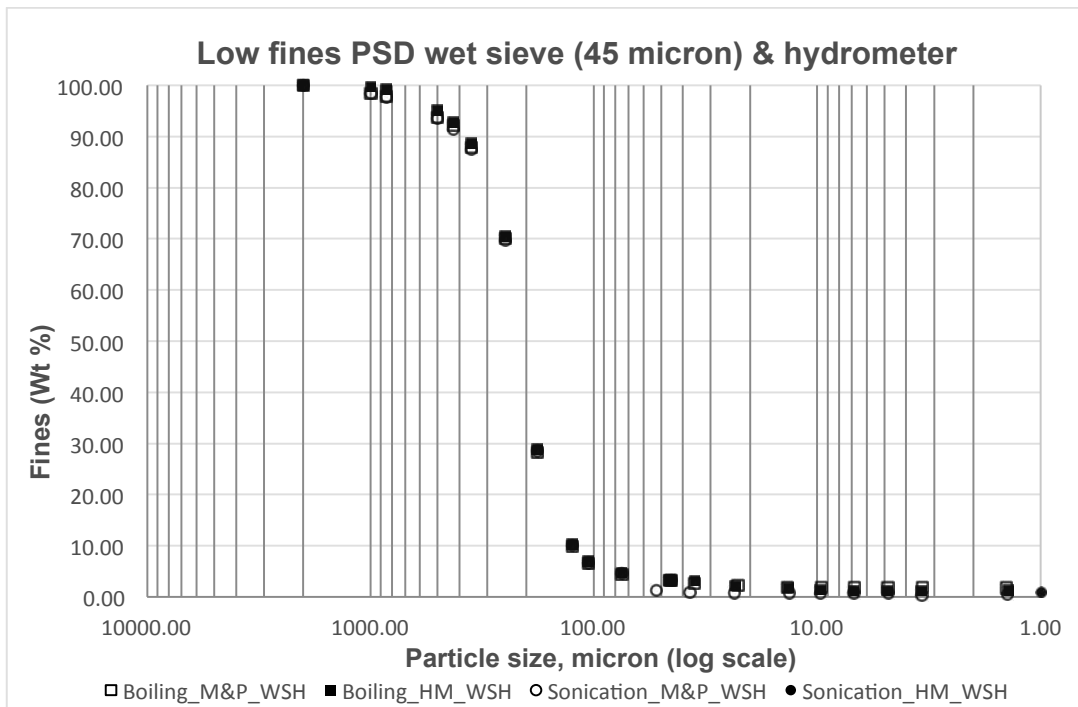


Figure 15. %Fines measured (low fines) using wet sieve and laser diffraction for different procedures

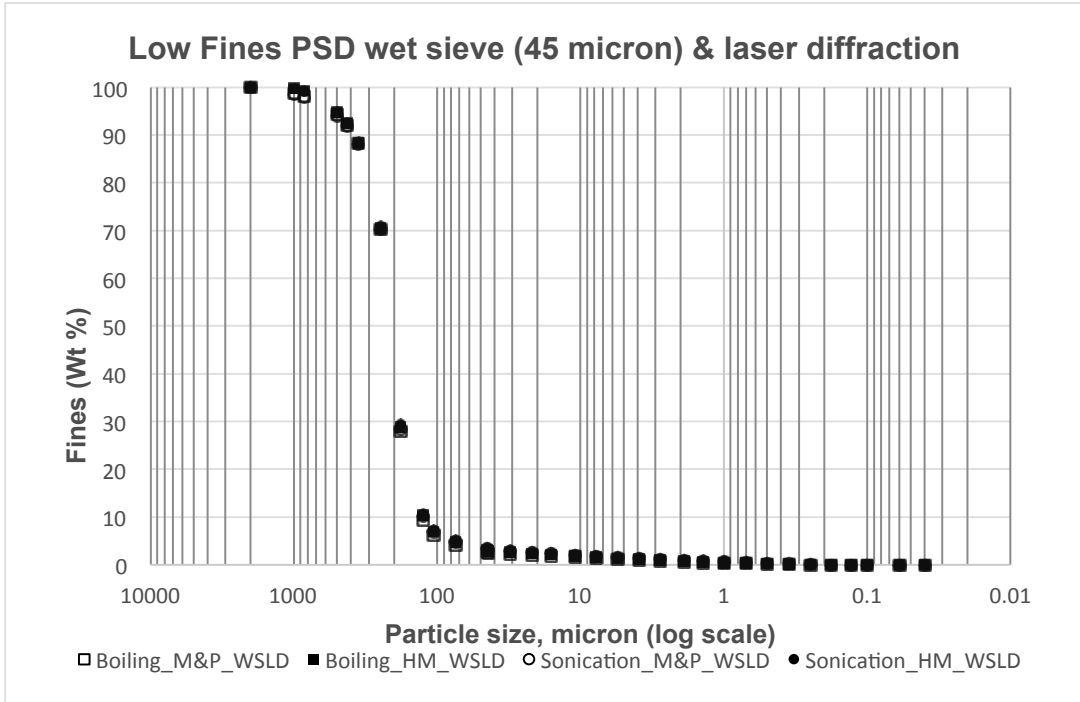


Figure 16. %Fines (low fines) measured using wet sieve and laser diffraction for different procedures

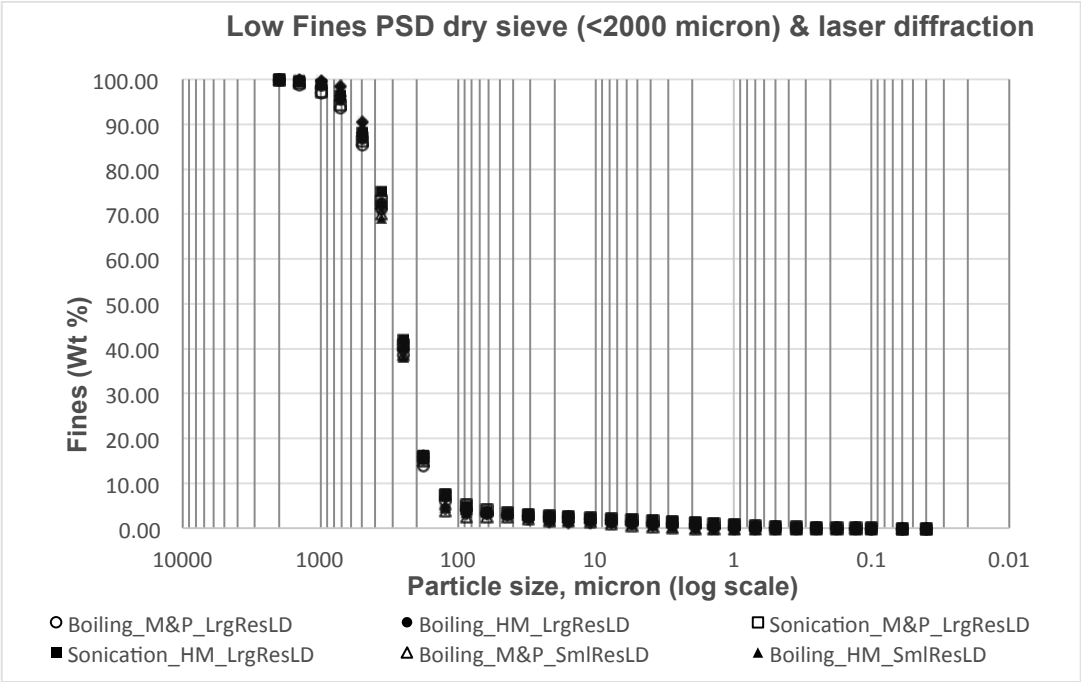


Figure 17. % Fines (low fines) measured using laser diffraction for different procedures

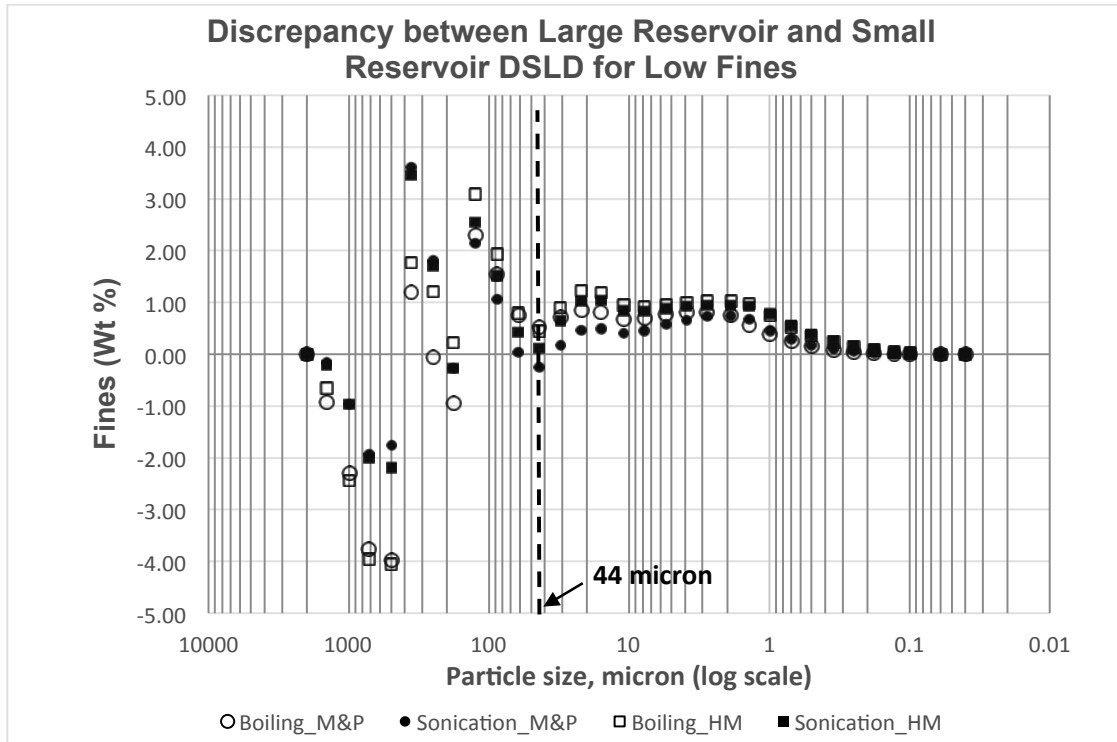


Figure 18. PSD variation (low fines) between small and large reservoir recirculators using laser diffraction

Session 6

COSIA Special Session II

DEMYSTIFYING THE METHYLENE BLUE INDEX

Heather Kaminsky
Suncor Energy Inc. Calgary Alberta

ABSTRACT

Clays & clay minerals have long been recognized as having a significant impact on oil sands tailings behavior, with increased clay content being associated with slower settling, higher required flocculant dosages and longer consolidation times. The Methylene blue index (MBI) is a simple index test that provides an indication of clay activity. This test has been in use in the oil sands for over 30 years and is routinely employed in test programs. This paper explains the Methylene blue test, the common sources of error in the method, the different way the results are reported and how to convert between them and the ranges of MBI reported in different tailings streams. The paper will also review how MBI is used to predict process or geotechnical behavior.

INTRODUCTION

The methylene blue index is a number used to describe the clay content and activity of a sample. The methylene blue test measures how much methylene blue dye can be absorbed by a sample as determined by a titration test. Methylene blue absorbs to clay surfaces – both external surfaces and internal surfaces through ion exchange. Methylene blue has a very strong affinity to clay surfaces and so will displace any other ion present on the surface. For this reason the methylene blue test is sometimes described as testing the cation exchange capacity of a material, however it is actually more useful to think of the methylene blue test as a measure of surface area as the methylene blue effectively covers the clay surface. Hang and Brindley described the surface area of methylene blue as 130\AA^2 . Therefore one can calculate the surface area of the sample by assuming that each titrated molecule covers 130\AA^2 of surface area.

$$\text{Thus: } SA = \frac{\text{mLs of MB}}{\text{g of Sample}} \times C \times NA \times A$$

Where SA is the surface area of the sample in m^2/g , C is the concentration of MB in mol/mL, NA

is Avogadro's number (6.022×10^{23} molecules/mol) and A is the surface area of the MB molecule in m^2 .

METHOD

The methylene blue index test most commonly used in oil sands was developed by Amar Sethi at MRRT labs (Sethi, 1995) as a modification from the ASTM test method. The test method has since been refined by various groups, most particularly CANMET energy (Omotoso & Morin, 2008) and more recently the Clay Focus Group.

The key steps in the test are:

- 1) Dispersion of the sample to be tested - the sample is dispersed using stirring, boiling sonication and sodium bicarbonate as a dispersing aid. Dispersion is achieved when the sample has a homogenous appearance with no clay lumps or floating pieces on the surface. The sample will also have an opalescent appearance when swirled. For a video showing a well dispersed sample see: <http://youtu.be/BTMk4hyiSpl>.
- 2) Acidifying the sample just prior to titration – this removes the effects of ion oxide-hydroxides from the titration.
- 3) Titrating the sample with methylene blue in 0.5-1 mL increments.
- 4) Determining the end point (usually using the "halo method" – where a drop of slurried sample containing methylene blue is placed on Whatman filter paper and examined for the presence of a blue halo which indicates an excess of methylene blue).
- 5) Calculating the methylene blue index.

ASTM vs Oil Sands Method Comparison

The key differences from the ASTM method are:

- the use of 0.006N methylene blue solution instead of 0.01 N methylene blue solution.
- The use of sodium bicarbonate as opposed to distilled water for sample dispersion.

- The use of sodium hydroxide to assist with dispersion.
- The use of sonication and heating with mixing in dispersion as opposed to mixing only.
- The option of using a larger mass (5+ g) for sandy samples vs. the use of a fixed sample mass (2g).
- The type of filter paper used (Whatman 42 ashless vs Baroid 987).

In general the changes were made to achieve more repeatable MBI data for oil sands samples. The change in the solution strength was made as the higher concentration is more prone to the formation of dimers or other orientations of methylene blue that cause an overestimate in surface area. In addition, lower concentrations produce more sensitive end points as you need more mLs of the methylene blue solution to achieve the same absorption. The use of sodium bicarbonate and sodium hydroxide are both to promote dispersion and to convert the clays to the sodium exchanged form, which provides the highest measure of MBI. The increase in sample size allows for lower MBI samples to be assessed accurately. Finally, the Whatman type of filter paper was found to produce a more distinct halo which improves the accuracy of end point detection.

In general, a significant portion of the oil sands test method is focused on ensuring that the sample is dispersed. It is CRITICAL that the dispersion of a sample be assessed by the physical appearance of the sample rather than by assuming the sample is dispersed because the dispersion steps have been followed. This is because different samples take a different amount of time to disperse. Samples that have been subjected to Dean Stark treatment, and in particular samples of froth solids, froth treatment tailings or flocculated samples, are extremely difficult to disperse.

When undertaking the testing of a set of samples for the first time, a best practice is to use a series of tests on the same sample at different dispersion times to determine whether the MBI is consistent between tests or if it is increasing as a function of dispersion time. If the MBI is changing, the sample was not sufficiently dispersed at the start of the test.

INTERPRETING MBI

The fundamental MB test measures the number of milliliters of MB solution absorbed a given mass of sample. Usually the mass of sample used is small so the end point of the titration is often less than 20 mLs. The standard titration step size is often 1mL and so the relative uncertainty of the end point is usually in the order of 5%.

One factor which complicates the understanding of MBI in the industry is that different units are used to present the MB index.

These are:

- MB index (MBI) – this is the milliequivalents of MB per 100 g of sample. It is calculated by multiplying the MB# by the molarity of MB used (0.006 N). For ores this number is usually between 0.25-2. For MFT this number is usually between 5 and 15. This number is the reporting units specified in ASTM and is in SI units. It requires no additional information in order to convert to other units.
- Methylene Blue # (MB#)- this is the number of mLs MB used to titrate 100 g of sample. This number assumes that the reader knows the concentration of the MB used (presumably 0.006N for oil sands) but can be ambiguous in the case that the ASTM procedure was used instead – For oil sands ores this number is usually around 100. For MFT this number is typically around 1500.
- MB weight (MBW) – this is the Weight of MB used to titrate 100g of sample. This requires knowledge of the molecular weight of MB used to convert. Molecular weight of Methylene Blue trihydrate (reagent specified in CANMET procedure) is 373.9 g/mol. The molecular weight of pure methylene blue is then 319.84g/mol.
- % Clay as determined by MB - this generally takes the measured MBI and applies an empirically derived conversion between the MBI and the % clay mineral as measured by Sethi by XRD&PSD on a few samples of oil sands clay:

$$\% \text{ Clay} = \frac{\text{MBI} \frac{\text{meq}}{100\text{g}} + 0.04}{0.14}$$

- Surface area as determined by MB – this is a conversion based on the assumption of a monolayer of methylene blue absorbed on all available surfaces and that the surface area of the methylene blue is as described by Hang & Brindley.

One important point to note is that the magnitudes of the numbers reported are VERY different depending on the method of reporting used

(illustrated in Table 1 and Table 2). This can lead to a false sense of precision in the test and therefore a sense that the test is unreliable because a 200 point scatter between similar tests appears inaccurate.

It should be noted that if the activity is low and the same mass of sample is used the uncertainties will be quite high because the end point sensitivity is usually ~1 mL. This is why it is important to re-test low activity samples with more material to achieve larger titration volumes/or reduce the titration step size.

Table 1. Example of different MBI values on high activity MFT

	mLs of MB titrated	Mass of Sample (g)	Normality of MB meq/mol	MW of MB g/mol	MBI meq/100g	MBW g/100g	MB # (mLs 0.006N/100g)	% Clay
Measured	20	1	0.006	319.84	12	3838	2000	86
Typical Uncertainty	1	0.001	0.00001	0	0.6	192	100	4
Relative uncertainty	5%	0.1%	0.2%	0.0%	5%	5%	5%	5%

Table 2. Example of different MBI values on low activity MFT

	mls of MB titrated	Mass of Sample (g)	Normality of MB meq/mol	MBI g/mol	MBI meq/100g	MBW g/100g	MB # (mLs 0.006N/100g)	% Clay
Measured	3	1	0.006	319.84	1.8	576	300	13
Typical Uncertainty	1	0.001	0.00001	0	0.6	192	100	4
Relative uncertainty	33%	0.1%	0.2%	0.0%	33%	33%	33%	33%

The other source of confusion around MBI is that the % clay determined by MBI can be greater than 100% and doesn't always correlate with the % clay measured by other methods. This is because the % clay assumes an "average" oil sands clay.

It is easiest to explain this in terms of surface area – the typical surface areas of the common clay minerals which occur in oil sands are listed in Table 3 along with the MBI and "% clay" one would expect to see for a sample containing only that mineral with that surface area. As you can see, a sample containing 100% kaolinite would have an MBI of only 3 but would show up as 100% clay

mineral by XRD and would probably show up as close to 100% less than 2 micron (clay size) by sieve hydrometer. On the other hand a sample containing only 2.5% smectite and 97.5% sand would still give an MBI of 3 but would show up as only 2.5% clay mineral by XRD (if it was even detected) and would probably show up as only 2.5% less than 2 micron by sieve hydrometer.

Oil sands typically contain several clays in various proportions but generally end up with surface areas between 100-120 m²/g of clay so the correlation between MBI and particle size and by clay mineral determined by XRD calculated by

Sethi works relatively well as a comparison between clay particle size and MBI (it is empirically derived but works out to an average surface area of 110 m²/g). The problem with the conversion is when a very active clay (i.e. high in smectite) or a very inactive clay (i.e. high in kaolinite) comes around and throws off the correlation. Ideally one would use both particle size and MBI to get information about the particle size distribution as well as the likely activity of the particles.

Table 3. Typical Surface area, MBI and % Clay for pure clay samples

Mineral	Typical Surface Area (m ² /g)	Expected MBI for pure sample (meq/100g)	Expected % Clay using Sethi correlation
Kaolinite	20	3	19%
Illite	100	13	92%
Smectite	800	102	730%
“Oil Sands Clay”	110	14	100%

USES OF MBI

The MBI is very useful in predicting the total surface area of a sample which in turn can help predict a variety of properties such as:

- Amount of water trapped as bound water given a variety of double layer strengths.
- Surface area available for chemical reactions.
- Exchangeable cation sites available for chemical reactions.

These fundamental properties can in turn be used to help predict the outcomes of the various processes in oil sands.

Bitumen Recovery

One of the early correlations noted is the relationship between the MBI of an ore and the expected bitumen recovery. Namely, as the MBI increases the likelihood of poor recovery also increases. This is because as the particle surface area increases there is an increased hindrance to the flow of water and hence an increase in viscosity of the fluid.

Ores that process well usually have an MBI of 0.6 meq/100g or less (<5 m²/g, <100 mls 0.006N MB/100g). Ores with an MBI greater than ~1.3 meq/100g (>10m²/g) usually process poorly unless significantly more water is used in the process. Ores with an MBI in between 0.6 -1.3 are typically very sensitive to water chemistry effects.

Predicting Flocculent dosage

Another well documented correlation with MBI is the flocculent dosage –as the MBI of a sample increases there is a trending increase in the dosage required to obtain specific settling objectives. This was documented by Kaminsky et al. in the CONRAD water conference in 2012 for settling tests on batch sample. Similarly, Suncor uses an MBI clay based dosage to report flocculent doses for TRO (Revington, 2014).

Correlation with Yield Stress

Suncor TRO has also found a direct correlation between the yield stress of MFT and the clay to water ratio of the slurry as determined by MBI MFT (Omotoso et al., 2014). If the MFT is then optimally flocculated, there is another direct correlation between the yield stress of the flocculated MBI and the MBI of the unflocculated MFT (Diep et al., 2014). Of course, other factors such as previous shear energy will also influence the yield stress of a system so these correlations are site specific. Yield strength, of course, can then be correlated with other properties such as pump demand and beach slope.

Correlation with MFT Volume

Since MBI can be used to estimate the amount of water associated with the surfaces of the clay at different double layer strengths, it can therefore also be used to estimate the total volume of water trapped by the clay at different double layer strengths and hence the expected total volume of MFT. Omotoso et al. have demonstrated an empirical correlation between volume of MFT and the MBI of the MFT. (Omotoso et al., 2014).

Correlation with Atterberg Limits

There are several published correlations between Atterberg limits and MBI in the geotechnical literature (Cerato, 2001). Unfortunately, none have been published for oil sands. Published data where Atterberg limits and MBI have both been measured on oil sands fine tailings show a disappointing

correlation. Atterberg limit tests are also an index test and as such the results are best compared when the tests have been conducted in the same mine. The 2013 presentation by Gidley highlighted that the test method used for Atterberg limit testing can have a significant impact on the results. As such, the lack of correlation from literature is unsurprising as there is a limited amount of data where MBI and Atterberg limits were tested over a significant range using consistent methods.

Identification of Unstable or Low Permeability layers

MBI has been used outside the oil sands industry to characterize the stratigraphy of soil foundations and identify unstable layers (Chiappone et al, 2004). It has also been used within the industry to identify low permeability regions within tailings ponds (Lovbakke, 2014).

CONCLUSIONS

The MBI test is a useful index test with a wide range of applications. As an index test, its power lies in the fact that it is a relatively quick and inexpensive test that can easily be applied to a large number of samples. Having a large number of data points means that more detailed characterization tests can be more carefully selected and therefore the highest value data achieved.

As with most index tests it is important to understand the principles behind the test and the factors that can influence the outcome when determining how to measure and use the index for a given application. In the case of MBI, the degree of dispersion is the single factor that most strongly influences the test outcome and therefore should be critically assessed when setting up a testing program.

REFERENCES

ASTM Standard: C 837 – 99 (Re-approved 2003)

Cerato, A. (2001). *Influence of Specific Surface Area on Geotechnical Characteristics of Fine Grained Soils* (Unpublished graduate dissertation). Department of Civil & Environmental Engineering, University of Massachusetts.

Chiappone, A., Mareello, S., Scavia, C., & Setti, M. (2004). Clay mineral characterization through the methylene blue test: comparison with other experimental techniques and applications of the method. *Canadian Geotechnical Journal*, 41 (6), 1168-1178.

Diep, J., Weiss, M., Revington, A., Moyls, B., & Mittal, K. (2014). In-line mixing of mature fine tailings and polymers. In Jewell, R., Fourie, A., Wells, P.S., van Zyl, D. (Eds.), *Proceedings of the 17th International Seminar on Paste and Thickened Tailings* (pp. 111-126). Canada: InfoMine Inc.

Gilley, I., & Moore, T. (2013, February). *Impact of Test Methodology on the Atterberg Limits of Mature Fine Tailings*. Paper presented at the CONRAD Oilsands Clay Conference, Edmonton AB.

Hang, P.T., & Brindley, G.W. (1970). Methylene Blue absorption by clay minerals – determination of surface areas and cation exchange capacities. *Clays and Clay Minerals*, 18, 203-212.

Kaminsky, H., Sedgwick, A., Clark, J., & Fan, A. (2012). *Importance of Clay & Water Chemistry in Flocculation*. Presented at the CONRAD Water Conference, Edmonton AB.

Lovbakke, D. (2014). *Methylene Blue Index – Applications to Tailings Issues*. Presented to the meeting of the COSIA Clay Focus Group.

Omotoso, O., & Melanson A. (2014). Influence of clay minerals on the storage and treatment of oil sands tailings. In Jewell, R., Fourie, A., Wells, P.S., van Zyl, D. (Eds.), *Proceedings of the 17th International Seminar on Paste and Thickened Tailings* (pp. 269-280). Canada: InfoMine Inc.

Omotoso, O., & Morin, M. (2008). *Methylene Blue Procedure: Dean Stark Solids*. CanmetENERGY: Devon.

Sethi, A. (1995, January 23). *Methylene Blue Test for Clay Activity Determination in Fine Tails*. MRRT Procedures.

APPENDIX A – CONRAD METHOD FOR MBI DETERMINATION – CONRAD CLAY FOCUS GROUP DRAFT (2012)–MODIFIED FROM CANMET PROCEDURE

1. OBJECTIVE AND SCOPE OF THE PROCEDURE

The Methylene Blue Procedure is intended to address dispersion of oil sands process solids prior to methylene blue adsorption described in general by the ASTM Standard Test Method for Methylene Blue Clay (C 837-99 (Re-approved 2003)). This procedure is designed to be effective for all oil sands process streams but it may not be optimal for all streams. In this method all samples/sub samples are assumed to be representative of the process being stream being tested, recognizing that care is required to ensure this is true.

A mature fine tailings (MFT) analog is used as a calibration standard, to monitor the level of dispersion provided by the dispersion equipment used for sample preparation. The MFT analog is comprised of sand, montmorillonite, de-ionized water and bitumen. Bitumen and water are removed using Dean Stark extraction, the same procedure used for extracting bitumen and water from test samples.

2. PURPOSE

This procedure was developed specifically for oil sands process solids but could be used for oil-free minerals as well.

3. APPARATUS

- 250ml beakers;
- 1L volumetric flasks;
- analytical balance, accurate to 0.001g;
- hotplate/magnetic stirrer and stir bars;
- methylene blue powder;
- mortar & pestle;
- top-loading balance, accurate to 0.01 g;
- disposable pipettes;
- ultrasonic bath (Cole Parmer 1 ½ gallon with 40kHz transducers & built in seep frequency);
- room temperature water bath;
- hand held pH meter;
- burette stand;
- 50ml burette with teflon stopcock;

- whatman 42 ashless filter paper;
- watchglasses;
- dean-stark extraction apparatus – for preparation of mft-analog calibration standard.

4. REAGENTS

Analytical grade reagents shall be used in all tests.

- De-ionized water shall be used unless otherwise indicated in the procedure.
- Methylene Blue trihydrate (M.W. 373.9) (1 ml = 0.006 meq). Dissolve 2.2436 g of Methylene blue powder in 1L de-ionized water (or 1.1218 g in 500 ml). Wrap volumetric flask in aluminium foil to keep the solution from degrading. A fresh batch should be used within a day.
- 10% w/w NaOH (sodium hydroxide). Dissolve 10g of NaOH pellets in 90g of deionized water.
- 10% v/v H₂SO₄ (sulfuric acid). Add 10 ml of concentrated H₂SO₄ to 90 ml de-ionized water.
- 0.015M NaHCO₃ (sodium bicarbonate). Add 1.26 g of dry NaHCO₃ to 1 L de-ionized water.
- pH 4,7 & 10 buffer solution (calibrating pH meter).
- Coarse Ottawa sand, retained on 200-mesh sieve.
- Na-montmorillonite, marketed as Bentonite by Fisher Scientific.
- Solids and toluene -free oil sands bitumen produced from a dean stark extraction of oil sand ore.

5. SAFETY PRECAUTIONS

Wear gloves and protective eyewear when handling methylene blue, caustic and acidic agents. It is particularly painful if it enters the eyes and will stain skin a very dark blue. If you get Methylene blue on your clothes or skin apply liquid dish-soap immediately to the area (without water).

6. MFT-ANALOG STANDARD PREPARATION

- 1) Add Ottawa sand (35 g), water (55 g), bitumen (5 g) and bentonite (5 g) into a clean glass jar.
- 2) Mix the 100-g mixture thoroughly.
- 3) Run the entire mixture through standard Dean Stark extraction. Sub-sampling without adequate homogenization may cause the bentonite to preferentially pass through the Dean-Stark thimble. Once bitumen and water have been extracted, the dried solid serves as a bulk standard sample containing 12.5-wt%

bentonite. The bitumen free standard is referred to as an MFT-analog.

- 4) Gently shatter the MFT-analog using a mortar and pestle to remove clumps of materials.
- 5) Store as bulk standard.

7. PREPARATION OF METHYLENE BLUE SOLUTION

Prepare 500 ml of 0.006 N Methylene Blue solution. Stir solution at 400 rpm for a minimum of 10 minutes to ensure that all the dye is dissolved. Prepare this solution fresh daily.

8. DISPERSION OF SAMPLES

- 1) The MFT-analog must have gone through the Dean Stark extraction process or equivalent bitumen removal process. All test solids are assumed to have gone through the Dean Stark extraction process or equivalent bitumen removal process. Bentonite is used as received.
- 2) Measure out in a clean beaker, approximately 1 g of MFT-analog on a top loading balance and record the weight.
- 3) In a second clean beaker, measure approximately 0.2 g bentonite on a top loading balance and record the weight.
- 4) For each test sample place a clean dry beaker on the top-loading balance and tare the weight. Before adding the sample please take the following into consideration:
- 5) Is the sample very sandy? If so, use 5 g of sample.
- 6) Does the sample contain large proportions of clay? If so, use 1-2 g of sample.
- 7) Add the sample to the beaker and record the weight of the sample used.
- 8) Add 50 ml of 0.015 M NaHCO_3 to each sample. Add NaHCO_3 carefully so that the solids don't get spread all over the inside of the beaker. Use a disposable pipette to rinse the sides of the beaker with some of the NaHCO_3 solution already in the beaker.
- 9) Add 2 ml of 10% w/w NaOH solution to each sample with a disposable pipette. Place a clean dry stir bar in the mixture. Cover the beaker with a watchglass to keep the sample from evaporating. This step is to try and improve the dispersion of a sample – the pH of the solution should be measured, if the pH of the slurry increases above 11.5 coagulation of the clays is likely and the amount of NaOH added just be lowered or eliminated entirely.
- 10) Soak samples overnight (minimum of 12 hours).

11) In the morning place samples on a hotplate/stirrer set to 120° C (the sample should not heat above 60° C with the hotplate set at this temperature – monitor temperature as different hotplates heat at different rates). Set the stirrer to a minimum of 250 rpm. Adjust the mixing speed as required. *Make sure the sample is mixing completely and that all solids are in suspension and should move freely around the beaker. Use a glass rod with a rubber policeman to dispel any agglomerations.*

- 12) Heat and stir the sample for 20 minutes then transfer to an ultrasonic bath operating at a 42 kHz for an additional 20 minutes.
- 13) The samples should now be dispersed. Check that the samples show full dispersion:
- 14) A fully dispersed sample will be free of floating particles such as small balls of clay that may have become impregnated with air. These particles should be captured using a glass rod and policeman and pulverised while inside the sonification vessel to ensure they are dispersed properly.
- 15) Solids should be move freely from the corners of the sonification vessel and not adhere in clumps. These agglomerations should be captured using a glass rod and policeman and pulverised while inside the sonification vessel to ensure they are dispersed properly.
- 16) Look for signs of streaming birefringence within the sample. Birefringence is the effect produced by the individual clay particles as they rotate violently by the sonic sound waves within the bath. The effect it produces is similar in appearance to a tornado inside the mixed sample with the clay particles turning in a cone-shaped column appearing a dark and then light brown in colour as they individually catch the ambient light at different angles and then reflect them outwards at two distinct angles of refraction.
- 17) If the sample is not dispersed repeat step 14 until the sample is fully dispersed.

NOTE: DISPERSION IS THE MOST IMPORTANT PART OF THIS METHOD. If the sample is not dispersed completely the titration results will be inaccurate.

- 18) The times and methods provided in this method are from extensive testing at CANMET. Equipment varies from lab to lab and it wears out. By periodically performing optimization testing on the equipment with a known sample such as bentonite, an MFT

analog, or an in-house standard, one can always know the amount of mixing and sonication time necessary to achieve an optimum dispersion (i.e. a level at which methylene blue index does not increase with mixing/sonication time).

9. TITRATION OF SAMPLE

- 1) Place the beakers in a room temperature water bath and let them cool for 3-5 minutes. The following steps are carried out for the Bentonite first, followed by the MFT-analog, then for the test samples.

Commentary –samples which are too hot will show diminished MBI's. Room temperature is optimal for this test.

- 2) Place the beaker on a stirring plate located underneath the burette and start stirring the sample (no heat).
- 3) Place the handheld pH meter in the solution of the sample. Add 10% v/v H₂SO₄ until the pH drops to 2.5-3.8.. Titrate the sample with 0.006 N Methylene Blue while the sample is stirring.
- 4) Commentary: a pH of 2.5-3 has been found to tighten the halo effect and make end point detection easier. There is a significant amount of buffering capacity in most oil sands samples making a precise pH difficult to achieve which is why the 2.5-3.8 is recommended.
- 5) Add the methylene blue solution in 1 ml increments. Switch to 0.5 ml increments when the sample is close to reaching the endpoint. From prior experience with pure bentonite, depending on the batch, the endpoint can range between 28 and 34 mls. If the pure bentonite sample is not within this range there may be an issue with the methylene blue or with the procedure and the test is not considered valid.
- 6) With a transfer pipette, remove an aliquot of the sample (after each titrant addition) and place one droplet on a piece of Whatman 42 ashless filter paper. Continue placing drops of sample on the filter paper after each addition of titrant until the endpoint is reached. The endpoint is observed when there is excess of methylene blue in the water phase of the sample indicating. A blue halo will form around the sample droplet on the filter paper. A UV lamp may be used to enhance the detection of the halo. Continue 2-3 drops passed the end point to allow for endpoint verification.

- 7) Record the ml's of methylene blue required to reach the end point. An MBI test is only considered valid if it has a precision of 5% or better for instance if the end point of a test is 10mL of methylene blue and step wise titration was done in 0.5mL increments this would lead to a precision of 5%. A maximum of 50mL of Methylene blue is recommend for a valid test. For tests of multiple samples the methylene blue test should be repeated on approximately 5% of the samples to ensure that the results are repeatable.

10. CALCULATIONS

METHYLENE BLUE INDEX (MBI)

$$MBI \left(\frac{meq}{100g} \right) = \frac{mls \text{ of } MB \times Normality \text{ of } MB}{mass \text{ of dried sample } (g)} \times 100$$

METHYLENE BLUE NUMBER (MB#)

$$MB\# \left(mls \text{ of } 0.006N \frac{MB}{100g} \right) = \frac{mls \text{ of } 0.006 N MB}{mass \text{ of dried sample } (g)} \times 100$$

11. OTHER CALCULATIONS

These calculations are often requested by oil sands operators but should be treated as useful correlations and not direct outputs of the methylene blue test.

WEIGHT PERCENT CLAY

$$Wt\% \text{ Clay} = \frac{MBI + 0.04}{0.14} \times 100$$

Note this can lead to a wt% Clay greater than 100%

ACTIVE SURFACE AREA (BASED ON REFERENCE 3)

$$Surface \text{ Area} \left(\frac{m^2}{g} \right) = MBI \times 130 \times 0.06022$$

12. STANDARDIZATION

$$MBI_{MFT \text{ Analog}} \left(\pm 0.25 \frac{meq}{100g} \right) = \frac{MBI_{Bentonite} \times Wt\%_{Bentonite \text{ in } MFT \text{ Analog}}}{100}$$

The precision is taken from the ASTM Standard: C837-99.

$$Wt\%_{Bentonite \text{ in } MFT \text{ analog}} = \frac{Mass \text{ of } Bentonite \text{ in } Analog}{Mass \text{ of } Bentonite \text{ in } Analog + Mass \text{ of } Sand \text{ in } Analog}$$

If the MFT-analog MBI is outside the specified range, the dispersion equipment should be checked and test samples repeated.

13. UNCERTAINTY ANALYSIS

Following the method for propagating uncertainties outlined in “An Introduction to Error Analysis” by John R. Taylor, the uncertainty in the methylene blue index can be simplified as:

$$\frac{\delta MBI}{MBI} = \sqrt{\left| \frac{\delta Normality}{Normality} \right|^2 + \left| \frac{\delta mlsMB}{mlsMB} \right|^2 + \left| \frac{\delta Mass\ sample}{Mass\ sample} \right|^2}$$

Since the values uncertainty in the concentration and the uncertainty in the weight are very small relative to the uncertainty in the volume, they can be neglected from the equation leaving:

$$\frac{\delta MBI}{MBI} \approx \left| \frac{\delta mlsMB}{mlsMB} \right|$$

Similarly, since the methylene blue surface area is given by Hang and Brindley 1970 as:

$SA_{MB} = MBI \times 130 \times 0.0602$, the relative uncertainty in the surface area is also the relative uncertainty in the volume.

MBI should therefore be reported to no more decimals than the uncertainty in the measurement.

For instance assuming 5mL of MB was used to titrate 2g of solids and the uncertainty in the end point was 0.5mL the result would be:

$$5\text{mL} * 0.006/2 * 100 = 1.5$$

$$\text{With an uncertainty of } 0.5 * 0.006/5 * 100 = 0.15$$

Therefore it is appropriate to report the result as 1.5 ± 0.2 – or 1.5 (i.e. to two significant figures)

Or for MB#

$$= 5/2 * 100 = 250 \text{ with an uncertainty of } 0.5/2 * 100 = 25$$

Therefore it is appropriate to report the result as 250 ± 25 or 2.5×10^2

ACKNOWLEDGEMENTS

The CONRAD Clay focus group would like to acknowledge the efforts of Amar Sethi, Michelle Morin and Oladipo Omotoso in their efforts to improve the application of methylene blue analysis in the oil sands industry.

CONVENTIONAL OIL SANDS TAILINGS CAN ACHIEVE FINES CAPTURES OF 60% AND HIGHER

Catherine Fear¹, Edward McRoberts¹, Reza M. Nik², and Gennaro Esposito²

¹AMEC Environment & Infrastructure

²Shell Canada Energy

ABSTRACT

Conventional oil sands operations deposit segregating tailings streams into tailings facilities, resulting in beaches above water (BAW), beaches below water (BBW) and fluid fine tailings (FFT). Pond soundings discriminate the boundary between FFT and underlying BBW. Operational approaches increasing fines capture in beaches would result in less FFT requiring secondary treatment with alternate technologies. Using information shared via COSIA or in the public domain, a review of several case records was completed, including commercial scale external tailings facilities (ETFs), field scale trials and flume tests. The case records indicate that segregating tailings streams directed to conventional facilities having large deep ponds can achieve overall fines captures (cell, BAW and BBW combined) from 60 to 70%, to almost 80% in some cases. At the other end of the range, BAW deposits have lower captures, in the order of 30 to 40% for typical whole tailings. Contained beaching creates a lower energy environment with some ponding, and some BBW, resulting in a higher total capture than an uncontained BAW deposit, but still less than the best commercial scale ETFs. Operational variability, a reality of oil sands extraction plants, will play a dominant role, but increasing slurry density and maintaining constant flow conditions, as much as practical, would increase capture. Co-disposal of fine and coarse tailings streams may result in more effective capture than spiking fines into a coarse tailings stream, all else being equal. A variety of operational factors appear to result in a range of fines captures for large ponds.

INTRODUCTION

Conventional tailings operations at oil sands mines consist of discharging segregating tailings streams into tailings facilities, resulting in beaches above water (BAW), beaches below water (BBW) and fluid fine tailings (FFT). The outer shell of an external tailings facility is often constructed using the coarser fraction of the tailings, mechanically compacted by dozers, a technique referred to as cell construction. In this paper, cell and BAW are

considered together as a single zone. Overlying the FFT is a water cap, used as a source of recycle water for the extraction plant; the water cap thickness varies, depending on the facility. Pond soundings (AK97 or CT09) are used to discriminate the boundary between FFT and BBW (typically referred to as the "pond bottom"). Fish finder type techniques and/or solids content testing is used to discriminate the boundary between recycle water and FFT (typically referred to as the "mudline"). Some fines in the tailings slurry (mineral solids < 44 microns) are captured in the cell and beaches, with the rest reporting to FFT.

In Fall 2012, COSIA's Enhanced Fines Capture Working Group commissioned AMEC to undertake a desk study summarizing available fines capture data for segregating whole tailings deposits. The study included a review of depositional processes, as understanding these processes could lead to implementation of operational changes that would increase fines capture and reduce the amount of fines forming FFT in the first place. This paper provides a high level summary of the final report that was prepared for COSIA (AMEC, 2013); the complete report is available on COSIA's website¹.

FINES CAPTURE DEFINITIONS

Mass Balance Considerations

Fines capture is the proportional ratio of the mass of fines in the beach divided by the mass of fines in the tailings slurry directed to the storage facility (i.e. net of any rejects). The mass of fines in the beach, and hence fines capture, can be assessed directly or indirectly (by subtraction), as follows:

Direct:

$$Fines\ capture = \left(\frac{M_{FD}}{M_{FS}} \right) \quad [1]$$

Indirect:

$$Fines\ capture = \left(\frac{M_{FS} - M_{FF}}{M_{FS}} \right) \quad [2]$$

where:

¹ <http://www.cosia.ca/initiatives/tailings/tailings-documents>

M_{FD} = Mass of fines in beach deposit
 M_{FS} = Mass of fines in tailings slurry
 M_{FF} = Mass of fines in fluid fine tailings

In addition to characterizing the tailings slurry, the direct method requires an assessment of beach volume, beach dry density and beach fines content. Given the inherent large variability of tailings beach deposits, this method is more difficult and has more uncertainties associated with it than the indirect method. All beach sampling techniques result in some degree of sample disturbance, with resulting effects on the beach properties, as measured by subsequent laboratory tests. Deposits that are not fully saturated further complicate assessment of beach dry density. The mass of fines in the tailings slurry can be based on measurements made directly downstream of the final tailings pump box, or based on the mass of fines in the ore, accounting for rejects, if any.

The indirect method also requires characterization of the tailings slurry, but is independent of beach volume, beach density and beach fines content. It requires an assessment of FFT volume, FFT density and FFT fines content. Given the inherent stratification of FFT deposits, this method is more straightforward and reliable than the direct method. Furthermore, fluid sampling methods likely have little effect on the properties of the FFT samples, as measured by subsequent laboratory tests.

Completing a mass balance for fines and obtaining a small percentage closure (i.e. obtaining similar fines captures calculated using both methods) adds confidence to the result. Completing a mass balance for all mineral solids (sand plus fines) and achieving a small percentage closure further enhances confidence. Any difficulties in obtaining small closures will be more likely due to the beach side of the balance, for reasons outlined above.

Sand to Fines Ratio Index

Sand to fines ratio (SFR) is defined as follows:

$$SFR = \left(\frac{M_S}{M_F} \right) \quad [3]$$

where:

M_S = mass of sand (mineral solids > 44 microns)
 M_F = mass of fines (mineral solids < 44 microns)

Substituting Equation 3 into Equation 1:

$$Fines\ capture = \left(\frac{SFR_S}{SFR_D} \right) \cdot Sand\ Capture \quad [4]$$

where:

SFR_S = SFR of the tailings slurry
 SFR_D = SFR of the beach deposit

Sand capture is the proportional ratio of the mass of sand in the beach divided by the mass of sand in the tailings slurry directed to the storage facility. Using equations similar to Equations 1 and 2, but using the mass of sand for each component, sand capture can also be calculated directly or indirectly. When considering an ETF as a whole, the term "beach" is often used to refer to the combined total of cell, BAW and BBW, and "beach" sand captures can approach 100%, as the FFT in the pond typically has a relatively low sand content. If one assumes that an ETF has an overall sand capture of 100% (i.e. no sand reports to FFT), Equation 4 simplifies to SFR_S/SFR_D . This ratio is a simple index parameter that can be used to estimate the global fines capture of a given ETF (i.e. capture by cell, BAW and BBW combined). In reality, a small amount of sand reports to FFT, and the overall sand capture for an ETF is less than 100%. When considering the BAW component of an ETF on its own, the sand capture is much less than 100%, as sand also reports to BBW. In general, operational approaches that increase sand capture will increase fines capture, all else being equal.

Fines Capture Effectiveness Ratio Index

Küpper (1991) proposed another simple index parameter to compare the relative fines capture efficiencies of different depositional environments. In the COSIA study, this was referred to as Fines Capture Effectiveness Ratio (FCER), as follows:

$$FCER = \left(\frac{\%F_D}{\%F_S} \right) \quad [5]$$

where:

$\%F_D$ = fines content of tailings deposit
 $\%F_S$ = fines content of tailings slurry

For a given case record, FCER can be used to compare the relative fines capture effectiveness of beach regions resulting from different depositional environments. However, FCER is not equivalent to fines capture; for the same FCER, different sand captures will result in different fines captures.

Fines Storage

Fines storage (mass of fines per unit volume of beach) can be useful for planning, but is a different metric than fines capture. For a given beach dry

density, higher beach fines contents mean higher fines storage. Fines content can be assessed by sufficient sampling and testing, but dry density can be difficult to assess, as discussed earlier.

CASE RECORDS CONSIDERED

Three main commercial ETFs were considered in detail, with comprehensive operational histories and data sets provided by operators, as follows:

- Canadian Natural's Horizon Mine ETF
- Shell's Muskeg River Mine (MRM) ETF
- Syncrude's Aurora Settling Basin (ASB)

Figure 1 presents air photos of the three ETFs. The Horizon Mine ETF dyke is being constructed entirely of overburden/interburden, while dykes for the MRM ETF and ASB have been constructed mostly of the coarser fraction of the tailings. Fines captures for these ETFs were taken as reported by the operators; completing an audit of an operator's mass balance was not part of the study scope.



Figure 1. Main Commercial ETF Case Records Considered (shown to about the same scale).

The following additional ETFs were considered at a high level, based on either limited information in the public domain or provided by the operator:

- Suncor's Tar Island Pond (data analysis

by Don Sheeran in early 1990's, reported more recently by Mikula et al., 2008, and data in MacKinnon and Sethi, 1993)

- Syncrude's Mildred Lake Settling Basin (MLSB), first 1,000 Mt of ore (Fair, 2008)
- BAW deposits at Syncrude's Southwest Sands Storage (SWSS) facility.

Laboratory flume tests and field trials were also considered, ranging from a series of 8 m long flume tests completed by Total in 2011 (Sun et al., 2012) to a 1,200 m long contained beaching toe berm at MLSB constructed by Syncrude in Winter 1989/90 (Plewes et al., 1995).

The study did not consider any case records for tailings slurries intended to be non-segregating, and did not assess the impacts, if any, of different operators using different measurement methods.

FINES CAPTURE SUMMARY

Table 1 summarizes the range in fines captures observed. The case records can be divided into three main groups, as follows:

- Group 1 (highest captures, ranging from 60 to almost 80%) – commercial scale ETFs with old, large, deep ponds and large volumes of BBW
- Group 2 (lowest captures, ranging from 20 to 40%) – uncontained BAW and small scale contained beaching
- Group 3 (relatively high captures of about 65%) – (a) large scale contained beaching of whole tailings; (b) subaerial co-disposal of fine and coarse tailings streams

Group 1 – Commercial Scale ETFs

The case records indicate that segregating tailings directed to conventional tailings facilities with large deep ponds, resulting in large BBW deposits, can achieve overall global fines captures (cell, BAW and BBW combined) from 60 to 70%, to almost 80% in some cases. The ETFs considered in this study had a number of operational similarities and differences, and the resulting range in fines captures reported in Table 1 represents the net effect of these operational factors. ASB had the highest fines capture of 77% (BGC, 2011). Factors contributing to higher captures include:

- Maturity and depth of the pond, as older,

- deeper ponds have more BBW
- Full perimeter discharge around a more circular facility, with more interfingering of beaches in the centre of the pond
- Internal cross dykes
- Lower flow rates and higher densities
- Lower energy depositional environments
- Downward drainage effects in beaches
- Favourable pond chemistry

Table 1. Summary of Fines Captures for Case Records Considered

Operator	Tailings Facility	Time Period	44 Micron Fines Capture
Commercial Scale ETFs			
Syncrude	Aurora Settling Basin (ASB) ¹	2000 to 2009	77%
Shell	Muskeg River Mine (MRM) ETF	2003 to 2011	70%
Suncor	Tar Island Pond (Pond 1)	Up to early 1990's	63%
Syncrude	Mildred Lake Settling Basin (MLSB)	1 st 1,000 Mt Ore	62%
CNRL	Horizon Mine ETF	2008 to 2012	62%
Commercial Scale Co-Disposal			
Shell	MRM ETF – NE Beach Only ²	2008 to 2011	65%
Field Monitoring, Flume Tests and Field Trials^{3,4}			
Syncrude	1200 m Long Contained Beaching Berm	1989/90	66%
Syncrude	Southwest Sands Storage (SWSS) Field Monitoring of Uncontained Beaches Above Water (BAW)	2004	37%
OSLO	Contained 100 m Long Beaching Trials	1991	30 to 40%
Syncrude	ASB Cell & BAW Only	2000 to 2009	31%
Syncrude	Contained 300 m Long Spiking Trials	1993	20 to 30%
Total	Contained 8 m Long Flume Tests	2011	25%
Syncrude	Uncontained Beaching Trials	1988	≤ 21%

Notes:

1. At Aurora, froth is directed to Mildred Lake, and the resulting tailings to MLSB. If the froth tailings were also directed to ASB, the fines capture for ASB could be between 70 and 77%.
2. The combined overall average fines content of the three separate tailings streams reporting to the northeast beach portion of the MRM ETF was significantly higher than that for the MRM ETF as a whole and the other commercial scale ETFs.
3. For each set of flume tests and field trials, a range of slurry properties was tested; the fines capture reported above is for the test or trial that had the slurry fines content closest to the overall averages for the commercial operations, for direct comparison.
4. "Contained" tests and trials included some degree of containment at the far end, causing some amount of ponding to develop. "Uncontained" trials were open-ended, and any solids that did not deposit on the beaches could flow directly to the pond.

Group 2 – BAW Deposits

Uncontained BAW deposits have much lower fines captures than commercial ETFs, with fines captures being in the order of 30 to 40%, but as low as 20% or less, for typical whole tailings. This is demonstrated by the following case records:

- Uncontained BAW field trials at Syncrude in 1988 (Küpper, 1991)
- Limited data for BAW deposits at SWSS (pers. comm., Mr. Nan Wang of Syncrude)
- The BAW portion of the ASB, including cell construction (BGC, 2011)

Operational processes that would increase fines capture in BAW may require additional "on-off" controls to limit fines content in the shell portion of an ETF, for geotechnical stability requirements.

Group 3(a) – Contained Beaching

Contained beaching creates a lower energy environment with some ponding, and some BBW, leading to higher overall captures than typical uncontained BAW deposits, but still less than the best ETFs. This is demonstrated by a long toe berm that Syncrude constructed at MLSB in 1989 to evaluate contained beaching construction techniques (Plewes et al., 1995). A relatively high fines capture of 66% was achieved. A summary of the operational details is as follows:

- Some pre-trial beaching was completed, to facilitate drainage towards the spillbox.
- Whole tailings were discharged into a full scale, 200 m wide by 1,200 m long, closed ended cell, with a spillbox at its far end.
- Tailings were discharged using four 24" offtake pipes, operated one at a time.

Over the two week pour, offtakes were extended by 175 m (in 24.4 m increments).

- The spillbox was operated such that a relatively large pool was maintained at the far end of the cell, extending about 100 to 250 m upstream of the spillbox. This was done to promote sand capture, but the resulting "mini-pond" created BBW and enhanced the overall fines capture.
- The tailings slurry, beach deposits, and spillbox runoff were all characterized, and a detailed mass balance was completed. The 1991 OSLO field trials (Shaw et al., 1993) and the 1993 Syncrude field trials (Cuddy et al., 1993) also involved contained beaching as tailings were deposited into a closed ended cell with a spillbox. However, the cells were much smaller (10 m by 100 m and 40 m by 300 m, respectively), and the resulting fines captures were much lower than the overall fines capture achieved by the Winter 1989/90 toe berm constructed at MLSB. Total's 8 m long flume tests also had containment (Sun et al., 2012). While the tailings slurry was being discharged into the flume, the outlet end was blocked. The mixture was allowed to settle for 1 hour before runoff was drained from the far end of the flume by slowly opening rubber plugs on the weir at the end of the flume. Fines captures achieved in the flume tests were similar to those in the 1991 and 1993 field trials. Extrapolating from small scale tests or trials to commercial operations is difficult, if not impossible.

Group 3(b) – Co-disposal

Co-disposal of fine and coarse tailings streams may be more effective at fines capture than spiking fines into a coarse stream, all else being equal. This is demonstrated by the NE Beach at the MRM ETF (Figure 2). From 2008 to 2011, inclusive, a relatively high fines capture of 65% was achieved in the NE Beach (Esposito and Nik, 2012).

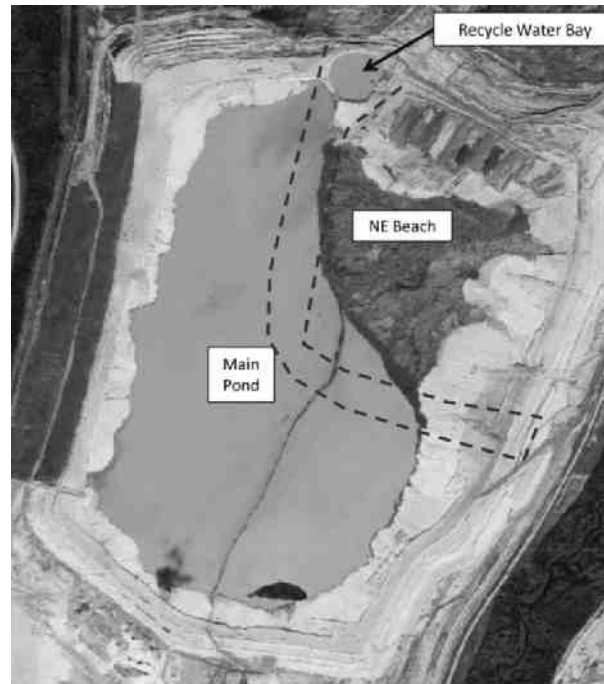


Figure 2. NE Beach at MRM ETF.

A summary of the operational details is as follows:

- MRM produces three tailings streams: coarse sand tailings (CST), thickened tailings (TT) and tailings solvent recovery unit (TSRU) tailings. At times, during various bypass conditions in the extraction plant, whole tailings (WT) are produced and discharged via the CST lines, rather than separate CST and TT.
- The ETF started out as a segmented facility, with a cross dyke separating the NE corner (NE Pool) from rest of the ETF (Main Pond); see Figure 2. The NE Pool initially received subaqueous deposition of TT, TSRU and some CST/WT.
- The cross dyke was not raised along with the ETF perimeter dykes, and eventually a long subaerial beach formed in the NE corner of the ETF, as a result of generally continuous deposition of TT and TSRU, with intermittent deposition of CST/WT.
- CST/WT were discharged into the Main Pond from the rest of the ETF perimeter.

SLURRY SFR

The ETFs considered in this study received all or virtually all of the tailings produced by the applicable mine during the time period over which they were constructed. For each ETF, the global SFR of all tailings streams combined ranged from about 3.5 to 5.0. The flume tests and field trials considered in this study covered a much wider slurry SFR range, from about 2 to 17. Therefore, to allow a direct comparison, the fines capture reported in Table 1 for each set of flume tests or field trials is for the test or trial that had a slurry SFR closest to the global values for the ETFs.

Figure 3 plots beach fines content versus slurry SFR for all case records considered in this study. Figure 4 presents a similar plot of fines capture versus slurry SFR. The flume tests and field trials indicate the following trends with increasing slurry SFR (i.e. decreasing slurry fines content):

- Decreasing beach fines content
- Increasing fines capture

While there are likely several potential factors at play, some of which may trade off with each other, a simple explanation of these trends is that a higher SFR slurry has more sand available to trap fines, but also fewer fines to trap in the first place.

At a given slurry SFR, the trends shown in Figure 3 and Figure 4 indicate lower beach fines contents and lower fines captures for the open ended BAW trials than for those tests/trials with containment.

From 2008 to 2011, if the three tailings streams that were directed to the NE Beach of the MRM ETF (CST/WT, TT and TSRU tailings) are considered together as a single combined stream, the overall average fines content was 33.5%; i.e. SFR of 2.0 (Esposito and Nik, 2012). As shown in Figure 3 and Figure 4, the beach fines content and the fines capture achieved at the NE Beach through co-disposal of these three streams was much higher than for those tests/trials that were run by discharging a single tailings stream at a similarly low SFR.

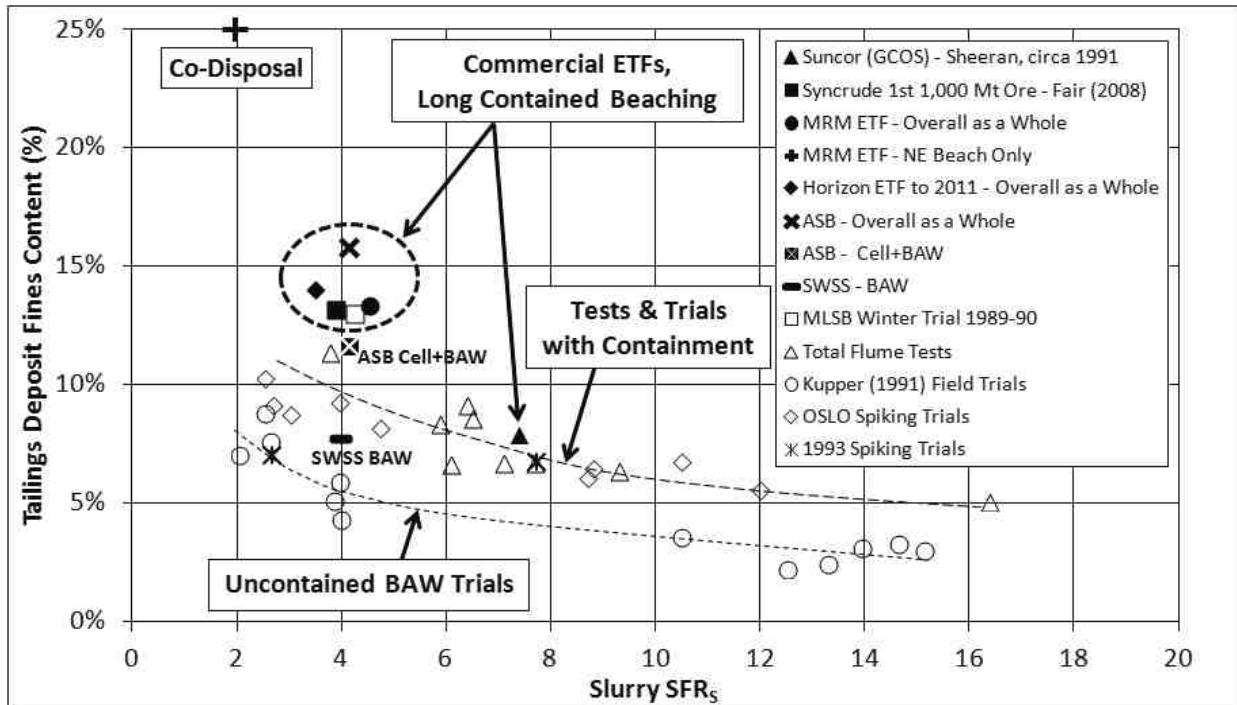
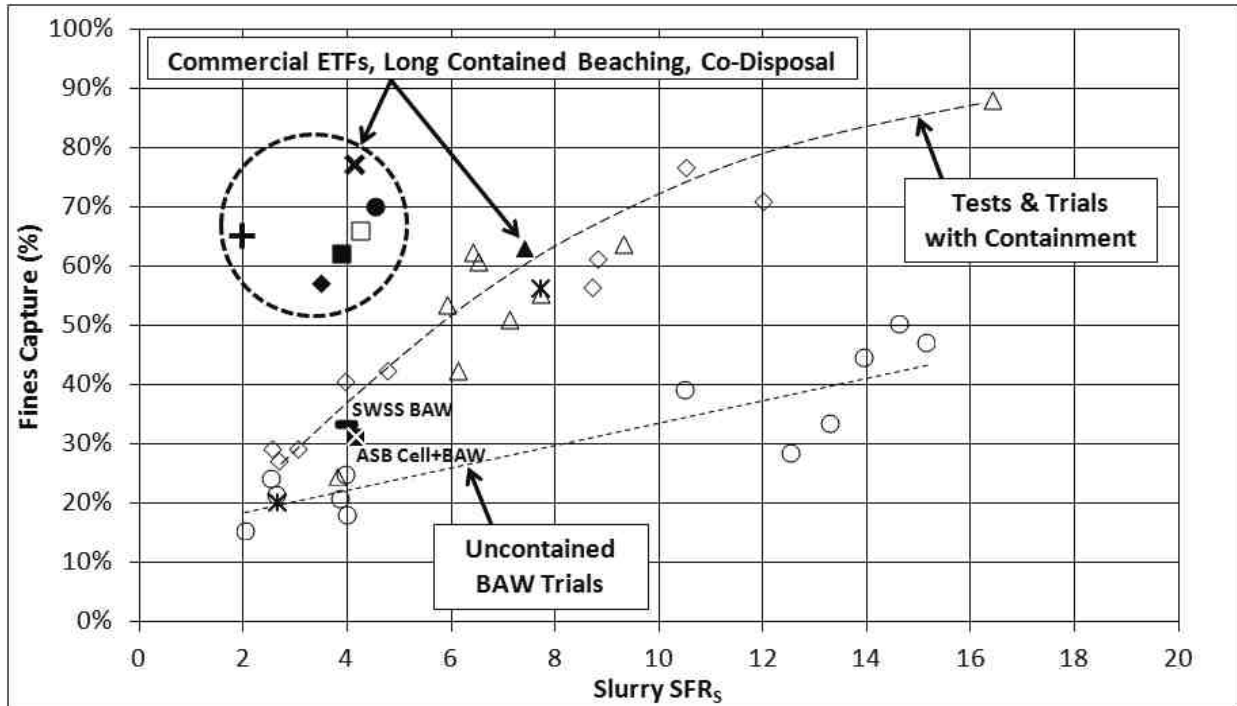


Figure 3. Beach Fines Content versus Slurry SFR Trends.



Notes:

1. The legend in Figure 3 also applies to this figure.
2. Fines captures for Küpper (1991) field trials, OSLO spiking trials, 1993 spiking trials and SWSS BAW are based on SFR_s/SFR_D , assuming 100% sand capture. Sand capture for the open-ended Küpper (1991) trials was likely less than 100%, and the actual fines captures are likely lower than shown here. Fines captures for all other case records are based on M_{FD}/M_{FS} .

Figure 4. Fines Capture versus Slurry SFR Trends.

OPERATIONAL VARIABILITY

Tailings slurry data were provided by the operators for the Horizon Mine ETF, the MRM ETF and ASB. The data indicate frequent large variations in slurry flow rate, slurry density and slurry fines content, consistent with typical operational variability of an oil sands extraction plant. The data also indicate that the total cumulative time that tailings lines are on flush is significant. At all three mines, about 10 to 20% of the data indicate that the coarse or whole tailings lines have slurry densities less than 1100 kg/m^3 , pumping essentially just water.

DEPOSITIONAL ENVIRONMENT

Depositional environment directly affects fines capture, with lower energy environments being more effective at capturing fines. To demonstrate the effects of depositional environment, the MRM ETF, Horizon Mine ETF and ASB were reviewed in further detail by dividing beaches into regions with different depositional environments and comparing

the fines contents and FCERs. This confirmed that subaqueously deposited BBW is more effective at capturing fines than subaerially deposited BAW.

Within BBW, fines contents increase as one moves from deposits near the shoreline to those farther out below a progressively deeper pond, ending with "pond centre" deposits. Physical mechanisms unique to BBW can result in BBW entrapping and entraining existing FFT, thereby increasing the overall fines capture for a facility, especially in older, deeper ETFs with large ponds. These include shallow and deep-seated slope instabilities and resulting turbidity currents created in the pond.

PREDICTING FINES CAPTURE

There are no existing models that can predict fines capture over the wide range of depositional environments that occur simultaneously in a typical tailings facility. Moreover, the typical operational variability of an oil sands extraction plant, as

discussed above, plays a dominant role that would be difficult, if not impossible, to model.

Historically, tailings planning has often made use of a pore capture model to estimate fines capture (developed by Mr. C. Marsh, working at Syncrude). The model assumes that all sand settles out as beach, forming a sand skeleton at an assumed dry density. The fines and water portions of the tailings being discharged are considered together as a slurry, with a portion of the slurry being trapped in the voids of the sand skeleton and the remainder reporting to the pond. However, the pore capture model is not applicable to BBW, given the different depositional mechanisms at play (slope instabilities, turbidity currents, etc.). While it may give reasonable results for BAW, inspections often indicate layers of concentrated fines within BAW that are not predicted by the model. Furthermore, open ended BAW deposits, with no containment, likely have sand captures that are less than 100%, thus reducing fines capture.

CONCLUSIONS

Segregating tailings directed to conventional commercial scale tailings facilities with large deep ponds, resulting in large BBW deposits, can deliver global fines captures as high as 70% to almost 80%. Older, deeper ponds, internal cross dykes, full perimeter discharge around a more circular facility, and downward drainage effects in beaches may assist fines capture in ETFs. However, large deep ponds may no longer be practical. Long beach / small pond type operations, with large uncontained BAW deposits, result in lower fines captures, in the order of 30 to 40% for typical whole tailings, but possibly as low as 20% or less.

The 1,200 m long contained beaching toe berm at MLSB achieved a high capture of 66%. Contained beaching creates a lower energy environment with some ponding and BBW. This results in a higher overall capture than a typical uncontained BAW deposit, but still less than the best commercial scale ETFs. Subaerial co-disposal of coarse and fine tailings streams in the NE corner of the MRM ETF resulted in a similarly high capture of 65%.

The case records indicate that segregating slurries with higher fines contents (i.e. lower SFR) result in beaches with higher fines contents, but the fines capture on a percentage basis drops. Co-disposal of fine and coarse tailings streams may achieve a

higher fines content and a higher fines capture than spiking fines into coarse tailings (co-mixing).

There are no existing models that can predict fines capture over the wide range of depositional environments that occur simultaneously in a typical tailings facility. Moreover, the typical operational variability of an oil sands extraction plant means that parameters playing a dominant role in tailings behavior upon deposition (slurry density, flow rate, fines content, etc.) are constantly varying and not predictable. Models do not, and probably could not, account for this operational variability. Directionally, increasing tailings slurry density and decreasing flow rate would increase capture. Upset conditions will play a role, and episodic periods of flushing lines with water are a typical part of operations at an oil sands extraction plant.

Pond chemistry is expected to also play a role, but was not part of the scope of this study. Both the ASB and the MRM ETF may have pond chemistries favourable to fines capture.

ACKNOWLEDGEMENTS

Angela Küpper (formerly AMEC, now BGC) played a key role in the study described in this paper, with a particular focus on depositional environment. This work would not have been possible without the contributions made by representatives from the following companies who, collectively, formed COSIA's Enhanced Fines Capture Working Group: Canadian Natural, Imperial Oil, Shell Canada, Suncor, Syncrude Canada, Teck and Total E&P Canada. Alexandre Goldszal (Total E&P Canada) was COSIA's working group lead over the study duration, and was integral to the successful execution of this collaborative project. Alan Fair (COSIA) provided valuable technical guidance over the course of the study. In addition to the Shell Canada authors of this paper, the following individuals collated and provided comprehensive operational histories and data sets for the main commercial ETF case records: Eric Coulombe (formerly Canadian Natural); Ross Young and Evan Davison (Shell Canada); and Nan Wang (Syncrude Canada). Chris Li (formerly Total E&P Canada) provided data for the Total flume tests. Bill Shaw provided data for historical field beaching trials at Syncrude and OSLO.

REFERENCES

AMEC Environment & Infrastructure. 2013. Beach Fines Capture Study, Report prepared for COSIA.

BGC Engineering Inc. 2011. Syncrude Aurora Settling Basin, 2000 to 2009 Fines Balance Update, Phase 5 Final Report, Report prepared for Syncrude Canada Ltd.

Cuddy, G., Lahaie, R. and Mimura, W. 1993. Spiking Tailings Slurry as a Method to Increase Fines Retention in Beach Deposits, Proceedings of Oil Sands – Our Petroleum Future Conference, Edmonton, Alberta.

Esposito, G. and Nik, R. 2012. Fines Capture in a Long Tailings Beach at the Shell Muskeg River Mine External Tailings Facility: Hydraulic and Depositional Aspects, Proceedings of the 2012 International Oil Sands Tailings Conference, Edmonton, Alberta.

Fair, A. 2008. The Past, Present and Future of Tailings at Syncrude. Presentation made at the 2008 International Oil Sands Tailings Conference, Edmonton, Alberta.

Küpper, A.M.A.G. 1991. Design of Hydraulic Fill, Ph.D. Thesis, U. of Alberta, Edmonton, Alberta.

MacKinnon, M. and Sethi, A. 1993. A Comparison of the Physical and Chemical Properties of the Tailings Ponds at the Syncrude and Suncor Oil Sands Plants, Proceedings of Oil Sands – Our Petroleum Future, Edmonton, Alberta.

Mikula, R.J., Munoz, V.A., Omotoso, O.E., and Kasperski, K.L. 2008. The Chemistry of Oil Sands Tailings: Production to Treatment, Presentation made at the 2008 International Oil Sands Tailings Conference, Edmonton, Alberta.

Plewes, H., Rice, S., Hitchman, R. and List, B. 1995. Syncrude Hydraulic Tailings Depositional Trial, Proceedings of the 1995 Canadian Geotechnical Conference, Vancouver, B.C.

Shaw, W., Beck, J. and Livingstone, W. 1993. Disposal of Fine Tailings Utilizing Hydrocyclone Techniques, Proceedings of Oil Sands – Our Petroleum Future Conference, Edmonton, Alberta.

Sun, R., Goldszal, A. and Li, C. 2012. Optimizing the Capture of Oil Sand Fines in Sand Beach Area, Proceedings of the 2012 International Oil Sands Tailings Conference, Edmonton, Alberta.

FLOODING OF IN-LINE FLOCCULATED TAILINGS AFTER THIN LIFT DRYING

Aref Najafi¹, Haneef Mian¹, Reza Salehi¹, Pierre Lacoste-Bouchet¹, Karen Friedrich¹, Howard Keele¹, Casey McWhan¹ and Joy Romero¹, Farzad Daliri², Silawat Jeeravipoolvarn², Jeremy Boswell² and Trempe Moore²

¹Canadian Natural Resources Limited, Alberta, Canada

²Thurber Engineering Ltd., Alberta, Canada

ABSTRACT

Over the last few years, Canadian Natural has been working to develop new technologies for treatment of Mature Fine Tailings (MFT) at the Horizon mine site. In 2013 Canadian Natural screened a number of tailings treatment technologies and selected dual polymer injection with thin lift deposition for further investigation both in the laboratory and in the field. Such an approach was selected to avoid material re-handling and to minimize the tailings operation footprint. The plan is to deposit the final treated product sub-aerially on the west side of the External Tailings Facility (ETF) thus utilizing the natural topography at the site, and surface area for evaporation and dewatering of the deposits. After one freeze-thaw cycle, the deposit is expected to be submerged under the rising ETF levels – creating a subaqueous Dedicated Disposal Area (DDA). Eventually, the DDA will be reclaimed as part of the ETF reclamation. The key elements for success are that the treated MFT dewater, gains strength with time, maintains the natural slope after deposition, and retains deposit integrity even after being submerged by the rising ETF levels. To support the concept and prove the feasibility of the subaqueous DDA approach, a series of bench scale tests were conducted. This paper provides some details of the approach, the behavior of the material, and preliminary results of the bench scale tests performed to investigate the strength degradation of the material under static flooding and flooding with wave action.

INTRODUCTION

Canadian Natural Resources Ltd is committed to develop energy resources in a sustainable and responsible way and to manage and minimize the environmental impact of operations during all phases of a project. To reach high standards of environmental performance and meet regulatory

compliance, Canadian Natural adheres to the principles of continuous improvement, efficient operations and technological innovation.

As part of its commitment to develop and commercially implement tailings treatment and management technologies that will successfully achieve the necessary performance to meet long-term reclamation and closure requirements at the Horizon oil sands mine site, Canadian Natural is investing in and exploring several innovative tailings treatment technologies. During 2012 and 2013 Canadian Natural identified approximately 100 tailings treatment technologies using the Tailings Roadmap Study (COSIA 2012) as a guideline. Using internal technology evaluation criteria, along with advice from industry consultants, Canadian Natural short-listed “Dual Polymer Injection Technology with Multi-Layer Thin-Lift Dewatering” as providing the best fit to Canadian Natural’s long-term environmental and strategic business goals. It was expected that this deposition approach would efficiently utilize both water release on a sloped surface and evaporation to dewater treated MFT. Such a treatment and deposition strategy is expected to avoid material re-handling and further land disturbance, which results in reduced future liability.

The gentle natural slope at the west side of the Horizon ETF (Figure 1) provides exceptional conditions for water release of treated MFT as well as a large area for thin lift deposition and surface evaporation. After a single freeze-thaw cycle, the deposit will slowly be submerged under the rising ETF levels. There were two major design considerations with this approach:

1. Strength degradation and stability of the subaqueous deposit after static flooding,
2. Re-suspension of the subaqueous deposit under wave action.

Canadian Natural decided to test the concept at bench scale, followed by lab pilot scale testing, and upon satisfactory results, field scale pilot testing for demonstration of the technology. In collaboration with Thurber Engineering Ltd. and SNF Energy Services, Canadian Natural designed a series of bench scale and pilot scale tests to prove the concept, and develop the design and operational parameters for larger scale demonstration of the technology. This paper provides some details of the test setup as well as preliminary test results and conclusions.



Figure 1. The Horizon ETF

EXPERIMENTAL SETUP

The main objectives of the test program were to:

- Investigate the effects of process water (PW) flooding on strength and solids content of SNF dual polymer treated MFT dried to selected solids contents.
- Investigate the effects of wave action on strength, solids content and re-suspension of SNF dual polymer treated MFT dried to selected solids contents.
- Provide preliminary data for subsequent evaporative drying and rewetting test programs.

Two tests were conducted – static flooding, and flooding with wave action. For both tests, MFT treated with SNF's dual (cationic and anionic) polymer was deposited into the test containers and dried to specified solids contents after which the material was inundated with PW. Solids content and shear strength of the materials were then measured before flooding, as well as at 7 days and 14 days after flooding for the static test; and 7 days and 12 days after flooding for the wave test. The materials used for these experiments were harvested from the Horizon ETF. Table 1 provides solids contents and index properties for the materials.

Table 1. Characteristics of raw materials

Material	Solids Content (%) ¹	Fines Content (%) ²	Gs	wL (%)	wP (%)
MFT	28.5	99.8	2.54	61	28
PW	0.34	-	-	-	-

1- Solids content includes bitumen.

2- Fines content of total solids by sieve-hydrometer test without bitumen extraction.

Dual Polymer Injection

An anionic polyacrylamide polymer with high molecular weight and medium charge density and a cationic polymer with low molecular weight and high charge density were used during this study. The treatment occurred in two stages:

- Stage 1: Anionic polymer added to MFT and mixed.
- Stage 2: Cationic polymer added to flocs generated by anionic polymer and mixed.

The major mechanisms of the flocculation in the dual polymer injection technology are bridging and charge neutralization, which occur in two steps as depicted in Figure 2. During the first step, macromolecules of the anionic polymer are attached to larger particles via bridging mechanisms as shown in Figure 2a. Some of the clay solids and most of the ultra-fine particles may not be attached to the anionic polymer branches due to their size. In the second step, the cationic polymer is added. During this step, the negatively charged smaller particles are attached together by bridging through the cationic polymer. In addition, the smaller particles are also attached to the larger particles via an electrostatic patch model mechanism. Cationic polymer also reinforces the

floc structure by entangling in the network of anionic polymer as shown in Figure 2b.

SNF polymers used in this study were prepared at a 0.4% concentration of polymer to water, by mass.

Quality of the treated material was identified by visual inspection of the floc sizes and initial water release rate.

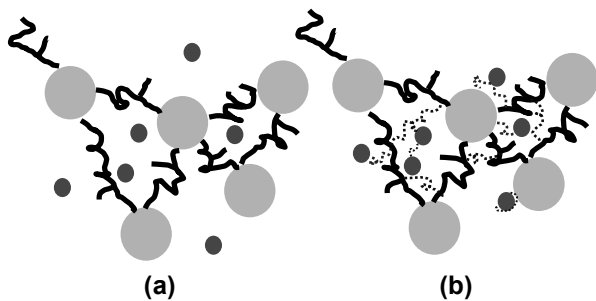


Figure 2. Dual polymer flocculation process (a) bridging mechanism of large particles (b) bridging and electrostatic patch model.

Static Flooding Test

Figure 3 shows the test setup for the static flooding test setup.



Figure 3. Static Flooding test setup.

To dry the materials, 90 W halogen bulbs and fans were used. In order to simulate a drainage condition, treated tailings were placed inside 10 litre pails with perforated bottoms. The 10 litre pails were then placed inside 20 litre pails to collect drained water. Four target solids contents (60%, 70%, 80%, and 90% by mass) were used for the test setup. All tests were conducted in triplicate to

ensure reproducibility of the results. Single layer tailings deposition and double layer tailings depositions were used in the tests.

Flooding with Wave Action Test

The flooding with wave action tests were conducted in a series of three flumes (2.0 m length \times 0.2 m width \times 0.6 m height). The test setup is shown in Figure 4. SNF dual-polymer treated MFT was prepared with two different mixing conditions – optimum mixing, and over mixing. The deposition method consisted of two 10 cm thick layers providing a final dried thickness of approximately 6 cm to 8 cm for the target solids content. Depth of water on top of the tailings was 35 cm. A pulse flow pump was used to generate waves with characteristics similar to those at the Horizon site. Two target solids contents (80%, and 90%) were used for the test setup. After the target solids content was achieved, the material was subjected to solids content and strength measurements. The deposit was then inundated and monitored for 12 days for strength degradation and solids content changes.



Figure 4. Flooding with wave action test setup.

WAVE ACTION AND POND BOTTOM SHEAR CALCULATION

Tailings re-suspension under water is a function of several factors. The process begins with energy delivered to the water surface through wind action. The amount of energy depends both on the wind velocity and fetch. The friction created initially between the wind (moving air) and the pond surface (motionless water) produces small surface deformations or ripples that progressively build into waves, as the wind continues to blow. Yanful and Catalan (2002) observed that bottom shear stresses produce a direct force on the sediment bed and they are responsible for erosion and re-

suspension. In this paper emphasis is placed on wind-induced-wave re-suspension.

Wind speed and fetch are two of the most important factors in controlling the size of waves and hence magnitudes of bottom shear stresses (Yanful and Catalan, 2002; Catalan and Yanful, 2002; Mian and Yanful, 2001). Since most researchers use the Sverdrup Munk Bretschneider (SMB) equations (Bretschneider, 1958) to calculate wave heights and hence the bottom shear stresses (e.g., Jin and Wang, 1998; Adu-Wusu et al., 2001; Yanful and Catalan, 2002), it was decided to use them in this study. US Army Coastal Engineering Research Centre (1984) provided the following equations for shallow-water waves ($D/L < 0.5$):

$$\frac{gH_s}{U_a^2} = 0.283 \tanh \left[0.53 \left(\frac{gD}{U_a^2} \right)^{0.75} \right] \tanh \left[\frac{0.0125 \left(\frac{gF}{U_a^2} \right)^{0.42}}{\tanh \left[0.53 \left(\frac{gD}{U_a^2} \right)^{0.75} \right]} \right] \quad \{1\}$$

$$\frac{gT_s}{2\pi U_a} = 1.2 \tanh \left[0.833 \left(\frac{gD}{U_a^2} \right)^{0.375} \right] \tanh \left[\frac{0.077 \left(\frac{gF}{U_a^2} \right)^{0.25}}{\tanh \left[0.833 \left(\frac{gD}{U_a^2} \right)^{0.375} \right]} \right] \quad \{2\}$$

where H_s is the significant wave height (m), T_s is the significant wave period (s), F is the fetch (m), U_a is the wind velocity (m/s), D is the depth of water cover along the fetch (m) and g is the gravitational acceleration (m/s^2). In the present study most of the conditions fell within the shallow-water wave range. The wavelength L was calculated iteratively using the equations given by the U.S. Army Coastal Engineering Research Centre (1984):

$$L = L_0 \tan h \left(\frac{2\sqrt{D}}{L} \right) \quad \{3\}$$

where L is the wavelength (m), and L_0 is the deep-water wavelength (m), which can be estimated by:

$$L_0 = \frac{gT_s^2}{2\pi} \quad \{4\}$$

Wave Orbital Velocity

The small amplitude wave theory suggested by Eagleson and Dean (1996) was used to determine the amplitude of the wave orbital velocity, U_w , just above the tailings bed due to a monochromatic wave of height H , given by:

$$U_w = \frac{H_s \sigma}{2 \sinh kD} \quad \{5\}$$

Where $k=2\pi/L$ is the wave number, and $\sigma=2\pi/T$ is the wave frequency (Dean and Dalrymple, 1984). Hence Equation [5] gives:

$$U_w = \frac{H_s \pi}{T_s \sin h \left(\frac{2\sqrt{D}}{L} \right)} \quad \{6\}$$

Shear Stress Due to Wind-Induced Waves

It is assumed that the flow in the Canadian Natural sub-aqueous deposit is hydrodynamically smooth. Flow characteristics over a smooth bottom depend on the Reynolds number, which measures the ratio of the inertial to viscous forces and indicates whether the flow is laminar or turbulent.

The calculated Reynolds numbers for the Canadian Natural DDA for wind speed up to 10 m/s fell between 1 and 63,000. This range of Reynolds number indicates that the flow occurred in the laminar range (for laminar flow $Re \leq 5 \times 10^5$; Whitehouse et al., 1999). Hence the laminar model for wave-induced oscillatory flow was used. For an oscillatory boundary layer, the maximum shear stress exerted on the bottom sediments due to wind-induced waves, τ_w , was estimated using the equation previously used by several other researchers including Bengtsson et al. (1990), Dyer (1986) and Soulsby (1997):

$$\tau_w = 0.5 \rho f_w U_w^2 \quad \{7\}$$

where τ_w is the bottom shear stress (Pa). In Equation [7], f_w is a bottom friction factor that depends on the surface roughness and flow characteristics (Reynolds number) in the wave boundary layer, both of which are related to the oscillatory particle velocity and the wave period. Ijima et al. (1966) noted that for laminar flow the smooth bed friction factor, f_w can be calculated as:

$$f_w = \frac{2}{Re} \quad \{8\}$$

Wind Speed and Direction at the Horizon site in 2011

Figure 5 shows the frequency distribution of average hourly wind speeds for the year 2011 at the Canadian Natural Horizon site. The wind speed in the field ranged from 1 m/s to 14 m/s with the

average wind speed at 2.7 m/s (Table 2). To mimic this average wind speed as well as an extreme condition for the Flooding with wave test, wind speeds of 3 m/s and 6 m/s were used for the wave height calculation.

To calculate the wave heights for the flume tests, the fetch for the Canadian Natural DDA was approximated for about 500 m, and the depth of water cover over the polymer treated MFT in the DDA was assumed to be 35 cm. With this assumption and application of Equations [1] and [2], the significant wave heights for 3 m/s and 6 m/s wind speeds were calculated to be 4.0 cm, and 7.5 cm respectively. It was then attempted to generate waves with similar significant height in the flumes using the wave generator.

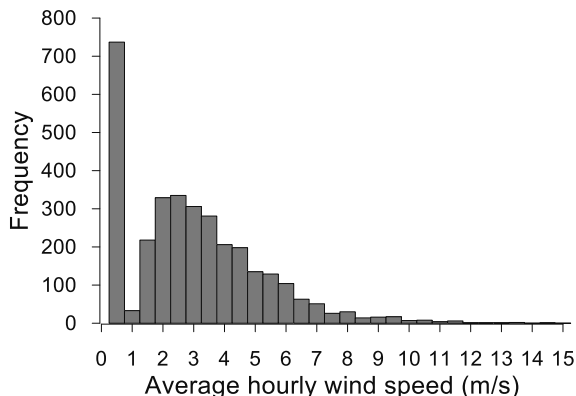


Figure 5. Frequency distribution of average hourly wind speed at the Canadian Natural Horizon Site during 2011.

Table 2. Average, minimum and maximum wind speeds at Canadian Natural’s Horizon Site during 2011

Statistics	Wind Speed (m/s)
Average	2.7
Minimum	0
Maximum	14.1
Median	2.5

Wind Generated Bottom Shear Stresses

Based on the selected wind speeds, fetch and water depth, the bed shear stresses induced by wave heights of 4.0 cm and 7.5 cm were calculated to be 0.26 Pa and 0.096 Pa respectively.

RESULTS OF STATIC FLOODING TEST (DOUBLE LAYER WITH BOTTOM DRAINAGE)

Net Water Release

One of the parameters used to evaluate the flocculation performance is Net Water Release (NWR). The NWR was found by measuring the total water input when preparing flocculated tailings and the water removed from the tailings after 24 hours, and was calculated as:

$$NWR = \frac{\text{Water release after 24 hr} - \text{Input water}}{\text{Total water in MFT}} \quad \{9\}$$

Treated material demonstrated NWR of 44% to 47% after 24 hours. This indicated that the produced material could be considered on-spec and well flocculated.

Average Solids Content after Flooding

Under static Flooding of all tailings samples, the deposits absorbed process water back into the tailings, showing a significant decrease in solids content after 7 days, after which small to negligible changes in the solids content were observed (Figure 6).

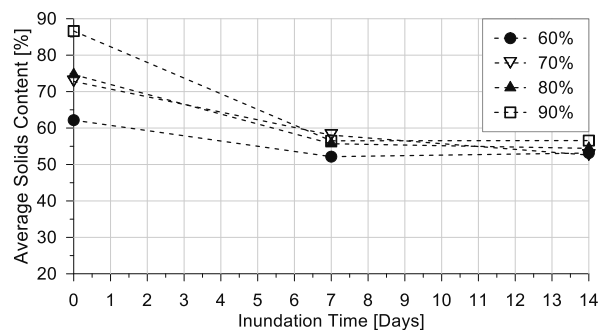


Figure 6. Average solids content vs. time for double layer with bottom drainage test during static flooding.

In general, for all samples, the solids content dropped from the original solids content to solids contents of between 50% and 60% after 7 days, and stayed in the same range up to day 14, which was the end of the monitoring period. The drier the material the higher the solids content after flooding typically.

Average Vane Shear Strength after Flooding

During static flooding, for all tailings samples, the materials showed a significant decrease in peak vane shear strength after 7 days of flooding, after which small to negligible changes in the vane shear strength were observed (Figure 7).

In general for all samples, the average peak vane shear strength dropped to a range between 2 kPa and 12 kPa after 7 days, and between 4 kPa and 12 kPa after 14 days. All samples (except samples dried to 90% solids content) exhibited peak vane shear strengths higher than 5 kPa after 14 days of flooding.

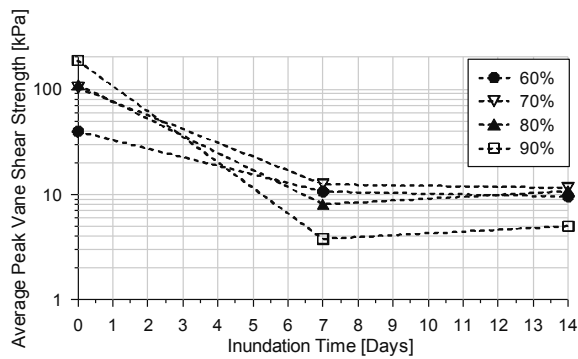


Figure 7. Average peak vane shear strength vs. time for the double layer tests with bottom drainage during static flooding.

Average Solids Content of Supernatant Water

The solids content of the supernatant water remained below 1% and there was no significant change to the supernatant within the test period (Figure 8).

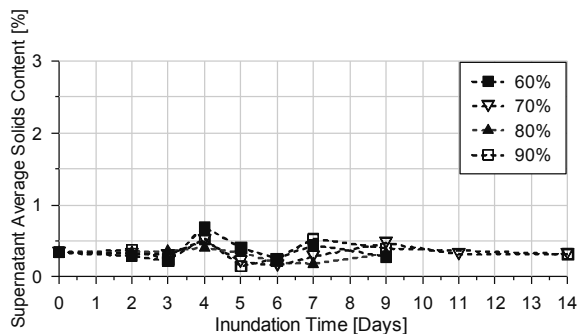


Figure 8. Average total solids of supernatant water vs. time for the double layer with bottom drainage test set during static flooding.

RESULTS OF FLOODING WITH WAVE ACTION TEST

NWR of the Flume Material

The over-mixed tailings in Flume 1 yielded a NWR of approximately 12%. The optimally mixed tailings in Flumes 2 and 3 demonstrated a NWR of approximately 18% and 19% respectively.

Average Solids Content after Flooding

After flooding with wave action for all the flumes, the treated MFT absorbed the process water, registering a significant decrease in solids content after 7 days, after which only a small to negligible change in the solids content were measured after day 12 (Figure 9).

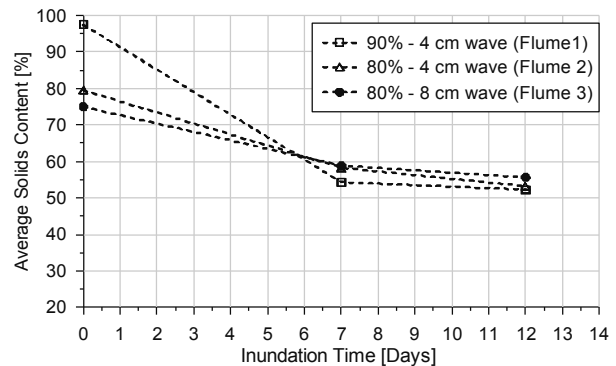


Figure 9. Average solids content vs. time of the tailings during flooding with wave action.

In general for all samples, the solids content dropped from the original solids content to solids contents of between 50% and 60% after 7 days, and stayed in the same range up to day 12, which was the end of the monitoring period.

Average Vane Shear Strength after Flooding

Treated inundated MFT in the flumes showed a significant decrease in peak vane shear strength after 7 days, after which only small to negligible changes in the peak vane shear strength were measured at day 12 (Figure 10).

In general for all samples, the peak vane shear strength ranged between 2 kPa and 8 kPa after 7 days and between 4 kPa and 9 kPa after 12 days. Except for Flume 1 (over-mixed with 90% solids content), the flumes exhibited peak vane shear strengths close or higher than 5 kPa after 12 days of flooding.

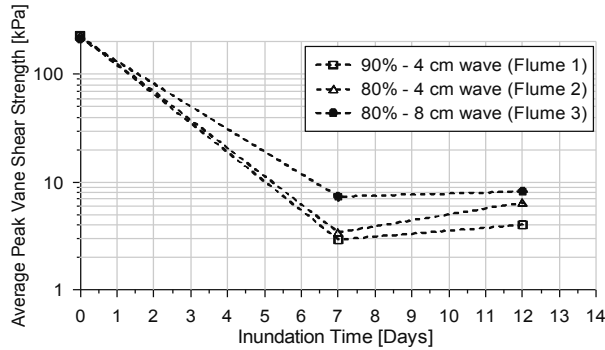


Figure 10. Average peak vane shear strength vs. time of the tailings during flooding with wave action.

Average Solids Content of Supernatant Water

The solids content of the supernatant water remained below 1% over the duration of the monitoring period (Figure 11).

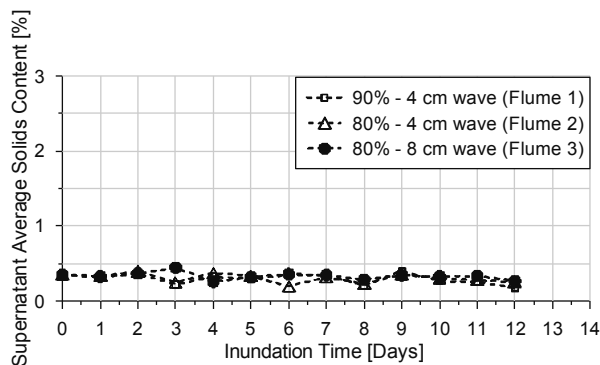


Figure 11. Average total solids of supernatant water vs. time during flooding with wave action.

DISCUSSION

Results from this feasibility study for the proposed subaqueous disposal of SNF dual polymer treated MFT with thin lift deposition show that the concept is feasible at the lab scale. Even though the deposit after flooding experienced a rapid degradation in strength and solids content, it

stayed above the AER Directive 074 requirements. In spite of induced shear on the deposit with wave action, treated material in the deposit stayed intact without considerable re-suspension.

It was also observed that the treated material that had reached a solids content of over 80% resulted in softening to a peak vane shear strength of less than 5 kPa after flooding. However, material that had reached a solids content of less than 80% resulted in retention of peak vane shear strength of over 5 kPa, but less than 10 kPa. In other words, the samples with slightly more moisture were less vulnerable to degradation upon rewetting than the more desiccated (and initially stronger) samples. The phenomenon of high strength vulnerability appears to follow a pattern similar to the shattering of a desiccated sample of dispersive clay upon rewetting.

From these early and limited lab tests, for the concept under consideration, the optimal target solids content prior to rewetting appears to be in the range of 70% to 80% solids content. The treated MFT which has not reached 70% prior to rewetting is not strong enough, and material over 80% appears more vulnerable to damage upon rewetting.

The addition of polymer adds slightly more strength to the treated MFT. At the liquid limit of the untreated MFT or typical natural clays., Peak shear strength of between 2 kPa to 5 kPa is expected (Sharma and Bora, 2003; Prakash, 2003); however, at this same water content the treated MFT has peak shear strength of just over 10 kPa.

The measured solids content of the supernatant water after the static and wave action flooding tests remains unchanged from the initial value of less than 1%, indicating that the extent of re-suspension and mobilization of solids back into the entire body of covering fluid is limited.

SUMMARY

Preliminary data has confirmed that a strength of greater than 5 kPa but less than 10 kPa appears possible with some level of surficial softening, and that the concept is feasible at the lab scale. It is expected that the tests will be repeated with a broader range of feed MFT, clay mineralogy, process water chemistry and polymer formulation, and that the impact of CO₂ injection or cessation of

CO₂ injection will also be investigated. It is also recommended to flood the samples for a longer time period to ensure no further degradation in strength occurs. The outputs from the lab scale studies will be combined with the field operation to focus on optimizing the following key parameters for the design and implementation of the scheme:

- Lift thickness, beach length and discharge rate;
- Target shear strength and corresponding solids content;
- Cycle time between subsequent lifts; and
- Annual rate of rise.

ACKNOWLEDGEMENTS

This program is comprehensive technology development program from idea stage to full commercial deployment in fast track manner. This made possible through the help and support from a team work among Canadian Natural, Thurber Engineering and SNF Energy. Here we acknowledge the individuals support and contribution to this work including Scott Ramey and Trong Vu Dong from SNF Energy, Darren Ritchie and Craig Graham from Canadian Natural, as well as Eric Coulombe from GCM Consultants (formerly from Canadian Natural).

REFERENCES

Adu-Wusu, C., Yanful, E. K. and Mian, Haneef. 2001. Field evidence of resuspension in a mine tailings pond. *Canadian Geotechnical Journal*, **38**(4): 796-808.

Bengtsson, L., Hellstrom, T., and Rakoczi, L., 1990. Redistribution of sediments in three Swedish lakes. *Hydrobiologia*, **192**: 167-181.

Bretschneider, C. L. 1958. Revisions in wave forecasting; deep and shallow water. *In* Proceedings of the 6th Conference on Coastal Engineering, 1958, ASCE Council of Wave Research, Ft. Blevior, VA, pp. 30-67

Catalan, L. J. J. and Yanful E. K. 2002. Sediment trap measurement of suspended mine tailings in a shallow water cover. *ASCE, Journal of Environmental Engineering*, **128**(1): 19-30.

COSIA 2012. Oil sands tailings technology deployment roadmaps. www.cosia.ca

Dean, R. G. and Dalrymple, R. A. 1984. *Water wave mechanics for engineers and scientists*. Prentice-Hall, Inc., Englewood Cliffs, N. J.

Dyer, K. R. 1986. *Coastal and estuarine sediments*. Wiley, New York.

Eagleson, P. S., and Dean, R. G. 1996. Small amplitude wave theory. *In: Estuary and coastline hydrodynamics*. McGraw-Hill, New York.

Ijima, T, and Tang, F.L. 1966. Numerical calculation of wind waves in shallow water. *Proceedings of the 10th Coastal Engineering Conference, Tokyo, Japan, September 1966*, ASCE, United Engineering Centre, N.Y., Vol.1, pp. 38-45.

Jin, K.-R., and Wang, K.-H., 1998. Wind generated waves in Lake Okeechobee. *Journal of the American Water Resources Association*, **34**(5): 1099-1108.

Mian, H. and Yanful, E. K. 2001. Wind induced waves and resuspension in two mine tailings ponds. *In* Proceedings of 2001 an Earth Odyssey, 54th Canadian Geotechnical Conference and 2nd Joint IAH and CGS Groundwater Conference, September 16 - 19, Calgary, Alberta, Canada, Bitech Publishers Limited, Richmond, B.C., Canada, pp. 1604-1611

Prakash, K. 2005. Discussion – Plastic limit, liquid limit and undrained shear strength of soil – Reappraisal. *Journal of Geotechnical and Geoenvironmental Engineering*, March 2005, pp. 402-403.

Sharma, B. and Bora, P. 2003. Plastic limit, liquid limit and undrained shear strength of soil – Reappraisal. *Journal of Geotechnical and Geoenvironmental Engineering*, 129(8): pp. 774-777.

Soulsby, R. 1997. *Dynamics of marine sands: a manual for practical applications*. Thomas Telford Publications, Inc., London.

US Army Coastal Engineering Research Center, 1984. *Shore protection manual*. US Army Coastal Engineering Research Center, Washington, D.C.

Whitehouse, R. J. S., Soulsby, R. L., Roberts, W., and Mitchener, H. J. 1999. Dynamics of estuarine muds. A manual for practical applications. HR Wallingford Rep. No. SR 527, Wallingford, OXON, U.K.

Yanful, E. K. and Catalan, L. J. 2002. Predicted and field-measured resuspension of flooded mine tailings. ASCE, Journal of Environmental Engineering, 128: 341-351.

DRYING OF THICK LIFT OIL SAND TAILINGS USING SMOLDERING

Babak A Jajuee¹, Scott R Hickman¹, and Greg Rockwell²

¹Imperial Oil, Calgary, Alberta, Canada

²Imperial Oil, Sarnia, Ontario, Canada

ABSTRACT

Thick-lift drying technology includes flocculation of tailings followed by formation of thick deposits for natural dewatering. The thick lift process is desirable owing to its simplicity, reduced operations, and smaller footprint compared to thin-lift drying. Although there is a significant performance improvement through optimization of this process, the biggest challenge remains to be insufficient strength in the internal layers of thick deposits due to high water content in the deposits. The dewatering performance of thick-lift deposits can be enhanced by smoldering a number of thickened TSRU or FFT columns (or tubes) embedded in the thick deposit as these tailings contain residual hydrocarbons. Thickened TSRU or FFT columns may be mixed with sand to improve their permeability for better aeration and smoldering. The heat generated from the smoldering reaction can accelerate the dewatering process of thick-lift deposits close to the TSRU columns. This process can be achieved with minimal investment in facilities. This paper describes the smoldering process, potential benefits, and results from laboratory experiments and modeling.

INTRODUCTION

Smoldering is a flameless combustion process that occurs at the surface of solids and liquids. It differs from flaming combustion, in which the fuel combusts in the gas phase. Smoldering is often associated with porous organic materials, with common examples including charcoal briquettes and cigars or cigarettes. Smoldering has also been tested for remediating soils contaminated with organic compounds¹.

Here, smoldering of TSRU tailings (“TSRU”) is examined as a method of thick-lift tailings dewatering. Several tests were performed to determine the combustion limits of smoldering

TSRU with air. Modeling was also performed to determine the extent to which the heat generated from smoldering TSRU would diffuse outward to dewater thick lifts of tailings.

Figure 1 and Figure 2 illustrate the proposed TSRU smoldering concepts for vertical columns and horizontal tubes. In both cases, air would be supplied to the TSRU in a preheated region to ignite smoldering. The temperatures attained during smoldering may be as high as 1000°C to 2000°C. The air would continue to be supplied during combustion-front propagation until all combustibles in the TSRU have been consumed.

Possible advantages for using this process to meet Directive 074 include: minimal fuel requirements, as the process is self-sustaining with an air supply; small infrastructure investment due to the *in situ* design; and the ability to readily control the process through the air supply, for example, if temperature adjustment or a quick shutdown were required.

EXPERIMENTAL

The experimental part of this program focused on determining the operational envelope for smoldering tailings and the maximum temperatures achievable. The experiments took place at Imperial Oil’s research center in Sarnia, Ontario.

A diagram of the experimental apparatus is shown in Figure 3. The TSRU column is 17.5 cm in height with a radius of 7 cm. At the bottom of the column, an air sparger covered with ceramic beads is used to create even air flow through the bed. The air is the oxidizer for smoldering combustion. Above the beads, a heater brings the base of the TSRU column to ignition temperature. The column is topped with additional ceramic beads to cool the off-gas. An array of thermocouples is positioned within the column to measure temperatures at locations of interest, in particular, at 2-cm intervals along the central axis.

¹ See, for example, P.I. Pironi and coworkers, *Environ. Sci. Technol.* 2011, 45, 2980-2986.

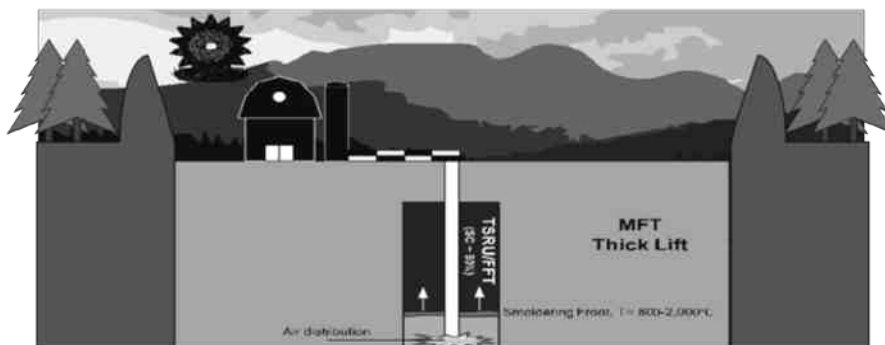


Figure 1. Vertical Smoldering configuration with TSRU Columns

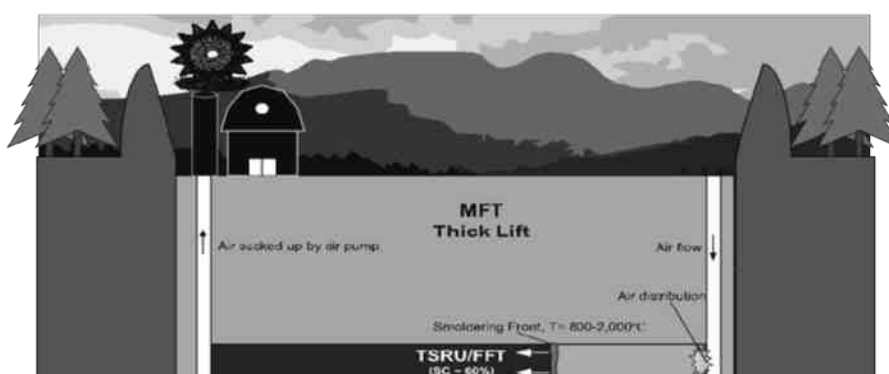


Figure 2. Horizontal Smoldering Configuration with TSRU Tubes

The experimental procedure consists of three primary steps: 1) heating, 2) ignition, and 3) propagation. The base layer is heated to create smoldering conditions, in this case a temperature of about 300°C. Air is then injected and blown upwards through the sample, igniting the base layer. In the present study, air flows were typically 80-100 SCFH. Following ignition, the heater is deactivated and the supply of air through the sample is maintained as combustion travels upwards. Eventually, the combustibles are consumed.

TSRU samples were prepared by a combination of blending in coarse sand (0.5-1 mm) and oven drying at 85-90°C. Sample moistures were determined by weight change before and after complete drying at 60°C. Hydrocarbon analyses were performed by Maxxam Analytics.

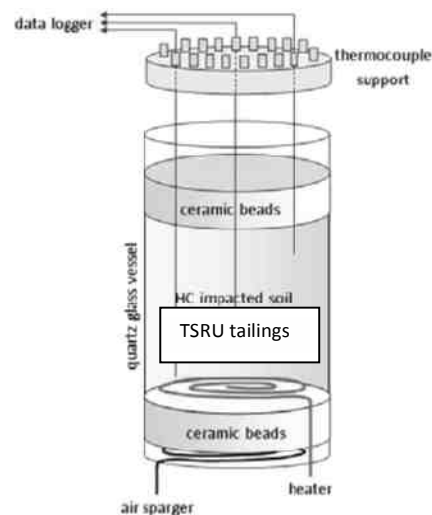


Figure 3. Experimental Setup

EXPERIMENTAL RESULTS

The samples used for all tests were flocculated TSRU tailings from Shell Muskeg River. The samples were left in pails for ~18 months for settling, after which surface water was decanted. The properties of the tailings post-settling included a sand/silt/clay ratio of 44/40/16 % by weight, a total organic carbon (TOC) of 20 % by dry weight, and a moisture content of 40% by weight.

A picture of the settled TSRU tailings loaded in the smoldering vessel is shown in Figure 4. As can be seen in the picture, the tailings are quite sludgy. The TSRU as presented would splatter and plug when moderate air flow was applied. To compensate, samples were prepared using a combination of sand addition and oven drying (Table 1). Pictures of blends 2, 4, and 5 are given in Figure 5.



Figure 4. Settled TSRU Tailings Loaded in Smoldering Vessel

From the test blends and smoldering runs, an operability map was constructed (Figure). The “Y” axis is the dry weight percentage of sand blended into the mixture, and the “X” axis is the blend moisture content. Sand blended at 80% and over leaves little or insufficient fuel for combustion. The other limits shown on this graph are where the sample is too dry or too sludgy, leading to plugging of the TSRU bed.

During runs, smoldering progressed bottom, top, and then middle in the tailings bed. A temperature trace from Run 5 at different vertical locations is given in Figure 7. The combustion front tended to move along the wall between the bottom and top of the bed before slowly penetrating to the middle.

Figure 8 shows an example of the front moving up the side of the column.



Test Blend 2



Test Blend 4



Test Blend 5

Figure 5. Test Blends of TSRU Tailings

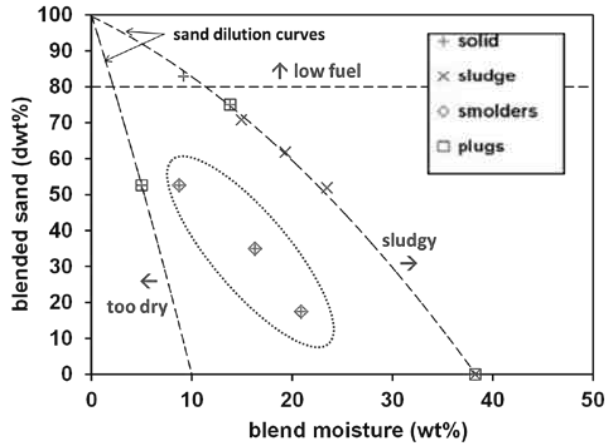


Figure 6. TSRU Smoldering Operability Map

Analyses were performed before and after smoldering to determine the residual hydrocarbons. Table 2 contains this data for Runs 5 and 6 and demonstrates that: 1) All F1BTEX, F2-F4, and F4G hydrocarbons were consumed, 2) no detectable PAHs formed from smoldering asphaltenes, and 3) most of the organic carbon (80%) was consumed despite slow air penetration.

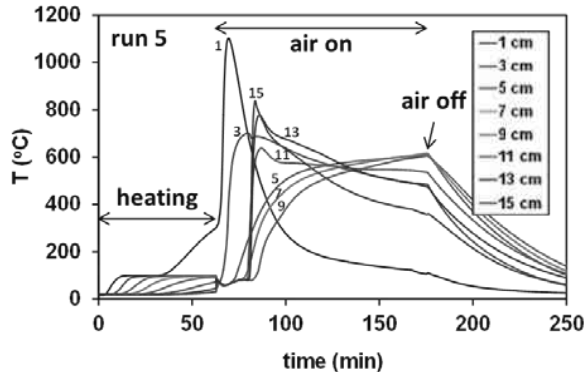


Figure 7. Combustion Temperatures at Different Heights in Column as a Function of Time for Run 5

Heat Transfer Results

Using the temperatures provided from the experimental portion of this work, a heat transfer analysis was done to estimate the degree of transfer to thick lifts of tailings from a single TSRU column. Figure 9 shows the control volume and boundary conditions used.

It should be noted that this is a one-dimensional model in which heat transfer only occurs radially through conduction. Convection in the tailings bed may carry the heat away from the TSRU column to

some extent further than what is shown here. It is also assumed that no heat is lost through the top or bottom of the column.

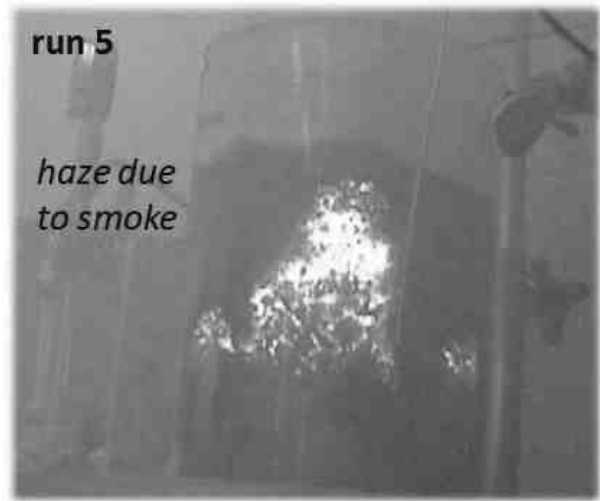


Figure 8. Picture of Smoldering Front Moving Up the Side on Run 5

With these assumptions in mind, the governing equation is:

$$\frac{\partial T}{\partial t} = \frac{\alpha}{r} \frac{\partial}{\partial r} \left(r \frac{\partial T}{\partial r} \right)$$

with the following boundary conditions:

$$\begin{aligned} T(r, 0) &= T_o \text{ for } 0 < r < R_1 \\ T(r, 0) &= T_{inf} \text{ for } R_1 < r < R_2 \\ T(R_2, t) &= T_{inf} \end{aligned}$$

An analytical solution was employed. A numerical solution was attempted, but the squared shape of the initial boundary condition at the radius of the TSRU column complicated this approach. The analytical solution in this case produces the following series solution:

$$\begin{aligned} T(r, t) &= T_{inf} + \sum_{n=1}^{\infty} \frac{2(T_o - T_{inf})R_1 J_1 \left(\lambda_n \frac{R_2}{R_1} \right)}{R_2 \lambda_n [J_1(\lambda_n)]^2} J_0 \left(\lambda_n \frac{r}{R_1} \right) \exp \left(-\frac{\lambda_n^2}{R_1^2} \alpha t \right) \end{aligned}$$

where λ_n are the zeros of the J_0 Bessel function (i.e., $J_0(\lambda_n) = 0$). The first 50 values of λ_n were used in the series solution. One thing to be noted about the equation above is that the thermal diffusivity, α , only appears in the time portion of the equation. This means that the TSRU column will cool more quickly if the thermal diffusivity is

higher, but the radial extent of the temperature profile curves will not be affected.

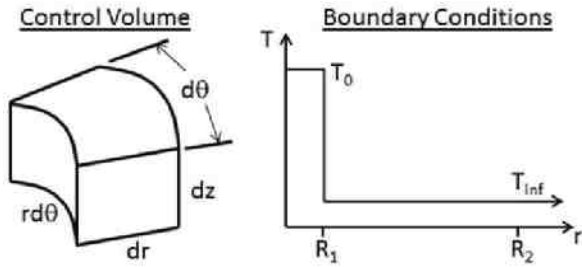


Figure 9. Boundary Conditions for Heat Transfer Analysis

Even with 50 terms, there is evidence of ringing in the analytical solution when time is close to zero, since at time equals zero, the derivative of the temperature curve at the radius of the TSRU

column is infinite. This ringing quickly disappears as the temperature front moves out and derivatives approach reasonable values. This infinite derivative is what complicated the numerical solution.

Figure 10 is a graph of the temperature profile using a smoldering temperature of 600°C. The graph is non-dimensional in both time and radial position. Using 80°C as a dewatering temperature, the temperature profile shows that dewatering will occur out to about 2 times the radius of the smoldered column. For 1200°C, the dewatering temperature will occur at approximately 2.7 times the column radius, and for 2000°C, the dewatering temperature will be reached at approximately 3.6 times the column radius.

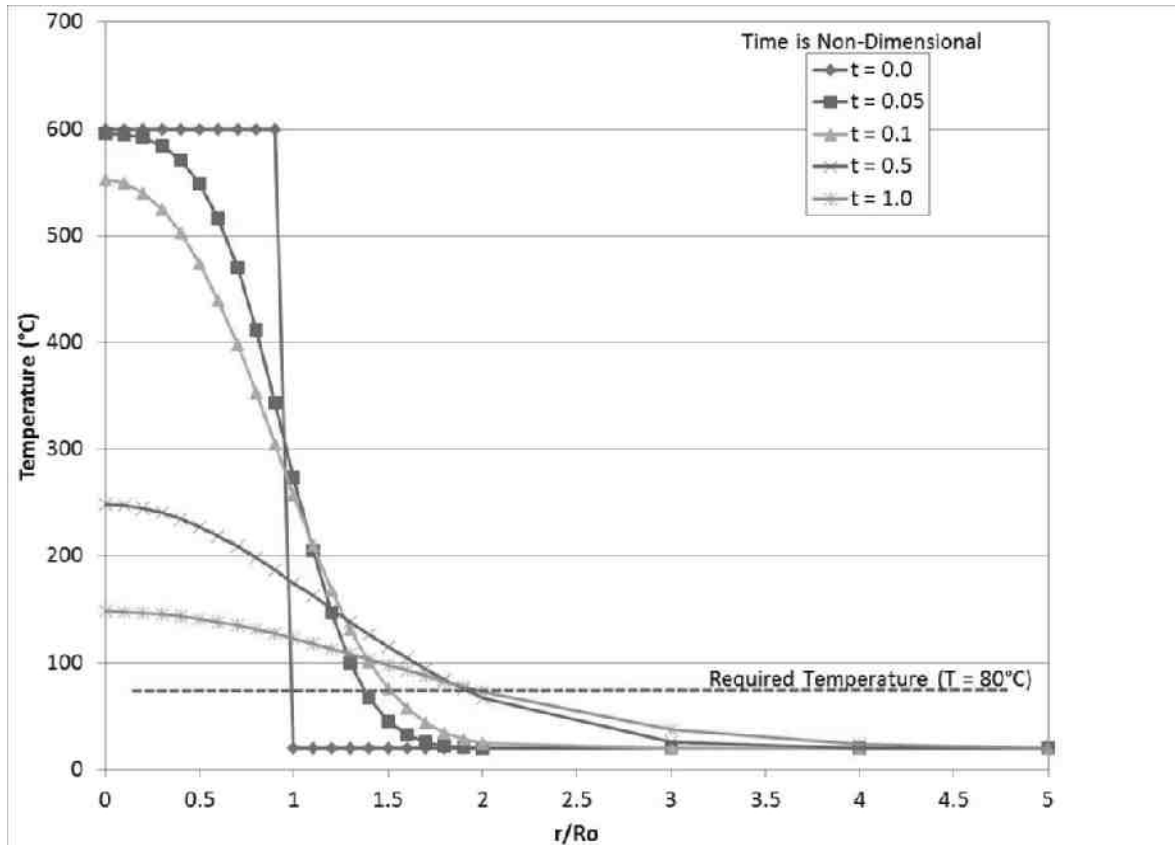


Figure 10. Temperature Profile for a Normalized Radius of TSRU at 600°C

CONCLUSIONS

From the experimental portion of this project, it was found that the moisture and air permeability are important variables to avoid plugging and ensure a viable smoldering process. The tailings column may require modifications such as drying to remove the sludgy texture, but no clear benefit was observed for sand addition. The hindered air permeability of the TSRU contributed to an atypical smoldering-front propagation and low temperatures based on fuel availability. The best-case temperatures were found to be between 700°C and 800°C for Run 6, which had the highest TOC. Potential future experimental work includes

evaluating the coarse component of non-flocculated TSRU tailings, which may improve air permeability, and characterizing the emissions.

The analytical portion of this project showed that realistic dewatering temperatures could occur out to a radius of 2 to 3.5 times the radius of the smoldered TSRU column. Adding additional columns of TSRU may increase the area dewatered, but a further heat transfer study would be needed.

Table 1. Test Summary

Run / Test Blend	Blended Sand (dry wt%)	Blend Moisture (wt%)	Calculated TOC (wt%)	Comments
run 1 (TSRU tailings)	0.0	38.2	20.3	sludge, splatters and plugs
test blend 1	51.9	23.5	9.8	sludge
test blend 2	61.8	19.3	7.8	sludge
test blend 3	70.8	14.9	5.9	borderline sludge (cakes on bottom)
test blend 4	75.0	13.4	5.1	solid, used for run 2
test blend 5	82.9	9.2	3.5	solid
run 2	75.0	13.8	5.1	solid, plugs after heating
run 3	52.6	~ 5	9.6	solid, plugs before heating
run 4	52.6	8.7	9.6	solid, smolders
run 5	35.0	16.3	13.2	solid, smolders
run 6	17.5	20.9	16.8	solid, smolders

Table 2. Analysis of Hydrocarbons Before and After Smoldering

Run	F1BTEX	F2-F4	F4G	PAHs	TOC
run 1*	140	9800	29000	-	200000
run 5 - before	12	6200	15000	ND	160000
run 5 - after	ND	ND	ND	ND	32000
run 6 - before	16	7400	18000	ND	200000
run 6 - after	ND	ND	ND	ND	34000

All Parameters in mg/kg

ND = Not Detected

*Settled TSRU Tailings without sand addition or oven drying

FURTHERING TAILINGS R&D VIA THE COSIA TAILINGS EPA AND THE RESEARCH WORKING GROUP

Andrea Sedgwick¹ and Alan Fair²

¹Total E&P Canada, Calgary, Alberta, Canada

²COSIA, Calgary, Alberta, Canada

ABSTRACT

This paper focuses on the history and evolution of Canada's Oil Sands Innovation Alliance's (COSIA) Tailings Environmental Priority Area (EPA). This group has a history that pre-dates COSIA by many years, including the Oil Sands Tailings Consortium (OSTC) and the Cooperative Oil Sand Tailings R&D Consortium. The COSIA Tailings EPA is enabling an unprecedented level of collaborative R&D, which is essential to accelerating the oil sand industry's ability to improve its environmental performance. Currently the COSIA Tailings EPA has several working groups that are intended to enable collaboration in a number of areas that are necessary to advance tailings technologies. In total there are nine Working Groups that are operating under the Tailings EPA umbrella.

One of those Working Groups is the Tailings Research Working Group. The premise for this group is to both identify research areas that will advance the knowledge in oil sand tailings in an effort to better understand the development initiatives that are taking place in the industry and to facilitate research work to address these needs. The areas were identified during a gap analysis. The main purpose of identifying these gaps is to attempt to resolve the gaps through targeted research. This paper will address the formation of the group and the gap analysis that was performed. It will also address some of the initiatives that are underway to address those gaps.

INTRODUCTION

Background

Oil sands were first found by the native Canadian peoples located along the Athabasca River. They used the heavy bitumen for sealing their canoes. It was not until the 1960's that this oil sand was used for bitumen production. In the early days of the oil

extraction process, it was assumed that the tailings would settle easily in the tailings ponds and that they would be reclaimed in an efficient manner. However, within a year it was determined that the clays in the pond take considerable time to settle naturally. The unsettled clay and water slurry was known as Mature Fine Tailings (MFT) or Thin Fine Tailings (TFT).

Almost immediately, research began. There were two major research areas that the oil sand companies were investigating:

- 1) MFT fundamentals to understand why the oil sand tailings were not settling; and
- 2) Mitigation measures that could aid in settling the MFT and thereby provide faster reclamation of the tailings ponds.

In 1995, a book was produced on the state of the art of oil sand tailings. It was instigated by a group formed in 1989 called the Fine Tailings Fundamentals Consortium which consisted of oil sand producers, federal and provincial research organizations and it is still considered an excellent reference.

Between 1995 and 2009 the oil sands companies continued to meet regularly to talk about tailings issues however there were two issues that limited the degree of collaboration:

- 1) Concerns in relation to anti-competition laws; and
- 2) The lack of company mandates to share information.

Another problem was that the oil sands companies were keeping the work that they were doing on tailings confidential as they were considering patenting new technologies. This led to discussions that did not allow for sharing of information and it was difficult to make significant advancements with each company doing their own research. Often there was duplication of efforts and that tended to be unnecessary.

As a result, most of the initial collaborative tailings work was related to “one-of” specific projects. In 2000, a collaborative project related to the use of thickening technology for oil sand tailings was initiated with the involvement of both industry and government. This subsequently resulted in the establishment of the Cooperative Oil Sand Tailings R&D Consortium. An agreement was put in place that focused on the sharing of much of the initial research work that had been conducted up until that time, including the results of the oil sand thickened tailings project and significant work that had been under-taken by Syncrude. Although this initiative was successful and fostered the sharing of data amongst the various surface mining companies who had an interest in tailings at the time, it had a limited scope and tended to focus on “pre-competitive” research.

Oil Sands Tailings Consortium (OSTC)

In 2009, the Alberta government instituted a new oil sand tailings directive which reflected a desire to put better regulatory controls in place to manage oil sand tailings. This focused the oil sand industry on the Social License to Operate by accelerating improved environmental performance. These concepts, combined with the desire to increase and enhance the research and development effort, led to several discussions within the oil sand companies.

The OSTC was first proposed by a small subset of the oil sand mining companies. In May of 2010, John Broadhurst (Shell) called a number of representatives from the other companies to a meeting where he pitched the idea of creating an organization that would focus on collaborative oil sand tailings Research and Development (R&D). An agreement was subsequently put in place (signed by all of the seven surface mining companies in April of 2011). The agreement was built around four principles: (1) A collaborative environment for conducting R&D work; (2) Transparency – a willingness to share results; (3) A bias to publish results and (4) Equitable sharing of costs. These same principles have been carried over into the COSIA Tailings EPA.

Alan Fair agreed to be the first Executive Director of the OSTC and assumed the role in July of 2011. The OSTC was very successful and it quickly became apparent that this model of collaboration

could, and should, be expanded to include other environmental areas.

COSIA

With the event of the OSTC, the CEO executives got together under the Canadian Association of Petroleum Producers (CAPP) umbrella and asked themselves if the collaborative effort in environmental areas could be expanded beyond tailings. The group of both mining and in-situ oil sands executives looked at the amount of large and small research groups in the areas of land reclamation, water, and greenhouse gases (GHG) and decided that a more focused and collaborative group was in order. By combining all of these into one group, the overheads would be simplified, the research and development would be more collaborative and there would be minimal duplication of work. In 2012, the oil sands executives agreed to form Canada’s Oil Sand Innovation Alliance (COSIA). Figure 1 shows the structure of the COSIA organization.

The Oil Sands Consortium was enveloped into this structure in the form of the Tailings Environmental Priority Area. The four Environmental Priority Areas (EPA) that make up COSIA are:

- 1) Tailings
- 2) Water
- 3) Land
- 4) GHG

COSIA Tailings EPA

For the Tailings EPA, it was quite easy to move to the new structure as it had been collaborating for a more than a year and was well on its way to a structured collaborative effort.

Under the new COSIA umbrella, the Tailings EPA now had vision, goals and plans for a portfolio of projects which would accelerate tailings innovation. Figure 2 shows the Innovation Funnel that each EPA follows. Its function is to provide a tool to ensure that there is a mix between incremental improvement and transformative technologies. Using tools such as these, allows the EPAs to provide focus to the overall portfolio.

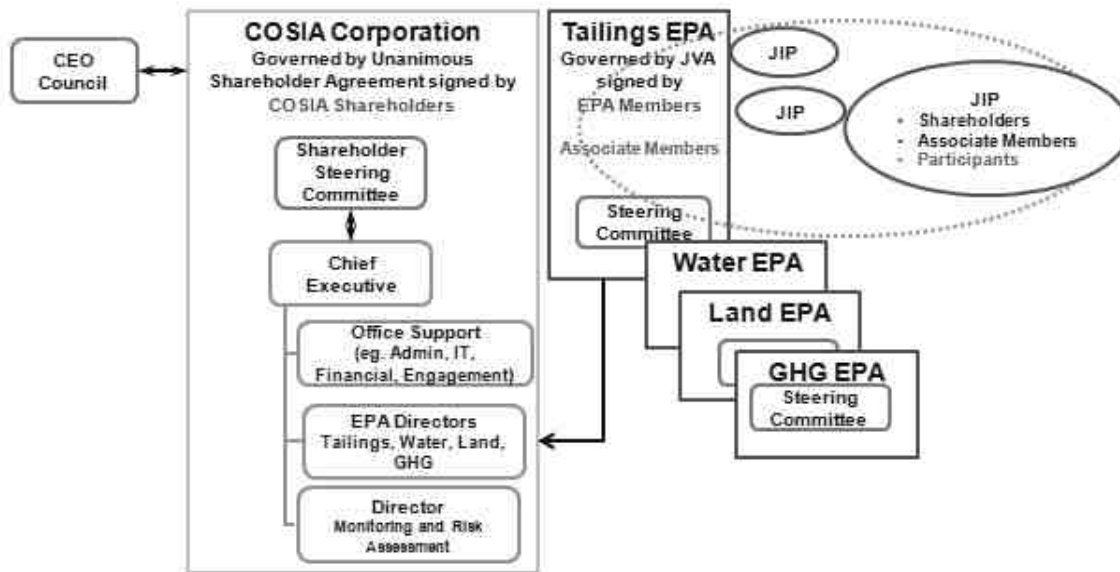


Figure 1. COSIA Governance and Structure

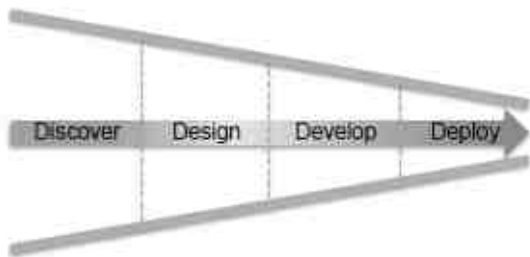


Figure 2. Innovation Funnel

Working Groups

In mid 2012, it was determined that there was a need to re-structure how technical issues and projects were managed. To ensure that enough time was spent sharing ideas about tailings topics, the Working Groups were formed. Initially there were only a few Working Groups however that amount has grown over the years with one new working group formed in 2013 and two more formed in 2014.

At this time, there are 9 Working Groups and 6 sub-groups:

- 1) Flocculant
- 2) Enhanced Fines Capture
- 3) Thickened Tailings
- 4) Deep Deposit
- 5) Research

- 6) Clay Focus
- 7) Integrated End Pit Lake
- 8) Technical Standards
- 9) Measurement Steering Committee
 - Deposit Sampling and Geostatistics
 - Ore Body and Rejects Sampling
 - Fines Balance
 - Pond Survey
 - Deposit Characterization
 - Fines Measurement

These Working Groups and Sub-groups are for information sharing and also provide the ability to promote projects which can be shared by the companies. The working groups can be created with an end goal in mind where when that goal has been achieved the working group will disband (such as some of the Measurement sub-groups) whereas others are planned to be longer-term (Research).

RESEARCH WORKING GROUP

In 2012, it was evident that there was a lot of work going on in the Tailings EPA that was focused on development projects however the research projects were hap-hazard with only general focus. At that time, it was proposed to create a Research Working Group which could consolidate all of the research that was going on at the time and provide focus for the future programs. In late 2012, the creation the Research Working Group was

approved by the Tailings EPA. Officially the group started work in January 2013.

The first task of the group was to identify the area in which it would be working. As the development areas were already quite advanced, it was decided to focus on two aspects of research:

- 1) Fundamentals; and
- 2) Very novel technologies

A key to focused research is identifying the perceived gaps and then directing research in those directions. Each company internally identified their gaps and then shared the gaps with the other companies. These gaps were then sorted and prioritized. There were four main areas that the gaps were segregated into (3):

- 1) Geotechnical
- 2) Process
- 3) Environmental
- 4) Analytical

The gaps that were identified were subjects that the companies felt there were little to no research in. Sometimes the companies had done some research in the area but it was not focused research and had not generated enough data that indicated that the gap had been fully understood and no further work was required to understand the subject. The Gaps List was meant to be updated periodically and was realized that it may be incomplete.

GEOTECHNICAL GAPS

There were several geotechnical gaps that were identified making it one of the high priority areas for research. These gaps were related to deposition and geotechnical properties of the tailings.

Lab Prediction Techniques

Techniques to determine long-term densification and consolidation for prediction of performance of flocculated tailings are required. Preferably this would be in the form of relatively quick, inexpensive tests which would be indicative of performance.

Currently, geotechnical centrifuges could be used to provide data however these techniques are

expensive and the labs that can provide these machines are few.

Freeze/Thaw

There is currently work being done on this application, particularly in providing models that can predict performance. Freeze/thaw for tailings treatment has been under investigation for years. However all of the mechanisms have not been investigated. For example, how freeze/thaw works under different water chemistries is not fully understood. Another area which could be investigated would be enhanced frost penetration methods for dewatering flocculated FFT and centrifuge cake particularly in deeper deposits (>1m).

Consolidation

Consolidation is extremely important in the long-term performance of tailings. There are several areas within this section which could be investigated.

Flocculated tailings are being used to improve dewatering and drying of the fluid fine tailings (FFT) or mature fine tailings (MFT). Further knowledge on ways to improve the permeability of flocculated tailings would be useful. At some point the clays start to touch at which time the permeability decreases as solids content increases.

There are several questions related to the topic of consolidation:

- 1) Is there an evening off of the permeability at some point and is it related to the clays or fines? Do different clay mineralogies impact consolidation? Which clays have more of an effect?
- 2) What can be done to improve the permeability/hydraulic conductivity of cohesive deposits?
- 3) What is the impact of polymers on consolidation?
- 4) How to you modify/improve the conductivity in a deposit?
- 5) Are there natural systems to increase dewatering and densification (plants, bacteria, etc)?
- 6) What is the effect of Particle Size Distribution (PSD) on Thickened Tailings' (TT) hydraulic conductivity and consolidation behavior?

- 7) What is the volume change behavior between hindered settling and consolidation of MFT?
- 8) It is difficult to move from 70% solids to 80%. Is it dependent on type of deposit? Is there a way to make higher solids TT consolidate faster by looking at "out of the box" methods?
- 9) It seems that oil sand tailings require a link between fluid mechanics and soil mechanics. Does there need to be correlations between chemical engineering tools and geotechnical tools?

Dewatering

It is understood that there are three stages of dewatering: initial dewatering, intermediate dewatering and long term consolidation. These stages of dewatering could happen under different conditions depending on the type of tailings (MFT, TT, CT/NST). The points where initial dewatering moves to intermediate dewatering and then to consolidation is not understood for the different types of tailings. Although work has been started on this topic, it has not been quantified fully.

Effect of Flocculants

The impact of flocculant selection and dosage on permeability, compressibility, dewatering and shear strength gain of treated tailings is not fully understood from the short term to the long term. The long-term effects of flocculation on geotechnical performance and reclaimability of the treated MFT (including cationic polymer stability) could be better defined.

Some questions that could be answered are:

- 1) Does chemical use need to be restricted to anionic polymers?
- 2) Is there really any benefit to cationic polymers?
- 3) How does the flocculant change the behavior of the clays? Is there the potential to change oil sand tailings to quick clays under some circumstances? When could those circumstances occur (in instances of over flocculation or lack of dewatering or in deep deposits)?
- 4) For flocculated materials, does high shear affect consolidation?

Drying

Tests on drying (desiccated layer) to assist or retard consolidation with intent of being able to control consolidation would be useful. This could

be through modeling and quantification of parameters. There is some continuing work by several researchers who are addressing this topic. It is a large topic which includes:

- 1) Impact of chemicals on evaporative drying of treated MFT (i.e. significance of osmotic suction development in flocculated deposits);
- 2) Impact of water chemistry on TT drying rate;
- 3) Impact of entrained water (and how it is entrained) on the release of water and subsequent drying of the tailings

Water Chemistry

The subject of the impact of inorganic minerals on MFT and TT thickening and consolidation (sulfates, soluble salts, water chemistry) requires some further research. High salinity deposits affect some oil sands producers and the affect of high salinity water chemistry on thickener performance and thereby deposition is important to understand.

Also, an area which has potential is to investigate in-situ chemical consolidation. Work could be done on introducing clay surface charge modifiers at the pond/FFT bottom to accelerate consolidation.

PROCESS GAPS

The process gaps are related to the upstream process, in other words – prior to the deposition of the tailings materials in the tailings deposition areas. Proper upstream manipulation of the tailings is extremely important to understand so that the deposited tailings can be optimized for drying and/or consolidation.

Understanding Bitumen Effect on Tailings

It has long been known that some bitumen is lost to the tailings. This bitumen is in two forms: free bitumen and bitumen attached to the solids particles. There are several questions surrounding this topic related to the effect of bitumen on tailings performance:

- 1) Polymer-particle (fines and clays) interaction in presence of bitumen;
- 2) Fundamental research on the relationship and interaction between flocculant molecules and bitumen in tailings;
- 3) Is there a difference in the effect of bitumen between MFT vs. TT?

- 4) Is there an effect of bitumen on consolidation and drying?

There has been some work done on a small portion of this topic by the University of Alberta (Klein et al) and Total (Santanach Carreras et al). However there is still more work to be done and the Tailings EPA is looking at proposals to address this topic.

Flocculation

Flocculation is a key topic in oil sands tailings management. Whether it is the flocculation of newly generated plant tailings or mature fine tailings, a fundamental understanding of the topic is important to proper tailings management. A lot of work has been done to understand flocculation for different types of processes and the work continues. There are three main types of tailings flocculation that are used in oil sands:

- 1) Thickening: small flocs with a good settling velocity
- 2) Centrifuge/Filtration technologies: medium sized, strong flocs are required
- 3) Drying technologies: large flocs with good dewatering characteristics upon deposition of the tailings.

Some of the questions that could be answered are:

- 1) Fundamentally, what cationic and anionic synergies exist for the different kinds of tailings (how the two are combined and how they work together)?
- 2) Are there transformative polymers for tailings treatment (better interaction with bitumen/particles, lower dosage, "greener", less shear sensitive)? These polymers would have to be significantly better performers to the current polymers being used.
- 3) A fundamental understanding of why one polymer may be better than another with different tailings and different processes (MW, long-chain, short-chain, etc).
- 4) What causes the tailings aging issue?
- 5) What microstructural changes in MFT fabric occur due to flocculation? Does flocculation change the arrangement of bitumen/clays?
- 6) Mixing: understanding the mixing of high density tailings with polymers (mixing not flocculation); Are there scale up issues and can they be quantified?

- 7) Is there any benefit to dilution vs. high density solids for the desired dewatering and consolidation?

- 8) What is the flocculent structure in different pumping regimes (turbulent, laminar, transition)?

Other Additives

The question was raised as to whether current chemicals are really the most optimal ones to use. Some research on replacing gypsum or alum with new additives in CT/NST (lower SFR, improve water chemistry and segregation) would be of interest. Are there alternative additives and/or combinations of additives that could increase tailings performance?

Rheology

Rheology is known to be a significant factor in characterizing tailings both with chemical addition and without. Questions that are related to rheology are:

- 1) Is there a relationship between flocculant dosage, rheology and shear-ability (shear thinning behavior)?
- 2) Rheology - getting a deeper understanding of what is affecting the rheology (water chemistry, clays)? Is there re-build of rheology after time (if so, how much time and what is it dependent upon)?
- 3) Minimum required yield stress of the carrier fluid to prevent dynamic segregation of the CT/NST during sub-aerial/sub-aqueous deposition? Does shear induced segregation occur?

Enhanced Fines Capture

Fines are captured in all of the tailings streams. There can be ways to increase the amount of fines that are captured without changing the integrity of the original tailings stream. Examples of this would be to add MFT to coarse sand tailings that is going to a beach or to add MFT to the thickener feed. This subject is a very promising area of research.

For spiking fines into coarse sand tailings, what is the effect of adding different types of fines (flocculated or unflocculated)? It is unknown as to the effect of clays on the combined stream. Is there a maximum amount of clays or specific clays that can be added without changing the overall

characteristics of the coarse stream? Is there an optimal PSD for enhanced capture for peak geotechnical stability?

It is important to understand the fundamental changes that occur when MFT is added to thickener feed. What is the impact on settling (is there preferential flocculation that occurs)? It is known that clays change the rheology, so what effect will that have in the thickener? Will bimodal distribution affect the efficiency of flocculation?

ENVIRONMENTAL GAPS

The environmental gaps identified were generally related to the long term effects of: chemical usage in tailings, froth treatment tailings and understanding the biological effects on tailings.

Chemical

From a fundamental perspective, it would be useful to understand the fate of polymers in tailings management to understand long-term reclamation aspects of the tailings. How do the chemicals break down over time (to monomers?)? This is very important in our long-term understanding of our deposits. It is unknown if there are fundamental changes in the water adsorbing capacity of polymer flocculants in FFT as they weather on the surface of flocculated FFT deposits. How long would this affect last after deposition?

Froth Treatment Tailings

In oil sands there are two types of froth treatment processes being used: paraffinic and naphthenic. These tailings consist of a solvent or diluent, some bitumen, fines, some coarse particles, and for paraffinic froth treatment, asphaltenes. These tailings may be separated from the other tailings, mixed into the pond, beached or deposited sub-aqueously. Each oil sand site has particular challenges related to their froth treatment tailings depending on their process and deposition strategy. Further research work, related to how these tailings in particular behave in a deposit and if there are any novel ideas as to how to treat them, is warranted.

ANALYTICAL

These gaps were related to areas in which it was thought that the methods of analysis could use some optimization or further understanding.

It is not clear as to the effect of bitumen on PSD of MFT using laser diffraction analysis. The industry could also use predictive tools for field performance based on lab measurements. For example, simulation of pipeline shear environment using a vane and cup geometry to predict in-line flocculation performance. Further data and subsequent analysis of rheometers vs. pipeloops and any recommendations would be helpful.

Planned Research to Address the Gaps

There are several ways that the gaps will be closed. Individually, the oil sand companies are doing research on some of these themes. Collaboratively, there are programs underway within the COSIA Tailings EPA, and specifically within the Research Working Group that will address the gaps detailed in this paper. Some of this work includes sponsoring Chair programs with universities, directed research and specific requests for proposals.

In 2013, the Research Working Group put out a Request for Proposals to a wide audience. The proposals that were received were from researchers from around the world including Canada, United States and Australia. There were proposals from research organizations, universities and consultants. The topics ranged within the geotechnical and process themes.

Nine projects were selected from over forty proposals. There are plans for another round of Request for Proposals which will occur in 2015 for projects starting in 2016. No dates have been selected yet.

CONCLUSIONS

In this paper, it may seem that there are more questions than answers; however the oil sand companies are working closely to better understand the fundamentals related to oil sand

tailings. COSIA's vision is to enable responsible and sustainable growth of Canada's Oil Sands while delivering accelerated improvement in environmental performance through collaborative action and innovation. Fundamental research is regarded as very important in ensuring this vision is met and it is through collaboration that the challenges in oil sand tailings can be resolved.

REFERENCES

Alberta Energy Regulatory (2009). Directive 074: Tailings Performance Criteria and Requirements for Oil Sands Mining Schemes.

Fine Tailings Fundamentals Consortium (FTFC). (1995). *Advances in Oil Sands Tailings Research*. Edmonton, AB: Alberta Department of Energy, Oil Sands and Research Division.

Klein, C. & Harbottle, D. & Alagha, L. & Xu, Z. 2013. "Impact of fugitive bitumen on polymer-based flocculation of mature fine tailings." *The Canadian Journal of Chemical Engineering*, Volume 91, Issue 8, August 2013, Pages: 1427–1432.

Santanach Carreras, E., Bourrel, M., Passade-Boupat, N., Sedgwick, A., Yang, X., Junaid, A. "Effect of Residual Bitumen on Flocculation." *Tailings and Mine Waste 2013*. Edmonton, Alberta.

Sedgwick, A. (2013). "Oil Sand Tailings Fundamental Knowledge Gaps." *Tailings and Mine Waste 2013*. Edmonton, Alberta.

Session 7

Tailings Management I

THE INGENUITY GAP IN OIL SANDS TAILINGS TECHNOLOGY

John Sobkowicz, Jeremy Boswell and Iain Gidley
Thurber Engineering Ltd., Calgary, Alberta, Canada

ABSTRACT

The challenges facing the Oil Sands industry in dealing with tailings are not new, and in the opinion of the critics, they are not being resolved quickly enough, despite the best efforts of many leading engineers and scientists, world-class organizations, and research and development entities.

Some have expressed the frustration that there is insufficient openness to new ideas, and that more could be done to unlock new ideas – to fire the imagination, to be truly innovative, to achieve step change, even sea change in what we are doing.

So, what roadblocks exist to applying ingenuity to develop new Oil Sands tailings solutions, and what avenues are open to promote ingenuity in the Oil Sands tailings industry? What else could we be doing? Are we wasting our efforts in certain areas and could our resources be better focused? The paper puts forward a number of questions to challenge current thinking and to provoke innovative efforts.

In suggesting a path forward for the Oil Sands tailings industry to close the ingenuity gap, this paper introduces the notion of a Tailings Social-Organizational Roadmap.

INTRODUCTION

“First Impressions” of the Oil Sands Industry

Many newcomers to the oil sands industry, and to the tailings side of the industry in particular, find themselves bemused by the apparent inability of mine operators and service suppliers alike to solve the fluid fine tailings (FFT) “problem”. Some (young engineers and scientists, staff of new oil sand mining companies, new regulators, and newly-aware environmentalists), become instant critics and form the opinion that a) little effort has been made to solve the oil sands fine tailings challenges, b) potentially applicable technologies from mines in other parts of the world have been

ignored, and c) progress on closure and reclamation of tailings ponds is painfully slow.

The first two of these concepts arise mostly from ignorance and have been disabused in a number of technical papers (Sobkowicz, 2010; Boswell et. al., 2012). The last criticism is more difficult to address because it is in fact true. The sense of bewilderment about progress on dewatering of FFT is not restricted to just the newcomers. There are many working on all sides of the industry who have not yet had the satisfaction of seeing a technically and cost effective solution emerge from the very large amount of research and development that has been expended to that end.

Technical Roadblocks to Research & Development Progress

Some of the technical roadblocks to progress are (Sobkowicz, 2013):

- Dewatering of oil sands FFT is technically difficult. For example, there is currently no tailings treatment technology that can produce the required amount of dewatering in one step; often several steps are involved and then additional dewatering is required to meet minimum reclamation requirements. At present this involves environmental assistance, which has limited effectiveness in northern Alberta (Boswell and Sobkowicz, 2010).
- Long research and development cycles are required to fully prove out technology concepts, partly due to technological complexity (Gidley and Boswell, 2013), partly due to the high “entrance fee” for new technologies, and partly due to regulatory pressure causing impatience and short-circuiting of the research and development process by oil sand operators.
- Late breaking technical issues arise that introduce serious performance problems into commercial scale operations (e.g., the current problems associated with fines segregation on discharge of CT or NST).

- Poor industry collaboration has, until recently, hampered research and development progress. With the formation of the OSTC (Oil Sands Tailings Consortium) in late 2010 and then of COSIA (Canada's Oil Sands Innovation Alliance) in 2012, this situation has improved.
- Unexpected environmental implications have arisen for several technological solutions that have been trialed at commercial scale. For example, thin-lift drying requires vast tracts of land to handle the volume of FFT produced each year – much more than is available on most leases and which carries, in any case, an additional environmental burden.
- Evolving regulations have introduced some uncertainties and inefficiencies into the research and development process. For example, Tailings Directive 074 (D074), while well meaning and in many respects well structured, introduced some artificial criteria for reclamation readiness which proved to be impractical and to introduce un-necessary cost into the treatment of FFT. Alberta Environment and Sustainable Resource Development has recently released a draft of its Tailings Management Framework, which as it evolves will hopefully allow a more ordered response from the oil sand operators.

Why is Progress on Solving the FFT Dewatering Problem so Slow?

If we understand many of the technical roadblocks, as discussed in the previous section, why is progress on solving the FFT dewatering problem so slow? This is a legitimate question – one that has been asked by many frustrated technocrats over the years, and one whose answer requires consideration of factors that lie outside the technical realm. The oil sands industry is not the first to have met an intractable social or technical problem. Perhaps insights from others who have encountered refractory problems before would be helpful in structuring a more effective approach to solving similar problems in the oil sands. This topic will be explored in greater detail in this paper.

THE INGENUITY GAP

The Concept

Thomas Homer-Dixon in 2000 published a landmark book addressing just the type of problem discussed herein. This book is called “The Ingen-

uity Gap” (Homer-Dixon, 2000). Some initial concepts are given below, which establish the meaning of this term, and the larger context within which intractable problems lie and which contributes to their unruly nature (all quotations unless otherwise indicated are from this book).

Homer-Dixon's book deals with large problems that afflict whole societies and encompass global changes in social structures, economics and the environment. But it starts with a relatively simple example of how systems can fail and how huge demands for ingenuity may be placed on a few people over a very short time period. This example is the explosion of a tail engine on United Airlines Flight 232 from Denver to Chicago on July 19, 1989, which ultimately led to a crash landing that killed 111 of the 296 people on board.

Homer-Dixon records that: “...the flight crew immediately faced a staggeringly complex task. Multiple, simultaneous, and interdependent emergencies converged on the cockpit. Some were recognized and understood, some were misunderstood, and some didn't even cross the crew's threshold of consciousness...For forty-four harrowing minutes the captain and his officers assessed a prodigious flow of incoming information, made countless inquiries and observations, and issued dozens of commands. Even with extra help from the check pilot, it was all they could do to keep the plane aloft and roughly on course to a crash landing...”.

Homer-Dixon suggests that United Flight 232 is a metaphor for an increasingly complex world, where decisions need to be made quickly, but where there exists also a high degree of uncertainty regarding the nature of the systems about which we are making decisions. He indicates that all successful societies need to provide a sufficient amount of *ingenuity*, sufficiently quickly to meet the demands placed upon them.

Ingenuity may be defined as the set of ideas and instructions that “...can be applied to solve practical technical and social problems....that tell us how to arrange the constituent parts of our social and physical worlds in ways that help us achieve our goals...”. In other words, when we are confronted with very real problems, we require ingenuity to solve them. Furthermore, Homer-Dixon states that: “I soon realized that ingenuity comes in two distinct kinds: the kind used to create new technologies....and the more crucial kind used

to reform old institutions and social arrangements and build new ones...”.

One final quote of relevance to the topic of this paper: “Our supply of ingenuity...involves both the generation of good ideas and their implementation...It’s not enough for a scientist, community or society simply to think up an idea to solve an environmental problem; the idea must also be put into practice...many of the critical obstacles occur not when the ingenuity is generated (there is usually no shortage of good ideas) but when people try to implement new ideas...it’s not lack of ingenuity that prevents us from solving our economic, social and environmental problems, but political struggles over power and values – struggles over what we want, where we should go, and who should benefit. If we resolve these struggles, then the problems we face become largely technical and are in most cases fairly easy to solve...”.

Application to Oil Sands Tailings Challenges

Homer-Dixon developed his concepts regarding ingenuity based on world-scale issues and problems that impact whole societies. However, in the authors’ opinion, the concept of ingenuity can also be applied with equal benefit and perspicacity to solving problems that arise at a smaller scale, such as that encountered in a large engineering project. It is thus useful to examine the challenge of dewatering FFT to a “reclamation-ready” state within the context of demand and supply of ingenuity.

Engineers and technological managers tend to be an optimistic group that believes that sufficient ingenuity can always be brought to bear to solve whatever problems arise in the course of doing business. One could say that this is a built-in, implicit, almost sub-conscious assumption.

One might wonder if such people are not viewing their world through overly rose-coloured glasses. What if this assumption does not always apply? What if continued effort over many years, involving a large number of resources, carried out at a high cost, does not solve the problem? Worse yet, what if the problem is not solved before the resources and the money run out, or before irreparable damage is done to some social, economic or environmental system? “If a society...” (*or an institution or a group of engineers and managers*) “...loses this race – if, in other words, it cannot supply sufficient ingenuity to meet its needs – it develops an **ingenuity gap** between requirement

and supply...” (*Italics comment and bold text added*). An ingenuity gap exists when the right set of ideas and resources cannot be brought to bear to solve a particular problem in a required (or reasonable) time frame.

Anyone reviewing the history of Oil Sands tailings research and development, the large effort expended in developing effective and cost-efficient methods of dewatering FFT with such limited success, and the various roadblocks to success that may exist (including those identified earlier and those as yet unidentified), could with good cause wonder whether the oil sand industry suffers from an ingenuity gap. And if they concluded that such a gap exists, they could also wonder why it exists, whether or not it is getting worse, and what could be done to alleviate the gap before there are irreversible consequences.

Action to close an ingenuity gap must address both the generation of new ideas (or new application of existing ideas) and the effective implementation of those ideas.

Questions We Should Ask Ourselves

Following are some questions that it would be useful to ask ourselves, as we ponder this question of how to overcome the ingenuity gap in Oil Sands tailings. Some of these overlap with and are in a sense generalizations of the technical roadblocks previously discussed; others are entirely new and/or address the non-technical side of the ingenuity gap.

1. **Do we understand the complexity of the natural systems that we disrupt and the effort needed to restore them post-mining?** Human beings are notoriously arrogant in over-simplifying natural systems that are incredibly complex and under-estimating their impact on the world. This is true in the fields of medicine, the natural sciences, the social sciences, and unfortunately also in engineering. In our haste to exploit our natural resources (to the betterment of society), do we suffer from environmental myopia? Homer-Dixon notes that “...Arrogance distorts our ability to see which challenges around us really need our attention; and that, in turn, distorts the amount and kinds of ingenuity we supply”. For example, is a focus on meeting a specific strength criterion for partly dewatered FFT within a specified time frame really that helpful,

or is it even hurtful? **On which aspects of the FFT problem should we really focus?**

2. **Do we understand the technical complexities of each potential FFT dewatering technology, including the environmental implications of their use?** A corollary question is: are all the elements of the tailings system and its treatment method deterministic, or do we need to deal with unpredictable elements, and if so, how does that impact the ingenuity required to develop our technological solutions?
3. There are some technological unknowns (in regards to dewatering FFT) of which we are aware and on which we are working. However, there must be other “unknown unknowns” – technological issues that have yet to rear their heads. **What demands will these “unknown unknowns” place on the ingenuity required to address them, when they do appear? Do we even now have or realize the expertise that will be needed? How quickly will we be able to recognize the need for and access that expertise?**
4. **Are we employing the right people to generate the ingenuity required to solve our tailings dewatering problems?** Our industrial system tends to favour “experts” or “specialists” as problem solvers, but complex problems often require people who can integrate knowledge from a number of different specialties. Are our problem-solving teams organized, resourced and empowered in such a way as to maximize the contribution of both types of “thinkers”?

In a previous paper, one of the authors (Boswell, 2010) describes five categories of skills required in Oil Sands tailings: technical, operational, environmental, legal and public. Some insight is provided as to how these skills might be integrated to provide solutions, and how other industries have addressed this challenge.

5. **Have we harnessed all of the productive ideas that could be used to solve our FFT dewatering problem?** Ingenuity may come from the generation of new ideas, but it may also come from the new application of effective ideas from other areas, requiring only the right mind to recognize its potential. Efforts have been made in the recent past to integrate knowledge from a number of areas by defining tailings technology suites and roadmaps to

improvement (Boswell et. al., 2012), but this is really just a first step in what needs to be accomplished (is “Round 2” just around the corner?). Some individual operators have also used the technologies listed as a useful starting point to extend the exercise into more specific investigations for their own unique needs, but have not necessarily collaborated more widely with other organizations.

6. **Are we maximizing our use of existing knowledge and ideas by communicating them effectively and making them fully accessible?** My use of an idea does not diminish its usefulness to you, but my hoarding of an idea does. Ingenuity is thus increased when ideas are shared fully and effectively. **Has the industry done all it can to be entirely open and transparent with all potential suppliers of ingenuity?**
7. Unlike ideas, human capital is “rival”, in that my use of it diminishes your unfettered access. **Are we organizing the human capital most important to our generation of ingenuity in a way that maximizes the delivery of that ingenuity?** In contemplating this question, we should challenge ourselves to think not only of improving the way we access and organize human capital within companies, but also between companies and from external sources.
8. **Is our focus on the need for technical ingenuity, almost to the exclusion of our need for social¹ ingenuity, hampering or even harming our progress?** Homer-Dixon points out that “...The two kinds of ingenuity, social and technical, are intimately interconnected. In fact, I came to understand that social ingenuity is a key pre-requisite to technical ingenuity. We need social ingenuity to set up and maintain public and semi-public goods such as markets, funding agencies, educational and research organizations, and effective government...”. When we reduce

¹ As defined by Homer-Dixon, the term “social” refers to the non-technical aspects of ingenuity, including organizational structure and institutions in societies, and political structure, institutions and influences. In this paper, the authors use the term in a non-standard manner to include these same influences, as they exist and also as they translate at the project scale, e.g., company and government organizational structure, management practices in companies and government, funding agencies, research and development practices, collaborative mechanisms with all stakeholders, etc.

these “big picture” comments down to the level of a group of operating companies, regulators and other stakeholders, we will find many novel ideas for providing social ingenuity. Co-operative efforts between regulators and mine operators to properly and usefully define the desired end product of dewatered FFT is one example; another is the formation of OSTC and later COSIA, to create a social framework (with a helpful “funding structure”) within which technical ingenuity can thrive; another is evolving (and improving) government policy and regulation. The authors believe that we have only begun to explore the opportunities for social ingenuity in the oil sands tailings context, and that both regulators and mine operators should challenge themselves to improve “funding agencies, ...research organizations, and effective government...”. For example, government agencies have for the most part focused on criteria to be met and penalties for not doing so; consideration could also be given (perhaps in a joint government-industry workshop) to incentives for increasing both social and technical ingenuity.

A less publicized and perhaps more enduring source of useful information which might contribute to our understanding of where we need to go in Oil Sands tailings was “Component 2: Objectives of the Tailings Roadmap Project”. The team also identified constraints and opportunities to Oil Sands tailings technology development. (Stephens et al, 2012).

9. **Are the existing incentives to supply ingenuity to solve the FFT dewatering problem sufficient, i.e., are they both appropriate and effective?** A common assumption in our modern world is that with sufficient incentive, mankind can supply the ingenuity to solve any problem. In essence, the argument is that with the right “raw materials”, with the right practical ideas, and with a sufficiently compelling reason, we can do anything. This premise is fallacious but it is also seductive, and we must therefore be cautious of over-confidence and even hubris. However, facing an apparently slow pace of progress, we should still examine if the existing incentives for ingenuity in Oil Sands tailings dewatering are sufficient? What are the current incentives? Some are internal to a mine operator (responsible corporate behaviour and profitability) and some are external (government policy and regulation, and meeting the needs

and expectations of stakeholders). **Have all incentives to improve ingenuity been explored, particularly incentives to small and medium sized entrepreneurs? Have existing incentives been described in a way that fully explains the implications to an operating company’s bottom line, which is such a strong driver of company behaviour. And described in such a manner, have those external incentives been incorporated within company policies and internal incentives for performance?**

10. **Are we ensuring that all of our resources are focused on increasing (rather than hampering) ingenuity?** It seems that the general view from “below” (i.e., from the perspective of those tasked with solving problems) of the helpfulness of certain groups such as managers and lawyers in promoting ingenuity, is often not positive. This may be an unfair view, but it is still worthwhile asking the questions: **Are the efforts of medium and high-level managers focused on increasing ingenuity – both technical and social? Are they thinking about how best to support the scientists and engineers who might generate the technical ingenuity? Are they re-organizing their own departments to best encourage social ingenuity? Is the legal profession engaged in supporting the drive for, and even providing, ingenuity (rather than throwing up road blocks)?** Just as scientists and engineers are being challenged to provide more ingenuity, so too should those who govern and lead business be challenged to support rather than “gate keep” or muzzle.
11. **How well do our scientific and engineering “institutions” function and what incentives do they give scientists and engineers to do good work?** This question is directed at the nature of these “institutions”, everything from the laboratories to the discipline used in carrying out research and development, and from its procedures for funding research to its mechanisms for peer review of scientific and engineering results. A previous paper by Gidley and Boswell (2013) addressed one of these issues (a description of the full cycle of research, development and commercial implementation, and how this cycle is often short-circuited). However, the question needs to be addressed by each operating company, in regards to its own scientific and engineering institutions, and by COSIA, who seeks to integrate the work done in the different companies.

Are there silos (either inter- or intra-company) within which scientists and engineers work that decrease the ingenuity that they generate? Are incentives clear or do the scientists and engineers receive mixed messages about the purpose of their work? Is funding sufficient and timely? Is research being done in an anticipative manner, such that the technology arrives in time, or are we consigned to driving while using the rear view mirror, or perhaps merely a more technologically upgraded rear view camera?

12. **Do we underestimate the time required to generate the ingenuity to solve the FFT dewatering problem?** It seems that there is a fundamental disconnect between the expectations of both regulators and company management to solve the FFT dewatering problem quickly, and the ability of the scientists and engineers so tasked, to do so. There are a number of reasons for this, as discussed previously in this paper. The point here is that unrealistic expectations sometimes create inappropriate priorities, focus efforts in the wrong direction, and result in a hugely excessive waste of financial resources. This can occur from a desire to shift operational practices before proven solutions are demonstrated. This issue is also closely tied to the provision of appropriate incentives for ingenuity. In the opinion of the authors, until the thinking of both the regulators and company management encompasses practical time frames to provide ingenuity, this situation will continue to fester, to the detriment of both the operating companies and society in general.
13. **Are we sufficiently open-minded about what constitutes an acceptable solution to the FFT dewatering problem?** It seems that an early draft of D074 anticipated that most fines capture would be accomplished by effective production and placement of CT or NST. By the time D074 was issued, that assumed solution had shifted to in-line flocculation and thin-lift dewatering / drying of FFT. Neither of these solutions has proven to be a panacea for all operators, and both still have significant technical and cost issues. Focus has shifted more recently to TT and centrifuged FFT as technical solutions offering some promise. The authors believe these approaches still have technical and cost issues, and may prove not to be sustainable solutions to the FFT dewatering issue (e.g., for a discussion of the required degree of dewatering to achieve a

geotechnically stable closure landscape, see Sobkowicz and Morgenstern, 2009). It is time for open discussion between regulators, mine operators and other stakeholders, regarding a full range of acceptable end scenarios for a reclaimed landscape. Some of the options “on the table” should include scenarios that are apparently not completely compliant with long held views of reclamation to an “equivalent” land capability.

14. **Do we have the political and business will to generate the needed ingenuity?** This question disguises a much deeper and more difficult one – are we willing to forgo some of our current benefits (company profit, employment of people, and local and provincial government revenues) to ensure that the solutions we provide return the land we have disturbed to a state that is suitable for use by future generations and by all the creatures that rely upon it for sustenance? By asking this question, we are not taking a rabid environmental point of view; we are simply asking how we define solutions to FFT dewatering and the creation of closure landscapes that meet socially responsible tests of acceptability, and what demands that will place on our ingenuity? It seems to the authors that the socially responsible end point should be a goal of which all suppliers of ingenuity, whether it be social or technical, are continually aware. Note that this comment is not aimed solely at government and business managers and leaders, but at every person who is involved in the production of social and technical ingenuity. Political and business will is generated at all levels in today’s society – not just at the “top”.
15. The fast pace of communications in today’s world creates unrealistic pressures to solve problems “instantly”. **Are we consciously taking the time required to generate the ingenuity to solve the FFT dewatering problem?** Pressure for instant solutions comes from many directions – internally, within each operator’s company, from government regulators and other officials, and from stakeholders with real concerns or with media points to score. Honest communication of realistic time frames to solve complex technical problems is needed, as well as an open and transparent discussion of research and development progress.

16. Experience shows that ingenuity is maximized when all stakeholders to a particular issue cooperate fully in solving serious problems. **What have both industry and government regulators done to increase communication and cooperation between stakeholders impacted by the Oil Sands tailings FFT dewatering challenge? What opportunities exist to increase ingenuity by harnessing the cooperative thinking of all stakeholders?**
17. **Are we doing all that we can to develop and then implement technical solutions in a rational and effective manner?** Homer-Dixon notes that there is seldom an insufficient generation of ideas but often many limitations on implementation of those ideas. **Do we follow a disciplined research and development process that gives us the best chance of proving out a technical idea and identifying its costs as early as possible? Do managers follow through with organizational changes to improve social and technical ingenuity, monitor progress, and make further changes if necessary? Do regulators monitor the impact of new or modified regulations and make the changes necessary to increase ingenuity and focus on practical goals?**

ALTERNATIVE APPROACHES

Lest we consign Homer-Dixon as overly negative or “left field”, two alternative approaches to the challenges of technology development are worth noting in brief, as they provide synergy with Homer-Dixon’s ideas and further guidance for Oil Sands technology development.

Technology Brokering

When searching for a solution to an idea, there is a romantic notion of a lone inventor, holed up in his or her garage, delivering the golden solution to the problem. While this makes for a good movie plot, and on rare occasion works in real life, it is not the normal script for leading technology development firms.

In examining the innovation centre IDEO (an international design and consulting firm), Hargadon and Sutton (1997), analyzed the steps taken to rapidly innovate and develop technologies. The processes

used at IDEO were similar to those found at 3M as well as those used by the Thomas Edison laboratory, which was responsible for many innovations. The main finding was that innovation often arrived through the cross pollination of ideas from a wide range of industries, related and seemingly unrelated. Ideas were not being created from whole cloth, but repacked and redesigned to create something new.

To foster the development of ideas there are five components. First an assessment of the gaps in the flow of information is made. Knowledge is then acquired, stored and retrieved for use on different projects. The end result is a collaborative effort that seemingly has created something new but in reality is the reworking of several old ideas into a new form.

There needs to be a realization that technology development and innovation cannot be managed as in a factory or a plant. While efforts are being made within the industry to foster collaboration, to develop a technology database and to reach out into other industries, the efforts require further investment, improvement of management and organizational structure (inter- and intra-company) and improved ability for collaboration.

The Risk Perception Gap

According to the principles espoused by Blake (1995), a gap exists in the perception of the treatment of FFT in the Oil Sands industry between those within the operators, consultants, regulators and the public at large.

If stakeholders were assigned rings on a bull’s-eye, with the smallest circle (i.e., the centre) being those who work in the industry and the largest circle being the public at large, opinion of how well the problem is being handled would become progressively more negative as one moved from the inner to the outer circles.

There is a tendency to view the negative opinions of those outside of the inner circles as inflammatory, bordering on wilfully ignorant. The difference between the viewpoint at the centre and the viewpoint on the outside is the risk perception gap.

Those in the inner circle may look at the more quantitative aspects of the problem. For example, asking questions such as: how much FFT is required to be treated, how can we deal with current demands for FFT treatment, how will we

deal with future demands, what environmental impacts are there, what progress is being made to address these issues?

As one moves further from the centre of the circle the perception and the questions change. For example, some of these questions might be asked: how am I and my family or community going to be impacted by this operation, how long will it take to return the land back to normal use, what do the various technical terms mean, can I trust these companies to do what they say they are going to do, will there be residual consequences or risks once this mine closes?

It is important to recognize that there is no “right” viewpoint. More work can be done to bridge the perception gap by understanding the values of those not intimately involved in the process, and by understanding that negative opinions arise from a lack of control of the issue and lack of trust of the industry, (since it is the primary benefactor of the product).

Thus, in order to make real progress, according to these two references we will need to:

- Broker technical solutions between disciplines.
- Bridge the risk perception gap with the public.

QUO VADIS?

So – where are we going as an industry? Can we find answers to the FFT dewatering problem, and if so where? As suggested earlier, as engineers we serve in an optimistic world, constantly working to find solutions. In acknowledgement of that noble calling, this paper suggests two additional ideas towards our framing of solutions to the challenges posed above.

A Tailings Social-Organizational Roadmap

The Tailings Technology Roadmap forged a path forward in regard to technological ingenuity. In the same way, what is now needed is:

- A critique of the organizational, regulatory, corporate, collaborative and societal structures (referred to herein as improving social-organizational ingenuity).
- A roadmap of “social-organizational ingenuity” improvement opportunities.

What is needed is a fundamental rethink on the above factors, thinking outside of the box. Some components might include:

- A think tank workshop to assess the existing state of social-organizational ingenuity, agree on a broad framework for action and improvement, and develop terms of reference for the creation of a social-organizational roadmap.
- This roadmap could be prepared by a consultant with leadership, legal, economic, sociological, community, environmental, cultural and technological resources. Individual teams working within each area would identify roadblocks and opportunities for outreach beyond their boundaries.
- A multi-stakeholder steering committee could support the process, maintain balance and ensure that the terms of reference are met.
- The Tailings Social-Organizational Roadmap could consider:
 - Benchmarking other industries.
 - Working with existing initiatives.
 - Introducing a scorecard approach.

Financial Incentive

The enormous cost in dollars and human effort of FFT reclamation is now a massive opportunity and economic incentive for us as an industry, as the potential savings are both high and necessary. It is also a threat, as this kind of spending cannot continue, especially if the price of oil were to drop. There is a window of opportunity for us right now. The question is – how can we provide incentives to ingenuity that address the cost factors of tailings treatment technologies?

CAN THE CONCEPT OF AN INGENUITY GAP HELP US?

This paper describes the concept of “ingenuity” as a set of ideas and instructions that can be applied to solve practical technical and social problems, and which involves both good ideas and the effective implementation thereof. An “ingenuity gap” exists when the right set of ideas and resources cannot be brought to bear to solve a particular problem in a required time frame.

By studying the forces driving our need for ingenuity and the factors that might limit our supply, we

can perhaps gain insight into the roadblocks to solving the FFT dewatering process. An attempt is made herein to pose questions that will help us to identify both the driving forces and the limiting factors, to more clearly see what we must do to be more ingenious in our approach to dewatering FFT and to produce sustainable closure landscapes.

It is the authors' belief that improvements can be made in a number of social and technical areas to narrow the ingenuity gap in Oil Sands tailings, so as to reach a technically and cost effective solution. Some of these improvements have been discussed or hinted at in this paper, but many will come only after some serious contemplation of the questions posed herein on the nature of ingenuity, and on our ability to apply greater ingenuity by accessing appropriate human capital and removing some of the social roadblocks.

Finally, ingenuity always thrives when ideas are shared fully and widely, and when all stakeholders to a problem co-operate in finding solutions. The provision of ingenuity is not the responsibility of one organization, or one group of managers, regulators or technocrats. It is a responsibility of every organization and individual that participates in the Oil Sands tailings industry. Each person's awareness of the path to ingenuity will allow him or her to participate more effectively in its generation.

REFERENCES

Blake, E.R., 1995. Understanding Outrage: How Scientists Can Help Bridge the Risk Perception Gap. *Environmental Health Perspectives*, Vol. 103, No. 6, pp 123-125.

Boswell, J.E.S. 2012. The Oil Sands Tailings Technology Roadmap Project: the Identification and Improvement of Tailings Technology Suites, and Pathways for Technology Development. 3rd International Oil Sands Tailings Conference, Edmonton, Alberta.

Boswell, J.E.S. 2010. Big Picture Thinking in Oil Sands Tailings. 2nd International Oil Sands Tailings Conference, Edmonton, Alberta.

Boswell, J.E.S. and Sobkowicz, J.C. 2010. Environmental assistance for tailings disposal, in *Proceedings of the 63rd Canadian Geotechnical Conference*, 12–16 September 2010, Calgary, Alberta.

Gidley, I. and Boswell, J. 2013. A generic model for technology development in oil sands tailings, in *Proceedings 16th International Seminar on Paste and Thickened Tailings (Paste 2013)*, R.J. Jewell, A.B. Fourie, J. Cadwell and J. Pimenta (eds), 17–19 June 2013, Belo Horizonte, Brazil, Australian Centre for Geomechanics, pp. 549–560.

Hargadon, A. and Sutton, R.I., 1997. Technology Brokering and Innovation in a Product Development Firm. *Administrative Science Quarterly*, Vol. 42, No. 4, pp 716-749.

Homer-Dixon, Thomas. 2000. *The Ingenuity Gap*. Alfred A. Knopf Canada, 480 pp.

Sobkowicz, J.C. 2010. History and Developments in the Treatment of Oil Sand Fine Tailings. *Proceedings of the 14th Annual Conference on Tailings and Mine Waste*, 17–20 October 2010, Vail, Colorado, pp. 11–30.

Sobkowicz, J.C. 2013. Developments in Treating and Dewatering Oil Sands tailings. *Proceedings 16th International Seminar on Paste and Thickened Tailings (Paste 2013)*, R.J. Jewell, A.B. Fourie, J. Cadwell and J. Pimenta (eds), 17–19 June 2013, Belo Horizonte, Brazil, Australian Centre for Geomechanics.

Sobkowicz, J.C. and Morgenstern, N.R. 2009. A Geotechnical Perspective on Oil Sands Tailings. *Proceedings of the 13th Annual Conference on Tailings and Mine Waste*, 1–4 November 2009, Banff, Alberta.

Stephens, B. 2012. Component 2 Results. Oil Sands Tailings Deployment Roadmaps. Report to Alberta Innovates – Energy and Environment Solutions. June 29, 2012.

GEOTECHNICAL INSIGHTS INTO DEPOSITION, DEWATERING AND STRENGTH PERFORMANCE OF THICKENED AND PASTE TAILINGS DEPOSITS AT SHELL CANADA'S TAILINGS TEST FACILITY

Srboljub Masala¹, Reza M. Nik², Gavin Freeman² and Robert Mahood²

¹Thurber Engineering, Calgary, Alberta

²Shell Canada Energy, Calgary, Alberta

ABSTRACT

Paste thickening produces a high density, high fines content and non-segregating thickener underflow product. Paste thickening process was trialed starting in 2007 at the Shell's Muskeg River Mine Tailings Test Facility to support the objectives of reducing fluid fine tailings inventory and accelerating the pace of reclamation of mined areas to terrestrial land uses.

The paper presents depositional and geotechnical data gained from three pilot-scale thickened tailings / paste deposition trials. Two of them were relatively thick deposits, about 4-5 m in depth (Large Cells 1 and 4) in which sedimentation and consolidation were the principal physical processes affecting tailings densification and strength gain. The third was a relatively thin deposit, less than a metre deep (Large Paddock) in which freeze/thaw consolidation and evaporative drying were the prevailing effects. Geotechnical performance of these deposits was used as a basis for qualitative comparisons of the relatively deep and shallow pond concept for oil sands tailings deposition.

Technical insights that are discussed include: deposit performance monitoring during filling and consolidation from 2007 to 2009, and *in situ* characterization and investigation of shear strength in 2008 - 2009. In addition, the paper presents the data from the field geotechnical investigations conducted in winter 2012, 3 to 5 years after deposition, in the conditions of stable, consolidated deposits which may be considered a desired pre-reclamation state.

INTRODUCTION

Tailings Testing Facility

Shell Canada commissioned the Tailings Testing Facility (TTF) at the Muskeg River Mine (MRM)

site in June 2007. The TTF was used to demonstrate the viability of various novel oil sands tailings treatment options at a pilot scale. The TTF was a 100 tons-per-hour (tph) dry solids capacity field pilot for tailings technology testing, consisting of a 10 m diameter paste thickener, rated for 20 tph dry solids capacity paste thickening, and a mixer and pumping unit with pertinent infrastructure (Shell Canada Energy, 2008 and 2009). Shell's focus at the TTF from 2007 to 2010 was on development of tailings thickening (TT) and non-segregating tailings (NST) processes (Matthews and Masala, 2009). This paper concentrates on the thickened tailings products.

Deposition cells and geotechnical monitoring instrumentation

Deposition cells 1 and 4 were constructed *in situ* overburden soil and oil sands ore, with design depth of 5 m. The cells had a rectangular base measuring (nominally) 20 m x 50 m with sloping sides of approximately 1.5H:1V. A one-metre high perimeter berm was constructed around the cells (Klohn Crippen Berger, 2011).

The cells were instrumented for monitoring the consolidation behavior of "deep" tailings deposits: settlements, total pressures, pore pressures and temperatures. The instrumentation was concentrated at two locations at approximately one-third and two-thirds of the cell length. All sensors at a monitoring location were attached to a wooden post, at different heights, to capture profiles of different geotechnical properties at various periods during the deposit history.

Each cell was instrumented with:

- one staff gauge for deposit surface elevation;
- one vibrating wire (VW) total pressure cell at the pond bottom near one of the posts;
- vibrating wire (VW) piezometers on both posts, at a one-metre vertical spacing from the base.

Approximate dimensions of the Large Paddock were 88 m x 15 m at the base, and 1.5 m of depth. Containment was provided by a one-metre high perimeter berm.

The Large Paddock was instrumented only for measurement of tailings settlement (deposit thickness) and temperature. The settlements were measured by staff gauges installed on 10 wooden posts (P1 - P10) distributed along the cell length, at variable distances from 5 m to 10 m. The posts were 2 m tall (above ground), with graduations at 1 cm. The geometry of the Large Paddock and the locations of the posts were surveyed after installation, in order to determine the elevations of other posts relative to post P1, which were required for the computation of tailings slopes.

Three posts - near the upstream (US) and downstream (DS) ends and in the middle - were equipped with thermistor strings for temperature monitoring, each string containing sensors at 10 cm separation, starting from the cell bottom.

All instrumentation was connected to a data acquisition system for automatic data collection and storage.

Deposition history

Cell 1 was filled with paste thickener underflow in 20 discrete deposition episodes from September to December 2007. This material was referred to as treated thickened tailings (TTT). The thickening process used gypsum and anionic flocculant to effect rapid settling and high overflow clarity in the paste thickener operation. A tremie with a radial diffuser at the end was used to reduce the discharge velocity and limit the amount of shear during sub-aerial placement of the TTT paste (Matthews and Masala, 2009).

As a part of the 2009 TTF testing campaign, the Jackpine Mine Thickened Tailings Analogue (JPM TT Analogue) was deposited into the Large Paddock and Large Cell 4. This tailings product was made according to a design premise intended to simulate the anticipated commercial-scale process conditions at Shell's other oil sands lease, the Jackpine Mine: the feed was not controlled for density and SFR; the thickener was operated without feed dilution; and deposition was maintained, as much as practicable, during thickener upsets. The thickener was operated with flocculant addition upstream only, and no treatment downstream.

Deposition of the JPM TT Analogue into Large Cell 4 was performed in two stages during about two weeks in October and November 2009. The tailings were discharged through an open pipe placed at the top of the perimeter berm (without a tremie/diffuser). The tailings was in a slurry (fluid-like) state throughout deposition. Large Cell 4 was filled to a depth of about 4.5 m with a JPM TT Analogue material with the solids content SC = 36-42% and the sand-to-fines ratio $SFR_{44} = 0.2-0.5$. During winter 2009-2010 the deposit was covered by an ice layer and did not freeze; its consolidation continued unobstructed by the weather.

Also in November 2009, between the two deposition events for Cell 4, a JPM TT Analogue material with slightly different properties - SC = 40-50% and $SFR_{44} = 0.20-0.65$ - was deposited in two lifts in the Large Paddock to a depth between 1.0 m US and 0.7 m DS. This tailings was also discharged through an open pipe placed at the top of the perimeter berm at the upstream end. The deposit was subject to a freeze-thaw consolidation (dewatering) in the winter 2009 - spring 2010 season and certain drying in the summer of 2010.

The thickening control process provided data on both feed and product (thickened tailings) properties: the pipeline instrumentation on flow rate and slurry density, and sampling on the physical and geotechnical index properties. The average in-line data for the two tailings types are presented in Table 1.

Table 1. Average in-line tailings properties

Property	TTT (Cell 1)	JPM TT Analogue (Cell 4)
Bitumen content (%) ¹	1.6	2.9
Solids content (%)	60 ³	40 ⁵
Void ratio	1.9	3.9
Fines content FC_{44} (%) ¹	60 ⁴	75 ⁶
Sand-to-fines ratio SFR_{44}	0.7	0.3
Atterberg limits LL/PL (%)	32 / 14	31 / 16
$C_{f44} = f_{44}/(f_{44}+w)$ ²	0.45	0.34

¹ Obtained by Dean-Stark.

² $C_f = f/(f+w)$, called "fines over fines plus water ratio", where f is the mass of mineral fines in total tailings and w is the mass of water in total tailings. Mineral fines may contain some bitumen.

³ Obtained by drying in muffle furnace at 550° C.

⁴ Obtained by washed sieve through No. 200 (75-micron sieve) and drying in muffle furnace at 550° C. Conversion from the 75-micron basis to the 44-micron basis was made using the TTF-specific formula: $SFR_{44} = 1.7 * SFR_{75}$.

⁵ Drying at 135° C in the Halogen Moisture Analyzer.

⁶ Obtained by washed sieving through No. 200 (75-microns) and oven drying at 105° C.

Geotechnical instrumentation data

Geotechnical instrumentation data for Cells 1 and 4 are presented as:

- time plots of tailings settlements, pore pressures at various depths, and total and effective stresses at the cell bottom in Figures 1 and 2; and
- temperature profiles in Cell 4 for selected times during cold and warm season in 2009-2010 in Figure 3.

The only presented monitoring data for the Large Paddock are settlement profiles during deposition and after freeze/thaw in winter 2009 and drying in spring 2010, shown in Figure 4.

Geotechnical characterization of the deposits

Tailings characterization, consisting of piston sampling with continuous profiling over deposit depth, laboratory testing for geotechnical index properties, and field strength testing (cone and ball

penetration and field vane testing), was conducted on:

- two occasions in Large Cell 1 (September 2008 and December 2012);
- four occasions in Large Cell 4 (December 2009, July and September 2010 and November 2012); and
- once in the Large Paddock (September 2010).

The sampling and testing was always conducted at three fixed locations in a cell: near its ends (US and DS) and in the middle (M).

Figure 5 presents profiles of selected geotechnical index properties - composition by Dean-Stark: oil-water-solids (OWS) and fines content FC_{44} - and undrained strength by the three field test methods in Cell 1, obtained during characterization in December 2012, about 5 years after deposition. The strength profiles include additional data from September 2008, representative of the conditions about a year after deposition.

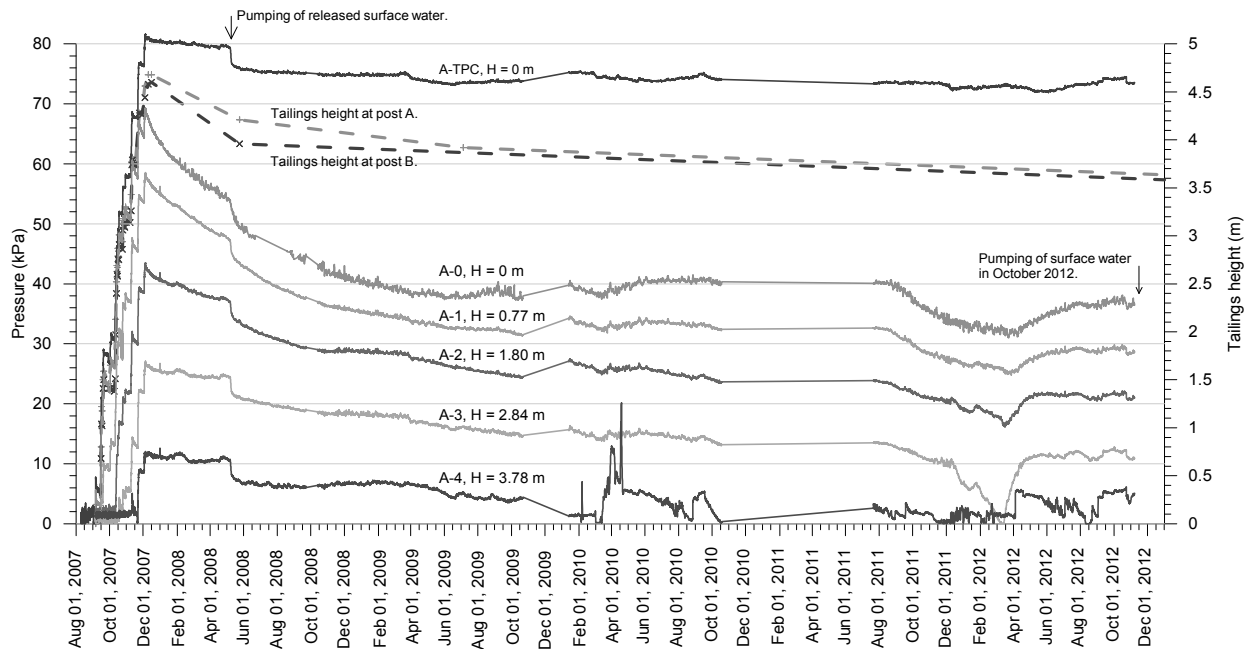


Figure 1. Cell 1, TTT - monitoring instrumentation data

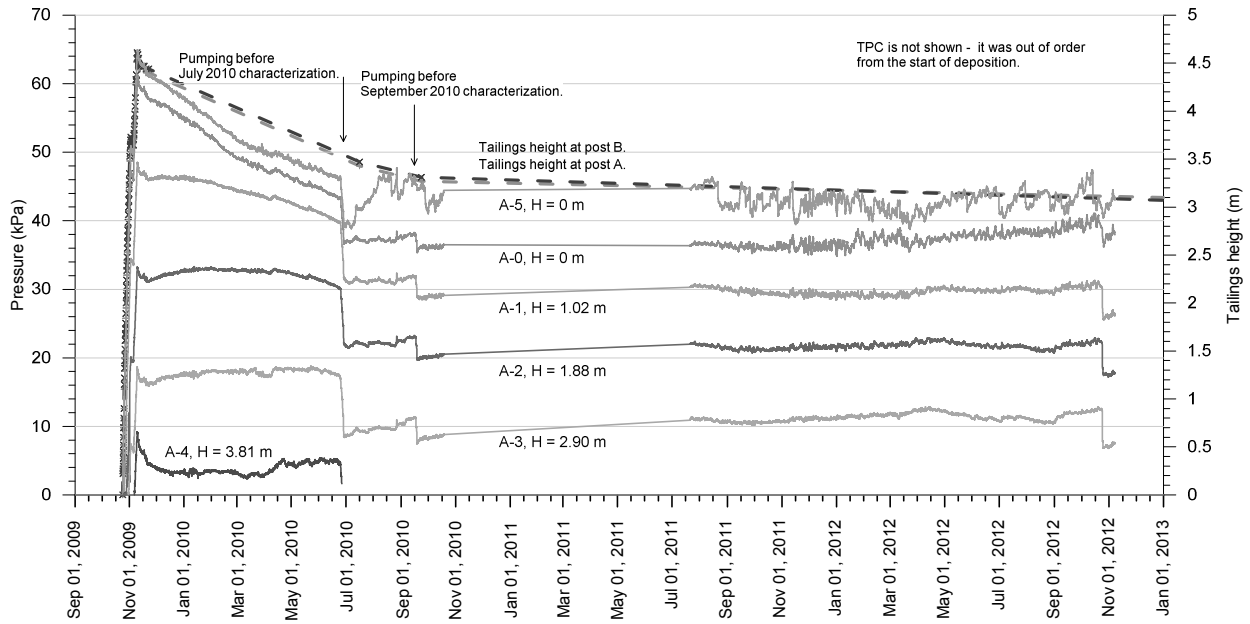


Figure 2. Cell 4, JPM TT Analogue - monitoring instrumentation data

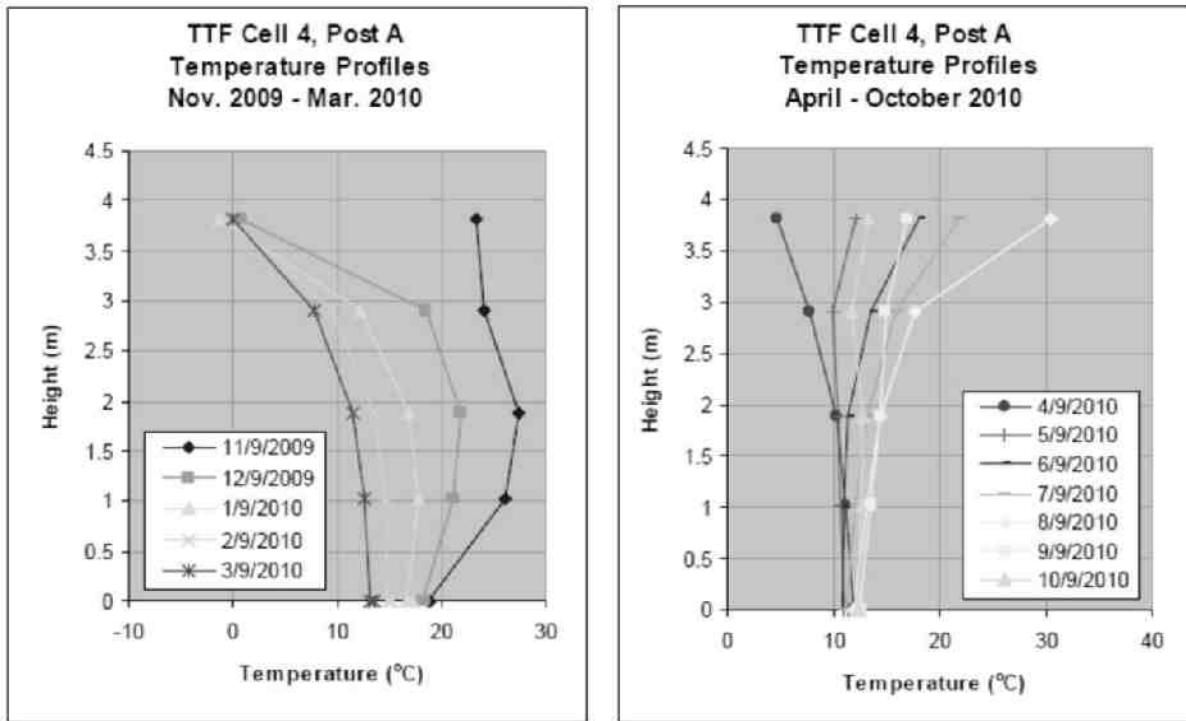


Figure 3. Cell 4, JPM TT Analogue – thermal profiles, cold and warm season in the first year after deposition

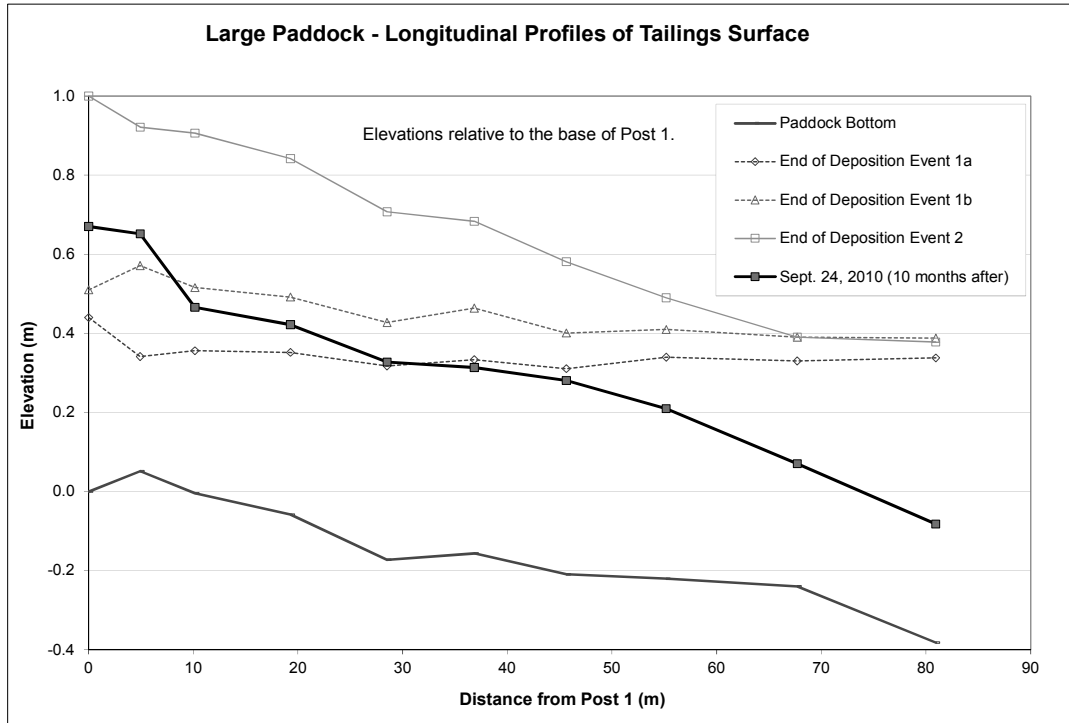


Figure 4. Large Paddock, JPM TT Analogue – settlement profiles, during deposition and after freeze/thaw

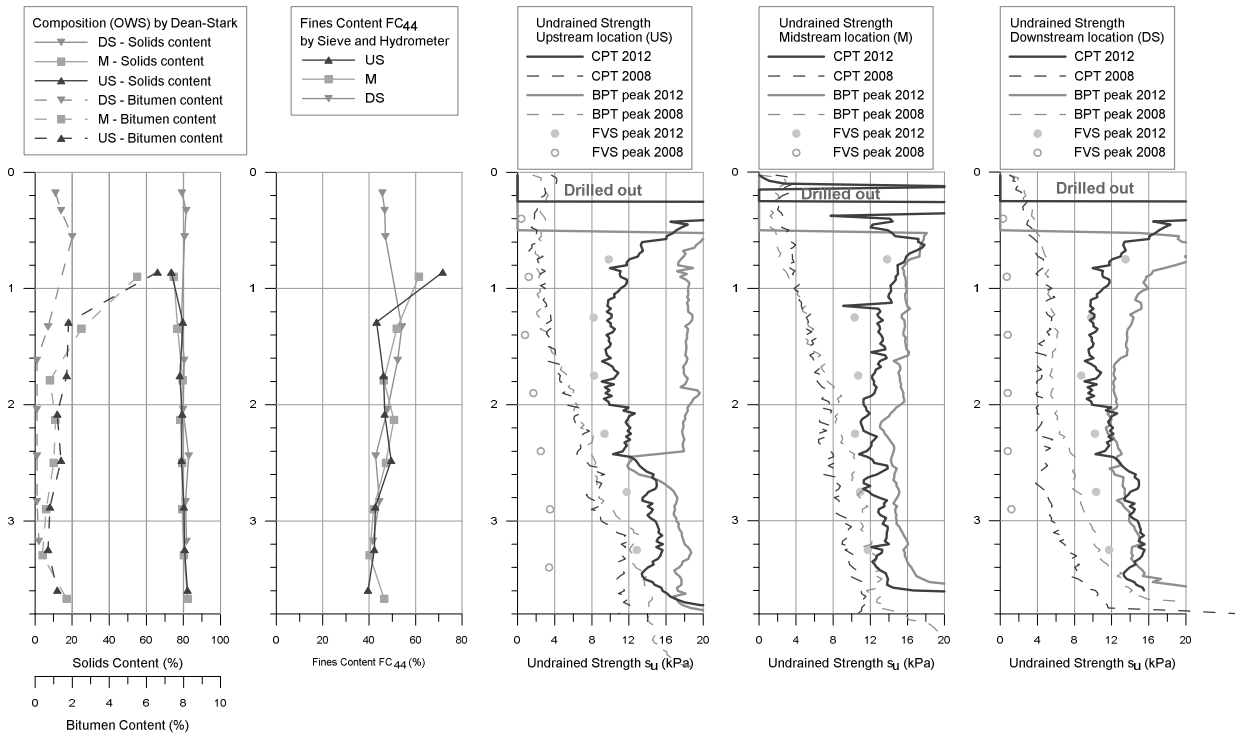


Figure 5. Cell 1, TTT – characterization in Dec. 2012: OWS, FC₄₄, undrained strength (including data from September 2008)

Figure 6 presents characterization data for Cell 4 from December 2012, which was about 3 years after deposition. Additional strength profiles from September 2010 correspond to the conditions a year after deposition.

Figure 7 presents the Large Paddock characterization data from September 2010, roughly a year after deposition. It was the only characterization campaign for this test cell.

DISCUSSION

Beach slopes

Tailings slopes in Cell 1 varied from 1% - 2% in the beginning of deposition to 0.2% - 0.3% at the end and post deposition (long-term). The steep initial slopes were not considered representative because of thin deposit at the time and the bottom boundary effect. A general tendency toward steeper slopes after shorter deposition events was noticed, probably because of accumulation of newly deposited material at the US side. This was estimated as a transitional effect; the commercial production slopes may be even gentler than the pilot-scale slopes.

Consistent with the JPM TT Analogue lower density at discharge, the deposition and long-term (post-deposition) slopes in Large Cell 4 were even gentler - in the range of 0.1% to 0.2%, practically horizontal.

The slopes of tailings surface in the Large Paddocks were measured from 0.3% to 0.6% (variable because of concavity) and were steeper than in Cell 4 because of the small deposit thickness and the bottom boundary conditions.

Segregation

The fines content profiles in Cell 1 show high uniformity below 1 m of depth, with FC_{44} about 45-50% ($SFR_{44} = 0.8-1.2$), while in the upper metre fines content increases to about 80% ($SFR_{44} = 0.2$), at the US and M locations. It should be noticed that these variations do not indicate segregation of TTT in Cell 1 (the fines

concentration is not at the DS side) but rather a variation in tailings production.

The JPM TT Analogue was a relatively thin slurry at discharge (with a SC of about 40% and C_{f44} of 0.34) and segregated upon deposition. The tailings was shown non-segregating in the static conditions (Shell Canada Energy, 2008) which pointed toward the open pipe discharge method as the cause for segregation. The open pipe method creates a high-energy depositional environment with poor control of flow velocity and shear energy dissipation.

Different modes of segregation in shallow and deep deposits of the JPM TT Analogue tailings can be observed in Figures 6-7, with characteristic patterns in variation of composition (bitumen and solids contents), fines content, and undrained strength. In the Large Paddock, the variation of these properties is primarily in horizontal direction; they are fairly uniform over depth. In contrast to it, in Large Cell 4 the direction of change of tailings properties is dominantly vertical. These different modes of segregation in shallow and deep deposits are considered typical for fine slurries (they have been observed in the existing oil sands tailings deposits) and can be explained by different modes of settling of a polydisperse tailings suspension in quiescent (Cell 4) and dynamic (Large Paddock) conditions.

Consolidation and pore pressure dissipation

Figures 1 and 2 present deposit settlement and pore pressure variations with time in Cells 1 and 4 (the piezometer readings were corrected for both temperature and barometric pressure). It can be seen that, in general, the settlement measurement frequency and accuracy are not sufficient for assessment of the end of consolidation. When surface settlements decay to imperceptible rates, excess pore pressures persist in the deposit, so that dissipation of excess pore-pressures lags behind the surface elevation changes. Therefore, measurement of excess pore pressures, and not settlements, is a more sensitive and reliable method for monitoring deposit consolidation.

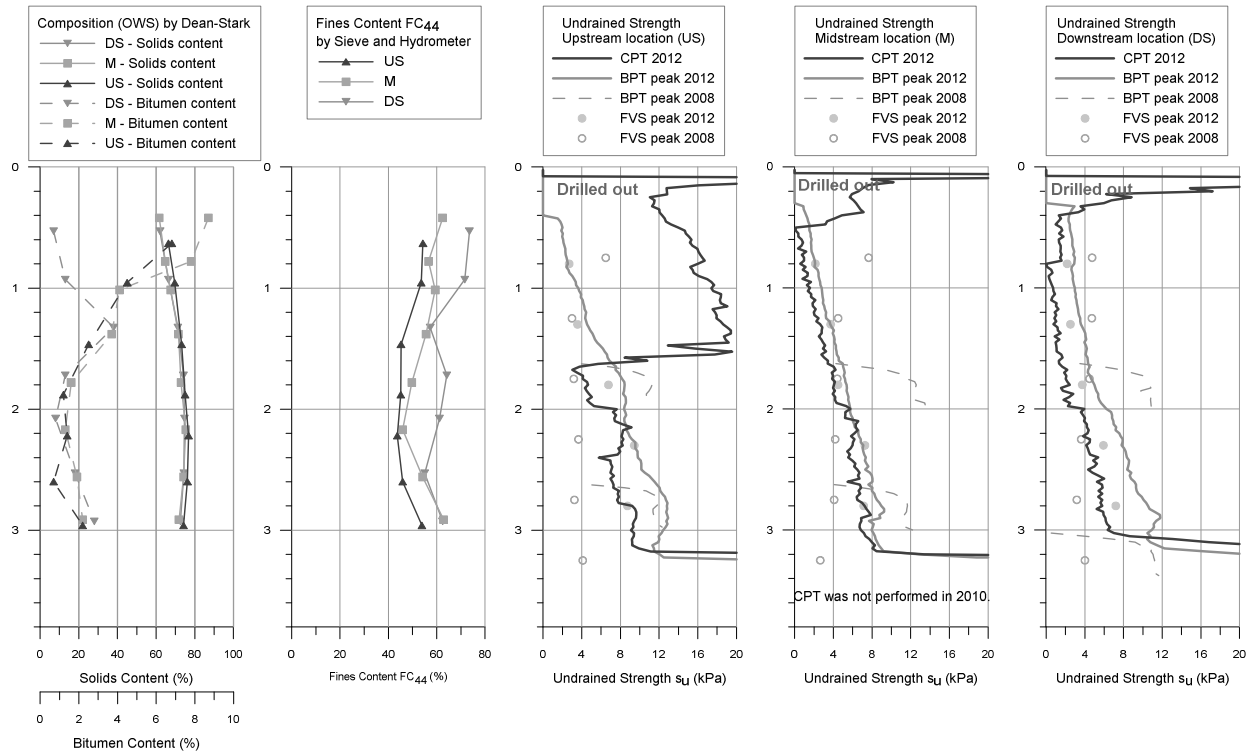


Figure 6. Cell 4, JPM TT Analogue – characterization in Dec. 2012: profiles of OWS, FC₄₄, undrained strength (including data from September 2010)

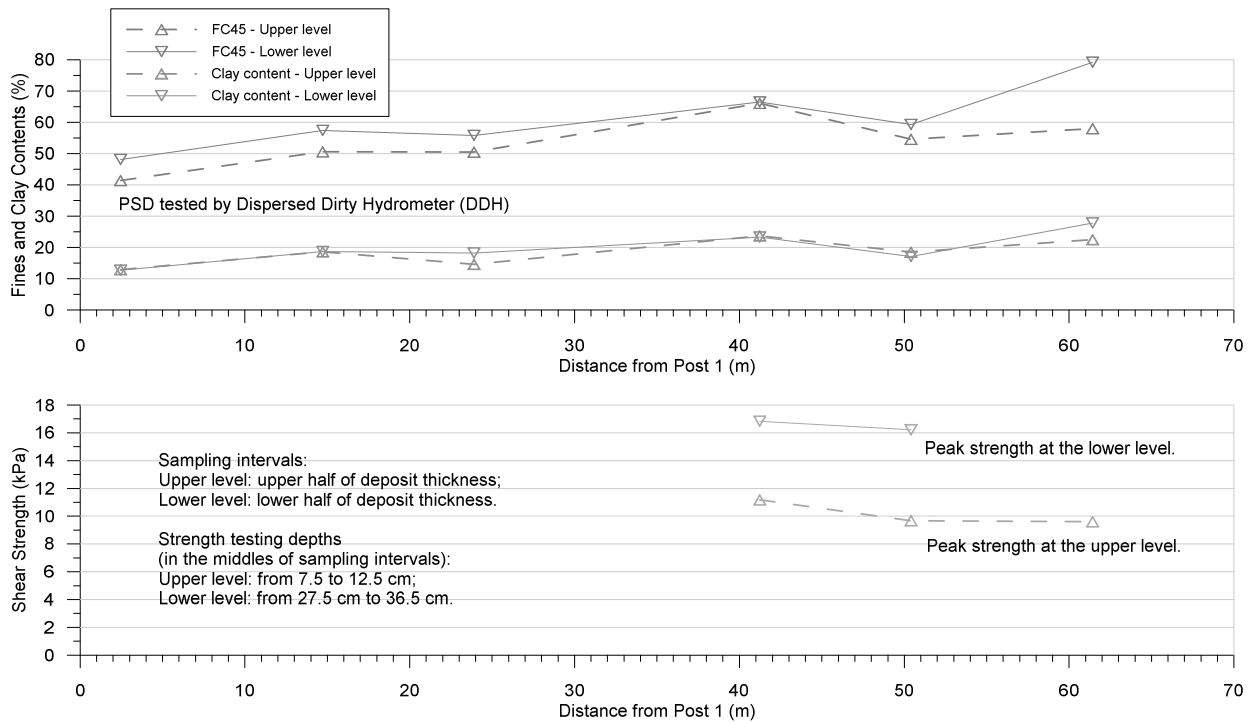


Figure 7. Large Paddock, JPM TT Analogue – characterization data from September 2010: longitudinal profiles of FC₄₄ and undrained strength.

However, beside the sensor sensitivity issues and corrections for temperature and barometric pressure variations, the in situ pore pressure measurements are subject to the boundary conditions effects. Consolidation process and pore pressure dissipation can be obscured by weather and seasonal variations in groundwater levels; see, for example, increases in pond water levels due to spring and fall precipitation and decreases due to evaporation in summer (Figures 1 and 2). In such a situation, it is better to make use of differential quantities like excess pore pressure or effective stress that cancel these effects. In our case we used the effective stress; the excess pore pressure required pond water level measurements which were not made with sufficient frequency.

Figures 1 and 2 show that the cell base was acting as practically impermeable boundary throughout

deposit consolidation. The pore pressure profiles were typical of the one-sided drainage case, with water flow toward the tailings surface and with the pore pressure profiles parabolic in shape, with the highest recorded values at the cell bottom. Since the cell bottom was the place where the pore pressure dissipation and the effective stress gain were the slowest, the effective stress at the base was a direct measure of the consolidation progress – when the effective stress achieved a plateau, a stable value, it marked the end of consolidation. The effective stress at the base of Cell 1 (Figure 8) was calculated from the total stress and pore pressure measurements at the base. The effective stress in Cell 4 (Figure 8) was calculated using the total stress obtained by integration of the density profile, since the total pressure cell was dysfunctional.

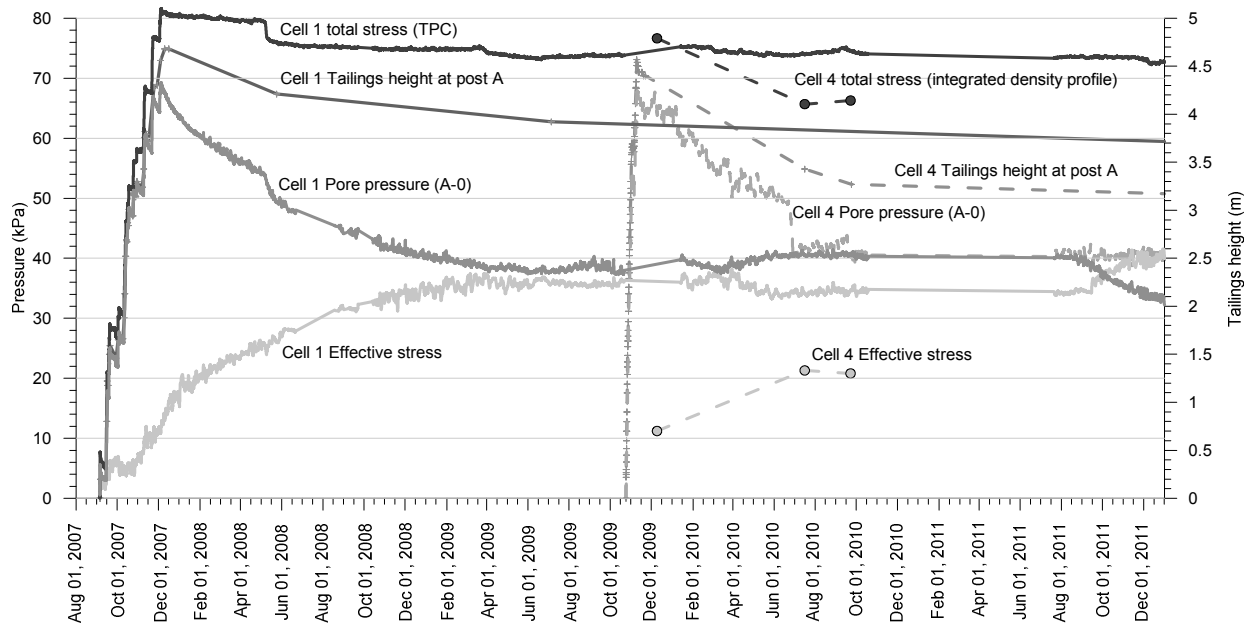


Figure 8. Cells 1 (TTT) and 4 (JPM TT Analogue) – effective stress at the cell bottom

It can be estimated that consolidation took about 20 months in Cell 1 and about a year in Cell 4 (the latter was based on point-wise information and was not as easy to decide).

It should be noticed that the consolidation times are specific for each deposit and depend on the deposit thickness (size) and on the boundary conditions. For predictive purposes at a commercial-scale level a proper consolidation model should be used, with the input

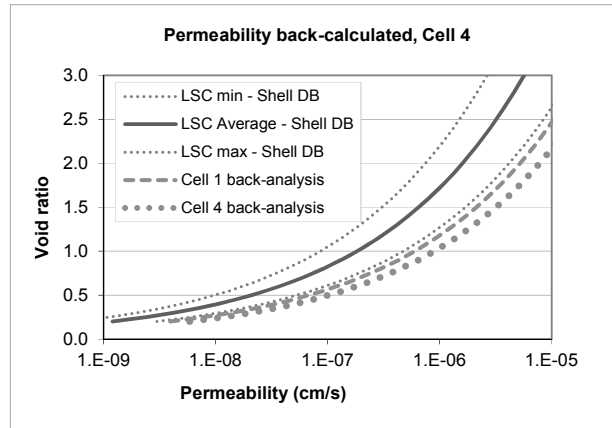
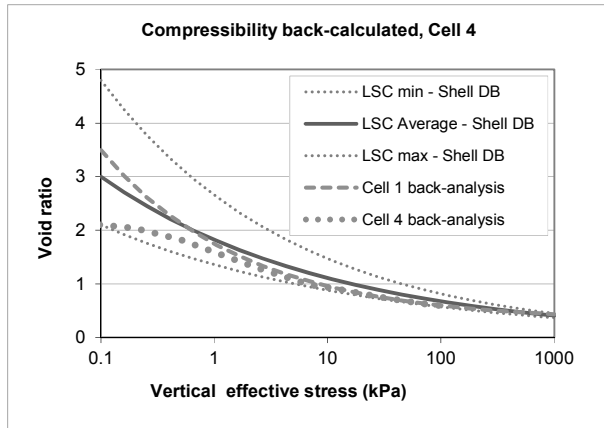
representative for the geometric scale of the analyzed deposit.

Consolidation parameters from monitoring data versus LSC tests

A methodology was developed for determination of the in situ representative material property functions in one-dimensional consolidation conditions by back-analyzing the monitoring and characterization data for an instrumented tailings deposit (Masala et al. 2014). The pilot-scale

compressibility and permeability functions for Cells 1 and 4 are shown in Figures 9-10, together with the ranges of the same functions obtained by the laboratory large strain consolidation (LSC) tests. It can be seen that the back-calculated compressibility functions, representative of the pilot-scale conditions, are close to those

determined by the laboratory testing. The back-calculated permeabilities are much higher than the laboratory counterparts – they are even slightly higher than the maximum permeabilities determined in the laboratory. This finding is consistent with anecdotal evidence from operational oil sands tailings ponds.



Figures 9(left) and 10 (right). Back-calculated compressibility and permeability functions for Cells 1 (TTT) and 4 (JPM TT Analogue)

Thermal behaviour

Freezing did not occur in the first year in a 4.5 m deep JPM TT Analogue in Large Cell 4, even when it was deposited during a cold winter, because of ice layer at the surface (Figure 3). However, freezing occurred in a 0.7-1 m thick deposit of the same tailings (Large Paddock). Therefore, the assumption of the freeze-thaw consolidation benefits may be overly optimistic for deep deposits with ponded water that can freeze in winter. Thermal behaviour of a tailings deposit is highly dependent on tailings properties, container geometry and deposition strategy (beside boundary – weather - conditions). The impact of surface ice on the thermal regime within deep tailings deposits is accentuated. To facilitate freezing, tailings must be discharged subaerially and should have high enough yield stress to create sufficiently steep beaches that will facilitate runoff of consolidation release water to the DS side of the pond. Then, freeze-thaw could possibly assist with a faster strength gain in the near-surface zones of tailings beaches that are not covered by water.

The thickness of a ‘thermally active layer’ responding to the seasonal temperature variations is about 3 m, based on monitoring of Cell 4 (Figure 3). This thickness is defined as the depth at which measured temperature variations drop below a

threshold value (e.g. 1°C) and is not the same as the frost penetration depth. The surface zone affected by daily variations of air temperature is about 0.3-0.4 m deep, based on monitoring in the Large Paddock (not shown). These depths are variable and depend on the tailings water content.

Shear strength gain with time

TTT in Cell 1

In September 2010, about 10 months after deposition, the tailings was still consolidating, with the solids content between 50% near the surface and 70% at depth. The measured water contents in the near-surface zone were higher than the liquid limit (LL), which was consistent with low measured undrained strengths in the top metre (only 2-3 kPa). The deposit strength was above 5 kPa in the lower half of the deposit on the US side and in the middle, while on the DS side the strength was still below 5 kPa.

A large increase in strength throughout Cell 1 deposit was recorded from September 2008 to December 2012, particularly in the upper parts of the deposit. This was caused by four cycles of seasonal effects - freeze-thaw and drying – since the last characterization in 2008. The strengths estimated from the penetration tests were

everywhere higher than 10 kPa. The vane strengths were consistently lower than the CPT and BPT estimates. The vane values were below 10 kPa at two depths in the middle of the deposit.

JPM TT Analogue in Cell 4 and Large Paddock

Measured undrained strengths in September 2010, about 10 months after deposition, were much higher in desiccated tailings in the Large Paddock than in Large Cell 4. The Large Paddock deposit achieved solids contents of 70-80%, with the minimum shear strength of about 10 kPa.

The strength in the Large Paddock was strongly related to suction (negative pore pressure) and varied with the degree of saturation, i.e. precipitation level.

The undrained strength in September 2010 in Cell 4 was below 10 kPa at all three test locations. The highest strength of about 7 kPa was measured at the US location, decreasing to roughly 5 kPa at the DS location.

Despite an overall increase in strength throughout the deposit measured after September 2010, the December 2012 strength measurements showed that Cell 4 tailings did not reach 10 kPa. The maximum strengths varied from 9.5 kPa at the US side to 7 kPa at the M and DS locations. As expected, the upper 1.5 m at the US side and 2 m at the M and DS sides still had strengths lower than 5 kPa. Until December 2012 Cell 4 was always covered with water, i.e. the deposit was fully saturated. The undrained strength in normally consolidated saturated deposits increases linearly with depth and must be zero at the surface. Since consolidation in Cell 4 ended before December 2012, no further increase in strength can be expected unless the deposit becomes exposed to environmental effects like drying or freeze-thaw (or engineered alternatives like surcharge loads and vertical drains).

CONCLUSIONS

The JPM TT Analogue was a relatively thin slurry at discharge which, combined with a high-energy deposition environment (open pipe) resulted in segregation in both thick (Cell 4) and thin (Large Paddock) deposit. The TTT in Cell 1, which was a paste and was discharged using a tremie/diffuser, did not segregate.

Consolidation of the two deep deposits, Cells 1 and 4, occurs between a year and a year and a half after deposition. The times needed for consolidation of a commercial-scale deposits must be estimated using an adequate consolidation model with representative input data.

Operational consolidation parameters at the pilot scale were obtained by back-analysis of the monitoring data. It was shown that the pilot-representative permeabilities were much higher than the values obtained by laboratory testing.

Measurement of excess pore pressures, and not settlements, is a more sensitive and reliable method for monitoring deposit consolidation.

The strength requirements for a pre-reclamation state 5 years after deposition were met by TTT in Cell 1 and JPM TT Analogue in the Large Paddock. This strength level could not be reached by the JPM TT Analogue in a shallow zone of the deposit in Cell 4, as its surface was always covered with release water and never exposed to climatic agents for freeze/thaw and drying effects.

Subaerial deposition was beneficial for JPM TT Analogue tailings in the Large Paddock. In general, subaerial deposition, in conjunction with a controlled low-energy depositional environment, may reduce segregation, if the tailings is prone to it, and it also allows early exposure of fresh tailings surface to weather agents, which facilitates freeze-thaw consolidation and drying.

Freeze/thaw was beneficial for thin JPM TT analogue deposit (Large Paddock) for both consolidation and strength gain. However, freezing did not occur in the thick deposits (4-5 m deep) of the same material, covered with release water. The pond design and operation should provide measures for draining of tailings surface to maximize the effects of subaerial deposition.

REFERENCES

- Klohn Crippen Berger. 2011. Shell Tailings Testing Facility (TTF), Geotechnical Investigations in Large Cell 4 and Large Paddock in 2010, March 01, 2011.
- Matthews, J. and Masala, S. 2009. Tailings research at Shell's Muskeg River Mine Tailings Testing Facility. Tailings and Mine Waste 2009, Banff, Alberta.

Masala, S.; Nik, R.; Freeman, G. and R. Mahood. 2014. Determination of field-representative consolidation properties of oil sands fine tailings by back-analysis of instrumented deposition trials. 67th Canadian Geotechnical Conference GeoRegina 2014, Regina, SK, Sept. 28 - Oct. 01.

Shell Canada Energy. 2008. Non-Segregating Tailings Technology Data Book, Revision 1

(Confidential Draft), Technology and Development, Shell Oil Sands, September 30, 2008.

Shell Canada Energy. 2009. Tailings Test Facility (TTF) Pilot Plant – Technical Objectives Summary. March 6, 2009.

DEVELOPING AN APPROACH TO PREDICT DEWATERING AND MATERIAL PERFORMANCE OF POLYMER FLOCCULATED MATURE FINE TAILINGS

Lois Boxill¹, Daryl Hockley¹, Dirk Van Zyl², Julie Thompson³ and Jeremy Olson³

¹SRK Consulting, Vancouver, British Columbia, Canada

²University of British Columbia, Vancouver, British Columbia, Canada

³Canadian Light Source, Saskatoon, Saskatchewan, Canada

ABSTRACT

Published in February 2009 by the Alberta Energy Regulator, Directive 74 provides operators of oil sands surface mines with criteria for desired rates of fines capture, shear strength development, and trafficability for oil sands tailings. Some operators have developed tailings management systems to address the regulation using polymers to flocculate fines from colloidal mature fine tailings (MFT). The resulting polymer-flocculated MFT (PF-MFT) appears soil like and demonstrates the ability to dry when deposited at thicknesses at which evaporation is still effective throughout the profile of the deposited lift. However, these polymer amended tailings are fundamentally new materials with complex physico-chemical interactions governing their dewatering characteristics and long-term performance. This fact is most evident when these materials are deposited in thicker lifts (>25 cm). When placed in thicker lifts a consistent crust forms (typically between 8-10 cm) above an even thicker layer of tailings in which the amount of secondary dewatering achieved appears to plateau. Ability to predict dewatering limits associated with PF-MFT enables better total cost accounting for tailings management using polymers and more accurate determination of reclamation costs. This paper describes a characterization framework being developed to support prediction of the amount of dewatering that can be achieved by treating MFT with polymers. The framework seeks to address the interplay of fundamental mechanisms of surface chemistry, material fabric and rheology, and the resulting material's geotechnical performance.

INTRODUCTION

Background

Directive 74 and its associated requirements were fundamentally intended to limit the quantity of fluid fine tailings stored on site and to provide criteria for

gauging how sequestered fines progress towards the goal of being incorporated into reclaimable landscapes. Surface mine operators, most notably Shell and Suncor, have made significant investments into researching, testing, and applying methods whereby MFT is flocculated with polymers and deposited in thin lifts. Released water and bitumen are returned to collection ponds while the deposited solids dry by natural evaporation processes (Matthews and Masala 2009, Wells et al. 2011, Charlebois, 2012, Suncor 2013, and Caldwell et al. 2014).

Experience to date with these methods has indicated several constraints:

- requirement for large amounts of space, which is particularly challenging for smaller mine sites;
- significant cost of polymer at the dosages needed to meet fines sequestration requirements;
- limitations of the effective drying period to summer months; and
- need to re-handle material in order to fully utilize existing disposal areas.

Mine operators seeking to address these limitations might consider a number of modifications. For example, increasing the thickness of the lifts in which the flocculated material is deposited would seem to allow a much better use of limited available space. Doing so would have significantly negative effects on evaporation. More generally, key performance indicators (KPIs) that focus on optimizing initial water release from PF-MFT may very well confound KPIs targeting additional dewatering and strength development.

Understanding these trade-offs requires first recognizing that PF-MFT is a complex synthetic material whose behaviour is impacted by complicated surface interactions between the bitumen, polymer, clay minerals, and cations

contained. As such, PF-MFT can exhibit characteristics quite different from those exhibited by conventional tailings or natural soils.

This paper describes an integrated material characterization framework aimed at describing the range of factors impacting the dewatering characteristics of PF-MFT and its ultimate performance as a reclamation media. The approach seeks to establish preliminary yet important linkages between fundamental material properties at the microscale and mesoscale for this unnatural material. This paper describes how characterization information obtained from the fields of surface chemistry, rheology, geotechnical engineering, mineralogy, and 2-D and 3-D sample imaging are complementary and can be powerfully combined to enhance overall understanding and assessment of the complex material that results when various MFTs are combined with polymer additives.

CURRENT OIL SANDS INDUSTRY APPROACHES TO CHARACTERIZING FINE TAILINGS

Chemical-Mineralogical Approaches

When viewed from the perspective of surface chemistry, it is clear that MFT is a stable colloidal suspension containing widely dispersed kaolinite, illite and illite-smectite clay minerals, residual bitumen, and ion rich process water at a pH ranging between 8 and 9 (Salehi 2010 and Masliyah et al. 2011). The surface area, surface charge, and cation exchange capacity of the clay minerals in suspension makes these minerals highly sensitive to their ionic environment and the pH of that environment.

The interlayer region of illite-smectite clays exhibits hydrophilic characteristics. While the role of residual bitumen is not conclusively known, experimental evidence at the laboratory and field scales indicates that bitumen can simultaneously exist in the form of distinct droplets or rafts and as coating on the surfaces of some clay minerals after flocculation with anionic polymers. Consequently, the hydrophobic-hydrophilic characteristics of bitumen may also impact the overall behaviour of PF-MFT.

Rheological Approaches

In the management of fluid fines tailings, rheology is often viewed as the domain that bridges the gap between mineralogical, chemical, and geotechnical perspectives of these complex materials (Vietti 2011 and Scales 2013). While most practitioners in this area would confirm that rheological characterization of input MFT and resulting PF-MFT enhances understanding of some of the tailings management implications for handling, deposition, and likely performance expectations for PF-MFT, it is doubtful whether rheologists would disagree about the complexity associated with rheological characterization of these materials or suggest that complete characterization and understanding of this material could be completed exclusively within this domain (Derakhshandeh 2014). Rheological characterization of MFT and PF-MFT confirms the importance of MFT heterogeneity, clay mineralogy, shear history, flocculation regime, and deposition environment. Said differently, rheologists easily recognize the impact seemingly small variability can have on the resulting product and the implications of these variations for flocculation and pipeline system design.

While rheological characterization is usually very helpful for optimizing flocculation and pipeline design, rheological characterization techniques have limited applicability to evaluation of the mechanical performance of deposited PF-MFT, especially when it is deposited in thick lifts. Also, rheological characterization of peak yield stress makes no assumptions about the test material's fabric. Said differently, rheological characterization recognizes that a measurement of shear stress can result from intrinsic properties of a material and does not solely require interlocking solid particles to exist.

Geotechnical Approaches

The field of geotechnical engineering seeks to apply principles of soil and rock mechanics to describe the engineering behavior of naturally occurring earth materials (minerals, rocks, soil, and water). The nature of the material typically characterized in this domain is not trivial as fundamental assumptions govern the applicability of critical theorem like those related to consolidation within soil mechanics. As such, geotechnical engineers struggle to meaningfully characterize fluid phase materials like MFT and approach characterization of PF-MFT using

techniques typically applied to natural soils. These include determination of particle size distribution and the associated material classification based on the nature and quantity of the solid particles present, determination of critical water contents for the material (aka Atterberg limits), shear strength characterization using field test methods normalized for “soil” systems, and consolidation testing (large strain and seepage induced) to directly measure compressibility and hydraulic conductivity (Znidarcic et al. 2011, Yao et al. 2012, Beier et al. 2013, Kabwe et al. 2013, and Estepho 2014).

The oil sands ternary diagrams (Figure 1) like the one developed by Azam and Scott (2005) attempt to establish boundaries between different types of engineering behavior and even material state by establishing relationships between solids content, fines content, and the ratio fines (minus 75 μm) in suspension.

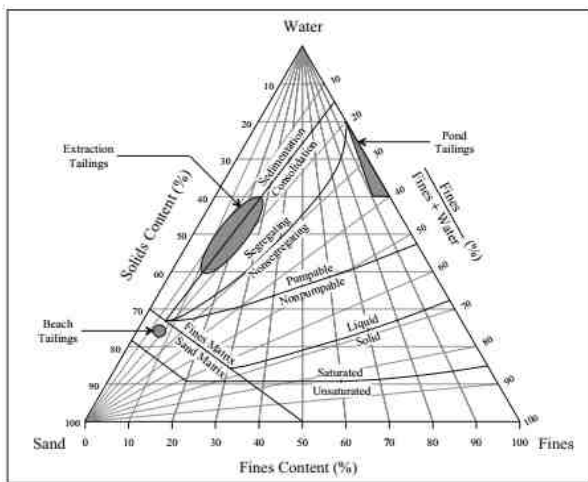


Figure 1. Geotechnically defined characteristic boundaries and zones of unflocculated oil sands tailings (after Azam and Scott, 2005)

However, research being undertaken by this paper’s authors suggests failure to account for how surface interactions impact the behaviour of solid particles can result in erroneous assumptions about the overall material phase, structure, and ultimate dewaterability. For example, colloidal stability is not limited to liquid phase interactions, impacts how the material interacts with its chemical environment, and impacts near and long-term material chemical and geotechnical stability.

The impacts of polymer flocculation of MFT on the geotechnical properties and behaviour of PF-MFT are in the relatively early stages of investigation. Yao et al. (2012) suggests that PF-MFT will likely continue to have large storage requirements and can be characterized by a large void ratio. This is consistent with ongoing research by this paper’s authors. However, correct interpretation of void ratio and permeability measurements must be informed by knowledge of actual material fabric and pore connectivity.

The use of shear strength to characterize the performance of PF-MFT further complicates matters because geotechnical engineers apply understandings of what shear strength implies from natural soil systems that are typically not dominated by polymer-flocculated clay minerals with residual bitumen. In natural systems, shear strength usually results from frictional interaction between hard/solid body particles that can be in intimate contact and exert force on each other. Likewise, application of consolidation theory assumes reduction in material volume is connected to the effective release of water from void spaces that in turn translate to increases in material strength (Kabwe et al. 2013). However, this line of reasoning does not account for the effects of soft particle deformation described by Mewis and Wagner (2012) or the impact of possible discontinuity in bi-modal porous networks that may be present in PF-MFT. These possibilities further underscore the need for enhanced understanding of the structure of PF-MFT on meaningful interpretation of measured shear strength values and confirming whether consolidation theory can be applied to these materials (Wells 2013).

CHALLENGES WITH CURRENT APPROACHES

Role of Clay Minerals

Understanding the impact of clay minerals on ore recovery and tailings management processes in the Alberta oil sands has been the topic of extensive research and continues to drive ongoing work by COSIA’s Clay Focus Group and others (FTFC 1995 and Mikula 2011). Mikula et al. (2008) also identified a reciprocal effect of clay mineralogy on water chemistry and the associated settling and rheological properties of the tailings suspension.

While it is widely acknowledged by geotechnical engineers that solids content, grain size distribution, clay content and mineralogy, and water chemistry impact fine tailings characteristics (Mitchell and Soga 2005, Sobkowicz and Morgenstern 2009, Miller 2010, and Scott et al. 2013), use of terms like “shear strength” and “consolidation” assumes a priori that models based on natural soil systems, which assume certain spatial relationships between solid particles, directly apply. Attempts at model simplification can also result in the removal or discounting of system components (e.g. bitumen) and complex interactions (e.g. between bitumen, polymer, clay minerals, and the ions present in the aqueous system) that are either not well understood and/or cannot easily be accounted for in mechanical models. In PF-MFT modelling, this limitation would extend to accounting for partial coating of clay mineral surfaces with bitumen and polymer, and the effects of the likely solubility of bitumen in polymer. As such, interpretation of results from these models must be done cautiously.

Initial vs. Ultimate Dewatering

While it has been demonstrated that flocculation of MFT with polymers can result in a rapid short-term release of water and fines sequestration, there is no guarantee that the ultimate geotechnical performance characteristics of the resulting PF-MFT will be desirable, especially when the material is deposited at thicknesses for which evaporative drying is ineffective. Field trials using polymers to flocculate MFT have been optimized for thin lift deposition. However, enhanced understanding of mechanisms governing dewatering has the potential of identifying ways to shorten the drying period for thin lift deposition and enable deposition of thicker tailings lifts.

PROPOSED COMPREHENSIVE FRAMEWORK APPROACH

Description of Proposed Approach

Complex, synthetic materials like PF-MFT require characterization input from the various fields best suited to analyze and quantify the factors governing various aspects of the material’s overall behaviour. In addition, characterization efforts must address the interfaces that exist between material components, as often the combination of components is not uniform and results in behaviour

different from the behaviour of the individual components.

The proposed approach combines compositional and mineralogical information with fundamental characterization data from the fields of surface chemistry, rheology, 2-D and 3-D imaging, and geotechnical engineering to develop a comprehensive characterization framework for PF-MFT. By establishing and describing the primary linkages between these fields illustrated in Figure 2, the framework seeks to identify and quantify the component interactions controlling dewatering along the continuum that exists from the micro-molecular level to field scale performance.

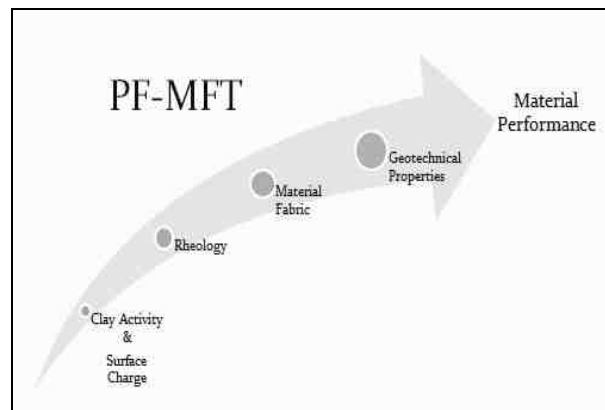


Figure 2. Proposed PF-MFT Characterization Approach

In this framework, impacts of charge density, surface reactivity, soft particle interaction, gel formation, colloidal stability, material fabric, and porosity can be quantified and used as input to additional testing to determine effective permeability. The characterization framework also provides a consistent approach to evaluating the performance limits of PF-MFT resulting from combination of different MFT and polymers.

Key Factors Governing Material Dewatering

The ability of a geomaterial to exhibit effective stress behaviour is directly tied to the physical interaction between solid particles within the material’s structure and the ability to remove fluids from the material’s pore spaces (Znidarcic 1999). However, the very existence of MFT demonstrates the profound impacts of activity at the microscale on overall material behavior.

The stability of a colloidal suspension like MFT is governed by where its pH is relative to the isoelectric point of the particles in suspension. In the range of pH 8 to 9, clay minerals exhibit strong electronegativity and remain widely dispersed as their isoelectric point generally occurs near a pH of 4 (Pecini and Avena 2013). Therefore, in the case of MFT, suspension stability results in the combined effect of widely dispersed clay minerals and a limited amount of water released from the suspension (Salehi 2010).

Therefore, the fact that MFT is a primary ingredient in PF-MFT is not a trivial point as the dominant properties of MFT as a stable gel would need to be substantially overcome or modified during polymer flocculation to produce a significant change in material behavior. As such, the chemical mechanisms enabling the initial release of water from PF-MFT must be understood. However, the factors impacting a polymer's dewatering limits when mixed with specific MFT samples must also be well understood (Fenderson et al. 2013).

The structure or fabric of the material that results from flocculation is also critical to understanding the physical mechanisms governing dewatering processes. X-ray computed tomography is a non-destructive, non-invasive technique that has been successfully used to examine the spatial configuration of natural soils (Taina et al. 2008). Knowledge of the resulting material fabric also enables development and calibration of representative computational models.

Ultimately, greater understanding of the properties governing fundamental dewatering aids enhancement of existing processes or informs development and trialing of secondary treatment processes (chemical and physical) that may be required to facilitate additional material dewatering. Operational experience and work by Mikula (2012) suggests that achieving solids contents in the 75% plus solids range results in a material that is trafficable and can be easily incorporated in primarily dry closure landforms.

PF-MFT Characterization Framework

Flowchart 1 illustrates the various test methods and analytical tools included in the proposed PF-MFT characterization framework. All test methods used are non-destructive and are aimed at characterizing the nature and response of the bulk material.

Baseline Characterization of PF-MFT Components

Given the heterogeneity of MFT within a single pond at a single site, it is important to characterize all material used in flocculation trials to enable meaningful interpretation of the study results and consideration of the implications of compositional changes. Characterization at this first stage includes percent-clay determination of MFT using the AST Methylene Blue procedure for sludges and slurries (Morin 2008); percent-bitumen, percent-solids, and percent-water determination; measurement of the pH and ζ -potential of MFT and process water used in flocculation; determination of the ionic composition and concentration of the process effected water being used to hydrate the polymer in the trial; and measurement of the methylene blue index (MBI) of the test polymer hydrated in process effected water being used in the trial. It is also important to note the type of polymer being used, namely its charge density, molecular weight, and a general understanding of its particle bridging mechanisms.

Input materials and flocculation methods used should be consistent so the PF-MFT is as consistent as possible for each of the tests to be completed.

Surface and Chemical Interactions

This category of tests is aimed at understanding the nature of and activity present on the surfaces of the PF-MFT being evaluated. Zeta-potential measurement provides an indication of the charge state of the resultant material that enables assessment of the stability of PF-MFT as it dries.

Determination of the MBI of PF-MFT enhances understanding about how the polymer functions during flocculation. Findings of elevated MBI post-flocculation suggest that the polymer used may provide reactive surfaces that exceed those provided by the clay minerals present and result in PF-MFT exhibiting hydrophilic characteristics post flocculation.

While certain anionic polymers, have been used to create linkages between the clay minerals (Ferrera and Pawlik 2009), the ability for similar polymers to liberate and disperse bitumen has been observed by this paper's authors in lab trials and has been documented by Arinaitwe (2013) and Gutierrez (2013). Where bitumen dispersion is observed, Raman Spectroscopy is used to identify the functional groups present in the bitumen released

either in “free” form or deposited on the surface of the flocculated clay minerals in PF-MFT.

Rheology

Rheological characterization of PF-MFT facilitates understanding not only of the material’s flow characteristics during and after deposition, but also enhances understanding of the viscoelastic properties that likely exist if PF-MFT remains in a saturated or near saturated state. The peak yield stress of PF-MFT is determined using a vane rheometer with wide gap geometry. Simple slump tests are also completed to get a sense of the flow characteristics of PF-MFT.

Visco-elastic material properties are determined using oscillatory flow rheology that also enables the phase of the PF-MFT (i.e. liquid or solid state) to be verified. This characterization is very important as it will inform design and modification of models used to analyze the overall performance of PF-MFT under a range of field conditions.

Primary Geotechnical Testing

Given the complexity of PF-MFT as a synthetic material, this characterization framework makes a clear distinction between primary and secondary geotechnical testing. Primary geotechnical testing measures the engineering response of the bulk material. Test methods include use of a field vane to obtain peak and residual “strength” values, cone penetrometer testing (static and dynamic if available), and determination of the Atterberg limits using the Cassagrande cup method.

A modified plate load test has also been devised to develop a relationship between measurements obtained with the field vane and a normal load applied at the surface of the PF-MFT. Within the proposed characterization framework, interpretation of measured values at this characterization phase is considered incomplete and lacking crucial information obtained during non-destructive imaging of the bulk sample.

Non-Destructive Imaging

Use of bulk imaging tools provides a means of looking at the microstructure of wet and dry PF-MFT. The objective of this phase of characterization is to obtain a clear image of the structures that existing within PF-MFT as it would exist after deposition and after removal of the initial water released.

Scanning electron microscopy under cryogenic conditions enables imaging of the clay minerals present in a wet sample of PF-MFT at $<1 \mu\text{m}$ scale. Using these images the nature of micro pore spaces and their physical arrangement can be investigated. The orientation and micro-fabric that exists between clay particles can also be investigated.

To probe the nature of the material fabric at a slightly larger scale, synchrotron based microtomography can be used to obtain 3-D imaging of PF-MFT. The biomedical imaging and therapy bending magnet (BMIT-BM) beamline at the Canadian Light Source Inc. in Saskatoon enables the entire domain of a 1 cm diameter by 5 mm thick sample to be imaged at an $8 \mu\text{m}$ voxel resolution using 25k electron volts (Wysokinski et al. 2007). While this technique does not characterize features smaller than $8 \mu\text{m}$, this scale of imaging allows characterization of the porosity structure, which may have significant implications for bulk water movement and evaporation.

While the presence of angstrom/sub-micron sized pores is being investigated, evidence of larger pores ($10 \mu\text{m}$ and $250 \mu\text{m}$) that are apparently disconnected, or at best connected by sub-micron sized pores, has significant implications for interpretation of field vane shear strength measurements and current estimation of consolidation parameters.

Dewatering and Material Performance

Use of a consistent and comprehensive characterization framework enhances interpretation of the individual data collected and understanding of the material as a complete system. Work by Laxton and Berg (2007) and Li et al. (2014) indicates the benefits of unifying different types of characterization data. The framework also provides a consistent means of understanding the effects of variability on the resulting material’s performance, structure, and behavior.

Comprehensive characterization of PF-MFT results in better interpretation of the complete data set and the selection and design of additional testing that may be completed to quantify porosity and dewatering rates. Enhanced understanding of the material results in better interpretation of data from more complex test methods. Furthermore, enhanced understanding of the material as a system enables selection and/or development of

performance criteria that is meaningful and accounts for the intrinsic properties of the material.

CONCLUSIONS

Operators and technology developers working in fine tailings produced at surface mines within the Alberta oil sands need a consistent way to characterize the ultimate performance of PF-MFT. The proposed characterization framework identifies the suite of information required to interpret primary geotechnical test data and to enhance understanding of the chemical and/or physical mechanisms affecting ultimate material dewatering. The combined results guide selection and interpretation of results from more sophisticated geotechnical testing and enhance development of effective and representative models designed to evaluate ultimate dewatering characteristics.

While it is true that much of data required in the proposed characterization framework already exists, the framework suggests the data must be unified to ensure the accuracy of any conclusions drawn about the ultimate performance of and associated costs related to PF-MFT.

REFERENCES

Azam, S. and Scott, J.D. 2005. Revisiting the Ternary Diagram for Tailings Characterization and Management. *Geotechnical News*, December 2005: 43-46.

Beier, N., Wilson, W., Dunmola A., Segó, D. 2013. "Impact of Flocculation-Based Dewatering on the Shear Strength of Oil Sands Fine Tailings" *Canadian Geotechnical Journal* 50: 1-7.

Caldwell, J., Revington, A., McPhail, G., Charlebois, L. 2014. Optimized seasonal deposition for successful management of treated mature fine tailings. In *Paste 2014*, Vancouver, June 8-12.

Charlebois, Lawrence E. 2012. "On the Flow and Beaching Behaviour of Sub-Aerially Deposited, Polymer-Flocculated Oil Sands Tailings: A Conceptual and Energy-Based Model." Master's Thesis. Mining Engineering, University of British Columbia, Vancouver, December.

Derakhshandeh, B. 2014. Rheological Analysis of Flocculated Suspensions. Coanda Research & Development Corporation, August.

Estepho, M. 2014. Seepage Induced Consolidation Test: Characterization of Mature Fine Tailings. Master's Thesis. Mining Engineering, University of British Columbia, Vancouver, January.

Fenderson et al. 2013. Understanding dewatering limits of polymer flocculated oil sands mature fine tailings. TWM, Banff, November 3-6.

Ferrera, V., and Pawlik, M. 2009. "Flocculation of Oil Sands Tailings," Proceedings from the Conference of Metallurgists, Sudbury, ON, August 23-26.

Fine Tailings Fundamentals Consortium (FTFC), ed. 1995. *Advances in Oil Sands Tailings Research*. I-IV Vol. Edmonton, Alberta: Alberta Department of Energy, June.

Gutierrez, L. 2013. A Role of Humic Mater and Ore Oxidation in Rheology of Oil Sands Slurries and in Bitumen Extraction. PhD Dissertation. Mining Engineering, University of British Columbia, Vancouver, April.

Kabwe, L., Wilson, G., Donahue, R. 2013. "Determination of geotechnical properties of in-line flocculated fine fluid tailings for oil sands reclamation." *Tailings and Mine Waste*, Banff, November 3-6.

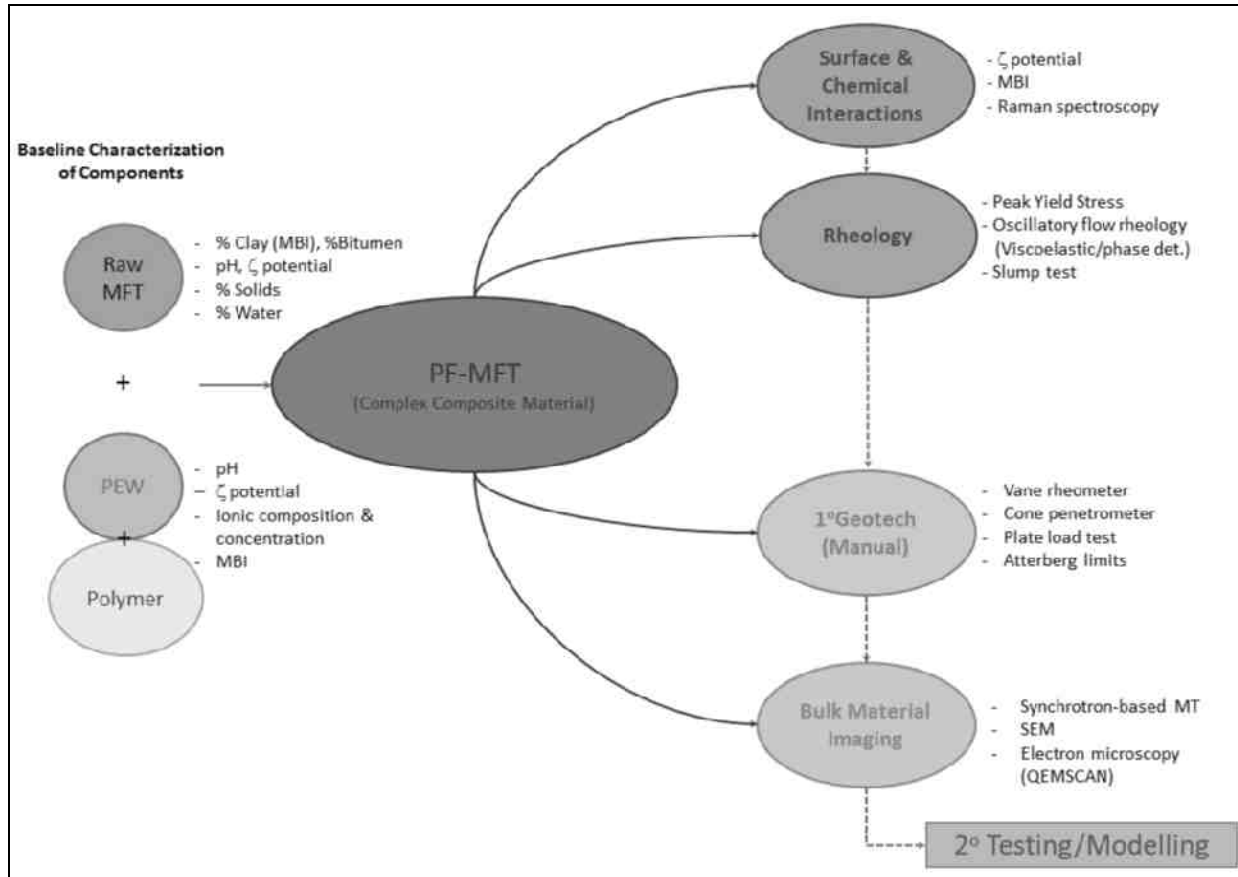
Laxton, P. B. and Berg, J.C. 2007. "Investigation of the link between micromechanical interparticle bond rigidity measurements and macroscopic shear moduli of colloidal gels." *Colloids and Surfaces A: Physicochemical Engineering Aspects* 301: 137-140.

Li, X., Zhang, L-M., Wu, L-Z. 2014. A Framework for Unifying Soil Fabric, Suction, Void Ratio and Water Content during the Dehydration Process. *Soil Science Society of America Journal*, vol. 78 No. 2: 387-399.

Masliyah, J., Czarnecki, J., and Xu. Z. 2011. *Handbook on Theory and Practice of Bitumen Recovery from Athabasca Oil Sands*. Volume I: Theoretical Basis. Kingsley Publishing.

Matthews, J., and S. Masala. 2009. "Tailings Research at Shell's Muskeg River Mine Tailings Testing Facility."

- Mewis, J. and Wagner, N. 2012. *Colloidal Suspension Rheology*. Cambridge: Cambridge University Press.
- Mikula, R. 2012. "Evaluation of Off the Shelf and Off the Wall Tailings Treatment Technologies: A Cautionary Tale". Third International Oil Sands Tailings Conference. December 2-5. p231f.
- Miller, W. G. 2010. Comparison of Geoenvironmental Properties of Caustic and Noncaustic Oil Sand Fine Tailings." PhD Dissertation, Department of Civil and Environmental Engineering, University of Alberta, Fall.
- Mitchell, J.K. and Soga, K. 2005. *Fundamentals of Soil Behavior*. 3rd Ed. Hoboken: John Wiley & Sons.
- Morin, M. 2008. AST Methylene Blue Procedure: Sludges and Slurries. Ottawa, ON: Natural Resources Canada, Canada Energy Technology Centre, Advanced Separation Technologies, Tailings and Emulsions.
- Pecini, E., and Avena, M. 2013. Measuring the Isoelectric Point of the Edges of Clay Mineral Particles: The Case of Montmorillonite. American Chemical Society, *Langmuir*, 29, 14926-14943.
- Salehi, M. 2010. Characterization of Mature Fine Tailings in the Context of its Response to Chemical Treatment. Master's Thesis, Chemical & Materials Engineering, University of Alberta, Edmonton.
- Scales, P. 2013. The Yield and Flow of Clay-non Clay Suspension Mixtures. 3rd CONRAD Clay Conference, Edmonton. February 20-21.
- Scott, J.D. et al. 2013. "Properties which affect the consolidation behavior of mature fine tailings." *Tailings and Mine Waste*, Banff, November 3-6.
- Sobkowicz, J. C., and N. Morgenstern. 2009. "A Geotechnical Perspective on Oil Sands Tailings." *Tailings and Mine Waste*, Banff, November 1-9.
- Suncor. 2013. "Tailings Management." Suncor Energy, www.suncor.com/en/responsible/3229.aspx#process, accessed on 25 September.
- Taina, I., Heck, R. and Elliot, T. 2008. Application of X-ray computed tomography to soil science: A literature review. *Can. J. of Soil Science*. 88: 1-20.
- Vietti, A. Clay Mineralogy and Water Chemistry on Tailings Settling and Rheology. Presentation at 2011 CONRAD Clay Conference, Edmonton, March 9-10.
- Wells, P.S. 2013. Clays and Oil Sands Tailings an Industry Perspective. Presentation at CONRAD Clay Conference, Edmonton, February 20-21.
- Wells, P.S., Revington, A. and Omotoso, O. 2011. "MFT Drying – Technology Update," in *Tailings and Mine Waste*, Vancouver, November 6-9.
- Wysokinski, T. et al. 2007. Beamlines of the biomedical imaging and therapy facility at the Canadian Light Source-Part 1. *Nuclear Instruments and Methods in Physics Research A*, Vol. 582, pp. 73-76.
- Yao, Y. van Tol, F. and van Paassen, L. 2012. The Effect of Flocculant on the Geotechnical Properties of Mature Fine Tailings: An Experimental Study. 3rd IOSTC, Edmonton, December 2-5.
- Znidarcic, D., van Zyl, D., Fredlund, M. and Wells, S. 2011. "Consolidation Testing of Oil Sand Fine Tailings." *Tailings and Mine Waste*, Vancouver, November 6-9.
- Znidarcic, D. 1999. Predicting the behavior of disposed dredging soils. Twelfth European Conference on Soil Mechanics and Geotechnical Engineering proceedings, vol. 2, p. 877-885.



Flowchart 1. Proposed Characterization Framework for PF-MFTs and Their Input Components

Session 8

Tailings Management II

MINING CUT-OFF GRADE POLICY AND TAILINGS PRODUCTION: COULD AN OUNCE OF PREVENTION BE WORTH A POUND OF CURE?

Ursula Thorley

Queen's University, Kingston, Ontario, Canada

ABSTRACT

Planning oil sands mines poses many challenges including the storage and treatment of fluid fine tailings (FFT) resulting from the bitumen extraction process. This paper explores the concept of mineable “ore” (the definition of a process cut-off grade) and presents a new research program that examines opportunities for improvements to the definition of ore in oil sands mining by explicitly considering tailings production potential.

The technical and economic concept of mineable ore in both an oil sands specific and a wider mining context is explored. Alberta *Directive 082*, governing the definition of mineable oil sands ore, and analogous approaches to the process cut-off decision from other commodities and jurisdictions are discussed. The economic and technical considerations involved in the best-practices definition of ore are reviewed. Consideration is paid to whether *Directive 082* may exacerbate tailings production.

A research program that aims to develop a new framework for defining oil sands ore is described. The research will explicitly consider bitumen recovery and tailings production associated with variable ores, including the explicit and implicit costs associated with FFT. The framework will incorporate these technical and economic considerations in defining ore to better support the mining and processing decision. Data limitations and a methodology for assessing the impact of this new framework on mine plans will be discussed.

INTRODUCTION

Background

Alberta's *Interim Directive 2001-7 Operating Criteria: Resource Recovery for Oil Sands Mine and Processing Plant Sites (ID2001-7)* was introduced in 2001. In 2013 the Interim Directive

was renamed Alberta *Directive 082: Operating Criteria: Resource Recovery for Oil Sands Mine and Processing Plant Operations (082)*, but otherwise remains unchanged from its introduction in 2001 (Alberta Energy Regulator, 2013).

The purpose of *082* is to define minimum criteria by which oil sands operators identify both the oil sand they are to mine and the amount of bitumen they are expected to recover from the mined oil sand. Previously, the individual operators negotiated operating criteria on a site-by-site basis.

As part of the broader set of regulations which exist under the *Oil Sands Conservation Act*, *082* is intended to reduce the potential waste of oil sands resources. This is presumably achieved by maximizing the amount of mineable bitumen that is processed while creating a predictable and evenly applied set of regulations under which oil sands mines operate.

The main stipulations of *082* with respect to bitumen recovery are:

- An in situ ore cut-off grade of 7% bitumen by weight.
- A minimum separable mining seam thickness of 3m, ore or waste.
- A minimum pit crest limit defined by a total volume to bitumen in place (TV/BIP) ratio of 12.
- A variable processing plant recovery based on the average bitumen content of the ore equal to 90% if the average bitumen content of the as-mined ore is 11% bitumen or greater, and defined by the following equation where x is the average % bitumen of the as mined ore when the average grade is below 11%

$$\text{Recovery} = -202.7 + 54.1(x) - 2.5(x^2)$$

The criteria are not enforced individually. Rather, each operator is responsible for ensuring that they have met the equivalent volume of bitumen

production indicated by the criteria on an annual basis.

A prescribed regulatory definition of ore is very rare in practice. The reasons that regulatory definitions are generally not pursued include: significant variation among mined deposits, even those that may share the same formation environment; the impact of dynamic economic forces on profitability; and the impact of technology advances on performance. Static criteria may also introduce a potential disincentive to continuous improvement.

Beyond the unusual nature of prescribing a regulatory definition of ore, the specific criteria defined under 082 are outdated from the perspective of modern mine planning. Some of the issues include:

- Criteria for defining pit limits and mineable ore and waste zones that are outdated. The criteria defined by 082 are appropriate to mine planning in the era before the widespread availability of powerful desktop computers and sophisticated mine planning software.
- No explicit consideration of the factors influencing bitumen recovery beyond ore grade. Other influencing factors include fines, clays, and ultra fines, chlorides, etc. Explicit modeling of recovery is now standard in metal mining and has been in use on a best-practices basis for over twenty years.
- No explicit consideration of the role of fines, clays and ultra-fines in the generation of fluid fine tailings, or of the economic and environmental liabilities associated with fluid fine tailings production. The consideration of variable waste costs associated with different ore types is critical to establishing economic cut-off grades and is widely employed by mining operations outside of the oil sands.

These issues are beginning to emerge in the scientific literature. Potential issues associated with 084 and proposals to address some of these issues, particularly as they relate to the concepts of mining selectivity and reserve modeling, have been presented (Chunpongtong, 2014; Manchuk et al, 2014; Thorley, 2012). The focus of the proposed research is on the consideration of tailings production in defining ore.

MODERN MATERIALS MANAGEMENT

Ore has many definitions, but most are firmly rooted in economics. When considering mineable deposits ore can be defined as any aggregation of metallic or non-metallic material that produces a profit when mined, processed and sold. A key concept is that each block of ore must carry its own costs; high-value material should not be used to subsidize sub-economic material.

The concept of ore control has undergone significant evolution in the last two decades. This evolution has been driven by improvements in available computing power, improved programming techniques, and the availability of commercial software packages for geologic and geostatistical modeling and mine planning. At most advanced mining operations the days of materials routing using a simple sample grade, an average process recovery, and uniform ore and waste mining costs are long past.

A typical metal mine may consider the following when determining the routing destination for a mining block. The list is not meant to be exhaustive:

- The grade of the material.
- The expected process recovery for the material. There may be multiple process options, each with distinct recoveries, throughput times, and costs. Recoveries may vary depending on the degree of weathering of the ore where it has been stockpiled.
- The haulage costs associated with routing the block as ore or waste.
- The treatment costs if the block is routed as ore.
- The costs associated with reclamation if the block is treated as ore or waste.
- The net return associated with the block once mining, processing, reclamation, transportation, treatment charges, etc. are considered.

The routing decision is supported by significant data relating to the physical properties of the materials including the ore type, the grade, expected fragmentation, grinding effort, reagent consumption during processing, expected recovery, impact of the material on the process (for example “preg-robbing” gold ores), the presence of deleterious materials (which may incur treatment penalty charges), etc. Normally, every blast hole is

sampled in ore, and at mines with environmental challenges related to acid rock drainage waste holes may also be sampled routinely.

Clearly, the definition of a “cut-off grade” can be quite complex and a significant body of literature exists in the fields of cut-off grade optimization specifically and mine optimization generally. A one-size fits all approach is not valid from a technical or economic standpoint.

As an example, Newmont Gold successfully moved in the 1990’s towards the integration and optimization of their Nevada operations (Clark and Dagdelen, 2007; Dagdelen and Kawahata, 2007; Hoerger et al, 1999). At the time the company operated 16 open pit mines, 4 underground mines, and 19 process facilities. The mines contained over 90 metallurgical ore types and over 60 potential process path options. Variable mine sequences, variable cut-off strategies, the cross-shipment of ore were all implemented as a result of the work. Significant savings, project value increases and synergies have been reported and Newmont, and other companies, have continued to fund research in this area and implement the results of the work.

MATERIALS MANAGEMENT AND THE OIL SANDS

Planning oil sands mines poses many challenges including the storage and treatment of fluid fine tailings (FFT) resulting from the bitumen extraction process. In recent years tailings storage and treatment have emerged as significant issues with respect to the public’s perception of the industry. Increased government scrutiny of the tailings issue, and the introduction of Alberta’s *Directive 074: Tailings Performance Criteria and Requirements for Oil Sands Mining Schemes* have undoubtedly increased the costs associated with tailings for all oil sands operators.

Despite the prominent role tailings considerations play in oil sands mine planning, 082 does not appear to include any consideration of tailings production, management, treatment, or prevention. This is problematic given that in oil sands mining 082 largely replaces the strategic considerations that drive materials management in the broader mining industry. Management of tailings begins in the mine with the definition of ore, not in the plant with the treatment of that ore.

It is not clear that the impacts of the directive on the performance of oil sands mines have been broadly assessed, but specific aspects of the directive have been analyzed. The potential limitations of 082 with respect to reserve calculations have been assessed using a nonconfidential data set (Chunpongtong, 2014).

By employing a narrow approach to the definition of ore (i.e. the operating criteria) the directive opens the possibility of unintended consequences with respect to the technical, environmental and economic performance of the oil sands. 082 ignores the consideration of well-documented variations in bitumen recovery among ore facies, instead favouring an “averages” approach. It also ignores the environmental and economic impacts of variable tailings production associated with different ores. It is quite likely that these issues were not considered important when the directive was originally conceived, developed and released as *ID2001-7*.

Potential concerns with the application of 082 related to waste production and specifically tailings generation include:

- Production of fluid fine tailings (FFT), which may render some material uneconomic. This FFT production is associated with a requirement to material that meets a bitumen content criterion but ignores the associated tailings production, which is variable and not dependent on bitumen content. Dilution of profit through the requirement to process sub economic ore may increase the total bitumen recovered, but it reduces the financial capacity of the mine developer to invest in other aspects of the business.
- Potential disincentive to increase resource recovery and utilization through expanded pit limits (higher TV:BIP ratio). This may actually reduce the total bitumen recovered.
- Potential disincentive to define the economic and environmental costs associated with the processing of different materials when the environmental costs associated with bitumen processing and FFT from certain processed materials are explicitly considered in defining ore.

The relationship between the properties of the various facies and both bitumen recovery and tailings production is significant. Ignoring these relationships under 082 is akin to a gold mine developing plans which ignore the variations in

gold recovery by ore-type, ignore the acid-generating and neutralizing potential of their various materials, and ignore the role of preg-robbing carbonaceous ores. There exists the potential to explore modern materials management practices to improve the performance of oil sands mines.

PROPOSED RESEARCH PROGRAM

A research program is proposed that will explicitly consider bitumen recovery and tailings production associated with variable ores, including the explicit and implicit costs associated with FFT. The research takes a broad view of the cut-off grade question and seeks to incorporate technical and economic considerations in defining oil sands ore. The research is underpinned by a belief that tailings production and management must begin with geology and be an explicit consideration in mine planning.

The hypothesis of the research program is that current mine planning approaches, developed in compliance with 082, result in sub-optimal mine planning and mine development. The plans may be sub-optimal in the context of government goals for resource development (rational, beneficial resource utilization); corporate goals for resource development (profit and shareholder return); and social expectations related to resource development (net-positive benefit and limited environmental impact). This sub-optimal performance is the direct result of the directive removing a robust consideration of economic and technical criteria from strategic mine planning decisions.

The goals of the research program include:

- Development of a mining model framework that incorporates technical and economic considerations in defining ore in order to better support the mining and processing decision. Rather than focusing solely on bitumen content the model framework will include recovery and tailings production, amongst other considerations, in the calculation of mining block value.
- Generation of mine plans using the new model framework and modern approaches to pit limit analysis and mine sequencing.
- Assessment of the performance of these plans vs. traditionally generated mine plans. The

assessment will consider: bitumen recovery/conservation; FFT production; mine footprint, including eventual reclamation activities; economic performance; and, other criteria as identified.

The framework will incorporate these technical and economic considerations in defining ore to better support the mining and processing decision.

One of the key questions the research seeks to answer is the impact that the criteria defined under 082 have on FFT production. The potential for “ore” as defined under 082 to actually be sub-economic when tailings production is considered will be explored. This is an important goal of the research, given the significant differences in the properties of the ore bodies under development in 2014 versus the ore bodies under development in 2001, when the directive was originally issued and on which the technical criteria were undoubtedly based.

The proposed research will rely on being able to identify the unique characteristics of individual mining blocks. As a result simulated or simplified data sets, average values and correlation-relationships will need to be replaced with the development of detailed data sets related to ore characteristics (including geologic and processing characteristics), costs (including those related to mining, processing, reclamation, and tailings treatment activities), and tailings production. The demands for these data are beyond what is normally incorporated in mine planning and will involve significant work to develop.

SUMMARY

- *Directive 082* establishes the criteria by which oil sands operators define ore, or the material they will route to their process plants.
- 082 relies on the modeling of average conditions, and does not consider variations in recovery associated with different ore types.
- 082 employs dated and simplified approaches to ore body modeling and cut-off definition/materials management that are not consistent with best-practices in modern mine planning.
- 082 does not consider the important question of tailings production in defining ore.
- The proposed research program will seek to develop a more holistic definition of ore by including a meaningful consideration of

bitumen recovery and tailings production, amongst other considerations.

- The proposed research program will assess the performance of a modernized approach to materials management for an oil sands mine relative to the performance of plans developed under the stipulations of 084.

REFERENCES

Alberta Energy Regulator, 2013. *Directive 082: Operating Criteria: Resource recovery requirements for oil sands mine and processing operations*. Edmonton, Alberta: Alberta Energy Regulator.

Chunpongtong, L., 2014. Overestimation of oil sands mining reserve caused by an archaic algorithm. *CIM Journal*, Vol.5, No. 3: 180-184.

Clark, L., and Dagdelen, K., 2007. Finding added value at Newmont through large-scale mining sequence, cutoff grade and process optimization using mixed integer linear programming. *SME Annual Meeting Preprint No. 07-004*, Denver, Colorado.

Dagdelen, K., and Kawahata, K. 2007. Cutoff grade optimization under complex operational constraints for open pit mines. *SME Annual Meeting Preprint No. 07-085*, Denver, Colorado

Hoerger, S., Hoffman, L., and Seymour, F., 1999. Mine planning at Newmont's Nevada operations. *Mining Engineering*, January, 1999, 5pp. Retrieved from onemine.org.

Manchuk, J.G., Babak, O., Deutsch, C.V., 2014. Numerical modeling of mining selectivity for oil sands. *CIM Journal*, Vol.5, No. 3: 159-170.

Thorley, U., 2012. Oil sands mine planning and design: Analysis and system modeling of conventional and oil sand applications (Ph.D. thesis).

INTRODUCING A HOLISTIC APPROACH FOR THE OPTIMIZATION OF TAILINGS SYSTEM

Houssein Kheireddine and Chiron Mukherjee
DNV GL, Katy, Texas, U.S.A

ABSTRACT

To maintain bitumen production in a sustainable manner tailings management is an important aspect of the process not only from an environmental standpoint but also from a production efficiency perspective. In DNV GL's work processes, methodologies incorporating cutting edge technology have been developed in order to measure risk and optimize performance. This has been implemented in a case study that will be discussed in this paper.

The objective of the case study is to demonstrate how to evaluate the availability of the tailings system taking into account the reliability, maintenance, design, configuration, and operational constraints of critical equipment needed to transport sands, fines, and water to the tailings deposition area. Also, risk ranking of the tailings system will be performed in order to highlight major contributors to availability losses. This paper will also quantify the impact of the tailings system on the production facility of the integrated oil sands development. A set of sensitivity cases will be evaluated in order to optimize the tailings system design and configuration.

Finally, the proposed approach can be used to help make critical management decisions regarding the tailings system. For example, the study will aim to identify opportunities to improve overall availability or debottleneck the system and assess whether adding additional equipment or lines would optimize overall performance.

INTRODUCTION

Along with proper plant design, asset management is a critical function of process development. It sets the basis for risk and economical evaluation. Each asset has unavailability associated with it. This unavailability comes as a result of unplanned and planned downtime. Predicting site-wide efficiency on an individual asset basis is not only time and energy intensive, it often leads to under or over

prediction of its impact on the overall system performance. Therefore, asset managers must target a more holistic approach for better utilization and risk assessment of a particular unit or system.

Plant owners and operators often seek new and creative opportunities to improve operational performance/efficiency yielding in an increase in production. The desire to keep the plant running at minimum cost and maximum production is usually faced with multiple challenges. It is impossible to reach optimal plant operation without the complete understanding of the system behavior or unit interactions as a whole. Reliability, availability, and maintainability (RAM) analysis is often conducted in order to provide a quantitative assessment of the level of performance that may be expected from the system as a whole over the design life. This analysis will also identify major systems, activities, and bottlenecks that contribute to production losses, as well as evaluate alternative design configurations to allow assessment and optimization of sparing philosophies and, in particular, storage volumes.

Because oil sands systems are complicated, assessing the performance metric of the system based on bitumen production efficiency only is not sufficient. As tailings are waste by-products of bitumen production, the availability of the tailings system is another important aspect of the performance metric that must be evaluated. This work will introduce a systematic approach to quantify the impact of tailings system downtime on the bitumen production as well as evaluate tailings system alternative design configuration to optimize its availability.

APPROACH

This section will introduce the generic approach used to conduct RAM analysis at DNV GL. Probability based simulation software, such as TARO (Total Asset Review and Optimization), software is usually used to run complicated RAM studies. It is a probability based simulation software. It analyzes event generations in order to

predict achievable asset performance and overall production. It is a very powerful tool that allows simulators to model complex systems based on raw data in order to assist with decision making in design, operation, and maintenance activities. It takes into account probable events that may affect production, and identify bottlenecks in the system. Not only does it aid the user in acquiring a better understanding of the system connectivity and unit

interdependencies, but it also assists with the generation of alternative designs and configurations. In this study, TARO will be used to rank assets by criticality of production, as well as design optimization. Figure 1, Modeling Strategy, is a schematic illustration of the proposed approach.

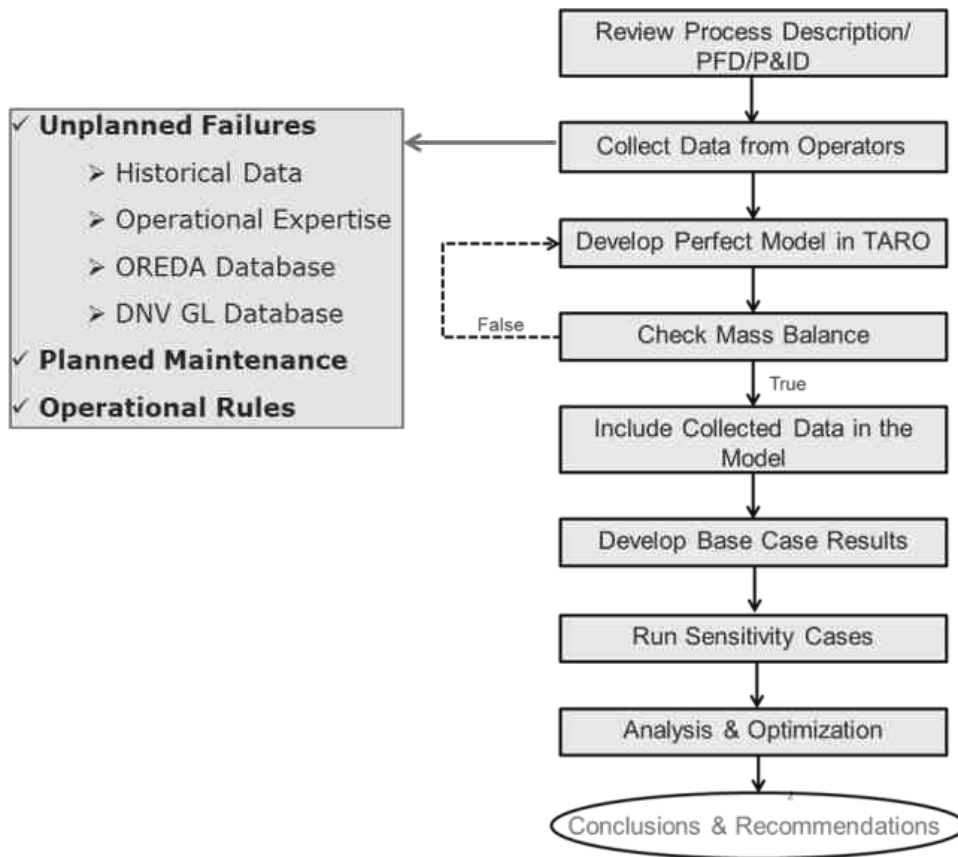


Figure 1. Modeling Strategy

A thorough revision of process description is an important first step for model development. Other initial documents to be reviewed include block flow diagram (BFD), process flow diagram (PFD), piping and instrumentation diagrams (P&ID), mass balance, and basis of design. This step helps the user to better understand the system, asset functioning mode, and sparing philosophies. Then, operational rules, maintenance strategies, and historical performance data (if available) will be collected and reviewed. A combination of site-specific historical failure data, data from similar assets operated by the same company and industry-typical data is recommended.

TARO simulation of a “perfect model” will be initiated. This could be done at equipment or unit level. The main concern at this stage is to model the correct flow sequence as well as feed and product ratios. Note that “perfect model” is the model that does not include any planned or unplanned downtime. This way, a maximum production is achieved. This should allow for validation of the mass balance in TARO compared to the actual mass balance provided. After the perfect model is validated, reliability and maintenance data will be included in the model.

After the Base Case model is built. Base Case preliminary results will be generated and analyzed. Based on preliminary results, sensitivity cases will be normally conducted around major contributors (unit/equipment) to production efficiency losses. Then, analysis and optimization of system performance will be executed. This is followed by development of conclusions and recommendations that intend to help make critical management decisions.

The key metric normally utilized to measure the performance of a system will be production efficiency and availability.

Production efficiency is the weight based proportion of production rate that can be expected over the normal production rate, and it will be calculated using the following equation:

$$\text{Production Efficiency (\%)} = \frac{\text{Predicted Achieved Production}}{\text{Normal Production}} \times 100$$

Predicted achieved production refers to the system production rate taking into account both planned and unplanned downtime. While normal production rate is the maximum production rate that could be achieved excluding the impact of any downtime.

Availability is the proportion of time that an equipment or unit is available to perform a required function under stated conditions. Availability is a function of equipment/unit reliability, maintainability, equipment configuration, logistical delays, mobilization of maintenance personnel, restart delays, including all planned and unplanned non-productive time. This value will not exceed 100%. It will be calculated using the following equation:

$$\text{Availability} = \frac{\text{Up Time [Mean Time Between Failures]}}{\text{Total Time [Up time + MTTR + Mean Logistic Delay]}}$$

Note that the availability of a unit/equipment does not account for the impact of other units/equipment on it.

STUDY CASE

In order to illustrate the applicability of the proposed approach, a high level oil sands system model is developed. Then, sensitivity analysis will be evaluated in order to optimize the tailings system design and configuration.

Note that the following description, assumptions and reliability data used to develop the base case do not mimic a specific site or project. They are hypothetical, and used for illustration purposes.

Base case

Oil sands ore is excavated by shovels and loaded into trucks in the mining area. Then, ore is transported to the ore preparation unit (OPU) where it is crushed and conditioned before entering the extraction unit. Extraction unit consists of two separation units to separate untreated bitumen, water, sands, and fines. Two tailings streams A and B of distinctive compositions are sent to the external tailings area. Tailings A stream leaves the bottom of first separation stage, and it is primarily composed of sands and fines. Tailings A stream is sent to Tailings A system/area. Tailings B stream leaves the bottom of the second separation unit and it is mainly composed of water along with oil, sands, and fines. Tailings B stream is sent to Tailings B system/area and a back-up route that connects Tailings B stream to Tailings A stream is built. The untreated bitumen is then directed to bitumen treatment unit (BTU) where solvent is used in order to remove any residual water, sands, and fines. Treated bitumen is finally stored and shipped via pipeline for further separation. Refer to Figure 2 Site-Wide Block Flow Diagram.

Key assumptions:

- System life is assumed to be 30 years
- System normal bitumen production capacity is 100 thousand barrels per day (KBD)
- In case of Separation II downtime, 10% bitumen production loss is expected (Back-up route)
- Storage and Shipping availability is 100%
- Utility System is assumed to be 100% available
- Tailings A system downtime will cause 100% bitumen production loss
- Tailings B system downtime may or may not cause 10% bitumen production loss (depending on the scenario-refer to the table 1)
- Because of the extensive planned maintenance required for such systems, planned downtime is assumed to contribute 15% absolute production losses

Schematic flow diagram of tailings system A and B is shown in Figure 3 Tailings System Configuration. Table 1 Tailings System Operating Scenario summarizes the operational logic for the tailings system.

Table 2 Base Case Reliability Data shows the availabilities that were used in the model.

Note that since TAP line is spared, so TAP planned downtime is assumed to not have impact on bitumen production.

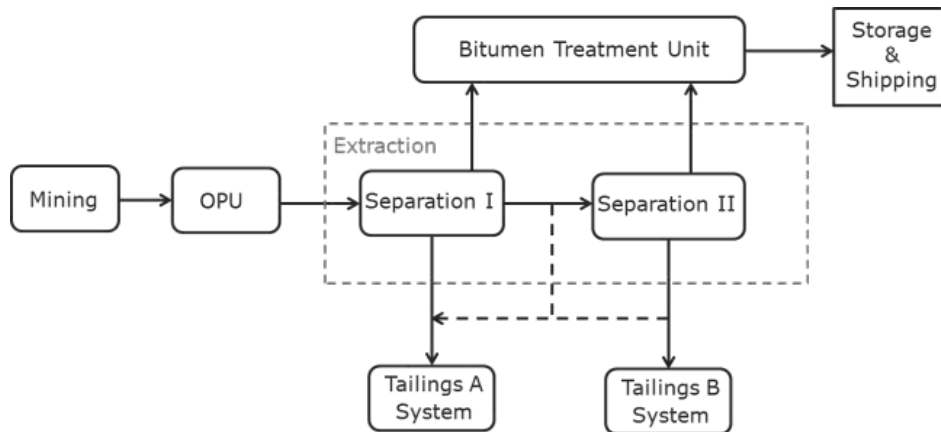


Figure 2. Site-Wide Block Flow Diagram

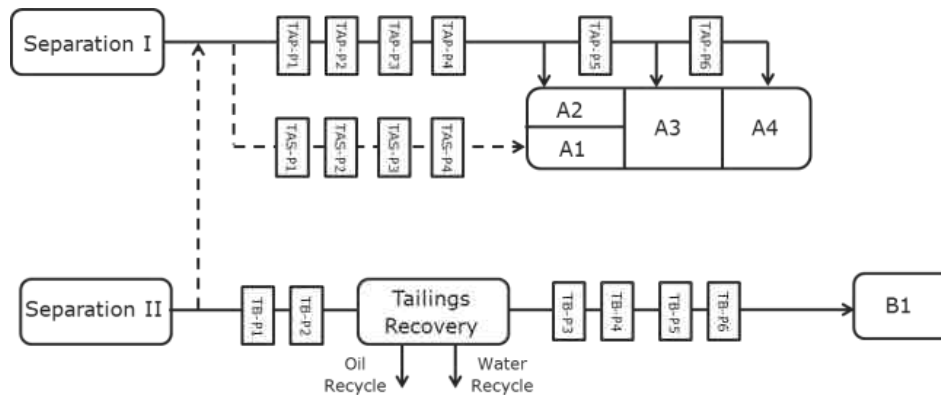


Figure 3. Tailings System Configuration

Base Case Results

The following results were obtained:

During the 30-year system life, the average production efficiency for oil sands development is predicted to be 65.6%. This corresponds to an expected average bitumen production of 65.6 KBD. Production losses include complete system

outages as well as periods of degraded production, and it is expected to be 34.4%. This is equivalent to 125.6 days' worth of bitumen production losses. Refer to Table 3 Base Case Result Summary for comparison.

Figure 4 Criticality Breakdown Pie Chart details the contributors to production losses by system. The average absolute loss of bitumen production is

predicted to be approximately 34.4%, which is associated with the high level breakdown of key contributors to such losses.

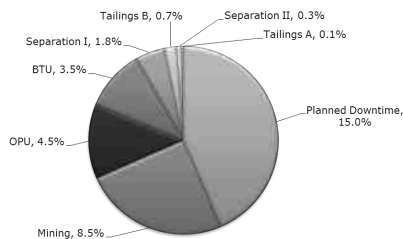


Figure 4. Criticality Breakdown Pie Chart

The planned downtime is the key contributor to production losses, accounting for approximately 43.6% of the total predicted losses (15.0% absolute). This is followed by Mining which contributes 8.5% of absolute bitumen production losses. The OPU alone accounts for 12.9% of the total predicted losses (4.5% absolute).

The tailings system cumulatively contributes 0.75% absolute bitumen production losses. Tailings A system only contributes 0.10% absolute production loss. The main reason is that the risk of simultaneous outages of TAP and TAS is relatively negligible (4 out of 8 pumps will need to be simultaneously down). A total of 0.65% absolute losses are incurred by Tailings B system. These losses are due to TB-P1 downtime which causes 10% bitumen loss.

Note that parts of the tailings system can be unavailable and although this does not have an impact on bitumen production, it may implicate that tailings cannot be deposited appropriately into specific tailings ponds. For instance, although the tailings system only contributes 2.2% of the total bitumen production losses, low availability of the tailings system may cause tailings management difficulties and eventually long term production constraints on the main plant.

Availability Results

For availability results refer to Figure 5 Availability Results Summary.

Sensitivity Case I

Sensitivity case I assumes that TAS does not exist. This sensitivity is performed in order to assess the impact of TAS on bitumen production. A total of 63.2 KBD bitumen production is achieved. This is equivalent to an increase of 2.4% absolute production loss. This should be followed by cost-benefit analysis to determine if the costs associated with the proposed redundant line would be justified against the incremental production increase.

Sensitivity Case II

Sensitivity Case II assumes that TB-P1 has a spare. This sensitivity is conducted in order to evaluate the impact of this spare pump on bitumen production and the Tailings B system availability. A total of 66.1 KBD bitumen production is achieved. This is equivalent to 0.5% absolute production efficiency increase. Note that 4.3% increase in TB availability is predicted. This should be followed by cost-benefit analysis to determine if the costs associated with the proposed process modification would be justified against the incremental production. Refer to Figure 6 Sensitivity Case II Availability Results Summary.

Sensitivity Case III

Sensitivity Case III assumes that a cross-over is built to connect TAS pipeline to TAP-P5. This sensitivity case does not have an impact on bitumen production. However, it has a large impact on the availability of Tailings A system. The availability to reach A3 and A4 increased by 18 and 17% respectively from the Base Case.

Although, this sensitivity does not have an impact on bitumen production efficiency, it is important to be able to manage tailings effectively within the area. In the Base Case, availability of pumping to A3 and A4 is below the target range of 75%. This means that most of the tailings will be deposited in the A1 and A2 regions causing long term problems. The cross-over helps relieve this problem and makes tailings management much easier. Refer to Figure 7 Sensitivity Case III Availability Results Summary.

CONCLUSION

Reliability analysis is a well-established methodology within the oil and gas industry, and for oil sands assets, to optimize design and help manage operational decisions. This case study demonstrates that similar methodologies can be readily applied to help tailings management tackle complex challenges. The impact of tailings

constraints on bitumen production can be predicted in terms of expected lost production and lost revenue. The availability of the tailings pumping and distribution system to deposit solids in different parts of the tailings area / ponds can also be determined. From this Base Case starting point, design and operational changes can be assessed and justified or optimized using a cost-benefit approach.

Table 1. Tailings System Operating Scenario

Item (s)	Scenario	Logic
Tailings A Primary Line (TAP)		
TAP-P1/2/3/4	2 pumps or more down	TAP Line shutdown, TAS is used as back-up route
TAP-P1/2/3/4	One pump down	Tailings A can only reach A2
TAP-P1/2/3/4/5	All pumps online	All pumps are required to reach A3
TAP-P1/2/3/4/5/6	All pumps online	All pumps are required to reach A4
Tailings A Secondary Line (TAS)		
TAS-P1/2/3/4	2 pumps or more down while TAP is down	Tailings A down causing site-wide shutdown
TAP-P1/2/3/4	one pump down while TAP is down	Tailings A can reach A1
Tailings B Line (TB)		
TB-P1	Pump is down	TB line is down causing 10% bitumen production loss
TB-P2/3/4/5/6	One pump is down while TB-P1 is online	TB line is down, Tailings B is routed to Tailings A

Table 2. Base Case Reliability Data

Unit/Item	Availability
Mining	90.9%
OPU	95.2%
Separation I	98.0%
Separation II	97.1%
BTU	96.2%
Tailings A Pump	92.6%
Tailings B Pump	94.3%
Tailings Regeneration	97.1%

Table 3. Base Case Result Summary

Model Performance Parameter	Base Case
Average Design Capacity Bitumen Production (KBD)	100
Predicted Annual Average Bitumen Production (KBD)	65.6
Annual Average Gas Production Efficiency (%)	65.6
Annual Average Gas Production Efficiency Loss (%)	34.4
Equivalent Annual Average Downtime (Days)	125.6

MINE CLOSURE PLANNING AND TAILINGS PLANNING TOOLS: SYNERGIES AND OPPORTUNITIES

Michael Alostaz¹, Julian McGreevy¹, Dylan Lee¹ and Carlo Cooper²

¹BGC Engineering
²MineBridge Software

ABSTRACT

Successful closure and reclamation planning of oil sands mines requires good understanding of the characteristics and long term behaviour of the tailings deposits included in the final landform design proposed for the mines. Nevertheless, tailings properties have an inherent variability that require considering multiple closure design options at the planning stage to accommodate the impact of the long term behaviour of tailing deposits on the performance of the closure landform. This paper explores the feasibility of using tailings planning tools and 3D software to evaluate the extent of the variation of closure landform performance based on anticipated range of tailing properties and behaviour characteristics, and to plan contingency measures to accommodate these variations.

INTRODUCTION

Closure planning is iterative. Several closure surfaces are typically required to arrive at a good design that satisfies the closure objectives. The availability of geographic information system (GIS) software, LiDAR imageries, and higher processing speed computers have made it more efficient to plan and design closure landforms in the oil sands industry. 3D tailings planning software can be used in tandem with GIS software to further expedite the process and quickly produce closure topography and designs for projects in the oil sands and other mine tailings projects.

APPLICATION OF TAILING PLANNING TOOLS IN CLOSURE DESIGN

Typically, the designer would work closely with a draftsman to design a CAD produced design of a closure landscape. Providing the designer with the tool to create the closure surface directly allows for better efficiency, examination of conceptual design

options, less iteration to arrive to the final design, and lastly, a more optimal design (ICMM 2014).

3D tailings planning software such MineBridge Software's Muck3D is typically used in the oil sands industry for tailings planning and scheduling (MineBridge 2014). However, this software has recently been applied to closure planning which one can argue is an extension of the tailings planning process.

As a tool for closure design, the software provides the closure planner with the means to quickly evaluate multiple design options for a variety of tailings properties and performance characteristics. From experience, producing designs options using 3D tailings planning software is typically 5 to 10 faster than the traditional approach. This significant time saving enables designers to consider more design options in the evaluation process, which leads to an increased closure design efficiency and accuracy (McKenna et al. 2013).

3D tailings planning software can quickly assess the volumetric and operational impacts of various design options. Such information is essential to evaluating the benefits and risks of the various closure design options under consideration and planning contingencies and mitigation measures in the design.

The software is particularly valuable for its ability to provide visual representations and apply colours, textures and geo-referenced aerial photos to the generated designs. This visual aid facilitates clear communications of design options under consideration.

There are three primary closure design areas which 3D design software could be used to support:

- Tailings facility closure design
- Overburden facility design
- Closure water management

The application of 3D design tools for each of these design areas is discussed below. These generic examples are drawn from experience in oil sands and metal mine tailings projects.

Tailings Facility Closure Design

Tailings facility design for closure in the oil sands region involves two main design components:

- Designing the facility to shed water towards a designed outlet
- Designing the facility to provide the desired closure land use.

Developing conceptual-level plans that meet these objectives has traditionally used traditional CAD tools such as Civil3D (Autodesk 2014). Now, specialized tailings modelling software provides the means to quickly model many different tailings deposition plans to identify the optimum deposition scheme that provides the closure conditions required for the internal drainage design of the closure surface. Figure 1 shows two tailings deposition schemes that will lead to different watershed designs for the closure surface.

In Figure 1a tailings are deposited from the discharge points arranged on the perimeter dyke, which would create a final tailings surface that slopes toward the central part of the deposit. At closure stage, this scheme will direct the surface water drainage toward the central part of the deposit, which will create a wetland at the center of deposit closure surface.

Alternatively, In Figure 1b tailings are deposited from the discharge point at the center of the tailings pond, which would create a final tailings surface that slopes toward the perimeter dyke. At closure stage, this scheme will direct the surface water drainage away from the central part of the deposit, which will require a collection channel around the deposit perimeter to manage the surface water runoff.

These deposition plans can be quickly integrated into the mine tailings planners deposition plans, which provides an opportunity to make the closure plans more real and better integrated into the mine and tailings plans.

Consideration of these facilities in 3D also provides opportunities to examine ways in which closure constraints may be addressed early in the tailings

deposition plan. Examples of these closure constraints include:

- Designing the Capping Material

Capping material surface over the top of final tailings surface can be generated either by hydraulic or mechanical placement. 3D tailings planning software provide the engineer the flexibility to make adjustments to the material placement to remold the capping surface such that it meets the closure goal by producing natural looking landforms (wetlands, uplands, shallow lakes, littoral zones, etc) and by controlling the direction of runoff at closure.

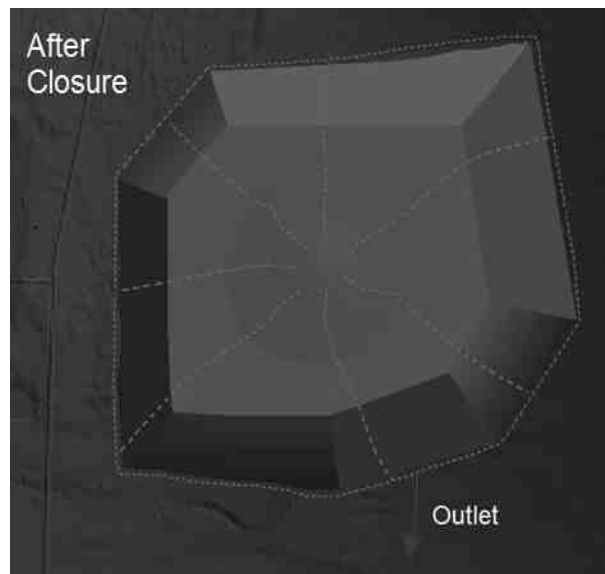
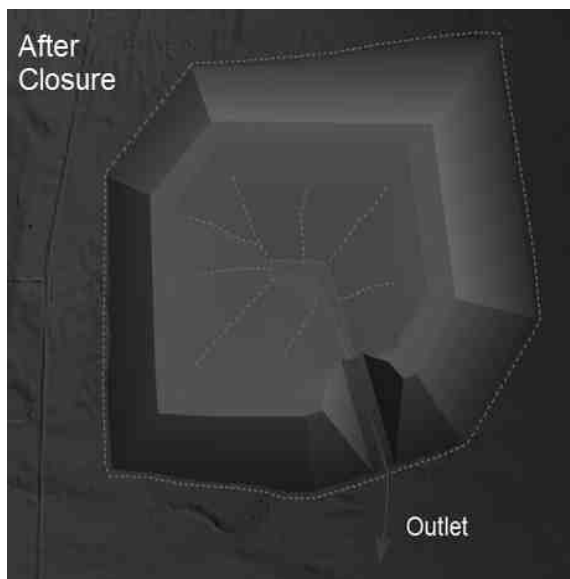
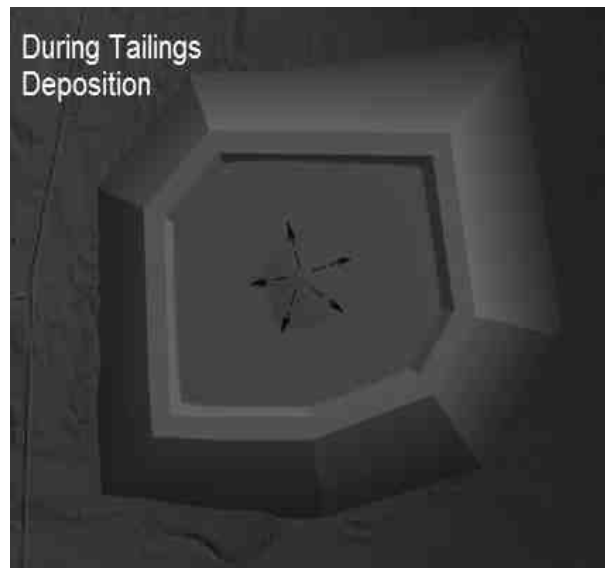
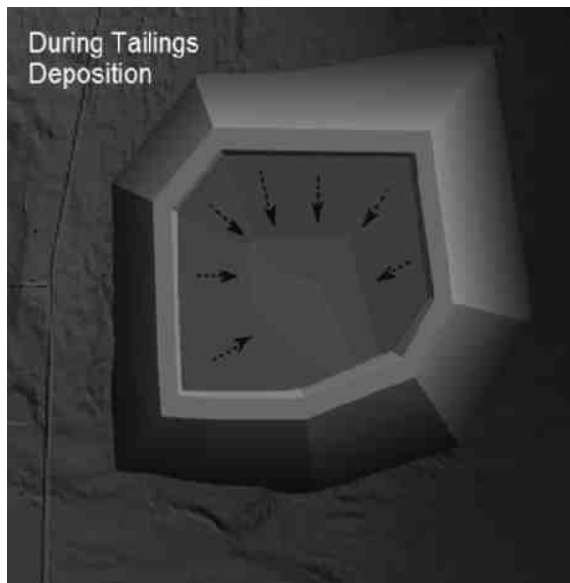
Furthermore, 3D tailings planning software provides the planner with the ability to minimize the capping material volumes required to achieve the desired surface water drainage patterns in the closed landform. This can be achieved by optimizing the tailings deposition schemes to allow increasing tailings deposition at the locations where water pending needs to be minimized or avoided. The end results are optimal locations for discharge points to pour tailings towards the eventual location of the tailings pond outlet.

- Accounting for tailings settlement / consolidation in the closure plans

Most soft deposits are expected to undergo settlement due to long term consolidation and release of tailings water (e.g. Jakubick et al 2003). Designing for settlement presents a challenge as tailings surfaces are generated to meet target volumes from a mine planning perspective and specific landform design criteria from closure planning prospective. Significant changes in the tailings surfaces can have a significant impact on the mine plans and could dictate the closure surface design by altering where the outlets or drainage are situated.

3D geometric models can be combined with consolidation modeling to:

- Identify the zones where the tailings deposit might experience higher settlement
- Generate a number of potential top of final tailings surfaces.



(a) Tailings are deposited from discharge points over the perimeter dyke

(b) Tailings are deposited from central discharge point

Figure 1. Closure drainage designs for alternative deposition schemes

Such data allows planner to identify the optimal location of drainage outlets in the closed landform. Furthermore, identifying the potential top of final tailings surfaces different tailings allows adjusting the tailings deposition schemes to provide higher tailing volumes at the areas where the deposit is expected to show higher settlement, or designing improvement techniques such as compaction to increase the density of the tailings deposit, where needed.

Figure 2 shows how compaction based on estimates of volume of material densified can be represented using 3D tailings planning tool.

By integrating closure planning into the tailings planning process, the resulting plans will be tailored towards the final closure goals, and minimize the amount of mechanical intervention that may be required at closure to achieve the desired closure surface.

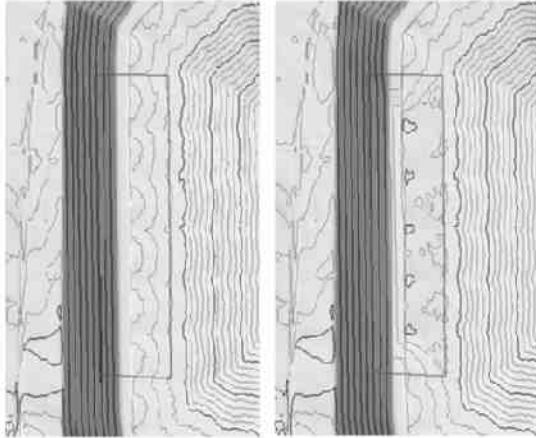


Figure 2. Surface contours before and after compaction

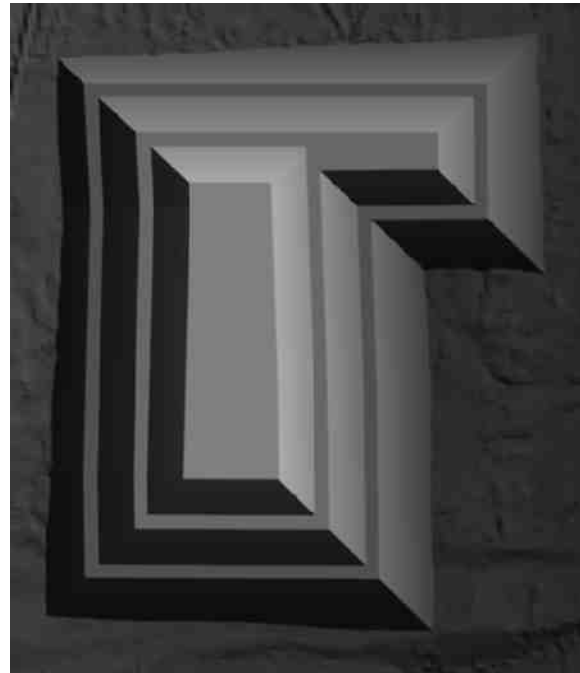
Overburden Facility Design

Overburden dump designs created for the mine plan are often adjusted for the closure design in three main ways (McKenna et al. 2011):

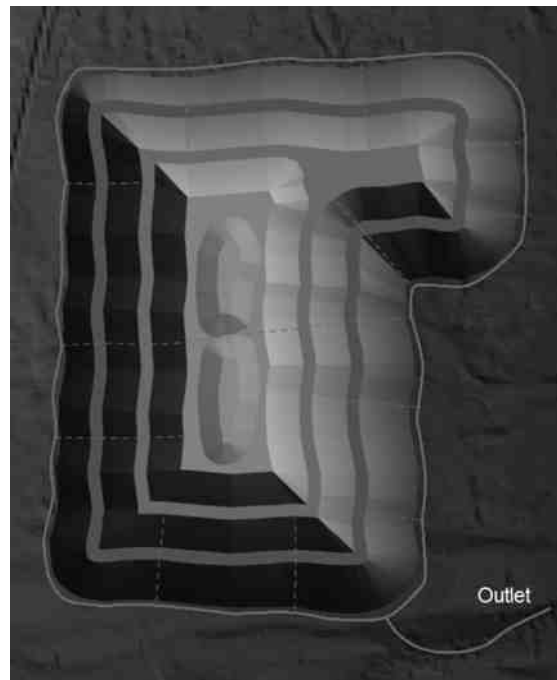
- Dump slopes are re-sloped.
- Drainage and watershed control features are incorporated into the design.
- The designs are changed to provide a natural aesthetic typical of the oil sands region.

For conceptual design, it's important to be able to rapidly develop surfaces which incorporate all three of these design features. If planners can quickly assess the volumetric impacts of the proposed changes, the closure design concepts can be evolved toward a suitable configuration which can then be considered at a higher level of detail. Figure 3 shows a dump reshaped to provide a natural aesthetic with cut/fill volumes balanced (i.e. both dumps contain the same volume of material).

With the aid of suitably specialized 3D tools, developed closure designs can be provided back to the mine planners for incorporation into the construction plan for the overburden dump. Incorporating the closure design into the initial construction design of the overburden dump reduces the cost for closure as compared to retrofitting the closure design into an already constructed overburden dump.



(a) Dump at the end of its operating life with unnatural appearance



(b) Dump reshaped to a more natural aesthetic

Figure 3. Representation of waste dump reshaping scenarios

Closure Water Management

Closure water management components including channel cuts, swales, outlets and mesotopography landform features such as breakwater islands, watershed berms, and domes are typically generated and merged onto the closure topography.

High-level design tools that provide the ability to quickly size closure channels and to integrate the channels into the surrounding landforms and natural environment allow engineers to explore different concepts and estimate the construction volumes. The cut volumes for these channels can be assessed, and the spoil dumps can be sized to ensure cut/fill balance. Figure 4 shows some closure water management features incorporated in the closure surface.

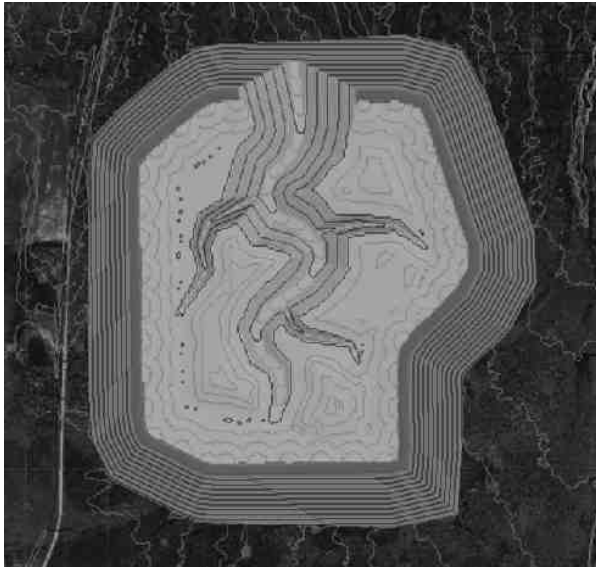


Figure 4. Closure water management features in the closure surface

3D design tools provide the opportunity to understand the ability of tailings facilities to contain flood events once the tailings facilities have been constructed to the closure design but which have not yet had an outlet channel constructed. This case “pre-closure” is a critical case for flood management for a tailings facility as the tailings facility has at that time reached the maximum dyke crest elevation and the maximum tailings surface elevation. Analyzing the flood storage capability of the pre-closure case pond provides mine operators with an initial understanding of any potential risks

associated with constructing a tailings facility to the closure condition without immediately providing an outlet channel.

LIMITATIONS

While programs like Muck 3D simplify the closure design areas as discussed above, there are some limitations in the program including:

- Topographic surfaces may be represented as gridded surfaces which in some instances may not provide the required resolution for features narrower than the model grid spacing.
- The tools for generating organic, non-linear shapes are in their infancy and so more refinement may be needed once the designs are taken to higher levels of detail in Civil3D.
- Limited ability for the program to perform spatial analysis of the statistics of a surface and hydrologic analysis.

These identified limitations can be reduced when GIS or CAD software is used in conjunction with geometric design tools and allow the utilization of the strengths of each program. Muck 3D provides an important tool for simplifying portions of closure design and for integrating closure planning with mine and tailings planning. The generated closure surfaces can be easily and imported into GIS software and stitched together in GIS software to create a site wide closure DEM which can be used for surface water and ground water modeling. Cross sections can also be easily constructed to view the closure surface along with other structural surfaces of interest.

SUMMARY

For closure design and for closure planners, 3D tailings planning tools provide an opportunity to quickly examine design components which may otherwise have been left to a more detailed design phase or modelled using more complex tools such as Civil3D. These conceptual design tools, in conjunction with other domain appropriate software give engineers the tools to produce more and provide a product that is of higher quality. This additional design detail provides an opportunity for the closure design to be more valuable to mine and tailings planners at an earlier time in the

closure design process. In the current digital media age and the emphasize on closure work requires that engineers are able to present to clients, regulators and stakeholders a 3D closure landscape that is tangible and realistic even before the first shovel hits the ground.

REFERENCES

Civil 3D AutoCAD. Web. 30 Sept. 2014
<<http://www.autodesk.com/products/autocad-civil-3d>>

International Council of Mining and Metals (ICMM). 2004. Planning for Integrated Mine: Closure Toolkit. London, UK.

Jakubick AT, McKenna GT, Robertson AM. 2003. Stabilisation of tailings deposits: international experience. Sudbury 2003. Mining and the Environment.

McKenna G, An R, Scordo E, McGreevy J. 2013. Toward Effective Closure Planning. From Progressive Reclamation to Sustainable Mining. Proceedings of the Tailings and Mine Waste 2013 Conference, Banff. University of Alberta Geotechnical Centre, Edmonton

McKenna G, Scordo E, Shuttleworth D, Straker J, Purdy B, and Buchko J. 2011. Aesthetics for mine closure. Proceedings of Mine Closure 2011 Conference (Lake Louise, Canada), Volume 1, pp. 603-612. Australian Centre for Geomechanics.

MineBridge. Web. 30 Sept. 2014
<<http://www.minebridgesoftware.com/>>

Session 9

Tailings Dewatering II

ADVANCES IN THE ELECTROKINETIC TREATMENT OF OIL SANDS TAILINGS

L. Richard Nelson¹, Paul Garcia², Ben Harris², and Doug Kimzey²

¹Alberta Innovates – Energy and Environmental Solutions, Edmonton, Alberta, Canada

²ElectroKinetic Solutions, Inc., Toronto, Ontario, Canada

ABSTRACT

Electrokinetic (EK) methods of de-watering and strengthening tailings are often considered too expensive for practical use in production. The results of the recent program to investigate EK treatment of oil sands tailings conducted by ElectroKinetic Solutions, Inc. (EKS) are showing potential for economical use at scale. Analysis of power consumption, water production, changes in water chemistry, solids content, and shear strength at medium scale for unit volumes up to 1,000 liters between 15% and 40% solids indicates that large scale treatment using the EKS process may be economically viable. Main and interaction effects for different configuration scenarios covering treatment duration, initial tailings properties, electrode materials, and suitability for recovered water for re-use in the bitumen extraction process are examined. Results from the EKS testing program are encapsulated in software models to predict the power usage, water recovery, and time to treat a volume of tailings. The model provides support for the selection of configuration parameters for different treatment scenarios. Relationships between configuration and cost factors such as electricity costs and material costs are being investigated.

BACKGROUND

Electrokinetic methods to de-water and strengthen clays are well represented in scientific literature. While many previous attempts at applying EK treatment to fluid tailings have shown promise, EK methods are typically regarded as involving high energy costs, operational problems with corrosion of electrodes, and difficulties removing supernatant fluid. EK treatment has been considered an “emerging technology with little-to-no plant scale use or information available (BGC Engineering, Inc., 2010).

Beginning in 2012, EKS embarked on research to investigate the feasibility of treating oil sands

tailings with a low current and low voltage application of electric fields to oil sands tailings. A series of tests conducted in a Sequential Design of Experiments (DOE) framework was conducted to optimize power consumption and water production. Factors such as electrode life, geometry, and spacing were analyzed. Water chemistry results between the surface water and water collected at the cathode were also analyzed.

The culmination of this work has led to a series of 1,000 liter tests that showed power costs to treat to 50% solids consistently under \$30 per dry tonne. EKS is also developing software that models power usage, water production, and time to treat tailings. The model under development is also used to quantify the effects of factors that drive variation in the consistency of treatment.

ELECTROKINETIC FORCES

Electrokinetic Reclamation (EKR) technology is uniquely suited to oil sands tailings reclamation due to the nature of the physical processes that keep the fines in suspension. Research has shown that a small percentage of nano-sized clay particles (20 to 300 nm) is responsible for the unique physical characteristics of mature fine tailings (MFT). These particles are polarized as a result of their physical structure and form fractal flocs that result in the formation of a thixotropic gel (L. S. Kotylar, 1996). Water and polarized organics adsorb to the clay surfaces and form bonds that are highly resistant to natural dewatering and consolidation processes. EKS utilizes these same characteristics to effect treatment in its EKR process.

Electrophoresis is the migration of a charged particle within a liquid due to the presence of an electric field. During EKR treatment the charged clay particles along with polarized organics migrate toward the electrodes where they begin to consolidate.

Electro-osmosis is the movement of fluid induced by an electric field as a result of ion flow. As consolidation of fines begins to occur around the electrodes via electrophoresis water begins to flow in toward the cathode. Positive ions flow toward the negatively charged cathode where they are removed to the surface.

These EK forces along with other electrochemical phenomena are the basis for EKR. The process is not thermally driven and depends largely on voltage potentials rather than large current flow to achieve results. EKR exploits the dielectric nature of MFT by using electrical signals that have been developed through large and small scale empirical testing. In doing so, EKS has been able to significantly reduce the power costs of EK dewatering and compaction.

EXPERIMENTATION

Initial Properties

Testing was performed using tailings with initial solids contents ranging from 15% to 40% solids by weight. For most tests, water was removed and sampled at regular intervals to track water recovery rates as well as water chemistry changes. The total power dissipated into the material was logged continually along with the total power consumption for the testing equipment. At the conclusion of each test, the electrodes were measured and weighed in order to quantify material losses.

Configurations

EKS performed tests on a variety of 1,000L configurations with electrode spacing up to 4.8m between anodes and cathodes. The 3D testing was performed in 1 cubic meter totes in vertical and horizontal configurations.

The 3D vertical configuration was approximately 50 times greater in volume, 3 times greater electrode spacing, and 7 times greater in thickness (height) than previous small scale testing.

The 3D horizontal test vessel was the same as the previous 1000L tests which used plastic 1,000L IBC totes, but with the electrodes oriented horizontally. The test vessel was filled with a low solids content (14.7% solids/wt.) tailings slurry produced by mixing 400L of high solids content MFT and 600L of process water.

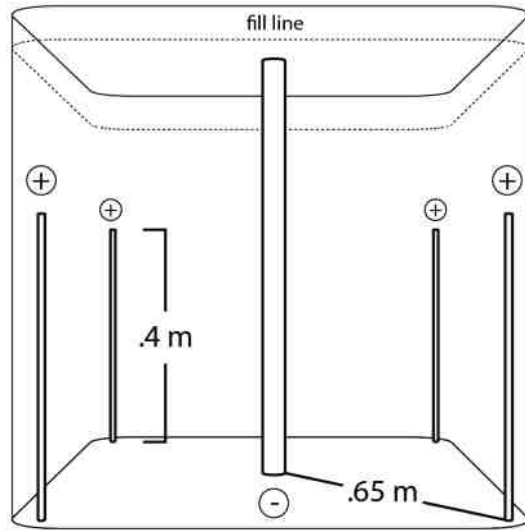


Figure 1. 1,000 Liter Vertical 3D Configuration

Two horizontal anodes were constructed of 6mm 304 stainless steel wire rope placed lengthwise along the bottom of the test vessel and spaced approximately 25cm from the long sides of the vessel and 25cm from each other. The cathode was constructed similarly to other 1000L tests; however, it was oriented horizontally and parallel to the anodes and then suspended approximately 30cm below the filled level.

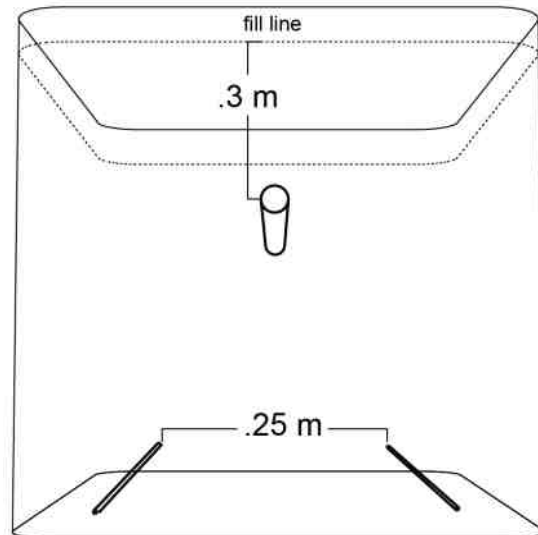


Figure 2. 1,000 Liter Horizontal 3D Configuration

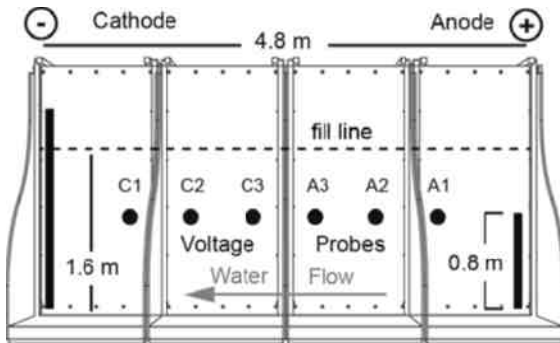


Figure 3. 1,000 Liter Vertical 2D Configuration

Larger electrode spacing was explored using a 2D test cell constructed to be 4.8 meters in length and 13 cm in depth. Acrylic walls allowed a cross section of the treatment to be visually tracked and recorded.

This test vessel was largely constructed using 2.5cm thick acrylic sheets spanning an area of approximately 5m wide x 2.5m tall x 13cm thick. The 83cm long anode was constructed of 1.6cm diameter aluminum pipe which contained a 6mm stainless steel core. In this and both 3D horizontal and vertical configurations the cathode consisted of a stainless steel woven sleeving supported by a 4.5 cm perforated PVC pipe. A wicking fiberglass sleeve surrounds the stainless steel and allows for water removal from the cathode.

The 2D vertical configuration used 1,000L of MFT containing 39.4% solids/wt. and ended with an average solids content of 49.3% solids/wt. after 7 weeks of treatment using a voltage gradient of 0.5v/cm. At the conclusion of the test, the anode was largely intact losing about 15% of its total length and 24% of its total mass.

The 2D horizontal configuration was meant to test the effectiveness of a horizontal arrangement over a distance. The electrodes were parallel stainless wire ropes. The vessel was filled with 15% material

Treatment duration

Treatment durations ranged from 2 to 7 weeks with the 2D 5 meter spacing test running the longest. Treatment was applied until the overall solids content in the vessel was approximately 50% solids by weight.

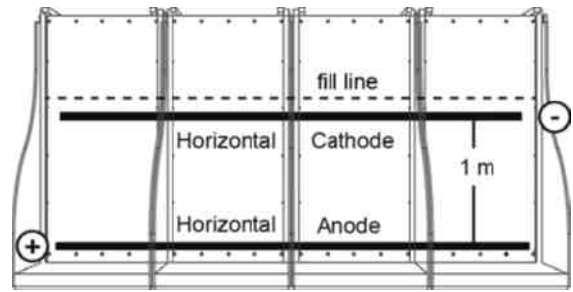


Figure 4. 1,000 Liter Horizontal 2D Configuration

RESULTS

Power consumption

Testing has shown that the EKR process can consolidate and dewater 1m³ of MFT containing ~40% solids/wt for about \$15/dry tonne (vertical configuration) and in 15% solids/wt material for about \$18/dry tonne (horizontal configuration). EKS believes that there could be significant economies of scale as the technology is scaled up to 5m electrode spacing in a 3D configuration.

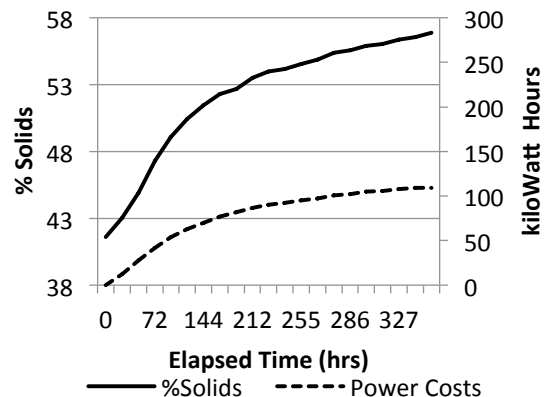


Figure 5. 1,000 Liter 3-D Vertical Test

Water Recovery

Water separation rates shown in Figure 7 are from the horizontal configuration test. This test was conducted on 15% solids by weight material.

Recovery averaged about 40L per day with peak production occurring within the first 2 days of treatment where water separation rates averaged about 200L per day. Approximately 600L of water was separated after 6 days of treatment and 9 days of post-treatment settling.

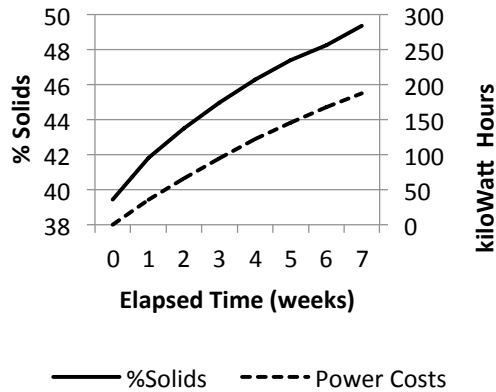


Figure 6. 1,000 Liter 2-D Vertical Solids Content and Power

Water Quality

Water chemistry results between the surficial and cathode water samples show distinguishing characteristics. Surficial water samples typically exhibited lower pH and conductivity values and lower values for sodium while still maintaining some bicarbonate in solution. Whereas the cathode samples typically had no bicarbonate, and had lower concentrations of total organic carbon and calcium.

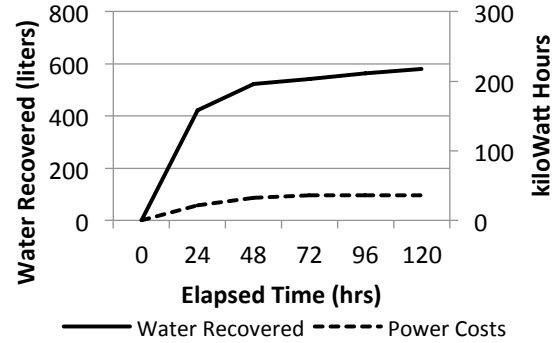


Figure 7. 1,000 Liter 3-D Horizontal Water and Power

Water chemistry results for the 15% 3D horizontal test, where cathode water was not removed, had slight variances with HCO_3 , TOC, Ca, and Mg decreasing over time for the surface water samples. No significant differences in chemistry were observed in samples collected between the surface and the mud line approximately 40cm below the surface.

Table 1. 3D Horizontal Configuration Water Quality Measurements

Parameter	pH	TDS	HCO_3	TOC	Ca	K	Mg	Na
Average Treated Value (mg/L*)	8.3	1263	470	38	21	29	13	324
Untreated MFT	8.4	2122	434	66	23	24	11	264
Untreated Process Water	7.9	1400	410	132	23	22	12	194

*except pH

Scanning Electron Microscopy (SEM) and Energy Dispersive X-ray (EDS) Analysis

Twenty-eight (28) samples collected from the 5m test vessel were sent to Water Planet Engineering (WPE) for Scanning Electrode Microscopy (SEM) and Energy Dispersive Spectroscopy (EDS) analysis. The purpose of this analysis was to determine if there were any differences in the microstructures and elemental composition of the

dewatered fines from various locations in the test vessel.

These samples were analyzed by a Jeol JSM-6610LV SEM and an IXRF EDS analyzer. The SEM produced two images at 500x and 5000x magnification for each sample while the EDS generated elemental color maps on the images to determine percent composition of each element present.

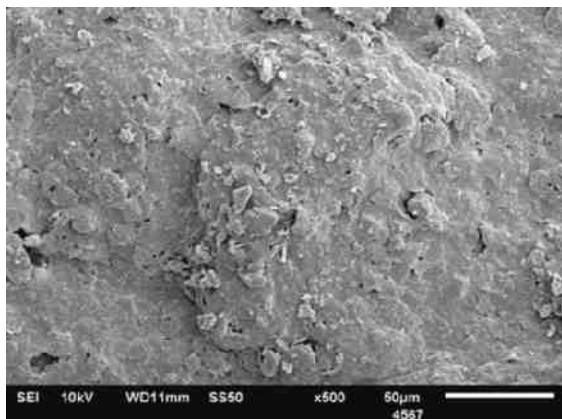


Figure 8. Treated Material SEM 500x Magnification

The particles visible on SEM images are plate like, thin particles, characteristic of a clay particle – predominantly kaolinite-like. Due to sample drying, most of the particles form larger aggregates, but average particle size is around 0.1 – 5.0µm.

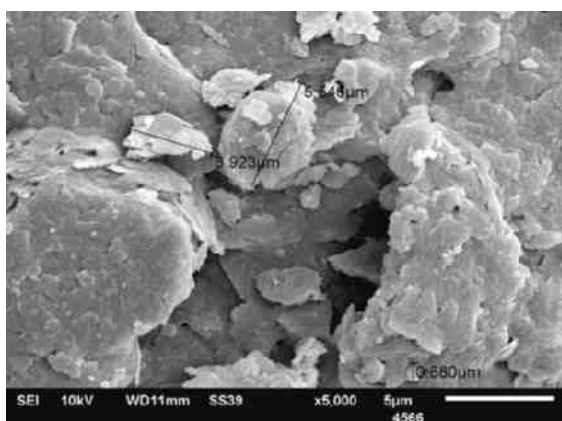


Figure 9. Treated Material SEM 5000x Magnification

Nearly all the samples show very similar morphology at a 5000X magnification. Significant differences in the morphologies could not be found under SEM. This indicates that the samples underwent the same type of morphological transition as they were dewatered and dried.

The elemental analysis of the solid particles using EDS showed that silicon, aluminum, and oxygen are the main elements of the particles, whereas potassium, calcium, magnesium, and iron are present as interlayer cations. Small amounts of titanium were observed on most of the samples. Such a composition is characteristic for kaolinite, which is composed of exactly the same elements.

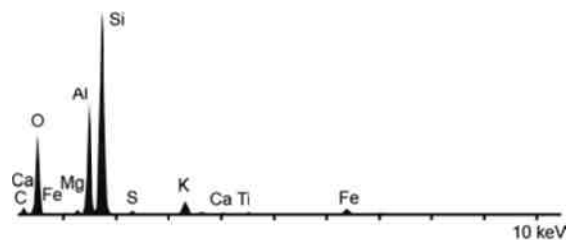


Figure 10. EDM Elemental Analysis

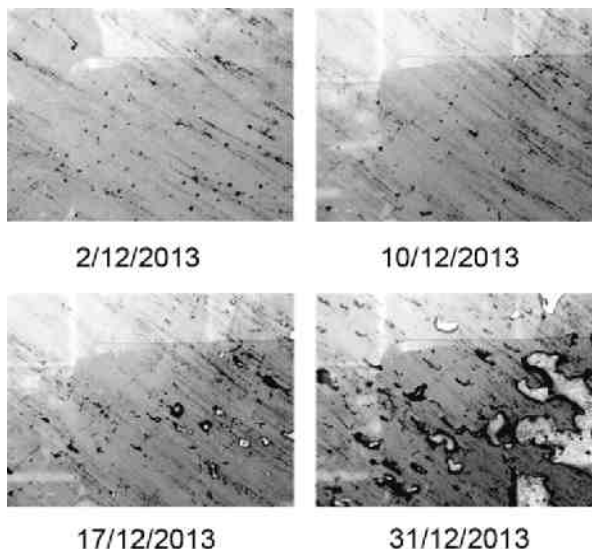


Figure 11. Bitumen Migration Time Series

Bitumen Migration

The EKR process causes the polarized bitumen adsorbed to the clays to migrate toward the electrodes as a result of electrophoresis. Bitumen migration could be seen through the acrylic walls of the electrode scale up vessel. Streaks of bitumen left on the acrylic panel tracked the movement of the organics.

Once reaching the region of compaction the bitumen forms larger groupings and displays signs of electrocoagulation. Also note the water vapor and gas generation that could be indicative of microbial activity.

Consolidation

EKR consolidates the solids primarily near the anode through a combination of coagulation, cementing, and aggregation, along with moisture removal from the interstices of the clays. The resulting microstructure of the compacted clays

appears to be the same as that obtained through drying of such clays.

Consolidation also occurs in the vicinity of the cathode with solids content by weight reaching as much as 60%.

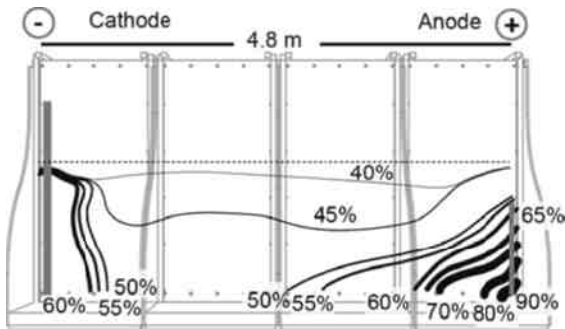


Figure 12. 2D 5m vertical horizontal test solids content distribution

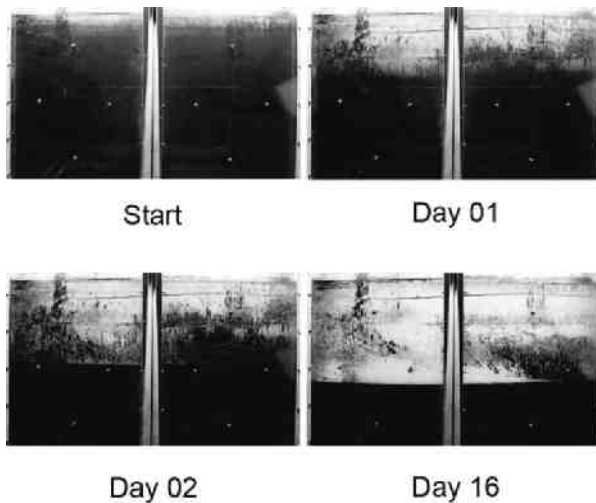


Figure 13. 2D Horizontal Configuration: Time Series of Consolidation

The 2D horizontal configuration was performed on 15% solids by weight material and showed a very rapid rate of consolidation with much of the separation occurring with the first 2 days of treatment.

Shear strength

Shear Vane testing was performed in the 3D vertical configuration near each anode, the cathode, halfway between the two and at various locations after 7 and 14 days of treatment and 10 and 19 days of post-treatment drying. Shear Vane

readings ranged from <1 to over 234 kPa with corresponding solids content measurements ranging from 47.7% to 76.6%. Shear values along the horizontal plane were greatest near the anodes in the corners of the treatment vessel and dropped off approximately halfway between the anode and cathode.

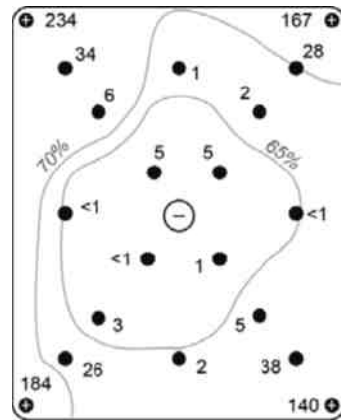


Figure 14. Post treatment shear strength (kPa) and solids content (percent by weight) distribution in vertical 3D configuration

Vertically, the shear values typically increased with depth generally along the vertical interval that had full exposure to the anode. A significant area of the treatment vessel, particularly at depth, had shear strengths values exceeding the target of 5 kPa. Long term post treatment evaluation is currently underway to determine the changes to the shear strength and solids content relationship over time.

PROCESS MODELING

EK forces such as electrophoresis and electro-osmosis are directly proportional to the electric field. Distribution of treatment is proportional to the distribution of the electric field throughout the volume of tailings being treated. By utilizing this and other relationships that have been identified through testing EKS is able to model the behavior of EKR treatment for a variety of scenarios.

Power Estimates

Power dissipation and energy storage are also functions of the electric field. The impedance of the material under treatment changes over the course of treatment in proportion to the rate of change of material properties such as solids content and salinity.

Time to Treat

A basic approximation of time to treat may be obtained by using the electro-osmotic flow rate to compute time required to produce a given volume of water. Both the The Helmholtz-Smoukowski and Casagrande versions of the electro-osmotic flow rates are dependent upon the electric field and subject to the same parameters of electrode module geometry, electrode degradation, and variation of material properties as power consumption.

Force Exerted by Electric Field

Force exerted by an electric field at any point in the volume of tailings being treated is a function of the charge distribution (or voltage), distance of the point to electrodes, and material properties. An electric field is typically expressed in terms of force per electrical charge (Newtons per Coulomb). Multiplying an expression for an electric field by a charge distribution produces an expression for force in Newtons. With care, an expression for Force per unit area or pressure may also be produced. All of the EK forces used by the EKS process are proportional to the electric field applied during treatment.

Voltage and Permittivity

Over the course of treatment, the permittivity of the tailings drops as water is removed. Monitoring permittivity throughout the treatment process allows progression to be assessed and predicted. A typical value for the relative permittivity of water is $\epsilon_r=81$. The relative permittivity of kaolinite clay is approximately $\epsilon_r=5$. Since the solids content of tailings changes from location to location as treatment progresses, permittivity also varies by location as well as with time.

Using a Cartesian coordinate system with the Five metre test cell, where the top of the anode is at coordinates $x_A = 4.88$ metres, $y_{A2} = 1.0$ metres and the bottom of the anode is at $x_A = 4.88$ metres, $y_{A1} = 0.17$ metres the general equation for the scalar voltage at any point (x, y) for $0 \leq x \leq 5$ and $0 \leq y \leq 1.6$ metres is given by:

$$V(x, y) = \frac{\rho_\ell}{4\pi\epsilon} \ln \left[\frac{y + \sqrt{(x-x_A)^2 + (y-y_{A1})^2} - y_{A1}}{y + \sqrt{(x-x_A)^2 + (y-y_{A2})^2} - y_{A2}} \right] \quad (1)$$

where ρ_ℓ is the line charge in Coulombs per metre and ϵ is the permittivity of the tailings where $\epsilon = \epsilon_0\epsilon_r$ with $\epsilon_0 = 8.854 \times 10^{-12}$ Farads per metre.

The electric field intensity calculated by Coulombs Law is given by (2):

$$|E(x, y)| = \frac{\rho_\ell}{4\pi\epsilon} \left[\frac{\tan^{-1} \left(\frac{y-y_{A1}}{x-x_A} \right) - \tan^{-1} \left(\frac{y-y_{A2}}{x-x_A} \right)}{x-x_A} \right] \quad (2)$$

The same voltage was applied across the anode and cathode for the seven week duration of treatment. Using an estimated charge density of $\rho_\ell = 5 \times 10^{-7}$ Coulombs per metre and assuming that the charge density on the anode remains constant, voltage at the probe locations A1 through C6 may be plotted using equation (1) over a range of relative permittivities.

Figure 16 shows voltage curves as a function of relative permittivity (ϵ_r) for each of the six voltage ports in the test cell at the beginning of the test and on the last day of the test after the loss of approximately 12.45 cm of anode length through degradation.

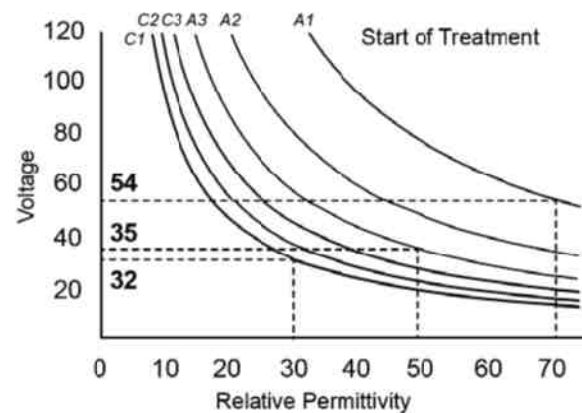


Figure 15. Voltage as a function of permittivity: Start of Treatment

Voltage data from probes A1, A2, A3, C3, C2 and C1 were collected over the duration of the test with 14-bit resolution. Using equation (1) and the voltage data, it is possible to approximate the spatial variation in permittivity throughout the five-meter scale-up test. Permittivity at different locations and the spatial variation of permittivity is an essential measure to approximate the impedance of the tailings during treatment. The RMS voltage over the duration of the test is shown in Figure 17. To make comparison to Figure 16 easier, the time scale is reversed in Figure 17 with the start of the test on the right and the end of the test on the left. As the solids content increases due to electro-osmotic flow and electrophoretic

finer migration, the permittivity of the water-clay tailings will drop closer to the permittivity of clay. As water is driven towards the cathode, the permittivity near the cathode may increase. Note that on the voltages for ports C1, C2 and C3, RMS Voltages by definition are always positive.

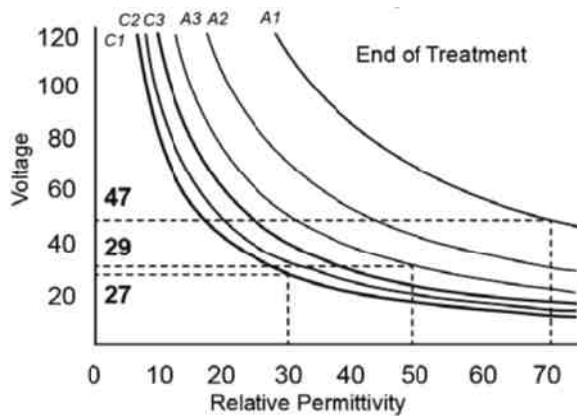


Figure 16. Voltage as a function of permittivity: End of Treatment

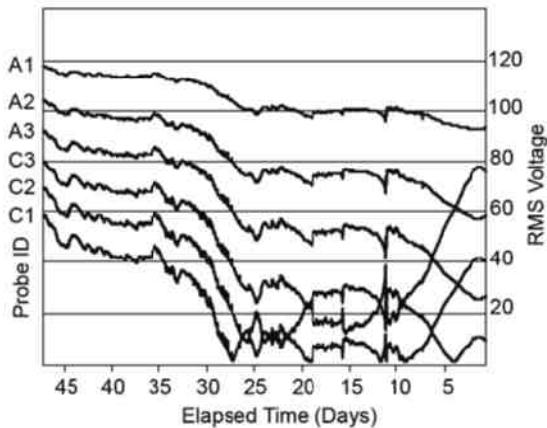


Figure 17. RMS Voltages at each port

The approximate relative permittivity at a port A3 at the test may be obtained by looking up the permittivity using the A3 curve for about 90 volts on the lower chart in Figure 16 for an anode length of 70.5 cm. This gives an approximate ending $\epsilon_r=17$ at port A3. Using a conservative 40 volts and the top chart in Figure 16, the initial relative permittivity at port A3 is approximately $\epsilon_r=44$. Port location A3 at $x=2.78$ and $y=0.95$ saw a drop in average relative permittivity of 27.

This exercise may be simplified by solving equation (1) for the relative permittivity.

$$\epsilon_r(x, y) = \frac{\rho_\ell}{V(x, y)4\pi\epsilon_0} \ln \left[\frac{y + \sqrt{(x-x_A)^2 + (y-y_{A1})^2} - y_{A1}}{y + \sqrt{(x-x_A)^2 + (y-y_{A2})^2} - y_{A2}} \right] \quad (3)$$

The electric field intensity at each voltage port location as a function of relative permittivity is shown in Figure 18.

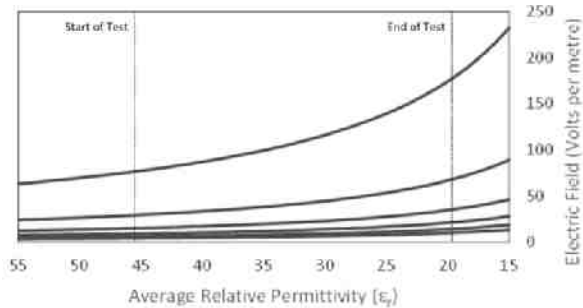


Figure 18. Electric field intensity at each port

The effects of distance on the electric field intensity are apparent in the curves for each voltage port location. Distribution of treatment is affected by the distribution of the electric field intensity throughout the volume of material being treated.

Aggregate Impedance

Capacitive and resistive elements of an analog circuit that describes the impedance of material undergoing treatment may be expressed in terms of the electric fields and properties of the material being treated. The values of each element in the analog circuit change over the course of treatment.

Since permittivity is a common parameter in the calculation of capacitance and conductivity, spatial variation in permittivity will carry forward into spatial variation in impedance. Over the duration of treatment, EK induced flow of water will also drive changes in permittivity and impedance over time.

An overall aggregate capacitance for the test cell at a given time and location during treatment is given by an evaluation of Laplace's equation $\nabla^2 V = 0$ and solving for $\frac{Q}{V} = \frac{\rho_\ell \ell}{V}$ for a constant potential and surface charge on the electrodes. This is the reason why electrode geometry has such a central role in capacitance.

For a simple approximation of an aggregate capacitance assume that each of the six ports A1, A2, A3, C3, C2 and C1 are the centroids of six volumes of adjacent tailings. An approximate aggregate capacitance may be estimated by (4).

$$C(t) = \frac{1}{\frac{1}{C_{A1}} + \frac{1}{C_{A2}} + \frac{1}{C_{A3}} + \frac{1}{C_{C3}} + \frac{1}{C_{C2}} + \frac{1}{C_{C1}}} \quad (4)$$

Where $C_{Ai}(t)$ and $C_{Ci}(t)$ are the corresponding capacitances for the volume of material currently around each port at time t .

The capacitance in each term in (4) is given by (5).

$$C(t) = \frac{Q}{V} = \frac{\left| \oint_s \epsilon \mathbf{E} \cdot d\mathbf{s} \right|}{\left| - \int_{x_1}^{x_2} \mathbf{E} \cdot d\ell \right|} \quad (5)$$

Each capacitance in (4) is accompanied by a frequency dependent reactance. The classic definition of reactance is given by (6).

$$X_c(t) = \frac{1}{2\pi f C(t)} \quad (6)$$

In a capacitive system, the time τ required to discharge 63% of the initial voltage is given by the product of the resistance R and the capacitance C.

By ohms law, the resistance of the volume of tailings around the ports is given by equation (7).

$$R(t) = \frac{v(t)}{i(t)} = \left| \frac{- \int_{x_1}^{x_2} \mathbf{E} \cdot d\ell}{\int_s \sigma \mathbf{E} \cdot d\mathbf{s}} \right| \quad (7)$$

Sigma (σ) in equation (7) is the conductivity in $(\Omega \cdot m)^{-1}$. Conduction of electrical current through porous media is primarily due to the movement of ions through bulk-saturating fluid. Factors affecting the conductivity of a clay-sand include porosity, clay content, salinity, permeability and degree of pore saturation. The properties for conductivity in the model include support for a statistical interval that describes variation of conductivity. Values for conductivity may also be supplied by a user-specified function.

Figure 19 shows the analog circuit for the aggregate impedance of a volume of material around voltage port C1. While the simple analog circuit shown in Figure 19 seems straightforward, each of the circuit elements changes over the course of treatment. Variation of material

properties also contribute to variation in electrical impedance.

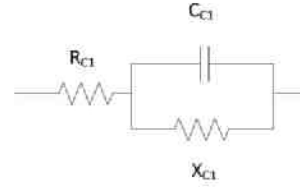


Figure 19. Analog circuit element for aggregate impedance

An analog circuit of the five metre test cell would include six of the analog circuit model shown in Figure 19 in series.

Equations (5) through (7) show that the resistive and capacitive elements are directly proportional to the strength of the electric field.

The migration of water from one area to another affects the impedance of a unit volume. If the individual capacitances in equation (4) represent the capacitances of six adjacent unit volumes, the migration of water will drop some capacitances of some unit volumes while raising the capacitance of others.

Electro-osmotic Flow Rate

The rate of electro-osmotic flow is dependent on the coefficient of electro-osmotic permeability of the tailings which in turn is dependent on the zeta potential (ζ). (Asadi, Huat, Nahazanan, & Keykhah, 2013). The Helmholtz-Smoluchowski electro-osmotic permeability in metres per second is given by equation (8).

$$q_{eo} = \frac{\epsilon_o \epsilon_r \zeta}{V_t} n |\mathbf{E}| \frac{A}{L} \quad (8)$$

Where V_t is the viscosity of the pore fluid, n is the soil porosity, $\epsilon_o \epsilon_r$ is the permittivity of the tailings, A is the gross cross sectional area normal to the flow of water and L is the length. $|\mathbf{E}|$ is the magnitude of the electric field inducing the flow.

The Smoluchowski equation (9) shows the relationship between the zeta potential (ζ) and the electrophoretic mobility.

$$\zeta = 4\pi V_t \frac{EM}{\epsilon_o \epsilon_r} \quad (9)$$

In clay the zeta potential (ζ) is usually negative, which causes the electro-osmotic flow to occur from anode to cathode. A positive ζ flows from cathode to anode. No electro-osmotic flow exists

for ζ near zero. Variation of ζ in kaolinite clay is a function of pH. Acidity increases as the magnitude of ζ decreases.

Equation (10) shows a widely used equation for electro-osmotic flow (Casagrande, 1949).

$$q_{eo} = k_e |E| A \quad (10)$$

Where k_e is the coefficient of electro-osmotic permeability. A typical value of k_e for Kaolin is 5.7×10^{-5} cm² per V·second.

CONFIGURATION OPTIMIZATION

The optimum configuration for EKR deployment is always going to be a trade-off between power requirements, time to treat and level of consolidation required. If longer treatment durations are acceptable then lower voltage gradients can be used and smaller power generation capabilities will be required. If more rapid reclamation is seen as a benefit then it may be worth the extra power to achieve reclamation management timelines.

EKR technology is designed to dewater and compact tailings deposits in place without requiring intermediate material handling steps or the addition of any additives or flocculants. This aspect of the technology has the potential to result in significant cost savings over approaches that require the tailings to be moved for treatment and then deposited one or more times after treatment.

EKR has the potential to serve as an enabling technology for multiple applications within the Alberta Oil Sands overall tailings management strategy. EKR can potentially be applied on a year-round basis. Installation of the electrodes and power distribution systems would need to occur during warmer weather. However, once these systems are in place, the system can primarily be managed remotely, and treatment can be applied throughout the year.

Holding facilities that may be reaching the end of their useful life could see new use as additional volumes are made available through the use of EKR. Volume reductions of as much as 70% have been achieved in laboratory testing.

Through the combination of electrode configuration design and treatment signal modification it is possible to obtain treatment homogeneity that will provide a sound geotechnical structure for reclamation activities. Additional research is under way to determine the effects of post treatment processes such as ionic diffusion and electro-cementation (S.Micic, 2002) in the long term distribution of EKR treatment.

NEXT STEPS

EKR treatment is currently being evaluated for a number of potential applications. In place densification of existing holding ponds is being developed as well as methods for facilitating the capping and loading of deep fines deposits. EKR is also well suited to targeted application for addressing areas of deposits that have not been treated to specification using other technologies.

EKS is in the process of demonstrating the potential of electrokinetic treatment at a scale of up to 130 cubic meters of tailings. If this testing shows that the treatment process is feasible at this scale, the next logical step will be completion of a field trial to confirm the commercial viability of the technology.

REFERENCES

- Asadi, A., Huat, B. B., Nahazanan, H., & Keykhah, H. A. (2013). Theory of Electroosmosis in Soil. *International Journal of Electrochemical Science*, 1016-1025.
- BGC Engineering, Inc. (2010). *Oil Sands Tailings Technology Review*. University of Alberta, School of Energy and the Environment. Edmonton, Alberta: Oil Sands Research and Information Network.
- Casagrande, L. (1949). Electro-osmosis in soils. *Geotechnique*, 159-177.
- Kotlyar, L. S., & Sparks, B. D. (1993). Characterization of Colloidal Solids From Athabasca Fine Tails. *Clays and Clay Minerals*, Vol. 41, No. 3, 341-345, 341-345.

L. S. Kotylar, B. D. (1996). Effect of Salt on the Flocculation Behavior of Nano Particles in Oil Sands Fine Tailings. *Clays and Clay Minerals*, Vol. 44 No. 1, 121-131.

S.Micic, J. a. (2002). Electro-Cementation of a Marine Clay Induced by Electrokinetics. *Proceedings of The Twelfth (2002) International Offshore and Polar Engineering Conference*. Kitakyushu, Japan: The International Society of Offshore and Polar Engineers.

CHEMICAL FREE MECHANICAL DEWATERING OF TAILINGS WHERE THE CAKE HAS SHEAR STRENGTH \gg 5 KPA

Hen Boele, Marco Brocken, Preston McEachern
Evodos, Raamsdonksveer, The Netherlands

ABSTRACT

The Evodos Dynamic Settler is a novel approach to 3-phase separation combining the principles of plate separators with the artificial high gravity of centripetal equipment. We report on a number of successful applications of this technology on problematic water, oil and clay mixtures including a kaolinite, a proxy for Mature Fine Tailings (MFT). An Evodos type 25 unit, originally designed to separate algae from aqueous culture, has now been broadly deployed for solids control.

The Dynamic Settler can process oil based drilling muds up to a specific gravity of ~ 1.35 and produce clean base oil in the 0.90 S.G. range. More solids rich muds must first be decanted to achieve the best capacity outcomes. When used on kaolinite, dry cakes averaged 60% wt solids from 2% and 5% wt suspensions. We subsequently performed a trial with an MFT feed mixture that had a water/clay/silt/bitumen mixture with a dry solid content $>30\%$ wt which in this case included total mineral solids ($>25\%$ wt) and bitumen solids ($>5\%$).

The Dynamic Settler produced a solid discharge from untreated MFT with an average dry solid content $> 65\%$ wt for a mineral recovery to cake of $>75\%$. The shear strength of the cake at discharge was $\gg 5$ kPa. The water effluent stream contained 5% mineral solids in our initial trial without optimization. A liquid bitumen stream was also produced containing $>25\%$ wt bitumen. Bitumen recovery was proven and optimization in design will greatly enhance recovery of a low water content bitumen stream.

INTRODUCTION

Background

Stokes' law explains the resistance or drag a particle experiences in a fluid and is used to interpret a particles settling behaviour as a function of the particle, gravitational force and the fluids viscosity. Laminar flow of the fluid is essential and

such conditions enhance the ability for a particle to settle under gravitational forces. Inclined plate separators (IPS) have long-exploited these characteristics to produce superior solids removal in water treatment (Davis 2010, Cheremisinoff 2002) and in dispersed liquid-liquid systems (Rommel et al. 1992). In bitumen processing, IPS have been deployed in froth treatment and achieve high efficiencies of bitumen recovery (e.g. 99%) and good solids removal (Tipman & Shaw 1993).

However, IPS are space intensive, prone to fouling and or produce a wet sludge (Davis 2010). In water treatment, typically 0.4 m² of plates are required per m³/hr of processing (AWWA 2012). At the large flow volumes of an oil sands mine, the size and capital cost of this approach is inhibitive unless artificial gravity can be used to increase the treatment efficiency per unit area of plate, decrease the water content of the sludge (cake) and provide an efficient means of handling the cake.

Evodos developed Spiral Plate Technology (SPT) that enhances gravitational forces, similar to centrifuges, but also minimizes settling distances and maintains laminar flow of the fluid during the treatment process.

The key characteristic is a plate pack where the surface of the plates runs parallel with the machine's axis of rotation (Figure 1).

The arrangement of these plates is such that the maximum swimming (settling) distance of a particle is $\ll 7$ mm. These plates form thin layers through which laminar flow is maintained as the influent mixture accelerates to the rotational speed. By creating artificial gravity through rotation, the settling process increases as per Stokes' Law. What is unique about this approach over scroll and disk stack designs is that fluid is accelerated to the rotational speed within each narrow vane; laminar flow is maintained, shear in the bowl is minimized and wear and floc breakdown are reduced.

The design is robust with respect to the high abrasion of fluid tailings. Because the plate-pack

and drum spin at the same speed, zones of acceleration are limited to the feed inflow through the central shaft. This is mitigated by the cartridge design that allows rapid replacement of the wear components at very low cost. Unlike scroll centrifuges, the wear of outer scroll flights does not occur in the Evodos dynamic settler because they are pressed to and rotating at the same speed as the drum.

The Evodos system has been effectively commercialized for the food industry, primarily for algae separation. Algae are a challenge because their specific gravity is similar to the water in which they are suspended and the goal of recovery is to do so without cell lysis (shearing the cells). The Evodos system has become the standard for algal recovery because it can accomplish both tasks more efficiently than competitive disk stack or scroll technologies. The need for separation of low gravity solids without shearing floc or pulverizing clay platelets makes the Evodos dynamic settler a valuable tool in oil sands tailings management.

METHODS

The Evodos T25 was deployed for trials with oil field wastes. Three mixtures were processed during the trials: MFT, flocculated MFT, sometimes referred to as Thickened Fine Tailings (TFT), and a simulated fluid fine tailings stream (symFFT) created from the effluent of an initial pass through the T25. The TFT feed was produced using an on-site thickener and the TFT was fed to the T25 within 15 minutes of production. The TFT was created with polymer SNF A3338 at a dose of 2.2 g/Kg clay. Methylene blue and XRD estimated clay contents for MFT are typically in the 75% and 50% ranges, respectively, resulting in a polymer dose rate of > 1 – 1.6 kg/tonne dry solids. Feed characteristics are presented in Table 1.

Table 1. Characteristics of feed

Type	S.G.	Solids (%wt)	Water (%wt)	Oil/bit (%wt)
Kaolinite	1.02	2	98	0
Kaolinite	1.05	5	95	0
OBM	>1.5	30	~5	65
MFT	1.26	28	64	8
TFT	1.10	14	86	<1*
Sim FFT	1.03	4	95	<1*

* bitumen not quantified due to low volumes



Figure 1. Evodos SPT plate pack.

Samples of the feed and the effluent were taken at incremental times during the test runs. In all applications, the clays stack along the vanes with finer particles concentrated at the top (Figure 2). Dry weight measurements (at 160C°) were performed on all samples to achieve an indication of the wt% of dry solids (minerals + bitumen). BMW analysis by retort was performed to give insight in the mass balance.

Kaolinite suspension (fine clay)

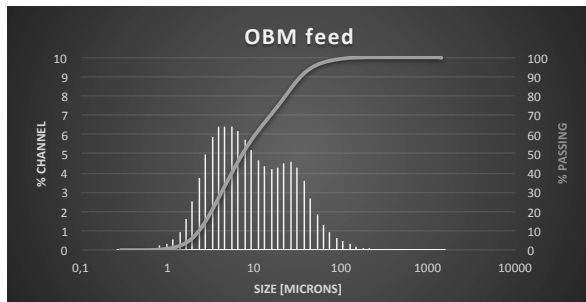
The results of kaolinite processing set the stage for use in oil field waste. Two and 5%wt suspensions consistently produced a clean water stream and a cake with 60%wt solids (Fig.2).

Oil Based mud (OBM)

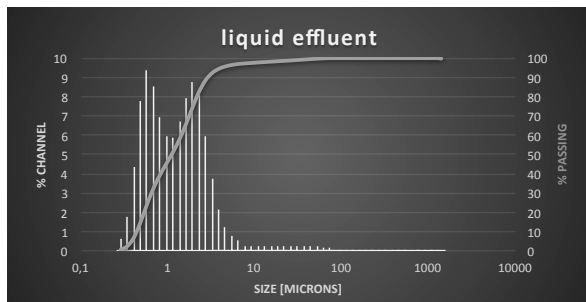
Processing of oil base mud to recover base oil is hampered by the occurrence of low gravity solids similar to kaolinite and the ultra fine clays. These clays are similarly problematic for fluid fine tailings. Trials have been performed on a range of OBMs including diesel-based, mineral oil based and proprietary mixtures containing weighting compounds such as barite.

Performance on OBM is a suitable proxy for treatment of oil sands tailings, the latter being somewhat easier from the perspective of requiring less focus on 3-phase separation but more difficult due to the existence of abrasive sands and higher capacity needs.

The particle size distribution (PSD) of oil based muds processed through the SPT are similar to MFT with d50 of approximately 8 μm and a d10 of about 2 μm . Figure 2 provides the PSD for a typical OBM processed through the SPT and the feed reported on in this paper. In this case, the S.g. of the OBM was 1.09 because it was first decanted to remove larger solids and we used the centrate from the decanter as feed for the SPT.



Following processing, the specific gravity was reduced to 0.91 and the d50 and d10 was reduced to 1.12 μm and 0.45 μm , respectively (Fig. 3). The water effluent contained < 2% wt solids and the oil phase < 1% vol solids and water.



Solids cake discharged from the SPT had an average mineral solids content of 65%. The SPT delivered dry cake with a low water content of 13%, the remainder being oil and organic solids bound to the mineral phase. Additional benefits of processing included a reduction in viscosity of the base oil from 17.9 cP to 11.2 cP and an increase in the electrical stability from 822 to 1893.

Fluid Fine Tailings

Tailings with 30%wt solids represents the upper range of effective processing because solids fill the spiral plates within 10 minutes requiring up to 5 discharge cycles per hour. We processed two MFT bulk samples with mean characteristics presented in Table 1. From this feed, a cake was produced that averaged 67%wt dry solids with a 7 kpa shear

strength. Of these solids, about 8% was bitumen bound in the mineral matrix, the remaining 33% was water. The liquid effluent (centrate) contained 5%wt solids and 2%wt bitumen. Total mineral recovery on MFT was estimated at 98%.



Figure 2. T25 opened to show kaolinite processing prior to solids discharge

For TFT, total mineral recovery was estimated at 99%. As is typical with TFT, the resulting cake was slightly wetter at 54%wt solids. Other trials with TFT suggest the polymer holds water in the mineral matrix but that the resulting cake may dewater better once placed in a deposition cell. The polymer did enhance mineral recovery resulting in an exceptionally clean liquid effluent with 0.2%wt solids and 99.8% water.

For the simulated FFT, a cake was created containing 52%wt solids from the initial feed stream containing 4% solids. This simulated FFT was comprised of entirely very small clays and silt, unlike conventional FFT that may contain a

broader particle size distribution including sand. The liquid effluent from this trial contained 2%wt solids.

DISCUSSION

A typical plate pack in a dynamic settler has ~ 65 m² of surface area for settling. With rotational acceleration, the SPT can achieve several thousand times the efficiency of a standard IPS or lamella clarifier. During the settling process, the 65 m² area gets covered with a thin layer of consolidated (soft) solids at an average layer thickness of 2 mm. The artificial gravity applied to the liquid mixture is 1700-4500 Gs creating a settling velocity in the SPT pack of about 0.23 mm/sec. Settling is highly efficient and has demonstrated success in a number of oil and gas applications including removal of low gravity solids from base oil and waste (slop) oil.

This was the first time the SPT was applied to oil sands mine tailings. Several improvements are required and are being incorporated in future generations of the equipment that will allow greater recovery of solids without the need for polymer.

Currently, the systems efficiency is diminished for single units because of the batch process for solids removal. The process runs until sufficient solids have been separated to fill the bowl to capacity. In the T25 this maximum volume for the solids is 15 L. Effluent is discharged on a continuous basis until this point is reached. Once full (approximately 10 minutes in this trial), the remaining fluid is drained as effluent and the solids are discharged into the solids tray through a counter rotation discharge cycle lasting approximately 3-4 minutes. However, when paired with multiple machines, the process can be run continuously and efficiency is greatly improved.

CONCLUSIONS

The SPT draws on advances previously deployed in liquid-liquid (e.g. oil extraction) and liquid-solids treatment (e.g. municipal water treatment, tailings treatment). By creating similar conditions such as the maintenance of laminar flow and high relative area for particle settling but under high gravitational forces, the SPT vastly improves the loading rates that can be achieved in a small

footprint. As well, fine solids that could not be separated under normal clarifier designs can be removed by the SPT. Applications include, recovery of drilling fluids, bitumen froth treatment and tailings treatment.

The accumulation of fines in drilling fluids is the primary reason for loss of recycling and their need for disposal. Present technology allows separation of about 50% of these fines between 70 microns and 40 microns. With Evodos SPT, these fines can be removed to the desired specific gravity. A standard feed has a SG of 1.2, which we have demonstrated can be successfully treated to SG 0.92. As the process is purely mechanical the physical and chemical profile of the oil is not altered. The flashpoint remains the same. No added chemicals are needed for this process.

Three phase separation is possible in the SPT with "tunable" phase separation in the SPT pack. High separation efficiency can be maintained despite changes in feed viscosity, temperature or oil/water composition, however, gravitational (ie rotational speed) and feed flow settings must be adjusted to maintain the location of the interfaces between phases.

Emulsions are a challenge for any physically based separation equipment. In the case of SPT, an emulsion creates an additional interface between the light (e.g. oil) and the medium (e.g. water) phases. We have found that an emulsion phase creates a barrier to both solids and water separation in a single-pass system. Ideally, the emulsion is broken with chemical treatment prior to feeding the SPT in a single pass system. However, the location of the interfaces in the SPT can be controlled to allow the removal of the emulsion interface with either the medium or the light phase with no chemical addition. Similar oil recovery can be achieved by removing the emulsion with either the light phase or the medium phase on a first pass then applying the chemical treatment (e.g. demulsifier) to the reduced volume stream. The choice of which phase to recover the emulsion in depends on the characteristics of the chemistry used to break the emulsion and the desired product. After chemical addition to this reduced volume stream, the first pass phase with emulsion is fed to a second pass to recover the remaining oil.

REFERENCES

American Water Works Association AWWA (2012). Water Treatment Plant Design, Fifth Edition. © McGraw Hill 1990.

Cheremisinoff, N.P. (2002). Handbook of water and wastewater treatment technologies. © Butterworth-Heinemann.

Davis, M.L. (2010) Handbook of water and wastewater treatment technologies: Design principles and practice. © McGraw-Hill.

Rommel, W. E. Blass, M. Meon (1992). Plate separators for dispersed liquid—liquid systems: Multiphase flow, droplet coalescence, separation performance and design. Chem. Eng. Sci.: 47, (3) 555–564.

Tipman, R. and R.C. Shaw (1993). Recent advances in the treatment of oil sands froth. Presented at AOSTRA. In. Masliyah & Gray 2007: Oil Sands Extraction and Upgrading – Intensive short course.

PERFORMANCE OF ELECTRICALLY CONDUCTIVE DRAIN-TUBE PLANAR GEOCOMPOSITES (eGCP) FOR DEWATERING OIL SANDS TAILINGS

Patricia Dolez¹, Sébastien Bourguès-Gastaud², Eric Blond¹ and Pascal Saunier³

¹CTT Group / Sageos, Saint-Hyacinthe, QC, Canada

²Irstea, Antony, France

³Afitex-Textel, Ste-Marie, QC, Canada

ABSTRACT

The oil sands industry generates large quantities of mineral waste called fluid fine tailings (FFT), whose disposal is challenging because of its very low consolidation rate and very poor geotechnical properties. Electrically conductive drain-tube planar geocomposites (eGCP) can be used to improve FFT dewatering by forcing water displacement through electro-osmosis and efficiently draining the expelled water. A laboratory device has been developed to simulate the FFT dewatering taking place as a result of self-weight consolidation, electro-osmosis and drainage. It allows recording the amount of expelled water by two geocomposites positioned horizontally on each side of the FFT as a function of time, normal stress and voltage applied between the two geocomposites acting respectively as anode and cathode.

Results obtained with mature fine tailings (MFT) provided by an Oil Sands Operator and a prototype of eGCP combining a three-layer nonwoven geotextile, a perforated tube and a tinned copper braid are presented. The MFT solids content increased from 44% to 70% as a result of the combined consolidation under self-weight and compressive stress and electro-osmosis treatment. This led to an improvement in the MFT shear strength from 0 kPa to a mean value of 25 kPa with a reduction in MFT volume of 51%. The power consumption associated with this experiment was 130 Wh, corresponding to 6.6 kWh/m³ of treated MFT. The MFT particles were efficiently retained by the geotextile filter, leading to clear water being collected. These results demonstrate the large potential of eGCP for accelerating FFT dewatering. Further experiments will investigate the dewatering efficiency of these geocomposites for treated FFT, i.e. after cycloning, consolidation with gypsum or addition of a flocculent for example.

INTRODUCTION

The recent surge in oil price has led to a major increase in oil sands mining. In Alberta for instance, which holds the largest world concentration in oil sands, the production of crude bitumen has reached 1.94 million barrels per day in 2013 (Alberta Government, 2014). This number is expected to double by 2020. Indeed, Alberta's three major areas are estimated to contain about 1.7 trillion barrels in bitumen, which represents 173 billion barrels of oil (Alberta Government, 2008).

Open-pit mining of oil sands generates large quantities of mineral waste. It is estimated that the production of 1 ton of synthetic crude oil requires 12.3 tons of oil sands and generates 15.6 tons of tailings (Allen, 2008). These tailings contain about 70-80 wt% water, 20-30 wt% sand, silt and clay, and 1-3 wt% residual bitumen. According to current mining procedures, the tailings are pumped in settling ponds where sand separates rapidly from silt and clay fine particles, forming perimeter beaches around what is called fluid fine tailings (FFT). On the other hand, the fine particles constituting FFT are held in suspension by electrostatic interactions. They display very low consolidation rates and reach a limit concentration of about 30 wt% solids after a few years, when they are called mature fine tailings (MFT) (Mikula et al. 1996).

MFT are then stored in containment basins, which will need to be monitored for very long periods of time because of the almost absence of further consolidation MFT will experience at that point (Well, 2011). One issue with these ponds is related to the very low bearing capacity of MFT (Mills, 2011). In addition, their very long drying time limits water reuse by the mining companies.

In order to lower the impact of oil sands mining on local communities and the environment, Alberta's Energy Resources Conservation Board has issued in 2009 a new directive on tailings which

complements the already existing regulations on water and air quality. Mining companies are required to reduce fluid tailings by capturing fines and storing them in dedicated disposal areas (DDAs) (ERCB, 2009). These fine tailings should also be processed as they are produced so that materials deposited in the previous year reach a minimum undrained shear strength of 5 kPa and 10 kPa within 5 years after active deposition has stopped.

Large efforts have also been devoted by the mining companies and research groups in order to find solutions for improved tailings management (Devenny, 2010). A first strategy is based on the pre-deposit treatment of FFT using flocculants (Mikula et al. 1998), thickeners (Chalaturnyk et al. 2002), centrifugation (Houlihan, 2009), filters (BGC Engineering, 2010) and super absorbent polymers (Farkish et al. 2013) for example. An alternative solution allowing preserving the conventional mining operations relies on post-deposit dewatering. For example, freeze-thaw has been shown to generate a substantial dewatering in FFT (Dawson et al. 1999). However, none of these methods appear to have provided yet the mining industry with the ideal solution to the tailings issue (Beier et al. 2012).

A new post-deposit dewatering technique is described in this paper. It is based on the use of electrically conductive drain-tube planar geocomposites (eGCP). eGCPs combine two mechanisms (Bourgès-Gastaud et al. 2014): the traditional in-plane water transport function of drainage composites; and an electro-osmosis phenomenon induced by the application of a voltage across the layer of tailings between conductive elements embedded in geocomposites, which produces the migration of water from the anode to the cathode (Figure 1).

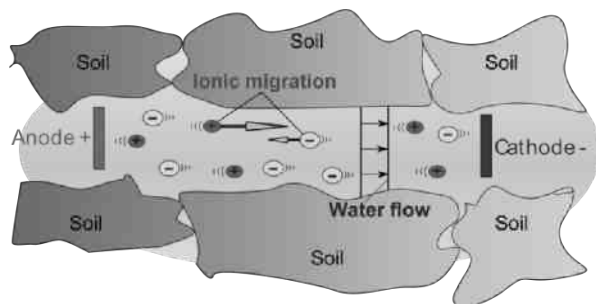


Figure 1. Principle of electrokinetic dewatering.

The efficiency of eGCPs to dewater FFT was tested with a laboratory device developed to simulate the path of water resulting from self-weight consolidation, electro-osmosis and drainage taking place in a real FFT disposal area dewatering scenario. Results obtained with MFT provided by an Oil Sands Operator and an eGCP prototype are presented. The dewatering efficiency is discussed in terms of MFT solids content, shear strength and power consumption.

MATERIALS AND METHODS

Electrically Conductive Drain-tube Planar Geocomposite

An eGCP prototype was developed by combining a drain-tube planar geocomposite and a metal electrode (Figure 2). Drain-tube planar geocomposites have gained acceptance within the geotechnical engineering community for transporting liquids and gases (Saunier et al. 2009). The drainage core is made of a 20-mm outer diameter perforated tube, which provides a high in-plane flow capacity. The eGCP prototype also includes a three-layer nonwoven geotextile, with two outer filter layers and a heavier central drainage one. The thickness of the geotextile is 5.9 mm (ASTM D5199), its masse per unit area is 553 g/m² (ASTM D5261), and its filtration opening size is 120 μm (ONGC 148.1-10). Finally, a cylindrical tin-plated copper braid (diameter 25 mm, resistivity 1.3 10⁻³ Ω.m) is positioned around the perforated tube, which is inserted in a gusset in the geotextile.



Figure 2. Picture of the eGCP prototype

Tailings

The dewatering experiments were carried out with a sample of MFT collected in August 2012 in a pond at the Muskeg River site (Alberta, Canada) and graciously provided by the Oil Sands Operator Shell Canada. An analysis of the MFT sample by

thermogravimetry revealed that they contain about 55 wt% water, 7 wt% bitumen and 35 wt% inorganic material. Grain size analysis was performed using the hydrometer method (ASTM D422). It showed that 72% of the particles are smaller than 45 μm . This sample thus appears to be slightly dryer and coarser than what is generally reported in the literature for MFT (Jeeravipoolvarn, 2010). Differences were also observed in the pH, with the value of 7.2 measured being slightly lower than the usual 8 to 8.5 range (Allen, 2008), as well as in the crystalline composition analyzed by X-ray diffraction, with 65% quartz, 14% kaolinite, 3% illite and no bentonite. The Zeta potential value of -31mV indicated a stable suspension.

Dewatering Test Setup

The experiments were carried out using a laboratory device specially developed to simulate the tailings dewatering taking place in a real FFT disposal area dewatering scenario as a result of self-weight consolidation, electro-osmosis and drainage (Bourgès-Gastaud et al. 2014). Two geocomposites are positioned horizontally on each side of the tailings (Figure 3). The test cell dimensions were selected to allow evaluating a representative area of the eGCP and to take into account the large strain deformation of the tailings: the internal width and depth are 270 x 270 mm^2 and the initial distance between the upper and lower eGCPs is 260 mm. The test cell can contain about 20 liters of tailings.

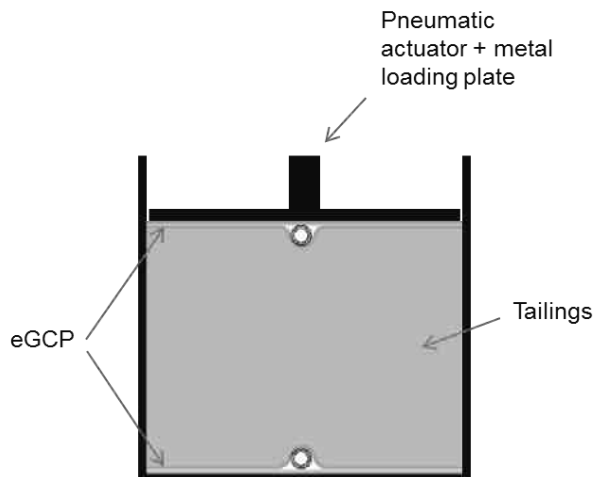


Figure 3. Schematic representation of the dewatering test setup

During the experiment, drainage is solely ensured by the upper and lower eGCPs: Particles are captured by the geotextile filter layers. Water flows in the geotextile central drainage layer and enters the drainage tube through the perforations in the tube wall. The lower eGCP tube goes through the cell wall and the filtrate is continuously discharged out of it by gravity. In the case of the upper eGCP tube, the filtrate is extracted with a Venturi pump. To avoid any pressure drop in the upper eGCP tube, it has an air inlet. Filtrates extracted by the upper and lower eGCPs are collected separately and weighted.

In order to simulate self-weight consolidation, normal stress of up to 60 kPa can be applied to the tailings by a system of pneumatic actuator and metal loading plate (Figure 3). The dimension of the loading plate is such that it slides with negligible friction along the cell walls.

The conductive components of the eGCPs are connected by copper wires to a DC power supply which can act either as a current or voltage source. Data acquisition is performed with a computer-controlled multimeter.

Test Protocol

For the experiment described in this paper, a sequence of steps was followed to simulate a typical dewatering scenario that would take place in a real FFT disposal area. It is illustrated in Figure 4.

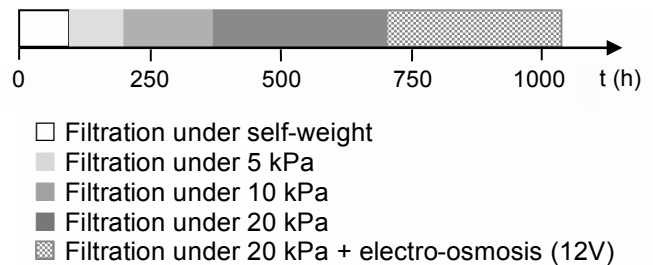


Figure 4. Dewatering experiment timeline

The first phase only involved filtration under self-weight exerted by the amount of tailings in the test cell. During that phase, only the lower eGCP was installed and its drainage tube constituted the sole outlet for the filtrate. This step allowed the formation of the filter cake on the geotextile filter. It ended when the filtrate expulsion had reached 60% of its asymptotic value. This first step lasted 96 hours.

The second step of the dewatering process started with the installation of the upper eGCP. Normal stresses of 5, 10, and then 20 kPa were applied to the MFT/eGCPs system with the pneumatic actuator and the loading plate to simulate the effect of overlaying layers as the pond is progressively filled. The value of 20 kPa corresponds roughly to the stress applied by a 1.5 m-thick layer of MFT. Each stress increment was applied when the expulsion degree had reached 60% of its asymptotic value. During that phase of filtration under compressive stress, the filtrate was collected both from the upper and lower eGCP tube. This second step lasted a total of 600 hours.

During the last phase of the dewatering experiment, the normal stress remained at 20 kPa and a voltage of 12 V was applied between the electrically conductive components of the upper and lower eGCPs. The cathode was positioned at the bottom of the cell and the anode at the top. This last electro-osmosis step lasted 335 hours and was also stopped when the expulsion degree had reached 60% of its asymptotic value.

RESULTS AND DISCUSSION

Figure 5 shows the cumulative weight of filtrate collected from the upper and lower eGCP tubes as well as the total collected filtrate as a function of time. The various phases of the dewatering experiment are also indicated. During filtration under self-weight, only the lower eGCP was installed and its tube was the sole outlet for the filtrate. As the normal stress was increased to 5, 10 and 20 kPa, the amount of filtrate that flowed from the upper and lower eGCP tubes was relatively similar. When the electro-osmosis (EO) phase started, only the lower eGCP, where was situated the cathode, collected filtrate.

The quantity of filtrate extracted during each phase is reported in Table 1. Mechanical dewatering under self-weight and compressive stress allowed the extraction of a significant quantity of filtrate. About 70% of the total quantity of filtrate was collected during these first two phases. This filtrate is thought to be composed of free water as well as part of interstitial water according to the categorization proposed by Smith and Vesilind (1995). A reduction in MFT volume of about 35% was achieved as a result of mechanical dewatering under a normal stress of 20 kPa. Therefore, eGCPs appear to provide a very efficient drainage for MFT.

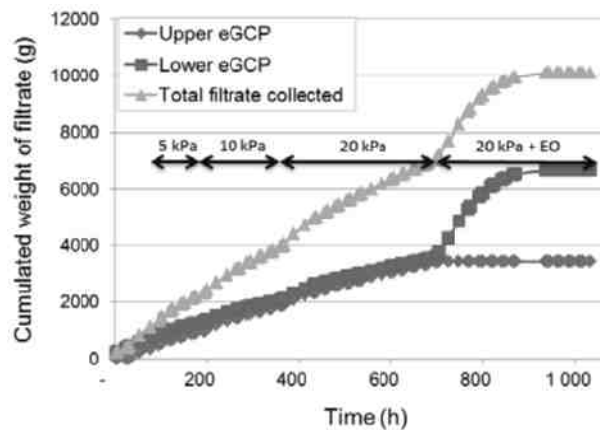


Figure 5. Filtrate collected as a function of time

Table 1. Quantity of filtrate extracted during each phase of the dewatering experiment

	Normal Stress (kPa)	Voltage (V)	Duration (h)	Filtrate collected (g)
Filtration	-		96	1 353
Normal stress	5		101	982
	10		170	1 698
	20		329	2 989
EO	20	12	335	3 066
Total			1 032	10 088

The additional treatment of the MFT by electro-osmosis allowed the extraction of another 30% of filtrate, possibly composed of the residual interstitial water and maybe some vicinal water. Indeed, electro-osmosis is expected to allow extracting water more tightly bound to solid particles. At the end of the electro-osmosis phase, the total reduction in MFT volume had reached 51%.

Except for the portion collected at the early stage of the filtration under self-weight phase, which was slightly cloudy, the filtrate was clear. An analysis of the filtrate by thermogravimetry provided a solids content value of 0.3%. The eGCP prototype tested is therefore very efficient to retain particles from flowing in the tubes.

The level of impregnation of the geotextile component of eGCP was measured to be around 1800 g/m² for the upper eGCP and 2700 g/m² for the lower eGCP. However, no trace of bitumen was visible to the naked eye on the geotextile grey filter or white drainage layer. The geotextile

impregnation is thought to be mostly attributable to clay particles. Therefore, filter clogging by residual bitumen does not appear to be an issue for MFT dewatering by eGCP.

The variation of the current as a function of time during the electro-osmosis phase is shown in Figure 6. The initial drop, from 111 to 88 mA within the first hour of treatment, may be attributed to a chemical polarization of the MFT. Then, a logarithmic decrease is observed. It can be attributed to the gradual dewatering of the MFT, especially around the anode, which lowers the electrical conductivity of the MFT. The power consumed during the dewatering experiment was equal to 130 Wh, which corresponds to 6.6 kWh/m³ of treated MFT.

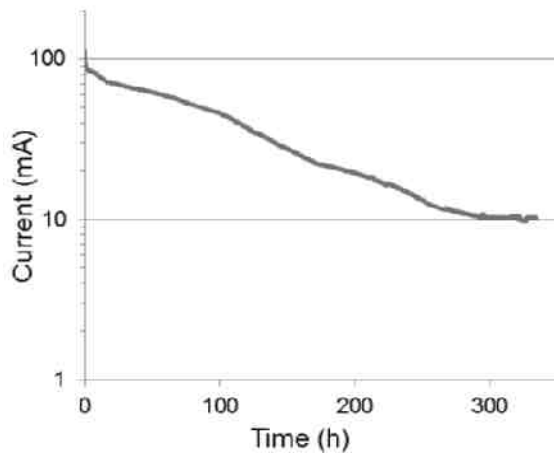


Figure 6. Current as a function of time

The long-term efficiency of the electro-osmosis treatment is limited by the durability of the electrodes, which may corrode over time. After the experiment was over, the side of the anode facing the cathode was strongly degraded (Figure 7). The weight loss of the anode was measured to be 47%. On the other hand, the cathode was still intact.

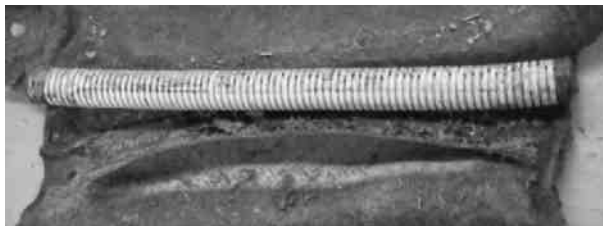


Figure 7. Condition of the anode after the electro-osmosis treatment

The solids content of the MFT after the dewatering experiment was completed was evaluated on two cores collected in the test cell. An average solids content of 70% was measured for the dewatered MFT, which corresponds to a 60% increase compared to the initial value.

Shear strength was also measured with a Geonor vane shear tester at three depths: just below the upper eGCP, at mid-height, and just above the lower eGCP. Figure 8 shows the results obtained. An increase in shear strength is observed with height, with a lower value being obtained in the vicinity of the cathode while the area close to the anode displayed higher shear strength. However, even the lowest value is well above the 10 kPa limit imposed by Directive 074 within 5 years after active deposition has stopped (ERCB, 2009).

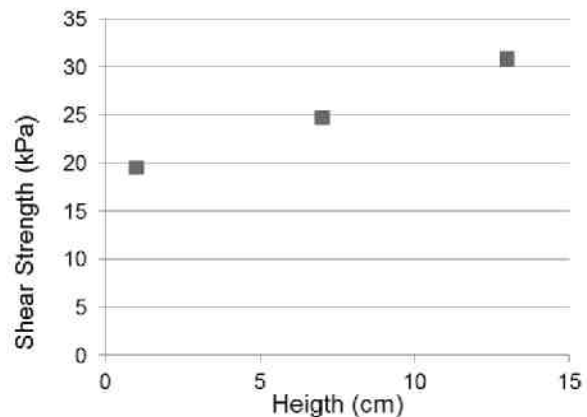


Figure 8. Shear strength of dewatered MFT as a function of height in the test cell

CONCLUSIONS

A study is currently conducted to evaluate the performance of electrically conductive drain-tube planar geocomposites (eGCP) for dewatering oil sands tailings. This paper reports the results of an experiment carried out on a mature fine tailings (MFT) sample provided by an Oil Sands Operator with a laboratory device developed to simulate the tailings dewatering taking place as a result of self-weight consolidation, electro-osmosis and drainage.

The dewatering protocol involved three steps: filtration under self-weight, filtration under compressive stress simulating a 1.5-m overlying tailings layer, and electro-osmosis. The eGCP prototype used combined a three-layer nonwoven

geotextile, a perforated tube and a tinned copper braid.

The results show that a large effect is produced by the mechanical dewatering processes, i.e. filtration under self-weight and filtration under compressive stress. A reduction in the MFT volume of about 35% is obtained at the end of the 20 kPa filtration phase simulating the action of a 1.5-m overlaying tailings layer. These data demonstrate the capability of drain-tube planar geocomposites for efficiently draining MFT.

The additional electro-osmosis treatment further improved the MFT dewatering. With 130 Wh corresponding to 6.6 kWh/m³ of treated MFT, the total MFT volume reduction produced reached 51%, with shear strength values above 20 kPa throughout the test cell.

These results show the large potential of eGCP for accelerating FFT dewatering. This type of treatment also offers the flexibility to stop the process when the desired result has been obtained. Further experiments will investigate the dewatering efficiency of these geocomposites for treated FFT, i.e. after cycloning, consolidation with gypsum or addition of a flocculent for example.

ACKNOWLEDGEMENTS

This project is carried out in partnership with Afitex-Textel (Quebec, Canada) as well as Canada's Oil Sands Innovation Alliance (COSIA). It benefits from a financial support from the Natural Sciences and Engineering Research Council of Canada (NSERC) through its Applied Research and Development program. The authors also want to thank Shell Canada for providing a MFT sample as well as Dr. Melissa Chappel and Mr. Maxime Lemire, who contributed to the experimental work.

REFERENCES

Alberta Government. 2014. Energy: Annual Report 2013-1014, 146p.

Alberta Government. 2008. Alberta's Oil Sands: Opportunity. Balance, 20p.

Allen, E. W. 2008. Process water treatment in Canada's oil sands industry: I. Target pollutants and treatment objectives. *Journal of Environmental Engineering and Science*, **7**: 123-138.

Beier, N., Sorta, A., Wilson, W., Segó, D. 2012. Challenges with meeting regulatory compliance in the oil sands industry. *Geotechnical News*, March 2012: 36-39.

BGC Engineering Inc., 2010. Oil sands tailings technology review. Oil Sands Research and Information Network, University of Alberta, School of Energy and the Environment, Edmonton, Alberta. OSRIN Report No. TR-1, 136p.

Bourgès-Gastaud S., Stoltz G., Dolez P., Blond E., Touze-Foltz N. 2014. A laboratory device to characterize electrokinetic geocomposites for fluid fine tailings dewatering. *Revue canadienne de géotechnique*. Accepted,...

Chalaturnyk, R. J., Scott, J. D., Ozum, B. 2002. Management of oil sands tailings. *Petroleum Science and Technology*, **20** (9-10): 1025 – 1046.

Devenny, D. W. 2010. A screening study of oil sand tailings technologies and practices. Alberta Energy Research Institute, 43p.

Dawson, R. F., Segó, D. C., Pollock, G. W. 1999. Freeze-thaw dewatering of oil sands fine tails. *Canadian Geotechnical Journal*, **36**: 587–598.

ERCB. 2009. Directive 074: Tailings performance criteria and requirements for oil sands mining schemes. Alberta's Energy Resources Conservation Board, Feb. 3, 2009.

Farkish, A., Fall, M. 2013. Rapid dewatering of oil sand mature fine tailings using super absorbent polymer (SAP). *Minerals Engineering*, **50–51**: 38-47.

Houlihan, R. 2009. Possibility of using centrifugal filtration for management of oil sands tailings, *OSTRF News*, March 2009: 1-2.

Jeeravipoolvarn, S. 2010. Geotechnical behaviour of in-line thickened oil sands tailings. PhD Thesis, University of Alberta, 410p.

Mikula, R. J., Kasperski, K. L., Burns, R. D., MacKinnon, M. D. 1996. Nature and fate of oil sands fine tailings. *Advances in Chemistry*, **251**: 667-723.

Mikula, R. J., Munoz, V. A., Kasperski, K. L., Omotoso, O. E., Sheeran, D. 1998. Commercial implementation of a dry landscape oil sands tailings reclamation option: Consolidated tailings.

7th UNITAR International Conference on Heavy Oil and Tar Sands, Beijing, China, 15p.

Mills, A. 2011. A case history on the use of high strength woven geotextiles to reinforce an oil sands tailings pond closure. Proceedings of the 2011 Pan-Am CGS Geotechnical Conference, Toronto, ON, Canada, 8p.

Saunier, P., Ragen, W., Blond, E. 2009. Behavior of 'Draintube' drainage geocomposites under high compression load. Proceedings of Geosynthetics 2009, Salt Lake City, UT, USA, 4p.

Smith, J.K., Vesilind, P.A. 1995. Dilatometric measurement of bound water in wastewater sludge. *Water Research*, **29**: 2621-2626.

Sunderland, J. G. 1987. Electrokinetic dewatering and thickening. I. Introduction and historical review of electrokinetic applications. *Journal of Applied Electrochemistry*, **17**(5): 889-898.

Wells, P. S. 2011. Long Term In-Situ Behaviour of Oil Sands Fine Tailings in Suncor's Pond 1A. Proceedings of Tailings and Mine Waste 2011, Vancouver, BC, Canada, 9p.

Session 10

Water Treatment

IMPACT OF CO₂ ADDITION ON INITIAL BASE MINE LAKE WATER CLARITY

Jordan Brandon, Weibing Lu, Vincent Duong and Ania Ulrich
Civil and Environmental Engineering, University of Alberta, Edmonton, Alberta, Canada

ABSTRACT

An end pit lake (EPL), with fluid fine tailings (FFT) below lake water, is a potential strategy to manage oil sand FFT in the reclaimed landscape while simultaneously allowing improvement in lake water quality. An essential requirement for this strategy to be successful is for sunlight to penetrate the lake water at least 2 m. Syncrude began the first full-scale oil sand EPL demonstration in 2013, called Base Mine Lake (BML). Previous studies indicate that lowering pH by adding carbon dioxide promotes flocculation of suspended clay particles and improves water clarity. Laboratory testing with 161 L columns containing BML water and FFT showed that bubbling CO₂ in the water reduced the pH from about 8 to about 6 but did not improve water clarity. To further reduce the pH to 3.5, hydrochloric acid was carefully added to the water after which water clarity improved to a maximum Secchi disk depth of 1.64 m. Light intensity measurements in the water produced a linear correlation between Secchi disk depth and light intensity: $I/I_0 = -0.0012D + 0.2445$ with $R^2 = 0.88$.

INTRODUCTION

The Alberta oil sands have seen rapid expansion in the last two decades. Two on-going challenges are managing oil sands process-affected water (OSPW) and fluid fine tailings (FFT). An end pit lake (EPL) with FFT below an initial lake water of OSPW, is a proposed strategy to incorporate FFT in the reclaimed landscape while allowing improvement in lake water quality to occur. The goal is to allow a viable aquatic ecosystem to establish while effectively sequestering FFT solids (McKenna and Hrynyshyn, 2012).

Suspended solids, released from the ore during bitumen recovery processing and subsequently dispersed in water contained in tailings impoundments, contributes to OSPW turbidity (Oil Sands Tailings Consortium (OSTC), 2012). A healthy aquatic ecosystem requires sunlight to penetrate through water to a depth of at least 2 m. A common simple field method to measure water

clarity is Secchi disk depth. It is determined by slowly lowering a Secchi disk and recording when its pattern is no longer visible through the water. Relative light intensity is a more rigorous water clarity measurement technique. A light sensor lowered in the water records the light intensity. The at-depth light intensity is divided by the light intensity measured at the water surface to determine the relative light intensity. This accounts for variations in absolute light intensity due to the light source and the time of day. Unless otherwise specified, light intensity in this paper will refer to relative light intensity.

Aas et al. (2014) introduces two estimations relating Secchi disk depth to relative light intensity; a) Secchi disk depth occurs at a relative light intensity of 10% and b) the depth of 1% relative light intensity is twice the depth of the Secchi disk depth. The depth of 1% relative light intensity is important because it is considered to be the minimum light required for photosynthesis (Luhtala and Tolvanen, 2013).

It is hypothesized that dispersed fine clay solids in lake water composed of some OSPW, and alkaline water pH (greater than ~8) significantly impairs light penetration, and that reducing the pH will flocculate many of these solids, improving water clarity. Previous studies have indicated that lowering the pH of the water causes positive charges to develop along the clay particle edges, promoting edge-to-face flocculation (Proskin et al. 2012). Carbon dioxide has been suggested to lower the pH because it is non-toxic, mimics natural carbon dioxide diffusion from air into water, and has a theoretical lower limit for pH reduction of around 5.7 in deionized water at $10^{-3.5}$ atm carbon dioxide partial pressure and 25°C (Lower 2014).

Two studies report success in using carbon dioxide in the densification of FFT. In the first study, Zhu et al. (2011) conducted a small-scale laboratory experiment where they lowered the pH of FFT to 5.8-6.0 by adding carbon dioxide directly into the FFT. Their experimental procedure added carbon dioxide to FFT in an autoclave at a pressure of 100 kPa and then allowed it to settle

for 24 hours in 100 mL graduated cylinders. As the carbon dioxide treated FFT settled, the released water was visually clearer than the released water from the untreated FFT column. In the second study, CNRL (2010) conducted a field-scale experiment where they introduced carbon dioxide directly into FFT and achieved a total suspended solids reduction in tailings pond water from 20,000 ppm to less than 500 ppm, five months after the carbon dioxide addition.

Following these reported results but recognizing the significant challenges of bubbling carbon dioxide into FFT in a uniform manner and not re-suspending solids, we tested bubbling carbon dioxide in BML lake water to see if similar effects on pH and water clarity could be achieved. The desired outcome is to have sunlight penetrate the lake water to a minimum of 2 m. Water clarity was measured using both a Secchi disk and a light intensity meter. In addition, we developed a relationship between light intensity and Secchi disk depth to validate the assumption that Secchi disk depth occurs at 10% of surface light intensity.

METHODS

Column set-up. A 2.5 m tall column was set up to simulate EPL conditions. The column had an outer diameter of 30.5 cm and was made of clear Townsend acrylic tubing with 0.635 cm wall thickness. A total of ten sampling ports were included in the design, two each at 40, 80, 120, 160 and 200 cm measured from the bottom of the column. Sampling ports were controlled by Swagelok SS Quarter-Turn Instrument Plugs, model SS-4P6T4. Figures 1 and 2 show the sample ports and the column. Approximately 20 cm of FFT from BML was placed at the bottom of the column. This was gently overlain with 2 m of BML water collected in 2013 with a composition of about 90% OSPW and 10% fresh water from Beaver Creek Reservoir. This composition mimics the approximate initial water composition of BML. The FFT and water were placed with a funnel and tube to minimize disturbance and mixing of the two layers. The top of the column was left open.

Lake water and FFT characterization. General water parameters were assessed for the lake water at day 0. One sample was taken at each sampling port and the results were averaged. pH and Redox were measured using an Accumet AR50 Dual Channel pH/Ion/Conductivity meter. Conductivity was measured with an Exstik II

EC500 portable meter and turbidity was measured using an Orbeco-Hellige Digital Direct-Reading Turbidimeter with readings taken five seconds after insertion into the instrument.

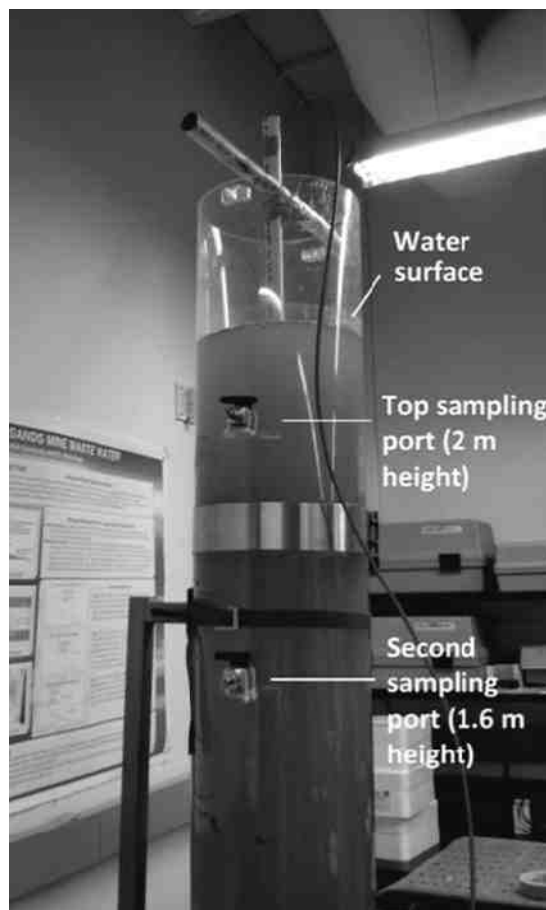


Figure 1. Top half of the water column at day 0 showing the top two sampling ports and water level at 2 m above the water/FFT interface (2.2 m height). The carbon dioxide addition tube and apparatus to keep it centred are shown on the top of the column.

Alkalinity was measured using an automatic titrator and 0.02N sulphuric acid. Hardness was measured during manual titration with Manver 2 hardness indicator and 0.01M EDTA following ASTM Standard D5907 (2012). Total dissolved solids (TDS) and total suspended solids (TSS) were determined following ASTM Standard D5907 (2013) with overnight drying at 105°C. FFT solids content was determined following ASTM Standard C324 (2001). Zeta potential was measured using a Malvern Zetasizer Nano ZSP and DTS1070

capillary cell at 25°C using electrophoretic light scattering.

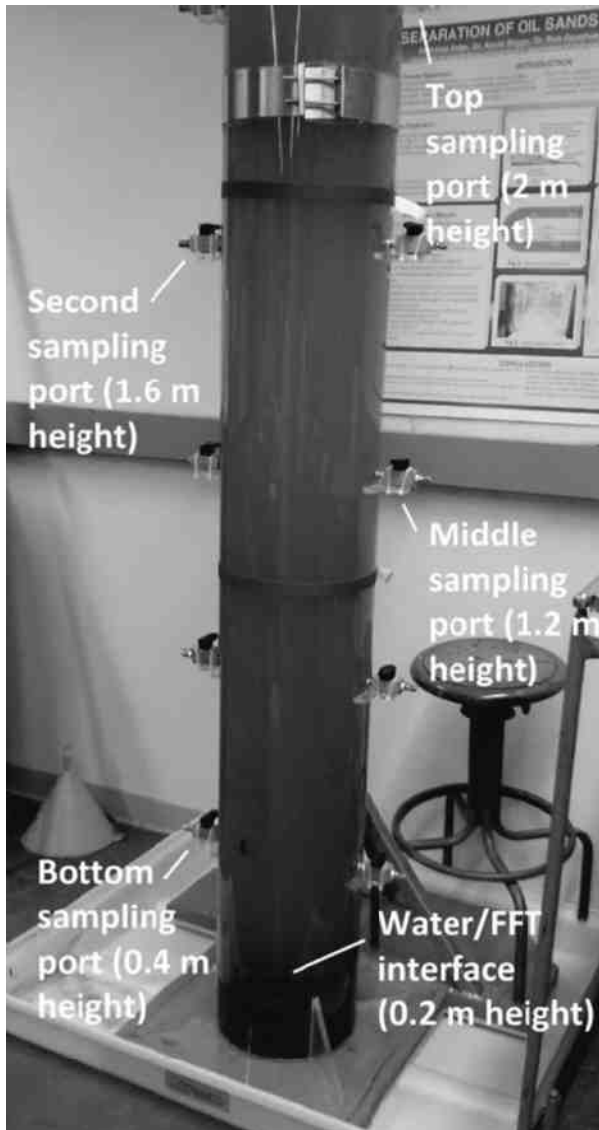


Figure 2. Bottom half of the water column at day 0 showing all sample ports and the water/FFT interface at a height of 0.2 m. An initial volume of 161 L of FFT and water combined were placed into the column.

Phase 1: Carbon dioxide addition. The first phase of the experiment used carbon dioxide gas (PRAXAIR, 99.9% purity) to lower the pH of the water. Table 1 summarizes the carbon dioxide addition for the duration of the experiment. Carbon dioxide was initially bubbled in at 0.14 m above the water/FFT interface at flow rates increased from

0.1 L/min to 0.3 L/min. Flow rate was measured using a Dwyer Cat. No. VFA-22 flow meter. The gas was bubbled through a Seal Plastics polyethylene tube (44D-1/4 OD) with a 4 mm opening positioned at approximately the centre of the column. The low flow rate was utilized to minimize disturbance of the FFT. Two days after the experiment commenced, the carbon dioxide outlet was moved from 0.14 m to 1 m above the interface to reduce potential disturbance to the FFT. No disturbance was observed but raising the discharge accommodated a higher flow rate of 0.3 L/min. Four days after the experiment commenced, a sparger (Corning, 39533-12C with pore size 40-60 μm) was added lowering the discharge point to 0.9 m above the FFT. The sparger was added to increase the diffusion of carbon dioxide into the water by creating smaller bubbles with larger surface area. At the same time the flow rate was increased to 1 L/min for 2 days. The pH did not significantly decrease after 2.2 days and this phase of the experiment was stopped at 9 days.

Phase 2: HCl addition. The second phase of the experiment used hydrochloric acid to lower the pH below 6. Initially small volumes of 16-19 mL of 0.1N hydrochloric acid were added but observing no effect on pH, the volumes and concentrations of the acid were increased. In total, 71 mL of 0.1N, 99 mL of 6N and 115 mL of 12N hydrochloric acid were added incrementally. Carbon dioxide was bubbled for a couple of hours after the addition of acid to aid in the acid distribution and to allow for uniform pH throughout the water.

pH readings. Sample ports on the sides of the column facilitated the taking of water samples at various depths. To measure pH, samples were taken at 20 cm and 180 cm above the water/FFT interface (the top and bottom sample ports in Figure 2). Initially these ports were 180 cm and 20 cm below the surface of the water respectively, but water levels decreased through the duration of the experiment due to evaporation and sampling. Measuring from the bottom of the column, water levels decreased from 2.20 m at the start of the experiment, to 2.10 m at 9 days (end of phase 1) to 1.96 m at the end of phase 2. The last two pH readings were taken at 140 cm above the water/FFT interface (second sample port from the top) instead of 180 cm because the water level was below the top sample port. For pH readings an Accumet Basic AB15 pH meter was used and the readings at both depths were averaged.

Table 1. Carbon dioxide addition to the water layer.

Duration of bubbling (days)	CO ₂ flow rate (L/min)	CO ₂ Volume (L)	Notes
0.0 – 0.2	0.1	29	CO ₂ introduced 0.14 m above water/FFT interface
0.2 – 0.9	0	0	
0.9 - 1.1	0.1	29	CO ₂ bottle changed at day 1
1.1 – 1.9	0.3	346	
1.9 – 2.2	0.3	130	CO ₂ introduced 1 m above water/FFT interface
2.2 – 4.0	0	0	
4.0 – 6.0*	1.0	2880	sparger added, CO ₂ introduced 0.9 m above water/FFT interface
6.0* – 7.9	0	0	*CO ₂ flow was interrupted during this time period but the exact time was not observed
7.9 – 8.9	1.0	1440	
	Total	4854	

Secchi disk depth. Secchi disk depth readings were done with a standard 20 cm Secchi disk with white and black markings and a braided polyester line (Science First 78-010 Fieldmaster Secchi disk). To ensure consistency, the same person did all of the Secchi disk readings. Two readings were done and averaged to get to the reported Secchi disk depth using the method outlined in Science First (2003). The first reading is determined by slowly lowering a Secchi disk and recording when

its pattern is no longer visible. A second reading is made by lowering the Secchi disk further and then slowly raising it and recording the depth at which its pattern reappears. For phase one of the experiment, Secchi disk depths were recorded with no side covering of the water column and no extra lighting other than those normally on in the room. The room contained 2 rows of double florescent tube lights (Philips 32T8/TL841 plus, 32 Watts). For the second phase (HCl addition), a blackout curtain was used to prevent light coming in from the side of the column and a Globe Workshop halogen work light (250 Watts, model no. 60568) was added at the top of the column. The work light was fixed above the column and directed downwards and not moved after initial installation. Secchi readings made in phase 1 and 2 were not mixed to ensure consistency.

Light intensity. Light intensity was measured using a LI-COR LI-192SA Underwater Quantum Sensor and LI-1400 datalogger. This LI-COR meter measures the intensity of the light in the photosynthetically active radiation (PAR) range of wavelengths between 400 nm to 700 nm (LI-COR, 2006; Alados and Alados-Arboledas, 1998). The sensor was attached to a lowering frame with the sensor pointing upwards to ensure the sensor was reading light intensity from the top of the column. Three 15-sec average readings were recorded at the surface and the Secchi disk depth. Light intensity is reported as light intensity at the desired depth (Secchi disk depth) over light intensity at the surface of the water. As mentioned before, during the second phase of the experiment, a curtain was used as well as the work light. The curtain and external light were added to reduce light interference entering the sides of the column and to ensure light intensity readings were only capturing the light penetration from the surface of the water.

RESULTS AND DISCUSSION

Once full lake water elevation was reached at Syncrude's BML the water composition consisted of about 90% OSPW and 10% fresh water. With fresh water inflow and outflow to maintain elevation, lake water composition will change over time. It is estimated that after 3 years the water composition will transition to about 20% OSPW and 80% fresh water. For this experiment, the lake water composition mirrors the initial water composition at BML (90% OSPW, 10% fresh). Initial water quality parameters and FFT

characteristics are shown in Table 2 and Table 3 respectively.

Table 2. Chemistry of initial lake water (90% OSPW and 10% fresh)

	Average	Standard Error	Number of Samples
pH	7.92	0.01	5
Conductivity (mS/m)	2.92	0.04	5
Redox (mV)	485	0.4	5
Turbidity (NTU)	88	4	5
Alkalinity (mg/L of CaCO₃)	588	2	5
Hardness (mg/L of CaCO₃)	39	1	9
TSS (mg/L)	29	3	3
TDS (mg/L)	1940	30	5

Table 3. FFT characterization completed on day 0 of the experiment.

	Average	Standard Error	Number of Samples
Solids content (% by mass)	37	4	4
Zeta potential (mV)	-28	1	3

Water and FFT characterization. The initial lake water is alkaline with high alkalinity levels. Both of these characteristics will impede lowering the pH. TDS, TSS, turbidity and conductivity are slightly below the values measured by Wang (2011) for OSPW, which can be explained by the addition of fresh water. For zeta potential, colloidal material is considered stable (and hard to settle) if the measurement is more positive than +30 mV or more negative than -30 mV (Moayedi et al., 2013). Measurements between -30 mV and 30 mV indicate the material can flocculate and settle (Moayedi et al., 2013). The FFT zeta potential is close to the dividing line of -30 mV for being stable. Lowering the pH will increase the zeta potential and improve flocculation and settling (Moayedi et al., 2013).

Phase 1: Carbon dioxide addition. The addition of carbon dioxide into the water column led to a

reduction in pH of the lake water as predicted. The pH was lowered from an initial 7.92 to 5.97 at its lowest point. Figure 3 shows the pH and Secchi disk depth profile during phase 1 of the experiment. After 2.2 days (after 500 L carbon dioxide addition), the pH at about 6 did not change significantly. At the end of the 9 days of intermittent carbon dioxide addition (an additional 4300 L between 2.2 days and 9 days), the pH of the lake water was 6.01. Neither did the Secchi disk depth change significantly during this time (17.5 to 19 cm) as shown in Figure 4.

Our results contradict those of Zhu et al. (2011) and CNRL (2013) where carbon dioxide addition into FFT improved lake water clarity. Zhu et al.'s (2011) lab study was conducted with 100 mL samples and carbon dioxide addition was through the use of an autoclave. Water clarity was visually observed after 24 hours. CNRL's (2013) study was completed at field-scale at their tailings pond and the carbon dioxide addition method is unknown.

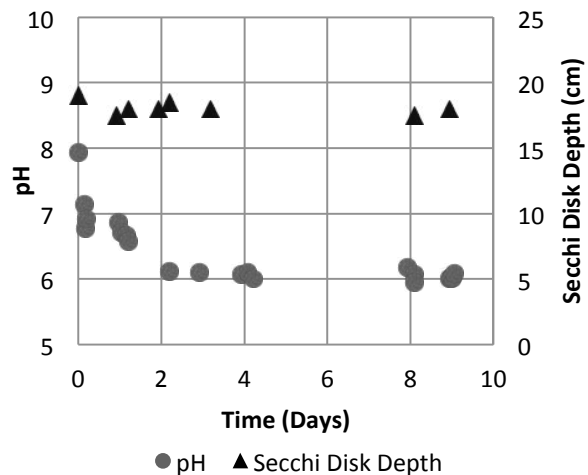


Figure 3. pH (●; primary y-axis) and Secchi disk depth (▲; secondary y-axis) profiles during carbon dioxide addition in Phase 1.

At the CNRL site, a lag period of one month was followed by a sharp decline in TSS between months two and three, followed by a more gradual decline in months four and five after which the TSS readings stabilized. Several factors could lead to the different results: (1) location of carbon dioxide addition – FFT versus lake water, (2) method of carbon dioxide addition – autoclave versus bubbling (3) scale of the experiments – 100 mL, 161 L or a tailings pond, and (4) duration of

experiment – 24 hours, 9 days or 5 months. Based on CNRL’s results there is a possibility that phase 1 of our experiment was not run long enough to see beneficial effects. Even though we had reached the saturation capacity of carbon dioxide under ambient conditions, more time may be necessary for water clarity to occur.

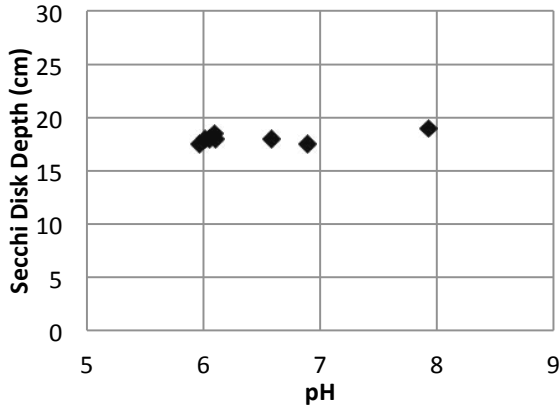


Figure 4. pH vs. Secchi disk depth over the 9 day course of the phase 1 experiment.

Phase 2: HCl addition. Hydrochloric acid was added after the completion of phase 1. Day 10 for the phase 1 experiment correlates to day 0 for the phase 2 experiment. Addition of small volumes of hydrochloric acid at the beginning of the experiment did not have any effect on pH. On day two, the addition of 100 ml of 12N hydrochloric corresponded to a drop in pH from 5.94 to 4.25 by day 5. Figure 5 shows the pH and Secchi disk depth profile for the duration of the phase 2 experiment. There is a clear increase in water clarity as measured by Secchi disk depth up to day 30. After day 30, the Secchi disk depth doubles in less than 30 days. The pH was not lowered during this time period and begins to rebound to pH 5. This indicates that time is a factor in increasing Secchi disk depth. Phase 1 of the experiment may not have been run long enough to see any of the effects on water clarity.

The increase in water clarity due to hydrochloric acid addition allowed us to study the relationship between light intensity and Secchi disk depth and to validate the assumption Secchi disk depth occurs at a light intensity 10% of the surface light intensity.

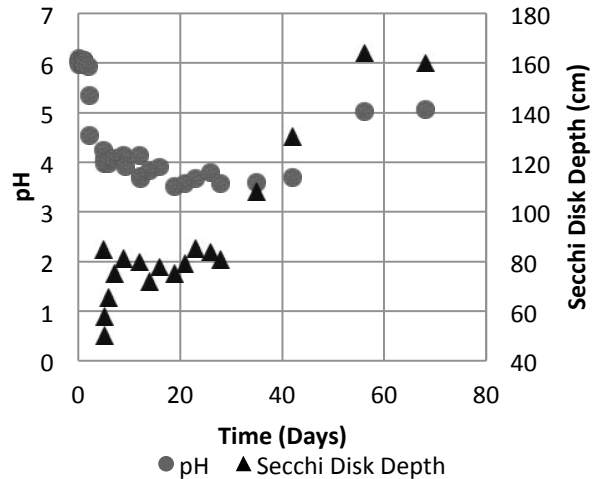


Figure 5. pH (●; primary y-axis) and Secchi disk depth (▲; secondary y-axis) profiles during hydrochloric acid addition in phase 2. Day 0 correlates to the start of the phase 2 experiment.

Our results are generally between 13% and 17% but a few measurements at the edge of our data range suggest a linear trend between Secchi disk depth, with larger Secchi disk depths leading to lower light intensity values. Secchi disk depth is often used as a substitute for light intensity (Aas et al., 2014; Holmes, 1970; Luhtala and Tolvanen, 2013), thus it would make sense for the light intensity to be the same at the Secchi disk depth regardless of where that depth occurs. Figure 6 shows the relationship between Secchi disk depth and light intensity. It is important to note that a Secchi disk reading is subjective and dependent on the person taking the measurements. We took this into account and ensured the same person did all Secchi disk depth measurements, therefore ensuring data was internally consistent. The line of best fit is drawn through the data assuming a simple linear relationship between light intensity and Secchi disk depth. There is a negative slope in the data collected. The equation for the linear line of best fit was found to be:

$$I/I_0 = -0.0012D + 0.2445; \quad R^2 = 0.88$$

Where, I/I_0 = Light Intensity (unitless)
 D = Secchi disk depth (cm)

Aas et al. (2014) did similar but more extensive experiments on Secchi disk depth and light intensity in coastal areas around Oslo. Their study

found the mean light intensity at the Secchi disk depth was 9% with a standard deviation of 6% (Aas et al. 2014) from several different sea bays. Data collected from one primary bay averaged 9% with a standard deviation of 4% (Aas et al. 2014). In comparison, our data ranged from 5%-26% with an average of 14% and standard deviation of 5%. We do not know the reason our data displayed a trend but two suggestions are offered for future research. First, Aas et al. (2014) did a field study in open ocean water while our experiments were conducted in a water column with blacked out sides. Light intensity measurements in the lab column may have been systematically lower than in the field because light penetration from the sides was eliminated. If light penetration from the sides is more important at greater depths, this could explain the reason light intensity at greater Secchi disk depths is lower than at shallower Secchi disk depths. Second, the parameters and composition of the BML lake water may somehow impact the Secchi disk depth and light intensity. It is recommended that future work, such as a field study comparing Secchi disk depth and light intensity at BML be conducted.

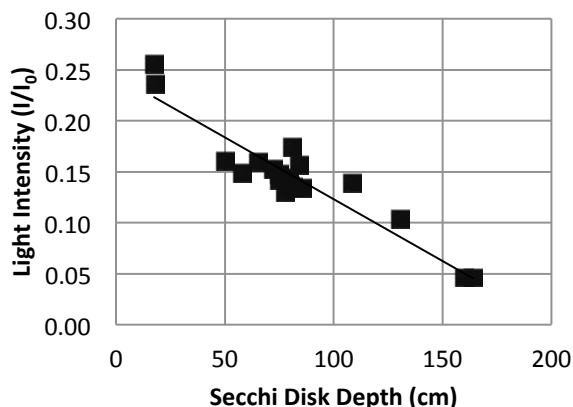


Figure 6. Correlation between light intensity and Secchi disk depths.

CONCLUSION

Two different relationships were explored through the two experimental phases. The effect of carbon dioxide on pH and water clarity was tested in phase 1 and the effect of hydrochloric acid on pH and water clarity was tested in phase 2. In addition, the relationship between light intensity (measured with a LI-COR PAR sensor) and Secchi disk depth was established in phase 2.

The addition of 4854 L of carbon dioxide to lake water over a 9 day period in an end pit lake scenario had no effect on water clarity. The pH of the lake water was reduced from 8 to 6 but no corresponding effect on water clarity was observed. Lowering the pH further using HCl led to an increase in water clarity, with Secchi disk depth doubling between day 30 and day 60. We propose that future research focus on determining: (1) if a lag period of one to three months is required before an improvement in water clarity is observed, and (2) to what extent water composition of 90% OSPW and 10% fresh water versus 20% OSPW and 80% fresh water plays a role in water clarity.

The relationship between light intensity and Secchi disk depth was examined. The assumption that the Secchi disk depth represents the depth at which 10% of the light at the surface is able to penetrate was not observed in this study. Instead, the data suggests that as the Secchi disk depth moved further into the water column, the measured light intensity reduced. The reason for this trend is not known. A field study on Secchi disk depth and light intensity in BML could validate the relationship found in this experiment and help to identify the reason for the trend found in our data.

ACKNOWLEDGEMENTS

The authors would like to thank Syncrude for providing the funding for this project and for access to their EPL FFT and lake water sources. As well, an NSERC CGS M scholarship helped fund Jordan Brandon. In addition, the authors would like to thank Dr. Lisa Brown for her expertise and advice before, during and after the experiment.

REFERENCES

- Aas, E., Høkedal, J. And Sørensen, K. 2014. Secchi Depth in the Oslofjord-Skagerrak Area: Theory, Experiments and Relationships to Other Quantities, 10:177-199.
- Alados, I and Alados-Arboledas, L. 1998. Direct and Diffuse Photosynthetically Active Radiation: Measurements and Modelling. *Agricultural and Forest Meteorology* 93:27-38.
- ASTM Standard C324. 2001 (2014). Standard Test Method for Free Moisture in Ceramic Whiteware Clays. ASTM International, West Conshohocken, PA, USA.

- ASTM Standard D1126. 2012. Standard Test Method for Hardness in Water. ASTM International, West Conshohocken, PA, USA.
- ASTM Standard D5907. 2013. Standard Test Method for Filterable Matter (Total Dissolved Solids) and Nonfilterable Matter (Total Suspended Solids) in Water. ASTM International, West Conshohocken, PA, USA.
- Charette, T. and Mooder, B. 2012 Regional Geography & Ecology. In: Cumulative Environmental Management Association ed. *End Pit Lakes Guidance Document*. Wood Buffalo, AB, Canada: Cumulative Environmental Management Association, pp. 101-137.
- CNRL. 2010. 2010 Stewardship Report to Stakeholders. Innovations in Tailings Management.
- Holmes, R. 1970. The Secchi Disk in Turbid Coastal Waters, *Limnology and Oceanography*, 15:688-694.
- LI-COR. 2006. LI-COR Underwater Radiation Sensors: Instruction Manual.
- Lower, S. 2014. *Carbonate Equilibria in natural Waters*. Simon Fraser University, Barnaby, BC, Canada.
- Luhtala, H. and Tolvanen, H. 2013. Optimizing the Use of Secchi Depth as a Proxy for Euphotic Depth in Coastal Waters: An Empirical Study from the Baltic Sea, *ISPRS International Journal of Geo-Information*, 2:1153-1168.
- McKenna, G. and Hrynshyn, J. 2012. Introduction and Background. In: Cumulative Environmental Management Association ed. *End Pit Lakes Guidance Document*. Wood Buffalo, AB, Canada: Cumulative Environmental Management Association, pp. 9-29.
- Moayed, H., Kazemian, S., Kassim, K.A., Nazir, R. and Raftari, M. 2013. Removal of Suspended Colloids through the Control of Their Zeta Potential, *Journal of Dispersion Science and Technology*, 34:1273-1279.
- OSTC. 2012. Technical Guide for Fluid Fine Tailings Management.
- Proskin, S., Seago, D. and Alostaz, M. 2012. Oil Sands MFT Properties and Freeze-Thaw Effects, *Journal of Cold Regions Engineering*, 26:29-54.
- Science First. 2003. 78-010 Fieldmaster Secchi Disk: Limnological, 200 mm. Yulee, FL, USA.
- Wang, Yingnan. 2011. Application of Coagulation-Flocculation Process for Treating Oil Sands Process-Affected Water. M.Sc. Thesis. University of Alberta, Canada.
- Zhu, R., Liu, Q., Xu, Z., Masliyah, J., H., Khan, A. 2011. Role of Dissolved Carbon Dioxide in Densification of Oil Sands Tailings. *Energy & Fuels*, 25:2049-2057.

THE POTENTIAL IMPACT OF DIFFERENT TYPES OF TAILINGS ON WATER QUALITY AND QUANTITY REPORTING TO OIL SANDS END PIT LAKES: A PRELIMINARY MODELING EXERCISE

Alexander Holden¹, Gord McKenna¹, Xiaoying Fan² and Kevin Biggar¹

¹BGC Engineering Inc.

²Suncor Energy Inc.

ABSTRACT

Oil sands tailings management has been evolving since mining began 50 years ago. Many technologies are currently used commercially to manage oil sands tailings. Each technology releases consolidation and seepage waters at different rates and with different chemistries. The flux and quality of these release waters in the closure landscape will affect proposed end pit lakes (EPLs) downstream – these effects may be relatively benign or adverse - and they may potentially change with the adoption of new technologies during mining operations. To explore the effect of various tailings technologies and tailings properties on water quality reporting to EPLs, a simplified spreadsheet model was developed. The model consists of a single tailings facility situated within a reclaimed watershed that sustains an EPL. The type of tailings in the deposit was changed with each model run. The model provided several unexpected insights. Notably, the loading and chemistry at the EPL inlet from the various tailings technologies tended to converge after about 10 years. Secondly, regardless of the technology used, the results suggest that EPL water quality is likely to be dominated by seepage and drainage from tailings sand deposits. Seepage from these sand deposits is expected to send large quantities of process-affected waters to the EPLs well into the future.

INTRODUCTION

End pit lakes (EPLs) in the Oil Sands region are being designed for passive treatment of process-affected waters, as a reclamation technology for mined-out pits, and in many cases, for storing fluid oil sands tailings under a fresh water cap (CEMA 2012). Ongoing industry research and development, stimulated in part by increasing regulatory pressures to reduce the volumes of fluid tailings, has led to examination of new tailings

technologies which are now at various stages of research, development, and commercialization. Each of these proposed tailings technologies results in different volumes of fine and coarse tailings, releasing process-affected waters with different chemistries and at different rates. The flux and quality of these release waters in the closure landscape will affect the chemistry and performance of EPLs downstream – these effects could be positive or negative for the EPL.

The objective of this study was to evaluate the potential impact of various tailings technologies on water quality reporting to EPLs as part of the reclamation and closure of oil sands mines.

Key tasks were to:

- List and group tailings technologies that are presently under consideration for the Oil Sands region using the list of CTMC Tailings Roadmap technologies (CTMC 2012)
- Conduct a literature review of water quality and release rates information for the tailings technologies identified
- Run model simulations of a generic EPL watershed to directly compare the influence of these tailings technologies.

METHODS

The study began with assessing the 101 technologies identified by the Tailings Roadmap (CTMC 2012) and creating a short list of 54 technologies for more detailed investigation. A literature review was conducted to characterize the properties of the tailings produced by each of the selected technologies, with a focus on consolidation rates, hydraulic conductivities, and release water quality.

To rapidly explore the potential effect of each type of tailings on water quality reporting to an EPL, a simplified spreadsheet model was developed. The

model consists of a simple, generic (or virtual) EPL watershed, and simulates the impact of a single tailings facility and the associated reclaimed watershed upon the water chemistry reporting to an EPL (Figure 1). The tailings facility was either a reclaimed tailings pond (Scenario 1) or an above-grade waste dump (Scenario 2). In both cases, the tailings facility was assumed to consist of an overlying deposit of tailings and a containment

structure or underlying base material (tailings sand or overburden). The type of tailings in the deposit was changed with each model run. The rate of water release and the water quality from the tailings deposit, dilution from the watershed, and the resulting water quality at the EPL inlet were estimated for each technology under consideration.

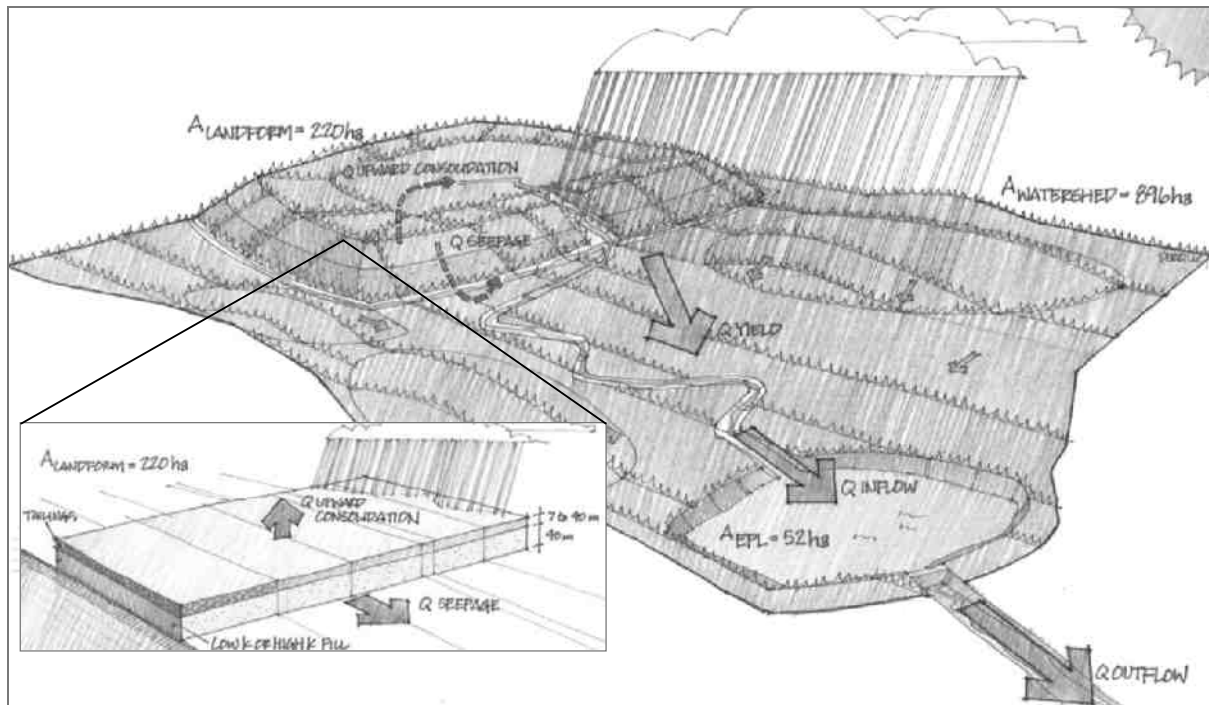


Figure 1. Virtual EPL watershed conceptual model. The watershed includes a single tailings facility (either a reclaimed tailings pond (Scenario 1) or above-grade waste dump (Scenario 2) – see inset).

While there are more complex consolidation, groundwater/seepage, and EPL models in use in the industry, the advantages of this generic model are its simplicity, transparency, and it allows for rapid comparison of different tailings technologies under the same conditions.

Inputs and outputs to/from the EPL included:

- Post-reclamation tailings consolidation water (at a declining rate)
- Yield (surface water runoff + groundwater discharge) from reclaimed and natural land
- Seepage from the tailings deposit (assumed, for simplicity, to report to the EPL after consolidation is complete)
- Re-use, treatment, or discharge of water from the EPL outlet, to maintain a constant lake elevation.

The potential location of different types of tailings in the closure landscape was determined by working with Suncor staff and using current mine tailings and closure plans. This information was used to refine the model scenarios (Table 1).

Chemical species of interest were identified by Suncor and included select major ions, trace elements, nutrients and organics. However, complete chemistry describing the tailings pore waters was not available for all technologies, therefore the study focused on sodium (Na), chloride (Cl), naphthenic acids, and total dissolved solids (TDS) (e.g., Table 2). Table 3 lists important input parameters and Table 4 lists assumptions and approximations.

RESULTS AND DISCUSSION

Modeling of the virtual EPL watershed provides an estimate of the quantity and quality of produced water that would affect the EPL, from the deposition of tailings in the closure landscape.

The modeled chemistry at the EPL inlet, accounting for release from tailings within a reclaimed tailings pond and site-wide yield (Scenario 1) indicated that:

- Release water from froth tailings caused the highest EPL inlet concentrations (Figure 2)
- The responses from all tailings types tended to converge after roughly 10 years (Figure 2).

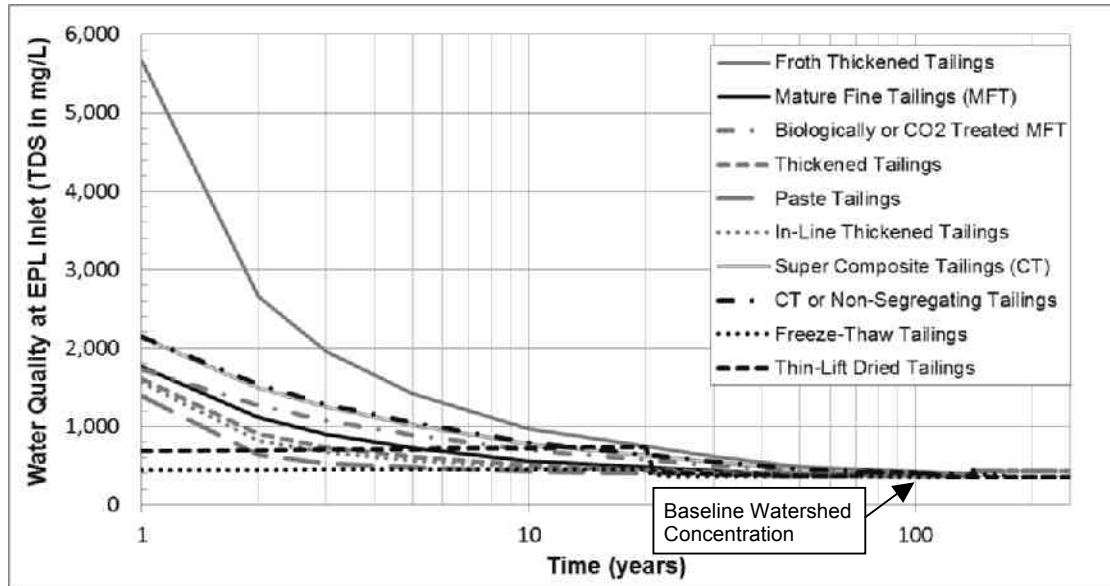


Figure 2. Simulated water quality (TDS) at the inlet of a virtual EPL, accounting for consolidation release from a single tailings facility (reclaimed tailings pond – deposited tailings type was varied) and yield from the reclaimed watershed. The results suggest that the response to the different types of deposited tailings converges after approximately 10 years.

The modeled chemistry at the EPL inlet, accounting for release from tailings deposited within a waste dump and site-wide yield (Scenario 2) indicated that:

- The responses from almost all tailings types tended to converge after roughly 10 years
- The response from tailings sand deposits (which includes Conventional Hydraulic Fill and similar technologies) did not show the exponential decrease in concentrations common to most technologies, but instead released elevated concentrations well into the future (Figure 3).

While most tailings technologies provide different means of transforming fluid tailings into more stable and solid deposits, the alternate extraction technologies – retorting (Taciuk 1981) and solvent extraction (Tis et al. 1984) - represent radical changes to ore processing that have important

repercussions that extend to reclamation and closure. These include the generation of 'dry' tailings. Little information was found concerning the properties of either technology's tailings during the review of publicly available literature. As these methods provide a major reduction in ionic loading rates, further investigation is likely warranted if an operator wishes to consider this change to its extraction process.

Chemistry and Peak Loading

Water quality and its implications on the receiving environment can be assessed in several ways, one of which is analysis of the peak concentrations released over time. For tailings deposited in tailings ponds and above-grade waste dumps, inorganic species loading was greatest from froth treatment thickened tailings (initial concentration of 5600mg/L TDS), and least from freeze-thaw

tailings (peak concentration of 450mg/L TDS). Because most reported water chemistries did not include complete trace element or polycyclic aromatic hydrocarbon characterization, comments cannot be extended to other chemical species. The order of decreasing ionic loading was: froth treatment > tailings sand > rim ditching > CT-like

tailings > MFT-like tailings > thickened tailings > thin-lift drying > freeze-thaw drying. It is noted that the volumes of each of these tailings varies considerably from plan to plan, and in particular, froth tailings is generally a low volume deposit relative to other tailings products.

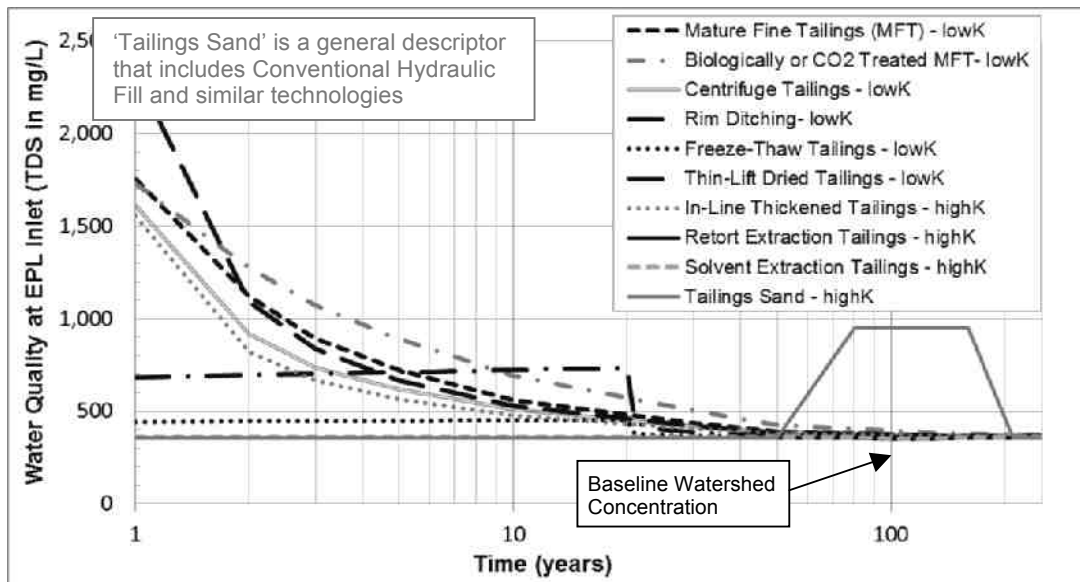


Figure 3. Simulated water quality (TDS) at the inlet of a virtual EPL, accounting for consolidation release from a single tailings facility (above-grade waste dump– deposited tailings type was varied) and yield from the reclaimed watershed. The dump base material was either low conductivity overburden (lowK) or high conductivity tailings sand (highK). The results suggest that seepage/drainage from tailings sand deposits and landforms will be a key driver of long-term water quality in EPLs.

Rates and Durations of Release

Equally important to peak concentrations are the rate and duration of release of process-affected waters from the tailings deposit. Three different patterns were observed.

- The most common was for a large initial release of process-affected water with a rate that decreased exponentially.
- A second type was for a single pulse of loading, observed in high conductivity, non-consolidating sediments deposited within high conductivity landforms (this pertained to tailings sand, retort extraction tailings, solvent extraction tailings, and sand or coke covers).
- The last type of behaviour was specific to thin-lift deposition technologies, and included a fairly constant release of consolidation water from the outset of deposition until shortly after

the last lift was deposited, at which point release decreased rapidly. In this last scenario, each lift behaves similarly to the first pattern, releasing process water in an exponentially decreasing manner. The net effect of adding a new layer each year is an approximately constant level of release.

Differences in the rates and durations of release can have important implications on water treatment and impact on the receiving environment. A high initial chemical loading that decreases rapidly with time may be suited to direct recycle to the plant or treatment by a water treatment facility. According to our simplified model, such a facility could be operated for relatively short duration (e.g., ten years following closure), and would treat the bulk of the loading. Thereafter, release rates and chemical loading drop significantly, to the point that

dilution or polishing by bioremediation may be sufficient before waters could be discharged into the environment.

Alternately, the opposite strategy might be warranted – rather than encouraging or accommodating initial high release of chemical species, use engineered measures to forcibly slow the initial release into the watershed so that the loading becomes more uniform, and can be treated or diluted by the closure watershed (e.g., Rowe 1990). Such a strategy may also be warranted for tailings which release a pulse of chemical loading, such as tailings sand deposits. This might include use of low permeability covers, containment within low permeability sediments or use of a liner, restricting drainage into the EPL to allow sufficient dilution from the watershed as a whole, or use of other watershed control measures.

The modeling suggests that thin-lift deposition technologies yield a more consistent release of chemical species that would seem to be amenable to a variety of strategies. For example, water treatment of such a constant loading may be easier to implement than for technologies which display an exponential decay of concentrations over time.

Seepage from Large Tailings Sand Deposits

The data suggest that tailings sand deposits will themselves yield significant chemical loading to the reclamation and closure watershed. Coarse tailings sand deposits or landforms are highly permeable, have a porosity of about 30 to 40% (McKenna 2002), are ten to fifteen times the volume of the fine-grained tailings deposits (the focus of the present study), and contain five to fifteen times the volume of process-affected water.

There are several important implications of the chemical loading from tailings sand deposits as they relate to EPLs:

- Long-term drain-down and flushing from large tailings sand deposits will typically take several centuries and produce large fluxes of process-affected waters reporting to the EPLs (e.g., Price 2005).
- These fluxes will typically be much larger and far outlive the fluxes from fine-grained deposits owing to the difference in relative volumes of the tailings sand landforms and the relatively low gradients driving seepage rates.
- The simple model used in this study shows this effect in Figure 3, but since the volume of sand

considered was small (to allow direct comparison with other tailings technologies), the effects are understated.

- Alternatives which dramatically change this outcome include non-water-based extraction technologies, which leave de-saturated sand-based deposits. However, the connate salts remain (though are not concentrated by multiple passes through the extraction plant) and will flush with time. If these technologies are considered further, prediction of their flushing rates and chemistries will need to be refined. Alternatively, coarse tailings could be filtered or cycloned to reduce the total ionic loading, and re-slurried with fresh water (as is done with some kimberlite tailings) if required, but again at considerable expense.

Thus, the long-term water quality and quantity from various tailings technologies reporting to EPLs may have a relatively small impact on EPL performance due to the large volumes from tailings sand deposits.

CONCLUSIONS

In this study, a simple Excel-spreadsheet-based model was created to rapidly explore the impact of different tailings technologies deposited in the reclamation and closure landscape on water quality reporting to EPLs.

Based on the results, the following conclusions are drawn:

- Regardless of which technologies are used to manage the oil sands tailings fines, the EPL water quality is likely to be dominated by seepage and drainage from tailings sand dumps and landforms. Seepage from these large tailings sand deposits will send large quantities of process-affected waters to the EPLs well into the future.
- The release water chemical loading and resultant EPL inlet water quality from the various tailings technologies tended to converge after about 10 years (well within the lifespan of the mine).
- The technologies can be grouped into four categories with respect to the effect on EPL water quality:
 - Non-aqueous extraction technologies (retort and solvent extraction) have the greatest potential to reduce naphthenic acid and salt loading reporting to EPLs.

These are step-out technologies not under active consideration and present other cost and environmental challenges. Further work to explore the potential benefits and risks to EPLs may be warranted.

- Technologies that de-saturate the tailings (thin-lift drying, accelerated dewatering, filtration) have the ability to remove ions from the deposits and have slow flux rates for long-term seepage compared to conventional tailings technologies.
- Other slurry-based tailings technologies all contribute consolidation and seepage waters to the EPL along a continuum of release rates.
- There are no indications that the major technologies under consideration have water chemistries that are significantly different from existing conditions to warrant further specific EPL water quality research on those technologies. One exception to this may be froth treatment tailings and reprocessed froth tailings due to the pH and organic solvent carry-over considerations. Methods of storing and potentially retreating froth tailings should be given a high priority.
- This paper provides the basis for a simple model. For design, more complex models will be employed for specific closure plans.

REFERENCES

- AECOM, 2012. Basis of design memorandum: Suncor Energy Tailings Water Treatment Plant. Suncor Project No.: 03-00093, AECOM Project No.: 60241853, 15 pp.
- Chapman, D. E., 2008. Hydrogeologic characterization of a newly constructed saline-sodic clay overburden hill. M.Sc. Thesis, Dept. of Civil Engineering, University of Saskatchewan, Saskatoon, SK. 154 pp.
- Cumulative Environmental Management Association (CEMA), 2012. End pit lakes guidance document. Available from: http://cemaonline.ca/index.php/administration/cat_view/2-communications/20-cema-news/22-the-insider.
- Consortium of Oil Sands Tailings Management Consultants (CTMC), 2012. Oil sands tailings technology deployment roadmap. Project report – volume 2 component 1 results. Consultants' report for OSTC and Report to Alberta Innovates – Energy and Environment Solutions. Available from: http://ai-ees.ca/media/7361/1906-component_1_report.pdf.
- Fedorak, P.M., Coy, D.L., Salloum, M.J., Duda, M.J., 2002. Methanogenic potential of tailings samples from oil sands extraction plants. *Canadian Journal of Microbiology*, 48:21–33.
- Headley, J.V., Armstrong, S.A., Peru, K.M., Mikula, R.J., Germida, J.J., Mapolelo, M.M., Rodgers, R.P., Marshall, A.G., 2010. Ultra-high resolution mass spectrometry of simulated runoff from treated oil sands mature fine tailings. *Rapid Communications in Mass Spectrometry*, 24:2400-2406.
- McKenna, G., 2002. Landscape engineering and sustainable mine reclamation. Ph.D. Thesis, Dept. of Civil and Environmental Engineering, University of Alberta, Edmonton, AB. 660 pp.
- Pollock, G.W., McRoberts, E.C., Livingstone, G., McKenna, G.T., Matthews, J.G., Nelson, J.D., 2000. Consolidation behaviour and modelling of oil sands composite tailings in the Syncrude CT prototype. IN: Tailings and Mine Waste '00, Proceedings of the 7th International Conference on Tailings and Mine Waste, 23-26 January, 2000, Fort Collins, CO, U.S.A. pp: 121-130.
- Price, A.C.R., 2005. Evaluation of groundwater flow and salt transport within an undrained tailings sand dam. M.Sc. Thesis, Dept. of Earth and Atmospheric Sciences, University of Alberta, Edmonton, AB. 129 pp.
- Proskin, S., Sego, D., Alostaz, M., 2010. Freezethaw and consolidation tests on Suncor mature fine tailings (MFT). *Cold Regions Science and Technology*, 63:110-120.
- Quagraine, E.K., Peterson, H.G., Headley, J.V., 2005. In situ bioremediation of naphthenic acids contaminated tailing pond waters in the Athabasca oil sands region – demonstrated field studies and plausible options: a review. *Journal of Environmental Science and Health*, 40:685-722.
- Rowe, R.K., 1990. Contaminant impact assessment and the contaminating lifespan of landfills. *Canadian Journal of Civil Engineering*, 28:244-253.

Sawatsky, L., Wislesky, I., Wu, S., 2012. Comparison of pore water storage requirements of several tailings management systems. IN: Proceedings: International Oil Sands Tailings Conference, 2-5 December, 2012, Edmonton, AB, Canada. pp: 93-101.

Total E&P Joslyn Ltd., 2010. Joslyn North Mine Project Additional Information February 2010 – Appendix J: Water Quality Supporting Information. Available from: http://www.total-epectanada.com/upstream/documents/Additional_Information/mainmenu.pdf.

Scott, A.C., Young, R.F., Fedorak, P.M., 2008. Comparison of GC-MS and FTIR methods for quantifying naphthenic acids in water sample. Chemosphere, 73:1258-1264.

Wells, P.S., J. Caldwell, 2009. Vertical "wick" drains and accelerated dewatering of fine tailings in oil sands. IN: Tailings and Mine Waste '09, Proceedings of the 13th International Conference on Tailings and Mine Waste, 1-4 November, 2009, Banff, AB, Canada. pp: 429-440

Taciuk, W., 1981. Apparatus and process for recovery of hydrocarbon from inorganic host materials. US Patent number 4285773. Alberta Oil Sands Technology and Research Authority (Edmonton, CA). August 25, 1981.

Tis, D. J., Culbertson, R. W., Kelley, M. N., 1984. Recent developments with the Dravo solvent extraction process for tar sand. Energy Progress, 4(1):56-58.

Table 1. Summary of scenarios modeled.

Location	Permeability of containment material	Permeability of fully consolidated tailings	Technologies included
Reclaimed Tailings Pond	Low	Varies	12 technologies were modeled in this scenario. Sand and coke covers were also modeled.
Above-Grade Waste Dump	High (tailings sand)	High	3 technologies were modeled: retort extraction, solvent extraction, and tailings sand (conventional hydraulic fill).
	High (tailings sand)	Low	2 technologies were modeled: In Line Thickened Tailings (ILTT) and Thin-Lift Drying.
	Low (Clearwater overburden)	Low	6 technologies were modeled: Mature Fine Tailings (MFT), biologically or CO ₂ treated MFT, Freeze-Thaw, Thin-Lift Drying, Accelerated Dewatering, Centrifuging.

Table 2. Concentrations of Na, Cl, TDS and naphthenic acids in select tailings and water types.

Tailings or Water Type	Na (mg/L)	Cl (mg/L)	TDS (mg/L)	NAs (mg/L)	Reference
Mature Fine Tailings	382	28	(1781)	48	Fedorak et al. 2002 Quagraine et al. 2005 Proskin et al. 2010
Composite Tailings	607	133	2235	62	Fedorak et al. 2002 Wells et al. 2009
Tailings Sand (whole tailings)	760	655	2395	n.m.	Suncor records McKenna 2002
Polymer-amended, dried MFT (thin-lift dried tailings analog)	517	337	(1655)	48	Headley et al. 2010
Athabasca River	21	11	200	<0.01	AECOM 2012 Scott et al. 2008
Reclaimed Overburden Runoff	16	9.2	358	1.2	Total E&P Joslyn Ltd. 2010

NAs = naphthenic acids, n.m. not modeled, TDS = total dissolved solids. Bracketed TDS were estimated from major ion content.

Table 3. Summary of parameters used in modeling.

	Parameter	Value	Comments
Tailings containment structure (underlying base material)	Thickness	40 m	
	Tailings sand (base material) porosity	0.35	
	Clearwater Formation overburden fill (base material) porosity	0.44	Chapman 2008
	Tailings sand (base material) vertical hydraulic conductivity	5×10^{-7} m/s	McKenna 2002
	Clearwater Formation overburden fill (base material) vertical hydraulic conductivity	8×10^{-9} m/s	Chapman 2008
Reclaimed tailings ponds	Seepage out through base	26 mm/year	
Tailings	Tailings deposit thickness	7-40 m	Depending on tailings type
	Tailings deposit area	220 ha	
	Terminal saturated density	85% solids (at 140 years)	
	Maximum net percolation (high hydraulic conductivity material)	180 mm/year	Price 2005
End pit lake	EPL size	51.7 ha	
	EPL watershed area	896 ha	
Watershed inputs	Average annual rainfall	437 mm/year	
	Average annual site-wide yield (surface water runoff plus groundwater discharge)	143 mm/year	

Table 4. Model assumptions, approximations and simplifications.

Assumption/Simplification	Reality	Hypothesized Impact
There is a single tailings facility in the EPL watershed	There will likely be many tailings facilities and vast volumes of tailings sand (10-15x that of fine tailings deposits) contributing waters to the EPL	Current model is structured for direct comparison of tailings technologies under identical conditions, though it will not accurately represent the net (site-wide) chemical loading to an EPL
Seepage from tailings facility base/containment materials was not included	Pore water from Clearwater Formation overburden dumps or tailings sand containment materials will also report to the EPL as either surface water from seeps, or as groundwater.	The net loading from each tailings facility will be greater than simulated. Concentrations, release rates and durations will reflect the net effect of release from the deposit and from the base material.
Covers were not included explicitly, except when the technology itself was a cover.	Seepage rates are governed by the performance of the reclamation covers and hence are implicitly included in the analysis.	Small
Consolidation rates were highly simplified and based on expert opinion and experience, including recent work by Sawatsky et al. (2012). Consolidation release was assumed to be upward only, and consolidation reached a maximum terminal tailings density either of 85% solids or after 140 years.	This simplified empirical approach was used in lieu of a more traditional large-strain consolidation approach, which would have required much more data and assumed filling rates and deposit geometries (e.g., Pollock et al. 2000).	Small for this simplified model, but would be an important aspect of a more complex model.
Seepage from the tailings deposit was modeled as plug flow pore water release, assuming a complete flushing of contents with one pore volume of flow, and a constant chemistry equal to that of the initial tailings pore water.	In reality, flushing will occur more slowly and concentrations will decrease with time.	Flushing rates will be highly dependent on dyke geometry and cover performance.
EPL inlet water quality was determined following a simple mass balance approach. Chemical reactions were not considered. At each time step, complete, instantaneous mixing of input waters was assumed to occur. Water quality and quantity in the EPL water cap were not considered.	A variety of biogeochemical reactions may occur, affecting water reporting to, and in the EPL. Stratification may occur across the EPL water cap. The water used to initially fill the EPL could vary from fresh water to process-affected, which could be more or less benign than other inputs reporting to the EPL.	These assumptions (particularly relating to the initial EPL water quality and quantity and assumptions of perfect mixing), could have significant effects at least on short-term EPL behaviour.
Yield was generalized as having the same chemistry as runoff over reclaimed overburden in the region (Total E&P Joslyn Ltd. 2010).	Yield would also be determined by the water quality of groundwater discharge from different deposits and formations. In addition, the initial water quality of yield from reclaimed landforms often has elevated salt and naphthenic acid concentrations.	Chemical loading to downstream EPLs from site-wide yield may be greater than modeled and vary with time.
Where technology-specific release water chemistry data were not available, reasonable approximations were made using data from other, similar technologies.	Most tailings waters have signatures similar to that of the recycle water system, allowing reasonable estimates based on existing data. Care is taken to assess the impact of any process aids in any novel tailings technology.	Small to moderate

BIOAMENDMENT OF OIL SANDS MATURE FINE TAILINGS ACCELERATED DEWATERING AND IMPROVED RELEASE WATER QUALITY

Emily Cao¹, Raymund Sampaga¹, Abi Olubodun², Todd Burns², and Ania C. Ulrich¹

¹Department of Civil and Environmental Engineering, University of Alberta, Edmonton, Alberta, Canada

²Cypher Environmental Ltd., Winnipeg, Manitoba, Canada

ABSTRACT

Bitumen is extracted from oil sands using a hot-water extraction process, producing a large tailings stream that is stored in impoundments. One of the major challenges facing the oil sands mining industry is efficient dewatering of the tailings and subsequent water treatment. UltraZyme HydroCarbon, a consortium of bacteria and enzymes, developed by Cypher Environmental Ltd. was investigated for its capacity to dewater mature fine tailings (MFT), which typically consists of ~30% fine clay particles. Two different MFTs were studied: "Mixed MFT" which was a MFT blend from several oil sands companies provided by COSIA with a solids content of 29.4%; and "Single MFT" which was MFT from a single company's tailings pond, with a solids content of 34.6%. Preliminary results proved promising where the addition of 1.5g UltraZyme/L MFT released approximately 130-170mL of pore water from 800mL of Mixed MFT. Meanwhile, approximately 65mL of pore water was released from 800mL of Single MFT when the dosage was 1.0-5.0g UltraZyme/L MFT. Solids content for both MFT types reached about 39% within 60 days after UltraZyme treatment. The real promise in the bioamendment strategy was in the improved water quality where 40% removal of the petroleum hydrocarbon F3 fraction was observed in Mixed MFT, and 30% removal of bitumen content was observed for Single MFT. The toxicity level of expressed pore water decreased significantly for the treatment of Single MFT with UltraZyme.

Keywords: dewatering, UltraZyme, mature fine tailings (MFT), solids content, water quality

INTRODUCTION

During bitumen extraction, large volumes of tailings are produced. Conventionally, whole

tailings are composed of sands, clay, water and residual bitumen. In the tailings ponds, sand particles segregate from the slurry upon deposition, while the clay and bitumen remain suspended and form mature fine tailings (MFT) (1, 2). MFT only settles to about 30% to 35% solids content after several years of placement (3, 4). The storage of large amounts of MFT precludes the efficient release of the water. One of the major challenges facing the oil sands mining industry is the economical and efficient dewatering of MFT. Thus, a large amount of work has been carried out to develop techniques to enhance this process. Ongoing work into removing water from MFT includes **1**) physical processes such as filtration of whole tailings (5), centrifugation of fine tailings, thermal drying of MFT (6), and freeze/thaw cycling (7); and **2**) chemical processes have focused on the addition of flocculants such as polyacrylamide (PAM), hybrid Al(OH)₃- polyacrylamide (Al-PAM) and poly (N-isopropyl acrylamide) (PNIPAM) (1, 8, 9). For example, Suncor's TRO™ process, where MFT is mixed with a polymer flocculent and deposited in thin layers over sand beaches, has been developed and tested since 2003 (10). However, cost for large scale physical treatment could be high; and degradation of flocculants could occur during the chemical treatment process. Biological amendments, on the other hand, may be applied for MFT dewatering without negatively affecting, and potentially even improving the water quality. Unfortunately, very little work has been done to examine which bioamendment treatments would be effective for MFT dewatering.

In this study, UltraZyme, a proprietary blend of bacteria developed by Cypher Environmental Ltd., which is designed to remediate organic wastes in a variety of water and wastewater treatment related applications, will be tested. Tests will focus on the capacity of UltraZyme to enhance the dewatering of MFT and improve water quality, with a preliminary examination of optimal dosages required.

METHODS

Materials

Two types of MFT were used for the tests. Mixed MFT was provided by Canada's Oil Sands Innovation Alliance (COSIA) and consisted of a mixture of MFTs from several of the oil sands companies, and Single MFT consisted of one type of MFT from a single tailings pond at a depth of 12m. Oil sands process-affected water (OSPW) was also taken from the same tailings pond as the Single MFT sample. The UltraZyme bioamendment was provided by Cypher Environmental Ltd.

Dewatering tests

The dewatering tests were first conducted at 22°C temperature with Mixed MFT at a dosage of 1.5g UltraZyme/L MFT. OSPW was used to dissolve UltraZyme. After proper mixing, 20mL of 60g UltraZyme/L OSPW, and 800mL MFT was added to a 1L graduated cylinder. The graduated cylinders had been autoclaved before adding the MFT to eliminate contamination. Triplicate test columns were set up and triplicate control columns with no UltraZyme addition were set up as well. The amount of dewatering, measured as the volume of expressed pore water above the water-MFT interface, was recorded once every week for 60 days.

The dewatering tests were repeated at room temperature with Single MFT at a dosage of 0.5, 1.0, 1.5, 2.5, and 5.0g UltraZyme/L MFT. Testing was carried out as described above in 1L graduated cylinders for a period of 60 days. Duplicates were set up for these treatment columns, as well as control columns which were made as described above. The precision of analyses were evaluated with the following formula for standard deviation used for duplicate results (11):

$$s = \sqrt{\frac{\sum_{i=1}^n (-x_{i1} - x_{i2})^2}{2n}} \quad (1)$$

Chemical properties

Prior to performing dewatering tests, samples were taken from the original MFT bulk, parameters were tested, and thus, "time 0" data was obtained. To obtain pore water from the original bulk MFT, MFT was centrifuged at 10000xg for 20min in plastic

centrifuge tubes and the resulting supernatant was filtered through 0.45µm filters and tested. After dewatering tests were complete, the same parameters were tested once again to determine the properties of the MFT and pore water post-treatment. For the controls, since very little or no pore water was released, pore water was centrifuged out of the MFT and tested as described above.

Solids content was determined using the industrial standard procedure, Dean Stark (12). The F2, F3 and bitumen fractions were obtained by analyzing the hydrocarbon fraction collected from the Dean-Stark extraction on a gas chromatograph equipped with flame ionization detector GC-FID (Agilent 7890) (13). The GC column used was an Agilent DB-1HT, 30m, 0.32mm; flow rate 27.130 ml/min; oven program 50°C for 5min, 30°C/min to 350°C and held at 350°C for 10min. Naphthenic acids (NAs) were extracted from pore water (14), derivatized by N-tert-butylidimethylsilyl-N-methyltrifluoroacetamide (MTBSTFA), and analyzed using GC-FID (Agilent 7890). The GC column used was an Agilent DB-1HT, 30m, 0.32mm; flow rate 48.347ml/min; oven program 50°C for 2.5min, 30°C/min to 320°C and holding at 320°C for 10min.

Pore water was filtered through 0.45µm filter and analyzed for dissolved organic carbon (DOC) using a total organic carbon analyzer (Mandel TOC - L).

Toxicity of pore water was analyzed using the Microtox Assay (Microtox® 500 Analyzer, Azur Environmental), with an incubation time of 5 min and the 81.9% Basic Test protocol (15, 16). The toxicological parameter EC50 (effective volume percent concentration required to decrease bacterial luminescence by 50%) was analyzed. EC50 was converted to toxicity units (TU), where TU=100/EC50 (15).

RESULTS AND DISCUSSION

Dewatering tests

The initial solids content was 29.4% and 34.6% for Mixed MFT and Single MFT, respectively (Table 1). By adding UltraZyme, the solids content increased to 38.4% in Mixed MFT. Meanwhile, the solids content increased about 3% at the 0.5g/L dosage and about 4% at the 1.0g/L, 1.5g/L, 2.5g/L, and 5.0g/L for Single MFT. Except for the 0.5g/L dosage, the solids content for all the other tests

reached about 38.5% after treatment. Regardless, of MFT type and with a minimum 1.0g/L UltraZyme dose, the highest solids content achieved was around 39%.

Table 1. Solids content (wt%) in Mixed MFT and Single MFT: before dewatering tests, samples were taken from the original bulk MFT, solid content was tested, and “time 0” data were obtained. After dewatering tests were completed, solid content was tested for both control and treated columns. Triplicate columns were studied for Mixed MFT, and duplicate columns were studied for Single MFT. Results are presented as an average ± one standard deviation.

Mixed MFT	
Sample I.D.	Solid content (wt%)
Time "0"	29.4
Control	31.3 ± 1.6
1.5g/L treatment	38.4 ± 0.5

Single MFT	
Sample I.D.	Solid content (wt%)
Time "0"	34.6
Control	33.2 ± 0.7
0.5g/L treatment	37.4 ± 0.1
1.0g/L treatment	38.3 ± 0.4
1.5g/L treatment	38.8 ± 0.4
2.5g/L treatment	38.4 ± 0.2
5.0g/L treatment	38.6 ± 0.3

The results of Mixed MFT dewatering are shown in Fig.1a. The most drastic dewatering in the columns with UltraZyme occurred early in the experiment, with 95.7mL of pore water being released over the first 28 days, followed by 40.6mL over the next 22 days. The dewatering rate was 3.4mL/day over the first 28 days followed by 1.8mL/day over the next 22 days. A total of 24.0mL of pore water was released over the 60 days for the control, with a dewatering rate of 0.4mL/day.

The results of Single MFT dewatering are shown in Fig.1b. The most drastic dewatering occurred in the first 25 days. The dewatering rate was 2.2mL/d, 2.0mL/d and 2.7mL/d over the first 25

days for dosages of 1.5g/L, 2.5g/L and 5.0g/L, respectively. After day 25 the dewatering rate slowed down. The volume of water released reached approximately 65mL by day 60. The dewatering rate was 0.9mL/d and 1.2mL/d for the first 45 days, for the lower dosages of 0.5g/L and 1.0g/L, respectively. After day 45 the dewatering rate slowed down. The volume of water released in total was 42mL and 57mL for dosages of 0.5g/L, 1.0g/L, respectively. No water was released over the duration of the experiment (60 days) for the control columns.

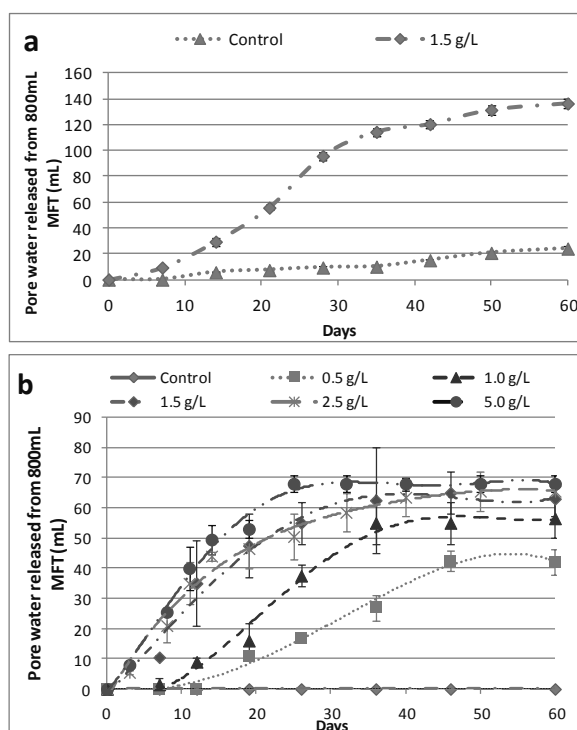


Figure 1. Volume of pore water released from MFT: 1a shows the volume of pore water released from 800mL of Mixed MFT with the addition of 1.5g/L UltraZyme over a period of 60 days. Triplicate columns were studied for each dewatering test, and error bars are one standard deviation. 1b shows the volume of pore water released from 800mL of Single MFT with the addition of 0.5g/L, 1.0g/L, 1.5g/L, 2.5g/L, and 5.0g/L UltraZyme over a period of 60 days. Duplicate columns were studied for each dewatering test, and error bars show one standard deviation.

Comparing the dewatering ability of UltraZyme on the Mixed MFT and Single MFT, it seems that UltraZyme has a stronger dewatering ability when applied to Mixed MFT, since the volume of pore water released is much higher. However, the solids content achieved by treating with UltraZyme was around 38.5% for both MFT types. The difference in pore water volume released is due to the difference in initial solids content for the two kinds of MFTs, where Mixed MFT had a lower initial solids content as compared to the Single MFT. Therefore, the volume of pore water released from MFT was associated with the initial solids content of the MFTs and the maximum solid content that can be achieved was around 39%. Meanwhile, the solids content was not affected by increasing the Ultrazyme dosage above 1.0g/L, which indicates 1.0g/L might be the optimal dosage for treating MFT.

Columns with UltraZyme addition and Control columns also displayed different physical appearances during the dewatering experiment, as shown in Fig.2. For columns with UltraZyme addition, for both Mixed and Single MFT, cracks developed in the MFT likely from biogenic gas production. This was observed during the first or second week and continued over the course of the experiment. Swelling of the MFT interface above the original level also occurred as a result of the biogenic gases forming in the MFT. Also, expressed pore water on top of the MFT interface was cloudy, with a layer of oily residue on top of the water, especially during the period of rapid dewatering. The released water gradually became clear once the dewatering rate slowed down.

Degradation of organic compounds

Hydrocarbons serve as the intended carbon/energy source for the UltraZyme bacteria consortium. Upon degradation of these substrates, biogenic gases are produced as a metabolic byproduct. Thus, it is of interest to study which hydrocarbon fraction serves as the preferred substrate for the UltraZyme, and how UltraZyme addition may change the hydrocarbon composition in MFT. For the Mixed MFT treatment, the F2 fraction did not change significantly as a result of UltraZyme addition, whereas the F3 fraction decreased about 40% (2.5mg/g MFT) compared to the control columns. Bitumen content of the test columns and control columns did not show a significant difference (Fig. 3a). On the other hand, UltraZyme treatment of Single MFT resulted in neither the F2 nor F3 fraction showing a significant

change in comparison to the control columns. However, the bitumen content for the treated columns decreased about 30% (10mg/g MFT) for all the dosages during the 60-day period (Fig. 3b).

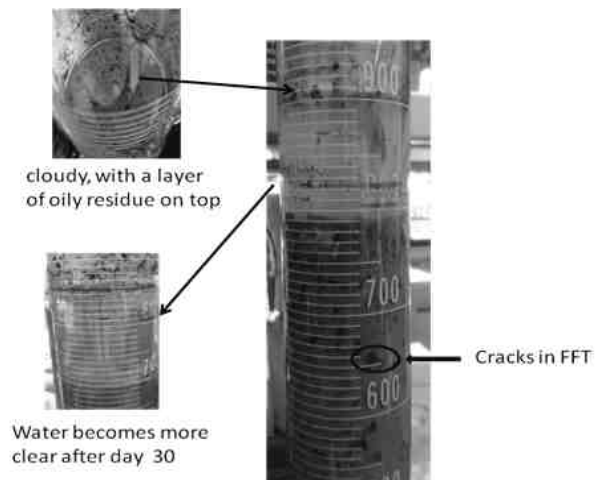


Figure 2. Observation of columns with UltraZyme addition: pictures were taken at day 21 and day 42 while treating Mixed MFT with 1.5g/L UltraZyme addition. Cloudy water on top of the MFT is shown, and one of the cracks is circled.

These results demonstrate that UltraZyme showed a different preference of substrate while treating the two types of MFT. The reason for this might be that different native microbial communities were present in the two different kinds of MFT. It is possible that these microbial communities interact differently with the UltraZyme microorganisms in terms of metabolic processes and thus, the carbon source preference may be different in each system. Also, the nutrient content such as N, K and P content could be very different in the two MFTs, which may also affect the substrate preference (17, 19).

UltraZyme is designed to degrade organic hydrocarbons in MFT, as a result, the chemical composition in released pore water may change as well, which can affect the quality of the expressed water. In order to study the water chemistry of the expressed pore water, parameters including pH, DOC and NA content were studied. For Mixed MFT, the pH and DOC levels remained relatively constant (8.5-8.7, and 110-120mg/L, respectively) both before and after treatment. While no

significant difference was observed for these two parameters, the amount of NAs decreased from 69.7mg/L to 37.4 ± 9.6 mg/L (30% removal) for treated columns. Meanwhile, for Single MFT, pH, DOC, and NA levels all remained relatively constant (8.5-8.9, 160-180mg/L, and 32-36mg/L, respectively) after treatment. There was no significant difference observed for any of these parameters.

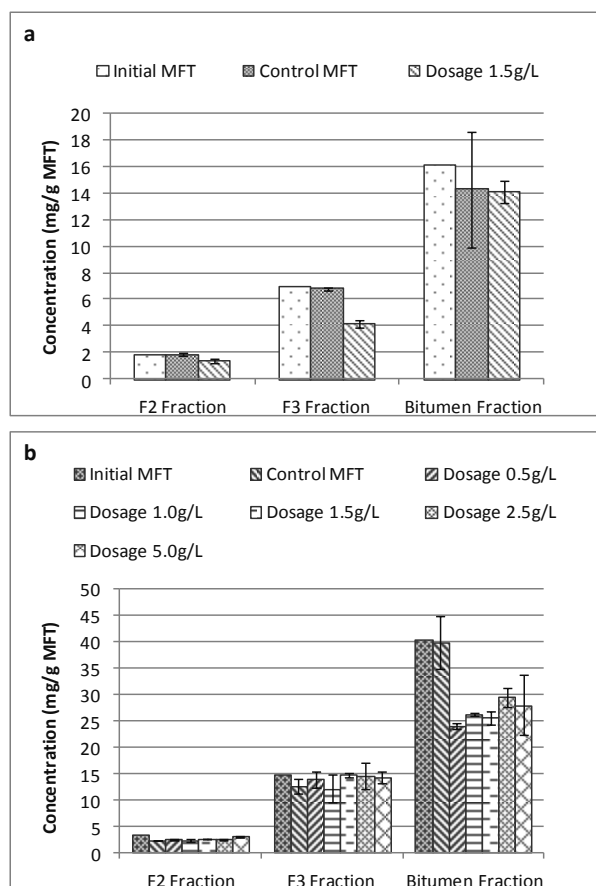


Figure 3. Hydrocarbon content of MFT before and after treatment: 3a shows the hydrocarbon content of Mixed MFT. A significant decrease of F3 content was observed for the treated Mixed MFT. 3b shows the hydrocarbon content of Single MFT. A significant decrease of bitumen content was observed for the treated Single MFT. Triplicate columns were studied for Mixed MFT controls and treated columns, and duplicate columns were studied for Single MFT. Results are presented as an average \pm one standard deviation.

Toxicity is an important parameter when studying water quality. Toxicity of the pore water was tested at “time 0” and after the dewatering test for Mixed MFT. The toxicity did not change with the treatment of UltraZyme, which stayed at about 1.4 TU (Fig 4a). In contrast, for Single MFT, the toxicity decreased significantly for the columns with UltraZyme treatment. The toxicity was around 1.7-2 TU for the control and initial MFT, and decreased to 1.0 TU for all the treated columns (Fig. 4b).

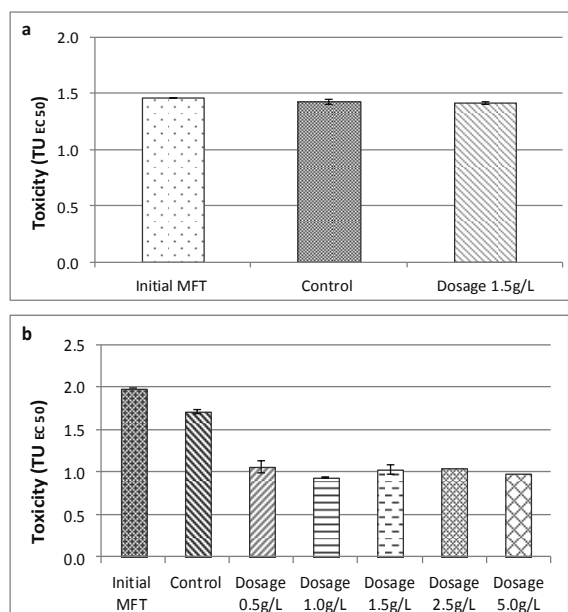


Figure 4. Toxicity of pore water before and after treatment: 4a shows the toxicity of pore water released from Mixed MFT. No difference was observed between pore water released from the treated Mixed MFT and pore water released from the control columns. 4b shows the toxicity of pore water released from Single MFT. A significant decrease of toxicity was observed for pore water released from the treated Single MFT at all UltraZyme dosages. Triplicate columns were studied for Mixed MFT controls and treatment experiments, and duplicates were studied for Single MFT. Results are presented as an average \pm one standard deviation.

Although the concentration of NAs and DOC did not decrease in the released pore water from the Single MFT, it is likely that the dissolved organic

fraction changed composition. For example, DOC is a measure of the total dissolved organic carbons in the pore water: if complex organic carbons are digested into simpler organic compounds, the DOC value will remain the same. During the treatment process it is possible that the more complex and toxic compounds are digested to simpler and less toxic compounds in the pore water released from the Single MFT (18, 19). As a result, the toxicity level goes down significantly.

CONCLUSION

We studied two treatments, one with Mixed MFT and the other with Single MFT. The two treatments showed similar results on the dewatering test, which indicated Cypher Environmental's UltraZyme could help release water from MFT, and that by using this treatment technique the maximum solid content that can be achieved was around 39%.

Different UltraZyme dosages were studied using Single MFT. The volume of water released increases only up to a dosage of 1.0g/L, at which point no change is observed. Different dosages showed very similar effects on the tested chemical properties of MFT and the toxicity of pore water. Therefore, it might be concluded that 1.0g/L is the optimal dosage for treating MFT.

UltraZyme addition may affect bitumen content or the F3 fraction differently when used in treatment of different MFTs. There was 40% removal of the petroleum hydrocarbon F3 fraction in Mixed MFT and 30% removal of bitumen content in Single MFT after treating with UltraZyme. NAs content also decreased 30% in Mixed MFT after treatment. The toxicity level of expressed pore water decreased 1 TU for the treatment of Single MFT with UltraZyme. It is promising that UltraZyme could improve the quality of the released pore water.

The preliminary results of this study proved promising, demonstrating that UltraZyme could help improve release water quality from MFT. However, little is known as to why UltraZyme affects the hydrocarbon composition of MFT differently when treating MFT from different sources, or why UltraZyme treatment decreases the toxicity level of pore water released from Single MFT, but not from Mixed MFT. Future work could focus on **1)** investigating the detailed chemical composition of hydrocarbons instead of simply the

fractions of hydrocarbons in the original and UltraZyme-treated MFT, in order to understand which groups of chemicals are desirable substrates for UltraZyme; **2)** studying changes in the chemical composition of released pore water, which could help explain the observed changes, or lack thereof, in toxicity of released pore water; **3)** studying the differences between microbial communities in different sources of MFT, which may be the key factor affecting the effectiveness of UltraZyme treatment; and **4)** testing the treatment efficiency of UltraZyme at different temperature ranges to determine the performance of UltraZyme under temperatures relevant to the environment, and therefore the conditions of in-situ dewatering treatment.

ACKNOWLEDGEMENTS

The authors are grateful to NSERC and Cypher Environmental Ltd. for providing research funding and to COSIA for providing materials.

REFERENCES

- Andersen, J.C., Wiseman, S.B., Wang, N., Moustafa, A., Perez-Estrada, L., El-Din, M.C., Martin, J.W., Liber, K., and Giesy, J.P. 2012. Effectiveness of Ozonation Treatment in Eliminating Toxicity of Oil Sands Process-Affected Water to *Chironomus dilutus*. *Environmental Science & Technology*. 46: 486-493.
- Bulmer, J.T. and Starr, J. 1979. Syncrude analytical methods for oil sand and bitumen processing. Alberta Oil Sands Technology and Research Authority. Method 2.10: 62-68.
- Dorn, P.B., 1992. Case histories—the petroleum industry. In: *Toxicity Reduction: Evaluation and Control*. Ford, D.L. (Ed.), Water Quality Management Library, vol. 3. Technomic Publishing Company, Lancaster, PA, pp. 183–223.
- El-Din, M.G., Fu, H.J., Wang, N., Chelme-Ayala, P., Perez-Estrada, L., Drzewicz, P., Martin, J.W., Zubot, W., and Smith, D.W. 2011. Naphthenic acids speciation and removal during petroleum-coke adsorption and ozonation of oil sands process-affected water. *Science of the Total Environment*. 409: 5119-5125.

- Li, H., Zhou, J., Chow, R., 2008. Comparison of polymer applications to treatment of oil sands fine tailings. In: First International Oil Sand Tailings Conference, pp. 77-84.
- Koerner, R.M. 1994 (3rd Ed.). Designing with geosynthetics. Prentice Hall, Inc., Englewood Cliffs, N.J., USA.
- Leahy, J. and Colwell, R. 1990. Microbial degradation of hydrocarbons in the Environment. *Microbiological Reviews*. 54: 305-315.
- Loick, N., Hobbs, P., Halea, M., and Jones, D. 2009. Bioremediation of poly-aromatic hydrocarbon (PAH)-contaminated soil by composting. *Critical Reviews in Environmental Science and Technology*. 39: 271-332.
- Lu, W., Ewanchuk, A., Perez-Estrada, L., Segó, D., and Ulrich, A. 2013. Limitation of fluorescence spectrophotometry in the measurement of naphthenic acids in oil sands process water. *Journal of Environmental Science and Health, Part A: Toxic/Hazardous Substances and Environmental Engineering*, 48: 429-436.
- Madill, R.E.A., Orzechowski, M., Chen, G., Brownlee, B.G., Bunce, N.J., 2001. Preliminary risk assessment of the wet landscape option for reclamation of oil sands mine tailings: bioassays with mature fine tailings pore water. *Environmental Toxicology* 16, 197-208.
- Pandey, J., Chauhan, A., and Rakesh K. Jain, R.K. 2009. Integrative approaches for assessing the ecological sustainability of in situ bioremediation. *FEMS Microbiology Reviews*. 33: 324-375.
- Schramm, L.L., Stasiuk, E.N., MacKinnon, M., 2000. Surfactants in Athabasca oil sands slurry conditioning, flotation recovery, and tailings processes. In: Schramm, L.L. (Ed.), *Surfactants: Fundamentals and Applications in the Petroleum Industry*. Cambridge University Press, Cambridge, pp. 365-430.
- Seifert, W.K. and Teeter, R.M. 1969. Preparative thin-layer chromatography and high resolution mass spectrometry of crude oil carboxylic acids. *Anal. Chem.* 41: 786-795.
- Seifert, W.K., Teeter, R.M., Howells, W.G., and Cantow, M.J.R. 1969. Analysis of crude oil carboxylic acids after conversion to their corresponding hydrocarbons. *Anal. Chem.* 41: 1638-1647.
- Shell Canada. 2005. The Athabasca Oil Sands Project. 2004 Sustainability Report. [online]. Available from http://www.shell.com/static/caen/downloads/about_shell/what_we_do/aosp_s-d_report.pdf
- Small, C.C., Ulrich, A. and Hashisho, Z. 2012. Adsorption of acid extractable oil sands tailings organics onto raw and activated oil sands coke. *Journal of Environmental Engineer.* 138: 833-840.
- Suncor Energy. 2005. Suncor Energy 2005 Report on Sustainability. [online]. Available from http://www.suncor.com/data/1/rec_docs/616_Suncor%20SD%20Report_2005%20.pdf
- Suncor Energy. 2010. Oil sands tailings technology: understanding the impact to reclamation. [online]. Available from <https://circle.ubc.ca/bitstream/handle/2429/30342/13%20Mamer.pdf?sequence=1>
- SynCrude Canada. 2004. SynCrude Canada Limited 2004 Sustainability Report. [online]. Available from <http://sustainability.synCrude.ca/sustainability2004/download/SynCrudeSD2004.pdf>

DEGRADATION OF NAPHTHENIC ACIDS AT 20°C AND 10°C BY A PSEUDOMONAS SP. NATIVE TO AN OIL SANDS TAILINGS POND

Sarah Miles, Dena Cologgi, Ania C. Ulrich
University of Alberta, Edmonton, Alberta, Canada

ABSTRACT

Extraction of bitumen from Alberta's oil sands requires large volumes of water, leading to an abundance of oil sands process-affected water (OSPW) that must be remediated prior to discharge or reuse. OSPW contains a variety of toxic compounds, including naphthenic acids (NAs). Previous studies have demonstrated the capacity of microorganisms to degrade NAs and decrease OSPW toxicity. To identify candidates for NA bioremediation, we obtained samples of OSPW from Suncor Energy and created microcosms with NAs provided as a sole carbon source. Through selective enrichment, a microbial community enriched in NA-degraders was established. From these enrichments we obtained a handful of microbial isolates, including bacteria, yeast, and fungi. The objective of this study is to establish the NA degradation ability of one isolate, a *Pseudomonas* sp. and the effect temperature has on this process. Microcosms were prepared with commercially available and natural NAs at 20°C and 10°C. Dissolved organic carbon (DOC) concentrations were monitored as a rough proxy of NA concentrations. It was determined that the bacterial isolate was able to remove 87% of the DOC in the microcosms with commercially available NAs, and 78-79% of the DOC in the microcosms with natural NAs, indicating that commercially available NAs were more readily degraded. It was also determined that temperature did not affect the total removal, but rates of removal were 4 times slower at 10°C than at 20°C. Further analyses will determine the NA degradation capacity and mechanism the *Pseudomonas* sp. isolate. Presently, this organism shows promise to effectively degrade commercial and acid extractable organics (AEOs) from OSPW. If successful, these experiments will provide the scientific framework necessary for the development of in-situ OSPW bioremediation schemes.

INTRODUCTION

The Athabasca, Cold Lake and Peace River oil sands in Northern Alberta, Canada, are one of the largest proven reserves of oil in the world, second only to Saudi Arabia (Government of Alberta, 2008). There are an estimated 1.69 billion barrels (269.2 m³) of recoverable bitumen in Alberta's oil sand region (ERCB, 2013). Approximately 2.21m³ of water is used per 1m³ of bitumen extracted (Syncrude Canada, 2004). With the production of 112 million m³ of bitumen per year ((ERCB), 2013) approximately 3.3m³ of raw tailings is created per 1m³ of extracted bitumen (Gosselin et al., 2010). This post extraction water is termed oil sands process-affected water (OSPW), and is stored in engineered tailings ponds in accordance with Alberta's Zero discharge policy introduced in the Alberta Environmental Protection and Enhancement Act (1993) (Giesy et al., 2010).

During the extraction process, organic compounds found naturally in the bitumen such as polyaromatic hydrocarbons (PAHs), benzene, toluene, ethylbenzene, xylenes (BTEX), and naphthenic acids (NAs) become concentrated in the OSPW. NAs are known to be a prevalent compound in, and the major contributor to the toxicity of OSPW (Kannel and Gan, 2012; MacKinnon and Boerger, 1986). NAs have a general structural formulae of C_nH_{2n+z}O₂ where *n* represents the carbon number and *z* is the hydrogen deficiency and is zero or a negative, even integer due to rings or double bonds (Dzidic et al., 1988; Fan, 1991; St John et al., 1998). In general, NAs are natural surfactants, and are a mixture of cyclic and acyclic alkanes possessing a single carboxylated side chain (MacKinnon and Boerger, 1986). As naphthenic acids are a natural component of bitumen, they are solubilized into the water during the extraction process. Their concentration in OSPW varies (<1mg/L to 120mg/L) based on the age of the tailings pond, the operator, and the extraction process used (Scott et al. (2008)).

NA degradation studies can be performed using either commercially available NAs (i.e. Merichem), or those from the environment (acid-extractable organics (AEOs)) obtained from OSPW). Microbial degradation of NAs extracted from OSPW is slower than degradation of commercial NAs. This is due to the chemical composition differences of the commercial NAs and AEOs (Clemente et al., 2004; Han et al., 2008; Herman et al., 1994; Scott et al., 2005). Grewer et al. (2010) determined that the classical formula of NAs given as $C_nH_{2n+2}O_2$ may only account for 10-36% of AEOs in natural OSPW, but will potentially account for 43.5% of the commercially available Merichem NAs. Holowenko et al. (2002) found that natural NAs are composed of a wide range of molecular masses, with n ranging from 5-28. Whereas the molecular mass of commercially available NAs is generally lower with n of about 10-14 (Clemente et al., 2004; Clemente et al., 2003). This large difference in composition and mass can account for the difference in biodegradability between commercial NAs and AEOs.

With the abundance of organic compounds present in tailings ponds, it is no surprise microbial activity is high (Holowenko, 2000; Holowenko et al., 2001). NAs are known to be weakly biodegradable (Meredith et al., 2000), however it has been shown that NAs, can be removed from OSPW through microbial degradation which is most effective under aerobic conditions (Nix and Martin, 1992). It was found by Herman et al. (1994) that aerobic cultures containing *Pseudomonas stutzeri* had the capacity to degrade commercial NAs. It was also determined that three aerobic bacteria, *Acinetobacter calcoaceticus*, *Pseudomonas fluorescens* and *Kurthia sp.*, were able to degrade naturally occurring NAs (Herman et al., 1994).

The goal of the current research is to establish the ability of an aerobic bacterial isolate from OSPW to degrade NAs. The objectives of this study were to determine i) if the bacterial isolate was capable of growing and degrading NAs as its sole source of carbon, ii) to determine the extent the bacterial isolate can degrade commercially available and naturally occurring NAs and iii) to determine the effect of temperature on degradation rates and capacity.

METHODS

Bacterial Isolate

The aerobic bacterial isolate used in this study was obtained through selective enrichment of NA-degrading organisms in OSPW from Suncor's South Tailings Pond (STP) as part of another project in Dr. Ulrich's lab group in the Civil and Environmental Engineering Department at the University of Alberta, Edmonton. Details of the enrichment and isolation procedure are described elsewhere (Hofstetter et al., Submitted 2014). It was determined through genetic analysis that the bacteria, was from the *Pseudomonas* genus (Hofstetter et al., Submitted 2014). Confirmation of isolate purity in each microcosm was done at the end of the experiment by plating and visual inspection.

Naphthenic Acids

Commercially-produced naphthenic acids were a gift from Merichem Chemicals and Refinery Services LLC. A 100mg/ml stock solution was prepared by dissolving the NAs in 0.22 μ m-filtered 0.1N NaOH.

The experimental AEOs were taken from a single OSPW source, Suncor's STP. This OSPW was collected in 2009 and stored at 4°C until used. The OSPW was first centrifuged at 8,000xg and then filtered through a 0.22 μ m filter. The extraction of AEO from the filtered OSPW was done by increasing the pH of 400mL of OSPW to 10 with 1.0N NaOH. The basic OSPW was washed two to three times with 50mL of dichloromethane (DCM), and the resulting DCM fraction was discarded. The OSPW was then acidified to a pH of 2 with 37% HCl. The acidic OPSW was then washed three times with 50mL of DCM, and the DCM fraction was collected. The DCM was then evaporated, leaving behind a residue consisting of the recovered AEO fraction. To quantify the mass of AEO collected, the residue was resuspended in a known amount of DCM, and derivitized using N-methyl-N-(*t*-butyldi-methylsilyl) trifluoroacetamide reagent (MTBSTFA) at 60°C for 20 minutes. Samples were allowed to cool, and then run on a gas chromatograph with a flame ionization detector (GC-FID). The GC-FID used was an Agilent Technologies GC system (7890A) with a (7693) auto-sampler running an Agilent Technologies 122-5512 column (15m x 0.250mm x 0.25 μ m).

Commercial Merichem naphthenic acids were used to prepare the calibration curve for quantification. Once quantified, the dried AEO were dissolved in an appropriate volume of 0.22 μ m-filtered 0.1N NaOH to obtain a 100mg/ml stock solution.

Microcosm Set up

Each microcosm consisted of a 1L Erlenmeyer flask with 500ml of Bushnell-Haas media, and an inoculation of *Pseudomonas* sp. to an optical density at 600nm (OD₆₀₀) of 0.005. Triplicate flasks were then fed 45mg/L of AEOs, or commercial NAs. Control flasks contained the same contents but were autoclaved twice, at least 24 hours apart, to create a killed control. Each experimental condition was set up in triplicate, and controls in duplicate, as shown in Figure 1. The entire experiment was performed at 20°C and 10°C, with microcosms shaking at 150rpm.



Figure 1. Experimental set up, 20 flasks total.

Sampling and analyses

The sampling of microcosms was done at room temperature in a biological safety cabinet to ensure sterility. 20mL samples were withdrawn and centrifuged at 8,000xg for 10min, then filtered through a 0.22 μ m filter and stored at 4°C for further analyses.

Dissolved Organic Carbon

Dissolved organic carbon (DOC) was measured to track potential degradation of organic compounds present. As NAs were the only organics provided, DOC measurements can be used as a rough proxy for NA concentrations. 8ml of the stored samples

were diluted with ultra-pure water to 25ml and run on a Shimadzu Model TOC-L with an ASI-L Shimadzu autosampler. The DOC concentrations were determined through external calibration.

Optical Density

Microbial growth was monitored throughout the experiment through OD₆₀₀ measurements. An additional 1mL sample was aseptically withdrawn from each flask and placed in a 1mL cuvette. The OD was then measured on a Thermo Scientific NanoDrop 2000c Spectrophotometer as an absorbance at 600nm.

RESULTS AND DISCUSSION

The growth of *Pseudomonas* sp. was monitored through OD readings, and the growth of bacteria in the live experimental flasks was compared to the relatively consistent OD readings of the control flasks. The results of the 20°C experiment (shown in Figure 2) clearly show the exponential growth of *Pseudomonas* sp. within a few days of it feeding on commercial NAs and AEOs, while the control flasks show no growth. The 10°C experiment (Figure 3) follows the same trend. These optical density growth curves confirm that the *Pseudomonas* sp. isolate can grow aerobically with either commercial NAs or AEOs as their sole source of carbon. Therefore, it can be determined that this *Pseudomonas* sp. isolate can degrade NAs under the conditions specified.

With the experimental set up allowing only commercial NAs or AEOs as the sole carbon source, DOC measurements were used as a rough proxy for NA concentration. The average initial (day 0) and final (day 31) DOC values are shown in Table 1 and Table 2 for 20°C and 10°C, respectively. Both control sets for commercial NAs and AEOs show little variation in DOC throughout the course of the experimental run (see Table 1 and 2).

The commercial and AEO control sets for both temperatures show a small net gain of DOC. This could be due to the release of carbon from the lysing cells during the autoclaving process (Schaller et al., 2011).

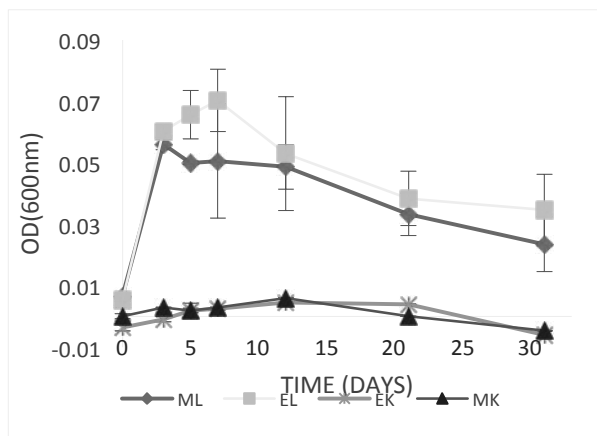


Figure 2. Optical Density of *Pseudomonas* sp. at 20°C. ML: Commercial NAs with live *Pseudomonas* sp., EL: AEOs with live *Pseudomonas* sp., EK: AEOs with heat-killed *Pseudomonas* sp., MK: Commercial NAs with heat-killed *Pseudomonas* sp. Values are averaged triplicates \pm standard error of triplicates.

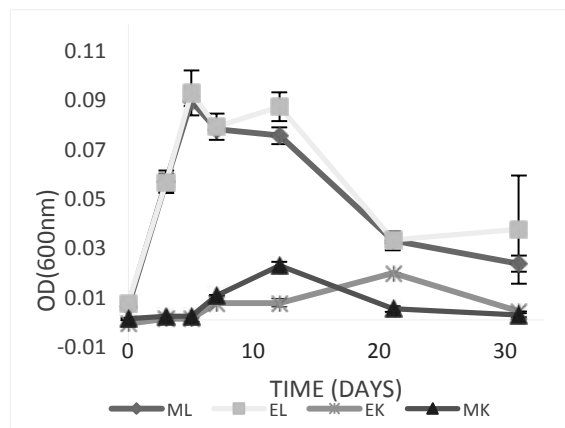


Figure 3. Optical Density of *Pseudomonas* sp. at 10°C. ML: Commercial NAs with live *Pseudomonas* sp., EL: AEOs with live *Pseudomonas* sp., EK: AEOs with heat-killed *Pseudomonas* sp., MK: Commercial NAs with heat-killed *Pseudomonas* sp. Values are averaged triplicates \pm standard error of triplicates.

Table 1: Dissolved organic carbon content and percent removal at 20°C

	Average DOC (mg/L) ¹	Initial	Average Final DOC (mg/L) ¹	Percent Removal (%) ¹
Commercial NAs Live	213.6 \pm 2.0	27.3 \pm 0.8		87.2 \pm 0.3
AEO Live	220.4 \pm 3.7	44.7 \pm 0.6		79.7 \pm 0.1
Commercial NAs Control	219.5 \pm 0.2	233.1 \pm 0.0		-6.1 \pm 0.0
AEO Control	239.5 \pm 2.3	251.2 \pm 1.		-4.9 \pm 0.4

¹Values indicated are averaged triplicates \pm standard error of triplicates.

Table 2: Dissolved organic content and percent removal at 10°C

	Average Initial DOC (mg/L) ¹	Average Final DOC (mg/L) ¹	Percent Removal (%) ¹
Commercial NAs Live	214.1 \pm 1.0	26.5 \pm 0.9	87.6 \pm 0.4
AEO Live	228.2 \pm 0.7	49.7 \pm 0.6	78.2 \pm 0.
Commercial NAs Control	213.8 \pm 0.9	225.0 \pm 0.3	-5.2 \pm 0.6
AEO Control	242.8 \pm 0.0	251.2 \pm 0.6	-3.4 \pm 0.3

¹Values indicated are averaged triplicates \pm standard error of triplicates.

The degradation of commercially available NAs by *Pseudomonas* sp. is consistently greater than that of AEOs. As demonstrated in Table 1 and Table 2, the percent removal of DOC is 7.5% greater for commercial NAs at 20°C, and is 9.4% greater than AEOs at 10°C. Thus, effectively demonstrating that commercially available NAs are substantially different than AEOs. Holowenko et al. (2002) found that AEOs are composed of a widespread range of molecular masses. However the molecular mass of commercially available NAs has been found to be generally lower (Clemente et al., 2004; Clemente et al., 2003). A large difference in mass between AEO and commercial NAs can account for the difference in biodegradability.

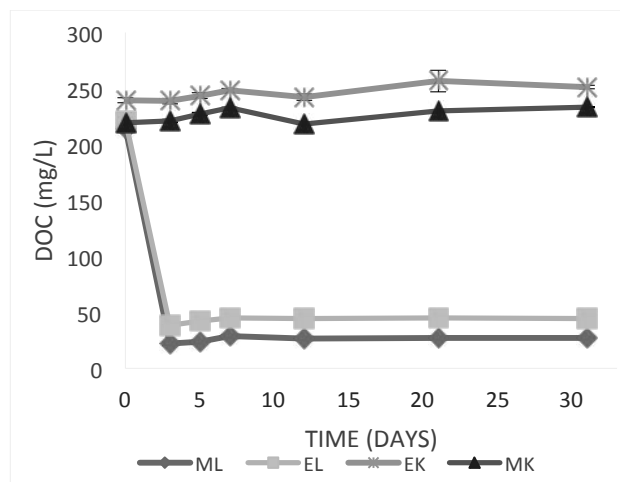


Figure 4. Dissolved Organic Carbon at 20°C. ML: Commercial NAs with live *Pseudomonas* sp., EL: AEOs with live *Pseudomonas* sp., EK: AEOs with heat-killed *Pseudomonas* sp., MK: Commercial NAs with heat-killed *Pseudomonas* sp. Values are averaged triplicates ± standard error of triplicates.

The consistent percent removals of dissolved organic carbon for 20°C and 10°C indicate that temperature is not a limiting factor for the overall capacity of the *Pseudomonas* sp. isolate to degrade the NAs. However, the temperature change does influence the rate of the process. As shown in Figures 3 and 4, the days required for the degradation of NAs is considerably different. For the experimental set up at 20°C it required up to three days for the isolate to degrade both NAs to its capacity. Conversely, for the 10°C experimental set up, it required up to twelve days for the isolate

to degrade the NAs to a consistent concentration. This equates to rate of removals shown in Table 3. These removal rates are distinctly different given the temperature change. Decreasing the temperature from 20°C to 10°C decreases the removal rate by 4 times for both commercial NAs and AEO removal. This implies the bacterial isolate is sensitive to temperature during the initial phase of degradation of commercial NAs and AEO, however the isolate will ultimately degrade to the same level given enough time.

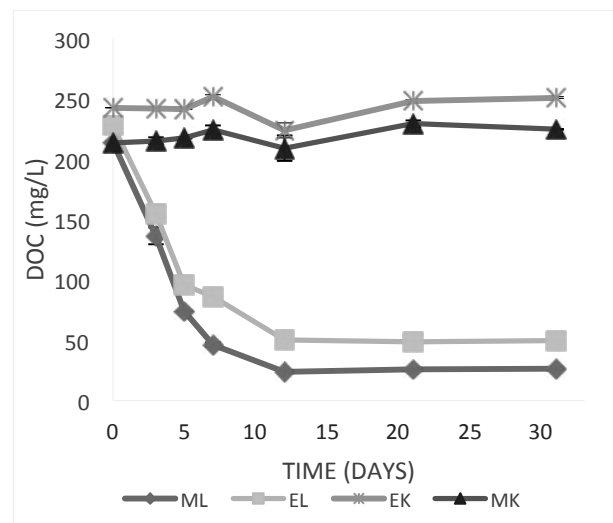


Figure 5. Dissolved Organic Carbon at 10°C. ML: Commercial NAs with live *Pseudomonas* sp., EL: AEOs with live *Pseudomonas* sp., EK: AEOs with heat-killed *Pseudomonas* sp., MK: Commercial NAs with heat-killed *Pseudomonas* sp. Values are averaged triplicates ± standard error of triplicates.

Table 3. Rates of DOC Removal

	20°C Rate (mg/L/day) ¹	10°C Rate (mg/L/day) ²
Commercial NAs Live	63.9±0.4	15.9±0.1 ^a
AEO Live	60.7±2.1	14.8±0.4 ^b

¹Rates were determined using zero order kinetics fit from day 0 to day 3 with an r-squared value of 1.

²Rates were determined zero order kinetics fit from day 0 to day 12, with r-squared values of ^a0.85, and ^b0.87

CONCLUSION

NAs are the main compound of concern in OSPW, and recent studies have demonstrated that microorganisms native to tailings ponds are capable of NA degradation. The bacterial isolate *Pseudomonas* sp. has shown that it has the capacity to degrade NAs and grow with commercially available NAs and AEOs as a sole carbon source.

It was determined that this bacterial isolate has the ability to remove approximately 87% of commercial NAs and 78-79% of AEOs, as measured as DOC. This difference in removal of DOC indicates that there are structural and compositional differences between commercially available NAs and AEOs that affect biodegradability. Although the final percent removal was very similar for both 20°C and 10°C, the rate of removal is 4 times different for the two temperatures. This finding has environmental implications as 10°C is much more representative of the cooler temperatures present in tailings ponds. It should be noted that total degradation is the same at warmer temperatures, so laboratory studies performed at room temperature still provide environmentally-relevant results, but in a shorter time frame.

To further explore the comprehensive aptitude for the *Pseudomonas* sp. isolate to degrade NAs, more analyses of samples will be required. Low resolution analyses of NAs will be done using the GC-FID, and high resolution analyses will be done using high pressure liquid chromatography (HPLC) with orbitrap mass spectrometry (Bataineh et al., 2006). In addition, Microtox™ toxicity assay analyses will be used to determine changes in toxicity level. Presently, these analyses have shown promise that the *Pseudomonas* sp. isolate effectively degrades commercial and AEOs from OSPW.

Future studies will include determining the ability of other bacteria, fungi and yeast isolated from tailings ponds to degrade natural AEOs, commercial NAs and model NAs. The feasibility of enhancing the NA degradation process using these isolates either in co-culture with one another, or in conjunction with chemical pre-treatment options will also be examined.

ACKNOWLEDGEMENTS

The authors would like to thank Suncor Energy for providing OSPW for this project. Special thanks to Simmon Hofstetter, Amy-lynn Balaberda, Timothy Edwards, and Elena Dlusskaya for their contributions to this work. The authors also thank Yan Cao for her technical expertise and advice throughout the project. This work has been financially supported by the Helmholtz-Alberta Initiative.

REFERENCES

- Bataineh, M., Scott, A.C., Fedorak, P.M. and Martin, J.W. (2006) Capillary HPLC/QTOF-MS for characterizing complex naphthenic acid mixtures and their microbial transformation. *Analytical Chemistry* 78, 8354-8361.
- Clemente, J.S., MacKinnon, M.D. and Fedorak, P.M. (2004) Aerobic biodegradation of two commercial naphthenic acids preparations. *Environmental Science & Technology* 38, 1009-1016.
- Clemente, J.S., Prasad, N.G.N., MacKinnon, M.D. and Fedorak, P.M. (2003) A statistical comparison of naphthenic acids characterized by gas chromatography-mass spectrometry. *Chemosphere* 50, 1265-1274.
- Dzidic, I., Somerville, A.C., Raia, J.C. and Hart, H.V. (1988) Determination of Naphthenic Acids in California Crudes and Refinery Wastewaters by Fluoride-Ion Chemical Ionization Mass-Spectrometry. *Analytical Chemistry* 60, 1318-1323.
- Energy Resources Conservation Board (2013) ST98-2013: Alberta's Energy Reserves 2012 and Supply/Demand Outlook 2013-2022.
- Fan, T.P. (1991) Characterization of Naphthenic Acids in Petroleum by Fast-Atom-Bombardment Mass-Spectrometry. *Energy & Fuels* 5, 371-375.
- Giesy, J.P., Anderson, J.C. and Wiseman, S.B. (2010) Alberta oil sands development. *Proceedings of the National Academy of Sciences* 107, 951-952.

- Gosselin, P., Hrudey, S.E., Naeth, M.A., Plourde, A., Therrien, R., Kraak, G.V.D. and Xu, Z. (2010) The Royal Society of Canada Expert Panel: Environmental and Health Impacts of Canada's Oil Sands Industry. December 2010.
- Government of Alberta(2008) Launching Alberta's Energy Future. Provincial Energy Strategy. . Government of Alberta.
- Grewer, D.M., Young, R.F., Whittal, R.M. and Fedorak, P.M. (2010) Naphthenic acids and other acid-extractables in water samples from Alberta: What is being measured? *Science of the Total Environment* 408, 5997-6010.
- Han, X., Scott, A.C., Fedorak, P.M., Bataineh, M. and Martin, J.W. (2008) Influence of molecular structure on the biodegradability of naphthenic acids. *Environmental Science & Technology* 42, 1290-1295.
- Herman, D.C., Fedorak, P.M., Mackinnon, M.D. and Costerton, J.W. (1994) Biodegradation of Naphthenic Acids by Microbial-Populations Indigenous to Oil Sands Tailings. *Canadian Journal of Microbiology* 40, 467-477.
- Hofstetter, S., Edwards, T., Dlusskaya, L., Brown, L.D., Whittal, R., Gänzlec, M. and Ulrich, A. (Submitted 2014) Resistance of Oil Sand Tailings Pond Microorganisms to Acid-Extractable Organic Compounds. *Science of the Total Environment*.
- Holowenko, F.M. (2000) Methanogenesis and fine tailings waste from oil sand extraction: a microcosm-based laboratory examination, *Biological Sciences*. University of Alberta, Edmonton, AB.
- Holowenko, F.M., Mackinnon, M.D. and Fedorak, P.M. (2001) Naphthenic acids and surrogate naphthenic acids in methanogenic microcosms. *Water Research* 35, 2595-2606.
- Holowenko, F.M., MacKinnon, M.D. and Fedorak, P.M. (2002) Characterization of naphthenic acids in oil sands wastewaters by gas chromatography-mass spectrometry. *Water Research* 36, 2843-2855.
- Kannel, P.R. and Gan, T.Y. (2012) Naphthenic acids degradation and toxicity mitigation in tailings wastewater systems and aquatic environments: A review. *Journal of Environmental Science and Health, Part A* 47, 1-21.
- MacKinnon, M.D. and Boerger, H. (1986) Description of Two Treatment Methods for Detoxifying Oil Sands Tailings Pond Water. *Water pollution research journal of Canada* 21, 496-512.
- Meredith, W., Kelland, S.J. and Jones, D.M. (2000) Influence of biodegradation on crude oil acidity and carboxylic acid composition. *Organic Geochemistry* 31, 1059-1073.
- Nix, P.G. and Martin, R.W. (1992) Detoxification and Reclamation of Suncors Oil Sand Tailings Ponds. *Environmental Toxicology and Water Quality* 7, 171-188.
- Schaller, J., Weiske, A. and Dudel, E.G. (2011) Effects of gamma-sterilization on DOC, uranium and arsenic remobilization from organic and microbial rich stream sediments. *Science of the Total Environment* 409, 3211-3214.
- Scott, A.C., MacKinnon, M.D. and Fedorak, P.M. (2005) Naphthenic acids in athabasca oil sands tailings waters are less biodegradable than commercial naphthenic acids. *Environmental Science and Technology* 39, 8388-8394.
- St John, W.P., Rughani, J., Green, S.A. and McGinnis, G.D. (1998) Analysis and characterization of naphthenic acids by gas chromatography electron impact mass spectrometry of tert.-butyldimethylsilyl derivatives. *Journal of Chromatography A* 807, 241-251.
- Syncrude Canada (2004) Syncrude Canada Ltd 2004 Sustainability Report.

Session 11

Tailings Deposition and Modelling

A NEW APPROACH TO OPTIMIZE THE CAPTURE OF OIL SANDS FINES IN SAND BEACH

Ruijun Sun¹, Jianmin Kan² and Alexandre Goldszal²

¹Saskatchewan Research Council, Saskatoon, Canada

²Total E&P Canada Ltd, as Operator of the Joslyn Joint Venture, Calgary, Canada

ABSTRACT

The concept of storing fines in voids of coarse sand when oil sand tailings are deposited in a sand beach area has been evaluated in many studies. It has been found that a sand beach is capable of capturing up to 50% of fines by mass upon initial placement. The objective of this study was to verify that the fines to fines plus water ratio of a tailings feed is a key parameter controlling the percentage of fines captured. A further objective was to evaluate any other parameter(s) that will affect the process, and to determine its impact on sand beach properties.

Mature Fine Tailings were used as the fines source in this study. Two types of commercial sand were blended to simulate coarse tailings from medium grade oil sand ore. The slurry mixtures were prepared based on their respective targets of feed solids concentration, fines to fines plus water ratio and sand to fines ratio. Slurry mixtures were prepared and tested in an 8 m long flume to simulate fines captured in beach deposition. After draining free flow runoff, the beach was allowed to settle for 7-30 days and beach strength was examined. Feed, beach and runoff samples were analyzed. The percentage of feed fines and volume captured in beach were inferred from the analytical results.

It was found feed fines to fines plus water ratio and feed carrier yield stress are two key parameters to control the percentage of feed fines and volumes captured in sand beach. This study demonstrated that adding sand to flocculated fines can achieve up to 80% w/w of fines captured and more than 2 kPa of beach shear strength 7 days after deposition.

INTRODUCTION

To reduce Fluid Fine Tailings (FFT) inventory in oil sands mining development, fines captured in a sand beach is a promising concept which consists

of mixing Mature Fines Tailings (MFT) or Thickened Tailings (TT) into coarse sand slurries. If done properly, this will maximize fines captured within the inter-particle porosity of sand particles. Using this technology it is estimated that coarse sand in a Sand Beach Area (SBA) can capture more than 50% of fines produced^[1] from oil sands mining process.

The concept of fines captured in SBA was first tested by Syncrude^[2] in early 1990's. A number of large scale tests were conducted to study mechanisms of fines captured from coarse tailings deposition and MFT spiked coarse tailings. A field demonstration test was conducted at the Syncrude site to prove the concept^[3]. W.G. Miller et al^[4] summarized the flume test results done by Syncrude and OSLO in the early 1990's, and concluded that flume deposition tests could provide a reliable and effective method to correlate the tailings beaching behavior.

In recent years, reduction of fines tailings inventory has become a critical issue, especially following the ERCB's Directive 074 issued in 2009^[5]. This directive states that a tailings disposal strategy must be able to reduce FFT stored in tailings ponds by increasing the fines capture in the Designated Disposal Area (DDA), and improve on the rate at which land is being reclaimed and made trafficable. Even though the directives are managed on a project-by-project basis, the same objectives must be met by all operators, specifically:

1. 50% of the fines in the total feed to be captured in the DDA (by 2013 annually and every year thereafter)
2. Minimum undrained shear strength of 5 kPa for the material deposited in the previous year, and a deposit which is ready for reclamation within 5 years after active deposition has ceased (with shear strength of 10 kPa).

To address the requirements of this Directive, the concept of beach fines capture has been revisited and further developed.

The Saskatchewan Research Council (SRC) and Total E&P Canada (TEPCA), conducted a Phase I study in 2011 which investigated the capabilities of a coarse sand beach in capturing fines from oil sand tailings. Actual oil sand materials were tested in an 8 m long flume. Coarse sands used in the Phase I study were produced from hydrocyclone underflow tailings during an extraction pilot conducted at SRC in 2009. The coarse sand was grouped as high grade (HG), medium grade (MG) and low grade (LG) based on bitumen content in the original ore. MFT used in the study was acquired from Syncrude's Aurora tailings pond.

The findings from the Phase I study [6] are summarized here:

1. For all three groups of coarse sand (HG, MG and LG) tested, more than 50% of fines from the feed can be captured in sand beach after the first placement;
2. The percentage of fines captured in sand beach was governed by the feed fines over fines plus water $[F/(F+W)]$ ratio. The optimum feed $F/(F+W)$ ratio was at 13-15%. Above this value, the percentage of fines captured decreased due to fines being suspended and lost in runoff;
3. LG sand's potential for capturing fines is limited due to its already high percentage of fines in feed solids;
4. Flocculation of feed could increase the fines captured in a sand beach; however beach strength needs to be evaluated over a longer period of time than the 24 hours tested in the Phase I study;

Due to limited materials and testing time available to the Phase I study, the beach was neither thick enough nor tested long enough to generate accurate beach shear strength data.

The overall objective of this Phase II study was to further develop the technology in two main tasks outlined below based on findings from Phase I:

1. Building on the Phase I results that identified the feed $F/(F+W)$ as a key parameter to control the percentage of fines captured, the Phase II study will investigate the limit of feed $F/(F+W)$ increase;
2. To investigate what other parameter(s) will affect the fines captured process, and how to further optimize the process.

The Phase II study involved tests at both lab scale

in the form of 2.4 m long wooden flumes and pilot scale in a larger 8.0 m long metal flume. For limited space available in this paper, only the results of the pilot scale flume tests are discussed in high level in this paper.

EXPERIMENTAL METHODS

Testing Materials

Due to the size of the sample requirements and limited availability of oil sand coarse tailings, two commercially available Lane Mountain sands (LM #70 and LM #125) were used to simulate oil sand coarse tailings in this study. They were blended to a ratio of approximately 24% LM #70 vs. 76% LM #125, so the properties of the blended sand mixture (SFR, d_{50} and fines fraction) were representative of coarse sand generated from medium grade (MG) oil sand ore. The blended LM sand mixture was used throughout the study, the exact blend ratio was adjusted periodically when a new batch of sand was used. Figure 1 shows the particle size distributions of blended LM sand and MG sand.

The MFT used as fines source was obtained from Syncrude Aurora tailings pond and received by SRC in the spring of 2013. Properties of feed material is presented in Table 1 (in Illustration section).

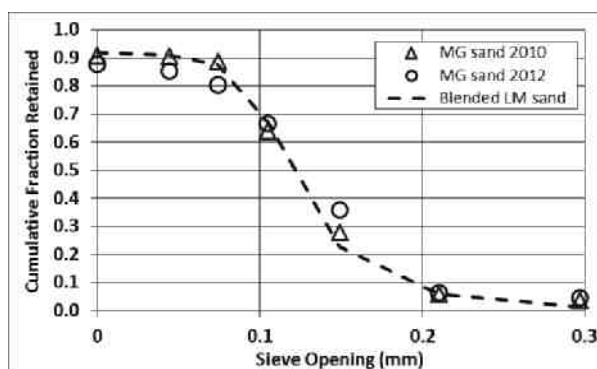


Figure 1. Particle Size Distributions of Blended LM Sand

Pilot Flume Apparatus and Test Procedures

The pilot flume used for this study has dimensions of 8.0 m (L) x 0.25 m (W) x 0.5 m (H). The pilot flume testing apparatus is shown in Figures 2 and 3 (Figure 3 in Illustration section).

A number of instruments were employed on this flume. Fresh slurry and beach height was measured by calipers at 8 locations at 0, 1.0, 1.7, 2.6, 3.6, 4.5, 6.4 and 8.0 m from flume inlet. Two traversing gamma-ray densitometers were used to monitor and measure vertical solids concentration distributions. The densitometers were denoted as gamma1 and gamma2 and were located 2.0 m and 6.0 m from the flume inlet respectively. Two low energy 100 mCi (3.7 GBq) Cesium-137 sources (Ronan Engineering) supplied the gamma ray radiation in the experiments. Figure 4 (in Illustration section) shows the schematic locations of different measuring devices.

Each flume test started by homogenizing blended LM sand, MFT and process water in a 1.5 m³ tank equipped with a 20 hp mixer. To ensure adequate mixing and to maintain feed consistency, 600-800 L of tailings mixture were prepared in the tank but only 400 L was discharged into the flume. Slurry mixtures were prepared based on their respective targets of feed solids concentration (C_m), $F/(F+W)$ ratio and Sand to Fines Ratio (SFR_{44}). If slurry flocculation was required, flocculent (AF3338 supplied by SNF) was pre-dissolved in process water followed by mixing the solution with MFT; known amount of coarse sand was then added to the flocculated MFT mixture. The flocculent dosage was based on gram of flocculent per tonnes of total solids (gpTs), dry basis.



Figure 2. Pilot Flume Apparatus

For every test, the flume was set at 1% slope to mimic the slope of a field SBA and help drain runoff. The homogenized mixture was discharged into the flume via a 0.025 m diameter pipe at the desired flowrate and a fixed discharge angle (45°).

The slurries were discharged at a flowrate of 100 L/min which was pre-determined as the optimum discharge flowrate during the Phase I study. Eight 250 mL cut-stream feed samples were taken during deposition. The mixture was allowed to settle for 1 hour before runoff was drained by slowly opening rubber plugs on a weir located at the end of flume. The runoff was collected in separate drum(s) for weight and composition analysis.

During pilot flume testing, vertical slurry solids concentration profiles were measured immediately after deposition by two gamma traversing densitometers. The same gamma measurements were repeated on the beach after draining the runoff, and then again 7 days after deposition. At the end of pilot flume testing, twelve vane shear stress were measured at 6 locations along the flume and 2 depths at each location. Beach samples were taken near these locations and 2 depths at each location. Beach samples, along with samples taken from feed and runoff, were analyzed for total solids concentration and particle size distributions.

RESULTS AND DISCUSSION

Calculation Definitions

As mentioned earlier, this study included tests in lab scale flumes as well as pilot flume testing. The lab scale tests were smaller and consisted of Group A tests using MFT as fines source and Group B tests using thickened tailings as fines source. These tests helped define the test parameters for the Group C tests which were conducted using pilot flume and MFT as a fines source. Only Group C test results are discussed in this paper.

Table 1 (in Illustration section) summarizes the test matrix and results. Mixture properties such as total solids concentration (C_m), density, SFR_{44} and $F/(F+W)$ ratio can be calculated from analytical results obtained from feed, runoff and beach samples. Mass balance of feed, runoff and beach can be derived from the weighted average of these results.

The following terms and definitions are used:

1. Fines captured in beach = ratio of mass of fines in the beach deposit to mass of fines in the feed (w/w)

2. Feed volume captured in beach = ratio of beach deposit volume to feed volume (v/v)

Effect of Feed $F/(F+W)$ and Carrier Yield Stress

Flume test results confirmed that feed $F/(F+W)$ is the controlling parameter for feed fines and volume captured in sand beach. Figure 5 shows that for capturing 50% w/w or more feed fines in sand beach (with strong feed volume captured results as well), the critical feed $F/(F+W)$ range was 0.125-0.130 (as in Tests C1, C3, C6 and C2 shown in Table 1). When feed $F/(F+W)$ was increased to 0.15 or above, the feed fines captured rate reduced to 40% or below (as in Tests C4 and C5 shown in Table 1).

Figure 6 shows that the fines captured rate is also correlated to carrier fluid yield stress. Carrier fluid is defined as the combined mass of fines ($-44 \mu\text{m}$) and water in the feed, which governs the flow behavior of the slurry. As the carrier yield stress increased, more fines were suspended in the carrier and lost as runoff, causing the fines captured rate to decrease. The critical feed carrier yield stress to cause the feed fines suspended and fines captured rate dropped to below 50% was only 0.05 Pa (which was surprisingly low) and it corresponded to critical feed $F/(F+W)$ value of 0.124.

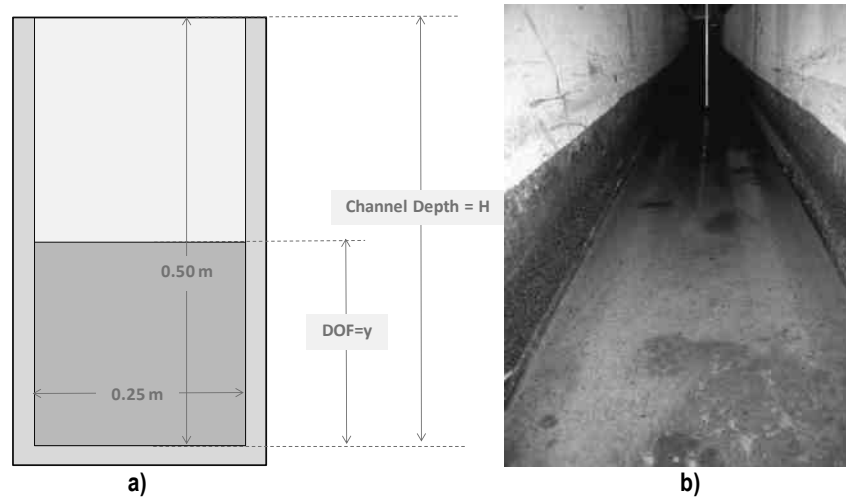


Figure 3. Pilot Flume Rectangular Cross-Section: a) Schematic, b) Photograph

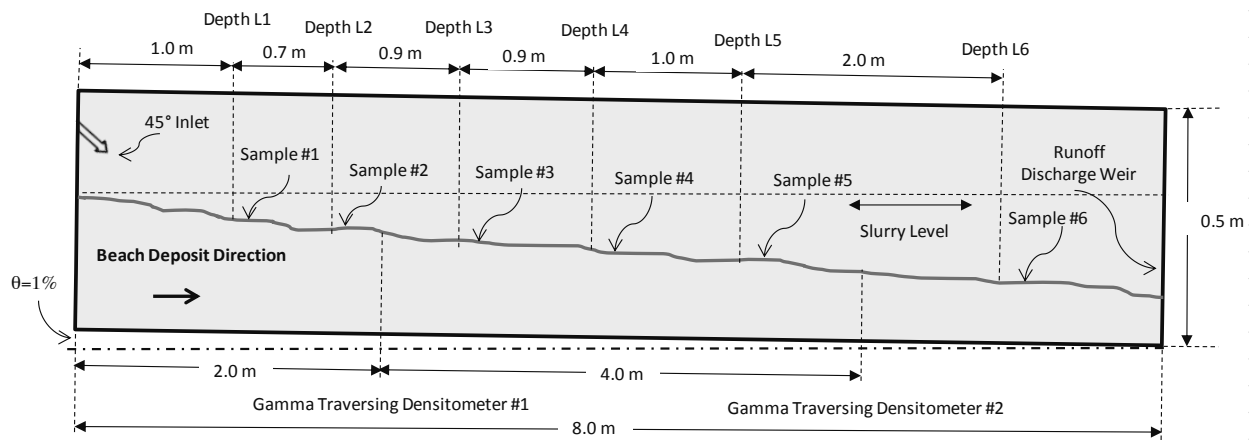


Figure 4. Schematic of Pilot Flume and Locations of Measuring Devices

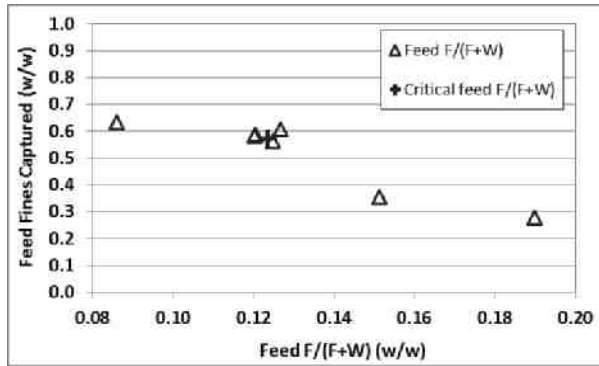


Figure 5. Effect of Feed $F/(F+W)$ on Feed Fines Captured

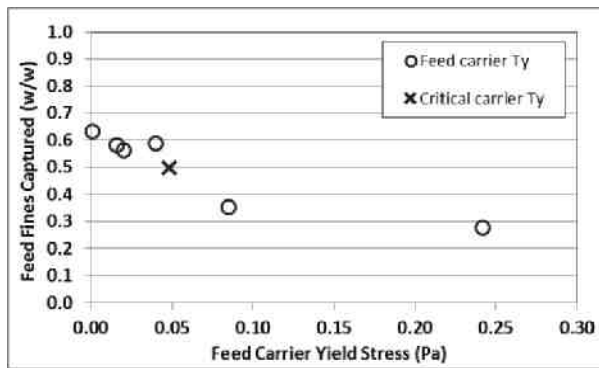


Figure 6. Effect of Feed Carrier Yield Stress on Feed Fines Captured

Effect of Flocculation and High Solids Concentration

Figure 7 and Table 1 show that Tests C2 and C7 had very similar feed properties (feed concentration at 0.55-0.57, $F/(F+W)$ at 0.12-0.13 and SFR_{44} at 8.1-8.3) with the exception of the addition of 150 gpTs of flocculent into the feed of Test C7. The test showed that low dose flocculation did not increase the fines or volume captured rate. However, when the feed concentration was increased to 0.65 in tests C8 and C10, and the same dose of 150 gpTs flocculent was added to the feed, the percentage of fines captured increased to 83.1% w/w (as Test C8) and 76.8% w/w (as Test C10) respectively.

The flocculent dosage used in the study was relatively low at 150 gpTs (based on total solids in feed), which was enough to increase the carrier yield stress and promote the suspension of fines in the carrier, however it was not enough to agglomerate majority of coarse sand particles

such that increase the strength of the deposit. Under this scenario, the suspended fines was lost as runoff.

Flocculation was more effective when enough sand particle population was present. Figure 6 and Table 1 shows when feed concentration increased from 0.55 to 0.65 (as in Tests C8 and C10), the increasing sand concentration promoted the agglomeration of all components in the deposit, it also increased the strength of deposit. For Tests C8 and C10, flocculation increased the fines captured rate to 83.1% and 76.8%, and achieved beach shear strength to 5.1 and 2.5 kPa respectively (7 days after deposition), despite the fact that feed $F/(F+W)$ was increased to 0.142-0.163, which exceeded the critical range of 0.125-0.130. Without flocculation, only 35.5% of feed fines were captured for the same range of feed $F/(F+W)$ (as in Test C4) and C4's beach shear strength was at 0.6 kPa, after the same 7 day consolidation period.

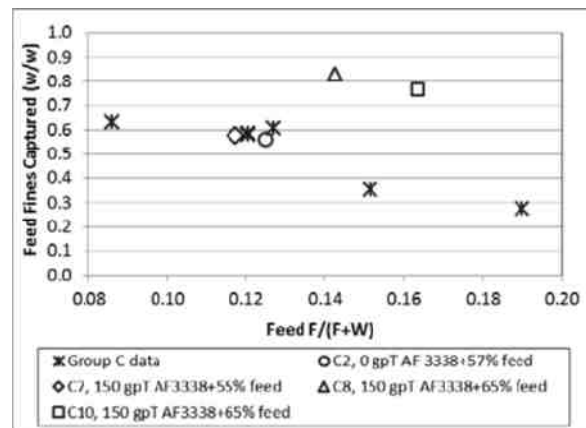


Figure 7. Effect of Flocculation and Feed Concentration on Feed Fines Captured

These results suggest that fines capture process can be optimized by adding coarse particles to flocculated fines stream. It will result in an increased rate of fines captured and still maintain the required shear strength of the deposit.

A Case Study on the New Approach

The new approach can be further evaluated by examining Tests C8 and C10 in more detail. Test C8 had a feed concentration of 0.649, $F/(F+W)$ of 0.142 and SFR_{44} of 10.1. The MFT stream of this mixture was flocculated with 150 gpT AF3338 (dosage based on total feed solids) before mixed

with coarse tailings. Test C8 achieved 83.1% feed fines captured and 87.0% feed volume captured. Figure 8 shows the beach shape and beach SFR distributions of Test C8. Although the SFR at lower beach layer was slightly higher than upper layer, the fines were not separated from coarse particles. The runoff layer was very thin. More beach SFR data can be found in Table 2 (Illustration section).

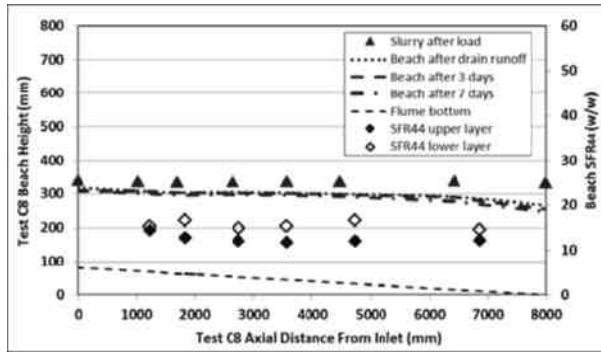


Figure 8. Beach Shape and Beach SFR Distributions of Test C8

Figure 9 shows the concentration distributions of Test C8's slurry just after it was loaded in the flume, and the concentration distribution of beach deposit after the runoff was drained from the flume. Gamma scans were conducted at two locations of the flume (2 m and 6 m from flume inlet, Gamma #1 and #2 respectively). The beach thickness and solids concentration at the two locations were very similar. The concentration of the top layer (runoff) was low at ~10%. After drained the runoff, only the top layer at the far end of flume (located at Gamma #2) had a slightly lower concentration. All of which indicated that majority of the material (87% v/v) was captured in the beach and loss of material to runoff was minimum.

Figure 10 shows Test C8's beach concentration distributions 7 days after deposition. The majority of the beach had consolidated with a uniform concentration distributions. For Test C8 the feed $F/(F+W)$ was increased to 0.142 which exceeded the critical value of 0.125-0.130, however coarse sand was added to bring the feed concentration to 0.65, which helped ensure that the beach shear strength was not compromised by the increased feed $F/(F+W)$.

However, adding more fines to the feed without increasing the flocculent dosage and/or coarse solids could compromise the fines captured and

reduce the beach shear strength. For Test C10 the feed $F/(F+W)$ was increased even more than C8, to 0.163 while keeping the same feed concentration at 0.656 and the flocculent dosage at 150 g/Ts. The fines captured and volume captured rates, while still high, decreased to 76.8% and 83.3% respectively, but more concerning was the drop in beach shear strength which only reached an average of 2.5 kPa for Test C10.

The average beach shear strength reached 5.1 kPa, 7 days after deposition (Table 1). Test C8 shows that adding coarse sand to flocculated fines is an effective approach to improve the fines captured process.

Figure 11 shows the beach shape and SFR distributions of Test C10. The beach is still thick, however the SFR on upper layer was lower than the bottom layer, and the difference widened as the beach developed further. This indicated more fines stayed on top of beach with the potential to be lost as runoff.

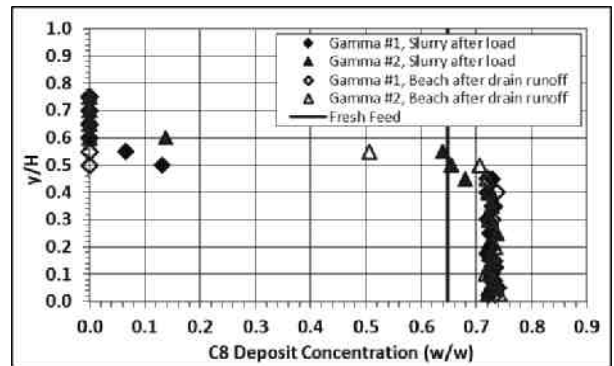


Figure 9. Beach Gamma Concentration Profiles of Test C8, Day 1

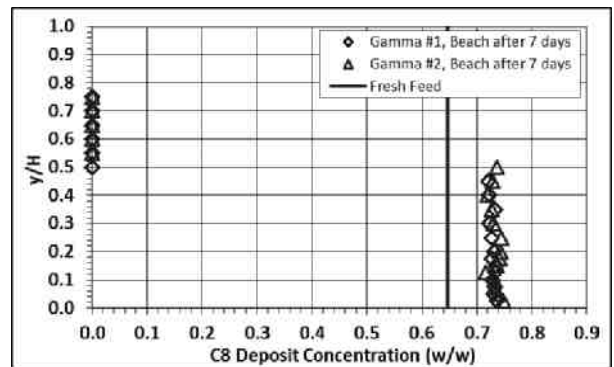


Figure 10. Beach Gamma Concentration Profiles of Test C8, Day 7

Figure 12 shows the concentration distributions of Test C10's slurry just after it was loaded in the flume, and C10's beach deposit after the runoff was drained from the flume. Although the concentrations in the lower half of beach were relatively uniform, the upper half of beach was stratified. There were more fines on upper layer of the beach, especially near the end of beach (location gamma2), an indication that fines were washed to the end of flume and could be lost as runoff.

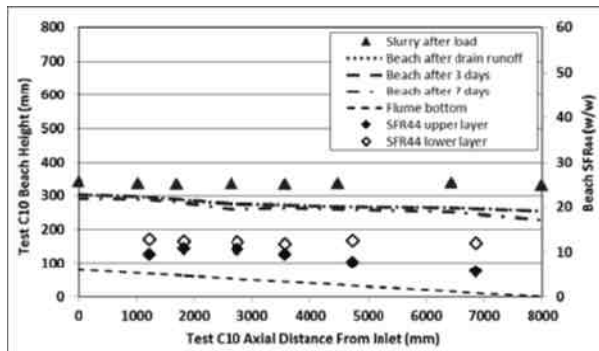


Figure 11. Beach Shape and Beach SFR Distributions of C10

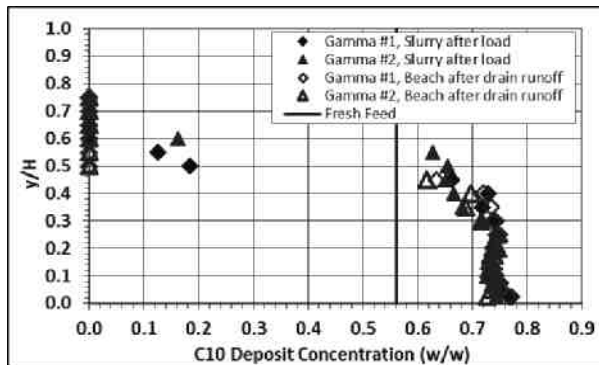


Figure 12. Beach Gamma Concentration Profiles of Test C10, Day 1

Figure 13 shows the beach concentration distributions of Test C10, 7 days after deposition. The upper layer of beach at both locations of gamma1 and gamma2 still remained stratified which contributed to a lower beach shear strength. To reduce stratification on the upper half of beach for Test C10, a higher flocculent dosage would be required to increase the carrier yield stress until it can form a fines network strong enough to reduce stratification and capture more coarse sand and

increase the network shear strength. The alternative would be to increase the coarse sand concentration and to improve the agglomeration and to reduce the watery upper layer and runoff.

Therefore, the dosage of flocculation has to be developed and selected carefully based on feed compositions, target fines captured rate and beach properties.

Figure 14 shows beach shear strength for selected Group C tests, which were measured 3 days and 7 days after each deposition respectively. Although majority of the shear strengths didn't reach 5 kPa during 7 days, the results suggested that most of them would exceed 5 kPa if given enough drying time (30 days or longer). The exceptions are Tests C4 and C5, both had low beach shear strength (~0.6 kPa after 7 days) due to high feed $F/(F+W)$ (0.15 and 0.19 respectively) and low rate of fines captured in beach (36% and 28% respectively).

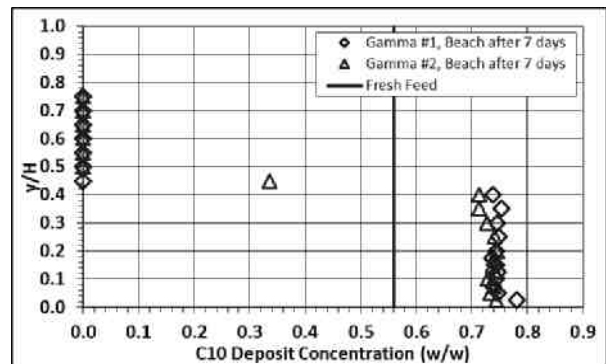


Figure 13. Beach Gamma Concentration Profiles of Test C10, Day 7

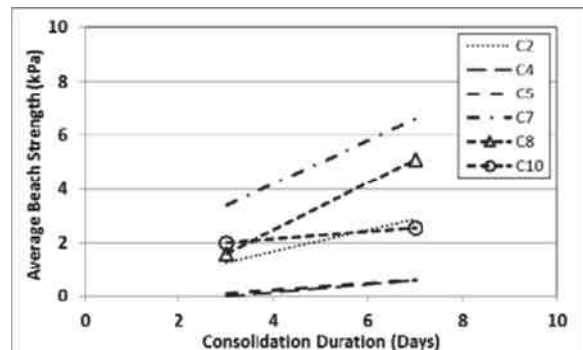


Figure 14. Beach Shear Strength as a Function of Deposition Duration for Group C Tests

KEY LEARNINGS

1. Feed $F/(F+W)$ is a key parameter to control the rate of fines captured on sand beach. Without flocculation, the critical $F/(F+W)$ value for capturing 50% or more feed fines is at 0.125-0.130.
2. Feed carrier yield stress is another key parameter that governs the rate of fines captured. Increasing feed $F/(F+W)$ ratio increases carrier yield stress. This makes the fines and partial coarse sand suspended in the carrier fluid and lost as runoff, which results in reduction of fines captured rate in the deposit. This influences the upper limit of the feed $F/(F+W)$ ratio that is effective for optimal fines capture.
3. Flocculation can improve the fines captured rate by agglomerating all feed components such that fines and coarse sand will be uniformly suspended so the slurry approaches non-segregating. To ensure this near non-segregating slurry remains on the beach instead of continuing as non-segregated slurry run-off, a new method is to add coarse sand into the flocculated fines to increase the strength of non-segregating deposit. This approach with higher feed concentration plus flocculation will improve the rate of fines captured.
4. Tests C8 and C10 results show that if feed concentration is increased to 65%, and feed $F/(F+W)$ is at 14-16%, adding 150 gpT AF3338 to MFT can achieve greater than 75% fines and volume captured. These experiments also obtained beach strengths of 5.1 kPa and 2.5 kPa, 7 days after deposition for tests C8 and C10 respectively.
5. Optimum flocculent dosage has to be developed to suit the feed composition and to optimize the beach strength.
6. Since higher feed concentration, feed $F/(F+W)$ and flocculation all contribute to the improvement of fines captured, the fines captured system needs to be designed and validated carefully to reach an optimum feed $F/(F+W)$, rheology and beach strength.

FUTURE WORK

1. Flocculation can improve the rate of fines captured by agglomerating fines, coarse sand and water together. More research is required to study the impact of flocculation on hydro-conductivity or permeability of the flocculated beach.
2. Larger than pilot flume scale tests are required to further develop the process of improving the rate of fines captured and beach strength by adding coarse sand into flocculated fines.
3. Although no wall effect was observed in the flume tests, wider (>0.25 m) flume or field tests are recommended for future fines captured in sand beach studies if adequate material and space are available.

REFERENCES

- P.S. Wells and R.A. Riley, MFT Drying-Case Study in the Use of Rheological Modification and Dewatering of Fine Tailings Through Thin Lift Deposition in the Oil Sands of Alberta, Paste 2007, 271-284, Perth, Australia, (2007).
- G. Cuddy, R. L. Lahaie, and D.W. Mimura, Spiking Tailings as a Method to Increase Fines Retention in Beach Deposits. Proceedings of the Fine Tailings Symposium. Oil Sands – Our Petroleum Future Conference. Edmonton, Alberta. Paper F21, pp. 1-21. April 1993.
- W. Shaw, J. Beck, W. Livingstone, Disposal of Fine Tailings Utilizing Hydrocyclone Techniques Oil Sands Our petroleum Future Conference, Fine Tailings Fundamentals Consortium. Edmonton, AB April 4-7, 1993.
- W.G. Miller, J.D. Scott, and D.C. Segó, Flume deposition modeling of caustic and non-caustic oil sand tailings, Can. Geotech. J. 46: 679–693 (2009).
- Energy Resources Conservation Board. 2009, "Tailings Performance Criteria and Requirement for Oil Sands Mining Schemes, Directive 074".
- R. Sun, A. Goldszal and C. Li, Optimizing the capture of Oil Sand Fines in Sand Beach Area, Third International Oil Sands Tailings Conference. Edmonton, AB December 3-6, 2012.

Table 1. Group C Test Matrix and Results

Test ID	Feed System	Average Feed			Feed Fines Captured (w/w)	Feed Vol. Captured (v/v)	Average Beach Strength (kPa)		
		Cw (w/w)	F/(F+W) (w/w)	SFR (w/w)			3 day	~7 days	~30 days
		C1	MFT, sand, P/water	0.578	0.086	13.587	0.635	0.674	0.1
C3	MFT, sand, P/water	0.545	0.120	7.741	0.587	0.677	1.5	4.0	
C6	MFT, sand, P/water	0.553	0.120	8.032	0.582	0.661	1.0	2.4	
C2	MFT, sand, P/water	0.566	0.125	8.145	0.562	0.670	1.3	2.9	
C4	MFT, sand, P/water	0.560	0.151	6.144	0.355	0.473	0.0	0.6	
C5	MFT, sand, P/water	0.555	0.190	4.314	0.277	0.293	0.1	0.6	
C7	150 gpT AF3338	0.554	0.117	8.369	0.579	0.684	3.4	6.6	
C8	150 gpT AF3338	0.649	0.142	10.142	0.831	0.870	1.6	5.1	
C9	MFT, sand, P/water	0.562	0.127	7.840	0.609	0.699	1.3	4.0*	
C10	150 gpT AF3338	0.656	0.163	8.78	0.768	0.833	2.0	2.5	

* Measured after 18 days for 30 days testing

Table 2. Beach Particle Size Distributions and SFR₄₄ for Selected Group C Tests

Test ID		C1	C3	C2	C4	C5	C7	C8	C10								
System		Normal MFT	Normal MFT	Normal MFT	Normal MFT	Normal MFT	+150 gpT AF3338	+150 gpT AF3338	+150 gpT AF3338								
Feed Cw (w/w)		0.578	0.545	0.566	0.56	0.555	0.554	0.649	0.656								
Feed FOFW (w/w)		0.087	0.121	0.125	0.151	0.190	0.118	0.143	0.163								
Feed SFR ₄₄ (w/w)		13.587	7.741	8.145	6.144	4.314	8.369	10.142	8.78								
Fines Captured (w/w)		0.635	0.587	0.562	0.355	0.277	0.579	0.831	0.768								
Volume Captured (v/v)		0.674	0.677	0.670	0.473	0.293	0.684	0.870	0.833								
Sample Location	Dist. From Inlet (mm)	SFR ₄₄ (w/w)	d ₅₀ (mm)														
L1D1	1016	23.8	0.125	6.0	0.149	9.4	0.129	11.7	0.154	8.0	0.137	14.1	0.161	14.5	0.166	9.5	0.251
L1D2	1016	24.9	0.132	20.3	0.154	17.0	0.125	20.3	0.175	8.0	0.137	20.3	0.175	15.5	0.158	12.8	0.172
L2D1	1702	21.5	0.119	18.4	0.214	14.0	0.127	13.1	0.183	9.3	0.141	14.4	0.147	12.8	0.146	10.9	0.135
L2D2	1702	21.1	0.127	18.2	0.167	16.3	0.128	19.7	0.142	9.3	0.141	19.7	0.142	16.8	0.152	12.4	0.215
L3D1	2642	24.5	0.131	18.1	0.152	17.9	0.157	11.3	0.158	9.8	0.141	21.3	0.170	12.1	0.136	10.7	0.212
L3D2	2642	22.2	0.121	17.9	0.149	17.1	0.151	21.1	0.152	9.8	0.141	21.1	0.152	14.9	0.168	12.3	0.143
L4D1	3556	26.5	0.127	19.8	0.155	15.5	0.230	12.8	0.167	8.1	0.153	15.8	0.165	11.8	0.140	9.5	0.144
L4D2	3556	23.2	0.129	18.5	0.148	17.0	0.137	19.1	0.135	8.1	0.153	19.1	0.135	15.5	0.147	11.8	0.169
L5D1	4470	26.8	0.259	16.6	0.157	16.1	0.184	12.7	0.163	7.9	0.137	19.1	0.135	12.0	0.163	7.8	0.133
L5D2	4470	27.2	0.152	16.7	0.142	16.2	0.144	18.8	0.135	7.9	0.137	18.8	0.135	16.7	0.138	12.6	0.139
L6D1	6418	11.6	0.226	7.8	0.189	13.3	0.116	10.6	0.226	6.0	0.134	12.9	0.137	12.3	0.131	5.7	0.140
L6D2	6418	11.6	0.226	7.8	0.189	13.3	0.116	10.6	0.226	6.0	0.134	17.6	0.119	14.7	0.157	12.0	0.213

MUDDY RIVER DELTAS AS ANALOGUES FOR OIL SAND TAILINGS BEACHES: IMPROVING FINES CAPTURE AND OPERATIONAL EFFICIENCY WITH TAILINGS BEACH MODELING

Ben Sheets¹, Timothy Wagner¹, John Swenson¹, John Horton¹, Jim Langseth¹, Luca Sittoni², Dirk-Jan Walstra², Han Winterwerp², Rob Uittenbogaard², Jan van Kestern², and Arno Talmon²

¹Barr Engineering, Minneapolis, MN

²Deltares, Delft, Netherlands

ABSTRACT

Subaerial and subaqueous beaching of tailings are common practices in Oil Sand mines. While a number of technologies exist for optimal tailings placement with respect to Directive 074, such as non-segregating slurries or atmospheric fines drying, these are not always operationally practical. Thus, beaching of whole tailings and related water-rich slurries is common in a variety of settings. Even modest (several percent) improvement in the fines content of such beaches would constitute a significant fines capture, and could significantly reduce costs associated with rehandling of MFT. This paper presents fundamental modeling research conducted by Barr/Deltares with the goal of optimizing fines content in beaches, both above and below water/MFT, based on their similarity to high-concentration natural sedimentary flows. We propose that river deltas are a viable analogue for such flows, and doing so opens the door to a wealth of existing literature and tools for advancing our understanding of important beaching processes. By modeling a generic range of scenarios involving variable tailings sediment concentration, rheology (Newtonian vs. non-Newtonian), solids content, and discharge configuration, we show that certain scenarios promote higher beach fines capture. The modeling presented here could be adapted to any particular geometry, and used to predict operational strategies to optimize fines capture and minimize operational costs.

INTRODUCTION

Background

Oil Sands operators have taken a broad range of approaches to tailings deposition and disposal. Nearly all of these are united by their focus on the

objectives laid out in Directive 074. Indeed, most are focused on capturing a significant fraction of fine sediments (< .044 mm) in deposits that are strong enough to allow reclamation within a reasonable time window. The full range of technologies currently employed by Oil Sands operators is beyond the scope of this paper, but is reviewed in detail by BGC Engineering (2010). New technologies under development are reviewed in the Tailings Technology Deployment Roadmaps (Sobkowicz, 2012). The reader is referred to these documents for detailed background on available technology.

Despite availability of a broad range of technologies, which range from deposition and drying of thickened or polymer-amended fine tailings to subaqueous emplacement of non-segregating tailings slurries, operational realities frequently require subaerial or subaqueous beaching of conventional tailings (whole tailings). For example, overboarding of whole tails is common practice when equipment required for the above technologies is unavailable due to scheduled maintenance. In this eventuality, whole tails with relatively low solids concentrations (ca. 30%) and high sand:fines ratios (ca. 4:1) are deposited in a variety of configurations, often depending on where space is available. Such deposits are typically very strong, but usually have very low fines content, and their deposition results in relatively high rates of fines segregation, production of fluid fine tailings, and eventually mature fine tailings (FFT/MFT).

The purpose of the present study is to investigate ways to optimize whole tailings deposition such that deposit fines content is maximized, and thus segregation is kept to a minimum. Even a modest improvement in the fines content of whole tails beaches would lead to significantly reduced production of fine tailings, and therefore appreciable cost savings by reducing the eventual volume of fine tailings rehandling.

River Deltas as Whole Tailings Analogues

The focus of the study presented in this paper is the hypothesis that subaerial and subaqueous whole tailings deposits can be reasonably approximated as analogous to natural river deltas. Doing so opens the door to a large existing body of literature regarding depositional patterns, fines content, and deposit slopes, each of which are relatively well understood in natural and man-made deltaic systems. Indeed, river deltas have been the focus of sedimentological and sediment transport study since the time of the ancient Greeks (hence their Greek-letter-derived name). Gilbert (1884) was among the first to identify deltaic deposits as having a distinctive layering geometry and sediment grain size distribution. The details of the subsequent 100+ years of deltaic research are not important here, but it is noteworthy that a significant fraction of the Earth's population lives on river deltas, and consequently their dynamics have been, and continue to be, the subject of intensive research by authors too numerous to list. Reading (2009) provides a thorough summary of the relatively recent state of the art in characterization of deltaic processes and deposits, including a review of the seminal work by Galloway (1975), which provides a framework for distinguishing the relative influence of either source characteristics (grainsize, flow rate) or external influences such as waves or base water level changes.

Perhaps the most important summary observation from the above referenced literature is that the processes that control sediment grain size distribution both above and below water are well understood in nearly all river delta environments. Sediment distribution across the subaerial portion of the delta (the delta top) is typically via a network of linked distributary channels and overbank flows that periodically migrate to fill accommodation space as evenly as possible. Subaqueous (clinoform or bottom set) processes range from gradual accumulation of suspended sediment in the quiescent ocean (or lake, pond, etc.) to active transport and deposition from sediment laden density currents. While other processes, such as debris flows or mass failures, operate in some environments, their deposits are easily distinguished from more conventional sediment transport phenomena (Reading, 2009).

As with many sedimentary systems, river deltas tend to produce deposits that become increasingly fine with distance from their source, due to

progressive loss of those grain sizes most difficult to transport. That is, the coarsest sediments (sand, gravel) tend to deposit on the delta top, and finer sediments (silt, clay) are transported farther into the basin where current velocities are smaller, and silt to clay sized particles are able to settle to the bottom of the stagnant water body.

While this general grain size distribution characterizes deltaic sedimentary environments as a whole, it is worth noting that non-channel (overbank) depositional environments on the delta top often lead to significant deposition of fine-grained sediments. Consider many of the Earth's largest deltas, in which sand- and silt-sized sediments are only found in or very near the active channels. The remainder of the sediment (all of which is fines) ends up in deposits either off the channel mouth, or deposited in delta top regions far from the channels via overbank flows. The archetypal example of this phenomenon is the Mississippi delta, in which more than 90% of the deltaic deposit is fine grained, in part due to the sediment load of the Mississippi River comprising more than 90% fine-grained sediments. More important for our discussion here, however, is the nature of the overbank flows that lead to delta top deposition of fine-grained sediment, which are reviewed by Roberts (1997), among others.

These overbank flows that lead to relatively fine-grained deposits are the flows that Oil Sands operations should seek to reproduce. Even with relatively sandy source streams, any strategy that maximizes these flows could be used to optimize whole tailings deposition.

Modeling Approach

The relative ubiquity of deltaic processes (and associated research) on Earth has led to the development of a number of numerical modeling tools that are considerably more sophisticated than any of the commonly used modeling approaches in the Oil Sands. Such tools are often publically available (open source), and the source code for many of the very best are downloadable through the Community Sediment Dynamics Modeling System (CSDMS; csdms.colorado.edu). Numerical models that are designed to simulate everything from the most basic deltaic processes (sediment transport and deposition) to the influence of changing water level and waves are available. The authors of this paper suggest that this body of numerical technology represents an important resource for the Oil Sands industry.

The research presented in this paper utilizes one of these tools, Delft3D, which is an integrated modeling suite designed to simulate the effects of not only basic sediment transport processes, but how they might be affected by wind, waves, ice and vegetation, as well as how water chemistry evolves due to all of the above (Gerritsen, et al., 2007; Delft3D Open Source Community Webportal: oss.deltares.nl/web/delft3d). Delft3D source code is available from both the CSDMS and Deltares websites.

The central question is whether an internationally recognized delta modeling software package can be applied to the specific case of Oil Sands tailings. The modeling program presented here, therefore, involves an adaptation of existing Delft3D deltaic modeling to the general geometric and sediment transport constraints of the Oil Sands environment.

Application of Delft3D to Oil Sands Scenarios

Adaptation of deltaic modeling, including Delft3D, to scenarios involving whole tails deposition is relatively straightforward. This is largely due to the fact that natural deltas, and particularly the physics that govern the transport and deposition of sediment are essentially the same. That is, in tailings streams in which solids content is low enough that flow dynamics can be considered Newtonian, traditional fluid mechanical approaches are valid for predicting their behaviour. Similarly, except for the most extreme high sediment concentrations, deposition and erosion behaviour is primarily a function of a balance between turbulent fluid velocity and particle settling rate. Even at relatively high concentrations a correction for hindered settling can be applied. Newtonian morphological evolution, such as channelization and delta lobe formation, is similar in any environment characterized by these behaviours. We contend that these behaviours are shared between natural deltas and whole tails beaches.

Thus, Delft3D, which is designed to simulate these processes across a broad range of scales (from small ponds and rivers to major oceanic river deltas) in natural environments, is well suited to simulation of whole tailings deposition.

The key to adaptation of Delft3D to Oil Sands tailings scenarios lies in proper definition of basin geometry (i.e.: pond extent, bathymetry, pond elevation), tailings stream characteristics (i.e.: sediment concentration, grain size distribution),

and operational history (i.e.: time evolution of discharge rate and pond elevation). As noted above, the focus of this study is to determine whether characteristic Oil Sand tailings pond geometries can be modeled stably and realistically.

Non-Newtonian Slurries

An approach based on Newtonian fluid dynamics, in which sedimentation rate is primarily a function of settling rate, is clearly not suited to simulating all possible tailings slurries. This is particularly true for slurries that include either thickened or polymer-amended fine tailings, due to the fact that these higher-solids content materials typically behave as non-Newtonian fluids (commonly as Bingham plastics).

While the primary focus of this paper is adaptation of Newtonian modeling to whole tailings scenarios, we would note that a secondary line of research involves addition of non-Newtonian fluid dynamics and sediment settling behaviour to the Delft3D framework. This approach is based on an analytical model for sand settling through non-Newtonian carrier fluids as a function of both fluid rheology and shear rate. This approach is described in detail in a previous contribution to the IOSTC (Sisson, et al., 2012), and progress on non-Newtonian modeling is discussed later in this document.

RESULTS

In order to investigate the general applicability of Delft3D to whole tailings scenarios we defined a series of generic tailings basin geometries and configurations that were intended to highlight particular aspects of tailings beach formation. Thus, the scenarios presented in this study are simplified versions of real tailings basins meant to illustrate basic behaviour. Table 1 lists several of these scenarios, which will be discussed in turn.

Table 1. Selected Model Scenarios

run	Qw [m ³ s ⁻¹]	Qs [kg/m ³]	wt. conc.	SFR
1	1.0	5	5.0%	1
2	1.0	10	10.0%	1
3 upr.	1.0	325	32.5%	3.3
3 lwr.	1.0	200	20 %	1

The first set of simulations undertaken for the purpose of evaluating the applicability of Delft3D to Oil Sand tailings scenarios involves relatively low sediment concentrations—analogue to those common in natural environments. Figure 1 shows an elevation/bathymetry map of one of these simulations, in which a steady discharge of $1 \text{ m}^3 \text{ s}^{-1}$ was delivered via a channel-like geometry from the left edge of the domain. Sediment feed rate was also constant. The boundary conditions for this simulation are given in Table 1. The simulation was set up in a generic square basin (500 x 500 m) with a sloping floor, in which the water depth at the inlet was 1 m, progressively deepening to 5 m at the right hand edge of the model domain. Two sediment size fractions were used in all simulations presented here: a sand fraction of 100-micron mean diameter, and a fines fraction of 44-micron mean diameter. Pond level was held constant for all simulations.

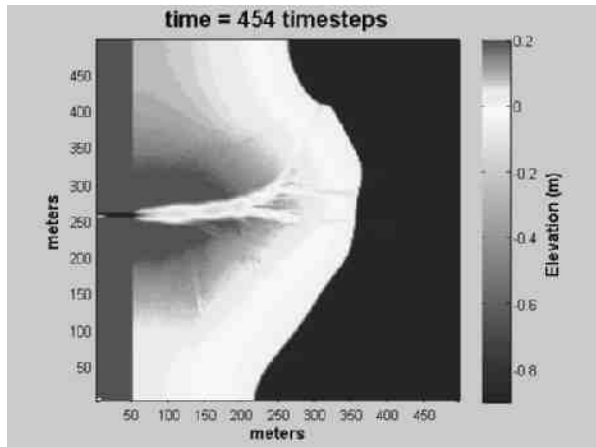


Figure 1. Low concentration simulation – elevation (run 1)

The approximate duration of this scenario was on the order of 6 – 12 months, though precise time is arbitrary in this sort of simulation. In order to keep computational time reasonable (less than one day), a morphological acceleration factor was applied that increases numerical transport, erosion, and sedimentation rates for each iteration of the model. Predicted beach above water (BAW) slopes range from 0.01 – 0.5 %, with slopes as high as 1% in certain locations. BAW slope varies due to the specific channel migration history, as well as where the measurement is made—the shortest path from inlet to shoreline will necessarily have a higher slope than longer flow paths.

Figure 2 shows the vertically averaged SFR of the deposit (mass of 100 micron sand divided by mass of 44 micron fines) at each point in the model domain. That is, the entire mass of sand at a particular X, Y location divided by the entire mass of fines at that same location at all elevations.

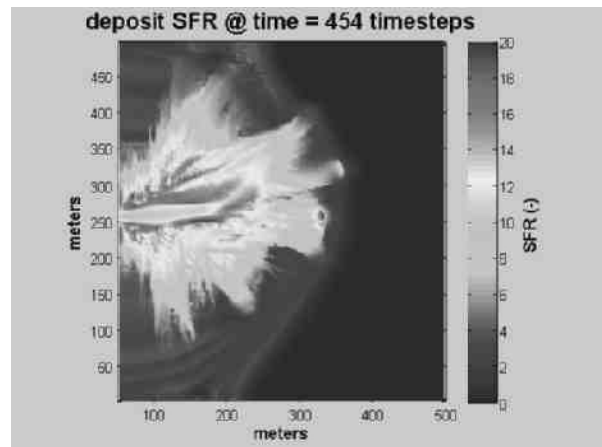


Figure 2. Low concentration simulation – SFR (run 1)

Note that higher SFR values are concentrated in areas where channelized flow was more common (through the center of the deposit), and that the deposits progressively fine towards the edges of the deposit.

Figures 3 and 4 show the topographic/bathymetric and SFR maps for run 2, which involved a doubling of sediment concentration over run 1. Otherwise, input conditions and basin geometry were held constant.

The fundamental difference in result between runs 1 and 2 is that run 2 shows significantly higher BAW slopes, locally as high as 2%, particularly near the inlet. Additionally, filling rate is significantly higher, due to the availability of twice as much sediment in the simulated tailings stream. SFR patterns are similar between the two runs, though the delta-average SFR is somewhat higher in run 2, due to a more restricted delta area, and therefore less BAW distance across which to segregate fine from coarse sediment. Vertically averaged SFR reaches a somewhat higher value in this simulation. Note that this simulation was run for a shorter model time: 3 – 6 months. This shorter period for deltaic evolution was necessary due to the higher slopes that occurred in this simulation, which led to overtopping of the

numerical dike along the left edge of the model domain.

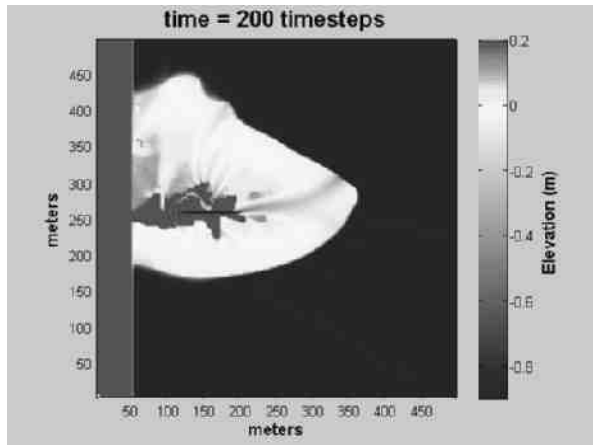


Figure 3. Mid concentration simulation – elevation (run 2)

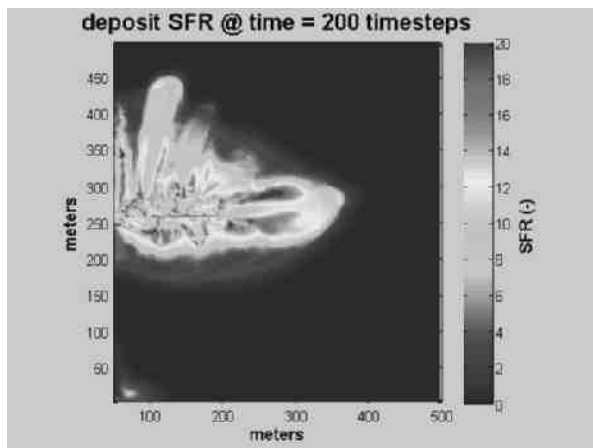


Figure 4. Mid concentration simulation – SFR (run 2)

Based on the results of these simulations, and many others that are not specifically reported here, it is clear that simulation of deltaic processes at the general scale of tailings deposits is possible. However, the sediment concentrations employed in runs 1 and 2 are considerably lower than those common in whole tailings streams (30%+). Additionally, the feed SFR is lower than common ore ratios (4:1).

Both of these discrepancies relative to average whole tailings properties were addressed in a new set of simulations, of which run 3 is an example (Table 1). In this simulation two tailings sources were introduced along the long wall of an enlarged generic basin (1500 x 1000 m). The bathymetry of

this basin was similar to that of runs 1 and 2. Figure 5 shows the elevation and bathymetry of the two run 3 deltas.

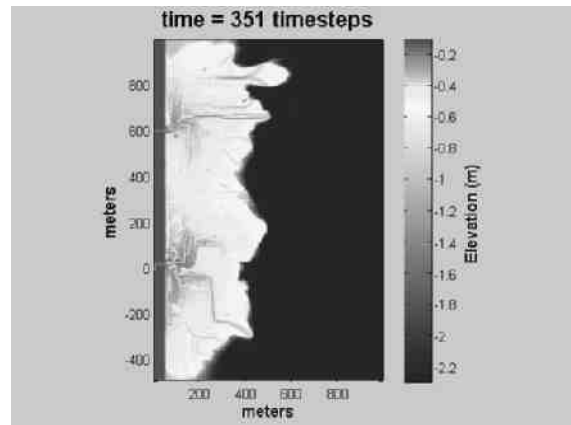


Figure 5. High concentration & SFR simulation (run 3)

Evolution of the run 3 deltas can be thought of as roughly 1 year of deposition, though precise time is not specified, for reasons discussed above. Overall, slopes on the upper delta are somewhat higher, due to the somewhat higher sediment concentration. The central result of run 3 is that simulation of higher concentration flows is, indeed, numerically possible, and the overall geometry and BAW slopes are physically reasonable.

Figures 6a and 6b show the deposit sand content along three flow-perpendicular sections cut numerically at the end of run 3. The more proximal of these (Fig. 6a) shows a relatively sand rich deposit near the channels, as well as a generally sandy deposit throughout its thickness. This stands in contrast to the more distal section (Fig. 6b), which shows coarse sediments concentrated around the channels, but a significantly finer deposit base. This fine-grained lower deposit is the distal equivalent (the delta toe) of the early sandy channels on the proximal section. Not until later in the simulation do coarse sediments come to dominate the deposit, after adequate slope has been built near the inlet to drive coarse sediment farther into the basin.

Figures 7a-c show flow parallel deposit sections through the center of the upper delta (Fig. 7a), lower delta (Fig. 7c), and through the region between the two (Fig. 7b). These sections illustrate how the two deltas, despite contrasting feed SFR, lead to similarly sandy deposits. As in the cross-sections of Figures 6a and 6b, the base of the

deposits tends to be relatively fine-grained, and the upper deposit progressively sandy, as the system fills the basin. The central flow-perpendicular section (Fig. 7b) shows overall lower sand content, due to its position away from the primary sediment sources. However, the same coarsening upward seen elsewhere in this system persists.

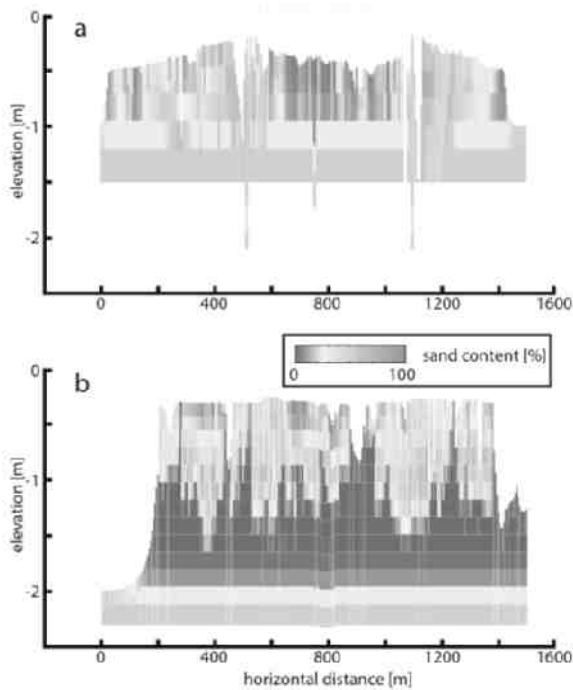


Figure 6. Proximal (a) and distal (b) flow-perpendicular deposit sections (run 3)

DISCUSSION

One of the major hurdles in numerically simulating realistic whole tailings streams is that their sediment concentrations tend to be relatively high in comparison to natural rivers. Indeed, most natural rivers have weight-based sediment concentrations an order of magnitude or more lower than a typical whole tailings stream (milligrams of sediment per kilogram of water). Thus, nearly all of the common sediment transport laws, which are calibrated to a natural range of conditions, are pushed to their reasonable computational limit by whole tails concentrations.

The results from run 3 presented above indicate that simulation of feed concentrations in excess of 30% by weight produce reasonable results, at least

when evaluated with respect to BAW slopes, channel patterns, and overall depositional patterns.

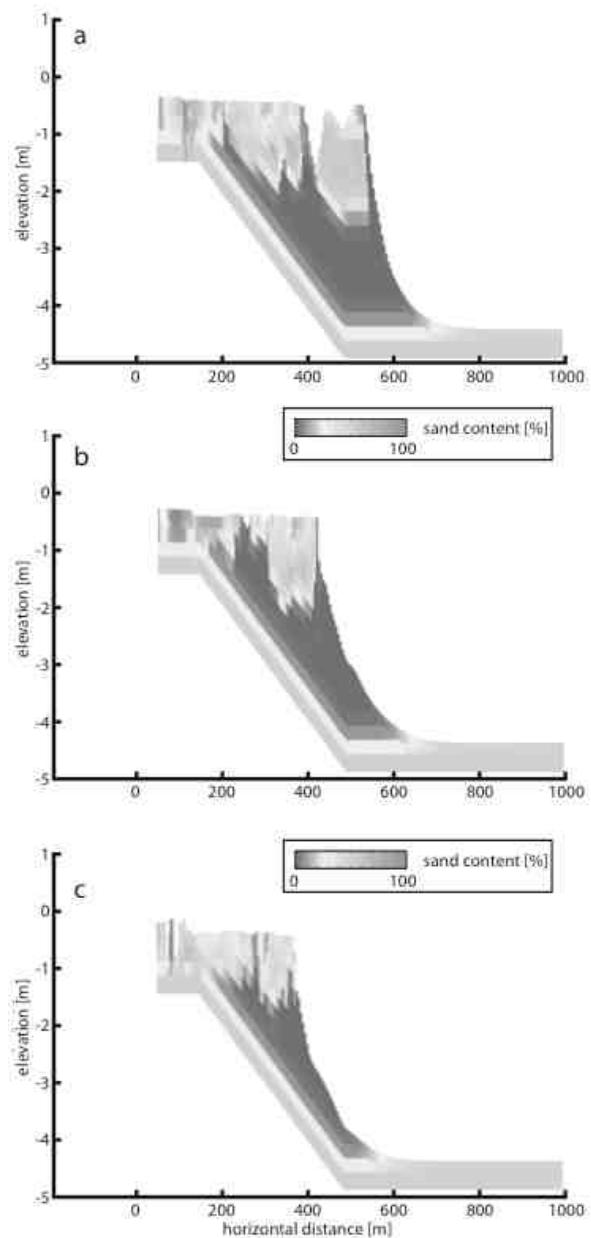


Figure 7. Upper (a), middle (b), and lower (c) flow-parallel deposit sections (run 3)

General Behaviour

While application of Delft3D to Oil Sands scenarios is relatively new, and specific numerical simulations tailored to a particular deposit are not yet available, several important phenomena are illustrated by the model results presented here.

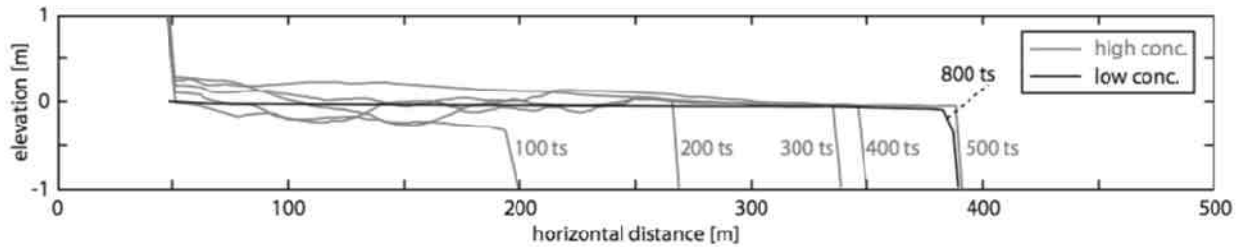


Figure 8. Timelines From Low (Black) And High (Blue) Concentration Simulations (Runs 1,2)

We would expect these behaviours to be universal, regardless of the specific geometry or tailings composition at a particular mine.

Runs 1 and 2 serve to illustrate the effect of sediment concentration on expected BAW geometry. Figure 8 shows superposition of topographic/bathymetric time lines from both runs along a flow-parallel section. The blue lines derive from the higher concentration run 2, and the single black line from the lower concentration run 1. Note that higher sediment concentration leads to both a higher BAW slope and a more highly dynamic channel network. These are common behaviours in deltaic systems at all scales, as increased sediment concentrations require higher slopes to move the increased load. When much of that sediment load is transported along the bed, as is the sand and coarse fines fraction in these simulations, channelization and bar formation processes tend to be more dynamic.

Another generic phenomenon illustrated by these simulations that we would expect to be universal, regardless of mine specifics, is the overall distribution of coarse and fine material within these deltaic deposits. The cross sections of Figures 6 and 7 show how, regardless of SFR and sediment concentration, the sand content of deltaic deposits tends to increase upward, as well as decrease with distance from the channels. This phenomenon would be expected in any deltaic system where water level is relatively constant. The degree to which this occurs will be a function of feed characteristics, such as SFR and grain size distribution, as well as pre-existing basin geometry. For example, deltas that prograde into relatively shallow basins tend to show less upward coarsening, as there is less space to accommodate distal fine-grained deposits.

That this is a generic deltaic sedimentation phenomenon suggests that manipulation of water level might be a strategy to promote deposition of

fines-rich layers. That is, periodic deepening of water leads to alternation of coarse and fine deposition in natural systems at all scales, and there is no reason to expect that similar processes would not operate in tailings ponds.

Figures 2 and 4, which show maps of depth-averaged SFR indicate how the particular SFR and grain size distribution of those simulated tailings streams (runs 1 and 2, SFR = 1:1, fines = 44 micron) leads to a relatively low SFR deposit away from the channels. Due to the numerical fines falling on the large end of the fines spectrum (silt sized) they are not as efficiently transported as clay sized particles, and thus tend to deposit on the BAW. This leads to relatively high fines contents away from the active channels—fines contents that are considerably higher than might be expected for a deltaic system dominated by sand and clay (with little in between). In such systems BAW fines content would be considerably lower than those simulated here.

More important than the specific SFR predicted in the runs presented here, however, is the overall distribution of fines content. Note how the sections of Figures 6 and 7 indicate higher fines content in the region between the tailings feed points. We would expect this trend to occur in any system with a distribution of grain sizes—finer grained sediments will be preferentially deposited (captured) away from the channels.

Ongoing Research

Several phenomena that are important for predicting Oil Sands tailings beach evolution are not included in the modeling presented here. Potentially foremost among these is the common production of tailings slurries that are best characterized as non-Newtonian plastics, and thus are not properly described by the conventional equations employed by Delft3D.

Incorporation of non-Newtonian flow equations into Delft3D is the subject of ongoing research. This work is based on a theoretical framework for describing non-Newtonian flows described in Sisson, et al. (2012), in which the velocity profile is a function of carrier fluid rheology following the method of Coussot (1997), and the rheological evolution, particularly sand settling behaviour, is a function of mixture density and shear rate (Sisson, 2012). The result of this theory is a prediction for not only non-Newtonian velocity profiles and flow behaviour, but for sand/mud sedimentation rates from such mixtures as they traverse tailings beaches. Figure 9 shows the contrast between Newtonian (blue) and non-Newtonian (red) velocity profiles with the same discharge as predicted in Delft3D. Note that the Newtonian flow is much thinner and higher velocity under the same driving conditions. The non-Newtonian flow shows a much higher equilibrium depth as well as an upper region of 'plug' flow, in which all particles are moving at the same velocity.

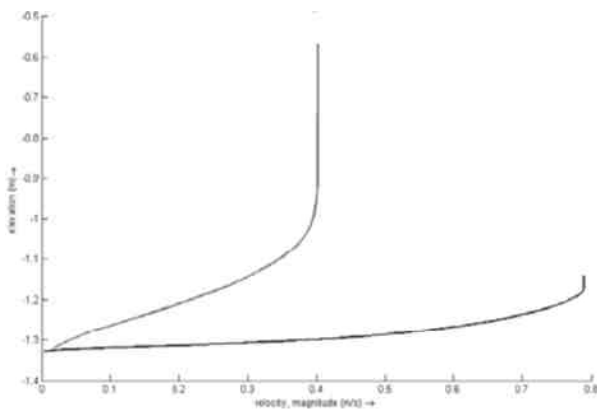


Figure 9. Delft3D velocity profile predictions for Newtonian (blue) and non-Newtonian (red) flows

This is a promising development, as it presages full inclusion of non-Newtonian flow processes in the Delft3D framework, and thus the ability to model the full spectrum of tailings slurries that are common in Oil Sands mines.

Two other areas on which we are focusing our ongoing development of Delft3D as a tool for Oil Sands modeling are subaqueous processes and improved understanding of high-concentration sediment transport. The latter is presently less important than the former, in part on the basis of the work presented here—the existing sediment transport formulation is able to handle realistic whole-tails concentrations with a numerically

stable simulation, and produces reasonable results (physically reasonable slopes, depositional patterns, etc.). Further, higher sediment concentrations are frequently associated with non-Newtonian flow, which is on the verge of full implementation.

The final direction of ongoing research that is of note for this discussion is subaqueous processes. They are of fundamental importance to prediction of fines capture, due to the frequent presence of FFT or MFT in many existing ponds. The importance of subaqueous processes arises from the potential for mixing between beach below water (BBW) flows and these existing FFT materials. While not implemented in the simulations discussed in this paper, the mechanism for doing so exists in Delft3D via equations developed for simulation of density/turbidity current processes. The flow of subaqueous currents driven by density contrasts (due to temperature, salinity, or sediment concentration) is a common process in natural systems at a variety of scales. The authors are currently working on adapting this framework to the specific issue of FFT/MFT entrainment by tailings flows. The results of this research will be the subject of a planned research article.

SUMMARY

The central conclusion of the research presented in this paper is that the Delft3D modeling software is applicable to Oil Sands tailings scenarios. Therefore, the Delft3D software, which is capable of simulating a broad range of geometric and rheologic situations, comprises an invaluable tool for prediction of everything from deposit fines content to optimal tailings basin configuration and operation.

Delft3D applicability arises from the geometric and process similarity between natural deltas (for which Delft3D was originally constructed) and tailings basin deposition. Both environments are governed by the same physical processes, and therefore produce deposits with comparable characteristics.

This applicability provides a critically important tool for mine and tailings planning, due to the fact that it can be used to predict tailings operations far into the future. Additionally, a modeling tool like Delft3D can be adapted to any particular basin geometry and tailings composition.

Basin planning of this nature will be invaluable for prediction of:

- fines capture
 - optimization of basin filling strategy to promote high fines content in reclaimable deposits
 - validation of long-range tailings plans
- tailings basin construction planning
 - such as long-range planning for dike construction
- tailings basin filling plans
 - BAW/BBW slope prediction
 - optimal discharge location planning (and long range procurement)

REFERENCES

BGC Engineering Inc., 2010. Oil Sands Tailings Technology Review. OSRIN Report No. TR-1. 136 pp. <http://hdl.handle.net/10402/era.17555>

Coussot P., 1997. Mudflow rheology and dynamics, IAHR Monograph, Balkema, Rotterdam.

Galloway, W.E., 1975. Process framework for describing the morphologic and stratigraphic evolution of deltaic depositional systems. *in* Deltas: Models for exploration. Houston Geological Society, p. 87 – 98.

Gerritsen, H., E.D. de Goede, F.W. Platzek, M. Genseberger, J.A.Th.M. van Kester and R.E. Uittenbogaard, 2007. Validation Document Delft3D-FLOW; a software system for 3D flow simulations. Version 1.0. 31 December 2007. WL | Delft Hydraulics report X0256, M3470.

Gilbert, G. K., 1884. The topographical features of lake shores. U. S. Geol. Surv. Annu. Rep., 5, 104–108.

Reading, H. G. (Ed.), 2009. Sedimentary environments: processes, facies and stratigraphy. John Wiley & Sons.

Roberts, H. H., 1997. Dynamic changes of the Holocene Mississippi River Delta Plain: The delta cycle. *J. Coastal Res.*, **13**(3), 605–627.

Sisson, R., Lacoste-Bouchet, P., Vera, M., Costello, M., Hedblom, E., Sheets, B., Nesler, D., Solseng, P., Fandrey, A., van Kesteren, W., Talmon, A., and Sittoni, L., 2012. An analytical model for tailings deposition developed from pilot scale testing. Proceedings of the IOSTC, 2012, Edmonton, AB.

Sobkowicz, J., 2012. Oil sands tailings technology deployment roadmap. Project Report–Summary Report.

SEDIMENT DEPOSITION – INTEGRATION OF PHYSICS AND ITS CONSEQUENCES FOR MODELLING

Dirk Luger¹, Rick Sisson², Luca Sittoni¹ and Johan Pennekamp¹

¹Deltares, The Netherlands

²Barr Engineering, USA

ABSTRACT

Correct understanding of the physics and modeling of sediment deposition is important for the optimal design of the operation and reclamation of tailings deposits. Reclamation landfills and tailings ponds design requires interaction between many disciplines of science and engineering. The authors backgrounds range from (geo-)chemical engineering to hydrodynamics, sedimentology and soil mechanics. The paper aims to integrate the physical background of the mechanisms involved in sediment deposition in order to deal consistently with all relevant mechanisms and models.

From slurry in a pipeline to firm soil within a reclaimed pond, tailings undergo different physical processes at different time scales. Rheology and (non-Newtonian) hydraulics, together with sand settling, dominate the deposition behavior. Flocculation, sedimentation, consolidation and creep lead the transition from fluid into soil. Soft tailings subjected to overlying loads may have stability problems and can experience large deformations.

Physics and practical modeling constraints determine models set-up. Generally full 3-D modeling, simultaneously capturing all processes over time scales that range from dynamic seconds to creeping years is not appropriate or feasible. A vertical 1-D model may work for flocculation, sedimentation, hindered settling, segregation, creep and consolidation; 2-D or sometimes even 3-D models may be necessary to capture realistic deposition patterns, involving meandering and beach formation, or to perform (large deformation) geotechnical stability analyses.

Specific tailings management technologies, such as e.g. “Enhanced Fines Capture”, “Capping” “Composite Tailings” and “Non- Segregating Tailings”, demand accurate understanding and modeling of this set of multidisciplinary processes. The paper outlines a coherent physical and modeling approach to serve as a reference for different tailings management technologies.

INTRODUCTION

Background

Understanding and being able to model the most dominant processes that describe the transition of a fluid suspension of fines into a weak but solid geo-material is essential for the sediment deposition design that is required to develop hydraulically placed landfills worldwide and to manage tailings deposits in particular.

Experience with the worldwide dredging industry is that ‘good’ materials for land reclamation projects (i.e. sands with little or no fines) have become more and more scarce. So-called inferior materials like sands containing significant amounts of fines are now considered and used as landfill construction materials. The maintenance dredging of waterways and harbors leaves us with significant volumes of (often contaminated) harbor sludges and dredge spoils. These materials need to be disposed of and are often stored in confined disposal facilities (ponds). The drive to put them to more beneficial use has turned these materials into landfill construction materials as well.

These developments have increased the need to understand the role of fines (silt and clay particles) in the long-term properties of landfills. While working with and using contaminated materials has challenging environmental aspects that need to be addressed, the mechanical behavior also is far from straightforward.

The parallels with the challenges that are posed by today’s tailings deposition management and tailings ponds restoration tasks are evident.

While this paper focusses on the mechanical aspects of fluid and sediment behavior it is since long recognized that this behavior is affected by chemical processes and properties (Sills, 1995, Winterwerp, 2004).

Sediment Deposition Engineering (SDE)

The term Sediment Deposition Engineering (SDE) is used to cover the study of deposition, consolidation, segregation, strength of sediment-water mixtures and covers the complete range from fluid phase via the transition between fluid and solid behavior into the solid range. Examples of engineering applications include prediction of beach slope and composition (sand settling and fines capture) in tailings basins, study of settling, particle segregation, compaction, consolidation and strength development of soft soils, sand capping of soft soils and biogenerated or other types of gas emissions from tailings basins.

SDE is interdisciplinary; it includes different expertise areas, such as chemistry, colloidal science, fluid mechanics, sediment transport and geotechnical engineering.

Using the term SDE aims to prevent any single one of the contributing disciplines to claim this field as its own and aims to promote cooperation and a joint effort to achieve practical as well as scientific progress in this field.

The Missing Link

SDE has been dubbed “The Missing Link” by some because it covers the grey zones between well-established disciplines (e.g. geotechnics, fluid mechanics and sedimentology). At these zones, each single discipline meets its boundaries of applicability or relevance.

The biggest challenge is to spur a dialogue and cooperation between representatives from these different disciplines, to keep that cooperation going and to prevent competition and claiming the art of Sediment Deposition Engineering as its own by any one of the single disciplines. Even in institutes or universities where these experts are found together under one roof this is easier said than done.

INTEGRATION OF PHYSICS

Multidisciplinary character of SDE

The multidisciplinary character of sediment deposition engineering is clear. The pitfall of that situation is that a single discipline can perform quite well in predicting and modeling the behavior of the fluids-sediment-soil medium for some range

of process. Practitioners may focus on their success, without adequately understanding or exploring the limitations associated with a single discipline approach

Hydraulic engineers and sedimentologists can explain the processes and model them well into the solid phase, but when the settling sediment starts to behave more and more like a firm soil Navier Stokes “fades away” and geotechnical models rather than sedimentation models apply.

Similarly geotechnical engineers can extrapolate and fit their models quite well into the early stages of sedimentation, but then the geotechnical constitutive models are “stretched” to be used in the near fluid phases and the behavior is extrapolated far from the “solid” experience.

Chemistry and biology play their role since it is now also recognized that, while “simple” mechanics serve perfectly well to describe interaction between coarser grained soils, inter-particle forces (measurable with e.g. zeta-potential) as exist between clay and silt particles play a role in the formation of flocs in the suspension and the subsequent structure of the unconsolidated sediment, e.g. (Zhu, 2011) and (Ibanez, 2014). Gas formation, as caused by chemical and biological processes has its impact on consolidation characteristics of the sediment, Biological activity can directly influence the strength of the top layer of a deposit e.g. through growth of plant roots and enhanced evaporation. The deposition of organic slimes can give some strength, but decreases permeability; for example, worms living at the tailings surface have shown to potentially increase the strength of the top layer.

The chemistry of suspension and sediment is therefore important. While the chemistry for oil sands is initially governed by the oil extraction process, it can of course be influenced by direct chemical treatment of the tailings (e.g. addition of a flocculant), but also bacterial treatment or introduction of plants or animals has shown to influence strength development and consolidation behavior (M. de Lucas Pardo, 2014).

As a geotechnical engineer, the main author feels he has the right to confirm that most practitioners of his discipline tend to shy away from chemistry and biology, instead preferring to create models that describe and fit the observed phenomena rather than proceeding with research into the underlying mechanisms and developing a thorough

physical understanding. This is a source of frustration for the chemical and biological scientists, who feel that their potential for a contribution is overlooked. It seems logical that some of the “experience values” in the geotechnical engineering practice, like the ratio between immediate and long-term settlements, the permeability of the soil for different void-ratios, its strength to stiffness ratio, the development of strength in the absence of effective stresses and the loss of strength upon remolding can be better understood and predicted when these chemical and inter-particle forces that affect the settling and deposition process, are taken into account.

Not or-or but and-and

Rather than a process being e.g. **or** chemical **or** hydrodynamical **or** geotechnical, it is preferable that a process is approached as being **and** chemical **and** hydrodynamical **and** geotechnical. All disciplines play their roles; it is just that the relative importance of the different disciplines varies along the fluid-suspension-floc-sediment-soil line.

SDE R&D ROADMAP

We need to understand and be able to model how the sediment laden fluid spreads itself, how the flocculation and sedimentation process develops, how segregation occurs over the deposition area, how subsequently the consolidation, compaction and strength development takes place and how this can be affected by drainage, drying, capping or any other technique.

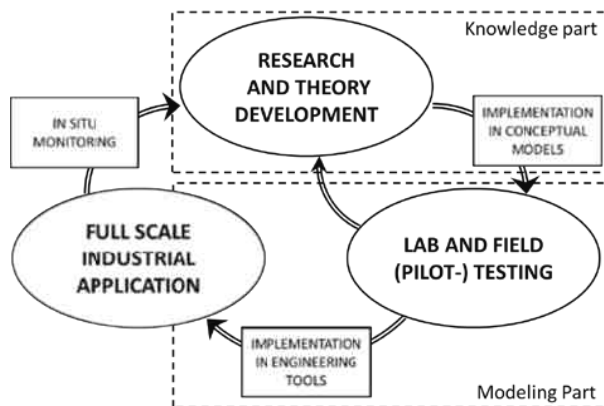


Figure 1. R&D Roadmap with feedback loops

To organize our R&D efforts a roadmap is being set-up. The ongoing and expected future projects in the area of SDE and the fluid to solid transition processes have been reviewed in the light of our current knowledge and modeling capabilities.

In summary the SDE-R&D Roadmap consists of:

The Knowledge Part

- Understanding processes as a function of multiple influence factors, both qualitatively and quantitatively. Defining the processes from the various disciplines that need to be implemented in numerical engineering models.

The Modeling Part

- Establishing effective ways and procedures to determine the quantitative parameters for the governing analytical models.
- Building these chemical, biological, rheological and constitutive models.
- Implementing the analytical models in numerical analytical tools, where necessary build or improve these tools, to enable prediction of the various sediment deposition engineering processes.

The SDE R&D Roadmap is split into two main parts: One part focusses on the acquisition of missing knowledge (“white areas”, the first bullet.) The second part focusses on putting new and existing knowledge to use, by developing proper in-situ and lab testing procedures, building the chemical, rheological and constitutive models and finally the implementation in conceptual and numerical models (the last three bullets), meanwhile providing feedback to the theory development and research.

The SDE R&D Roadmap needs feedback loops: they exist in the form of measurements that confirm or disprove the assumptions that are made and the adequacy of the theoretical and numerical models. Feedback loops form an integral part of what is called the innovation circle: from theory into models and lab or pilot-tests to industrial applications (Figure 1).

Up-scaling of the processes is one of the biggest challenges (P.S. Wells, 2014) and feedback through the in-situ-monitoring of pilot- and full-scale applications is indispensable to achieve further optimization and understanding.

SDE ROADMAP - KNOWLEDGE PART

An overview of the required knowledge areas is obtained by following the subsequent stages and transition phases that a hydraulically placed fill or tailing passes: Flow, deposition, consolidation and restoration.

Table 1 presents such an overview, without claiming to be complete. The stages go from pipeline transport, to deposition in the pond or fill area, to consolidation and finally to a state where the area is either restored to a proper ecological status (lake or land) or put to use for building or other economic benefit. The “white areas” are all processes that are not understood well enough.

Table 1. Stages, Processes and Phenomena

Stages	Processes	Phenomena
Flow	pipeline-, open channel- and beach-flow, transport	segregation, sedimentation, erosion, mixing, flocculation, in-flow state changes, thixotropy, chemical balance, temperature effects
Deposition	sedimentation, beaching, dumping, raining	biological and chemical effects, flocculation, binding, hindered settling, gel-formation, transition fluid > gel > solid, segregation and generation of heterogeneity, gas injection, flocculant degradation, weathering, beach-/cap-/internal (in-) stability, strain softening, thixotropy
Consolidation	compaction, dewatering, vertical-drainage	strength increase, stiffness built-up, permeability changes, strain softening, densification, groundwater flow, leaching, creep, weathering, heterogeneity, (cyclic loading)
Restoration	drying, capping, soil-improvement, containment	strength increase, stability, permeability changes, desiccation, cracking, accessibility, groundwater flow, leaching, in-situ mixing, chemical binding, weathering

SDE ROADMAP – MODELING PART

Similar to the identification of “white areas” where knowledge is missing one needs to identify “white areas” where the modeling and application capabilities are missing or lacking.

Managing hydraulically placed fills, including deposition, consolidation and strengthening of the fill material requires the design of:

- Transport process (power requirements, dimensioning);
- Flocculation or other thickening treatment (improvement of sedimentation and future consolidation behavior);
- Pond lay-out (storage and segregation optimization) (avoiding or promoting of heterogeneity);
- Beaching strategy (storage and segregation);
- Land reclamation (designing for future settlement and stability requirements);

- Vertical drainage (speeding up consolidation);
- Compaction techniques (dynamic-, RIC-, vibro-floatation-, etc.);
- Sand-capping strategies.

The application of numerical models (design tools) is only possible with appropriate parameter determination before use and verification measurements after use.

Physical Modeling And Data Acquisition

Physical research and testing tools within the roadmap that we are aiming for comprise various systems, from small scale property tests to larger scale model tests:

- Chemical analysis tools
- Zeta-potential measurements
- Rheology tests
- Suction induced consolidation (SIC-) tests
- Sedimentation basins and columns

- Standard and advanced geotechnical classification and testing tools, like sieve analyses, density and permeability tests, static and cyclic triaxial and direct simple shear tests
- Laboratory centrifuges to perform accelerated sedimentation and consolidation testing
- Various model bins to model sedimentation and sand raining processes (capping) at scales of decimeters to tens of meters.
- A large scale GeoCentrifuge (1x2m @ 300g).
- Pipeline transport and erosion models (o-tubes)

In addition facilities are available for field testing and in-situ monitoring.

Numerical Models

Constitutive or analytical conceptual models are implemented in numerical models, which are powerful tools for quantitative analysis and prediction of effects of different operational and design scenarios. More than one numerical model is associated with the SDE Roadmap: because the actual size, time scales and number of relevant dimensions vary widely for the processes to be modeled, a single numerical tool is not likely to cope with these effectively.

Chemical, Biological, Rheological, Geotechnical, Or Any Combination Thereof...

Some of the relevant questions that come to the mind of the modeler while tackling a SDE task may include: Which processes can and which processes must be combined in the model? Is the analysis of gas-formation and subsequent cavity or channel forming required? Do we need to incorporate chemical or biological effects in our design tool? Do we need dynamics and fluid flow analysis or are simple statics adequate? These processes need different models or, most often, a combination or the integration of different models.

From Micrometer To Kilometer Scale

Chemical and inter-particle effects take place at a very small scale. Sediment heterogeneity exists at scales that vary from centimeters in vertical direction to tens of meters in horizontal direction. Pond and landfill sizes range from tens of meters in vertical direction to kilometers in horizontal direction.

If small scale heterogeneities trigger large scale events the required local refinement of large 3-D meshes is almost impossible. Similar to other

types of engineering, e.g. where cracks in solids are not modeled one by one, but taken into account by a “smeared crack” concept, similar techniques may be in order in the modeling of small scale heterogeneities in tailings pond design.

From Seconds To Decades

Chemical processes, flows and geotechnical instabilities may take place over a short time span, and in particular when an instability in a soft sediment leads to strain softening (thixotropic behavior) the incorporation of inertia effects and strain rate effects is needed (if only for numerical reasons) since these effects may limit the extent of the instability. A dynamic large strain FE formulation like e.g. a Material Point Method (Beuth, 2014) may be in order to model the process. On the other hand, consolidation and creep take very long times and the use of static numerical codes may be more appropriate.

From 1- via 2- and 2.5- to 3-Dimensional

For pipeline transport as well as for sedimentation, consolidation and creep modeling simple 1-D models can suffice for the engineering and design. The simplest geotechnical stability analysis tools are based on 2-D models, where slip-circles or other failure modes can be described.

When the deposition and segregation needs to be modeled the distribution of the sediment laden flow over the area of the pond comes into play and at least a quasi-3-D (2.5-D) method is required, like provided in the public domain Delft3D program (<http://oss.deltares.nl/web/delft3d>). (2.5-D, since the program simplifies the model in the vertical direction.)

For the analysis of general flow problems or the stability of arbitrary geometries (i.e. not axis-symmetric or plane strain) full 3-dimensional analysis tools are required. Numerical models for the fluid phase range from full 3-D computational fluid dynamics programs (e.g. COMFLOW, <http://www.comflow.nl/>) to public domain programs like Delft3D.

Table 2 provides an overview of the programs that are currently part of or associated with our SDE R&D Roadmap and gives an impression of their range of applicability.

Table 2. Numerical models & their applicability

Fluid → Soft Sediment → Competent Soil			
Flow	Deposition	Consolidation	Restoration
2.5 to 3D high tech flow and/or mesh-free (large strain) numerical models			
COMFLOW			
Delft3D			
←----- Delft3D-mud -----→			
←----- MPM -----→			
1-D high tech models			
←----- Delcon -----→			
←----- FS-conbag -----→			
←----- TUD drying model -----→			
1-, 2- and 3-D engineering models			
←----- D-stab -----→			
←----- D-settle -----→			
Licensed commercial software			
←----- PLAXIS -----→			
←----- ABACUS -----→			

Overview of the programs(*) in table 2, proprietary or public domain(**):

COMFLOW:

3D CFD method for fluid flow.

Delft3D (public domain):

2.5 D fluid flow analysis.

Delft-3D mud:

As above, with capability to model thick non-Newtonian mud movement at bed level, and sand settling behavior.

MPM:

Material Point Method, “meshfree” 3-D large strain dynamic FEM model, including liquid and solid phase (grain skeleton) interaction.

Delcon:

1-D large strain model for the analysis of sedimentation, consolidation and strength development with incorporated bio-gas generation and dynamics (ebullition).

FS-conbag:

As Delcon, without the gas effects, but with more flexibility regarding void-ratio vs effective stress and void-ratio vs permeability relations.

D-settle:

Engineering tool for settlement analysis.

D-stab:

Engineering tool for analysis of geotechnical stability.

Programs in Table 2, licensed from 3rd parties (both with options to accommodate user-defined constitutive models):

PLAXIS:

FEM software for geotechnical engineering used for 2-D and 3-D modeling.

ABACUS:

General purpose FEM software, used for 2-D and 3-D modeling.

Note(*): For quite a few of these programs alternatives exist, both commercial and as open source software in the public domain. The authors simply want to give an overview of the tools that they currently consider suitable for further development.

Note(**): It is believed that open source software is a valuable means of spreading knowledge, mobilizing a contributing community and creating auditability of the numerical analysis tools. Where possible this is an integral part of our R&D strategy.

THE WAY AHEAD: ONGOING AND FUTURE R&D WORK

The research area comprises so many different fields of interest that not all aspects can be taken

on simultaneously. With the R&D activities in our roadmap we aim to make progress in some of the areas where the industry appears to have the greatest need and where the greatest knowledge gaps are present.

Tailings dewatering (consolidation) and strength development are key topics across the board of tailings treatment technologies. Dewatering is essential to reduce the volume of legacy and current fluid tailing. Dewatering amount and rate is closely correlated to strength and strength development. Strength is crucial for mine closure planning and as well as for promising and potentially very cost effective technologies such as sand capping.

Parallel to dewatering through consolidation, technologies like Atmospheric Fines Drying have their potential. Drying rates and the tailings strength that develops through capillary suction in the evaporation process are of interest.

Fines Capture is another critical issue in the Oil Sands Industry. Fines are required to be captured within sand grain deposits (beaches). The development of beaches and the consequent distribution of fines and sand are correlated with deposition operation: flow rate and velocity, solids concentration and particle size distribution, the location and re-location schedule of discharges. Optimization of these operational parameters can have a tremendous impact on fines capture within the sand beaches. Predictive numerical tools to optimize such operations are potentially very valuable.

With these key issues in mind, we have developed a SDE Roadmap that focuses R&D on knowledge gaps and critical numerical tools. The following list of ongoing and future research projects aims to illustrate this.

Consolidation And Stability Of Very Soft Soil

- Measuring of the effects of zeta-potential on flocculation, sedimentation and strength development. (Ibanez, 2014): correlates the dewatering and geotechnical properties of soft tailings with small scale particles interaction and settling history;
- Adaptation and implementation (in PLAXIS and DELCON) of creep in a hypo-plastic constitutive model. (Beuth 2014): critical for the improvement of the prediction of consolidation

and strength development of very soft, very slow consolidating soils (e.g. MFT);

- Modeling the stability of very soft – very large strain soils (e.g. MFT) with MPM (Beuth 2014) for technology applications (e.g. Sand Capping): allows prediction of failure and especially the extent of failure;
- Coupling geotechnics and biology to understand the effect of biota (worms) on improving the strength of the top layer via experimental observation and theoretical analysis;

Atmospheric Fines Drying

- Understanding and modeling dewatering of tailings in Atmospheric Fines Drying applications. (van Tol, 2014); for optimization of AFD technology.
- Modeling of unsaturated soil behavior with MPM. Unsaturated flow modeling and effects of capillary suction on soil behavior, three phase modeling of solids, fluids and gas.

Prediction Of Fines Capture Within Beaches

- Modeling of deposition patterns and bed heterogeneity with Delft-3D mud (Sheets, 2014): allows prediction of Fines Capture in beaches above and below water for different discharge conditions. It includes non-Newtonian for Non-Segregating Tailings technology (NST).

CONCLUSION

Apart from giving insight in the developments that are going on in the Netherlands with regard to the behavior of soft sediments the aim of this paper is twofold:

Missing Link

The authors wish to identify Sediment Deposition Engineering as a multidisciplinary work field, which bridges gaps between other engineering and science disciplines. It is in many ways the “Missing Link” between fluid-mechanics and geotechnics, integrating (amongst others) chemical and biological processes in these mechanical disciplines.

R&D Cooperation

The other aim is to provide a starting point for cooperation between research institutes, academia and industry to make further progress in the challenges of fluid to solid transition behavior. Authors will continue to seek actively contact with other researchers as well as the industry to accomplish this.

ACKNOWLEDGEMENTS

Authors are grateful for the interesting discussions they had with experts from UoA and COSIA and acknowledge the opportunity provided by their employers to prepare this paper.

REFERENCES

Beuth, L., Dykstra, C. & Jacobs, W. 2014. Modelling of Hydraulic Sand Capping on Creeping Ultrasoft Tailings. IOSTC 2014.

Ibanez, M., Wijdeveld, A. & Chassagne, C. 2014. Role of Mono- and Divalent Ions on the Stability of Kaolinite Suspensions and Fine Tailings. *J. Clay & Clay Minerals* (under final review)

Jacobs, W., Dykstra, C. & van Kesteren, W. 2012. In Situ Hydraulic Capping of Soft Tailings. Proceedings International Oil Sands Tailings Conference, Edmonton.

Lucas Pardo, M. de 2014. Pers. communication.

Sheets, B. et.al. 2014. Muddy River Deltas as Analogues for Oil Sands Tailings Beaches: Improving Fines Capture and Operational Efficiency with Tailings Beach Modeling. IOSTC 2014.

Sills, G.C. 1995. Time Dependent Processes in Soil Consolidation. Intern. Symposium on Compression and Consolidation of Clayey Soils, IS-Hiroshima'95, pp. 59-72.

Wells, P.S. 2014, Keynote address, 17th International Seminar on Paste and Thickened Tailings, 8-12 June 2014, Vancouver, Canada.

Winterwerp, J.C. & Van Kesteren, W.G.M. 2004. Introduction to the Physics of Cohesive Sediment in the Marine Environment. Series Developments in Sedimentology **56**. Amsterdam: Elsevier.

Zhu, R. et.al. 2011, Role of Dissolving Carbon Dioxide in Densification of Oil Sands Tailings. *Energy & Fuels*, **25**. pp. 2049-2057.

SEMI-ANALYTICAL MODELING OF THICKENED TAILINGS FLOWS

John B. Swenson¹, Ben Sheets², Dale Kolstad² and Walther van Kesteren³

¹Barr Engineering and Dept. Earth & Environmental Sciences, University of Minnesota Duluth

²Barr Engineering, Minneapolis, MN

³Deltares, the Netherlands

ABSTRACT

This paper presents a modelling framework for thickened tailings (TT) flows developed using the common approach of solving the balance between density driving and yield strength resisting forces. Several model versions are presented that simulate TT flow under a range of field situations, from laterally constrained to fully unconstrained two-dimensional radial flows under subaerial and subaqueous regimes. The models have been adapted to cases where bed slope varies between pours, as well as along the flow path during a single pour, and thus are useful for investigating the effects of multiple lifts or deeper stacks. Further, the models are designed to predict flow depth and mudline elevation during a pour by using a novel semi-analytical technique for finding the toe position at particular times as a function of volumetric flow rate. This technique is validated against repeat LiDAR topographic scans taken during a field TT deposition event. Though this modeling approach does not explicitly compute flow dynamics such as velocity profiles or particle size distribution, the results provide valuable insight into first-order mudline evolution, and are useful for investigating how surface slope and flow depth change when flows encounter basin walls, thus providing a long-term basin planning tool.

INTRODUCTION

Predictive modeling of polymer-amended 'thickened tailings' (TT) flow is a nascent field, and while the path forward ultimately may involve/require complex hydrodynamic models adapted to non-Newtonian flows, our objective here is to explore the utility of a relatively simple modeling approach. There are several reasons that a simplified modeling approach is advantageous for Oil Sands applications. Foremost among these is the fact that the complete dynamics of plastic flow (like tailings slurries) is not well-understood (c.f., Ancey, 2007),

and thus a comprehensive modeling approach is not yet available.

A second reason for exploring the utility of a properly framed simple model is that such an approach can provide valuable insight into first order behavior of tailings slurries and thus baseline predictions of their flow and deposition geometry. That is, despite omission of certain processes that might occur in some tailings deposition scenarios, a properly formulated simple model can bound the physically reasonable possibilities. Thus, physically reasonable ranges for important flow and deposit properties (such as slope, depth, or velocity) can be predicted, and long-term tailings basin planning improved.

Additionally, a simple modeling approach is ideally suited for predictions in environments where relatively few field-scale data are available for model calibration and validation. This is the situation for most Oil Sands operators. As model complexity increases, the required number of calibration parameters typically expands, and validation against detailed field measurements becomes increasingly important in order to assess the quality of the model predictions.

The simplified modeling approach presented in this paper, which is guided in part by field observations of TT behavior, is based on the simplified dynamics of 'thin' flows, in which, to a good approximation, the downslope driving force of gravity balances the shear stress of the flow on the underlying bed (e.g., Liu & Mei, 1990). We add to this the key simplifying assumption that the TT slurry operates in a 'critical' state, whereby it adjusts its depth and slope such that the bed shear stress is everywhere equivalent to the slurry yield stress. The basis of the relatively simple approach discussed here is not new. Rather, its applicability has been demonstrated by numerous authors, including Nye (1952), Liu and Mei (1990), Coussot & Proust (1996), and Soleimani *et al.* (2013). Ancey (2007) provides an insightful review of this approach in the context of other techniques for modeling plastic flows.

The overarching goal with this simplified modeling approach is to predict the interaction of thin TT flows with their underlying (basement) surface and overlying ambient fluid. This requires that we address explicitly the transient behavior of the flow, i.e. the lateral expansion and vertical accumulation of the TT slurry. An important element of the transient model is our treatment of the terminus of the laterally expanding flow; the position of this slurry ‘toe’ is unknown *a priori*, thereby making this—from a mathematical perspective—what is known as an implicit moving-boundary problem. The model we develop here is best suited to thin, transient TT flows; by definition, it cannot resolve the complex velocity structure of thick flows, nor can it address such potentially important behavior as channelization, water release, or thixotropy. Nonetheless, as we demonstrate below, the model provides insight into the transient behavior of thin TT flows interacting with their surroundings, and thereby allows predictions of TT behavior over a range of scales, from laboratory to field-pilot to commercial.

THEORY

We constructed a cross-sectional (one dimensional), semi-analytical model of TT slurry behavior applicable to ‘thin’ flows, i.e. slurries in which the vertical flow component is insignificant relative to lateral flow. Such flows are well described by a classical ‘lubrication theory,’ in which the streamwise momentum equation reduces to a balance between the depth-slope product and the boundary shear stress (τ_b), e.g. Liu and Mei (1990). We assume that the flowing TT slurry adjusts its depth-slope product to maintain the basal shear stress at the slurry yield stress (τ_y). Under these conditions, the slurry free-surface elevation, h , obeys the following governing equation:

$$\Delta\rho gh \left(S - \frac{dh}{dx} \right) = \tau_y \quad (1)$$

where g is gravitational acceleration, S is the local slope of the ‘basement’ material over which the slurry flows, dh/dx is free-surface slope, and x is the distance ‘downstream’ from the feed point along the basement surface. Implicit in Equation (1) are a local, topography-following coordinate system and small basement and free-surface slopes, i.e. $S \ll 1$ and $dh/dx \ll 1$. The reduced density, $\Delta\rho$, driving slurry flow is the difference

between the slurry density, ρ , and the density of the overlying ‘ambient’ fluid, ρ_a . Borrowing from the geologic nomenclature, a ‘subaerial’ flow corresponds to a scenario in which the overlying fluid is the atmosphere ($\rho_a \sim 0$), and a ‘subaqueous’ flow has an overlying ambient fluid, e.g. water or MFT, with density of comparable magnitude to that of the slurry.

Our model is fully transient: The flow expands continuously in response to upstream input of material and, by extension, the free-surface elevation varies in space and time, i.e. $h = h(x,t)$. A transient model provides the ability to predict rates and patterns of basin infilling in response to system geometry and the arrangement of slurry feed points. Note that Equation (1) does not contain time explicitly; rather, time enters the model through 1) the downstream slurry boundary condition and 2) an additional, ‘global’ equation for mass conservation. The downstream boundary condition enforced on the slurry is a function of the basin geometry and the instantaneous position of the downstream boundary itself. The current model configuration addresses two scenarios: In the first, the slurry is flowing across the basement surface in an unconfined manner and the slurry thickness decreases downstream. The position where the flow thickness vanishes defines the downstream ‘toe’ ($x = s$) of the slurry; thus, at the toe, $h(s) = 0$. This position is unknown *a priori*, which makes this system a moving-boundary problem. A solution to Eq. 1 requires an additional condition—a closure condition—to locate the toe.

In the second scenario, downstream expansion of the slurry has been halted by the presence of an impermeable boundary, i.e. a vertical wall. Continued input of material from the upstream feed point drives thickening—but not downstream expansion—of the slurry deposit. In this scenario, at any instant in time, the lateral extent of the slurry is known but the downstream thickness of the slurry is unknown *a priori*; as in the first scenario, a solution to Eq. 1 requires an additional closure condition.

The closure condition in both scenarios is a statement of global slurry volume conservation:

$$q_{so} = \frac{d}{dt} \int_0^{s(t)} h(x,t) dx \quad (2)$$

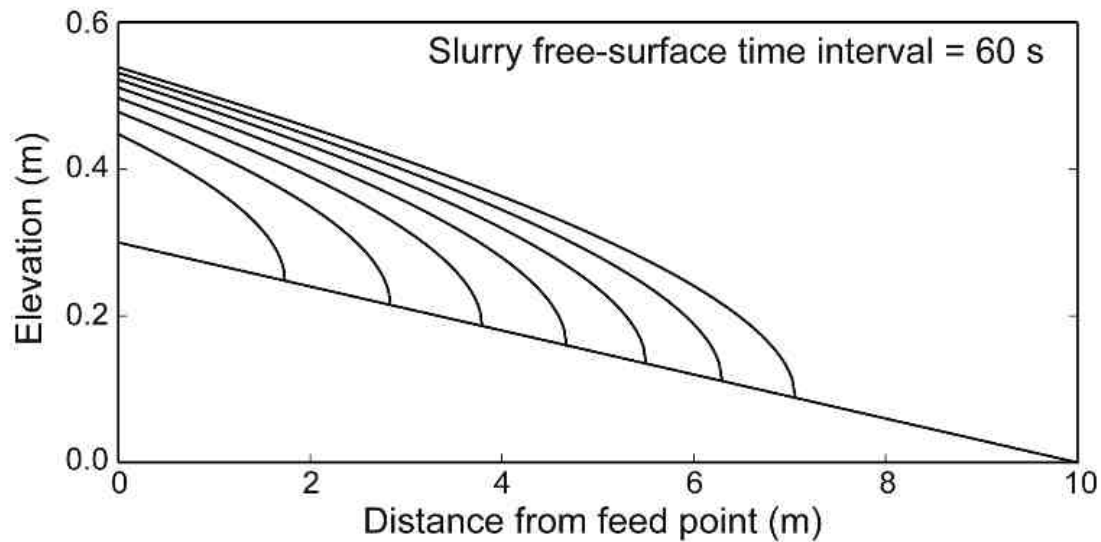


Figure 1. Model prediction for TT slurry flow over a uniform sloping basement surface with steady feed rate. Temporal spacing of slurry free surfaces (mudlines) is 60 s. Refer to text for flow parameters. Note approach to equilibrium flow conditions in the upstream section.

where q_{so} is the slurry feed rate per unit basin width (m^2/s). Physically, Equation 2 relates the feed rate to the rate of change in the volume of the slurry. A solution to Eq. 1 proceeds as follows: Assuming a known slurry profile from the previous time, the model makes an informed estimate for either the toe position (scenario 1) or the downstream slurry thickness (scenario 2) a time increment Δt later; the model integrates Equation 1 for arbitrary underlying basement geometry; based on the solution to Equation 1, the model computes the change in total slurry volume across the time increment (Δt) and compares that change to the *known* change in slurry volume ($q_{so}\Delta t$); the difference between these volume increments is the residual; the model uses the magnitude and sign of the residual to generate a new estimate for toe position or slurry thickness. Iteration proceeds until the residual is less than some tolerance. Depending on the geometric complexity of the basin and the basement surface, integration of Equations. 1 and 2 is in part analytical in nature.

RESULTS

General behavior

Consider first model predictions for slurry behavior in the simplest scenario of a uniform basement slope and constant tailings feed rate. (The

mathematical solution for this system is given below in Equation 6.). Figure 1 shows the predicted slurry free surface at equally spaced time intervals (60 s) for a system characterized by $S = 0.03$, $q_{so} = 0.003 m^2/s$, $\rho = 1150 kg/m^3$, and $\tau_y = 60 Pa$. Under these conditions, the fundamental prediction of Eq. 1 is a slurry profile that decreases in thickness with distance downstream of the feedpoint and possesses negative curvature, i.e. the mudline profile is 'convex up.' The convexity is a direct consequence of the depth-slope product in Equation 1: As the flow thins downstream, the free-surface slope increases accordingly so as to maintain a uniform basal shear stress. With sustained input of tailings, the slurry expands downstream and thickens. At any location in the basin, after passage of the slurry toe, the rate at which the slurry thickens decreases monotonically with time and the flow thickness evolves to a steady state. This approach to steady state is evident in the upper section of the model basin in Figure 1, where the separation between progressively 'later' timelines becomes indiscernible.

Dimensional analysis of Equation 1 shows that the slurry flow will approach a 'uniform' state, analogous to that of standard open-channel hydraulics, in which the slope of the slurry free surface matches the slope of the underlying basement ($dh/dx = 0$) and the flow depth approaches the 'normal' depth (h_o) given by:

$$h_o = \frac{\tau_y}{\Delta\rho g S} \quad (3)$$

The slurry flow can evolve to this uniform state at any location where the basement slope does not vary significantly for a length scale L_o , where

$$L_o = \frac{h_o}{S} \quad (4)$$

Note that L_o is the standard ‘backwater length’ from open-channel hydraulics. At a given location in the basin, the flow will approach steady state on a timescale (T_o) given by:

$$T_o = \frac{h_o^2}{q_s S} = \left(\frac{\tau_y}{\Delta\rho g} \right)^2 \frac{1}{q_s S^2} \quad (5)$$

From the scaling in Equations. 3-5, we see that a relatively ‘strong’ (large τ_y) slurry flowing on a shallow basement slope will be relatively thick and require a relatively long distance and/or time to reach equilibrium. Note that the scaling—particularly the timescale—is sensitive to basement slope and that h_o , L_o , and T_o are undefined for a flat-bottomed basin.

With a uniform basement slope and constant feed rate, Eq. 1 has an analytical solution:

$$\frac{h}{h_o} + \ln\left(1 - \frac{h}{h_o}\right) = \frac{1}{L_o}(x - s) \quad (6)$$

where h_o and L_o are the flow depth and backwater length defined above, respectively. We determine the slurry toe position, $s(t)$, by integrating Equation 3; due to the transcendental nature of Equation 6, we perform this integration numerically, making the full solution to this system semi-analytical in nature. Building on the lubrication theory of Liu and Mei (1990), Soleimani et al. (2013) used a steady-state version of Equation 6 to model thickened tailings as Bingham fluid. The key difference with the model we present here is our treatment of transient slurry behavior as a moving-boundary problem.

Flat-bottomed basin

If the basin floor is flat-lying, i.e. if $S = 0$, Eqs. 6 and 3 simplify to:

$$h = \sqrt{\frac{2\tau_y}{\Delta\rho g}(s - x)} \quad (7a)$$

$$s = \left[\frac{3}{2} q_{so} t \sqrt{\frac{\Delta\rho g}{2\tau_y}} \right]^{2/3} \quad (7b)$$

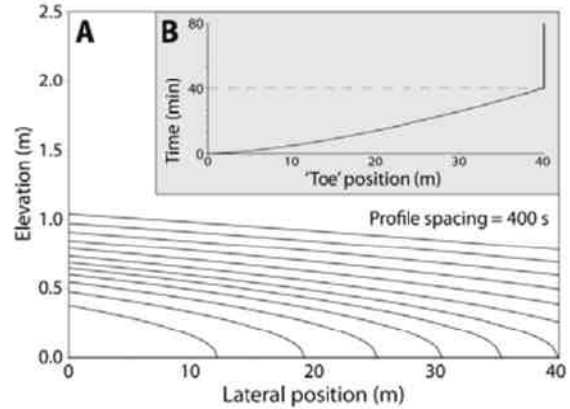


Figure 2. Model predictions for basin infilling with downstream-boundary interaction. (A) Model mudlines (uniform spacing of 400 s) for 80 minutes of slurry runout. (B) Corresponding trajectory of slurry toe; note interaction with downstream boundary after approximately 40 minutes.

In this limit ($S = 0$), the above concept of flow equilibrium disappears, and the slurry free surface will evolve in a self-similar fashion, maintaining a parabolic profile as it expands basinward at an ever-decreasing rate ($ds/dt \sim t^{-1/3}$). Physically, in the absence of a basement slope, the slurry must always thicken in proportion to its lateral expansion in order to maintain the surface slope necessary to drive flow across the flat surface in the assumed critical state ($\tau_b = \tau_y$).

Boundary effects

The above model results apply to ‘unconstrained’ slurry flow across the basin floor. In a finite basin, the slurry eventually interacts with downstream and lateral boundaries, which typically have the form of sub-vertical walls. This interaction changes the nature of slurry growth from dominantly lateral expansion (progradation) to vertical accumulation (aggradation); in this ‘constrained’ or ‘bounded’ scenario, the footprint of the slurry no longer

changes with time. To investigate the effects of basin boundaries on the evolution of the slurry free surface, we modified the above cross-sectional model to allow for interaction of the slurry with a downstream vertical wall at $x = L$. Mathematically, once the slurry toe interacts with the downstream wall, the moving-boundary nature of the problem changes somewhat: The position of the toe is known, i.e. $s = L$, but the thickness of the slurry at $x = L$ is unknown *a priori*; we must use the aforementioned iterative scheme (involving Equation 3) to determine $h(x=L)$ at any time.

Figure 2 shows model predictions for TT ($\rho = 1275 \text{ kg/m}^3$; $\tau_y = 75 \text{ Pa}$) flowing across a flat-bottomed basin and encountering a downstream wall at $x = 40 \text{ m}$. (The results we present below show a flat-bottomed basin, i.e. $S = 0$, but the methodology is easily generalized to systems with sloping basement surfaces.) Prior to interaction with the downstream boundary, the slurry free surface

evolves in a self-similar fashion given by Equation 7, i.e. the flow thickens in proportion to its lateral expansion. Interaction with the downstream boundary (wall) after 40 minutes of basin infilling arrests lengthening of the flow (Figure 2, panel B) and forces the system into a mode of vertical growth (aggradation). As the slurry aggrades, the slope of the free surface shallows through time, particularly in the downstream (distal) portion of the system; consequently, with time, the flow loses its characteristic 'bullnose' (convex up) geometry. The reason for the reduction in surface slope is tied to the basic model assumption of Equation 1: During aggradation, the flow thickens continuously without elongating; as a result, its surface slope must decrease in order to keep the slurry in the critical state whereby the boundary shear stress balances the yield strength.

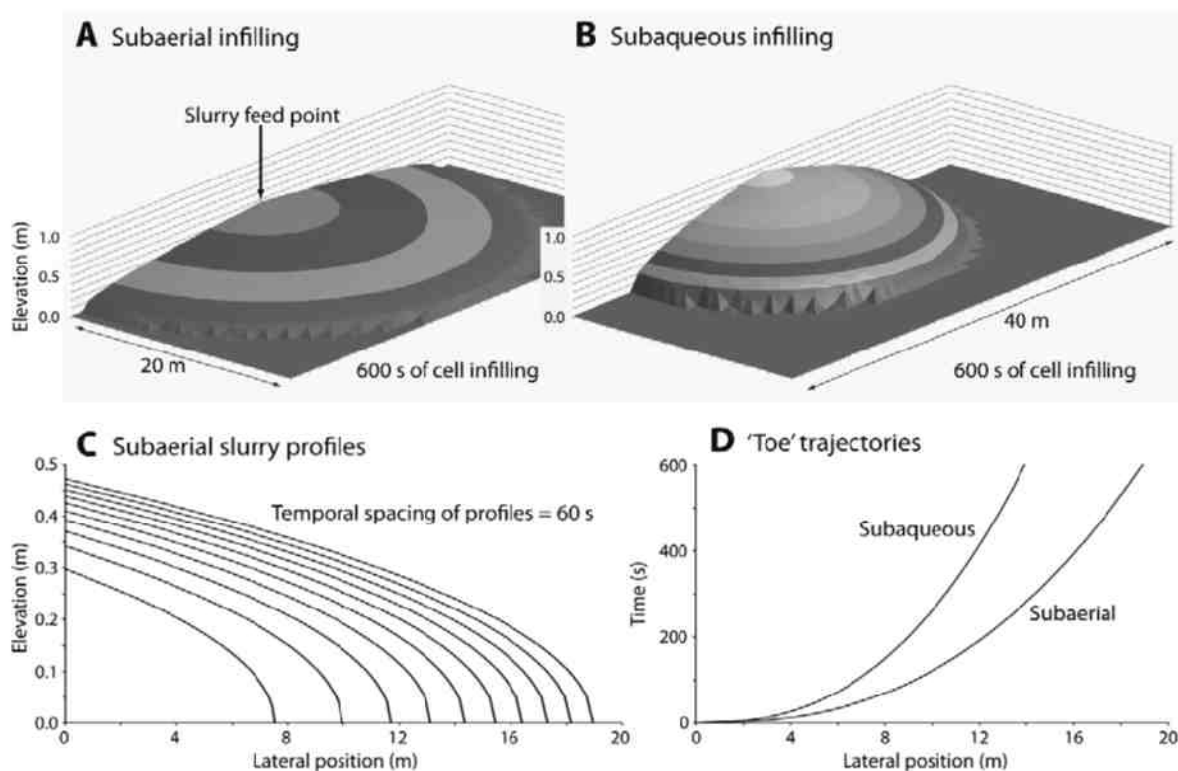


Figure 3. Slurry geometries after 600 s of basin infilling under (A) subaerial and (B) subaqueous conditions. The cone-shaped volumes in (A) and (B) are equivalent. (C) Slurry profiles at 60 s intervals for the subaerial infilling scenario. Note the self-similar profile geometry. (D) Slurry-toe trajectories for subaerial and subaqueous infilling scenarios.

Subaqueous behavior

In some field settings, TT might be emplaced in a subaqueous basin, in which the overlying fluid (e.g., water and/or MFT) has a density comparable to that of the slurry. Under such conditions, the gravitational driving force for flow is reduced significantly. By the scaling in Equations. 3 – 5, a subaqueous slurry flowing over a sloping basement ($S > 0$) will be thicker and require a greater length and/or time to equilibrate than its subaerial equivalent. The same basic reasoning holds true for TT flow across a flat-bottomed basin. The effects of subaqueous flow conditions are illustrated in Figure 5 (see the Discussion section below).

Three-dimensional flow

The cross-sectional model developed above, which provides basic insight into TT behavior, cannot capture the three-dimensional aspects of flow expansion associated with delivery of TT from a single feed point. We generalized the above theory to address slurry flow across a flat-bottomed basin in response to a constant

discharge of TT. In this highly idealized scenario, slurry behavior shows radial symmetry. The three-dimensional equivalent of Equation 7 is:

$$h = \sqrt{\frac{2\tau_y}{\Delta\rho g} (s - r)} \quad (8a)$$

$$s = \left[\frac{15 Q_{so} t}{4 \theta} \sqrt{\frac{\Delta\rho g}{2\tau_y}} \right]^{2/5} \quad (8b)$$

where r is radial distance from the feed point, Q_{so} is volumetric feed rate, and θ ($0 < \theta < \pi$) is an arbitrary opening angle for flow expansion. (Note that a sloping basin floor, i.e. $S > 0$, destroys the radial symmetry in the system; relative to the slurry morphology of Figures 3A and 3B, a system with $S > 0$ will show enhanced ‘downslope’ flow at the expense of lateral widening. A solution to this problem is relatively straightforward but requires a full numerical approach.)

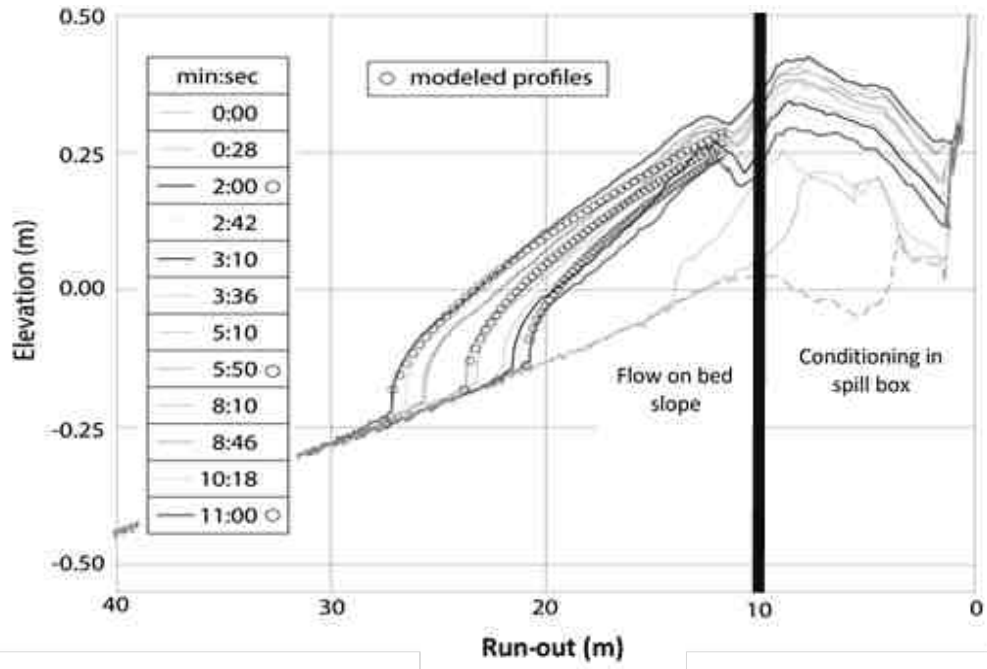


Figure 4. Comparison of model predictions to experimental observations for slurry surface in a field depositional event. For clarity, only three modeled profiles are superimposed on the observed slurry profiles.

Figure 3 shows model predictions for slurry evolution with $\theta = \pi$ for both subaerial and subaqueous (i.e., beneath a water cap) conditions. Similar to the cross-sectional model presented above, at any time during basin filling, the free surface displays a convex-up ‘bullnose’ geometry that is characteristic of the assumed ‘critical state’ of flow, i.e. the surface slope must increase with distance from the feed point to offset the reduced flow thickness and thus maintain a uniform boundary shear stress ($\tau_b = \tau_y$). In cross-section, the self-similar free-surface profile (Fig. 3c) has the identical parabolic form (Eq. 8a) as its cross-sectional equivalent (Eq. 7a). However, relative to the cross-sectional model, the rate of slurry toe advance is less in the three-dimensional case: $s(t) \sim t^{2/3}$ in the cross-sectional model (Eq. 7b), whereas $s(t) \sim t^{2/5}$ in Eq. 8b. This decreased rate of slurry expansion in the three-dimensional model results from flow expansion: In plan view, the area of the slurry, i.e. its footprint, increases quadratically with the length (radius) of the flow.

The effects of a water cap in three dimensions are similar to those observed in the cross-sectional model. The reduced gravity driving the slurry under subaqueous conditions produces a thicker and steeper flow (compare Fig. 3a and 3b) and, by mass conservation, a reduced rate of slurry advance across the basin floor (compare subaerial and subaqueous trajectories in Fig. 3d).

MODEL VALIDATION

To validate our modeling approach, we used repeat LiDAR topographic scans taken during a field-scale TT deposition event. The depositional event involved the emplacement of thin TT flow (a ‘lift’) from a single spill box on the edge of a 40 m x 40 m cell with a uniformly sloping basement ($S \sim 1.7\%$). The TT feed rate was approximately constant; the effective opening angle for the flow was approximately 45° (i.e., $\theta \sim \pi/4$). The finite width of the spill box and the relatively narrow opening angle of the flow present challenges in applying the above theory. Nonetheless, we modeled (‘hindcast’) the depositional event using the cross-sectional model of Equation 1 with a uniform yield stress, steady feed rate, and a characteristic basin width representative of the flow at the cell midpoint. Figure 4 shows a comparison between model predictions and observed slurry surface profiles. The only ‘tuned’ model parameter was the slurry feed rate, q_{so} , which we adjusted to

account for the aforementioned geometric complexities. We obtained a best fit between modeled and observed slurry profiles for an approximately 20% reduction in model q_{so} relative to the reported feed rate. This reduced feed rate likely captures the effects of 1) slurry trapping in the spill box (note the significant volume of material deposited in the spill box) and 2) modest flow expansion. Overall, the model captures successfully the first-order behavior of the slurry behavior. The theory appears to capture the curvature of the profile near the slurry toe but tends to under-predict slightly the flow thickness in the proximal portion of the cell, i.e. near the spill box, which is a region of rapid flow spreading.

DISCUSSION

Our goal was to develop a simple theory that captures explicitly the transient interaction of thin TT flows with underlying basement geometry and overlying fluids. Despite its simplicity and inherent limitations, limited observational data from a field depositional study suggest that the model captures the basic features of TT behavior.

While our modeling approach is not designed to capture certain phenomena, including the effects of water release, shear thinning or thickening, its fundamental shortcoming—a shortcoming it shares with all current TT models—is an inability to treat channelization. In contrast to fluvial (river) systems, which involve the interaction of a Newtonian fluid with a mobile (sediment) bed, relatively little is known about channelization in non-Newtonian slurry flows. We lack basic knowledge of the 1) flow instabilities that trigger channelization, 2) the intrinsic depth and length scales of channels, and 3) the timescales for channel migration and switching. Clearly, channelization is an important area of ongoing research.

Despite its inherent limitations, our modeling approach is informative in that it allows for rapid determination of flow characteristics (thickness, slope, toe positions, arrival times) as functions of material properties (density, yield stress), boundary conditions (pour rate, overriding fluid), and basin geometry (basement slope, locations of feed points); as such, it is a useful tool for guiding basin design and developing deposition strategies. To that end, consider Figure 5, which shows model predictions for TT behavior in a hypothetical,

scaled-up, in-pit scenario. This hypothetical basin contains multiple basement slopes and multiple overlying fluids designed to illustrate the

capabilities of the model. The basin geometry has an overall length of 1000 m and pit depth of 20 m.

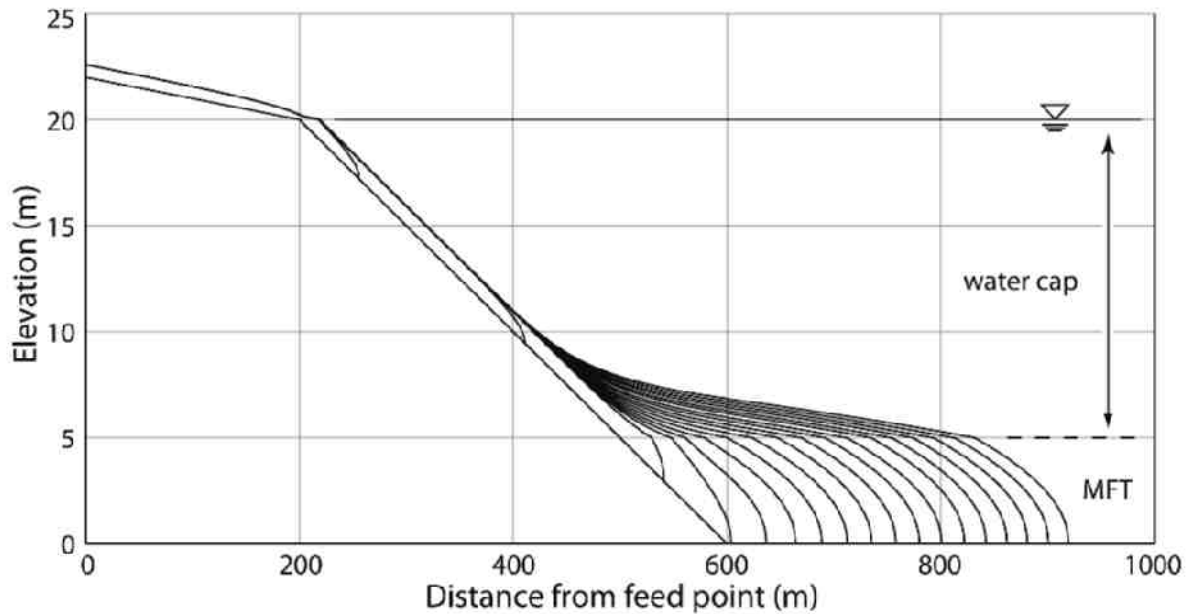


Figure 5. Model predictions for 9 hours of sustained TT flow in a hypothetical in-pit scenario with basal MFT and water cap. Uniform timeline spacing is 0.5 hours.

A steady discharge ($q_{so} = 1 \text{ m}^2/\text{s}$) of TT enters the basin from a point source (left edge of system) and flows across a gently-dipping ($S = 0.01$) 200 m stretch, a steeply-sloping ($S = 0.05$) 400 m section, and, finally, 400 m of flat basin floor. The distal boundary of the pit is a vertical wall. The model TT has a density of 1150 kg/m^3 and yield stress of 70 Pa. The lowermost 5 m of the pit is filled with MFT (nominal density of 1050 kg/m^3), which is capped by 15 m of clear water. The elevation of the water-cap free surface corresponds to the elevation of the slope break separating the first two basin sections; the slurry flow is thus subaerial for approximately the first 200 m and subaqueous thereafter.

Figure 5 shows model predictions for 9 hours of sustained TT flow; slurry profiles ('mudlines') are shown at uniformly-spaced 0.5 hour intervals. In the broadest sense, Figure 5 illustrates the rich interaction between the flow and basement slopes and overlying fluids. The slurry traverses the sloping portions of the basin relatively quickly, before slowing considerably and spending a

majority of the 9-hour model duration filling the flat-floored section of the pit. The flow reaches equilibrium, in the sense of Equation 3, in two locations—in the subaerial reach, several backwater lengths upstream of the shoreline, and again in the sloping subaqueous reach, several backwater lengths upstream of the density discontinuity between water and MFT. The combined effects of basement slope and ambient fluid are apparent in the flow thickening immediately outboard of the shoreline, where, by Eq. 3, the five-fold slope increase is more than offset by the nearly eight-fold decrease in effective density. Moving basinward, the flow thickens again at the interface between water cap and MFT, where ambient-fluid density jumps. Finally, the flow thickens considerably upon encountering the flat ($S = 0$) floor of the pit at $x = 600 \text{ m}$. As the flow expands across the flat pit floor, it thickens continually in order to maintain a free-surface slope sufficient to overcome friction (τ_b) and thus advance the slurry toe.

SUMMARY

Relatively simple modeling approaches can provide both valuable insight and important predictions of tailings slurry flow behavior at commercial Oil Sands scales. The simplified model provides physically reasonable bounds on mudline slopes associated with arbitrary basin geometry and boundary conditions for non-channelized TT flow. Such insight is critically important for assessing the viability of proposed tailings deposition strategies, as well as for long-term basin management planning.

ACKNOWLEDGEMENTS

The authors would like to acknowledge and thank Shell Canada for both funding support and for permission to use field data originating from the Atmospheric Fines Drying (AFD) test cell program.

REFERENCES

- Ancey, C. 2007. Plasticity and geophysical flows: a review. *Journal of Non-Newtonian Fluid Mechanics*, **142**: 4-35.
- Coussot, P. and Proust, S. 1996. Slow, unconfined spreading of a mudflow. *Journal of Geophysical Research: Solid Earth*, **101**: 25217-25229.
- Liu, K. F. and Mei, C. C. 1990. Approximate equations for the slow spreading of a thin sheet of Bingham plastic fluid. *Physics of Fluids A: Fluid Dynamics*, **2**: 30-36.
- Nye, J. F. 1952. A Method of Calculating the Thicknesses of the Ice-Sheets. *Nature*, **169**: 529 – 530.
- Soleimani, S., Simms, P.I., and Wilson, W. 2013. Optimizing deposition of polymer-amended mature fine tailings. *Proceedings of GeoMontreal*, 2013.

Session 12

Chemical Applications

OIL SAND TAILINGS POND RECLAMATION BY MFT POLYMERIZATION CAPPING AND CHARACTERIZATION OF THE MFT POLYMER

Jibin Zhao and Guoxing Gu

Oil Sands Environmental Development & Services Inc., Edmonton, AB

ABSTRACT

Polymerization capping is a newly developed technology to facilitate oil sand tailings reclamation process. It uses approximately 90% mature fine tailings (MFT) and 10% chemicals to form a layer of MFT polymer on top of a soft tailings deposit. The resultant MFT polymer layer combines chemically with the tailings deposit and its surface is able to support heavy reclamation equipment for forestation and vegetation after completion of the polymerization process. The tailings deposit (mud) can be any soft tailings with solids content $\geq 30\%$, preferably $> 40\%$ by weight, such as composite tailings, thickened tailings and centrifuged tailings. It is estimated that a 5-15 cm MFT polymer capping layer should be able to support heavy reclamation equipment, meeting the ERCB directive 074 requirement for oil sands tailings disposal.

The polymerization capping can be implemented in all seasons by mixing MFT and the chemicals in a vessel, and then spreading the resultant mixture on top of a soft tailings deposit area by area. The areas are arbitrary places without the need to pre-build any cell boundaries. Following benefits can be realized,

1. faster reclamation of oil sands tailings ponds than ERCB Directive 074 required,
2. significant overall reclamation cost reduction,
3. extensive suitability for CT deposit, thickened fine tailing deposit, centrifuged fine tailings deposit, and
4. minor current process modification.

Conceptual processes for polymerization capping and reclamation of oil sands tailings ponds are provided, various characterizations of the MFT, mixture of the MFT and the chemicals as well as resultant MFT polymer were conducted, such as rheological test for shear stress and viscosity, geological test for consolidation and hydraulic conductivity, and structural test for yield strength, Young's modulus and Poisson's ratio.

INTRODUCTION

In Northern Alberta's oil sands mining operations, it takes about two tonnes of oil sands and 2-5 barrels of river water to produce a barrel of synthetic crude oil (SCO) and 1.5-2.0 barrels of mature fine tailings (MFT) typically containing 30% solids and 70% water by weight, a by-product of mining operations. Currently, there are more than 800 million m^3 tailings holding in more than 180 km^2 of tailings ponds in the Alberta oil sands region. The tailings inventory is increasing at a rate of 50 million m^3 per year. Based on a centrifuge simulation study, the tailings in tailings ponds need more than 130 years to settle by themselves, holding a significant amount of water and occupying a huge area of disturbed land. The legislations of Alberta require reclamation of both the land disturbed by oil sand mining activities and the land occupied by tailings ponds to self-sustaining ecosystems. According to Directive 074, oil sands mining companies are required to reduce 50% of their fine tailings by the year of 2013 and turn their processed tailings into tailings deposits with trafficable surfaces within 5 years of their disposals.

Some attempts have been made to improve oil sands tailings consolidation, such as composite tailings process that combines fine and coarse tailings at a coarse to fine ratio of approximately 4.25 with the addition of gypsum as a coagulant, thickening process that uses polymer flocculants in a thickener to turn fluid tailings into soft mud, centrifugation process that also uses flocculants in centrifuges to enhance dewatering. All of the three processes produce soft tailings deposits that can not meet the criteria of Directive 074.

Recently, Suncor Energy in conjunction with Shell Canada developed an atmospheric drying process and is implementing Tailings Reduction Operation (TRO). In this process, MFT is mixed with a polymer flocculant, and then deposited in thin layers over sand beaches with shallow slopes. The water in the tailings drains back to the tailings pond and the resulting product becomes a dry material over approximately one month time period. Then the dried or semi-dried material can be relocated to

a new place making room for depositing new tailings. This atmospheric drying process is expected to improve tailings management going forward, and can also be used to reduce existing tailings inventory at Suncor's operations. However, it is seasonal dependent, its performance compromises in summer raining seasons and the operation has to cease in whole winters. Canadian Natural Resources Limited is implementing CO₂ injection process to mitigate its oil sands fine tailings to achieve a fast solids settling and water recycling. The solids settling performance at 6 months after CO₂ injection is equivalent to the performance at 24 months with no CO₂ injection into the fine tailings stream. However, it has been found that the remaining fluid tailings becomes more difficulty in flocculation dewatering process, our understanding is that CO₂ injection turns the remaining fine tailings into a gel, reducing mobility of the pore water. It is highly desirable to develop a tailings processing technology that can be used in all seasons and make tailings deposit trafficable as required by Directive 074.

This paper is to provide an in-situ polymerization method for capping soft oil sands tailings and making the capping surface trafficable and ready for further reclamation. It will also provide a method for capping the soft tailings using MFT as a major material, hence reducing fluid tailings storage in tailings ponds, eventually eliminating tailings storage ponds.

PRINCIPLE OF POLYMERIZATION CAPPING

The polymerization capping is a newly developed technology to facilitate tailings consolidation and reclamation process. It uses approximately 90% MFT and 10% chemicals to form a layer of polymer on top of a soft tailings deposit as shown in Figure 1.

The resultant MFT polymer layer combines chemically with the tailings deposit and its surface is able to support heavy reclamation equipment for forestation and vegetation after completion of the polymerization process. The tailings deposit (mud) can be any soft tailings with solids content $\geq 30\%$, preferably $> 40\%$ by weight, such as composite tailings, thickened tailings and centrifuged tailings. It is estimated that a 5-15 cm polymer capping layer should be able to support heavy reclamation equipment, meeting the ERCB directive 074 requirement for oil sands tailings disposal.

The polymerization capping can be implemented in all seasons by mixing MFT and the chemicals, and then spreading the resultant mixture on top of a soft tailings deposit area by area as illustrated in Figure 2. The third area can be covered once the first and second areas are completed. The areas are arbitrary places without the need to pre-build any cell boundaries.

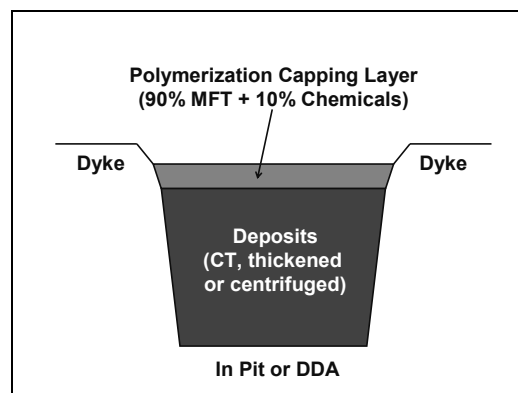


Figure 1. Principle of polymerization capping.

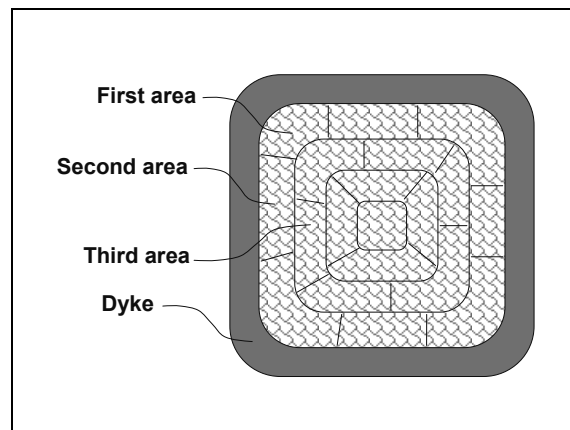


Figure 2. Implement of polymerization capping.

STEPS TO RECLAIM OIL SANDS TAILINGS PONDS

For a tailings pond holding mature fine tailings (MFT), there are three steps to reclaim a pond to a trafficable surface as illustrated in Figure 3.

Step 1: Fluid tailings flocculation and disposal – MFT or fluid fine tailings (FFT) is dredged and mixed with a flocculant solution in a pipeline, and solids in the MFT are flocculated and then

discharged into a disposal pond (or pit), where water is released and withdrawn for preparing the flocculant solution and recycling back to extraction.

Step 2: Released water removal – When the disposal pond is close to full, the MFT flocculation is stopped, and remaining release water in the disposal pond should be removed completely prior to subsequent polymerization capping.

Step 3: Polymerization capping – MFT or fluid fine tailings (FFT) is dredged and mixed with chemicals (monomers, additives and initiators) in a mixing tank, the resultant fluidable mixture is discharged onto the surface of the previously flocculated MFT, on which the resultant mixture spreads to form a layer of polymer after completion of the polymerization reaction. The step 3 uses not only the same tailings pipeline but also the tailings pump.

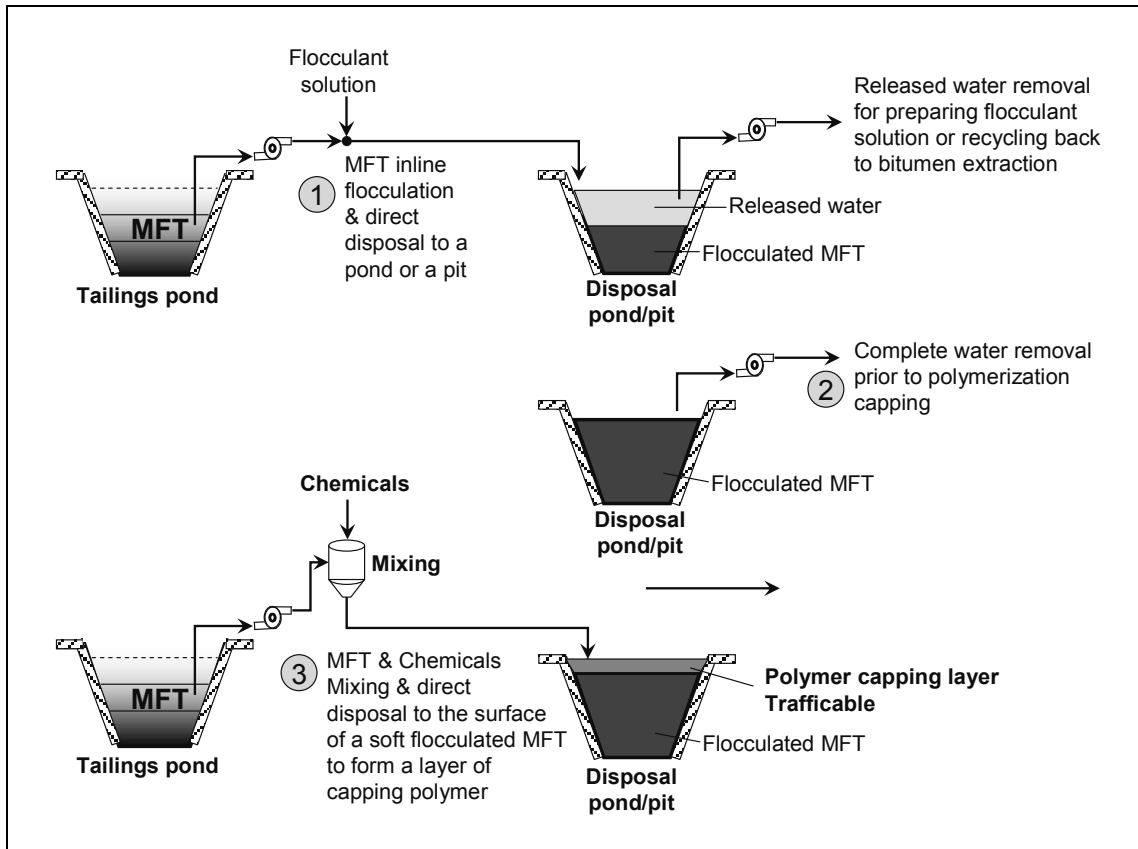


Figure 3. Steps for implementing polymerization capping.

The total dosage of all chemicals is approximately 10% of the polymer layer by weight. The polymerization reaction can be well controlled by adjusting chemical composition to achieve a desired gelation time, e.g. 10-30 minutes. The gelation time is defined as the time period from the time when the initiator is added to the system to the time when the gelation starts due to polymerization reaction. The longer the gelation time, the longer the resultant mixture can flow and spread to cover a larger area.

Assuming that a recipe having 10 minutes gelation time is used to make a 10-cm capping layer on a

flat soft deposit, based on volume conservation, the calculated coverage of the capping layer using different pipe sizes and flow velocities is shown in Figure 4. It can be readily found that a 6-inch pipe is required to cap a swimming pool size area with 10 cm thickness within 10 minutes; while an 18-inch pipe is required to cap a soccer field size area with 10 cm thickness within 10 minutes. This is just a rough estimation, in reality, many factors must be taken into consideration to predict the coverage, such as, surface roughness and slope, fluid viscosity, yield stress, heat transfer, ect. A numerical simulation is required to achieve such an objective.

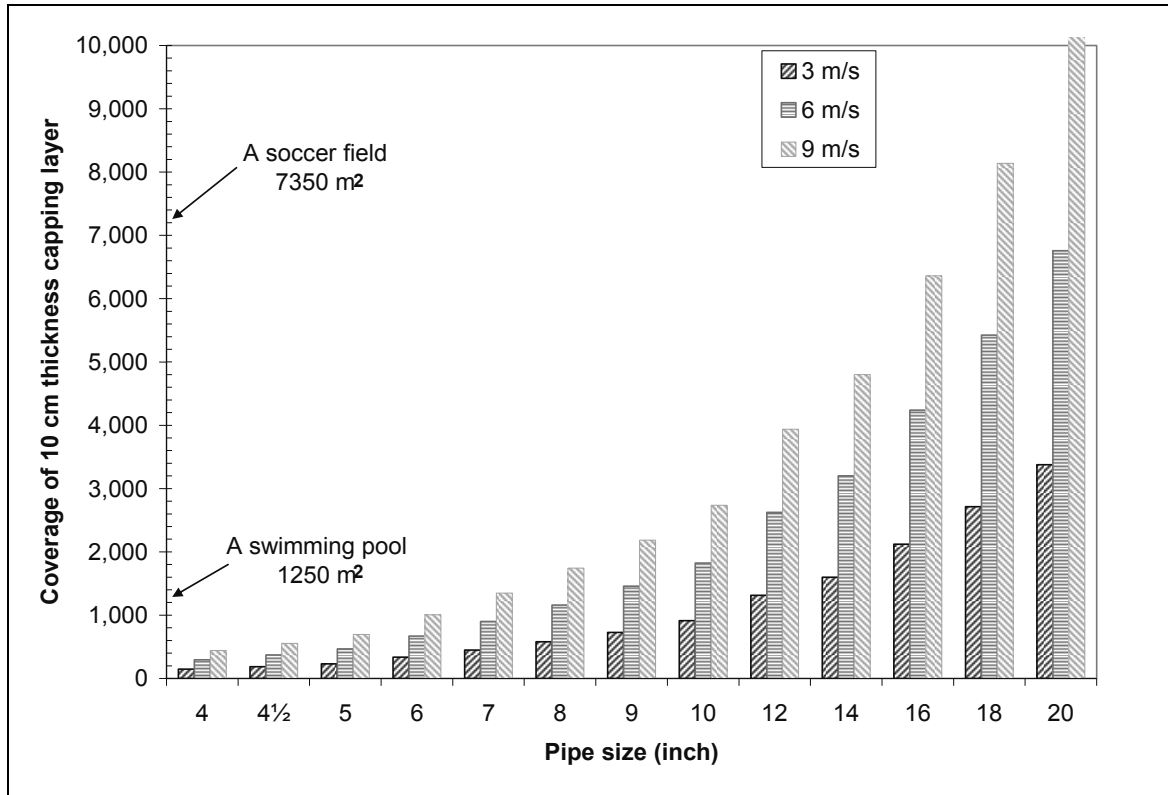


Figure 4. Calculated coverage of a 10 cm capping layer using different pipe sizes at different flow velocities.

CHARACTERIZATION OF THE MFT, MIXTURE FOR SPREADING AND THE RESULTANT MFT POLYMER

Determination Of Gelation Time

Gelation time is one of the most important factors controlling the capping process. A longer gelation time is desirable so as to allow the mixture spreading and covering a larger area of a soft deposit. The polymerization reaction is an exothermic process; hence the process can be monitored precisely by measuring its temperature as illustrated in Figure 5. A 100 g sample (mixture of 90% MFT and 10% chemicals, proprietary recipe) was used for the tests. The MFT, received from a COSIA member, contains 32.4% solids, 3.7% bitumen, of the solids 93.7% is fine. A rubber-like polymer cake was formed after each test. Fig. 5 shows progresses of the polymerization

with different gelation times achieved by using MFT containing 25-35% solids and different chemical recipes. R-0 is the case with only one monomer and one initiator, which had a gelation time less than 30 seconds, the polymerization reaction started immediately after mixing the MFT and the initiator, and gave off heat to rise its temperature; the polymerization reaction reached its highest rate at approximately 10 minutes then slowed down, which is reflected by the temperature curve with a maximum point. The curves of R-1 through R-5 represent the cases when different recipes were used, achieving a gelation time ranging from 5 minutes to 60 minutes, a time range broad enough to meet any implementation requirement. Figure 5 also shows that the polymerization reactions completed within 30-60 minutes with changing cases from R-0 through R-5, meaning that the polymer layer, if used to cap a soft tailings deposit, is trafficable after its temperature returns to ambient temperature within 3-4 hours.

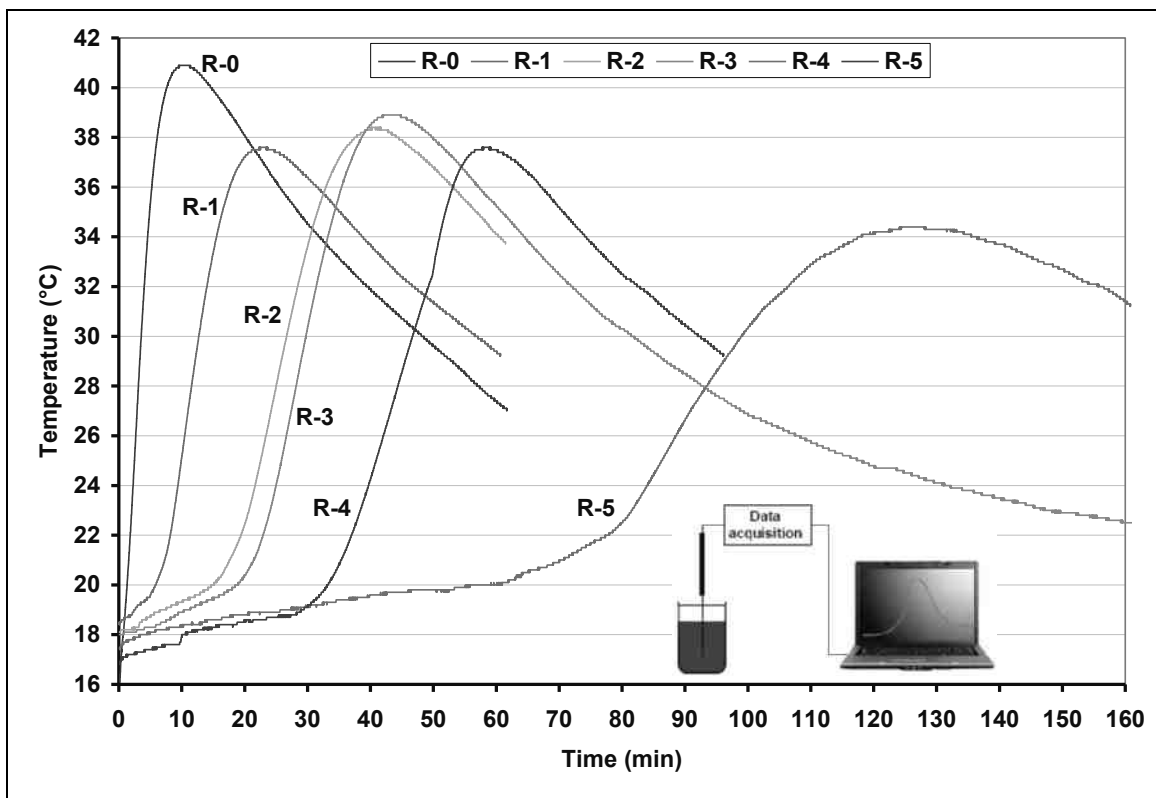


Figure 5. Progresses of the polymerization with different gelation times achieved by using MFT containing 25-35% solids and different recipes. R-0 is the base case with only one monomer and one initiator, R-1 through R-5 are the cases for different recipes.

Rheological Characterization Of The Mft And Mixture (Mft + Chemicals)

Viscosity and shear stress are two important factors controlling the spreading and polymerization process. Both of them were measured using a Brookfield vane rheometer at 0.3 RPM as a function of time. MFT and all chemicals were firstly mixed using a proper mixer at 600-900 RPM for 5 minutes to ensure thorough mixing, and then the mixture was transferred to a measuring cell for rheological property measurement immediately. Shear stress and viscosity results are both shown in Fig.6 for recipe R-2. Viscosities of the MFT and the mixture (MFT + R-2 chemicals) at different RPMs before gelation are shown in Fig. 7. The results show that, before

gelation, both shear stress and viscosity of the mixture kept unchanged, however, after gelation, viscosity and shear stress both increased dramatically, reflecting the vigorous polymerization reaction started once it passed its induction threshold (gelation time). This suggests that viscosity can also be used to determine gelation time. The viscosity of the mixture is lower at all shearing RPMs, and both decreased with increasing shearing RPM slowly, indicating a shear thinning behaviour for the both. The low viscosity of the mixture is favourable for its spreading on a soft deposit to cover a larger area. Addition of chemicals to MFT decreased viscosity, which is very favourable for the mixture to spread on a soft deposit.

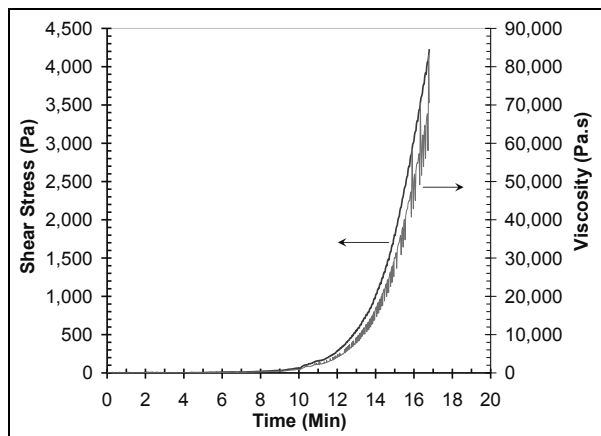


Figure 6. Shear stress and viscosity of the mixture of MFT and added chemicals vs time at 0.3 RPM.

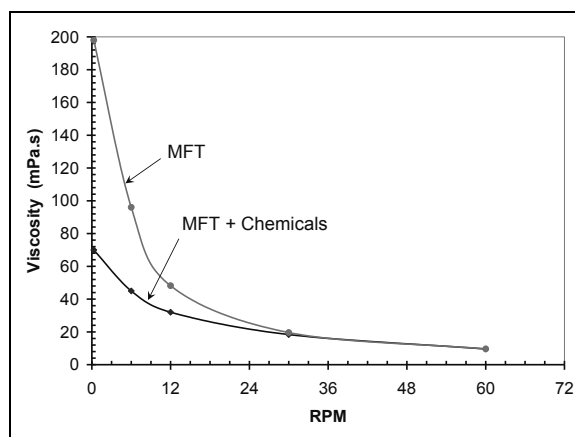


Figure 7. Viscosity of MFT and the mixture (MFT + chemicals) at different RPMs before gelation.

Rheological Characterization Of The Flocculated Mft (Soft Mud)

Rheological property (shear stress and modulus) of the flocculated MFT is also measured using the vane rheometer. Two flocculated MFT samples were prepared using our own developed flocculant, VitalFloc GO-20, at dosages of 550-650 g/t solids. Shear stress and modulus were measured and summarised in Figure 8. The result shows that the flocculated MFT had a yield stress greater than 300 Pa.

One Dimensional Consolidation Test

In order to find out geological and structure properties of the MFT polymer, 1-D consolidation test was performed at Golder Associates. The MFT polymer was directly casted to the size of test

ring, both ends trimmed, inundated in tap water for 24 hours for saturation assisted with vacuum and vibration. For loading over 50 kPa, each loading stage was held for 6 to 12 days until primary consolidation was completed. The Result is summarized in Fig. 9. Vertical strain and void ratio as a function of vertical effective stress were calculated from the test result and are shown in Figure 10. The Coefficient of volume compressibility, coefficient of consolidation and hydraulic conductivity were also derived from the consolidation test, they are summarized in Table 1. The results show that the MFT polymer basically is an elastic material having a little plastic property. The void ratio changed from 4.5 to 1.1 with increasing vertical stress from 10 kPa to 825 kPa. The low hydraulic conductivity indicates that the MFT polymer is impervious; nevertheless it has a good water adsorption property.

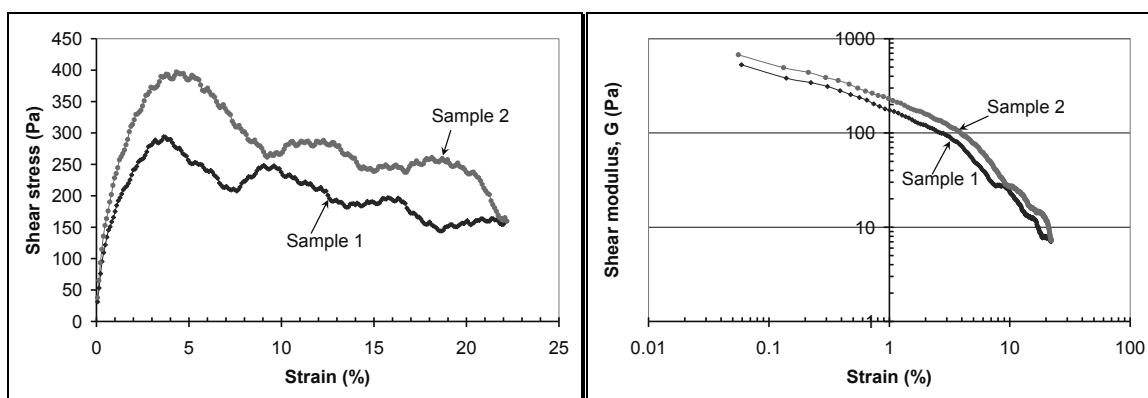


Figure 8. Shear stress and shear modulus (G) of the flocculated MFT (soft mud).

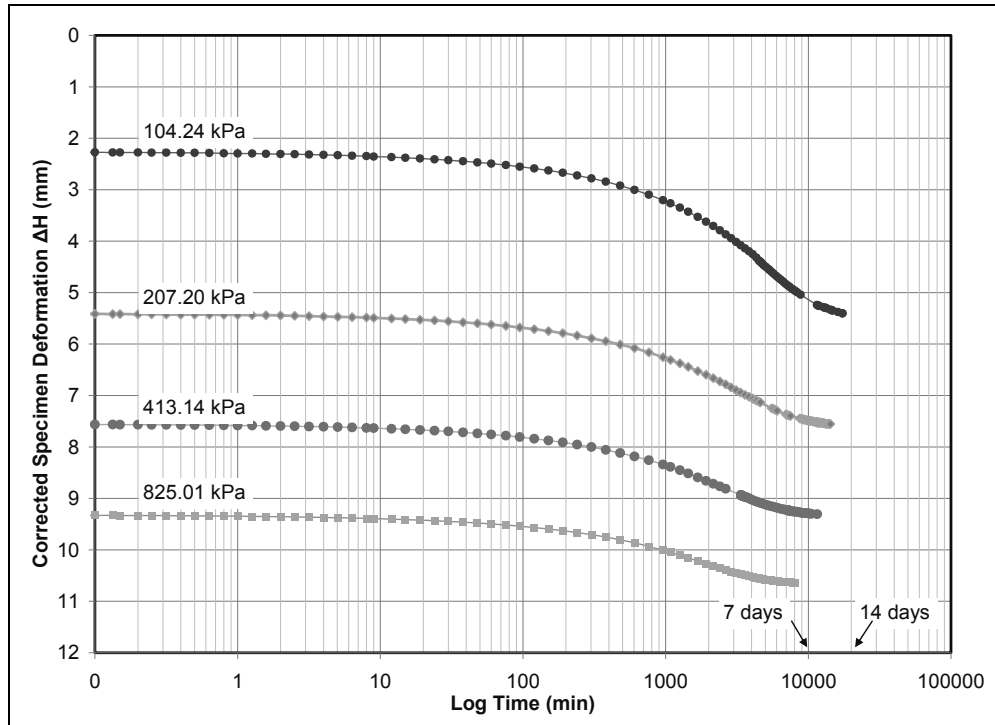


Figure 9. Deformation vs. time (log scale).

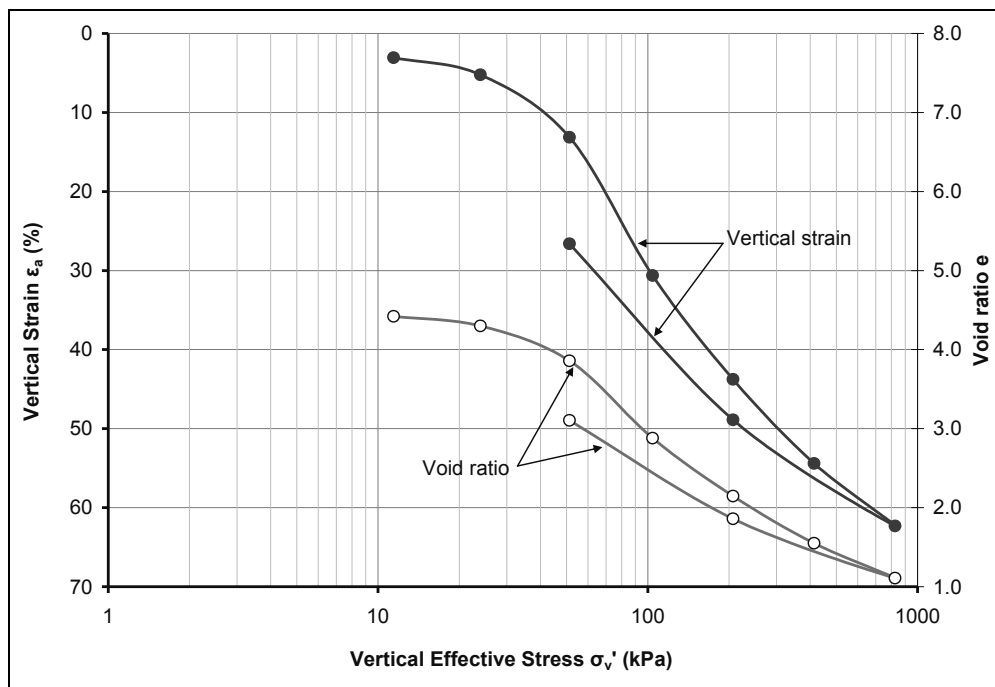


Figure 10. Vertical strain ϵ_a and void ratio e vs. vertical effective stress σ_v' .

Table 1. Coefficient of Volume Compressibility, Coefficient Of Consolidation and Hydraulic Conductivity Derived From the Consolidation Test.

Vertical Stress σ_v' (kPa)	Coeff. of Vol. Compressibility m_v (m^2/MN)	Coeff. of Consolidation c_v (m^2/yr)	Hydraulic Conductivity k (m/s)	Coeff. of Secondary Consolidation. C_α
0.00				
11.43	2.69			
23.96	1.73			
51.27	2.89			
104.24	3.30	2.07E-03	2.13E-12	0.323
207.20	1.28	2.09E-03	8.30E-13	0.132
413.14	0.52	1.58E-03	2.55E-13	0.076
825.01	0.19	1.58E-03	9.41E-14	0.072
207.20				
51.27				

Yield Stress And Young's Modulus Measurement

Yield stress and Young's modulus of the MFT polymer were measured at different conditions; four sets of samples were prepared. 1) The raw MFT polymer containing 38% solids; 2) the raw MFT polymer was dried to contain 60% solids; 3 & 4) both MFT polymer samples containing 38% and 60% solids were separately prepared in the same way as for 1) and 2), then the samples were kept in a refrigerator for 24 hours and then left for 24 hours at room temperature to allow the samples to resume its property as much as possible. All MFT polymer samples were casted in a 1 inch pipe. The drying test was to study the impact of solid content vertical gradient distribution due to water evaporation; the frozen test was intended to study how winter climate would affect the capping layer's mechanical performance. Force was measured using a setup as shown in Fig. 11. An electronic scale equipped with a PC was used as a force sensor; one end of the MFT polymer sample was clamped on a cantilever and another end was clamped on a mass that is placed on the scale. The scale was zeroed when all set, the PC

recorded the weight changes while the cantilever was cranked up manually. Three different cranking speeds were used, 2, 4 and 8 cm/min. It was realized that a cranking speed of 2 cm/min was too slow and 4 and 8 cm/min were confirmed to produce acceptable repeatability. Stress was calculated using the weight change divided by the sample's original sectional area. Stress vs strain plots are shown in Fig. 11. The result show that MFT polymers with higher solid content have greater mechanical strength and better elastic property, which is indicated by the higher strain than the MFT polymers with low solid content. Freezing the MFT polymer sample for 24 hours had minor impact on the mechanical property. These results suggest that the MFT polymer capping layer will have much stronger mechanical strength when it is semi or fully dried than its fresh one, winter climate will not reduce its mechanical strength.

Ultimate yield stress of the samples containing 60% solids is significant higher than the samples containing 38% solids, so does the Young's modulus (slope of the curves).

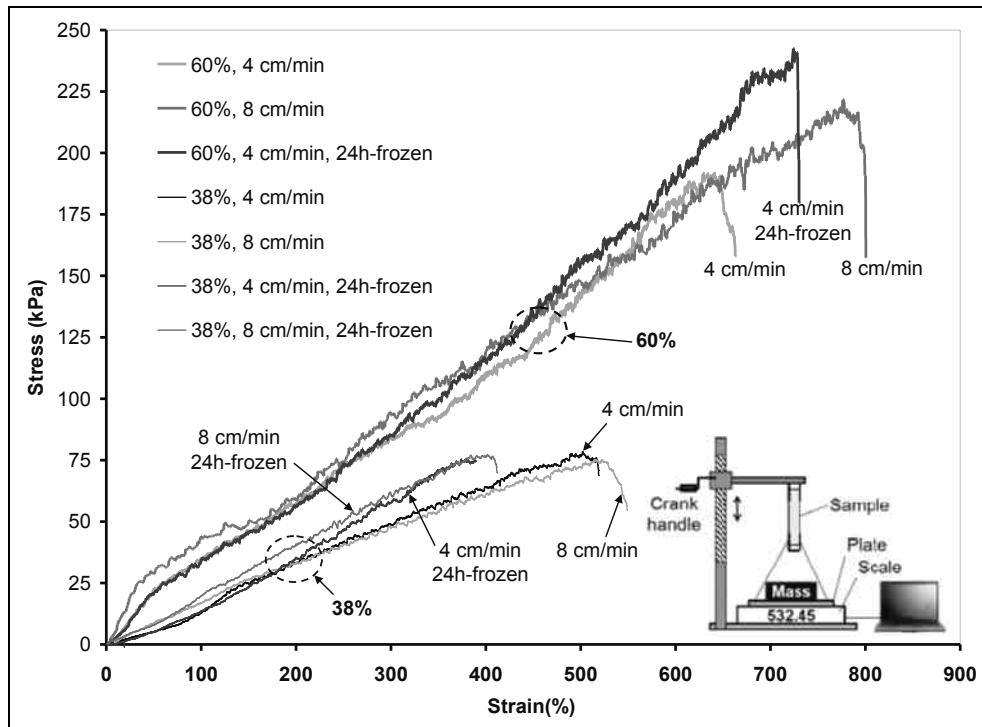


Figure 11. A comparison of stress vs strain for the MFT polymer samples with different solid contents.

SUGGESTIONS FOR TAILINGS POND RECLAMATION

Four steps are suggested to implement the polymerization capping technology as shown in Figure 12,

1. polymer capping as illustrated in Figure 3 to turn the fluid tailings into a trafficable surface;
2. making some holes for water release to overcome its impervious nature;
3. cover the holes with MFT polymer pads to enhance local mechanical strength and allow release water to pass through the gaps;
4. and loading sand or soil on top of the trafficable capping layer when the capping layer is semi or fully dried.

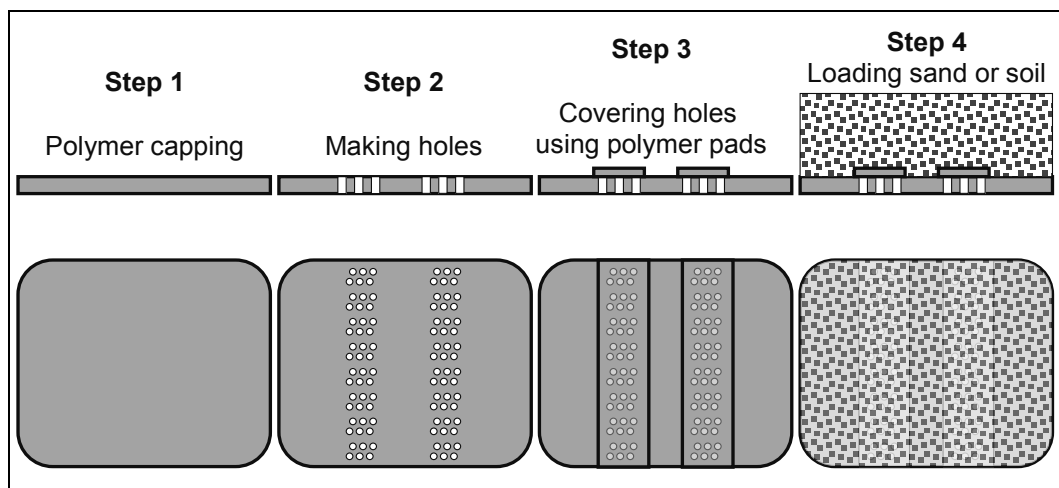


Figure 12. Steps for tailings pond reclamation.

Holes can be made using special aeration equipment similar to lawn aerator. MFT polymer pads can be made in any size. A photo of the MFT polymer pads is given in Figure 13. Each pad is approximately 2 square feet in areal size and 2

inches in thickness. The pads are wrapped using plastic wrap to avoid moisture loss. Due to its good elasticity, MFT pads can be made long strips for rolling and placing in the same way as laying sod.

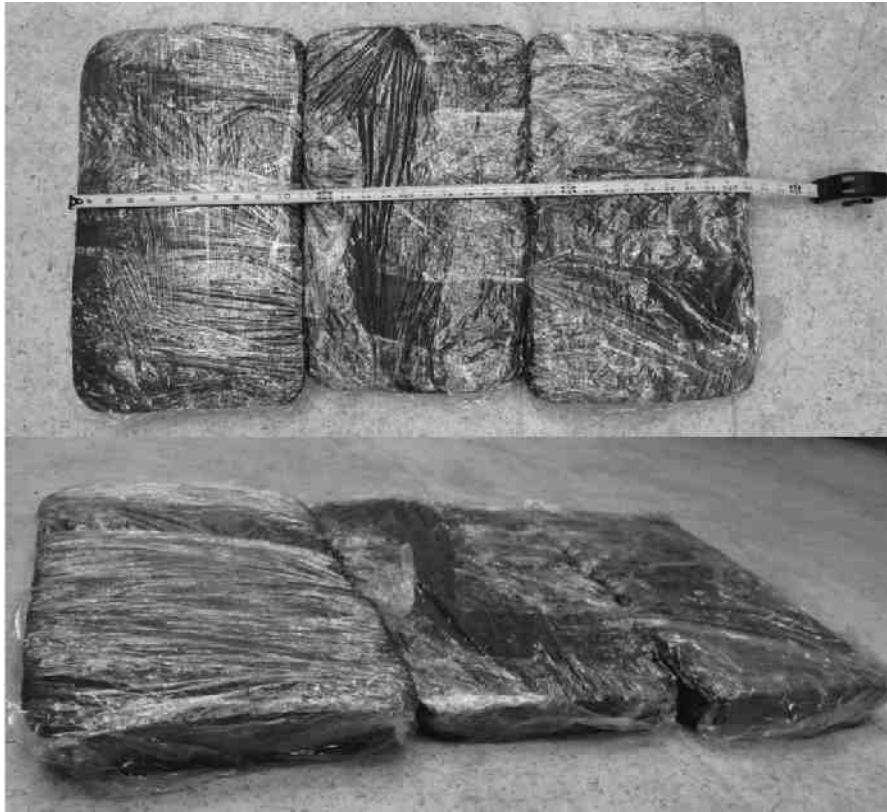


Figure 13. A photo of MFT polymer pads.

ACKNOWLEDGEMENTS

National Research Council-Industrial Research Assistance Program is appreciated for financial assistance.

CLAY-FLOCCULANT INTERACTIONS IN DEVELOPING NEXT GENERATION FLOCCULANTS FOR OIL SANDS FLUID FINE TAILINGS MANAGEMENT

Carol Mohler, Michael Poindexter, Claribel Acevedo, Tom Sanders Jr, Gregory Meyers, Carl Reinhardt, Wu Chen, Harpreet Singh and Jesus Atias
The Dow Chemical Company, Midland MI, Freeport TX and Calgary, Alberta

ABSTRACT

Oil sands mining companies face significant challenges to reduce the size of tailings ponds, and to increase the speed of pond reclamation. A variety of technologies are under consideration to improve tailings management, most of which rely on an effective chemical treatment. These include the use of chemical flocculants to reclaim large quantities of fluid fine tailings generated during oil sands surface mining. Chemical flocculants are typically high molecular weight polymers, which are thought to remove clay particles from tailings by a bridging flocculation mechanism. Flocculation efficacy is affected by many variables including clay content, clay species, particle size and distribution, bitumen content, pH, ionic strength, polymer charge, polymer conformation and mixing efficacy. Furthermore, the pond-to-pond and within-pond variation for many of these variables poses additional challenges to achieve a robust flocculation process.

One of the keys in designing a successful flocculation system is to improve the understanding of clay-flocculant interactions and how these interactions are affected by process variables. This paper describes the use of surface-sensitive methods such as atomic force microscopy and quartz crystal microbalance to provide insight into flocculant interactions on prototype clay surfaces, as well as the effect of solution properties. Unique high-throughput imaging methods are also leveraged to quantify the settling of various clays using different flocculants. Building the understanding of these flocculant-clay interactions will accelerate the development of more effective and robust chemical treatments for fluid fine tailings.

INTRODUCTION

The aqueous discharge stream from the bitumen extraction process used in processing surface-mined Alberta oil sands ore consists of a variable

mixture of clay, silt, sand, water soluble organics and residual bitumen. Clays, which are classified by both size ($<2 \mu\text{m}$) and chemical composition (phyllosilicates) (Kaminsky, 2008) are particularly resistant to consolidation even over long times. When stored in massive holding ponds, the suspended solids (mostly clays and silts), gradually densify to ~25-40 wt% solids in 2-5 years. However, these consolidation levels are far below what is needed for effective treatment in terms of strength of the deposited material and amount of fines capture. Numerous approaches are being studied to address the remediation of oil sands tailings, and many of these rely on the use of chemical flocculants to assist in dewatering and consolidating the tailings. A multitude of different chemicals have been studied as flocculants over the years, with variations in chemical composition, charge density, molecular weight, and molecular architecture (Li, 2007; Michaels, 1954; Yang, 2004; Moffett, 2010; Wang 2010). To develop more effective, robust flocculants, it is critical to use methods which elucidate clay-flocculant interactions in order to understand how variations in flocculant structure and chemical composition affect those interactions.

The flocculation process is typically characterized by bulk methods, such as settling tests to monitor dewatering and the increase in solids concentration, capillary suction time (CST) tests for drainage capacity, and consolidation testing to assess compaction and mechanical strength increase on drying (Longo, 2010; Wells, 2011; Kasperski, 1992). These tests can give meaningful predictions of initial and end-use performance, but may not give sufficient insight into how the chemical structure of the flocculant can be manipulated to further improve performance. For this reason, additional experimental techniques are needed which are sensitive to the flocculation process on a molecular level. Both atomic force microscopy (AFM) and quartz crystal microbalance with dissipation (QCM-D) have shown promise in defining forces between model clay surfaces and high molecular weight flocculants, as well as

flocculant adsorption kinetics in model clay systems (Long, 2006; Alagha, 2011, 2013; Gupta, 2010). These surface techniques help to bridge the gap between bulk solids settling and dewatering and the effect of flocculant-clay interactions on short and long term performance. In addition to utilizing recently developed high throughput screening methods to rapidly evaluate settling performance of flocculants (Mohler, 2012), it is also desirable to correlate and leverage learnings derived from molecular-level experiments to optimize flocculant performance determined on a bulk scale.

EXPERIMENTAL

Materials

Clays were obtained from the Clay Minerals Society Source Clay Repository at Purdue University, with chemical composition reported by Purdue listed in Table 1. The clays were first ground using a rotor mill (Retsch GmbH, Germany) equipped with a 0.08 mm ring sieve. To achieve a smaller particle size, the clays went through an additional grinding process in recycle water obtained from Alberta operator sources. The recycle waters used had a range of pH (8.0 to 8.4) and ionic content (calcium 23-27 ppm, magnesium 14-17 ppm, sodium 258-755 ppm and sulfur 60-152 ppm). The wet grinding was accomplished using a Soil Dispersion Mixer (Humboldt H-4260A) at 14,000 or 24,000 rpm for several minutes, at times in the presence of a small amount of a dispersing aid such as sodium hexametaphosphate. The clay solutions were then transferred to a 500 mL settling column with additional recycle water and mixed via plunger for 30 seconds; after an hour a portion of the top part of the settled solution was removed for the rest of the settling tests. The particle size and size distribution of the clay solutions was determined using a Laser Diffraction Particle Size Analyzer (LS 13 320 MW, Beckman Coulter) with a Universal Liquid Module (ULM). The mean/median particle sizes of the kaolinite and illite were 5.6/3.4 μm and 8.0/5.7 μm respectively.

Stock solutions of flocculants were prepared at 0.5 wt% (5000 ppm) by dissolving the solids in operator recycle water, and stirring magnetically at 130 rpm for 1 hour. Flocculant solutions were equilibrated for at least 2 hours at room temperature before use. For AFM experiments, flocculant stock solutions were prepared at a

concentration of 5,000 ppm by directly dissolving polymer powders in milli-Q water (resistivity $>17 \text{ M}\Omega\text{-cm}$) using magnetic stirring at 130 rpm for 1 hour, and diluted to 100 ppm using milli-Q water.

High Throughput Settling Rate

Clay settling was measured using a high throughput apparatus described elsewhere (Mohler, 2012). Experiments were performed in small scale ($\sim 4 \text{ mL}$) with samples arranged in a 4x6 plate array. Appropriate amounts of clay and process water were added to maintain a constant solids loading.

A diagram of the high throughput settling test workflow is shown in Figure 1. Clay solutions were dispensed manually by pipette into 10 mL glass vials. The filled vials were placed in a plate tray on the deck of a liquid handling robot (Extended Core Module, FreeSlate Inc., Sunnyvale, CA), and any additional recycle water required to dilute the clay was added to the individual vials by a robotically-controlled 250 μL disposable positive displacement (PD) pipette. The vials were then stirred on-deck at 100 rpm for 5 minutes using a magnetic mini-stir disk (V&P Scientific, CA) to ensure homogeneity.

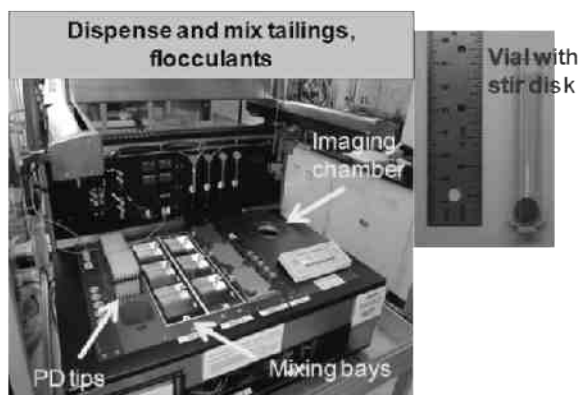


Figure 1. High-throughput method to prepare flocculant/clay formulations and assess settling behavior. Flocculant solutions were automatically dispensed into 10-mL vials (see insert) containing clay solution while stirring. Digital images of the samples were collected robotically as a function of time.

The vials were stirred for an additional 2 minutes at 100 rpm immediately before the addition of the stock flocculant solution, which was delivered to

each vial robotically with a 250 μL PD pipette while stirring at 100 rpm. Stirring was allowed to continue for 3 minutes. The total weight of material was controlled to be the same in each vial and was approximately 4 grams.

To determine the settling rate, individual vials were removed periodically from the plate by one of the robotic arms and placed in the imaging chamber on the robot deck, where a digital image of the sample was collected. Significant attention was paid to design an imaging chamber with sufficient lighting and lens systems to obtain high quality images of the settling clays and exuded water, since the clays themselves are opaque and challenging to image in detail. The robotic protocol allowed images to be collected as quickly as 15-20 seconds after the cessation of mixing, and as rapidly as 5 seconds between images, enabling rapid settling to be observed. Settling tests were usually conducted over a 20 hour time period. Digital images were processed using an automated digital analysis algorithm which automatically picks the bottom of the vial, the top of the original solution and the top of the settling clay which in the oil sands industry is often called the mudline. Clay heights were normalized to the initial clay line and used to quantitate the relative settling properties of the clay-flocculant slurries.

Quartz Crystal Microbalance

Measurements of flocculant adsorption on surfaces were made using a quartz crystal microbalance with dissipation factor (QCM-D E4, Biolin Scientific, MD). Both silica (SiO_2) and alumina (Al_2O_3) coated quartz crystals were purchased from Biolin, to simulate different basal surfaces found in clays. The AT-cut quartz crystal sensors had a 14 mm diameter and a fundamental shear oscillation frequency of 5 MHz. The temperature of the sample chamber was controlled to 0.02 $^\circ\text{C}$, and all experiments were run at 20 $^\circ\text{C}$ to minimize bubble formation. Solutions of flocculant in recycle water were prepared at 4,000 ppm (0.4 wt %), and then diluted to 500 ppm for the QCM-D experiments. Solutions were flowed over the substrates using a low volume peristaltic pump (Ismatec IPC), operating at a constant flow rate of 0.10 mL/minute. All measurements were made by running the water over the substrate until a stable background was achieved. Changes in frequency and dissipation were measured simultaneously at multiple frequencies (overtones) of the fundamental oscillation frequency of 5 MHz.

Atomic Force Microscopy

The substrates used for AFM/colloidal probe force measurements quartz crystal microbalance (QCM) sensors coated with alumina (Al_2O_3) or silica (SiO_2) (Biolin Scientific, MD). The sensors were treated by UV-ozone for at least 10 minutes to ensure any organic contaminants were removed from the surfaces, and were mounted on an AFM specimen disc mount using an adhesive (hot melt Paraffin wax).

Colloidal probe experiments were performed using a Dimension Icon[®] AFM (Bruker Corp.) equipped with ScanAsyst[®] tool for automated scanning parameter optimization. Silica colloidal probes consisting of a SiO_2 particle (2.5 μm nominal diameter) mounted on a silicon nitride cantilever (0.6 N/m nominal spring constant) were purchased from NovaScan Technologies. The spring constant of the cantilever was calibrated using the thermal tune method (Butt, 2005). Probes were characterized for shape irregularities and size by imaging a TGT1 test grating (NT-MDT North America). A scanning electron microscopy (SEM) image of a typical colloidal probe (Figure 2) indicated a probe diameter of 2.07 μm , in reasonable agreement with the nominal specification of 2.5 μm .

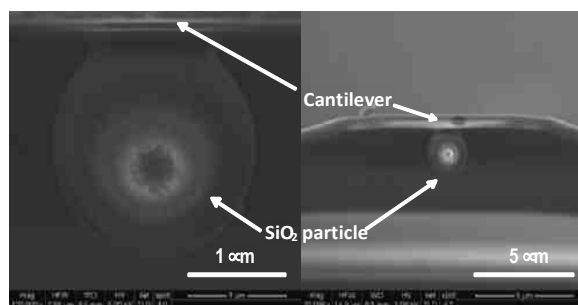


Figure 2. SEM micrographs of SiO_2 colloidal probe and calibration of probe diameter using the SEM micrograph on the left side (bottom). The size of the silica sphere by this analysis is in agreement with the nominal manufacturer specifications (2.1 vs ~ 2.5 μm).

Force curves were recorded using a 500 nm ramp at a 1 Hz cycle time with a forward and reverse velocity of $\sim 1,000$ nm/sec, and a contact force trigger of 10 nN (trigger threshold to avoid probe and surface damage). Force curves were acquired

on multiple locations over a 500 nm x 500 nm area on each sample surface. Each force curve represents the average of 50 to 100 force curve acquisitions. The substrates were contained in a Petri dish, and immersed in solutions exchanged using a syringe. Milli-Q water was used to rinse the probe and substrate thoroughly between measurements involving different solutions.

RESULTS AND DISCUSSION

High Throughput Settling Rate

Small scale high throughput settling tests have been shown to be useful in screening the performance of flocculants in tailings slurries (Mohler, 2012). Similarly, it can be instructive to utilize this approach to gain information on flocculant efficacy in different types of clays. Images are shown in Figure 3 for the settling of two different types of clay (kaolinite and illite) after 20 hours, as a function of flocculant dose, for two flocculants with different chemistries. Regardless of clay type, the best performance was observed for Flocculant X at 1,000 ppm, based on enhanced dewatering and water clarity. Flocculant X was also more effective at dewatering kaolinite compared to illite, indicating that flocculant performance can strongly depend on the clay type. The floc size was also smaller in illite (Figure 3), regardless of flocculant identity or dose.

In addition, Flocculant X was able to flocculate kaolinite far more effectively than Flocculant H. A dense layer of floc was visible at the bottom of the vial even at 200 ppm, and is even more distinct at 500 ppm. At 1,000 ppm, almost all the clay was flocculated from solution and only a slight opacity was observed in the supernate. By comparison, little flocculation was observed, if at all, for Flocculant H in kaolinite over the 200 to 1,000 ppm range. Neither flocculant was as effective on illite and may indicate that this TOT (tetrahedral-octahedral-tetrahedral) type clay is more challenging to flocculate overall compared to the TO (tetrahedral-octahedral) kaolinite structure.

These results suggest some improvement in flocculant performance in tailings might be achieved if new chemical flocculants can be developed that are more effective in treating illite. Flocculant performance was dependent on both clay type, as well as flocculant chemistry; this knowledge can in principle be used to design

flocculants whose effectiveness is optimized relative to the clay identity, clay mixtures and clay content of the tailings stream.

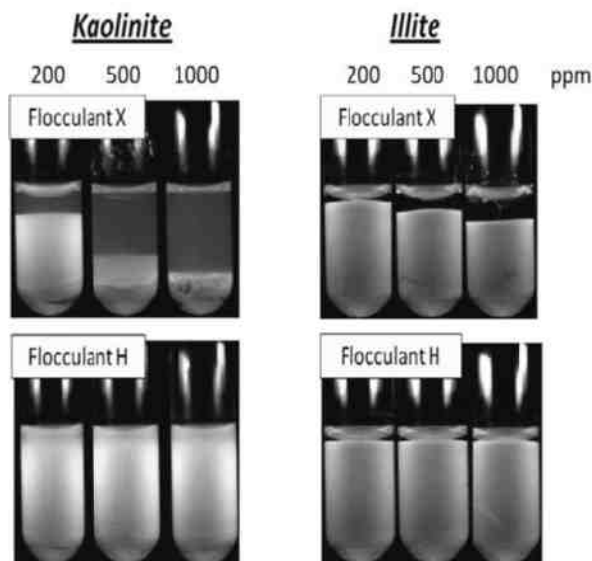


Figure 3. Settling of kaolinite and illite clays in recycle water after 20 hours, as a function of flocculant dose. Images are shown for two flocculants with different chemistries.

Quartz Crystal Microbalance

To complement the more macroscopic or bulk settling results, the QCM-D technique was used to monitor the adsorption and desorption of nanogram quantities of flocculant on surfaces. The frequency shift of a piezoelectric quartz crystal sensor set into oscillation at its resonance frequency, can be related to the mass change resulting from material adsorbed on the sensor (Marx, 2003; Rodahl, 1995). The kinetics of the adsorption and desorption processes can be followed, and the mass of the adsorbed layer extracted. In addition, the dissipation of the sensor oscillations also gives information about the viscoelastic properties of the adsorbed film (Reviakine, 2004; Voinova, 2004).

The adsorption characteristics of 100 ppm aqueous solutions of two different flocculants with different chemistries are shown in, on a model clay surface (silica coated QCM sensor). Flocculant H shows very little if any adsorption onto silica (no appreciable frequency or dissipation shifts), while Flocculant Z strongly adsorbs onto this substrate (negative frequency shifts). The adsorption of

Flocculant Z is fairly rapid; the adsorbed film appears to be “soft” and viscoelastic, since the dissipation factor is nonzero, and the harmonic responses do not overlap. In contrast, based on differences in frequency shifts, Flocculant H adsorbs onto the alumina coated sensor while Flocculant Z does not (Figure 5). Qualitatively, the adsorption of Flocculant H on alumina seems to be a somewhat slower process than that of Flocculant Z on silica since the frequency shift on adsorption has a much shallower slope, and the mass of the adsorbed Flocculant H on alumina appears to be smaller than that of Flocculant Z on silica. Adsorption kinetics of flocculants on clay surfaces can be important in determining flocculant efficacy, since flocculant reformation rates on the surface depend in part on the amount of adsorbed flocculant (Gregory, 2011).

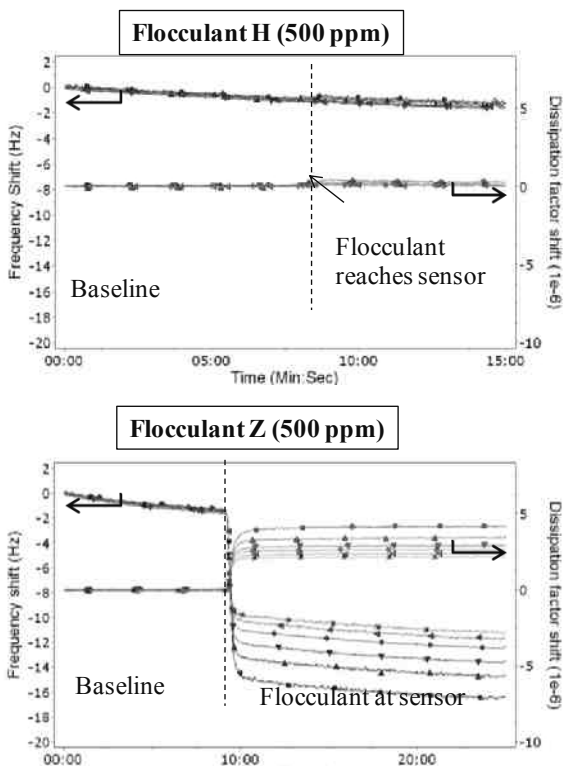


Figure 4. Frequency and dissipation factor shifts as a function of time for two different flocculants on silica substrate, in recycle water. The family of curves for both frequency and dissipation factor represent the respective responses at different harmonics of the fundamental oscillating frequency.

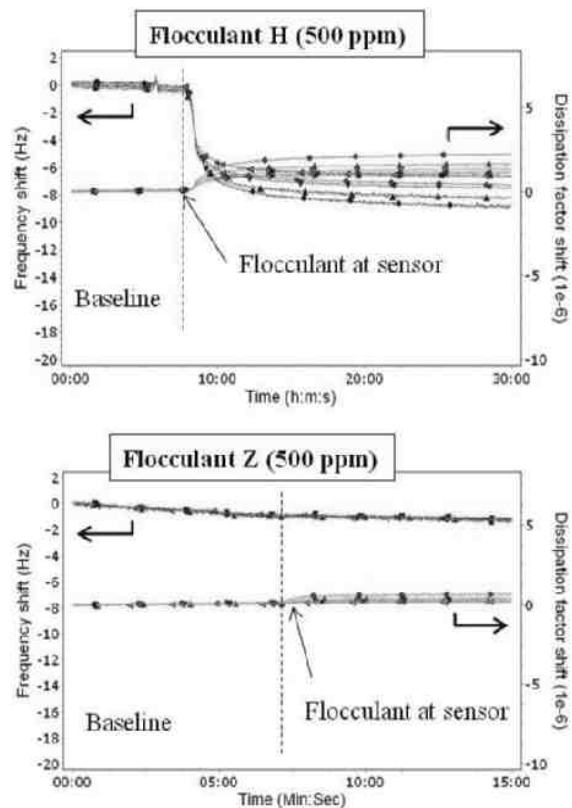


Figure 5. Frequency and dissipation factor shifts as a function of time for two different flocculants on alumina substrate, in recycle water. The family of curves for both frequency and dissipation factor represent the respective responses at different harmonics of the fundamental oscillating frequency.

Since both TOT and TO clay types are typically present in oil sands tailings, the complementary aspect of the adsorption on silica and alumina surfaces suggests a mixture of these two flocculants may be more effective than either flocculant alone.

Furthermore, the viscoelastic properties of the adsorbed films of Flocculants Z and H are different (Figures 6, 7). The slope of the dissipation factor versus frequency shift curve is small for adsorbed Flocculant H on alumina substrate, reflecting an adsorbed film that in the initial adsorption phase is rigid enough to oscillate in phase with the sensor. The molecular conformation of this initial adsorption is consistent with “train” arrangements of the flocculant on the surface in Region 1, most

likely with low surface coverage. As the adsorption continues, the dissipation factor increases and the adsorbed film shows more elasticity (slope increases), suggesting a regime (Region 2) where the film contains more loosely bound species such as “loops” and “tails”. The adsorbed film of Flocculant Z on silica similarly shows a reformation during the adsorption process, but the adsorbed Flocculant Z film has a higher dissipation factor and a higher slope ($\Delta D/\Delta f$) throughout the adsorption on silica, compared to adsorbed Flocculant H on alumina. Adsorbed Flocculant Z may be more loosely packed than Flocculant H on their respective surfaces both initially and throughout the adsorption process, so that Flocculant Z may be more likely to form additional flexible structures such as loops and trains, which are more effective at bridging to adjacent clay particles.

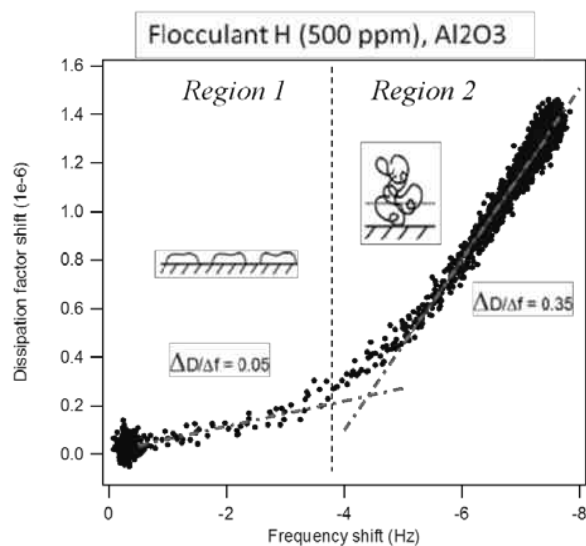


Figure 6. Change in dissipation factor with adsorption for Flocculant H on alumina substrate in recycle water.

Atomic Force Microscopy

Atomic force microscopy gives yet another way to probe the interactions between flocculant molecules and clay surfaces, by discerning the effect of added flocculant on the forces between a model clay surface and a colloidal probe of similar or different composition than the surface. In AFM the force is measured between the tip attached to a soft cantilever and the surface (Butt, 2005). The cantilever acts as a spring that allows forces between the tip and the sample to be measured with pico-Newton sensitivity. The deflection of the

cantilever is detected using a laser beam, which is focused on the free end of the cantilever and reflected into a photodetector. This deflection is converted into a force by Hooke's Law.

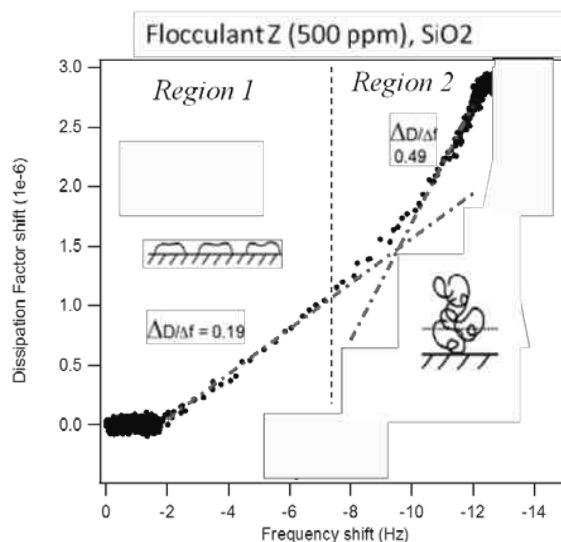


Figure 7. Change in dissipation factor with adsorption for Flocculant Z on silica substrate, in recycle water.

AFM enables a quantitative determination of the type of forces (repulsive or attractive) between flocculant molecules and various surfaces, the relative magnitude of these forces and their length scale. The interactions of model clay surfaces (represented by a SiO₂ colloidal probe and either a silica or alumina surface) in aqueous solutions containing two different flocculants revealed interaction force profiles that change depending upon flocculant chemistry and surface type (Figures 8, 9). For interactions between silica surfaces (Figure 8), the presence of 100 ppm Flocculant X in milli-Q water led to approach and retraction force profiles that were comparable to those measured in milli-Q water alone. Addition of the flocculant at this dose level introduced no specific interactions between the SiO₂ probe and the silica substrate. This flocculant does not appear to preferentially change the surface charge on either surface compared to water alone, and only some small attraction at short distances was observed on the retract curve. Different behaviour was observed for Flocculant H, which showed exclusively repulsive interactions between negatively charged surfaces on approach or retraction.

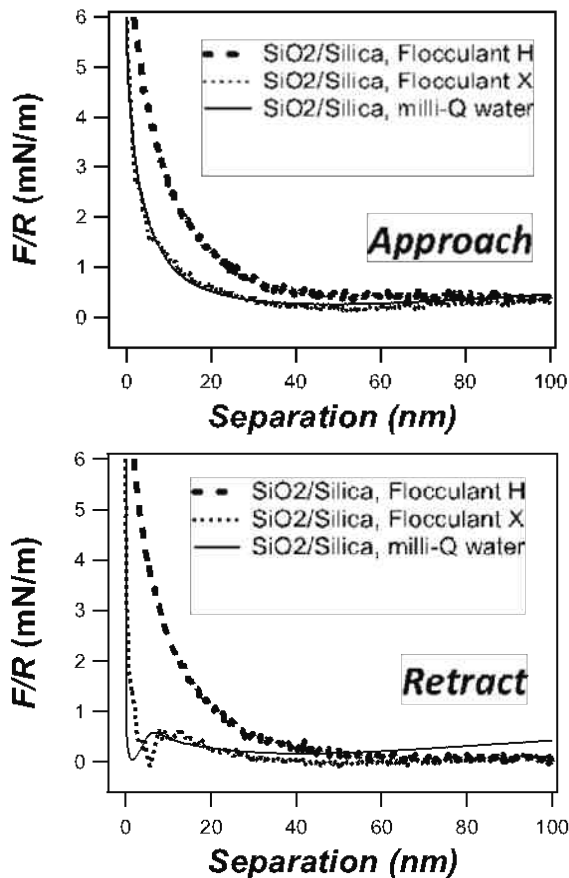


Figure 8. Force profiles for SiO₂ colloidal probe and SiO₂ surface, in milli-Q water and 100 ppm aqueous solutions of two different flocculants.

For oppositely charged surfaces (Figure 9, silica probe and alumina), as expected an electrostatic attraction at short distances was observed in water alone, with significant pull-off in the retraction curve. The presence of 100 ppm of Flocculant H negated this electrostatic attraction, resulting in solely repulsive interactions between the surfaces, whether in approach or retraction. This may be due to a rapid coating of the alumina with Flocculant H, which might screen the surface. Flocculant X displays different behaviour than Flocculant H for oppositely charged surfaces, producing adhesion forces similar to water alone. Slightly less attraction (approach) and adhesion (retract) is observed in 100 ppm Flocculant X solutions compared to water. If there is some small amount of adsorption of Flocculant X to either surface at this pH, surface coverage is insufficient to substantially negate the intrinsic

electrostatic attraction between the SiO₂ probe and alumina surface.

Future studies which vary the flocculant concentration, molecular weight and molecular architecture are planned, since the specific nature of flocculant interactions and surface adsorption is expected to change the interaction forces. The effect of residual bitumen and the presence of clays coated with polar organic species will also be addressed.

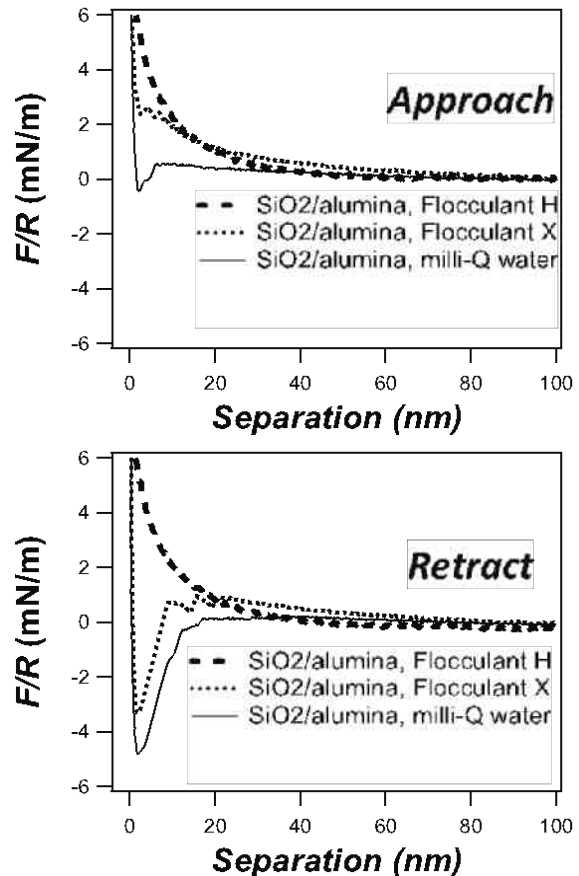


Figure 9. Force profiles for SiO₂ colloidal probe and Al₂O₃ surface, in milli-Q water and 100 ppm aqueous solutions of two different flocculants.

CONCLUSIONS

Small scale digitally-imaged high throughput settling experiments, atomic force microscopy and quartz crystal microbalance with dissipation have been used to probe flocculation behaviour for

various flocculants in mixtures with different clay types. All three of these methods were shown to be sensitive in detecting the effects of flocculant chemistry, molecular architecture and clay type or model clay surface. While bulk methods to characterize flocculant performance such as solids level, settling, capillary suction time, and yield stress are important predictors of end-use performance, they do not give clear insight into the molecular process of flocculation and are of somewhat limited utility in driving the development of new and innovative flocculant systems. Ultimately, the complex, variable, and time-dependent nature of interactions in clay-flocculant systems requires the use of multiple techniques to fully define the clay flocculation process.

With the combination of high throughput settling imagery, AFM and QCM-D, our ability to understand clay-flocculant interactions at a molecular level is greatly improved. This enabling combination of technologies is critical to build understanding of clay-flocculant interactions and is being used to design and optimize flocculants with improved performance for oil sands tailings having a wide range of compositions.

ACKNOWLEDGEMENTS

The authors acknowledge Chris Alvey for acquiring the SEM images and Saul Garcia for the source clay milling.

REFERENCES

- Alagha, L.; Wang, S.; Xu, Z.; Masliyah, J. H.; Adsorption Kinetics of a Novel Organic-Inorganic Hybrid Polymer on Silica and Alumina Studied by Quartz Crystal Microbalance; *J. Phys. Chem. C*, **115**, 15390-15402, 2011.
- Alagha, L.; Wang, S.; Yan, L.; Xu, Z.; Masliyah, J.; Probing Adsorption of Polyacrylamide-Based Polymers on Anisotropic Basal Planes of Kaolinite Using Quartz Crystal Microbalance, *Langmuir*, **29** (12), 3989-3998, 2013.
- Butt, H.J.; Capella, B.; Kappl, M.; Force Measurements with the atomic force microscope: Technique, interpretation and applications, *Surf. Sci. Reports*, **59**, 1-152, 2005.
- Gregory, J.; Barany, S.; Adsorption and flocculation by polymers and polymer mixtures, *Advances in Colloid and Interface Science* **169**, 1-12, 2011.
- Gupta, V.; Miller, J. D.; Surface force measurements at the basal planes of ordered kaolinite particles, *J. Colloid Interface Sci.*, **344**, 32-37, 2010.
- Kaminsky, H. A. W.; Characterization of an Athabasca Oil Sands Ore and Process Streams, PhD thesis, University of Alberta, 2008.
- Kasperski, K. L.; A Review of Properties and Treatment of Oil Sands Tailings, *AOSTRA J. Res.*, **8**, 11-53, 1992.
- Li, H.; Long, J.; Xu, Z.; Masliyah, J.; Flocculation of Kaolinite Clay Suspensions Using a Temperature-Sensitive Polymer, *AIChE J.*, **53**(2), 479-488, 2007.
- Long, J.; Li, H.; Xu, Z.; Masliyah, J. H.; Role of Colloidal Interactions in Oil Sands Tailings Treatment, *AIChE J.*, **52**: 371-383, 2006.
- Longo, S.; Francoeur, R.; Labelle, M.; Wislesky, I.; Tailings Dewatering in the Oil Sands; 2nd International Oil Sands Tailings Conference, Edmonton, 5-8 December 2010 (p 43).
- Marx, K. A.; Quartz Crystal Microbalance: A Useful Tool for Studying Thin Polymer Films and Complex Biomolecular Systems at the Solution-Surface Interface, *Biomacromolecules*, **4**(5), 1099-1120, 2003.
- Michaels, A. S.; Aggregation of Suspensions by Polyelectrolytes, *Ind. Eng. Chem.* **46** (7), 1485-1490, 1954.
- Moffet, R.H. Treatment of Oil Sands Mature Fine Tailings with Silica. 2nd International Oil Sands Tailings Conference, Edmonton, Alberta (Dec 5-8, 2010)
- Mohler, C.E; Poindexter, M. K.; Atias, J.; Chen, W.; Witham, C. E.; Development of Flocculants for Oil Sands Tailings Using High-Throughput Techniques; 3rd International Oil Sands Tailings Conference, Edmonton, 2-5 December 2012 (p 113).
- Reviakine, I; Morozov, A; Rossetti, F; Effects of finite crystal size in the quartz crystal microbalance

with dissipation measurement system: implications for data analysis, *J. Appl. Phys.*, **95**, 7712, 2004.

Rodahl, M; Hook, F; Krozer, A; Brzezinski, P; Kasemo, B; Quartz Crystal microbalance setup for frequency and Q-factor measurements in gaseous and liquid environments, *Rev. Sci. Instrum.*, **66**(7), 3924 (1995).

Voinova, M. V; Jonson, M; Kasemo, B; On dissipation of quartz crystal microbalance as a mechanical spectroscopy tool, *Spectroscopy.*, **18**, 537-544, 2004.

Wang, X; Feng, X; Xu, Z; Masliyah, J. H.; Polymer Aids for Settling and Filtration of Oil Sands Tailings, *Can. J. Chem. Eng.*, **88**, 403-410, 2010.

Wells, P.S., Revington, R., and Omotoso, O., 2011. Mature Fine Tailings Drying – Technology Update”, *Proceedings of the 14th International Seminar on Paste and Thickened Tailings*, R.J. Jewll, A.B. Fourie (eds) 5-7 April 2011, Perth, Australia, Australian Centre for Geomechanics, 155-166.

Yang, W; Qian, J; Shen, Q. J.; *J. Colloid Interface Sci.*, **273**, 400-405, 2004.

Table 1. Chemical composition of clays (wt%)

	Kaolinite KGa-2	Illite IMt-1
SiO ₂	43.9	49.3
Al ₂ O ₃	38.5	24.25
TiO ₂	2.08	0.55
Fe ₂ O ₃	0.98	7.32
FeO	0.15	0.55
MnO	ND	0.03
MgO	0.03	2.56
CaO	ND	0.43
Na ₂ O	<0.005	0
K ₂ O	0.065	7.83
P ₂ O ₅	0.045	0.08
S	0.02	

ND = not detected

CONSOLIDATION RATES AND RESULTING PHYSICAL PROPERTIES OF PARTICLEAR™ SILICA TREATED FLUID FINE TAILINGS

Robert H. Moffett¹ and Fred D. Godbille²

¹DuPont Chemicals & Fluoroproducts, Wilmington, DE USA

²DuPont Centre for Process Innovation, Canada

ABSTRACT

In-situ polymerization of silica has recently been proposed as a treatment method for fluid fine tailings (FFT). Silica treatment has been shown to increase the wet strength of FFT by more than an order of magnitude and to maintain this strength advantage throughout the dewatering process. FFT treated by in-situ polymerization of silica has been shown to evaporatively dry at rates essentially equal to that of water. Silica treatment of FFT has been demonstrated to be relatively insensitive to oil sands tailings mineralogy.

This paper will focus on silica's positive effect on FFT consolidation rate and the improved physical properties of the consolidated FFT. Conditions which favor faster consolidation rates for silica treated FFT will be discussed. Comparison to FFT treated with anionic polyacrylamide will be included.

INTRODUCTION

Fluid fine tailings are an undesirable consequence of the current oil sands aqueous extraction process. In an effort to reduce FFT inventory, many oil sands producers have attempted to chemically dewater FFT, relying principally on traditional coagulation and flocculation chemicals. More recently, these same chemical processes have been combined with highly capital intensive centrifuge plants. Consistent and reproducible flocculation and coagulation of oil sands FFT is highly challenging as changing FFT solids concentration, mineralogy, and surface area all affect flocculant performance. A more robust, simple treatment process with low capital intensity would be a desirable position.

SILICA TECHNOLOGY

In-situ polymerization of silica within the water phase of FFT has been disclosed as a simple, robust process for treatment of FFT (Moffett 2010). Tailings when initially treated have reduced viscosity (Godbille 2014) compared to untreated tailings allowing for long flow distances (Tilton 2013). As describe by Sobkowicz (2013), the silica treatment ultimately produces a continuous network of linked nano-sized silica particles resulting in a synthetic soil structure within the water phase of the tailings.

The silica synthetic soil structure creates a significant increase in FFT strength prior to and during the dewatering process (Moffett 2013). Large strain consolidometer testing has shown silica treatment has no measurable effect on hydraulic conductivity of the tailings at any given void ratio (Moore 2013). However silica treated tailings maintain a higher void ratio at low stress levels which result in faster dewatering than untreated tailings (Moore 2013). The synthetic soil structure has been demonstrated to permit self-weight consolidation of FFT in a 10 meter standpipe test (Moore 2013).

Minimal data exists however directly comparing the consolidation rates of silica treated FFT to tailings treated with anionic polyacrylamide.

TAILINGS CHARACTERIZATION

Various types of fluid fine tailings types were utilized for this study. General physical properties of the tailings are shown in Table 1. Particle size distribution was determined by static light scattering using a Malvern Instruments Mastersizer 2000. Fines as reported in this paper are those particles

Table 1. Sample Characterization

Sample	A	B	C	D	E
Tailings Type	Mature Fine Tailings	Mature Fine Tailings	Thickened Tailings	Centrifuge Tailings	Mature Fine Tailings
Source	Alberta Oil Sands	Alberta Oil Sands	Alberta Oil Sands	Alberta Oil Sands	Alberta Oil Sands
Wt% solids (includes bitumen)	39.5	32.3	50.1	57.9	26.7
pH	7.7	7.5	7.6	8.0	8.2
SpG (g/cc)	1.26	1.22	1.42	1.50	1.16
Particle Size Distribution (µm)					
D(0.1)	1.7	1.8	2.4	1.7	1.4
D(0.5)	10.8	13.4	23.6	10.4	8.1
D(0.9)	46.9	66.8	120.6	56.4	42.6
SFR	0.14	0.25	0.51	0.16	0.08
Solids Composition					
SiO ₂ (wt%)	64.4	63.4	76	66	50
Primary Clays (wt%)					
Kaolinite	17.9	17.0	14	18	30
Illite	3.5	4.6	5	14	15
Impurities	Balance	Balance	Balance	Balance	Balance
Major Cations Dissolved in Pore Water (ppm)					
Ca	15	19	7	26	28
K	17	15	24	15	19
Mg	9	12	5	13	13
Na	379	378	623	565	950
S	3	3	50	54	216

having a particle size of < 44 microns. Sand to fines ratio (SFR) is the ratio of > 44 micron particles to those particles < 44 microns in diameter. Tailings solids mineralogy was determined by XRD. Major cations dissolved within the pore water of the tailings were determined by ICP.

CONSOLIDATION TEST METHODOLOGY

Consolidation rates of the various FFT samples and treatment methods were evaluated using a custom fabricated test apparatus referred to as a rapid screening consolidometer (RSC). The RSC has 8 independent stainless steel test cells 9.73 cm in diameter. Vertical effective stress ranging from 10 to 200 kPa can be applied to the test samples. The test cells are loaded with a fixed mass of tailings (approximately 1200 grams). Vertical stress is applied to tailings through an air cylinder to a floating piston positioned above the tailings. The bottom of the test cylinder is equipped with a filter paper supported by a wire mesh screen. Exuded water from the test cell is collected in a bottle beneath the cell. Displacement (consolidation) is measured by a linear potentiometer connected to the air cylinder piston (Figure 1).

Treated FFT samples were prepared and placed into the RSC test cells, covered and allowed to set for 24 hours. Any water that was released to the surface of the sample was removed prior to insertion of the floating piston and start of the compressive dewatering test.

For this report, silica dose rates are reported in wt% SiO₂ relative to the water content of the FFT. APAM dose rates are reported in grams of polymer/tonne of MFT solids (including bitumen).

Figure 2 is typical of the results from RSC testing, showing how increasing the Particlear™ (silica) dose increases the rate of consolidation. Samples treated with higher silica dose rates generally compress slightly less since they have higher yield strength and are therefore more resistant to compressive force.

Total reduction in height (consolidation) from the start of compressive dewatering is determined for each test. The time to reach 90% of the total consolidation under compressive force is then determined from the data recorded by the RSC. The effect of silica dose on time to 90% consolidation is shown in Figure 3. This methodology is used to report the remainder of the compressive force dewatering experiments.

RSC Cell Construction

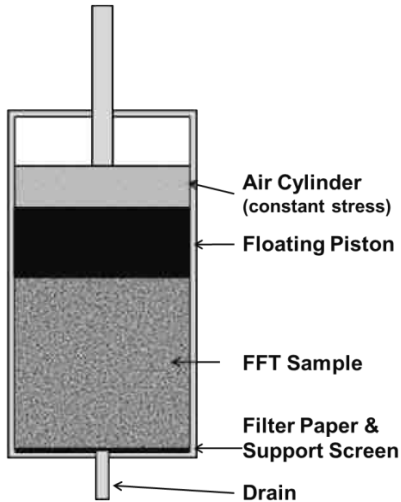


Figure 1. RSC Cell

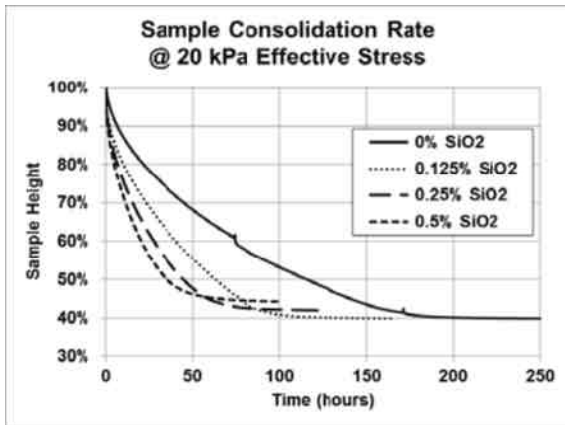


Figure 2. RSC “Typical” Results

Consolidation Rate Comparison to Linear APAM – MFT “A”

Figure 4 shows the comparative consolidation times for MFT “A” treated with a high molecular weight linear APAM (L-APAM) and those results achieved with silica treatment. Time to 90% consolidation was determined for vertical effective stress values between 10 and 200 kPa. Silica treatment was conducted at 0.25 and 0.35% SiO₂. As a result of its high starting yield strength, essentially no water was released from the silica treated samples in the RSC cell after 24 hours when no compressive force was applied.

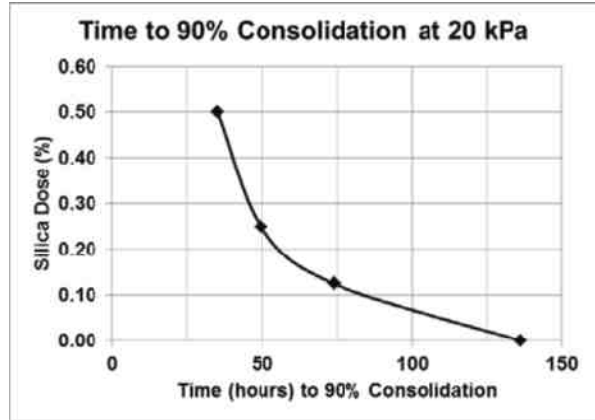


Figure 3. RSC “Typical” Time to 90% Consolidation

The L-APAM solution was prepared at 0.2 wt% due to its very high viscosity. L-APAM was tested at 500 and 750 gram/tonne of dry MFT solids. As a result of the high starting solids concentration of the MFT “A” the 24 hour water release from L-APAM was essentially the same volume as that added by the APAM solution. Therefore, both the silica treated and APAM treated samples started the compressive force portion of the test at the same solids concentration. As can be seen in Figure 4 the consolidation rate of both silica samples was faster than both APAM samples. For example at 40 kPa effective stress, 0.35% SiO₂ reached its 90% consolidation point in approximately 40% less time than the L-APAM at 500 g/tonne.

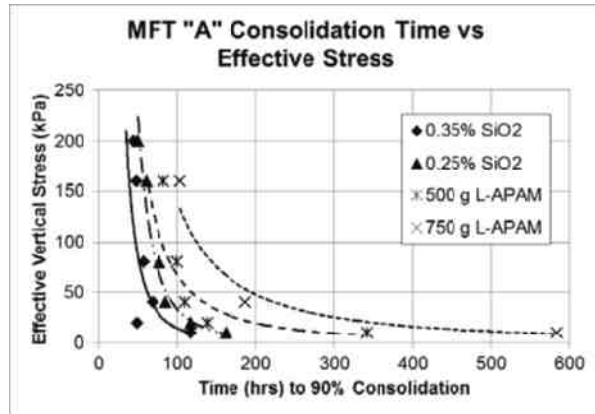


Figure 4. 90% Consolidation Time; MFT “A”

Consolidation Rate Comparison to Branched APAM – MFT “B”

Comparison between silica treatment and branched APAM (B-APAM) was conducted with MFT “B”. Silica treatment was conducted at 0.35% SiO₂. Again essentially no water release occurred from the silica treated sample over the first 24 hours in the RSC cell when no compressive force was applied. Optimum B-APAM dose was determined previously in separate laboratory experiments to be ~ 900 grams/dry tonne of MFT solids. As a result of its lower viscosity, B-APAM was capable of being prepared at 0.4% solids. In this case the B-APAM was able to release a greater amount of water prior to application of compressive force than the volume of water introduced with the APAM solution. B-APAM increased the solids concentration of MFT-B from 32.5 wt% to an average of 38.1 wt%. Interestingly, this was essentially the same solids concentration as L-APAM yielded with MFT “A”. Figure 5 shows again the silica treated MFT reached its 90% consolidation point faster than the B-APAM even though the B-APAM sample started the compressive force dewatering test at a higher solid concentration.

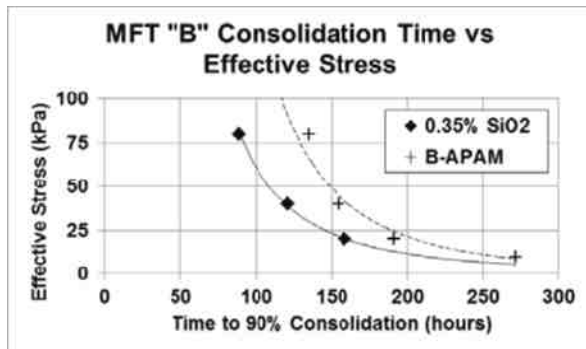


Figure 5. 90% Consolidation Time; MFT “B”

Consolidation Rate - Thickened Tailings (TT) and Centrifuge Tailings (CFT)

Silica treatment demonstrates a positive effect on the consolidation rate of both TT and CFT. Consolidation of silica treated TT takes about ½ as long as untreated TT (Figure 6). Limited testing with CFT has shown silica treatment has a large effect on consolidation rate reducing consolidation time by > 5x over untreated CFT (Figure 7).

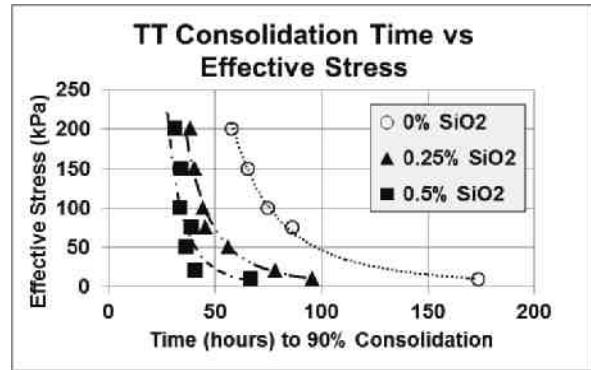


Figure 6. 90% Consolidation; Time TT

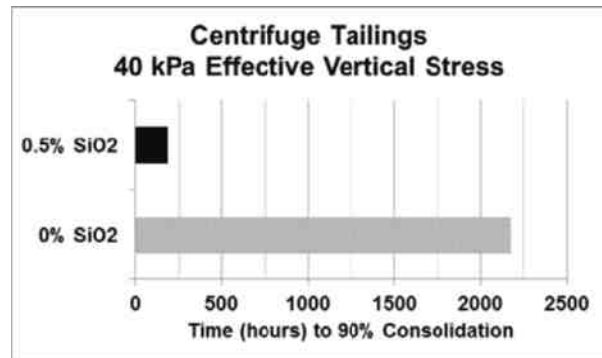


Figure 7. Consolidation Time; CFT

DEWATERED YIELD STRENGTH TESTING

The solids concentration and the yield strength of the compressed samples from the RSC tests were determined. Peak yield strength was determined using a rheometer equipped with a vane spindle rotating at 0.1 rpm

Figure 8 and Figure 9 show that silica treated MFT “A” or “B” has substantially higher yield strength than either L-APAM or B-APAM through the entire dewatering process. The yield strengths of silica treated MFT “A” and “B” (Figure 10) were found to be identical. Interestingly, both L-APAM and B-APAM also produced essentially the same strength as each other at the same solids concentration.

As shown in Figure 11 the yield strength of TT can also be substantially improved by silica treatment.

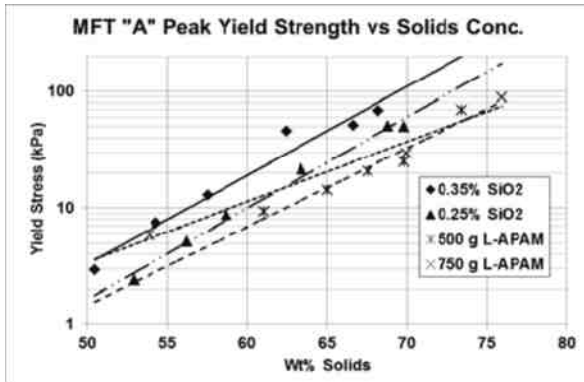


Figure 8. Peak Yield Strength; MFT "A"

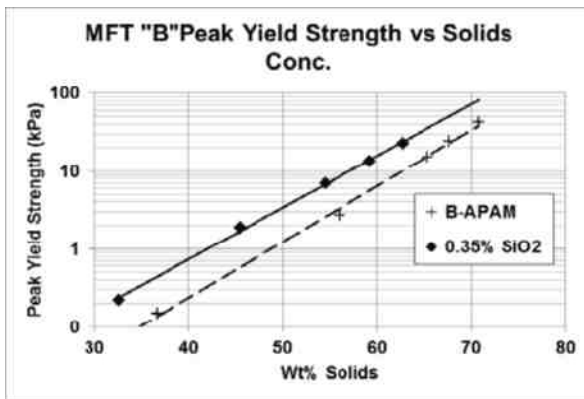


Figure 9. Peak Yield Strength; MFT "A"

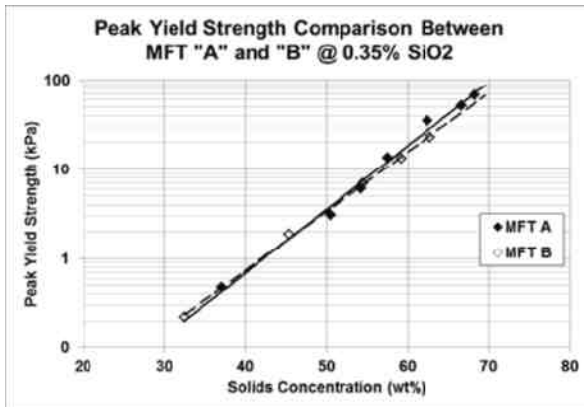


Figure 10. Peak Yield Strength Comparison; MFT "A" vs MFT "B" Treated with SiO2

REMOLDED YIELD STRENGTH TESTING

The remolded yield strength of the various RSC cakes was determined following the peak yield strength test. Remolded yield strength was determined by increasing the speed of the rheometer spindle from 0.1 rpm to 1 or 10 rpm as listed. Ten revolutions were conducted at the higher speed, followed by a 1 minute rest period. The rheometer was then restarted at 0.1 rpm and the peak (remolded) yield strength then re-measured.

Figure 12 shows that silica treated MFT "A" has significantly higher remolded yield strength than L-APAM at any solids concentration. Silica treated MFT "B" also demonstrates higher remolded yield strength than B-APAM over the entire dewatering curve (Figure 13).

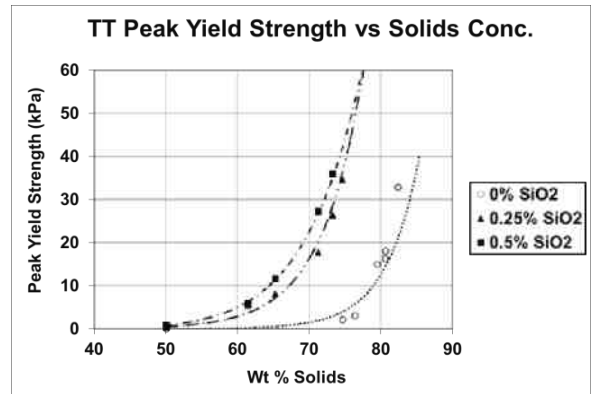


Figure 11. Peak Yield Strength; TT

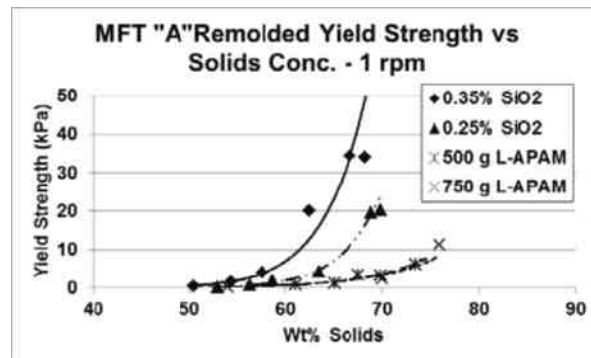


Figure 12. Remolded Yield Strength; MFT "A"

Figure 14 shows how silica treatment improves the remolded yield strength of TT also.

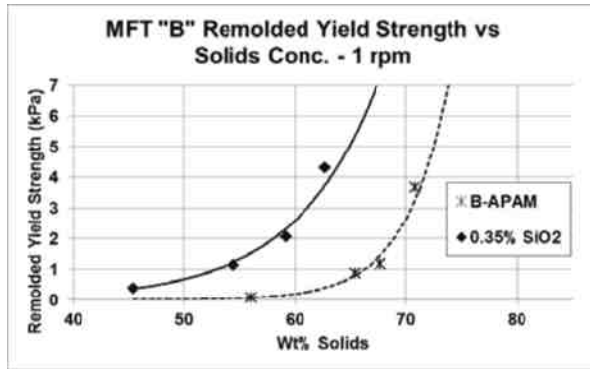


Figure 13. Remolded Yield Strength; MFT "B"

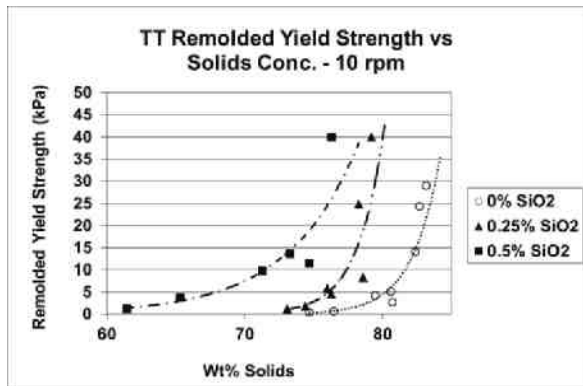


Figure 14. Remolded Yield Strength; TT

RELEASE WATER QUALITY

Moore described filling a 10 meter high consolidation column with FFT A treated by 0.35% SiO₂. During filling of this column approximately 5% of the total water associated with the MFT was released to the surface of the MFT prior to opening the column's under drainage pathway. Characterization of this release water is compared to the water released to the surface by B-APAM in the RSC experiment. Chemical analysis (Table 2) shows the silica treated release water has a high bicarbonate anion concentration and a corresponding high sodium concentration. This is the result of activation of the sodium silicate solution with carbon dioxide. Suspended solids concentration of the silica treated MFT release water is extremely low as a result of entrapment of the fines by the silica network. Industry standard BEU tests have shown no negative impact when using 100% silica treated release water compared to industry process water obtained from an oil sands producer.

B-APAM release water is chemically more similar to release water from untreated MFT. Fine solids in the B-APAM treated MFT release water can potentially be quite high (Table 2 and in Figure 15) and could require additional treatment. These unhindered fine solids can have a potential negative influence on bitumen extraction (Wallace 2004) if they escape the deposit and are entrained in the recycle water stream.

Table 2. Release Water Chemical Analysis

Sample Description		pH	Entrained Solids mg/L	Alkalinity mg/L as CaCO ₃	Bi-carbonates mg/L as CaCO ₃	Carbonates mg/L as CaCO ₃	Total Inorganic Carbon mg/L	Ion Chrom Major Anions				ICP Major Cations			
								F	Cl	NO ₂ -N	SO ₄	Ca	K	Mg	Na
MFT	Treatment														
"A"	None	8.41	NA	584	584	0	135	3	156	ND	<5	15	17	9	379
"A"	0.35% SiO ₂	8.2	5	2305	2305	0	560	ND	194	ND	<5	52	27	42	1002
"B"	None	8.76	NA	601	540	61	132	7	184	ND	<5	19	15	12	378
"B"	900 g/tonne B-APAM	8.57	500	514	466	48	110	2	209	4	20	16	15	10	356

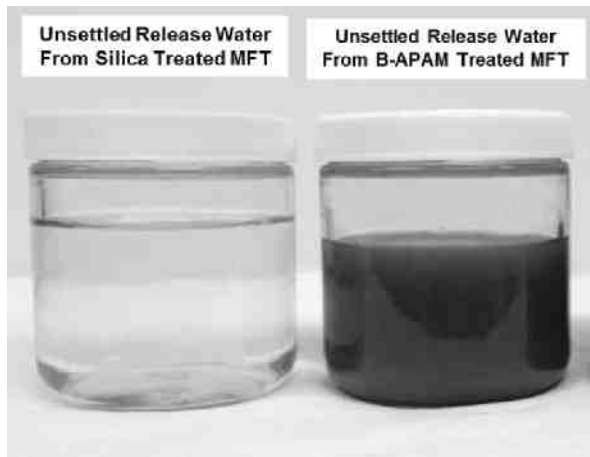


Figure 15. Release Water from MFT “B” Treated with Silica vs MFT “B” Treated with B-APAM

RECOVERY AFTER SHEAR

Dunmola (2013) discloses that shearing APAM flocculated MFT results in the deterioration in rheological properties, dewatering and shear strength gain of MFT. Silica treated MFT has the ability to regain yield strength after shear to essentially the same value as if it had not been sheared. MFT “A” was treated with 0.5% silica and the peak yield strength was determined. The treated sample was divided into three sub-samples (X, Y, and Z).

- Sample X was consolidated under 35 kPa vertical effective stress.
- Sample Y prior to any consolidation step was remolded by hand. Peak yield strength of sample Y four days after remolding was determined to be 49% of the undisturbed sample. After remolding Sample Y was consolidated under 35 kPa effective stress.
- Sample Z was consolidated to an intermediate point (effective stress 14 kPa). Peak yield strength was determined and then Sample Z was remolded by hand. After 5 days Sample Z recovered 31% of its undisturbed strength. After remolding Sample Z was consolidated under 35 kPa effective stress.

As can be seen in Figure 16, all three samples reached the same peak yield strength and solids concentration after final consolidation at 35 kPa.

Similar recovery results can be seen with evaporative drying. MFT “E” was treated with 0.5% silica and compared to L-APAM dosed at 1000 g/tonne. The treated samples were divided into two sub-samples each. Sub-sample B (silica treated) and sub-sample D (L-APAM treated) were highly sheared using a planetary gear food mixer. All four sub-samples were allowed to evaporatively dry. Solids concentration and peak yield strengths were measured for all samples during the drying process. As can be seen in Figure 17 the sheared silica treated samples have essentially the same strength as the unsheared silica samples. The sheared L-APAM treated sample has consistently lower yield strength than the unsheared L-APAM sample.

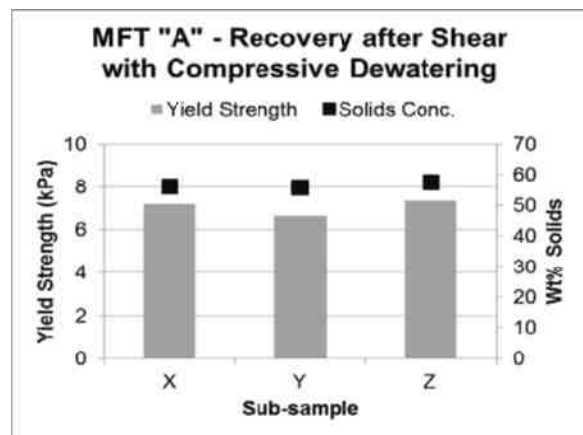


Figure 16. Shear Recovery – Compressive Dewatering

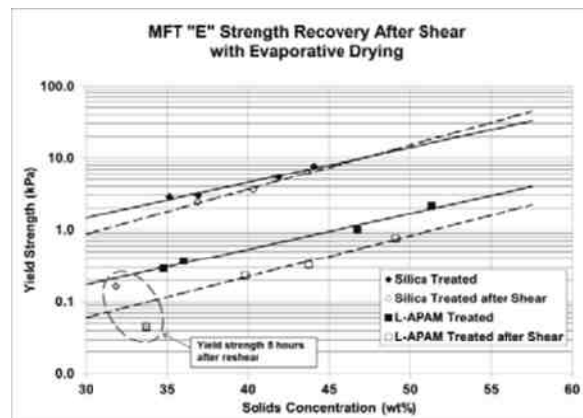


Figure 17. Shear Recovery – Evaporative Drying

INDUSTRIAL IMPLICATIONS

As discussed in the previous sections, the time for FFT consolidation can be substantially reduced by in-situ polymerization of silica. In the field, consolidation rates can be further improved by incorporation of drains or drainage layers and by surcharge loading. Silica treatment can be varied as necessary to provide FFT strength and erosion resistance for drains and/or drainage layer installation. Immobilization of fines by the silica network protects the drains and drainage pathways from fines infiltration allowing them to function as designed. Yield strength of the silica treated FFT can be varied as required to support higher surcharge loading by simply adjusting the silica dose.

The impact of functioning drains and higher surcharge loading can be appreciated by modeling a 20 meter deep deposit of MFT which is filled over a two year period. For this study MFT “B” treated with 0.35% Particlear™ was compared to MFT “B” treated with 900 g/tonne B-APAM. Compressibility and hydraulic conductivity of treated MFTs (Figure 18 and Figure 19) were determined in large strain consolidation experiments as described by Moore (2013). FSConsol software was used to model the deposition conditions shown in Table 3. Top and bottom drainage is assumed for each layer. Each surcharge is assumed to be added linearly over a 3 month time span.

In the study two solids contents after placement for B-APAM treated MFT were modeled; 35 wt% and 43 wt%.

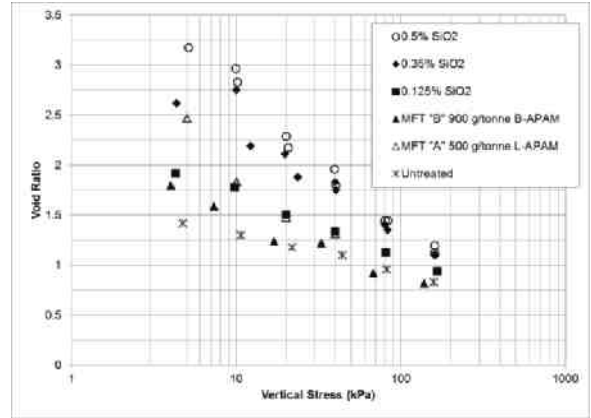


Figure 18. MFT Void Ratio vs. Effective Stress

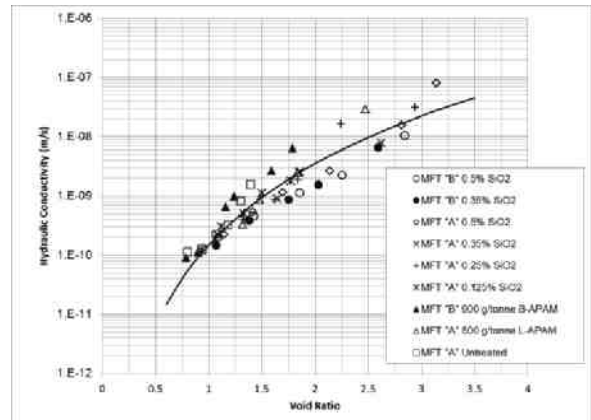


Figure 19. MFT Hydraulic Conductivity vs Void Ratio

Table 3. 20 m Deposit Modeling Parameters

FSConsol Modeling Conditions						
Case	% SC as MFT	Layer Depth	Treatment	% SC after Placement	Surcharges (kPa)	Timing of Surcharges
A	32.5	20 m	900 g/tonne B-APAM	43.0	25 kPa 25 kPa	End of Fill + 1 yr End of Fill + 2 yr
B	32.5	20 m	900 g/tonne B-APAM	35.0	25 kPa 25 kPa	End of Fill + 1 yr End of Fill + 2 yr
C	32.5	20 m	0.35% Particlear™	33.5	25 kPa 25 kPa	End of Fill + 1 yr End of Fill + 2 yr
D	32.5	9 m (bottom)	0.35% Particlear™	33.5	25 kPa	End of Fill + 1 yr
		8 m (middle)	0.35% Particlear™		25 kPa	End of Fill + 2 yr
		3 m (top)	0.75% Particlear™		25 kPa	End of Fill + 3 yr

Figure 20 clearly shows all four treatment schemes dewater and consolidate during the 2 year placement period and therefore do not reach 20 meters in depth. Figure 20 also shows a single

layer of Particlear™ treated MFT consolidates faster than a single layer of B-APAM treated MFT at either starting solids content. Addition of intermediate drainage layers further increases the rate

of consolidation. The time necessary to attain 95% consolidation (end of deposition depth to final depth) is shown in Table 4. A single layer of Particlear™ treated MFT “B” is predicted to achieve this level of consolidation in 63% less time than a single layer of B-APAM treated MFT starting at 43% solids. Addition of intermediate drains and an additional 25 kPa surcharge on Particlear™ treated MFT “B” is predicted to require 88% less time than a single deposit of treated with B-APAM starting at 43% solids.

Table 4: 20 m Deposit; Time to 95% Consolidation

Case	Time to 95% Consolidation	Remaining Settlement
A	51 yrs.	0.35 m
B	46 yrs	0.50 m
C	19 yrs.	0.44 m
D	6 yrs	0.32 m

Figure 21 shows the yield strength predicted for each treatment 10 years after deposition is complete. The bulk of the B-APAM treated MFT has a yield strength < 5 kPa, whereas the entire single layer of Particlear™ treated MFT is projected to have a yield strength > 10 kPa. The Particlear deposit with the intermediate drains and higher surcharge is predicted to have a yield strength over 40 kPa at all depths.

CONCLUSIONS

Silica treatment has a positive impact on FFT consolidation as well as peak and remolded strength. Within the scope of this study;

- Silica treated FFT reached its 90% consolidation point in less time than the same FFT treated with either linear or branched APAM.
- Silica treated FFT was shown to have higher peak and remolded yield strength than either APAM.
- Silica treated FFT was demonstrated to recover full strength after being sheared whereas APAM recovers only partial strength.
- Release water from APAM treated FFT is chemically more similar to untreated FFT pore water. However, APAM treated FFT release water contains a significant level

of entrained fines that may reduce effectiveness of drainage pathways in FFT deposit and may negatively impact bitumen extraction if recycled without further water treatment.

- Silica treatment immobilizes fines in the FFT deposit, protecting drains and drainage pathways.
- Release water from a 10 m consolidation column filled with silica treated FFT has shown no negative impact on bitumen extraction in laboratory BEU experiments.
- A deep deposit of silica treated FFT was predicted to consolidate in 63% less time than an APAM treated FFT.
- Addition of intermediate drainage layers and increased surcharge was predicted to dramatically influence consolidation rates.

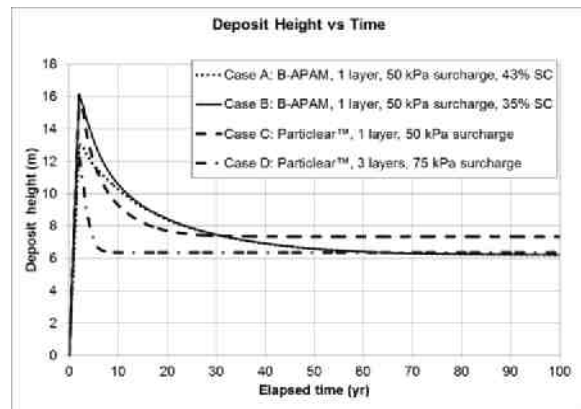


Figure 20. 20 m Deposit Height vs Time

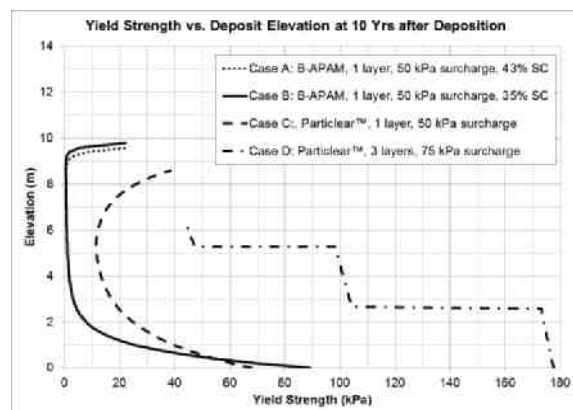


Figure 21. 20 m Deposit; Strength vs Depth

REFERENCES

Dunmola, A. Geotechnical benefits of flocculation in dewatering oil sands mature fine tailings. In: Proc. GeoMontreal 2013, the 66th Annual Canadian Geotechnical Conference, Montreal, Quebec, September 29-October 3, 2013, paper number 209.

Godbille, F.D. 2014. Modification of fluid fine tailing's rheological and stacking properties by in situ silica polymerization. In: D. Van Zyl, R.J. Jewell and A.B. Fourie, Paste 2014, Vancouver, British Columbia, pp. 201-214.

Moffett, R.H. 2010. Treatment of fluid fine tailings with silica. In: Proc., 14th Annual Conference on Tailings and Mine Waste, Vail, Colorado, October 17-20, 2010, pp. 347-353.

Moffett, R.H. 2013. Chemistry and geotechnical properties of fluid fine tailings treated by in-situ polymerization of silica. In: Proc. 17th Annual Conference on Tailings and Mine Waste, Banff, Alberta, November 3-6, 2013, pp. 57-67.

Moore, T. Laboratory Investigation of the Large Strain Consolidation Behaviour of Oil Sands Fluid Fine Tailings Treated with DuPont Particlear™. In: Proc. GeoMontreal 2013, the 66th Annual Canadian Geotechnical Conference, Montreal, Quebec, September 29-October 3, 2013, paper number 528.

Moore, T. Self-weight consolidation of Particlear™ treated fine tailings in a 10 meter column. In: D. Van Zyl, R.J. Jewell and A.B. Fourie, Paste 2014, Vancouver, British Columbia, pp. 231-244.

Sobkowicz, J.C. 2013. Predictive model for thick lift placement of silica-treated fluid fine tailings. In: Proc. 17th Annual Conference on Tailings and Mine Waste, Banff, Alberta, November 3-6, 2013, pp 181-189.

Tilton, J.N. 2013. Preferred rheological attributes for deposition of tailings slurries. In: Proc. 17th Annual Conference on Tailings and Mine Waste, Banff, Alberta, November 3-6, 2013, addendum.

Wallace, D. Fines/water interactions and consequences of the presence of degraded illite on oil sands extractability. The Canadian Journal of Chemical Engineering, Volume 82, August 2004, pp. 667-677.

FLOCCULATION OF ULTRA-FINE PARTICLES OF MATURE FINE TAILINGS

Reza Salehi¹, Zhenghe Xu² and Jacob Masliyah²

¹Canadian Natural Resources Limited, Calgary, Alberta, Canada

²University of Alberta, Edmonton, Alberta, Canada

ABSTRACT

To reduce the inventory of mature fine tailings (MFT) through development of novel tailings treatment technologies, it is essential to understand the stabilization mechanism of ultra-fine solids of MFT. This study aims at characterizing the MFT ultra-fine solids. The outcome of this study shows that MFT contains ultra-fine solid particles of different surface characteristics that respond differently to macromolecule flocculant in the context of flocculation and settling. This response depends not only on the size of particles but also on the presence of organic matter. Organic-rich particles exhibit lower settling rate than organic-lean particles of the same size, where the presence of organics is shown to decrease the adsorption of macromolecule flocculant. The lower affinity of hydrophobic organic matter on the surface of organic-rich particles to the macromolecule flocculant appears to be responsible for poor response of organic-rich fine particles to flocculation by macromolecule flocculant.

INTRODUCTION

A novel method is developed in this study to understand characteristics of ultra-fine particles in MFT by studying their response to chemical treatment. Through analysis of settling and rheological response of fractionated ultra-fines combined with solids characterization of the different layers of the settled MFT, an enhanced understanding of stabilization mechanisms of ultra-fine solids in MFT is gained.

BACKGROUND

Ultra-Fine Particles in MFT

Mature fine tailings are formed after two to three years due to slow sedimentation of fine solids in

fine tailing zone of an oil sands tailings pond. After reaching certain solid concentration, MFT slurry becomes stable and forms a gel which entraps both coarse and fine solids in a network. As a result, there is very little further consolidation beyond typically 35 wt% solids. Numerous researchers have emphasized the importance of the ultra-fine clays in MFT gelation which results in high water holding capacity of MFT [1, 2]. Ultra-fine particles in MFT mainly fall into two different types, hydrophilic ultra-fine solids and bi-wettable ultra-fine solids. Ultra-fine particles are the fraction between 0.02 to 0.3 μm . The bi-wettable ultra-fine solids contain strongly bonded organic materials. These ultra-fines are known to be responsible for gel formation in MFT [3].

Gelation of Ultra-Fine Particles

Ultra-fine clay particles (<0.3 μm) suspended in the water interact with each other and produce a highly stabilized structure. The slurry in this case is non-Newtonian with thixotropic and shear thinning properties [1]. Kotlyar et al. showed the dependency of the degree and rate of gelation on the size of the fine particles. They showed that as the size of particles decreases the degree of gelation (gelation index) increases [2].

Tu et al. [1] showed that ultra-fines and clay contents increase linearly with fines content. Here the fines content refers to the mineral solids smaller than 44 microns. They suggested that regardless of the initial ultra-fines concentration in the suspension they settle down to a final sediment volume containing a specific solids content of ultra-fine solid particles. This value is known as the critical gelation concentration (CGC). Thus, if the original concentration of ultra-fines is equal or greater than the CGC, gel structure will form and no sedimentation will take place. This value for ultra-fine particles is 1.5 wt% of the suspension. Clay particles (<3 μm) also can form gel networks in the suspension but their critical concentration is around 16 wt%.

Flocculation

Flocculation is a complex process involving a number of stages [4]. These stages occur simultaneously, and often compete against each other. Some of the most important parameters affecting the flocculation include mixing, polymer molecular weight, charge density and dosage and rate of polymer addition, background electrolyte as well as particle concentration and size.

Aggregation of ultra-fine particles of different sizes could lead to formation of different types of aggregates. Formation of the aggregates from different sizes of ultra-fine particles extracted from MFT slurries using NaCl as the coagulant has been investigated [2]. It has been suggested that smaller particles seem to have longer induction time i.e. the period before settling gets started. It has been also shown that smaller particles form larger aggregates with higher water to solid ratios.

EXPERIMENTAL

Materials

Mature fine tailings samples were obtained from West in Pit (WIP) pond of Syncrude Canada. Chemicals such as sodium hexametaphosphate (Calgon) used as dispersant and Magnofloc 1011 (anionic polyacrylamide flocculant), used in different stages of experiments were obtained from Fischer Scientific. For dilution of the samples and for polymer solution preparation, deionized water with conductivity of 15 MΩcm was used.

Equipment

For the purpose of mixing the slurries a standard geometrical configuration of beaker and baffle was used. A standard 250 ml beaker with diameter and height of 7.5 cm was used as the container for mixing the slurry and rheological analysis. Four baffles with the width of 1/10 of the beaker's height (T) were used to prevent vortex formation while mixing. A Rushton turbine impeller with the diameter of 1/2 T was used for mixing with the impeller clearance of 1/6 to the bottom of the beaker.

Rheological behaviour of samples was measured by an ARG2 rheometer from TA instrument. Due to the settling of the particles especially where the samples were flocculated as the result of polymer addition, Vane rotor geometry was used. The

particle size distribution (PSD) of the samples was measured using Malvern Mastersizer 2000. To measure the particle size distribution in different MFT samples, samples were taken from different locations while being mixed in the beaker. For the cases where samples were naturally flocculated, sonication and dispersing of the particles were implemented prior to particle size analysis. Sodium hexametaphosphate (Calgon) was used in these situations. STA 409 PC Luxx thermal analyzer from Netzsch Instrument was used for thermogravimetric analysis of the samples.

In order to study the properties of the clays, the organic fractions on their surface need to be removed. One may seek a procedure which does not alter the phases of the clays. Plasma ashing is a proper method in this case as the combustion happens at low temperature. A K1050X plasma asher was used for the removal of organic content from clays. Identification of different types of minerals in clays was conducted using a Rigaku Rotaflex X-ray diffractometer.

Experimental Procedures

Fine particles separation

Fractionation by centrifugation

Two types of ultra-fine particles were separated from the original untreated MFT sample. The procedure of the fractionation is illustrated in Figure 1. A 50 mL of MFT was diluted with 150 mL deionized water. The resulting slurry was left to settle for two days. The coarse particles in the slurry settled after two days and the suspension of the fine particles on top of the coarse sediment was separated using a disposal pipette. The separated top suspension was sieved to obtain a suspension of fine particles of sizes smaller than 28 μm. For this purpose wet screening method was applied, using sieves of 75 μm, 45 μm and 28 μm. The sieves of 75 μm and 45 μm were only used to separate coarse particles which could block the 28 μm sieve. The undersize fraction of 28 μm sieve was then centrifuged, which resulted in the formation of two layers of solids, one is light color sediment in the bottom of the centrifuge tube and another on the top of the sediment with a dark color. The dark sediment was separated from the light sediment using a pipette. The separated fine particles were washed twice with Syncrude tailings process water. This water has a similar chemistry to MFT water from the WIP pond. The purpose of using process water as washing water was to

make sure that the surface properties of clays were preserved after dilution. The washed clays were then centrifuged and put aside for further characterization. In this work whenever the terms light and dark fine particles are used they refer to particles fractionated by the method described above. The particle size distributions of the separated fractions are shown in Figure 2.

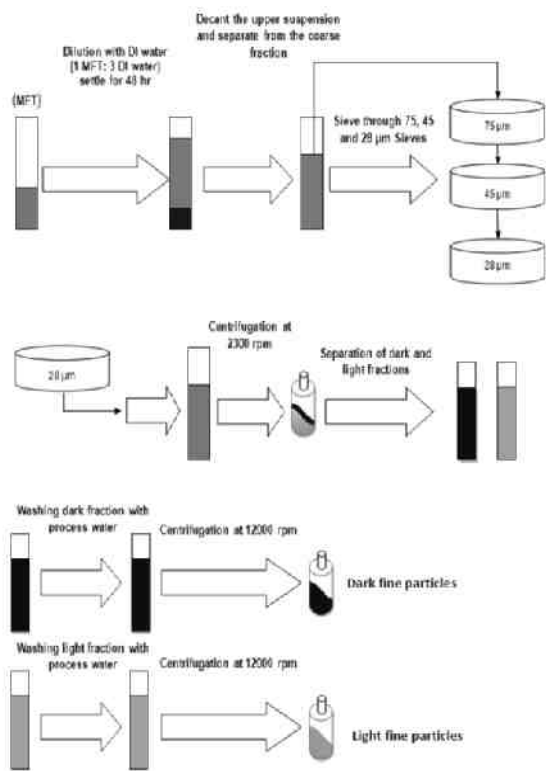


Figure 1. Schematic diagram of fractionation of fine particles from Syncrude WIP MFT.

Fractionation due to flocculation

Ultra-fines particles in MFT obtained from Syncrude WIP pond were also fractionated into three layers in the top, middle and bottom of a graduated cylinder after treating the slurry with polymer as shown in Figure 3. Polymer was added to light and dark fines particles fractionated by centrifugation and their properties and rheological behaviour were compared to the top and middle layer ultra-fines.

Flocculation Treatment

A 50 mL of MFT with solids content of 16 wt% was diluted with process water to 4 wt% solids. Diluted

slurry was premixed for 5 minutes at 1000 rpm followed by the addition of 5 ml of 1000 ppm polymer solution over 90 seconds while mixing the slurry at 350-370 rpm. The slurry was then poured immediately into a graduated cylinder through a funnel and left for sedimentation test.

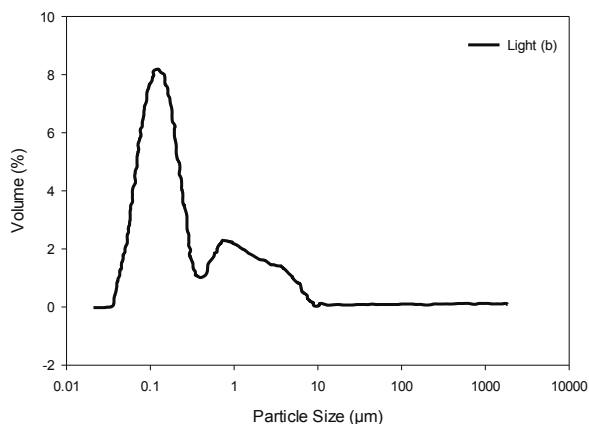
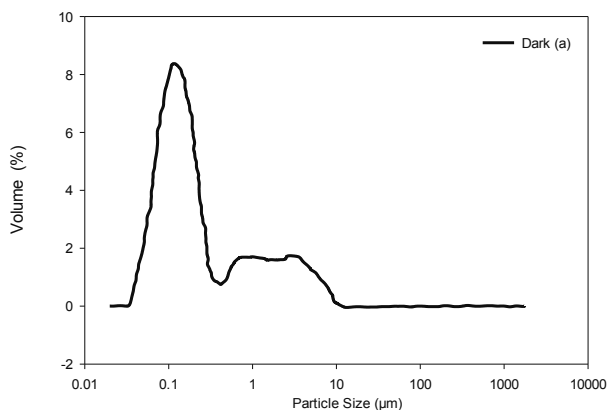


Figure 2. Particle size distributions fractionated from Syncrude WIP MFT, (a) dark fines sediment, (b) light fines sediment.

MBI Analysis

Methylene blue analysis method was used to compare the cation exchange capacity (CEC) of the dark and light fine particles. In this experiment, 213.6 mg of light fine particles and 200.3 mg of dark fine particles after ashing by low temperature ashing technique were dispersed in 50 ml of 0.015 M NaHCO_3 and 2 ml of 10 wt% NaOH . The mixtures were mixed using a magnetic stirrer for 30 minutes until the complete dispersion of the

particles was achieved. During this period, sonication was applied to assist the dispersion of the particles. Following the complete dispersion of the particles, 2 ml of 10 wt% H₂SO₄ was added into the slurry to make sure that the pH is lower than 3. Each sample was titrated with a 0.006N solution of methylene blue with the slurry being stirred. Detailed procedure of MBI analysis can be found elsewhere [5].

Rheological Analysis

For gelation rate tests, viscosity measurements and viscoelasticity measurements, suspensions of 10 wt% fine particles were prepared by adding 10 g of desired fine solids to 90 g of Syncrude process water and mixing the resulting slurry for 25 minutes. For these tests the temperature was set to 25°C in the conditioning and post experiment steps. For gelation rate measurement, time sweep test was conducted over 30 minutes with an oscillatory stress of 0.001 (Pa) and angular frequency of 0.3926 (rad/s). For viscosity measurements steady state flow tests were performed in shear rate range of 0.1 (1/s) to 10 (1/s). For viscoelasticity measurements strain sweep test was conducted in strain range of 0.0001 (%) to 0.1 (%).

RESULTS AND DISCUSSION

Applying flocculant treatment on MFT sample from Syncrude WIP pond resulted in the formation of three layers after sedimentation for two days as shown in Figure 3. The particle size distribution of the original sample as well as those for the top and middle sediment layers are shown in Figure 4.

Figure 4 indicates that the particles with sizes between 5 µm to 100 µm settle at the bottom of the cylinder after 48 hours. Particles in the middle and top layers have sizes between 0.03 µm to about 5 µm. The PSD in the figure above suggests that a large fraction of the particles in the middle and the top layer are ultra-fine particles smaller than 0.5 µm. The cumulative PSD shows that 99% of the particles in the top and the middle layers are less than 2 µm, i.e., the particles in these two layers have similar sizes. Thus particle size is not the dominant variable, which governs the

sedimentation in this case. Further characterization was performed to probe other properties of the

solids in the top and the middle layers. It is more interesting to probe particles in these two layers, specifically the particles in the top layer, as they do not settle by polymer addition in contrast to particles in the middle layer.

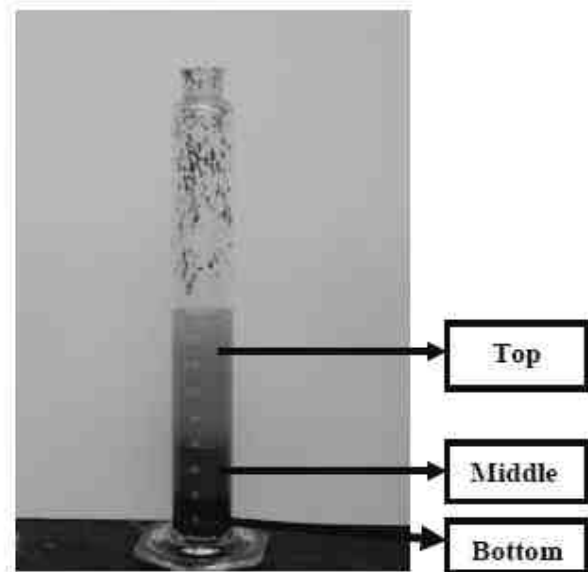


Figure 3. Sedimentation of WIP MFT after 2 days of flocculant addition.

Thermogravimetric analysis was used to measure the amount of organic content on the solids in the top and middle layers. Figure 5 shows the percent weight loss of the particles as a function of temperature. The temperature was increased from 30°C to 900°C at rate of 10°C /min. The solids samples were taken from the top and middle layers after 20 hours, 46 hours and 6 days of settling to investigate the change in the organic content of each phase with time.

Figure 5 shows that the amount of organic material on the solids in the top and middle layers obtained after 20 hr of sedimentation is nearly the same. On the other hand, the amount of weight loss in the top and the middle phase after 46 hours and 6 days shows the increased concentration of organic content in the solids from the top layer with increasing the settling time.

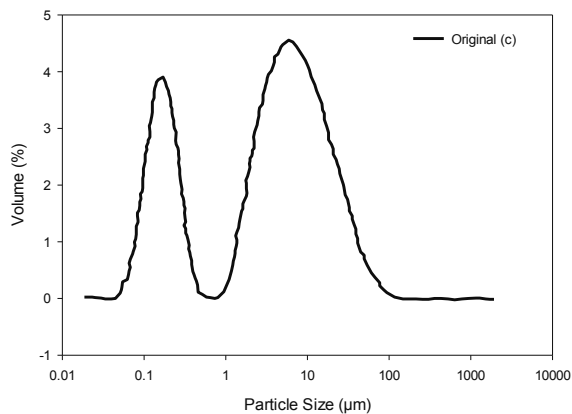
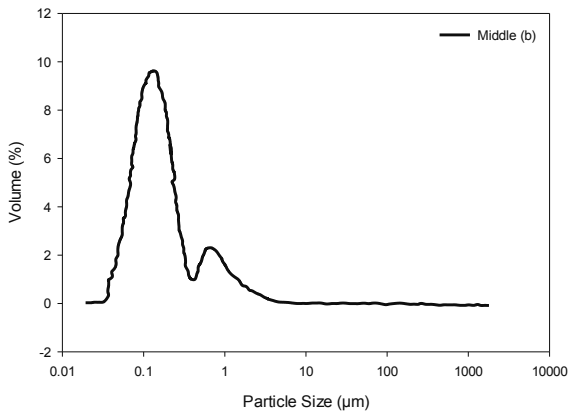
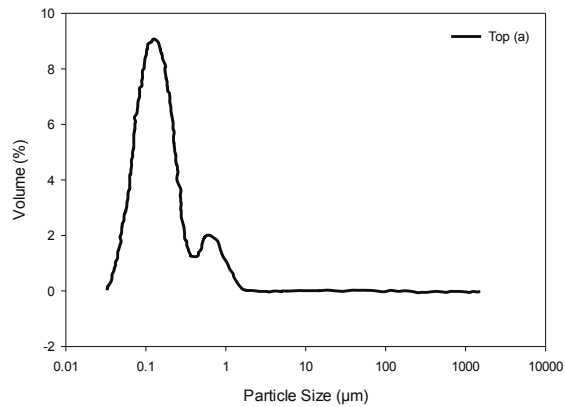


Figure 4. PSD of particles in the (a) top and (b) middle layers (separated due to flocculant addition to WIP MFT) and (c) original WIP MFT.

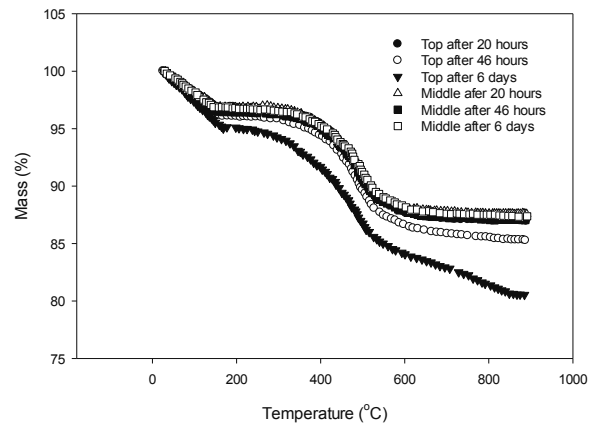


Figure 5. TGA analysis of solids from the top and middle layers (separated due to flocculant addition to WIP MFT) after 20 hr, 46 hr and 6 days of settling.

Although the particles in the top and the middle layers have the same PSD, it appears that the difference in the organic content makes them settle at different rates. Compared with solids in the middle layer solid particles in the top layer have slower settling rate possibly due to their poor response to flocculant addition as a result of higher organic content. It could also be that the effective solids density is affected by the organic matter or the presence of surface slippage.

Comparisons between solid particles from the top and middle layers and physically fractionated light and dark fine particles

As shown earlier in Figure 3, three different layers were formed after settling of the MFT slurry upon flocculant addition. The solids in the top and middle layers are fine particles. The fine particles in the MFT can also be separated using the method described in section 3.3.1. For this purpose physical fractionation was done by dilution, sieving and centrifugation. The resulted fractions were named light and dark fine particles according to their colours. The particle size distribution, the XRD patterns and the TGA analysis results of these two fractions and the ultra-fine solids from the top and the middle layer are compared in the following sections.

Comparison of the XRD patterns of light and dark fine particles with solid particles from the top layer

XRD patterns of light and dark fine particles show the presence of a variety of minerals. Background scattering is an issue which makes the interpretation of the patterns more difficult. This background scattering is supposed to occur in XRD patterns due to the presence of amorphous compounds such as those described by Majid et al. [6]. To solve this problem, particles were treated with low temperature plasma asher (LTA). Organic material in light and dark fine particles and the solids from the top layer were removed via 10 cycles of LTA with a power of 50 watt and duration of 30 minutes.

Siroquant X-ray diffraction analysis software was used for quantitative analysis of minerals in light and dark fines as well as fine particles separated from the top suspension of the cylinder. These results are presented in Table 1.

Table 1. Quantitative XRD (wt%) of light and dark particles (fractionated by centrifugation from WIP MFT) and solids from top layer fines (separated due to flocculant addition to WIP MFT)

	Kaolin	Illite	Quartz
Dark fines	8.2	91.5	0.3
Light fines	37.5	56.5	6
Top layer fines	14.1	71.5	14.3

Comparing the mineral contents of light and dark fine particles in Table 1 suggests a higher amount of illite in the dark fine particles and higher amount of kaolinite in the light fine particles. The solids from the top layer would be mostly a mixture of the particles similar to the dark and light fine particles.

Comparison of the TGA analysis results of light and dark fine particles with solid particles from the top and the middle layers

Figure 6 shows the TGA results for light and dark fine particles. This graph indicates the presence of higher amount of organic material bounded to the dark fine particles. Comparison between Figure 5 and Figure 6 suggests that the particles in the top layer are mostly similar to the dark fine particles as

they have higher organic content in comparison with solids from the middle layer.

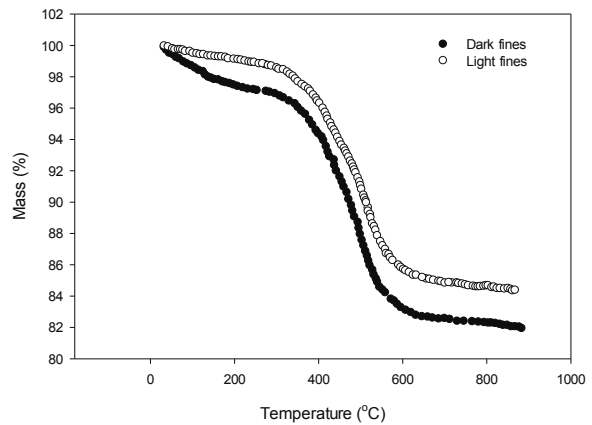


Figure 6. TGA analysis for light and dark fine particles fractionated from WIP MFT.

Comparison of the particle size distribution of light and dark fine particles with solid particles from the top and middle layers

Comparison between Figure 2 (a) and (b) and Figure 4 (a) and (b) suggests that physically fractionated light and dark fine particles and solid particles from the top and middle layer have similar sizes. All four fractions mostly consist of ultra-fine particles smaller than 0.5 µm.

The comparisons made in Sections 4.1.1 to 4.1.3 suggest that the fine particles in the top and middle layer of Figure 3 are similar to the physically fractionated dark and light fine particles. In other words the particles in the top and middle layer of Figure 3 are mixtures of physically fractionated light and dark fine particles. Comparisons of the TGA analysis results described in Section 4.1.2 also suggest that the amount of particles similar to the dark fines are more in the top layer than that in the middle layer as the solids in the top layer have higher organic content.

Polymer Adsorption

XPS results

As mentioned earlier it seems that the slower settling rate of the solids in the top layer is due to the presence of more organic matters on these solids. Another factor to be considered is the adsorption level of flocculant on the solids in the

top layer. Lower settling rate of the solids in the top layer could also be due to less adsorption of flocculant as a result of lower affinity of hydrophobic organic matter on the surface of organic-rich particles to the macromolecule flocculant. To investigate the adsorption of flocculant (Magnofloc 1011) on the surface of fine particles, rheological tests and XPS analysis were conducted. For these tests, comparisons had to be made between solid particles without polymer (before flocculation) and with polymer (after flocculation). The solids in the top and middle layer

could not be used for this purpose as they were separated from each other due to flocculation by polymer. Thus instead of using these solids, light and dark fine particles were analyzed as there was no flocculant on their surfaces. Magnofloc 1011 is a copolymer of acrylamide $(C_3H_5NO)_m$ and sodium acrylate $(C_3H_3NaO_2)_n$. Changes in the mass concentration of nitrogen can be used as an index of polymer adsorption on particles surface. The results in Table 2 show the mass fraction of nitrogen, oxygen and carbon on the surface of the particles before and after polymer adsorption.

Table 2. Results of XPS analysis on polymer adsorption on light and dark fine particles fractionated from WIP MFT

Peak	Light fine solids		Dark fine solids	
	Without polymer	With polymer	Without polymer	With polymer
Mass concentration %				
O	71.6	60.8	83.2	82.3
N	0.4	0.8	0.6	0.6
C	28.00	38.5	16.2	17.1

As shown in Table 2 the mass concentration of nitrogen is doubled after the adsorption of polymer on the light fine particles but there is no change in nitrogen concentration on the dark fine particles. It can be concluded that the level of polymer adsorption on the dark fine particles is limited in comparison with that on the light fine particles.

Rheological properties of light and dark fine particles before and after polymer adsorption

In order to investigate the adsorption of polymer on surfaces of light and dark fine particles the rheological properties of these solids are investigated in their original state and after the addition of flocculant. The rheological properties of the solids from the top and middle layer (shown in Figure 3) are also compared with the rheological properties of light and dark fine particles.

Viscosities of suspensions of light and dark fine particles before and after flocculant adsorption

The rheological analysis on suspensions of 10 wt% fine particles were conducted by the methods described in Section 3.3.4. Results from the Figure 7 show that the viscosity of the suspension

of dark fine particles is higher than that of the light fine particles. By adding equal amount of polymer (the polymer concentration was adjusted to be 1000 ppm with respect to the solids content of each suspension) to the two suspensions, their viscosities are altered. Comparison between the results in Figure 7 and Figure 8 shows that after flocculant addition, the viscosity of suspension of the light fine particles increased considerably while no change in the viscosity of dark fine particles was detected. This finding supports the hypothesis of a lower flocculant adsorption on the surface of dark fine particles.

Suspensions of 10 wt% of solids from the top and middle layer (shown in Figure 3) were also prepared by the method described in Section 3.3.4. Results from the Figure 9 show that the suspension of solids from the middle layer has higher viscosity than that of top layer. Comparison between the results in Figure 8 and Figure 9 suggests that the solid particles from the top layer are similar to dark fine particles. This finding again supports the hypothesis that the solid particles in the top layer adsorb flocculant to a lesser extent.

Comparison of the elastic and viscous moduli of light and dark particles with particles from the top and middle layers

Strain sweep test results show that the suspension of 10 wt% of dark fine particles (without flocculant) exhibit more elastic properties (G') in comparison with the suspension of light fine particles (also without flocculant) at the same solid concentration. The magnitude of the viscous modulus for these two fractions is similar as shown in Figure 10. A similar test was conducted for the suspensions of solid particles from the top and middle layer of the cylinder shown in Figure 3.

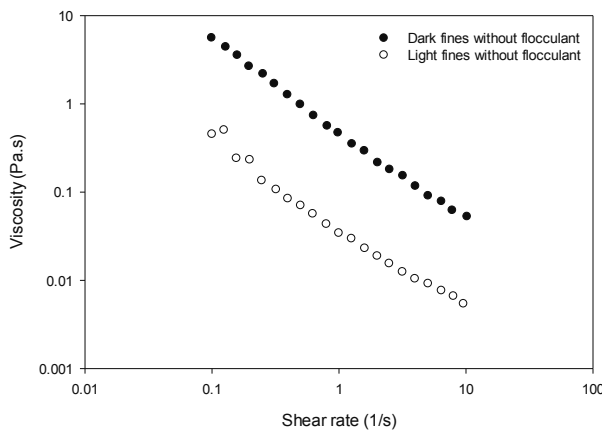


Figure 7. Viscosity of suspensions of 10 wt% light and dark fine particles (fractionated from WIP MFT) before flocculant addition at 25°C.

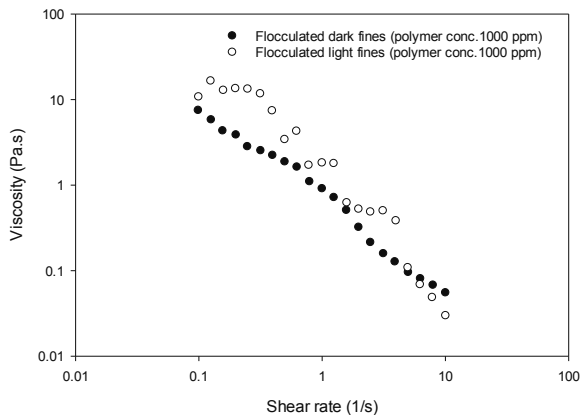


Figure 8. Viscosity of suspensions of 10 wt% flocculated light and dark fine particles at 25°C (fractionated from WIP MFT, polymer concentration 1000 ppm).

The results from Figure 11 suggest that elastic and viscous moduli of the suspensions of solids from the middle layer are higher than those for the top layer by about one order of magnitude.

This finding shows that solid particles from the middle layer (which are similar to light fine particles and contain lower organic content) were highly flocculated, exhibiting higher elastic properties (G') in comparison with solid particles from the top layer (which are similar to dark fine particles and contain higher organic content).

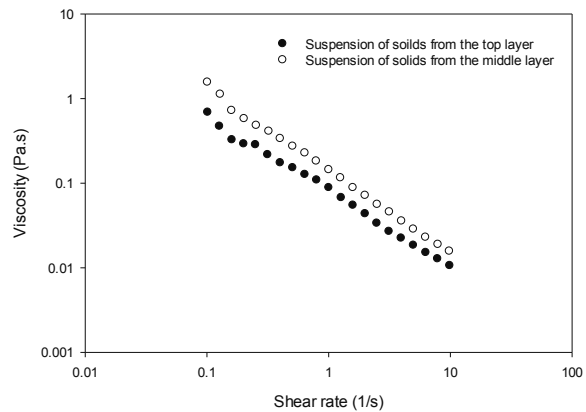


Figure 9. Viscosity of suspensions of 10 wt% solid particles from the top and middle layers (separated after flocculant addition) at 25°C.

Comparison of the gelation rate of light and dark fine particle suspensions (without flocculant) with suspensions of particles from the top and middle layers

Another important aspect in rheological properties of suspensions is the rate of gelation which can be measured by a method known as time sweep test. As mentioned in Section 2.2, ultra-fine solid particles form a gel due to the formation of a structural network. One can measure the gelation rate of the suspensions by pre-shearing them and measuring the rate of increase in elastic modulus after the mixing is stopped. The elastic modulus of 10 wt% light and dark fine particle suspensions was measured for half hour after pre-shearing the suspension for 10 minutes at 100 rpm. Figure 12 shows the rate of gelation for dark and light fine particle suspensions. Result suggests the higher gelation rate of dark fine particles. A similar test was conducted for the suspension of solids from the top and middle layers. Results from Figure 13

show that the gelation rate of the suspension of solid particles from the middle layer is higher than the top layer.

These results are consistent with the results of the viscoelasticity and viscosity measurements described earlier.

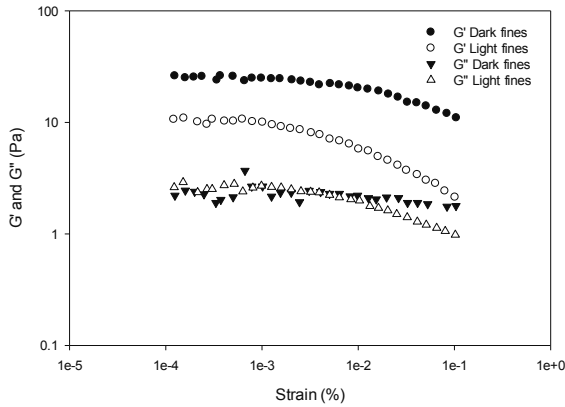


Figure 10. Elastic and viscous moduli of suspensions of 10 wt% light and dark fine particles (without flocculant) fractionated from WIP MFT at 25°C

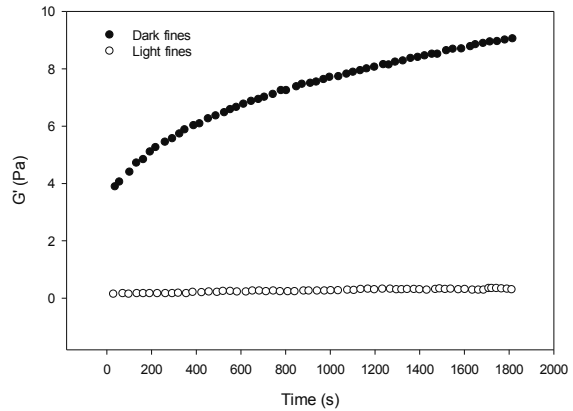


Figure 12. Gelation rate of suspensions of 10 wt% light and dark fine particles (without flocculant) fractionated from WIP MFT at 25°C.

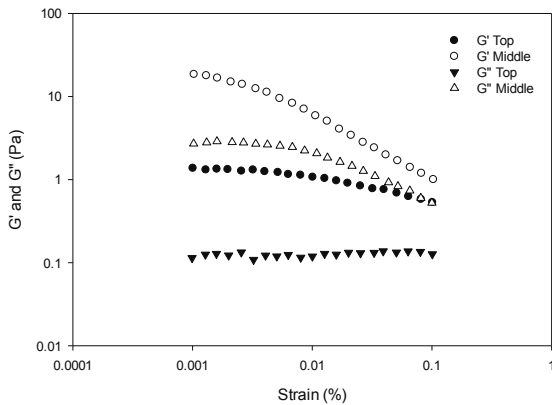


Figure 11. Elastic and viscous moduli of suspensions of 10 wt% solid particles from the top and middle layers (separated after flocculant addition to WIP MFT) at 25°C.

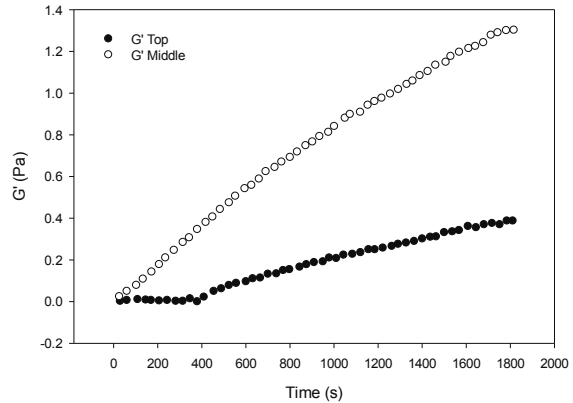


Figure 13. Gelation rate of suspensions of 10 wt% solid particles from the top and middle layers (separated after flocculant addition to WIP MFT) at 25°C.

Comparing the results in Figure 12 and Figure 13 suggests that after the adsorption of polymer, the solid particles containing lower amount of organic material, in the middle layer, exhibit more elastic behaviour and higher gelation rate, while in the original state, dark fine particles, containing more organic material had higher elastic modulus and gelation rate. This again is due to higher degree of flocculation in solid particles from the middle layer.

Cation Exchange Capacity (CEC) for Light and Dark fine particles

The CEC and surface area of the particles are calculated using the following two equations:

$$MBI\left(\frac{meq}{100g\ solids}\right) = \frac{vol.MB \times normality\ of\ MB}{weight\ of\ solids\ (g)} \times 100$$

$$SA \left(\frac{m^2}{g} \right) = MBI \times 130 \times 0.0602$$

The MBI (methylene blue index) for dark and light fine particles is 32.9 meq/100 g solids and 19.2 meq/100 g solids, respectively, and SA (specific surface area) is 257.9 m²/g and 150.5 m²/g for dark and light fine particles, respectively. The higher specific surface areas of dark fine particles than light fine particles after removal of organic material with LTA, suggests smaller average particle size or more porous structure of particles in this fraction.

This finding can also explain the lower settling rate of the fine particles in the top layer of cylinder shown in Figure 3. Without removal of organic matters the dark fine particles appear to have similar particle size to the light fine particles as shown in Figure 2. Thus the dark fine particles with higher amount of organic content respond to flocculant addition much more weakly than the light fine particles.

CONCLUSIONS

The results of this study suggest that fine solid particles of different surface characteristics in MTF respond differently to macromolecule flocculant in the context of flocculation and settling. This response not only depends on the size of particles as described in [7] but also on the presence of organic matter. The organic-rich (dark) particles were found to be richer in illite than organic lean (light) particles, resulting in a lower settling rate than particles of the same size. More importantly, organic-rich ultrafine particles responded to flocculant addition poorly, most likely as a result of lower affinity of hydrophobic organic matters on the surface of the particles to the Magnofloc polymer.

Although the suspension of the dark fine particles has a greater elastic modulus and viscosity than the suspension of the light fine particles in the original state, treating the sample with polymer,

Magnofloc 1011, reversed the situation. Ultra-fine particles containing a higher amount of organic matter, i.e., dark fines have more porous structure in comparison with the ultra-fine particles containing a less amount of organic matter, i.e., light fines.

REFERENCES

- Tu, Y., O'Carroll, J.B., Kotlyar, L.S., Sparks, B.D., Ng, S., Chung, K.H., and Cuddy, G., 2005, "Recovery of Bitumen from Oil Sands: Gelation of Ultra-Fine Clay in the Primary Separation Vessel", *Fuel*. 84(6) pp. 653.
- Kotlyar, L.S., Sparks, B.D., Lepage, Y., and Woods, J.R., 1997, "Effect of Particle Size on Clay Flocculation Behavior of Ultra-Fine Clays in Salt Solutions", *Clay Minerals*. 33 pp. 103.
- Fine Tailings Fundamentals Consortium, 1995, "Advances in Oil Sands Tailings Research", Alberta Dept. of Energy, Edmonton.
- Elimelech, M., 1995, "Particle Deposition and Aggregation: Measurement, Modeling and Simulation", Butterworth-Heinemann, Oxford.
- Hang, P.T., and Brindley, G.W., 1970, "Methylene Blue Adsorption by Clay Minerals-Determination of Surface Areas and Cation Exchange Capacities", *Clays and Clay Minerals*. 18(4) pp. 203.
- Majid, A., Argue, S., Boyko, V., Pleizier, G., L'Ecuyer, P., Tunney, J., and Lang, S., 2003, "Characterization of Sol-Gel-Derived Nano-Particles Separated from Oil Sands Fine Tailings", *Colloids and Surfaces A: Physicochemical and Engineering Aspects*. 224(1-3) pp. 33.
- Yuan, X.S., and Shaw, W., 2007, "Novel Processes for Treatment of Syncrude Fine Transition and Marine Ore Tailings", *The Canadian Metallurgical Quarterly*. 46(3) pp. 265.

OIL SANDS MATURE FINE TAILINGS SPIKING FOR THICKENER APPLICATION

Trong Dang-Vu¹, Reza Salehi² and Scott Ramey¹

¹SNF Energy Services, Canada

² Canadian Natural Resources Limited, Canada

ABSTRACT

The objective of this study is to evaluate the settling behaviour of tailings slurry resulting from blending mature fine tailings (MFT) and flotation tailings (FT) treated with various anionic and cationic polymers. The selected polymers will be used in developing a new method for improving fines capture by adding MFT to a gravity thickener feed (FT). The process performance targets are: 1) thickener underflow with a minimum solids content of 55%; and 2) thickener overflow with a maximum of 0.5% solids. Test conducted by the SNF Technology Development Group Laboratory conclude that these performance targets can be achieved using an anionic polyacrylamide flocculant. Additionally, it was found that a program combining the same anionic polyacrylamide with a secondary addition of cationic flocculant will result in higher sediment solids content, reduced supernatant solids content and wider range of control.

INTRODUCTION

Mature fine tailings (MFT) are one of the biggest challenges for oil sands operations due to their extremely slow settling rate. With an increase in bitumen production, MFT becomes an even more significant problem for the oil sands industry. Many technologies have been developed to treat the MFT on a large scale, for example, beach drying and centrifugation. In addition, filter presses, screw presses, rapid dewatering system, etc. have also been tested on a smaller scale. However, key disadvantages of all these technologies are the requirements for high capital and operational costs. To overcome this, Canadian Natural Resources Limited (CNQ) has been moving forward with contemplating a new concept of adding MFT to the thickener feed to be treated in existing thickeners when the plant SFR would allow. Schematic diagram of CNQ's Horizon thickeners with MFT spiking is given in Figure 1. Thickeners are currently used successfully at oil sands operation

and will be implemented by many other oil sands operators to treat FT and to recover heat from the warm overflow water. This new approach of blending MFT with FT not only reduces MFT inventory, increasing fines capture but also requires no additional cost for new equipment. SNF has partnered with CNQ in developing a chemical treatment solution for this treatment. This paper presents the outcome of this flocculant screening investigation, focusing on CNQ's specific blending recipe given in Table 1.

METHODOLOGY

Material

MFT, FT and process water samples were provided by CNQ and their characteristics are given in Table 2. Due to low solids content and SFR, part of FT sample was screened for sand fraction which was used later to blend back with FT to generate a new FT sample with required solids content and SFR. For the test the new FT sample was diluted down to 10% using supplied process water. This diluted sample is referred to as thickener feed.

SNF's flocculant products with different ionicity, charge density, molecular weight and molecule structure were used in this evaluation. In total, eight anionic products and four cationic products were tested. Properties of the selected anionic flocculant and cationic flocculant were given in Table 3. The selected anionic, Flopam® A-3332, outperformed other anionic products. Solutions of anionic and cationic flocculants were prepared at 0.4 wt.% using process water.

Procedure

For each test one litre of thickener feed was poured into a 1 litre beaker. A given amount of polymer solution was added, followed by mixing. Two stages of mixing were conducted at high speed, 300rpm, and low speed, 40rpm, using a portable

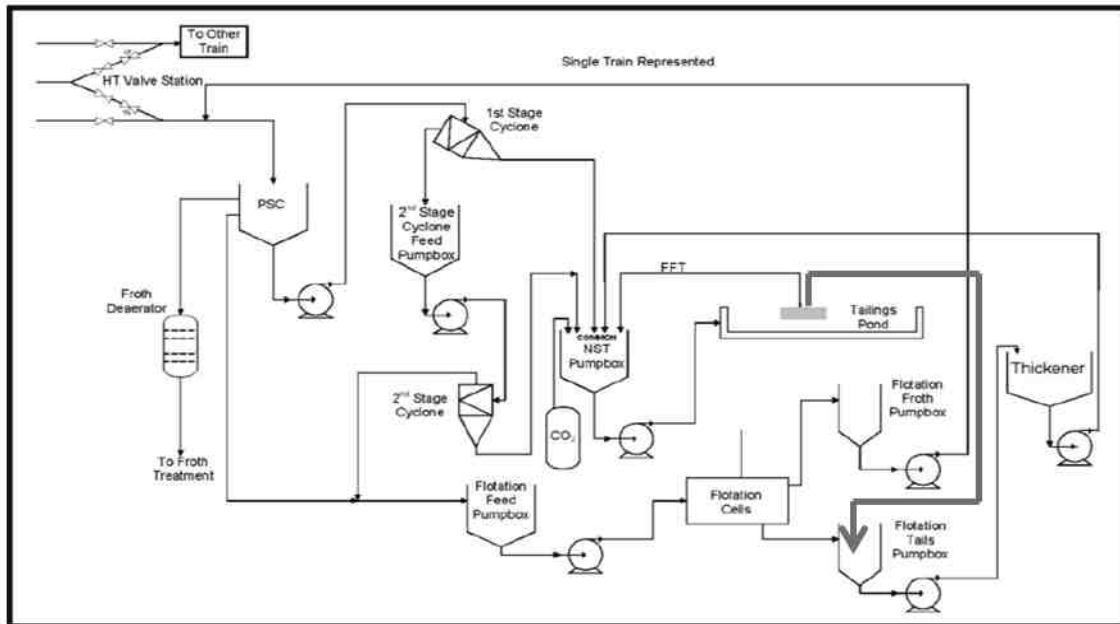


Figure 1. MFT spiking of Horizon thickeners schematic diagram

mixer equipped with a paddle-mixing blade. After mixing, the treated material was allowed to settle for 5 minutes and the solids content of overflow and compaction (density) of underflow were determined. The measurements of overflow solids and underflow density were repeated at 60 minutes after mixing, i.e. 55 minutes after the first measurement.

RESULTS AND DISCUSSION

Settling test results

Snapshots of treated thickener feed at different mixing times were given in Figure 2. Prior to polymer addition, the mineral solids were uniformly dispersed in suspension (Figure 2.A). Polymer was then mixed with the thickener feed at high rpm creating large flocs (Figure 2.B). Under this mixing condition the flocs sheared forming smaller flocs, which settled quickly when the mixing speed was reduced (Figure 2.C). Low speed mixing improved compaction of sediment (Figure 2.D).

Supernatant quality and sediment compaction for the Flopam® A-3332 addition at dosage of 150 g/t were illustrated in Figure 3. As can be seen, the solids content of supernatant was around 0.5 wt.% and it was independent of settling time. However,

the solids content of sediment improved significantly with time. Sediment's solids content increased from 46 wt.% for 5 minutes of settling to 54 wt.% after 60 minutes of settling. These results also indicated that the Flopam® A-3332 met the performance targets.

Results presented in Table 4 indicate an improvement of settling performance with additional cationic flocculant with different mixing times in two cases. In the first case, the Flopam® NRG 2880 produced very high quality overflow OF 0.2 wt.% solids but lower sediment density (45 wt.%). Note that process water used for preparing polymer solution contained the same solids content of 0.2 wt.%. In the second (lower) case, the supernatant quality was lower than the first one, but the sediment compaction increased significantly. Without cationic addition, the sediment solids content was around 50% while with 100 g/t of cationic addition, it increased to 65%. These results suggest a potential opportunity for thickener operation to produce a very high overflow quality or a very high underflow density.

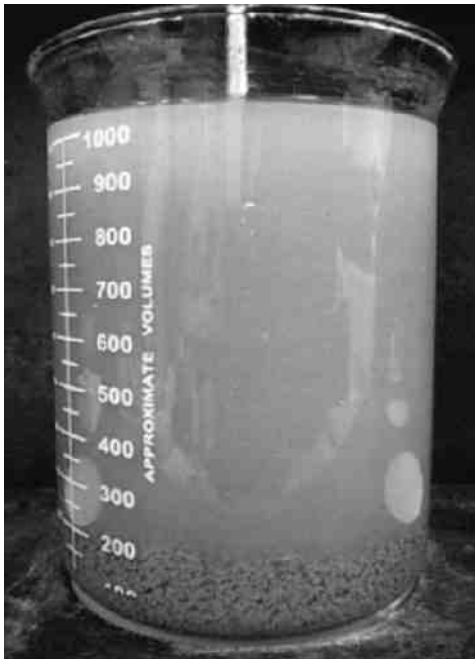
Figure 4 represents a relationship between overflow quality and cationic product dosage. A higher cationic product dosage results in a higher supernatant quality (lower solids content).



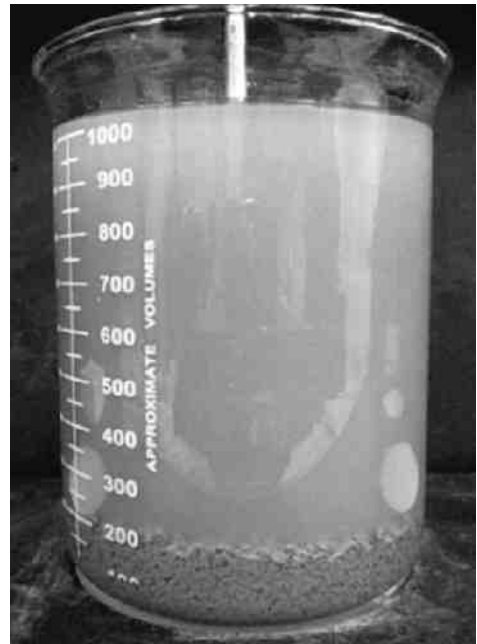
Before polymer addition



B. Polymer addition at high rpm mixing



Polymer addition at low rpm mixing



D. After mixing

Figure 2. Snapshots of treated thickener feed at different mixing time

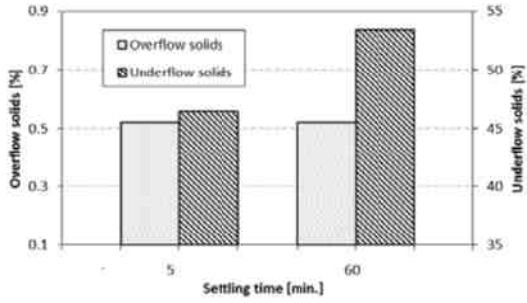


Figure 3. Overflow and underflow solids with Flopam® A-3332 addition

CONCLUSIONS

Based on the results and discussion presented above, the following conclusions can be drawn:

- Supernatant and sediment solids contents targets were achieved using a single SNF's anionic flocculant, Flopam® A-3332, at dosage of 150 g/t.
- Addition of cationic flocculant improved supernatant clarity and sediment density.



Figure 4. Overflow quality as function of cationic product dosage

Table 1. CNQ's blending recipe

Sample name	SFR [wt/wt]	Solid content [wt.%]	MFT/FT solids ratio [wt/wt]
Fall average (FA)	1.35	29.26	0≤MFT/FT solid ratios≤0.14

Table 2. CNQ's blending recipe

Sample	Solids content [wt.%]	Fines content [%]	SFR [wt/wt]	pH
MFT	33.3	97	0.03	7.8
FT	14.5	57	0.75	8.2
Process water	0.2	N/A	N/A	7.9
Sand (from FT)	100	0	N/A	N/A

Table 3. Properties of the selected products

	Flopam® A-3332	Flopam® NRG 2800
Molecular weight	Low	Very low
Ionicity	Anionic	Cationic
Charge density	Medium	Very high

Table 4. Effect of cationic flocculant addition on performance

A-3332 dosage [g/tonne]	NRG 2880 dosage [g/tonne]	Supernatant solids [%]		Sediment solids [%]	
		5 min.	60 min.	5 min.	60 min.
150	100	0.2	0.2	44.3	44.3
150	100	0.4	0.4	60.5	64.1

Session 13

Instruments and Parameter Measurement Techniques

SOIL PARAMETER ESTIMATION AND SAMPLE COLLECTION USING AN UNMANNED GROUND VEHICLE

Nicolas Olmedo and Mike Lipsett
University of Alberta, Edmonton, Alberta, Canada

ABSTRACT

Robotic systems can be integrated into industrial operations as part of autonomous ground surveys for environmental monitoring. In this paper we present the design and development of a prototype mobile robot for characterizing soft soil deposits. A mobile platform was modified for wireless teleoperation on rough terrain. Drilling and sampling payloads were designed to collect subsurface samples from deposits with a hard top layer. These payloads were integrated into the prototype with a sample collection capacity of 1500 cubic cm at up to 3 meters depth. The prototype was instrumented for terramechanics studies. The cohesion stress and internal friction angle of the terrain can be estimated using slip-based models of the wheel-soil interaction. The functionality of the prototype was tested in laboratory and outdoors settings.

INTRODUCTION

Unmanned ground vehicles (UGVs) have been used to explore environments that are not accessible to workers. There have been advances in the technologies and methods required for sample collection and soil parameter estimation using UGVs. Lunar prospective platforms have been developed to traverse loose soil and capture rock samples autonomously (Wettergreen *et al.*, 2010). Freitas *et al.*, developed an amphibious mobile platform for environmental monitoring in the Amazon basin (Freitas *et al.*, 2011). Other studies have used methods for soft soil parameter estimation to characterize unknown terrains (Yoshida, 2003).

Technologies and methods developed for planetary exploration with autonomous robots and payloads can be used to study industrial environments that are too dangerous or costly for manual data collection. Industrial operations on surface-mineable deposits create large amounts of tailings which do not readily consolidate. Variations

in soil strength can lead to sinking of equipment and vehicles. The need to determine the trafficability of the terrain drives the requirement of accurate and low-risk estimates of key soil parameters (Lipsett *et al.*, 2009). In this paper we present the development of a prototype robotic system for soft soil sample collection and parameter estimation.

PROTOTYPE DEVELOPMENT

The UGV prototype is composed of four main subsystems: (1) mobile platform, (2) drilling mechanism, (3) sampling mechanism, (4) instrumentation for terramechanics studies. A schematic of the subsystems and components is presented in Figure 1. In the following subsections we discuss the details of each subsystem and their interactions.

Mobile Platform

The Husky-A200, made by Clearpath Robotics (Clearpath-Robotics, 2014), is an electric skid-steer (differential drive) platform (Figure 2). Its chassis is made of two aluminum C-channels supported by a bottom and side plates. The C-channels provide the support and rigidity for the locomotion mechanism. Standard T-slotted aluminum railings are fixed to the top of the chassis to provide mounting points for additional payloads (Figure 3).

Each side of the robot uses a MMP S22-346F-24V brushed DC motor to drive both wheels with a belt transmission. The motors have a rated continuous torque of 172 in-lbs and a peak rated torque of 443 in-lbs. The maximum speed of the motors is 57 rpm. US-Digital E2 rotary encoders are used to measure the speed of the motor shaft. The resolution of the encoders provides over 320000 pulses per revolution (1024 steps quadrature encoder with a gear ratio of 78.71:1). The maximum speed of the platform is approximately 1 m/s with 330 mm diameter wheels.

Each motor is controlled by a Stellaris Brushed DC Motor Controller. The motor controllers can be interfaced by industry standard remote control (RC) servo type (pulse width modulated) interface, Controller Area Network (CAN) interface and RS232 serial interface. The motor controllers use the motor encoder inputs to modulate the voltage

supplied to the motors. Open-loop and close-loop controls are possible. Additionally, the motor controllers provide sensory feedback including motor position, speed, current and input voltage. Actuator temperature is measured using a K-type thermocouple fixed to the motor enclosure.

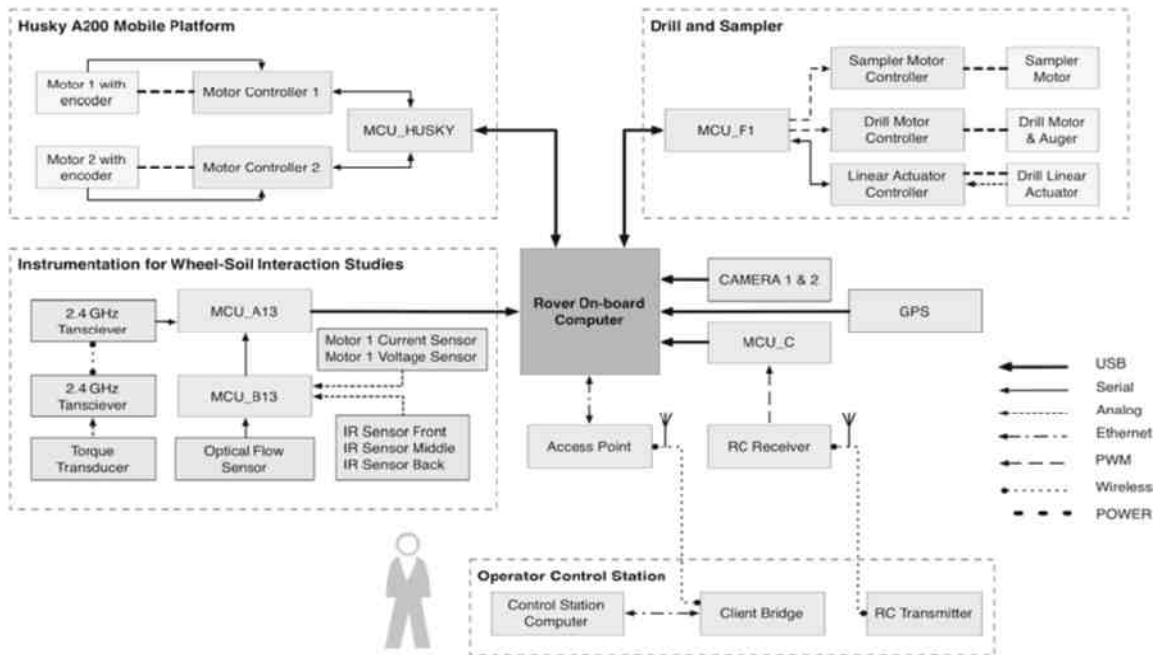


Figure 1. Schematic of the prototype's subsystem and components.

The mobile platform has a dedicated 24 V 20 Ah sealed lead-acid battery. The battery power is managed by a micro-controller unit (MCU) that triggers relays to connect or disconnect power to the motors. An emergency-stop button can be used to disconnect the motors at any time. The MCU also monitors battery voltage levels and current. The MCU board interfaces with the mobile platform's motor controllers and an on-board computer using an RS232 serial interface.

The Husky-A200 mobile platform has been tested in outdoors environments extensively. Under normal operation, the runtime of the system is approximately 4 hours. Under heavy operation, the runtime can decrease to 2 hours.

Modifications to the Mobile Platform

The mobile platform was modified to be able to carry additional payloads and traverse soft deposits. The modifications included a redesign of the electronics bay, the construction of a structural

frame on top of the rover, and improvements to the locomotion system.



Figure 2. Husky A200 mobile platform.

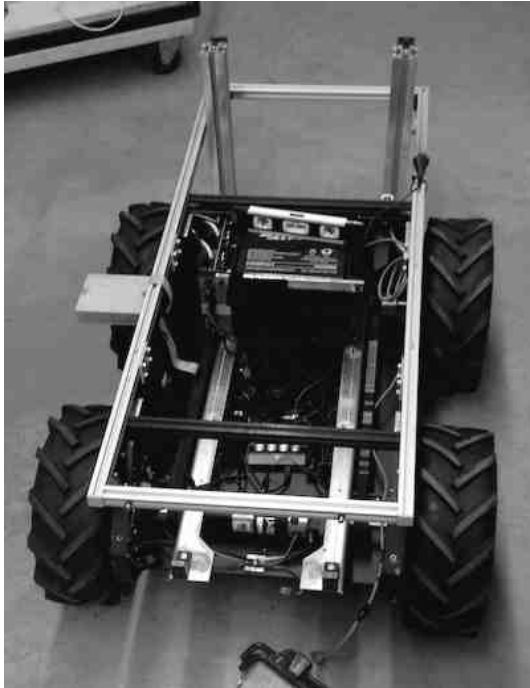


Figure 3. Husky A200 chassis.

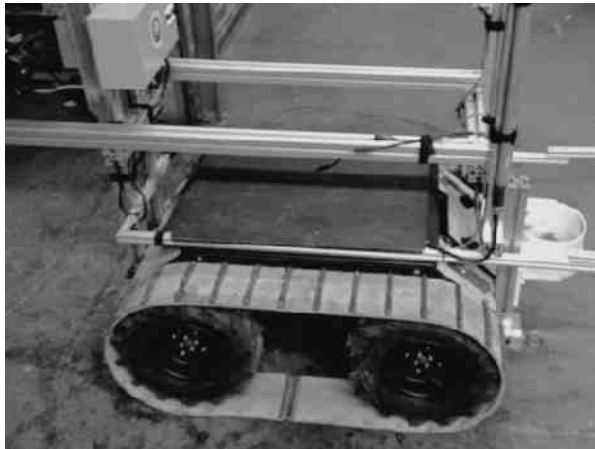


Figure 4. Modified Husky A200 with tracks.

We redesigned the electronics bay inside the chassis of the robot to accommodate for an on-board computer, an additional battery, and other electronics. The C-channels along the chassis are used to support a metallic structure that holds the on-board computer, and the additional battery.

A P8H61-I ASUS motherboard was selected as the on-board computer. The Mini-ITX form factor allows for a high performance computer to be easily integrated into the platform. It uses an Intel Core i7 processor and has 4GB of DDR3 RAM

installed. The computer is powered by the 24 V battery and is enclosed in a stiff metallic shell. A solid state drive is used to increase reliability in high vibration environments. An additional 12 V 10 Ah lead-acid car battery installed inside the electronics bay supplies power to high current devices. Having an extra battery increases the operating time of the platform and payloads.

We built a high strength and stiffness aluminum structure that supports the payloads used for collecting samples. Stiffness and strength are necessary to transmit the vibrations that can occur while conducting high reaction forces operations such as drilling and sampling. Vibrations can also occur while traversing uneven terrain. The frame is made of standard T-slotted aluminum framing of 40 mm and 20 mm. The frame design allows the payloads to be mounted on the front and back of the robot, keeping the centre of mass close to the centre of the vehicle.

Lower ground pressures are required for the robot to traverse low bearing strength deposits. We built tracks that increase the surface area under the robot (Figure 4). They are made using styrene-butadiene rubber (SBR) flat belts around the tires. The belts are cut to length and the ends are joined using alligator clips. To increase traction, V-belts are riveted across the flat belts every 3 inches. This design is quick and inexpensive to manufacture and is easy to mount to the existing platform. To put the tracks on, the robot's tires are deflated and the tracks are wrapped around the wheels. Once the tracks are aligned with the wheels, the tires are inflated to 20psi. Preliminary testing over pavement, compacted soil, loose soil, and grass demonstrated that no slipping or misalignment occurs between the tires and the tracks.

Drilling Mechanism

In many cases, a hard dry layer of material on the surface of the deposit prevents the collection of samples from the subsurface unconsolidated material. The dry material is usually referred to as a crust. A drilling mechanism is required to make a hole through the crust of a deposit to allow other equipment into the unconsolidated material.

We designed a drilling mechanism that drills holes through hard dry soil. It is mounted on and controlled from the rover (Figures 5). It consists of an electric motor mounted on a vertical linear actuator. A retrofitted brushless motor from an electric ice auger is used. An electronic speed

controller is interfaced with an MCU on-board the mobile platform to control the motor. The MCU modulates a signal to communicate on/off commands to the motor controller. A switch was mounted on the handles of the motor for manual on/off control. A 40 V lithium-ion battery mounted on the motor enclosure supplies power to the brushless DC motor. The battery is designed for high current applications in low temperature environments.

The motor is attached to a four inch diameter earth auger (Figure 6). The auger has a usable length of 2 ft. A plastic guard is mounted around the auger to prevent accidents during operation. The plastic guard also prevents the auger from slipping off its axis of rotation while it is in contact with the ground. At this point, no speed or torque feedback is used to control the drill.

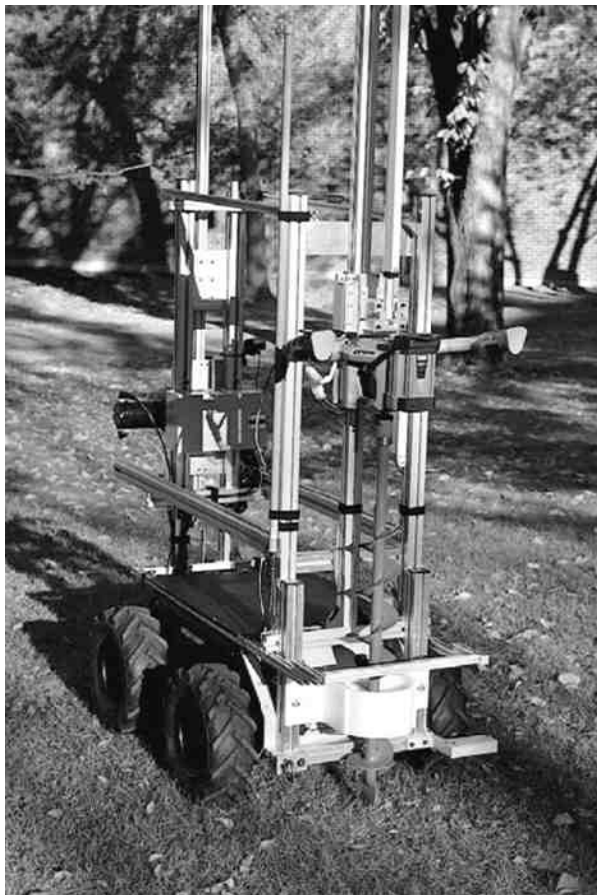


Figure 5. Drilling mechanism mounted on the aluminum frame.

The drill is mounted on a vertical electric linear actuator. The linear actuator has a maximum extension of 2 ft and can produce up to 150 lb of weight on bit on the auger. Preliminary laboratory experiments confirmed that this force is sufficient to drill through dry soils. The linear actuator is supported by linear bearings for T-slotted framing; they prevent the motor assembly from rotating due to high reaction torques. A DC motor controller is used to control the vertical position of the drill. The linear actuator has an internal variable resistor that is used as a linear potentiometer. The analog position feedback is required by the MCU as part of the input to a PID controller to control the linear actuator. The PI controller proved to be sufficient as the velocity of the linear actuator is very small.



Figure 6. Earth auger and brushless DC motor mounted on linear actuator.

Sampling Mechanism

A sampler mechanism was designed to collect soft material samples from up to 3 m depth. It consists of a sample container that is lowered into the deposit by a rack and pinion linear actuator (Figure 7).

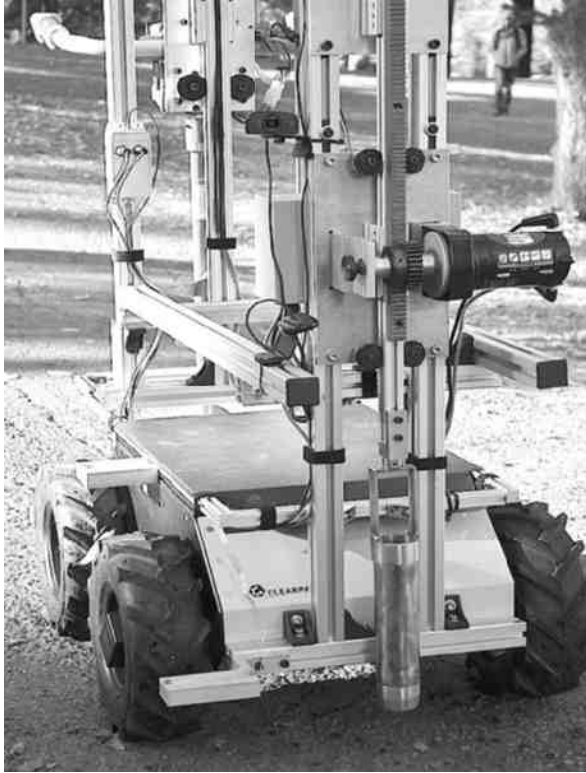


Figure 7. Rack & pinion sampler mechanism.

The sample container is designed to allow soft material to flow through it as it is lowered through the deposit; one-way valves capture the sample as the tool is raised. A plastic tube is placed inside the sampler to contain the captured material. This tube can collect samples with a volume of 1500 cubic cm. The plastic tube can be capped and be used to transport the sample with minimal disturbance.

A potential problem of the sample container is that hard or dry soil can obstruct it and prevent material flow. One way to mitigate this problem is to improve the design of the container and replace the one-way valves with an actuated mechanism. The mechanism would keep the container closed as the sampler is lowered, and will open it when the sampler has reached the sampling depth. Work on this design improvement has already been conducted, but further testing is still required.

Visual feedback to the operator is required to successfully operate the sampler. A front facing video camera is required to navigate and position the robot on the sampling location. In many deposits it is required to drill a hole through a hard surface layer to be able to reach the soft material under it. A second video camera is used to align the sampler to the hole. This camera points at the sampler's point of contact with the ground, giving the operator a direct view of the sampling process.

Terramechanics Modeling

Terramechanics models are used to study the stresses generated under a wheel moving over soft soil (Bekker, 1969). Slip-based models can be implemented to estimate the cohesion stress and internal friction angle of the terrain. From these parameters the drained shear strength of the soil can be calculated using Coulomb's equation:

$$\tau_{max} = c + \sigma_{max} \tan(\phi) \quad (1)$$

where c is the cohesion stress, ϕ is the internal friction angle, and σ_{max} is the maximum normal stress on the soil. Previous studies have simplified quasi-static models and estimated key soil parameters using a linear least-squared method (Iagnemma *et al.*, 2004). The simplification yields an equation of the form:

$$A = c - B \tan(\phi) \quad (2)$$

Where A , and B are functions of the wheel geometry, linear velocity, angular velocity, sinkage, normal loads and torques. The details of this equation and estimation method have been summarized in previous studies (Olmedo *et al.*, 2012).

Instrumentation for wheel-soil interaction studies

In order to implement the least squares estimation of cohesion stress and internal friction angle using equation 2, the values of A and B are required. This motivates the measurement of the wheel's linear velocity, angular velocity, sinkage and torque. The wheel geometrical parameters are known, and the normal load of the wheel is assumed to be constant and is calculated from the robot's weight distribution on flat terrain.

The front-right wheel of the prototype is instrumented to obtain the measurements required. The angular velocity of the wheel is

calculated using quadrature encoders on the axes of the motors; the linear velocity is estimated using an optical-flow sensor mounted over the wheel's track; the sinkage of the wheel is measured using infrared distance sensors. We developed a wireless torque transducer that measures the torque applied to the wheel. It is composed of a balanced Wheatstone bridge to measure the strain in the shaft of the wheel, a signal amplifier and a wireless transmitter. A wireless receiver is mounted inside the electronics bay and interfaces with an MCU. The MCU collects the measurements and transmits them to the on-board computer for processing.

TELEOPERATION AND CONTROL

Software

All software for the prototype was developed using the Robot Operating System (ROS). ROS is a set of software modules and tools that are commonly used in mobile robotics. ROS is open source and has an active community of developers. It is a meta-operating system which provides a hardware abstraction layer, package management and communication between processes (Quigley *et al.*, 2009). ROS software modules, called nodes, are used to create modular systems. Nodes can send information to other nodes using standardized messages sent through topics. Nodes can subscribe or publish messages to topics. In general, nodes do not need to be running in the same computer, but can be distributed over several computers running ROS in a local area network (LAN). The functionality of the rover is divided into interchangeable modules. Each module is tested independently before being integrated into the main platform's application. The main nodes developed are: rover motion control, controller selection, drill and sampler control, and sensory feedback interfaces. The built in ROS logging feature is used to record all information transferring between nodes. All measurements, states, commands and triggers are logged during operation. We can use ROS to replay this information or export it to other formats for analysis.

Operator Control Station

The successful operation of the rover relies on the communication link between the operator control station (OCS) and the robot. The OCS is composed of a computer, a client bridge and an

RC transmitter. We use redundant communication links to transmit motion commands to the rover. The first link is a 802.11g 2.4GHz wireless link with high bandwidth. A wireless access point is installed on the rover to create a LAN to connect the rover's computer and other wifi-enabled devices. A client bridge is used to connect the OCS computer to the LAN network. A high gain antenna is used to increase the wireless range to approximately 150 m. All the operator's commands to the platform and all the sensory feedback from the rover are transmitted through this link. Video feedback from the rover is transmitted in real time with unnoticeable delays. The operator uses a joystick and keyboard to input commands to the OCS computer; these include motion commands, emergency-stop triggers and control actions for the drilling and sampling mechanisms.

A secondary communication link between the rover and the OCS is implemented to maintain control of the robot even after a failure of the main link. This backup communication link consists of a standard 2.4GHz RC transmitter and receiver. The RC inputs are mapped to velocity commands for the mobile platform and emergency triggers. No sensory feedback can be transmitted back from the rover. The teleoperation software module running on the robot's computer is designed to monitor the status of the main communication link. If the main link fails or timeouts, the robot's payloads are retracted from the ground automatically, allowing the operator to use the secondary communication link to drive the robot back to safety. A steel cable is attached to the chassis of the robot so that it can be retrieved in case of wheel actuator malfunction or loss of both communication links.

EARLY FUNCTIONAL TESTS

Preliminary testing on an outdoors environment has been conducted to verify the functionality of the mobile platform and payloads. The tests were conducted by teleoperating the mobile robot from a distance, approximately 20 m, and performing a simulated sample return mission. All navigation and payload control was conducted from the OCU using the sensory feedback transmitted from the robot (Figure 8).

The first task of the operator was to teleoperate the rover to a preselected sampling location on a patch of loose soil. Next, the operator tested the drilling mechanism by tuning on the auger and lowering it

by 15 cm into the soil (Figure 9). Then, the operator lifted the drill and repositioned the robot to align the sampler with the hole (Figure 10). The repositioning was successfully completed using the visual feedback from the on-board cameras only (Figure 11). The functionality of the sampler container was tested with saturated sand in a laboratory setting. The mechanism was successful in capturing material that could flow through the one-way valves as the tool was lowered.



Figure 8. Teleoperation of the robotic system.



Figure 9. Drilling mechanism on loose soil.

CONCLUSIONS AND FUTURE WORK

A robotic system was designed for the characterization of soft soil deposits. We presented the developments of the technologies necessary for subsurface sampling and soft soil parameter estimation. We detailed the modifications required to a mobile platform and discussed the design and development of mechanisms for drilling and collecting samples. The challenges with



Figure 10. Sampler mechanism repositioned.



Figure 11. OCS view of the sampling process.

teleoperation and control of the system were also presented. Preliminary outdoors testing was conducted to show the feasibility of the system.

Near term future work will focus on improvements in the ergonomics of the mobile platform. These would include handlebars for ease of transportation and visual signals for alerting people when the robot is operating. Longterm objectives include the development of a multi-sample

mechanism to be able to collect up to 12 samples per trip. Fieldwork would include mapping a soft soil deposit using the technologies presented in this paper.

ACKNOWLEDGEMENTS

Financial support is gratefully acknowledged from the Natural Sciences and Engineering Research Council of Canada (NSERC) and the University of Alberta. The authors wish to thank the Mechanical Engineering Machine Shop staff for their technical support.

REFERENCES

M. G. Bekker, *Introduction to Terrain-Vehicle Systems*. Michigan: University of Michigan Press, 1969.

Clearpath-Robotics, "Husky," www.clearpathrobotics.com/husky/, 2014.

G. Freitas, F. Lizarralde, L. Hsu, V. Paranhos, N. R. S. dos Reis, and M. Bergerman, "Design, modeling, and control of a wheel-legged locomotion system for the environmental hybrid robot," in *Proceedings of the IASTED International Conference*, no. CMU-RI-TR-, November 2011.

K. Iagnemma and S. Dubowsky, *Mobile Robots in Rough Terrain Estimation, Motion Planning, and Control with Application to Planetary Rovers*, ser. Springer Tracts in Advanced Robotics. Springer Berlin / Heidelberg, 2004, vol. 12.

M. Lipsett and S. Dwyer, "A robotic system to characterize soft tailings deposits," in *Proceedings of Mine and Tailings Waste Conference 2009*, Banff Alberta, November 2009.

N. Olmedo and M. Lipsett, "Oilsands tailings characterization using a robotic system," in *Earth and Space 2012*, K. Zacny, Ed. American Society of Civil Engineers, 2012, pp. 1167–1176.

M. Quigley, K. Conley, B. P. Gerkey, J. Faust, T. Foote, J. Leibs, R. Wheeler, and A. Y. Ng, "Ros: an open-source robot operating system," in *ICRA Workshop on Open Source Software*, 2009.

D. Wettergreen, S. J. Moreland, K. Skonieczny, D. Jonak, D. Kohanbash, and J. Teza, "Design and field experimentation of a prototype lunar prospector," *International Journal of Robotics Research*, vol. 29, no. 12, pp. 1550 – 1564, October 2010.

K. Yoshida, "Slip-based traction control of a planetary rover," *Experimental Robotics VIII*, vol. 5, pp. 644–653, 2003.

ROBOTIC SYSTEMS FOR MEASURING PROPERTIES OF TAILINGS DEPOSITS AND COLLECTING SAMPLES

Michael G. Lipsett, Nicolas Olmedo, Benoit Rivard and Ward Wilson
University of Alberta, Edmonton, Alberta, Canada

ABSTRACT

Robotic systems can be used in industrial environmental monitoring to go beyond remote sensing to interacting with the environment. This paper discusses four applications of field robotics for monitoring oil sands tailings processes and post-depositional performance, and describes technology development, results of laboratory experiments, and in some cases field trial results. Several robots are presented that have been used for field surveys, including unmanned aerial vehicles that fly autonomously and can carry very light instrumentation packages. Tooling is described that measures soil properties and acquires surface and subsurface samples. Careful attention is paid to managing risks so that robots do not pose a threat to personnel, and the equipment is not operated when it may be lost in the deposit.

INTRODUCTION

Background

There are many potential applications of robotics and automation technologies in extractive industries, especially in mining and oil & gas. Key areas of application promise improved productivity, reducing environmental impact, and improving safety and reliability. In tailings, the opportunity lies in operation of remote tailings treatment processes involving dredging, pipeline operation, and thickening processes (chemical addition, mechanical separation, electrokinetics, or a combination). Automated systems also allow for anomalous conditions to be detected and controlled immediately, mitigating process upsets, leaks, and other risks to the operation.

Coordinated technology development programs are required for integration of automated mining equipment. Some vendors are developing and deploying robotic trucks for surface operations in hard rock mines; and partial autonomy is already

possible underground. There are opportunities in partial and fully autonomous shovels, and in linking production scheduling to path planning for individual machines for blending and optimal material handling. Other applications related to earthmoving are rovers for environmental monitoring, tele-operation and autonomous dozers and scrapers for tailings placement and reclamation, and automatic control of dredges (cable-driven or otherwise actuated) for mature fine tailings removal for treatment. Camera and gas sniff-equipped rovers can be applied for inspection and emergency situation awareness, either as ground vehicles with stair-ladder-climbing capability, or unmanned aircraft. The key challenge is design for reliability in rugged environments (cold, dust, explosion-proof), that are not well characterized – meaning that navigation has to include collision-avoidance, simple operation, with care to integrate autonomous technology into operating environment with explosion hazards and personnel.

Field robotics systems have been in development for many years. They have typically been deployed in extreme environments, such as nuclear plant inspection, industrial firefighting, volcano exploration, and security. These systems tend to be fairly small, wheeled units; but robotic boats and aircraft have also been used for monitoring of remote locations. To date, field robots have been used almost exclusively to measure what is going on in a hazardous environment. But new developments allow these systems to perform useful work.

Mission Profile & Measurement Requirements

With such a range of possible applications, it is important to choose missions where there is an advantage to adding the complexity of instrumentation packages and control systems. Those scenarios are typically ones where it is unsafe or very expensive to have people doing the work. Simply modifying equipment to be operated remotely seldom has a big advantage. Automation instead allows for very different ways of achieving

a task, because there is not the limitation of having to have a human on board.

The focus of our investigations to date have been to make measurements of soil characteristics using noncontact optical techniques, to deploy tools to take measurements of soil strengths, and to collect samples to bring back for analysis.

Oilsands tailings deposits can have highly variable shear strength. Even engineered tailings that have been densified may be prone to liquefaction when subjected to a dynamic load. For this reason, it is not currently possible to monitor the depositional performance of fresh soft tailings deposits without some risk to personnel. The near-term goal of

robotic systems development for tailings monitoring is to demonstrate the use of robotic vehicles to navigate on very soft terrain and collect information on the geotechnical properties of the terrain. This project entails two technology areas: vehicle design and navigation with stable control on soft ground conditions (up to and including saturated soils with no bearing strength), and design and integration of instrumentation to measure surface properties as well as access a subsurface zone and estimate soil properties on a periodic basis for navigation and mapping.

Four mission types are of interest when deploying a robot on a tailings structure. Key technology elements of a mission are illustrated in Figure 1.

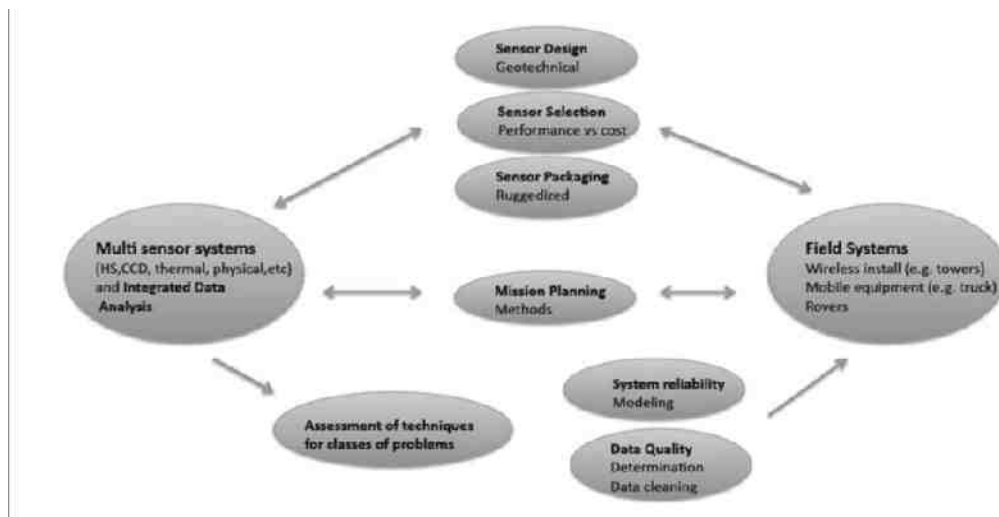


Figure 1. Elements of a Soil Characterization Program Using Remote Sensing & Robotics

To map the characteristics of a tailings structure, a robot can traverse the terrain. This is harder than it sounds, because locomotion on soft tailings can be very difficult when the shear strength is very low. A robot can estimate the properties of the soil, by measuring forces and torques, sinkage, and motion while interacting with the mud or soil. Soil parameters estimated can then be mapped using the robot's navigation system. For unmanned vehicles that operate on saturated soils, the vehicle must be buoyant; and the machine must be capable of freeing itself when stuck.

Second, a robot can collect surface and subsurface samples from the deposit. Robotic tooling can be used to make preliminary core sampling surveys for more timely assessment of geotechnical performance, as an adjunct to

conventional sampling campaigns, which are costly and would benefit from having lower accuracy survey to target specific locations for detailed analysis.

Third, a robot can move between pouring locations to watch the process of pouring treated tailings, and use machine vision to detect features that relate to early dewatering performance and to how the deposit will gain strength over time.

Fourth, a robot can deploy instrumentation onto a deposit without putting personnel at risk, and retrieve the instruments at a later time.

This paper describes some of the technological challenges and progress to date in each of these areas, for application in oil sands tailings.

MISSION CONCEPT FOR AUTONOMOUS MAPPING OF OILSANDS TAILINGS PROPERTIES

Amigoni et al., suggest that modern society needs to address problems related to environmental pollution and destruction of ecosystems through large-scale environmental monitoring (Amigoni et al., 2005). They discuss the necessity of efficient and affordable sensor systems that show autonomous and intelligent capabilities. Artificial intelligence (AI) would not only allow perceptive agents to autonomously reconfigure their measurement capabilities to environmental conditions, but also to share data and cooperate with other agents to enhance information gathering (Amigoni et al., 2005). The quality of perception increases with robotic systems that are mobile and work cooperatively.

Advances in navigation and perception allowed robots to conduct autonomous missions in unknown environments. Simultaneous localization and mapping (SLAM) was achieved using LASER, LIDAR and Vision. Computer vision techniques can be used to calculate robot translation and rotation from images. Visual odometry can be more accurate and reliable than wheel odometry, specially when slipping occurs. Probabilistic methods such as Kalman Filters (KF), Extended Kalman Filters (EKF) and Particle Filters (PF) have been used to compute maximum likelihood estimates of position of the robot and landmarks. LASER and LIDAR systems can collect point-clouds to map an environment in three dimensions. High volumes of data are generated and must be processed in real time. These advances were demonstrated in various applications such as underground mine mapping (Nuchter et al., 2004) and simulated lunar mission exploration (Wettergreen et al., 2010).

SLAM allows the robot to interact with the environment in useful ways. A classical example application is museum tour guides (Thrun et al., 1999). In an industrial setting, robotic systems can be used to map areas inaccessible to workers. Besides building a geometric map of the environment, a robot uses other technologies (payloads) to collect georeferenced measurements, such as gas compositions, electromagnetic field strengths, and soil properties. These extra dimensions to the map are important for the study of the environment and to pinpoint locations of interest such as sources of pollution. In

industrial sites, robots collect measurements of variables that determine a process performance or risk. Robotic systems implement AI techniques to identify hazards in multidimensional maps. Additionally, robotic systems remap an area to identify changes on process variables. The gradients of process variables help predict the future states of the process which are evaluated to improve process control.

The process of characterizing an environment is optimized by using perceptive agencies. A perceptive agency is composed of agents that form a multi-sensor cooperative intelligent system (Amigoni et al., 2003). Such a system of agents manages the complexity of environmental monitoring applications, the large number of observations required, and the geographical scale of the operation (Amigoni et al., 2003). Generalized perceptive agencies are constructed from modular agents specialized to a particular application. A simple architecture comprises of a coordinator agent, to manage the system, and multiple explorers, to collect data from the environment. AI routines are used to incorporate all the measurements gathered into a single map, from which specific hazards or other areas of interest can be identified (such as estimating the location of a pollution source). This information can be used to select areas for further studies. Previous work on monitoring electromagnetic pollution has demonstrated that this approach is effective (Amigoni et al., 2004).

Autonomous Unmanned Ground Vehicles (UGVs) can be used to map properties of oil sands tailings deposits. Reclamation processes of industrial sites can be accelerated by understanding sedimentation processes by measuring terrain parameters. Robotic systems can collect information on the geotechnical properties of the terrain without putting workers at risk. Perceptive agencies, as described previously, manage and optimize the environmental monitoring operation and aid workers in geotechnical characterization campaigns. Mission planning, task allocation, and information consolidation are conducted by a coordinator agent. Tailings operator can provide basic inputs to the coordinator, such as the boundary of the deposit to be characterized and the target spacial resolution of measurements. The coordinator will use AI to determine tasks for the rover explorers, and to interpret the information they transmit back. In many cases, not all robot explorers will be the same; limitations on the weight allowable for each vehicle will determine the

payloads that each rover carries. Specialization classes of robot explorers are required.

Robotic Explorer for Tailings Monitoring

A robotic vehicle that explores a tailings area to monitor the structure requires three key features: a low ground pressure locomotion system, a navigation system, and payloads for geotechnical characterization. One such system architecture is shown in the system diagram of Figure 2.

(1) The robot requires a locomotion system that is capable of traversing low bearing strength deposits and possibly saturated soils. Amphibious rovers

have been developed and tested in the Amazon basin, with favourable results (Freitas et al., 2011). These robots primarily move on sandy beaches, mud and over water. It is still undetermined if similar technologies can be used on saturated clays, on which traction needs to be carefully controlled to avoid excessive sinkage and slipping. Low ground-pressure track systems have been built for soils with bearing strengths of approximately 15 kPa and locomotion systems for soils with bearing strengths less than 5 Pa are being developed.

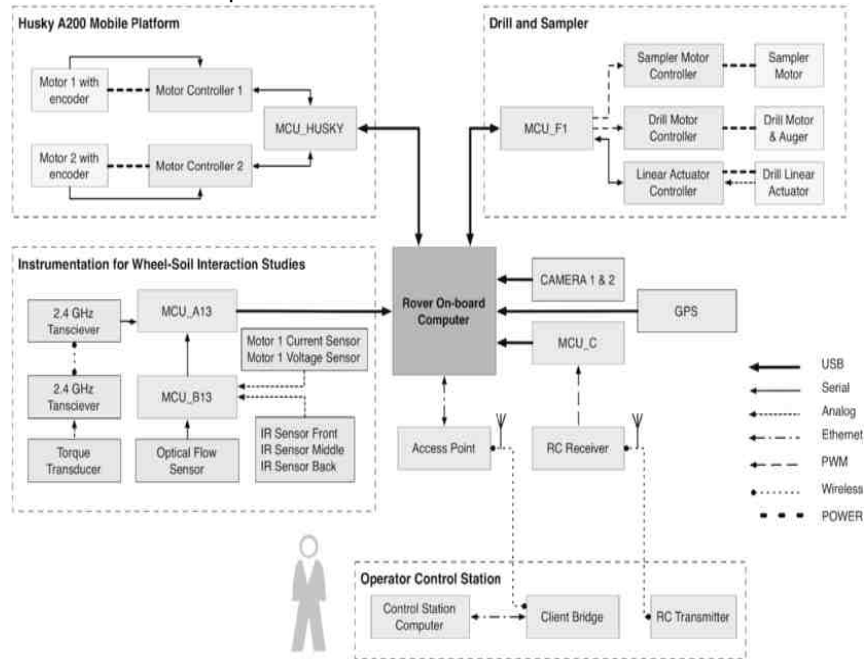


Figure 2. A System Architecture for Rover, Tooling, and Operator Ground Station

(2) An advanced navigation system is required for stable control on soft ground conditions. This system would include path and trajectory planning, geolocation, traction estimation, and ground pressure sensing. Low level controllers are required to modulate inputs to the actuators of the locomotion system to move through the terrain safely. Tailings deposits have high variability in shear strength and can be prone to liquefaction under dynamic loading, therefore it is likely that the robot will get stuck. The navigation system must be able to identify and correct trajectories that might put the robot in danger of becoming immovable, and must include fault recovery routines to free the robot when it gets stuck. Figure 3 shows one

approach to the logical flow of program control for sensing and navigation.

(3) Rover explorers will gather information from the environment using payloads for geotechnical characterization. Previous work has identified tooling for key soil parameter estimation: Fourier Transform Infrared Radiometer (FTIR) for non-contact reflectance spectrometry, automatically controlled penetrometer and shear-vane viscometer for shear strength estimation, and surface & subsurface sample collectors (Olmedo et al., 2012). The rover explorers will deploy these payloads at predetermined locations in the deposit, and cooperatively build a map of key soil

parameters. The spatial frequency of the measurements collected can be optimized for increased map resolution while taking into consideration power and time requirements.

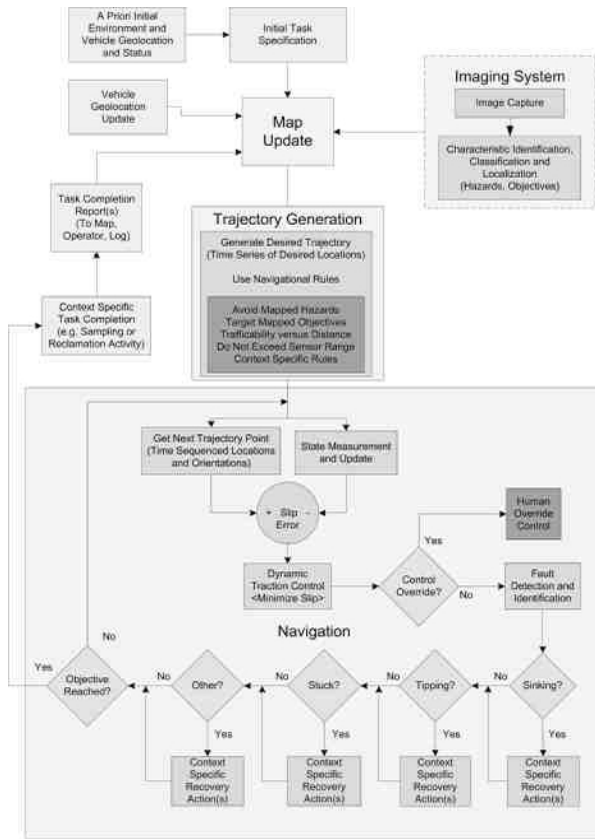


Figure 3. A Simple Rover Navigation Scheme with Fault Recovery

The geotechnical measurement tools are intended to provide sufficiently accurate characterization of the terrain at specific locations. As well, rovers can provide estimates of soil parameters in between tool deployment locations by using the locomotion system as a terrain parameter sensor. Soil properties can be estimated by measuring forces, torques, sinkage and motion while interacting with the terrain. For a very soft soil, an implement can be pushed through the material to estimate shear strength - or even viscosity of a fluid. These continuous estimates can greatly increase the resolution of the terrain map, and most importantly, ongoing estimates can be analyzed to identify areas of high interest for tool deployment and even potential hazards for other robots and vehicles.

Continuous estimates of soil properties are obtained by studying wheel-soil interactions.

Previous efforts on planetary rovers have studied terramechanics models to determine the rough terrain mobility and evaluate the traversability of an environment (Iagnemma et al., 2004). The cohesion stress and internal friction angle of the terrain can be approximated using slip-based terramechanics models. These models have been used to calculate the stress distribution under a moving wheel on soft soils (Bekker, 1969). Experimental validation of these methods have already been conducted for a wheel in quasi-static motion (Olmedo et al., 2012), and work has been proposed for expanding these models to dynamic systems.

SURFACE AND SUBSURFACE SAMPLE COLLECTION

Sampling surveys are required to target hazards and specific locations for detailed analysis. Autonomous sample collection can be part of conventional sampling campaigns that are costly and dangerous to workers. Robotic systems can estimate terrain properties on a tailings deposit, but it is necessary to verify these estimates with surface and subsurface samples. Rovers can be used to collect samples from areas inaccessible to humans. Surface samples are required to validate methods of stationary environmental monitoring equipment, such as hyper-spectral imaging of a deposit.

Surface Sample collection

Advanced robotic manipulators have been developed to collect surface samples from tailings. The manipulators require high repeatability in sampling, low weight and cost, suitable range of motion, and ruggedness for dirty environments. A key challenge of surface sampling, is to maintain soil integrity. Hyper-spectral analysis requires undisturbed samples that have the top 3 mm intact.

We have completed the design of a robotic manipulator to collect surface samples. The manipulator is configured as an articulated arm that carries a surface sampling mechanism, as shown in the computer graphic design image in Figure 4. Linear actuators move the arm's joints with high precision and repeatability. The sampling mechanism consists of a V-shaped end effector that is indented into the soil to obtain a sample, as illustrated in Figure 5. Laboratory tests are being conducted to evaluate the design.



Figure 4. CAD As-Built of Robotic Manipulator Mounted on Mobile Platform

Subsurface Sample collection

Autonomous sample return missions in oil sands tailings deposits can allow researchers to gather sufficient information to study consolidation processes. Work has been started on the design and integration of instrumentation to collect subsurface samples from up to 3 m depth.

As soft soil deposits dry, a hard crust forms on the surface, while saturated material remains trapped underneath. It is necessary to make holes through the top layer in order to deploy tooling under it. We have proposed a combination of drill and sampler pictured in Figure 6. An earth auger is used to drill a hole through the crust, and a soft soil sample catcher is lowered into the deposit to collect up to 1500 cubic cm of material. Work is being conducted to design a system that would allow full length stratified samples to be collected.

MACHINE VISION FOR DEWATERING PERFORMANCE ASSESSMENT

New methods for reclaiming tailings impoundments involve dredging MFT from ponds, and then processing the fluid-solid mixture to release water and develop strength in the resulting soil. Dredge positioning, pumping rates, and chemical addition processes are all currently controlled manually.

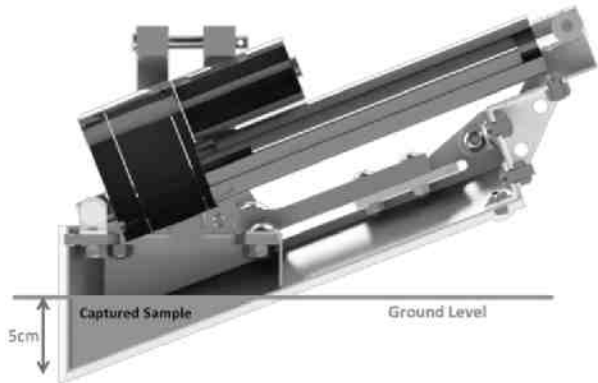


Figure 5. V-shaped Mechanism for Undisturbed Soil Sampling

In tailings thickening by polymer addition to MFT, prompt release of water occurs when the dosage matches the characteristics of the tailings feedstock. Changes in polymer dosage rely on qualitative assessments of dewatering effectiveness. Similarly, the performance of separation devices such as hydrocyclones and disc centrifuges are dependent on the concentration of solids, solids density, solids size distribution, and system throughput. To achieve densification with strength, favourable interfacial conditions must also be present to impart negative pore pressure in soil interstices.

Machine vision would allow for textural features of a surface to be identified, with potential applications for process control if features can be detected at the discharge of the pipe with sufficient predictive capability to allow for the process to be changed (primarily through changes in reagent addition). A knowledgeable operator can tell when a pour is going well, by the amount of water that is being expressed and by the texture of the proto-soil that wells to the surface of the sub-aerial discharge box and then flows into the main deposit. There is noticeable variability in the colour of the discharge. This means that characteristics of the solids can be detected optically.

When near infrared spectral information is also available, mineral type and abundance can also be assessed to determine the amount of clay from features at the surface of a sample. It is also possible to estimate using optical methods the surface activity of the clay solids. The Methylene

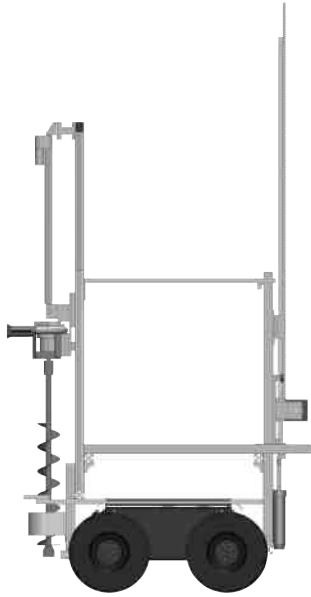


Figure 6. Drilling & Sampling Subsystems on a Mobile Platform

Blue Index (MBI) is an ASTM standard method for estimating the surface activity of a solid, and so comparison of methods to estimate MBI can be readily done. The standard technique relies on fully dispersed solids. A hyperspectral technique that can be done on ore (or MFT) will make that assumption, as it is based on surface solids. Work to date has shown promise of a hyperspectral set of features that can estimate clay surface activity (and particle size) in near real time.

Hyperspectral methods have also been demonstrated, not only in the laboratory but also under field conditions, to estimate the particle size distribution of solids in oilsands ore, and to detect different types of particles in oilsands froth. It is thus reasonable to assume that particle size distribution could be estimated for the solids in a saturated fluid as well, although this has yet to be demonstrated.

This combination of measurements of dewatering effectiveness and mineral properties (concentration, particle size distribution, and surface activity) would reveal relationships as to how dewatering is affected by the feed at the given dosage (or other process conditions such as hydrocyclone cyclopac configuration and inlet pressure, for example).

A shortwave infrared imaging camera would allow for both textural and spectral features to be

extracted using a single instrument. Such sensors are fairly expensive, and would be required at every pouring site. One solution would be to have a portable camera, perhaps mounted on a pickup truck (or on a robotic vehicle) that moves from one pouring location to the next. Alternatively, a suitable camera can be installed at each pouring location, with infrastructure for power and wireless communication of the features extracted from images to process decision-makers. A less expensive approach would be to use commercial grade visual-spectrum cameras with an infrared sensor. In that case, it would be important to have the hyperspectral instrument properly aimed. In any spectral observation, it is important to have proper illumination and periodic calibration with standard targets.

Tailings In-Pipe Characteristics for Process Control

Measurements made at the discharge pipe are useful for assessing how a deposit will behave. But measurements taken at the end of the pipe are not very useful for process control. It is important to make measurements as far upstream in the process as possible.

It is likely possible to adapt the hyperspectral techniques described above for measuring the characteristics of solids early in the process. This can be done by making samples from the pond in advance of the dredge operation. This could be done using a separate platform that samples ahead of the path of the dredge (for example, a robotic boat with a subsurface sampling system), or it could be done manually (although likely at higher expense). Simpler would be to mounted a sampler on the dredge head to withdraw samples of MFT as the dredge is working, or to use an autosampler to subsample the flow of slurry from the dredge pipeline system. Some preparation of the sample of the slurry will be necessary to reveal the necessary features (solids type, psd, and surface activity). The slurry flow rate, with a density measurement, will yield the solids flow rate. Particle size distribution then gives the amount of surface area. With an estimate of surface activity and surface area per unit time, dosage can be controlled downstream at the point of polymer injection.

As for dredge mass flow rate control, three variables need to be monitored in real time: density, flow rate, and pressure drop in the system. For effective control of a dredge-based engineered

tailings process, several technology steps are needed.

The first part would entail modeling the motion of a dredge and positioning of its submerged pumping head, along with the pumping of the fluid through a piping network, to predict the rate and concentration of solids through the system. Observability of the system is a key issue, because correct reagent addition depends on flow rate, solids concentration, solids particle size distribution, and cation exchange activity of the solids in the fluid. It is not critical that there be dredge dynamics included in the overall tailings process modeling. It is, however, necessary to know the flow rate and solids concentration from a mass balance standpoint. From a process operability view, PSD and BMI allow understanding of how much surface active solid material needs to be treated. It would be highly advantageous to know the dredge head location, which is readily done using GPS and some dredge ladder positioning and depth sensors, to map the MFT characteristics in the pond as dredging proceeds. With a validated model for dredge positioning and the process of solids flow and dosing, closed-loop automatic process control becomes possible.

In the case of bitumen production, clay activity directly affects the addition of reagents to generate surfactants or to modify water chemistry to improve interfacial tension amongst water, solids, air, and bitumen. A process instrument capable of measuring clay abundance and characteristics during pipeline transport would also be very useful for bitumen extraction processes.

TOOL DEPLOYMENT FOR ADVANCED STUDIES

As discussed, a robot can carry instruments, such as a hyperspectral sensor that estimates moisture content over a surface as the robot crosses terrain. (In some circumstances this will be an advantage over using a tower mounted imaging camera that collects an image with spectral information.) In other cases, there is no substitute for having an instrument on the deposit itself. A robot can be used to install piezometers to measure pressure at depth, used to estimate the rate of water percolation into the soil at the base of a deposit. More importantly, a robot can also position instrumentation for assessing the rate of evaporation from the surface. Eddy covariance units and evaporative flux chambers are used to

estimate evaporation from a surface. Evaporation estimates are important for understanding the rate at which drying occurs. A robot can tow such a unit to a location, as well as other instruments. Surface shear strength can be measured using a penetrometer. On muds and other saturated soils, an amphibious robot can carry a viscometer.

This approach allows instrumentation to be deployed and retrieved without putting personnel at risk.

With the recent developments in embedded systems and wireless communication, autonomous robots have become a viable technology option for monitoring in these regions. They can be designed to be lightweight, precise, robust, and inexpensive. This is not enough for successful integration of robots into an operating environment. A clear set of technical and functional requirements is necessary, along with processes and training to ensure that the robotic technology can be integrated into the operating environment without putting others at risk. In this way, robotic technologies can enhance overall system reliability. Among the risk controls that need to be in place are: risk assessments, safe work planning, appropriate alarms, signage, procedures to prevent people and equipment from interfering with robots, training for interactions with robots, fail-safes on the robot to prevent unexpected moves when people are in proximity to the system, and procedures for approaching a robot in a fault condition without putting personnel at risk.

CONCLUSIONS AND FUTURE WORK

A number of technology development initiatives are in progress related to designing and deployment of a mobile platform and tooling for very soft and even saturated soils. As well, optical methods are in active development and field testing.

Future work will report on system development, further testing of autonomous transportation, programming responsive control systems, adding new sensors, and testing at tailings sites. Based on successful prototype tooling tests, a fully functioning soft soil sampler will be produced for field testing by end of 2014. A control framework will be tested for deploying the current rover system for mapping of a crusted deposit (with accompanying conventional measurement results

for verification, including sampling and eddy covariance measurements), and design of a soft soils mobile platform to carry the sampler is in progress. Work may also be pursued on a simplified laboratory-scale dredge to investigate the interrelated dynamics of dredging and tailings treatment methods such as flocculation and centrifugation. A suite of robotics technologies may be useful for the range of challenges in managing tailings.

ACKNOWLEDGEMENTS

Financial support is gratefully acknowledged from the Natural Sciences and Engineering Research Council of Canada (NSERC), COSIA, and the University of Alberta.

REFERENCES

- F. Amigoni, A. Brandolini, V. Caglioti, C. Di Lecce, A. Guerriero, M. Lazzaroni, F. Lombardo, R. Ottoboni, E. Pasero, V. Piuri, and D. Somenzi, "Agencies for perception in environmental monitoring," in *Instrumentation and Measurement Technology Conference, 2005. IMTC 2005. Proceedings of the IEEE*, vol. 2, may 2005, pp. 1266–1271.
- A. Nuchter, H. Surmann, K. Lingemann, J. Hertzberg, and S. Thrun, "6d slam with an application in autonomous mine mapping," in *Robotics and Automation, 2004. Proceedings. ICRA '04. 2004 IEEE International Conference on*, vol. 2, April 2004, pp. 1998–2003 Vol.2.
- D. Wettergreen, S. J. Moreland, K. Skonieczny, D. Jonak, D. Kohan-bash, and J. Teza, "Design and field experimentation of a prototype lunar prospector," *International Journal of Robotics Research*, vol. 29, no. 12, pp. 1550 – 1564, October 2010.
- S. Thrun, M. Bennewitz, W. Burgard, A. Cremers, F. Dellaert, D. Fox, D. Hahnel, C. Rosenberg, N. Roy, J. Schulte, and D. Schulz, "Min-erva: a second-generation museum tour-guide robot," in *Robotics and Automation, 1999. Proceedings. 1999 IEEE International Conference on*, vol. 3, 1999, pp. 1999–2005 vol.3.
- F. Amigoni, A. Brandolini, G. D'Antona, R. Ottoboni, and M. So-malvico, "Artificial intelligence in science of measurements: from measurement instruments to perceptive agencies," *Instrumentation and Measurement, IEEE Transactions on*, vol. 52, no. 3, pp. 716–723, June 2003.
- F. Amigoni, V. Caglioti, and G. Fontana, "A perceptive multirobot system for monitoring electro-magnetic fields," in *Virtual Environments, Human-Computer Interfaces and Measurement Systems, 2004. (VEC-IMS). 2004 IEEE Symposium on*, July 2004, pp. 95–100.
- G. Freitas, F. Lizarralde, L. Hsu, V. Paranhos, N. R. S. dos Reis, and M. Bergerman, "Design, modeling, and control of a wheel-legged locomotion system for the environmental hybrid robot," in *Proceedings of the IASTED International Conference*, no. CMU-RI-TR-, November 2011.
- N. Olmedo and M. Lipsett, "Oilsands tailings characterization using a robotic system," in *Earth and Space 2012*, K. Zacny, Ed. American Society of Civil Engineers, 2012, pp. 1167–1176.
- K. Iagnemma and S. Dubowsky, *Mobile Robots in Rough Terrain Estimation, Motion Planning, and Control with Application to Planetary Rovers*, ser. Springer Tracts in Advanced Robotics. Springer Berlin / Heidelberg, 2004, vol. 12.
- M. G. Bekker, *Introduction to Terrain-Vehicle Systems*. Michigan: University of Michigan Press, 1969.

DEPLOYMENT OF HYPERSPECTRAL IMAGING INSTRUMENTS FOR REMOTE MONITORING OF SOFT TAILINGS WATER CONTENT

Iman Entezari, Benoit Rivard, Michael G. Lipsett, Jilu Feng and Gordon W. Wilson
University of Alberta, Edmonton, Alberta, Canada

ABSTRACT

A remote sensing method is proposed to address the challenge of measuring water content of soft tailing surfaces. Dehydration tests were conducted in the laboratory on four Mature Fine Tailing (MFTs) samples displaying varied swelling potential and bitumen concentration. Each experiment started with a sample that was fully saturated and terminated when the sample reached an air-dried state based on mass measurement. Spectral measurements were collected during the drying process to assess the potential of spectral sensing to estimate water content. Spectral features including absolute reflectance, absorption depth, and the normalized soil moisture index (NSMI) were evaluated for the estimation of water content of MFT. Results demonstrate that the spectral features examined show a good correlation with water content. The NSMI, however, seems to be the best moisture content estimator, as it shows a good level of robustness against the composition of tailings, and it is robust against the atmospheric conditions.

INTRODUCTION

Canada's oil sands deposits in northern Alberta represent one of the largest reserves of oil in the world. The oil sands are natural mixtures of inorganic materials (primarily quartz sands and clays), bitumen, and water (Kasperski, 2001). The bitumen is extracted either by open-pit mining or in-situ production. Open pit mining is viable for deposits at a burial depth of less than approximately 75 meters (National Energy Board, 2004) whereas in-situ methods extract deeper underground deposits. In surface mining, the bitumen is recovered through the general method developed by Karl Clark, where the oil sands ore is mixed with hot water and caustic, and the slurry is then sent to the extraction plant for bitumen flotation and froth production. This procedure is water-intensive and approximately 2.6 m³ of water is needed for production of each barrel of bitumen (0.16 m³) although much of the water is recycled

(Western Oil Sands, 2002; MacKinnon, 1989). Ultimately, large volumes of oil sands tailings composed predominantly of water with sand, silt, clay, and residual bitumen are produced during the open-pit mining process. The tailings are discharged to tailing ponds, where the coarse sand particles quickly settle to the bottom but the fine particles (mainly clays) remain in suspension in water and over a few years form a layer known as mature fine tailings (MFT) which still contains approximately 70 wt% water. Such MFT cannot be reclaimed and revegetated due to its poor water release and consolidation rate. The separation of water from MFT is thus an operational and environmental challenge for tailings management, and the subject of considerable technology development. The estimation of water content is an important task in the monitoring of the state of tailings surfaces.

Hyperspectral sensors measure the natural radiation reflected or emitted from the surface of an object across a portion of the electromagnetic spectrum, from which unique features about the measured surface are revealed. Advances in high spatial resolution hyperspectral imaging systems allow collection of an array of spectra in which every pixel of the acquired image is associated with a small area on the surface of interest. This allows for analysis of variability of features over the surface. Water content, particularly the moisture content from the soil surface, can be estimated and quantified using measurements of spectral features related to the overtones and combination absorption bands of water molecules near 900 nm, 1400 nm, and 1900 nm as well as the fundamental absorption band near 2800 nm. Multispectral measurements can also be made on a tailored set of frequency bands. Multispectral and hyperspectral remotely sensed data have been used to estimate moisture content of natural soils from a distance (Whiting et al., 2004; Haubrock et al., 2008). The overall reflectance in the optical spectral range can also be used for water content quantification, as the overall reflectance dramatically changes with water content. The present work discusses a laboratory-based investigation to estimate the moisture content of

soft tailings. Developing spectral features and models that are robust to environmental variations, including atmospheric conditions, is the subject of ongoing research.

METHODS

Sample description

A suite of 20 MFT samples collected in the summer of 2011 from the Muskeg River mine was provided by Shell Canada Energy. The samples were characterized for the Methylene Blue Index (MBI), yield stress, water content and contained various amount of residual bitumen. MBI is an indicator of the swelling potential of the tailings and is dependent on the type and relative abundance of clay minerals, total clay content, and particle size distribution of the sample. Four samples spanning a range of MBI were selected for the dehydration tests to assess the sensitivity of the spectral measurements to the composition of samples. Each sample was stirred to create a homogenous mixture before conducting the experiments. Air-dried samples examined are shown in Figure 1.

Laboratory measurements

The experimental approach was selected to derive a prediction the moisture content of MFT samples using hyperspectral observations. Spectral time-series data were collected for MFTs at variable moisture conditions to determine the spectral metrics of greatest sensitivity and derive predictive models. A sample thickness of approximately 1mm resided in a 150mm diameter petri dish, and reflectance spectra and the weight of the sample were collected every 4 minutes, starting from a saturated state.

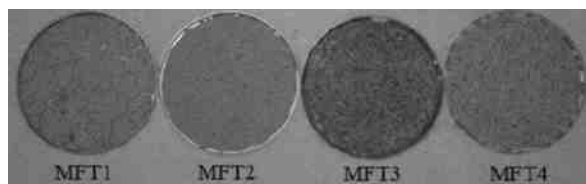


Figure 1. Air-dried state of the samples examined.

The experiment ended when no changes in the mass of a sample were observed, which took between 2–2.5 hours. Spectra in the 350-2500 nm range were collected with an Analytical Spectral

Device (ASD) spectrometer positioned at a normal viewing angle to the sample surface. A 50W quartz halogen lamp illuminated the sample at an incidence angle of 20°. The sample diameter footprint sensed was almost equal to the petri dish's diameter (150mm). The spectrum acquired at each time interval was the results of averaging 25 measurements. Spectrum acquisition took less than 3 seconds. Normalization of each measurement to that of a standard white reference panel for calculation of reflectance was conducted at the beginning of each experiment. The soil moisture corresponding to each of the measurements was calculated by:

$$SM = \frac{W_{\text{sample}} - W_{\text{solids}}}{W_{\text{sample}}} \cdot 100 \quad (1)$$

where W_{sample} and W_{solids} are the weight of the sample (water plus solids) and weight of dried solids, respectively.

Spectral features were derived from the collected spectral time series and regression analysis was used to link the spectral features to the moisture content. Coefficients of determination (R^2) were calculated to assess the accuracy of the spectral models. The summary of the dehydration tests is provided in Table 1.

Table 1. Summary of dehydration tests.

Sample No.	MBI (meq/100g)	Initial water content (wt%)	Test duration (min)
MFT1	9.1	47.84	108
MFT2	8.0	53.45	136
MFT3	7.1	55.34	120
MFT4	6.8	52.04	140

Spectral metrics evaluated

The reflectance spectra collected from the tailings samples during dehydration are affected by the variations in sample water content over time. Using the time series data, different spectral metrics were compared in terms of their ability to estimate the water content of MFT samples. The spectral features examined comprised absolute reflectance values, absorption depths, and the normalized soil moisture index (NSMI) (Haubrock et al., 2008). To determine the best wavelengths at which to examine absolute reflectance, a correlation analysis was performed between the absolute reflectance at all bands in the short-wave infrared

(SWIR) and water content, taking all the samples into account. Also, the absolute reflectance at 2205 nm attributed to clays was tested, as this spectral feature is not affected by the atmosphere and is thus applicable to the use of field imagery. The depth of absorption features attributable to water and centered at 1450 and 1925 nm was evaluated as potential spectral metrics for moisture content estimation. For this purpose the depth of the absorption band at 1450 nm and 1925 nm were calculated respectively using the continuum removed spectra between 1375 and 1550 nm and 1850 and 2150 nm. Lastly this study examined the normalized soil moisture index (NSMI) suggested by Haubrock et al. (2008). NSMI is calculated as the normalized difference of the absolute reflectance at 1800 and 2119 nm wavelengths.

RESULTS AND DISCUSSION

Absolute reflectance

The correlation coefficient between water content and absolute reflectance for each SWIR wavelength is shown in figure 2a. In general, reflectance in the SWIR has a high negative correlation with water content. The highest correlation was observed at 1985 nm. Plots of water content versus absolute reflectance at 1985 nm for all the samples are shown in figure 2b. MFT samples 1 & 3 show almost the same behaviour below 30 wt% water; however, MFT3 shows a lower reflectance than MFT1 below 10 wt% water content, likely because of a higher bitumen concentration. It can be concluded that when a sample is wet (above 10 wt% moisture content), the impact of bitumen on the reflectance is insignificant but it starts to impact the reflectance when the sample surface becomes very dry (below 10 wt% water content). As the reflectance at 1985 nm is affected by the atmosphere in field applications, the reflectance at 2205 nm was also examined, as shown in figure 2c. The behaviour observed at 2205 nm is similar to that at 1985 nm; but variability is lower (0.1 to 0.3 compared to 0.05 to 0.33 at 1985 nm). Because the variability in reflectance at both 1985 nm and 2205 nm above 30 wt% water content is attributed to the variation in standing water, the potential of these spectral

features was only evaluated below 30 wt%. By fitting a second order polynomial to the data, R^2 values of 0.95 and 0.94 were achieved for reflectance at 1985 and 2205 nm, respectively. Although both these features can be used successfully for water content estimation in a laboratory setting, only the reflectance at 2205 nm can be used in a field scenario due to its robustness against outdoor atmospheric conditions.

Absorption depth

Changes in absorption depth at 1450 and 1925 nm with respect to water content are shown for each sample in figures 2d and 2e.

Both of these features seem to be sensitive to changes in water content for the entire moisture regime with a slight decline in sensitivity of the 1450 nm depth below 8 wt% moisture content. The absorption depth at 1925 nm shows a higher range of variation than that for the 1450 nm band depth. The range of variation for the 1925 nm depth is roughly between 0 and 0.7 compared to 0 to 0.35 for the 1450 nm depth. R^2 values of 0.96 and 0.95 were obtained by fitting a second order polynomial considering the entire data points for 1450 and 1925 nm absorption features, respectively. Although there is a strong correlation between these absorption bands and water content, in a field scenario they would suffer from the impact of water vapour in the atmosphere and thus are of limited value in such a setting.

NSMI

Figure 2f shows the relationship between NSMI and water content for each tailing sample. The data shown in this figure suggest that NSMI shows a good level of robustness against tailings composition. Furthermore, it is sensitive to the variation in water content for the entire moisture regime. A R^2 of 0.97 was achieved by fitting a second order polynomial to the data. This high R^2 value - and the fact that this index is not affected by the atmosphere - makes the NSMI an appropriate water content estimator in field conditions.

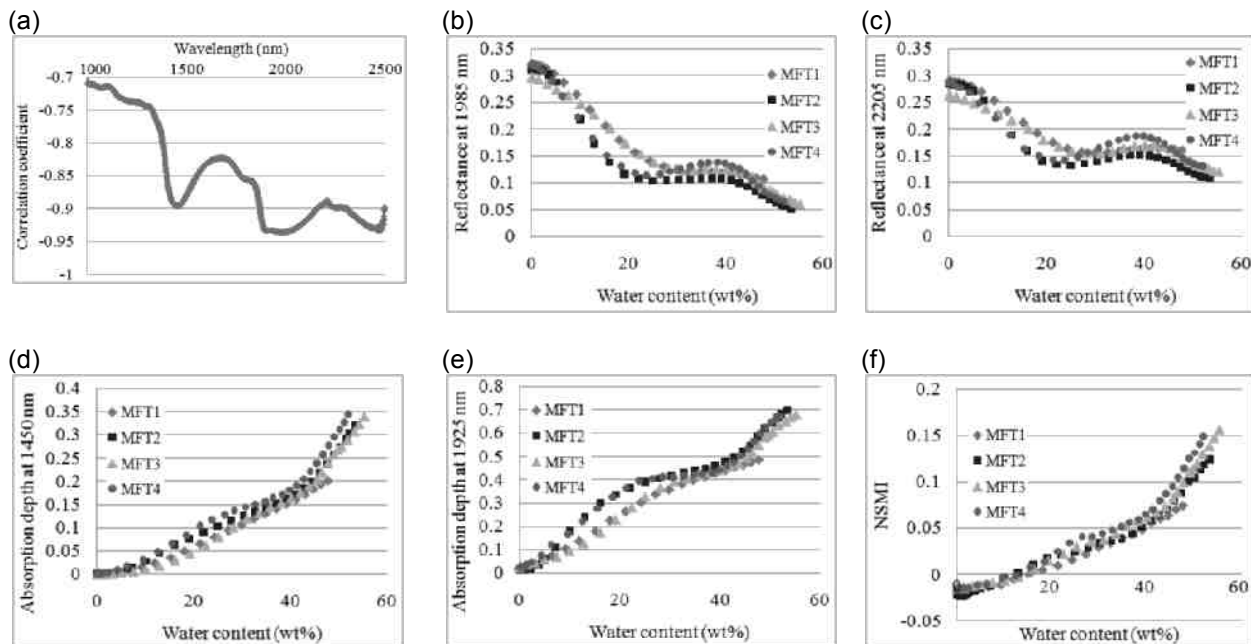


Figure 2. (a) Correlation coefficient between absolute reflectance and water content as a function of wavelength. (b) Absolute reflectance at 1985 nm versus water content. (c) Absolute reflectance at 2205 nm versus water content. (d) Absorption depth at 1450 nm versus water content. (e) Absorption depth at 1925 nm versus water content. (f) NSMI versus water content

CONCLUSIONS

This paper investigated the capability of hyperspectral remote sensing for estimating the moisture content of oil sands soft tailings. All spectral features examined were of value for the estimation of water content of the MFTs. The best result was achieved using NSMI ($R^2 = 0.97$). As NSMI is more robust against variability in atmospheric conditions, this feature seems to be the optimal estimator in field applications.

In future efforts, the models obtained from this laboratory investigations will be assessed for their applicability in field settings with verification by sampling, with the goal of not only estimating the moisture content of the surfaces of engineered tailings deposits but also showing when the deposit has stopped drying through evaporation.

ACKNOWLEDGEMENTS

The authors would like to acknowledge the Institute for Oil Sands Innovation (IOSI) at the

University of Alberta and Canada's Oil Sands Innovation Alliance (COSIA) for research support. Shell Canada Energy is also acknowledged for provision of samples.

REFERENCES

- Haubrock, S. N., Chabrillat, S., Lemmertz, C., and Kaufmann, H., 2008, Surface soil moisture quantification models from reflectance data under field condition: *International Journal of Remote Sensing*, vol. 29, no. 1, pp. 3-39.
- Kasperski, K. L., 2001, Review of research on aqueous extraction of bitumen from mined oil sands. [Division No. CWRC 01-17 (CF)]. Natural Resources Canada, CANMET-WRC.
- MacKinnon, M. D., 1989, Development of the tailings pond at Syncrude's oil sands plant: 1978–1987. *AOSTRA Journal of Research*, vol. 5, no. 2, pp. 109–133.
- National Energy Board, 2004, *Canada's Oil Sands: opportunities and challenges to 2015* [Pamphlet], Calgary, AB.

Western Oil Sands, 2002, Western Oil Sands annual report.

Whiting, M. L., Lin, L., and Ustin, S. L., 2004, Predicting water content using Gaussian model on soil spectra, Remote Sensing of Environment, vol. 89, no. 4, pp. 535-552.

TIME DOMAIN REFLECTOMETRY (TDR) SENSORS – APPLICATION TO FLOCCULATED MATURE FINE TAILINGS PERFORMANCE MONITORING

Jason Song¹ and Mike O’Kane¹, Robert Mahood² and Cynthia Cote² and Dale Kolstad³

¹O’Kane Consultants Inc.

²Shell Canada Energy

³Barr Engineering Company

ABSTRACT

The oil sands industry is developing and improving several tailings treatment technologies at various scales. Both automated monitoring (instrumentation) and manual measurements are employed in performance monitoring of treated deposits. Advantages of instrumentation include continuous tailings monitoring, *in situ* measurement without tailings disturbance, pre-installation before tailings placement so there is no access required after the tailings placement, and remote data download.

Monitoring tailings pore water is important as it is correlated to tailings solids content and indicative of shear strength, two key performance indicators for tailings deposit management. A time domain reflectometry (TDR) sensor measures volumetric water content in the tailings and is essentially a cable (and probe) radar in which a very fast rise-time voltage pulse is propagated down a cable, through the soil and reflected back. The tailings water content change (hence the change in impedance of the tailings) is recorded by the signal travel time along the cable (transmission line). The correlation between the signal travel time and the tailings water content is based on TDR calibration with the site-specific material.

Tailings volumetric water content when combined with other tailings geotechnical parameters (e.g. specific gravity), can be used to calculate tailings solids content. In addition, tailings water content change can be used to evaluate re-wetting of underlying layer(s) when multiple lifts are deposited, water flow within tailings deposits, and tailings water balance. This paper presents TDR sensor calibration and applications to flocculated mature fine tailings (MFT) performance monitoring for Shell’s Atmospheric Fines Drying (AFD) Deposition Optimization program. TDR measurements provide fair comparisons with data

obtained for tailings core samples taken at the same locations as the TDR sensors.

INTRODUCTION

The oil sands industry continues to explore new technologies for applications to soil sands tailings management. These explorations can be conducted at all levels from laboratory tests to bench scale, to pilot scale, to prototype, and to commercial scale. A number of tailings parameters can be categorized to be affecting evaluation of a tailings management technology. These parameters include rheological properties (e.g. slump, viscosity, etc.); strength properties (e.g. yield strength, peak and residual undrained shear strength, etc.), geotechnical index properties (e.g. particle size distribution, Atterberg limits, sand fines ratio, etc.), tailings compressibility and consolidation properties (e.g. compressibility coefficient, consolidation coefficient, etc.), tailings hydraulic properties (e.g. soil water retention curve, saturated and unsaturated hydraulic conductivity), and tailings sensitivity to above properties. With the increasing scale of tailings deposition, challenges to tailings geotechnical performance evaluation are increasing as uncertainties of tailings deposits uniformity are increasing. In addition, boundary conditions can also add uncertainty to tailings geotechnical performance when tailings deposition scales increase from laboratory scale to commercial scale. Boundary conditions include climatic conditions at the tailings pouring sites, surface water management strategies to tailings deposits or tailings containers, local and regional hydrological and/or hydrogeological settings of the tailings deposits, and tailings deposition plans (single lift deposition vs. multiple lift deposition).

Testing trials of all scales require geotechnical performance monitoring to evaluate feasibility and efficiency of the investigated technology. Solids

content and undrained shear strength of tailings deposits are two key parameters that are usually used to identify tailings geotechnical performance. Solids content increases when water in the tailings deposit is removed. Both sedimentation and consolidation can lead to densification of tailings deposits and increase solids content in the tailings mass. Generally, undrained shear strength of tailings deposits increases with increases of tailings solids content. Furthermore, tailings undrained shear strength may be obtained from tailings solids content based on empirical relationships (e.g. Masala and Matthews, 2012).

More often, tailings deposit solids content is measured from tailings core sampling. Direct *in situ* measuring tailings solids content is not common practice. However, *in situ* solids content values of tailings deposits can be calculated from monitoring *in situ* water content based on conversion relationships between solids content and water content in tailings deposits. Time domain reflectometry (TDR) technology is commonly employed to measure water content in tailings deposits.

Shell Canada Energy (Shell) initiated a field test program in 2012, at their Muskeg River mine (MRM) site, north of Fort McMurray, to assess various depositional strategies for in-line flocculated mature fine tailings (MFT) in order to maximize the tonnage of fines that can be processed per unit footprint and minimize associated operational efforts. Three instrumented test cells, namely: Thin Multi-lift (Thin ML), Thick Multi-lift (Thick ML) and Deep Stacking (Deep Stack) were constructed at MRM's atmospheric fines drying (AFD) operations site in summer 2012 to investigate depositional strategies. Deposition into the test cells began in late summer 2012 and completed in late summer 2013. According to the program plan, these three test deposits will be left in place, monitored and tested until late summer 2014. *In situ* volumetric water content (VWC) of the MFT deposits is measured with a TDR100 system supplied by Campbell Scientific Canada Corporation (CSCC).

This paper presents applications of TDR sensors in tailings geotechnical performance monitoring. Specifically, the paper presents the calibrated TDR sensors for water content monitoring in Shell's Atmospheric Fines Drying (AFD) Deposition Optimization program. The measured *in situ* tailings water contents are used for evaluation of tailings solids content, density, water

balance, re-wetting of the tailings deposits, and indicative of tailings undrained shear strength. The calculated solids content values derived from water content values measured with TDR are compared with core samplings results. Calibrated TDR equation enriches the TDR calibration database.

MEASUREMENT OF TDR SENSORS AND TAILINGS GEOTECHNICAL PERFORMANCE

TDR sensors used for VWC measurements for Shell's AFD Deposition Optimization program are Model CS645, supplied by CSCC. The CS645 TDR sensors have 7.5 cm long rods, recommended for high conductivity soils (soil bulk conductivity ≤ 5.0 dS/m) (Campbell Scientific, 2013). Measurement resolution of the CS645 TDR probe is $0.006 \text{ cm}^3/\text{cm}^3$. The TDR100 system was controlled by a data acquisition system (DAS).

A TDR is essentially a cable radar in which a very fast rise-time voltage pulse is propagated down a cable, through the soil and reflected back. The TDR reflectometer (e.g. TDR100) is used to generate an electromagnetic signal that will propagate along a transmission line. The TDR probe and the connecting coaxial cable are the transmission line of a typical soil water measurement system. A portion of the applied signal will be reflected back to the source when there is a change in impedance. Changes in water content cause changes in dielectric permittivity, which is related to impedance. A TDR system basically measures the propagation time of an electromagnetic signal along the transmission line, which allows for the computation of the apparent dielectric permittivity (or dielectric constant) of the material surrounding the rods. Empirical equations are then used to convert apparent dielectric permittivity into water content in the material. This can be achieved because a significant difference exists between the dielectric constant (defined as permittivity of material over permittivity of vacuum) of the soil matrix ($K_{soil} \approx 5$) and water ($K_{water} \approx 80$). The most commonly used empirical equation is a polynomial function derived by Topp et al. (1980) (Eq. 1) (referred to as Topp Equation in this paper).

$$\theta_{TE} = -0.053 + 0.0292\epsilon_m - 5.5 \times 10^{-4} \epsilon_m^2 + 4.3 \times 10^{-6} \epsilon_m^3 \quad (1)$$

where θ_{TE} is the VWC calculated with Topp Equation; and ϵ_m is the apparent dielectric permittivity measured with the TDR probe.

The TDR100 system converts recorded propagation time into apparent probe rod length (L_a). The ratio (L_a/L) of L_a to actual rod length (L) is equal to the square root of ϵ_m . Once a material-specific calibration curve is available, it can be applied to the L_a/L (or ϵ_m) value output by the TDR sensor to obtain VWC in the MFT deposits. It is important to note that a TDR system only gives an indication of the volumetric liquid water content of non-frozen soils because the dielectric constant of ice is approximately 3.2 (Spaans and Baker, 1995).

With saturated condition in the tailings deposit, measured VWC value is equivalent to the tailings porosity. Then tailings dry density can be calculated as:

$$\rho_d = G_s \cdot (1 - \theta_m) \quad (2)$$

where ρ_d is the tailings dry density; G_s is the specific gravity; θ_m is the measured VWC from TDR sensors.

Gravimetric water content in the tailings deposit can be expressed:

$$W_w = \frac{\theta_m \cdot \rho_w}{\rho_d} \quad (3)$$

where W_w is the tailings gravimetric water content; and ρ_w is the density of water.

The tailings bulk density and solids content can be calculated when the tailings gravimetric water content and dry density are known.

$$\rho_b = (1 + W_w) \cdot \rho_d \quad (4)$$

$$S_c = \frac{1}{1 + W_w} \quad (5)$$

where ρ_b is the tailings bulk density; and S_c is the solids content of the tailings deposit.

In addition to informing calculations of tailings solids content and bulk density, the measured VWC in the tailings deposit is also an important component for evaluating the tailings water balance. Figure 1 illustrates four TDR sensors installed for monitoring in a tailings deposit. The water balance equations for the top sub-layer,

middle sub-layers, and the bottom sub-layer can be defined as:

$$\Delta S_T = P + RI - RO - AE - NP_{OUT} \quad (6)$$

$$\Delta S_M = NP_{IN} - NP_{OUT} \quad (7)$$

$$\Delta S_B = NP_{IN} - UD \quad (8)$$

where ΔS_T , ΔS_M , ΔS_B are the water storage change from time t_1 to t_2 in the top sub-layer, middle sub-layer and bottom sub-layer, respectively; P is precipitation; RI is run in water to the tailings deposit; RO is runoff water; NP_{IN} and NP_{OUT} are net percolation into and out of the sub-layer respectively; and UD is the under-drainage of the bottom sub-layer.

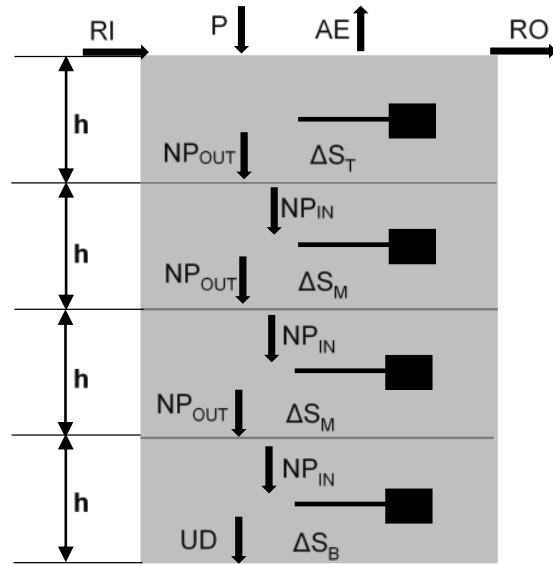


Figure 1. Illustration of TDR sensors monitoring volumetric water contents and water balance in a tailings deposit.

Change in water storage from time t_1 to t_2 can be calculated by Equation (9) when the sub-layer thickness does not change or Equation (10) when the sub-layer thickness changes:

$$\Delta S = (\theta_m^{t_2} - \theta_m^{t_1}) \cdot h \cdot A \quad (9)$$

$$\Delta S = (\theta_m^{t_2} \cdot h_2 - \theta_m^{t_1} \cdot h_1) \cdot A \quad (10)$$

where ΔS is the change in water storage from time t_1 to t_2 in a selected sub-layer; $\theta_m^{t_1}$ and $\theta_m^{t_2}$ are measured VWC in the sub-layer at time t_1 and t_2 ,

respectively; h is thickness of the sub-layer (when the thickness is not changing); h_1 and h_2 are the thicknesses of the sub-layer at the time t_1 and t_2 , respectively (when the thickness of the sub-layer is changing).

When TDR sensors are installed at fixed depths within the tailings deposit, distance between sensors will not change. However, the thickness of the top sub-layer is changing with tailings settlement.

Above water balance equations (Eqs. (6)-(8)) can be used to evaluate under-drainage (UD) when boundary conditions at tailings surface are available (i.e. P, RI, RO and AE are known). In addition, calculated changes in water storage also provide indicative of water flow in tailings deposits. It is not common practice to use change in water storage to address water flow in tailings deposits because pore-water pressure measurements with piezometers can provide direct evidence on water flow directions in the tailings deposits. However, water flow evaluation with piezometer data should match calculated change in water storage obtained from TDR readings.

It is a challenge to directly calculate undrained shear strength from the measured VWC values. However, two methods can be used to build connection between VWC and undrained shear strength. One method is the empirical relationship between solids content (and/or gravimetric water content) and undrained shear strength. Another method is to use VWC value to calculate tailings void ratio, then void ratio can be associated with effective stress (e.g. void ratio versus effective stress relationship obtained from tailings consolidation tests) that is further used for evaluation of undrained shear strength in the tailings deposits. Based on these connections, the measured VWC values, at the least, provide an indicative of undrained shear strength in the tailings deposits.

CALIBRATION OF TDR SENSOR TO OIL SANDS TAILINGS

A material-specific calibration curve is desirable when using TDR measurements for calculations of absolute VWC values (e.g. Take et al., 2007). For Shell's AFD Deposition Optimization program, the TDR sensor CS645 was calibrated with the site deposited flocculated MFT material. Table 1 lists

basic geotechnical properties of the flocculated MFT poured in the field.

A calibration cell was designed specifically for purposes of TDR calibration. The calibration cell is made of acrylic, and measures 30 cm x 30 cm x 50 cm (thickness x width x height). It has double base plates separated by a height of 5 cm. The inside base plate is perforated for tailings under-drainage, while the bottom plate is fitted with a hose and tubing to collect under-drainage outside the cell. A ledge to secure the TDR sensor head is located 12 cm above the inside base plate. A perforated plate is also placed over the tailings surface during the test to allow water release at the surface.

Table 1. Geotechnical properties of the flocculated MFT material in the program.

Property	Value
Specific gravity	2.0-2.5
Solids content (%)	33-35
Bitumen content (%)	4-8
Sand content (%)	5-55
Fines content (%, <0.074 mm)	45-95
Plastic limit	20-30
Liquid limit	45-70

Installation is important to a successful calibration test. During setup, initial conditions of flocculated MFT in the cell should be known. Initial conditions include total mass, total volume, water volume, solids volume, water mass, solids mass, initial void ratio, initial VWC and tailings bulk electrical conductivity. The test setup includes following steps:

- Record inside dimensions of the TDR calibration cell;
- Place two layers of geotextile on the base drain plate;
- Stop the bottom outlet;
- Attach a TDR probe to the ledge and connect the probe to the TDR100 reflectometer and datalogger;
- Set the TDR test cell on a scale platform;
- Record the weight of the empty test cell (complete with attached equipment);
- Pour MFT material into the cell; to a layer thickness of about 30 – 35 cm;
- Record the weight of the cell filled with MFT and the actual tailings layer thickness; and,
- Start test.

Calibration tests include three stages: self-weight settling, consolidation with surface loading, and consolidation with surface loading and bottom vacuum. Each stage lasted for one to two weeks. Surface loading was 2 kPa for one week and then increased to 5 kPa. The 5 kPa surface loading was maintained until the end of the test. Exerted bottom vacuum was 50 kPa and lasted two hours. The remainder of time allowed tailings to settle

and pore-water equilibrate in the deposit profile. Manual measurements were taken during the test. These measurements include measuring date and time, effluent volume (under-drainage and surface drain), effluent electrical conductivity (EC) value, tailings layer thickness, and total cell and MFT weight. Figure 2 shows a view of the TDR calibration test cell with applied surface load.



Figure 2. View of the calibration test cell with applied surface load.

At the conclusion of each test, three samples are collected from different depths in the MFT layer for water content determination. The water content values determined from samples are then compared to the latest values output by the TDR probe before the test is completed. Three TDR probes are used for calibration, with one TDR probe per each test run.

Volumetric water content (VWC) values of MFT tailings in the test cell were calculated using two methods: measurement of changes in tailings thickness and measurement of volume of drainage water (collected both at the base of the test cell and at the top of the surface loading plate). The measured tailings thickness can be used to calculate VWC because shrinkage (away from the walls of the cell) did not occur due to minimum evaporation during testing. Average VWC obtained from both methods is defined as the laboratory-measured VWC and is used for TDR calibration computation. Figure 3 presents a

calibration curve of TDR sensor CS645 for the flocculated MFT. As a comparison, the universal TDR calibration curve obtained from the Topp Equation is also presented in Figure 3.

The calibration equation is:

$$\theta_m = -0.079 + 0.042\epsilon_m - 8.08 \times 10^{-4} \epsilon_m^2 + 5.59 \times 10^{-6} \epsilon_m^3 \quad (11)$$

Although Equation (11) can express the entire range of VWC from 0 to 1.0, the actual calibration range of VWC is between 0.5 and 0.8. Figure 3 indicates that VWC values obtained from the calibrated equation for flocculated MFT are greater than those obtained from the Topp equation assuming measured apparent dielectric permittivity values are consistent. The difference in VWC values obtained from the calibrated equation and from Topp equation is presented in Figure 4.

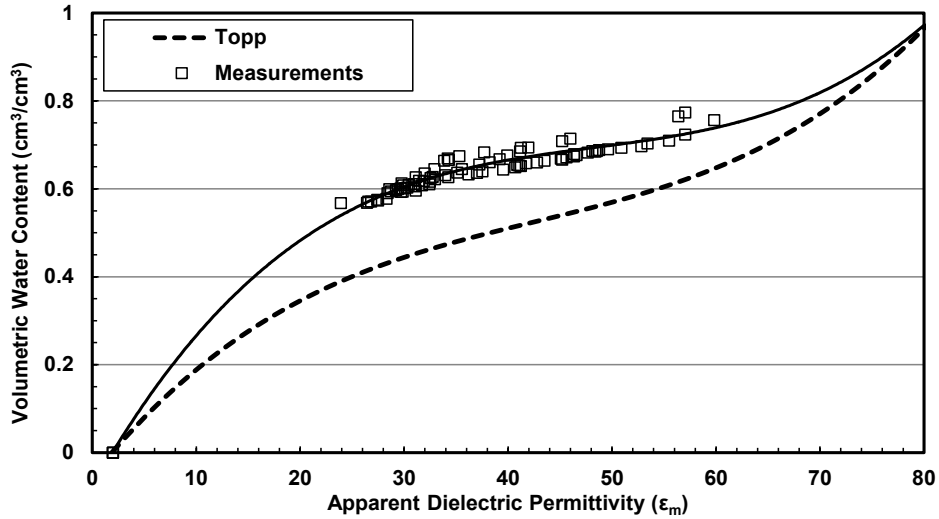


Figure 3. TDR calibration results for the flocculated MFT.

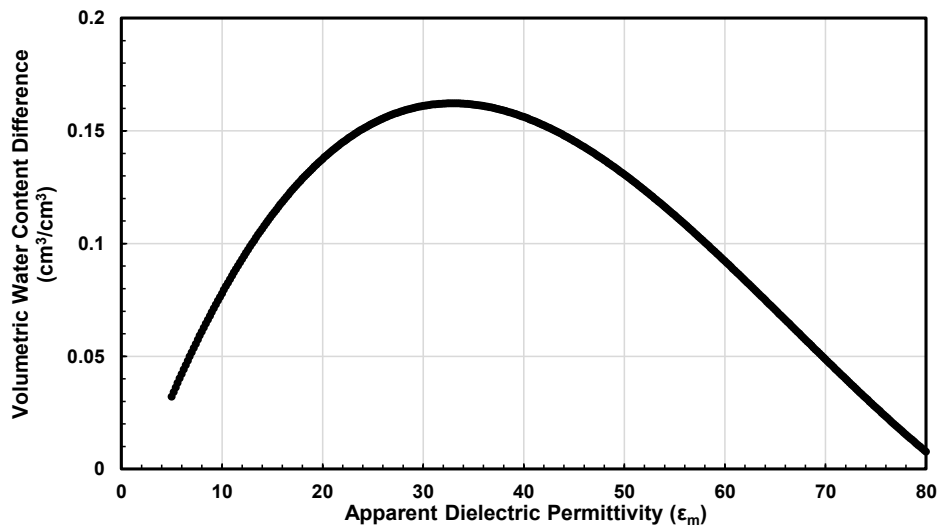


Figure 4. Volumetric water content difference ($\theta_m - \theta_{TE}$) against apparent dielectric permittivity.

According to Figure 4, the maximum difference of VWC occurs when ϵ_m is approximately 32. For flocculated MFT material, its VWC value is approximately 0.78 (with a solids content of ~40%) after pouring, decreasing with time due to tailings densification. When tailings solids content reaches 65%-70%, VWC approaches ~0.5-0.55. The measured apparent dielectric permittivity should be in the range between 20 and 65 (figure 3) when VWC values are in the range between 0.5 and 0.78. This range includes apparent dielectric permittivity value (32) at which the maximum

difference of VWC occurs (Figure 4). Therefore, it is necessary to calibrate TDR sensors for site-specific material in order to obtain reliable VWC values.

Figure 5 presents further TDR calibration curves for comparison. The TDR calibration materials used represent organic soils by Stein and Kane (1983) and Roth et al. (1992), peat substrates by Pepin et al. (1992) and Paquet et al. (1993), oil sands tailings (with ~0-7% bitumen) by Sorta et al. (2012).

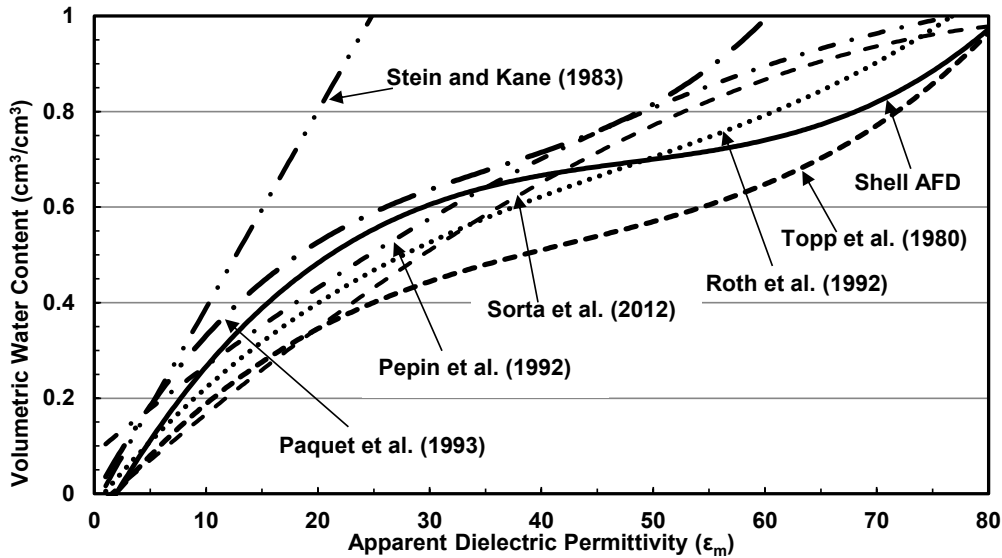


Figure 5. TDR calibration equations for various materials.

Although each calibration curve has its suggested interval of VWC where applicable, the general trend is that VWC is greater for organic materials than in mineral material when the apparent dielectric permittivity is the same. In addition to material constitution, factors such as temperature, TDR type can also affect VWC measurement accuracy using TDR.

TDR APPLICATIONS TO FLOCCULATED MFT PERFORMANCE

A direct application of VWC obtained from TDR readings in the MFT deposit is to evaluate solids content gain with time. Figure 6 presents average solids content values calculated from TDR readings versus average solids content values obtained from core sampling program.

Figure 6 indicates that generally, average solids content values obtained from TDR readings are in good agreement with average solids content values derived from core sampling with differences less than 2-3%. Obtained *in situ* solids content from TDR readings increased from 49% to 59% over one year in the Deep Stack deposit. This solids content increase does not include solids content gain, which is approximately 10%, in the MFT's initial dewatering. Although average solids content values are presented in Figure 6, solids content profiles can also be obtained as TDR sensors are usually placed at various depths in the

MFT deposit. Thus readings from TDR sensors provide continuous monitoring of solids content gain in the MFT deposit.

VWC values obtained from TDR readings are usually used to evaluate water volume in tailings deposits. Water volume obtained from TDR readings in the Thin Multi-lift (Thin ML) cell matches well to water volume obtained from core sampling (Figure 7). Calculated water volume in the deposit can be further used to evaluate under-drainage through the water balance method. Furthermore, a VWC profile along the deposit depths can be used to identify water flow in the deposit.

Empirical relationships between undrained shear strength and solids content can be used to evaluate undrained shear strength once solids content is known from the TDR measurement. Figure 8 shows relations of measured peak undrained shear strength and solids content in three test cells for Shell AFD Deposition Optimization program. It appears that different depositions have different solids contents corresponding to a peak undrained shear strength of 5 kPa. In the Deep stack cell, solids content is 55% to achieve a peak undrained shear strength of 5 kPa, while the solids contents may be 60% and 65% to achieve a peak undrained shear strength of 5 kPa in the Thick Multi-lift (Thick ML) cell and Thin ML cell, respectively.

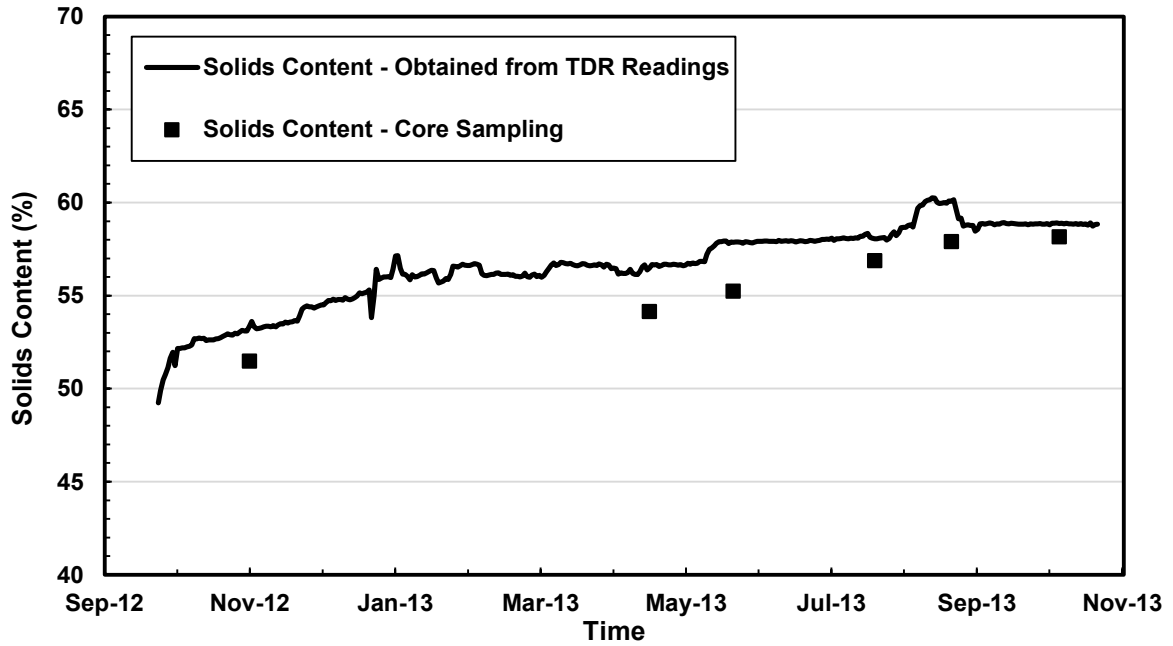


Figure 6. Comparison of solids content values obtained from TDR readings and from core sampling in Deep Stack deposit.

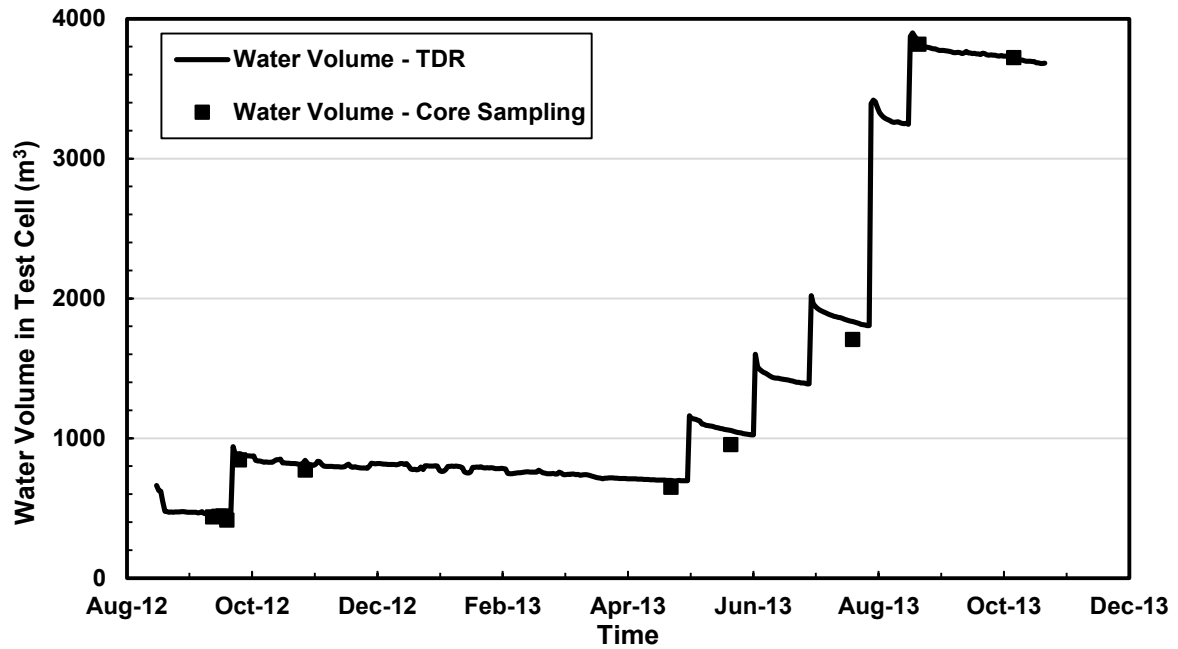


Figure 7. Water volume in the Thin Multi-lift cell obtained from TDR readings versus water volume obtained from core sampling.

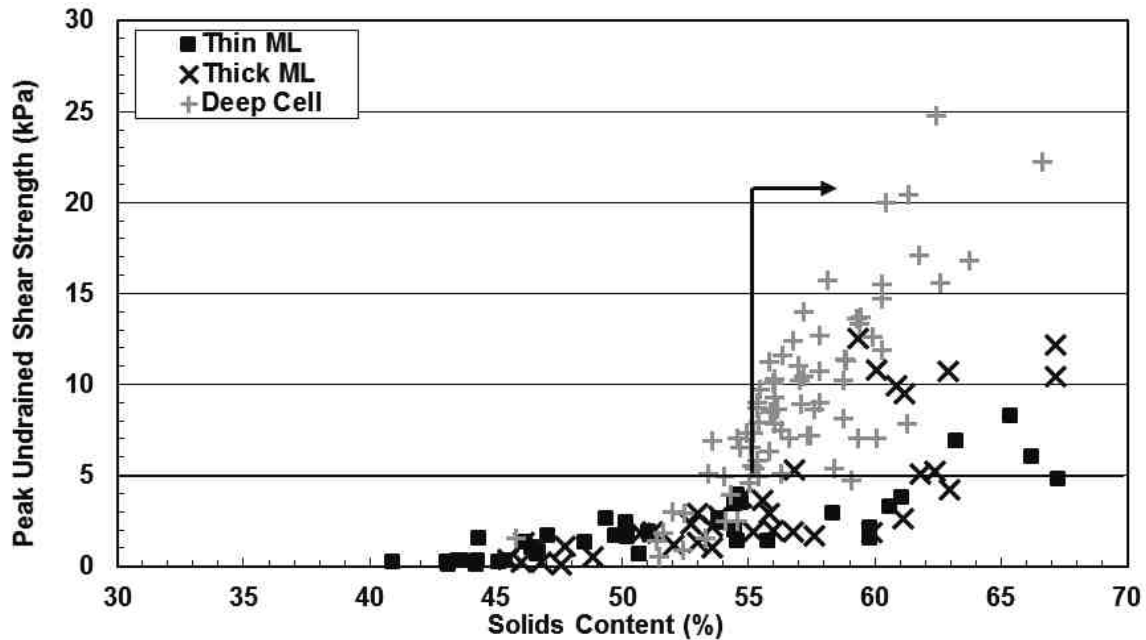


Figure 8. Peak undrained shear strength versus solids content in the deposits.

SUMMARY

The tailings solids content and undrained shear strength are key parameters to evaluate the tailings geotechnical performance for all scales of tailings tests. VWC measured using TDR sensors can be used to calculate solids content and also provide an indication of undrained shear strength. In addition, VWC values obtained from TDR readings can also be used for calculations of other geotechnical parameters such as void ratio and bulk density in tailings deposits. Calibrating TDR sensors to site-specific tailings is important to achieve accurate VWC measurement for geotechnical performance evaluation.

ACKNOWLEDGEMENTS

Many thanks to Dr. Adedeji Dunmola, who initiated and managed the Shell AFD Deposition Optimization program when he worked with Shell Canada Energy. Special thanks to Ms. Sophie Kessler, who helped conduct TDR calibration tests in OKC's Fort McMurray Office. The authors would like to thank Shell Canada Energy for publication permission of this paper.

REFERENCES

- Masala S. and Matthews J. 2012. Predicting development of undrained shear strength in soft oil sands tailings. International Oil Sands Tailings Conference 2012. December 2-5, 2012, Mayfield Inns and Suites, Edmonton, Alberta, Canada.
- Paquet, J.M., Caron, J. and Banton, O. 1993. In situ determination of peat water desorption characteristics of peat substrates. Canadian Journal of Soil Science, **73**: 329-339.
- Pepin, S., Plamondon, A.P. and Stein, J. 1992. Peat water content measurement using time domain reflectometry. Canadian Journal of Forest research, **22**: 534-540.
- Roth, C.H., Malicki, M.A. and Plagge, R. 1992. Empirical evaluation of the relationship between soil dielectric constant and volumetric water content as the basis for calibrating soil moisture measurements by TDR. Journal of Soil Science, **43**: 1-13.
- Sorta, A., Sego, D. and Wilson, W. 2012. Evaluation of time domain reflectometry (TDR) for use in centrifuge testing. International Oil Sands Tailings Conference 2012. December 2-5, 2012,

Mayfield Inns and Suites, Edmonton, Alberta, Canada.

Spaans, E.J. and Baker, J.M. 1995. Examining the use of time domain reflectometry for measuring liquid water content in frozen soil. *Water Resources Research*, **31**: 2917-2925.

Stein, J. and Kane, D.L. 1983. Monitoring the unfrozen water content of soil and snow using time domain reflectometry. *Water Resources Research*, **19**: 1573-1584.

Take, W.A., Arnepalli, D.N., Brachman, R.W.I. and Rowe, R.K. 2007. Laboratory and field calibration of TDR probes for water content measurement. The 60th Canadian Geotechnical Conference, Ottawa Geo2007, 1865-1871.

Topp, G.C., Davis, J.L. and Annan, A.P. 1980. Electromagnetic determination of soil water content: Measurements in coaxial transmission lines. *Water Resources Research*, **16**: 574–582.

SCALING INLINE STATIC MIXERS FOR OIL SAND MATURE FINE TAILINGS FLOCCULATION

Alebachew Demoz

Natural Resources Canada, CanmetENERGY Research Centre, Devon, AB

ABSTRACT

Current operations to reclaim mature fine tailings (MFT) ponds involve flocculation steps utilizing high-molecular-weight polymers. Static inline mixers are well-suited for this application. We performed MFT flocculation tests in 1-inch pipes utilizing commercial inline mixers by Chemineer-Kenics-KMS™, Koflo 275™, and Komax™. The objective was to determine an index or mixing parameter corresponding to optimal dewatering performance of flocculated MFT.

MFT was mixed with polymer solution at a dosage known to produce readily dewatering flocculated MFT. Treatment conditions using each of the static mixers was varied by changing the flow rate and number of static mixer elements. The Reynolds number, Re , mean fluid flow velocity, V , and the specific mixing energy dissipation rate per unit mass, ε , of the flocculated material were examined as likely parameters that can be associated with dewatering rate. The dewatering rates of the flocculated MFT passed through a peak with increasing V and Re , as evaluated by capillary suction time (CST) and/or the settling rate of the water/mud interface. For a given static mixer, the greater the number of elements in the inline mixer, the lower were the values of V and Re at which the peak dewatering rate occurred. Setting equal values of V or Re did not produce similar dewatering rates of flocculated MFT. On the other hand, the peak dewatering rates occurred within a narrow range of ε for the different types of static mixers used. These results suggest that as long as equal ε is dissipated by the mixing process, a variety of static mixers and configurations will produce flocculated MFTs having similar dewatering behaviours. In short, ε can be used to scale inline static mixing to produce flocculated MFT with optimal dewatering properties.

INTRODUCTION

Disposing of fines from a fluid waste stream requires aggregation of the solid particles such that

larger and denser solids masses settle out, which, in turn, improves dewatering. This aggregation (flocculation) can be accomplished by addition of a single polymer flocculant or a combination of flocculants to the tailings stream. A pretreatment step in which inorganic coagulants supplement the polymer action may also be used. Dispersion of the additives in oil sand mature fine tailings (MFT) and shear compaction of the resulting flocs requires mixing.

Inline mixing, when feasible, has a number of operational and cost advantages over dynamic mixing, which utilizes rotating impellers inside tanks. Static mixers are compact, low in cost, consume less power, and do not have any moving parts that require regular maintenance or result in sealing problems. Unlike dynamic batch mixing, inline static mixing is a continuous process. Inline static mixers are often employed as single-pass mixers. There is no need to maintain an inventory of feed as the MFT can be treated on demand directly from the tailings pond. The material residence time is short and good mixing is achieved owing to near-plug-flow behaviour. The capital and operating costs of dynamic mixers capable of handling the large inventories of MFT in a timely manner would be very high.

Static mixers consist of specially designed rigid structures inserted end-to-end in pipes in order to enhance turbulent mixing. The mixing elements split and recombine the mixture radially while the flow continues axially. This repeated action achieves uniformity in composition. Static mixer elements are broadly categorized into helical or twisted-ribbon, corrugated plate, and structured geometries (grids) mentioned below. Corrugated plate static mixers such as the Sulzer SMV™ have low porosity and are impractical for MFT flocculation. The Koflo and KMS static mixers used in this study are about 85% porous and are better at coping with plugging and deposition (fouling) problems during flocculation. From the perspective of static mixer selection, high-pass static mixers with blades protruding from the wall, such as the Chemineer-Kenics HEV™ mixer, provide improved

avoidance of flow restrictions associated with accumulation of deposits from the MFT.

Field observations and investigations of the dewatering rate of MFT flocculated using both static and dynamic mixers have proved that the dewatering rate is dependent on aspects of mixing, especially mixer type, mixing time, and mixing intensity (Demoz and Mikula 2012, 2010, Hogg 2000, Gillis et al. 2013). While static mixers are widely used in food processing; the manufacture of paints, polymers, and pharmaceuticals; and water treatment (Etchells 2004, Thakur 2003); the literature on their application in oil sands MFT flocculation is limited. Management of oil sands MFT operations currently appears to rely on experience and some trial and error, an approach that is normally fraught with start-up problems, time losses, and a lack of guidelines for restoring upset operations. This study examines the effects of three different commercial static mixers, the number of static mixer elements, and flow rate on MFT flocculation and dewaterability. Dewatering performance was evaluated based on capillary suction time (CST) and/or the settling rate of the water/mud interface (Sholz 2006). The overall goal is to determine an index or mixing parameter that correlates well with optimal dewatering of flocculated MFT. Such a mixing parameter could then be applied to optimize static mixer flocculation systems and for use as a scaling parameter.

EXPERIMENTAL

Some of the mixing tests required as much as a drum of MFT for every 5 minutes of test run. The tests were conducted in a pilot plant equipped with process units and sumps adequately sized to handle the relatively large volumes of material as shown in Figure 1. The MFT was fed from a 1.2-m³ tank using a progressive cavitation pump (capacity of 45 L/min). To maintain uniformity, the feed in the tank was continuously stirred during the flocculation process. The polymer solution was pumped using another smaller progressive cavitation pump (capacity of 10 L/min). The volume of added polymer solution was changed in proportion with the MFT flow rate such that the experimental polymer dosage was maintained. The flow rates of the pumps were set using their own variable frequency drives.

A high-molecular-weight, partially charged anionic polyacrylamide macromolecule was used as

flocculant. The flocculant dosage was 1000 g/ton of dry polymer to solids in the MFT. The feed was preconditioned with gypsum at the same concentration as the flocculant. The flocculant solution concentration was 0.1% (w/w). The polymer was injected at the centerline of the 1-inch diameter pipe, as close to the static mixer inlet as possible so that the flocculant wouldn't drift to low-turbulence areas and stream out before being dispersed in the tailings.

Three different types of commercial stainless steel static mixers from Chemineer-Kenics, Koflo, and Komax were used in this mixing study (see Figure 2). The Koflo and Komax mixers were acquired as units of 12-element mixers with 1-inch MNPT (male national pipe thread) connections. The adjoining pipes were 1-inch nominal diameter schedule 40 pipes.

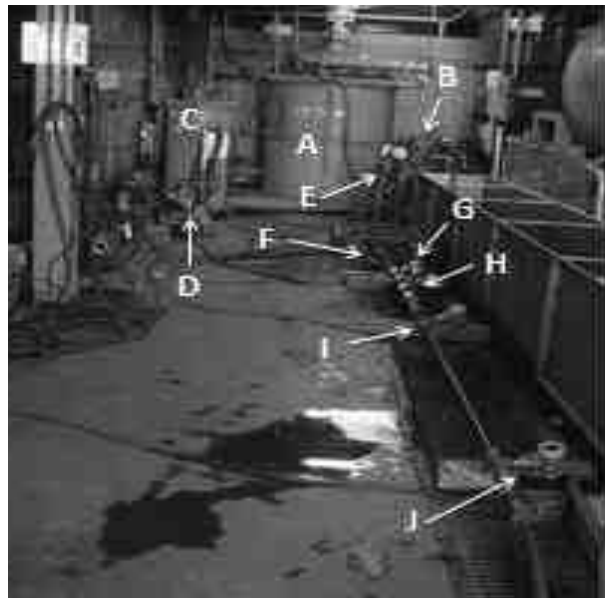


Figure 1. MFT flocculation test setup. A-MFT tank, B-MFT pump, C-Polymer solutions tank, D-Polymer pump, E-Flowmeter, F-Polymer injection point, G-Inlet pressure gauge, H-static mixers, I-Outlet pressure gauge, J-pipe pressure gauge.

An Andreas+Hauser™ Coriolis, PromasI flowmeter was placed upstream of the polymer injection point to measure the MFT flow rate. The pressure drop across the static mixers was measured using Andreas+Hauser™ Cerabar S PMC71 pressure transmitters (see Figure 1). The flowmeter and pressure transmitters all had 4 mA to 20 mA

analog signal outputs. These signal outputs were digitized and recorded by a PC interfaced with an Instronet 100™ data acquisition system. Pressures and flow rates were recorded every 4 s.

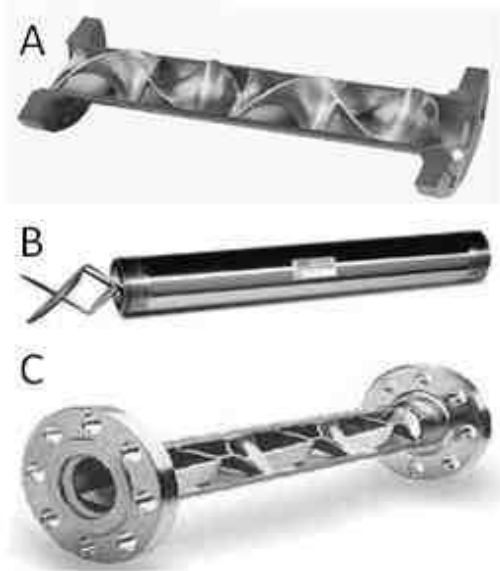


Figure 2. Cut-out figures of inline static mixers used. A) Kenics-KMS, B) Koflo 275, C) Komax-triple action.

Since the aim of this work was to produce rapidly dewatering flocculated MFT, the results of the mixing evaluations were evaluated in terms of dewaterability measures: capillary suction time (CST) and the initial settling rate of the mud/water interface. Measurements of the initial settling rate were done by collecting samples in a 1-L graduated cylinder at the discharge point of the 1-inch pipe. Some of the product was transferred to five CST cells. The CST measurements were conducted using a Triton Electronics meter and type 319 single-radius cell heads 10 mm in diameter. Whatman #14 filter paper was used to measure the CST. Results given are the means of at least triplicate CST measurements.

Feed materials characterization and rheological measurements are given in detail in Demoz and Mikula (2012).

RESULTS AND DISCUSSION

Pressure drop is a critical parameter of MFT flocculation using an inline static mixer. It dictates the energy dissipation rate of the mixing and is

related to the mixer geometry and the material properties of the MFT. The material properties, such as viscosity and density, can change as the flocculation process progresses, resulting in changes in pressure drop (see Figure 3). The pressure drop of the static mixers using MFT under conditions when the flow is Newtonian (as shown in Figure 3) is given in Figure 4. Gypsum-preconditioned MFT at 16% (w/w) solids is Newtonian at high shear rates, as shown in Figure 3 (shear rate $> 100 \text{ s}^{-1}$).

For the eight-element KMS mixer, more than one flow region can be distinguished based on the slope. In a laminar flow field, viscous forces dominate and the pressure drop has a linear dependence on flow rate. The KMS mixer was the only one where the flow rate was low enough to have a flow zone near the laminar region (Figure 4a). As the figure shows, ΔP was nearly linearly dependent on flow rate for flow rates below 5 L/min. It is well known that, under laminar flow, the pressure drop is proportional to the mean velocity. The additional static elements promote turbulence. In turbulent flow regimes the pressure drop is roughly a square function of velocity (Massey and Ward-Smith 1998). The slope of the log-log plot of the pressure drop vs flow rate for higher elements of the KMS mixer was between 1.9 and 2.

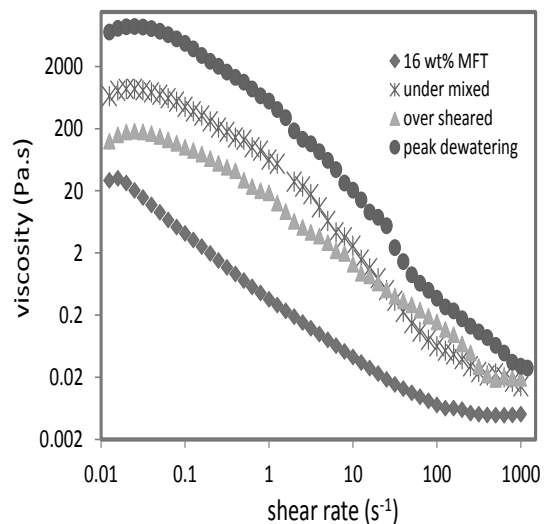


Figure 3. Progress of the steady-shear viscosity of 16% (w/w) solids MFT as it was flocculated using the Komax inline static mixer.

At all flow rates used, no similar breaks in the slopes were observed when using the Koflo and Komax static mixers as illustrated by the Komax pressure drop in Figure 4b. Moreover, the slopes of $\log\Delta P$ vs $\log Q$ were close to 2, indicating that all of the flocculations by Komax and Koflo were carried out in turbulent flow (Massey and Ward-Smith 1998).

In laminar flow, the mixing proceeds by alternating splitting and remixing at the junction and stretching and folding within the elements in a sequential fashion. Such mixing action may be adequate for blending but cannot create locally high shear stress required to form compact flocs that dewater well.

In turbulent flow the elements intensify the turbulence by creating eddies of higher energy. This leads to more intense shearing and radial mixing that, up to a point, are necessary to produce readily dewatering flocs. In all cases the pressure drop across the static mixer increases linearly with the number of mixing elements. The dependence of pressure drop on the number of elements in static mixers is analogous to the dependence of pressure drop on pipe length in pipes. In fact, authors use the same pressure drop flow equation for static mixers as for open pipes:

$$\Delta P = f \frac{L \rho V^2}{D} \quad (1)$$

where, f is the Fanning friction factor, V is the mean superficial velocity of fluid (m/s), ρ is the density (kg/m^3), and D and L are the diameter and length of the static mixer (m). For static mixers, f additionally depends on the geometry and arrangement of the elements. In the literature, f for static mixers is presented in two ways: first, as the ratio of the pressure drop across the static mixer to that across an open pipe of the same diameter, and, second, as empirical correlations based on measurements of flow rate and the pressure drop across the static mixer. In other words, the friction factor calculated from measurements of pressure drop and flow rate is mathematically correlated with Re :

$$f = g(Re, geometry) \quad (2)$$

The friction factor is an alternative way of expressing energy dissipation rate as given by equation 3. Figure 4 shows that the friction factor of a Komax static mixer is higher than that of a KMS mixer at the same Re . Comparing the three

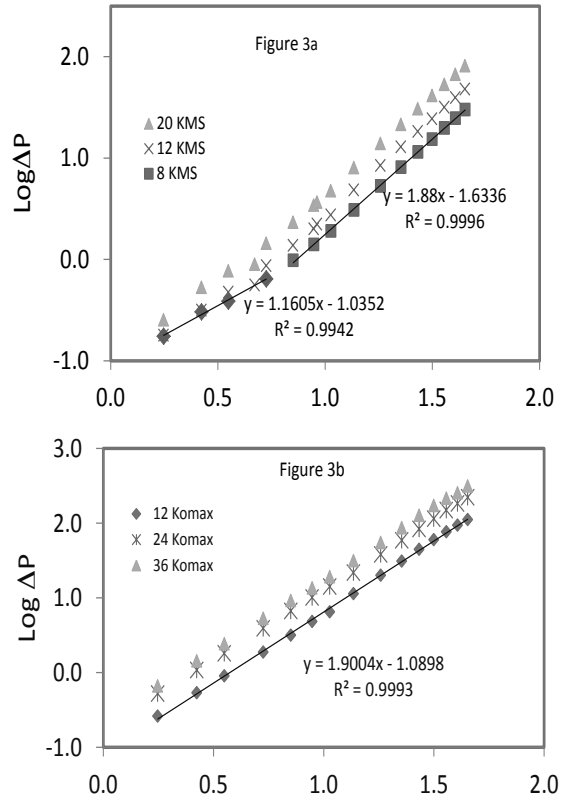


Figure 4. Empirical pressure drop across KMS (4a), and Komax (4b) static mixers for flow rates from 1.8 L/min to 45 L/min of 15% (w/w) solids MFT.

commercial static mixers used in our studies, the friction factors of Koflo and Komax mixers are 1.85 and 2.3 times that of the KMS static mixer, respectively. This is in agreement with the general observation that static mixers with helicoil surface elements show less pressure drop than those that utilize grids.

$$f = \frac{\varepsilon D}{2V^3} \quad (3)$$

The dewatering rate of MFT flocculated using different impellers in stirred tanks was shown to pass through a peak with increasing mixing energy input. The energy dissipated by the agitation was shown to be the salient property regardless of changes in mixing conditions and the dewatering rates of the flocculated MFT (Demoz and Mikula 2012). The inference from this is that other mixing systems can also be examined using the same energy density criterion. Kinetic energy supplied by the pump provides the mixing energy input that produces pressure drops across the inline static

mixers. The mixing energy density, also referred to as the specific energy dissipation rate, can be expressed as

$$\varepsilon = V \frac{\Delta P}{L} \frac{1}{\rho} \quad (4)$$

where ε is the specific energy dissipation rate per unit mass (W/kg). The other often-mentioned flocculation parameters in oil sand tailings management are fluid velocity and Re . These and other mixing parameters are well understood in many other applications while the same is not true for oil sands MFT flocculation (Thakur 2003). For plug flow, the mean velocity for static mixers is obtained from

$$V = \frac{4Q}{\pi D^2 \psi} \quad (5)$$

where ψ is the porosity of the static mixer representing the void space. The static mixers used have $0.8 < \psi < 0.85$. The superficial velocity of the fluid reported in this paper is in reference to the 1-inch pipe (Felicie et al. 2010).

There is ambiguity related to true shear rate in the choice of a suitable Reynolds number expression for non-Newtonian fluids. The Metzner-Otto Reynolds expression, Re_g , is recognized as a generalized Re definition (Chhabra and Richardson 2008):

$$Re_g = \frac{\rho D^{n'} V^{2n'}}{8^{n'-1} k'} \quad (6)$$

where k' and n' are the apparent consistency index and power index (different from the rheological power law model equation index). Re_g calculation following the approach of Haldenwan et al. (2010) to obtain k' and n' , is not applicable for our static mixer data because the analyses gave $n' > 1$. This would contradict the fact that MFT and flocculated MFT are shear thinning, i.e., $n' < 1$ (see Figure 3).

Figure 3 shows that MFT and flocculated MFT have steady viscosity at low and high shear rates. The fluid is constantly evolving from the moment when the MFT and flocculant enter the static mixer to the time they leave the static mixer. The floc sizes, size distribution, and viscosity are in flux during flow through the static mixer. A plausible approach supported by the rotating vane shear rheological measurements (see Figure 3) is to use the pseudo-Newtonian plateau viscosity at high shear to approximate the viscosity of the mixer

fluid. In this case, Re can be calculated using its common definition

$$Re = \frac{VD\rho}{\eta} \quad (7)$$

where η is the apparent viscosity of the flocculated MFT (Pa.s, N.s m⁻³).

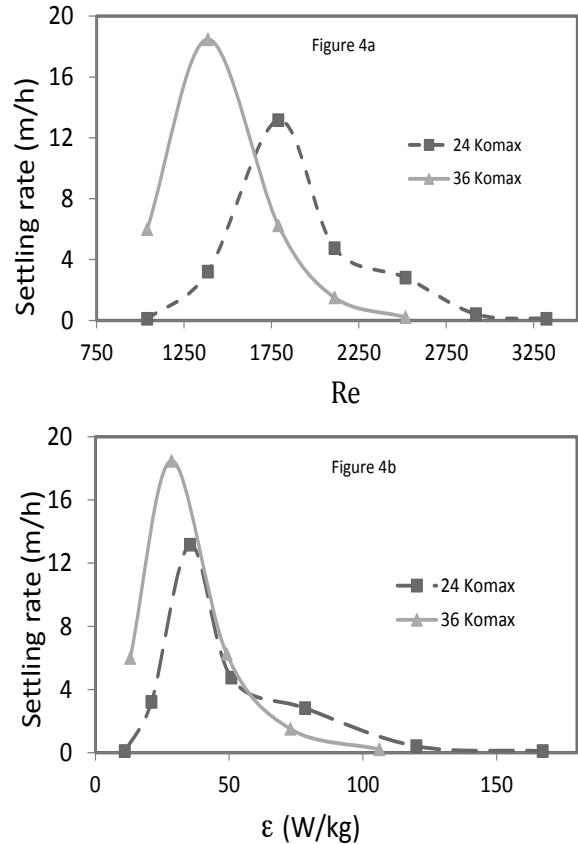


Figure 5. Initial settling rate dependence with Re (5a) and specific energy dissipation rate (5b) of MFT flocculated using 24- and 36-blade Komax static mixer elements.

The CST and initial settling rate of the mud/water interface represent the long- and short-term dewaterability of the flocculated MFT. Figure 5 presents the initial settling rate of flocculated MFT using two Komax static mixer combinations: 24- and 36-element mixers. Inline static mixing gave poorly dewatering flocculation at low and high flow rates, with better dewatering occurring in the intervening range. There is a clear peak in the settling rate of the flocculated MFT with increasing Re and ε . The higher-settling-rate samples gave

correspondingly shorter CST values. The CST is known to be inversely related to water release tendency (Sholz 2006). The Re dependence is a scaled version of V dependence (see equation 7) as the flocculated MFT is considered to have a pseudo-Newtonian apparent viscosity at high shear rates. In other words, the dewatering analyses by Re and V are not independent of each other. Therefore, Re dewatering dependence applies equally to V dependence.

The dewatering rates of flocculated MFT produced by the two other static mixers (Kenics-KMS and Koflo 275 static mixers) gave the same trend as described above for Komax. The Re at which peak dewatering of flocculated MFT was obtained varied with the number of static elements. Longer static mixers (more elements) produced optimally dewatering flocculated MFT at lower Re compared to the same type of static mixer having fewer elements. That is, the Re or V for the optimally dewatering mixing using the same static mixer was dependent on the number of elements used. However, the difference in ε of the optimally dewatering flocculation produced by static mixers differing in the number of elements is small enough that it can serve as a basis for scale-up or optimization of inline static mixer flocculation. The specific energy dissipation rate is directly related to the pressure drop as given by equation 4. The dewatering rate results show that excessive pressure drop leads to overshearing of flocculated MFT and poor dewatering performance, while mixing with inadequate pressure drop does not produce the energy necessary for floc formation and compaction.

CONCLUSIONS

Inline static mixers are appealing for large-throughput, continuous, MFT flocculation. Commercial applications often follow pilot-scale evaluations and success is dependent on proper scale-up. Our pilot-scale investigations of MFT flocculation by inline static mixing demonstrate that different styles of static mixers can be used to flocculate MFT. Multiple static mixer elements promote radial flow such that, starting from the lowest flow rates of 2 L/min, the flow was determined to be turbulent. Even in turbulent mixing, there is a low-threshold flow rate range, depending on the mixer design and number of

elements, to achieve satisfactory flocculation. Accordingly, MFT flocculation utilizing static mixers in laminar flow is totally ineffective.

Inline static mixing was investigated for the process requirement of producing readily dewatering flocculated MFT. The values of V , Re , and ε were examined to correlate with the peak dewatering performance of flocculated MFT. The results demonstrate that

1. For time-invariant fluid, the pressure drop is directly proportional to the number of elements for a given flow rate.
2. For a given inline mixer setup, flocculation to produce the best-dewatering MFT passes through a peak with increasing flow rate.
3. The greater the number of static mixer elements, the lower the flow rate at which the peak dewatering performance is obtained.
4. There is no similitude of V and Re with respect to the peak dewatering of MFT flocculated by different static mixers. V and Re are poor scaling parameters for MFT flocculation.
5. The specific energy dissipation rates of the optimally dewatering flocculated MFTs produced by different inline static mixers were comparable. These results suggest that prospective static mixers and their arrangements can be based on equivalence of ε . In other words, ε can be used to scale the flocculation of MFT by inline static mixers. At the field operator level, this means implementing control of the line pressure drop with flow rate for a consistent MFT feed.

ACKNOWLEDGEMENTS

The author is thankful for support and funding for this project provided by the office of Energy Research and Development under the ecoENERGY Innovation Initiative (ecoEII) program. All of the pilot plant tests were conducted with help from Dexter Woo, Craig McMullen, and others from the Tailings and Water team. Vincent Castonguay and Nirpal Dhillon from the Engineering faculty of the University of Alberta also participated as part of their student co-op program.

REFERENCES

- Chhabra, R.P., Richardson, J. 2008. Non-Newtonian Flow in the Process Industry, Oxford: Butterworth-Heinemann.
- Demoz, A., Mikula, R.J. 2012. "Role of mixing energy in the flocculation of mature fine tailings", *J. Environ. Eng. ASCE.*, 138, 129-136.
- Demoz, A., Munoz, V. & Mikula, R. 2010. Optimizing MFT Dewatering by Controlling Polymer Mixing, 2nd International Oil Sands Tailings Conference, Edmonton, Alberta.
- Etchells, A. W. and C. F. Meyer: *Mixing in pipelines*. 2004, In Paul, E.L, Atiemo-Obeng, V.A., Kresta, S.M., (editors): Handbook of industrial mixing. Wiley-Interscience, Hoboken (USA), chapter 7.
- Felicie, T., Sauze, L.N, Ricard, A., 2010 Turbulent liquid-liquid dispersion in Sulzer SMX mixer, *Ind.Eng.Chem.Res.* 49, 623-632
- Gillis, P.A. Moore, J.S., Poindexter, M.K., Witham, C.A., Chen, W. , and H. Singh, H, Mohler, C.E., J. Atias, J, 2013, The effects of in-line static mixer flow loop operational parameters on flocculant performance in mature fine tailing, in Tailings and Mine Waste '13, pp 137-146, Nov 3-6, 2013, Banff, AB, Canada
- Godfrey, J.C. 1992. "Static mixers", Chap 12 In Harby, N. Edwards, M.F., Nienow, A.W, (editors; Mixing in the process industries. Butterworth-Heinemann, Oxford, G.B.
- Haldenwang, H., Slatter, P.T., Chhabra, R.P., 2010. An experimental study of non-Newtonian fluid flow in rectangular flumes in laminar, transition and turbulent flow regimes, *J. S. Afr. Inst. Civ. Eng.* 52, 11-19.
- Hogg, H. 2000. Flocculation and dewatering., *Int.J.Miner.Process.*, 58, 223-236.
- Massey, B., Ward-Smith, J., 1998 Mechanics of fluids, 7th ed., (Cheltenham, U.K. Stanley Thorns Pub. Ltd, p. 197 and Ch. 7.
- Scholz, M. 2006. "Revised capillary suction time (CST) test to reduce consumable costs and improve dewaterability interpretation." *J. Chem. Technol. Biotechnol.*, 81, 336-344.
- Thakur, R.K, Vial, Ch., Nigam, K.D.P., Nauman, E.B., Djelveh, G., 2003. "Static mixers in the process industries", *Trans. IChemE*, 80

DEVELOPMENT OF STANDARD OPERATING PROCEDURES FOR STORAGE AND HANDLING OF WATER SAMPLES CONTAINING NAPHTHENIC ACIDS

Hamed Mahdavi¹, Haneef Mian¹, Steven Hepperle¹ and Zvonko Burkus²,

¹NAIT Applied Research Centre for Oil Sands Sustainability (NARCOSS), Edmonton, AB, Canada.

²Alberta Environment and Sustainable Resource Development (AESRD), Edmonton, AB, Canada.

ABSTRACT

Naphthenic acids (NAs) are considered as the main source of chronic and acute toxicity in oil sands process-affected water (OSPW). In this research NA losses due to storage in different materials, various preservation conditions, and due to separation of suspended solid were investigated. The other objective of this research is to provide recommendations how to minimize the NA losses before analytical measurements take place.

For separation of solids, two methods were compared - filtration and centrifugation. Our results indicate that there is no significant influence on NA concentration between these two methods.

Four type of glass bottles, 3 type of plastic bottles along with 2 type of centrifuge tubes were tested to determine the NA partitioning (losses) during storage. Lime-soda glass bottles demonstrated a better performance comparing with plastic bottles. In addition, polystyrene centrifuge tube had lower NAs losses than polypropylene (PP) centrifuge tubes.

Four type of bottle cap liners were tested. PTFE caps had the lowest NA losses; however, it is possible that polyethylene, and white rubber leak pollutants in OSPW solution and cause false-higher NA concentration measured by fluorescence spectrophotometer.

Preservation conditions including storage in fridge, at room temperature, low and high pH, and addition of methanol were studied. Our observations imply that the best storage conditions are preservation in the fridge without any pH change or methanol additive.

INTRODUCTION

Bitumen recovery from oil sands ore, either through surface mining operation or steam assisted gravity drainage (SAGD), is associated with the production of oil sands process-affected water - OSPW (Allen 2008). Because of inorganic and organic pollutants, OSPW is collected and impounded in tailings ponds according to environmental regulations and practice.

The Canadian Association of Petroleum Producers (CAPP 2014) predicts that the oil production from oil sands will increase by 4-5% annually over the next 15 years (www.capp.ca). Between 10-15 bbl of water is required to process a barrel (bbl) of bitumen. Oil sands tailings ponds, besides OSPW contain sands, clay, and hydrocarbons, such as unrecovered bitumen, polycyclic aromatic hydrocarbons (PAHs), lost diluent, and NAs. Naphthenic acids are the focus of this research. Tailings ponds are utilized for two distinct reasons: 1) to act as reservoirs for process-affected water to be re-used, and 2) to act as settling basins for tailings clays so that they can eventually release trapped water.

NAs have been recognized as the primary source of toxicity in OSPW (Whitby 2010). Despite numerous publications on identification and biological elimination of NAs, there is a gap in knowledge of the standard operating procedure for sampling, storage and handling of OSPW. Being polar compounds with relatively long hydrophobic chain, naphthenic acids have tendency to partition to plastics, organic sediments and other materials potentially affecting mass balances (losses) that need to be accounted. For the lack of a standard procedure, articles and industries have employed various protocols for sampling, storage, monitoring, and measurements of NAs, while the potential loss of NAs through those methods is

unknown. Partitioning to different glass bottles, storage and centrifugation containers during handling or storage have never been considered as variables that can affect quantitative or qualitative results. Initial research by Martin et al 2014 identified the influence of such conditions on commercial NAs, while the behavior of tailings-associated NAs is less known.

In this research, suspended solids separation, suitable container and conditions for preservation of OSPW are investigated. For suspended solids separation, centrifugation at different times and filtration were compared. Various containers including glass bottles, plastic bottles, and centrifuge tubes were tested for preservation of OSPW samples to find out the bottle with minimum NAs losses. Cap liners, made of 4 different materials were evaluated in terms of NA adsorption. In addition, the best storage condition in terms of temperature, pH, and addition of methanol was investigated. It is believed that results from this investigation will elucidate many unknown aspects of NA losses through sample handling and preparation before NA measurement.

MATERIALS AND METHODS

All glassware were trace cleaned with a detergent (Sparkleen1, Fisher brand or Liqui-Nox Precision Liquid Detergent), rinsed with tap water, pure methanol (Fisher brand, Certified A.C.S) and Milli-Q water (three times each). All chemicals and solvents were Certified A.C.S. All tests were done in triplicates along with a negative control (blank sample). Except in suspended solids separation tests, filtered OSPW samples (0.45 μm , Durapore PVDF Membrane, Millipore) were used for all the experiments. OSPW sample, used in this research, was taken from the surface of the oil sands tailings pond water with initial NA concentration of $46.6 \pm 1.6 \text{ mg L}^{-1}$, total suspended solids (TSS) of $40.53 \pm 3.56 \text{ mg L}^{-1}$, and pH of 8.6.

Naphthenic Acid Measurement

Naphthenic acid measurement was conducted using a Varian fluorescence spectrophotometer model Cary Eclipse from Agilent Technologies (Scan Software Version: 1.1(132)) in a quartz cuvette (10mm \times 10mm) with a PTFE stopper (VWR, Canada). For quantitation of NAs, OSPW and pure methanol (Fisher brand, Certified A.C.S) were mixed (1:1) and scanned by fluorescence spectrometer in synchronous mode at following

settings: start and stop wavenumbers (nm): 250 and 400 respectively, delta wavelength (nm): 18 nm, emission and excitation slit: 5 nm, scan control: medium, and excitation-emission filters were in auto condition. The fluorescence intensity (a.u.) at 280 nm wavenumber was used for quantification of NAs.

Standard curve preparation 5 L of OSPW were filtered through 0.45 μm filter paper (Durapore PVDF Membrane, Millipore) using vacuum Erlenmeyer flask and filter holder. pH was raised to > 10 by adding NaOH solution, followed by three times extraction using 50 mL of dichloromethane (DCM HPLC grade, BDH, Radnor, PA) per liter of sample in consecutive steps using 2-L glass funnel to remove non-polar polycyclic aromatic hydrocarbons from OSPW. Afterwards, pH was reduced to $\text{pH} < 2$ using HCl solution. Another 3 \times 50 mL DCM extraction (per liter of sample) was performed to extract NAs this time. The weight of extracted NAs was measured in a pre-weighed glass bottle after overnight evaporation of DCM under fume hood. The stock solution of 2500 mg/L of NAs in methanol was prepared and used for making standard solutions. A phosphate-methanol solution (containing 50% v/v of 0.05M phosphate buffer ($\text{pH}=8.5$) and pure methanol) was prepared and used for diluting NAs stock solution to make standard solutions in low concentration (0, 0.2, 0.5, 1, 2.5, and 5 mg L^{-1}) and high concentration (0, 5, 12.5, 25, and 50 mg L^{-1}).

Influence of Suspended Solids

50 mL of original OSPW sample (containing suspended solids) was added to each of 3 \times 6 glass centrifuge tubes (100 mL, Pyrex) and centrifuged at 3500 \times g for 5, 15 and 30 min. Same volume of methanol was added, followed by fluorescence. Supernatant (from 3 remaining centrifuge tubes) was filtered (0.45 μm , Durapore PVDF Membrane, Millipore) and filtrate was scanned for NA content. Suspended solids on the surface of filters were rinsed by 5 mL of 50% phosphate buffer-methanol solution and scanned for NAs content. The control samples (no centrifugation time, 3 \times 50mL of OSPW) was filtered and NAs contents of filtrate and suspended solids on the surface of filter were measured as previously explained.

Container for Storage

All containers, except trace cleaned borosilicate glass bottles and centrifuge tubes, were trace

cleaned as explained before. 50 mL of filtered OSPW was added to each 60 mL bottle. 10 mL of filtered OSPW was added to each 15 mL centrifuge tube. The cap liner materials for all glass bottles were PTFE, while for the plastic bottles, the cap was made of the same material as.

All containers were kept in fridge for 8 days and then the concentration of NAs in OSPW was measured using fluorescence. To measure the adsorbed NAs, OSPW was discarded and the internal surface of each container was rinse three times with 50% phosphate-methanol solution to the final volume of 5 mL, and then scanned for NA content.

Silanization protocol glass bottles were heated at 80°C for two hours in an oven and cooled down in a desiccator. Each bottle was filled to top with silanization solution (5% dichloromethylsilane in toluene) and left under fume hood overnight with closed cap. Then, the glass bottles were washed with pure toluene, followed by rinsing three times with methanol. Each bottle was filled to the top with pure methanol and left under fume hood for 30 min. All bottles were heated again in oven at 80°C for two hours, followed by cooling in the desiccator.

Influence of Bottle Cap Liners

Four different types of cap liners (cap size 38-400) were tested for influence on OSPW: PTFE, Polyvinyl, Polyethylene, and White Rubber. 12 glass bottles (125 mL, type III soda-lime glass) were trace washed as explained before and filled with 50 mL filtered OSPW. 3 caps for each liner were used to fasten the bottles. Bottles were stored in a fridge at ≈4°C upside-down for 7 days to expose OSPW to cap liner.

After 7 days of exposure, OSPW was scanned to determine the NA content. To measure the adsorbed NAs, the inner surface of each bottle and its cap liner was rinsed three times with the phosphate-methanol solution to the final volume of 5 mL. NA concentration in the 50%phosphate-methanol solution, was measured using fluorescence spectrophotometer.

Storage Conditions

Trace cleaned borosilicate glass bottles with PTFE caps (60 mL) were used to evaluate the impact of temperature, pH and addition of methanol on the

NA losses during storage of OSPW. 50 mL of filtered OSPW were added to each glass bottle.

Three bottles were stored in the fridge (≈4°C) and three were at room temperature (≈22°C) with presence of natural light. To evaluate the effect of pH, different pH solutions (pH=2.1 - 11.1) of OSPW were prepared by adding NaOH and HCl solutions and stored in the fridge for 8 days. Before measurement of NAs, pH of the samples was adjusted to pH ≈8.6 (the original pH of OSPW). To study the impact of methanol addition to OSPW (to potentially reduce NA losses), a 50% v/v methanol-OSPW solution was prepared and used for this experiment. All the samples were kept for 8 days in triplicate.

Statistical analysis

To determine the significance of difference in NA concentrations for more than two samples, one way analysis of variance (ANOVA) and for two samples simple student T-test was performed (P-value < 0.05) using MS Excel. Error of the mean is indicated using plus and minus one standard deviation in graphs and text.

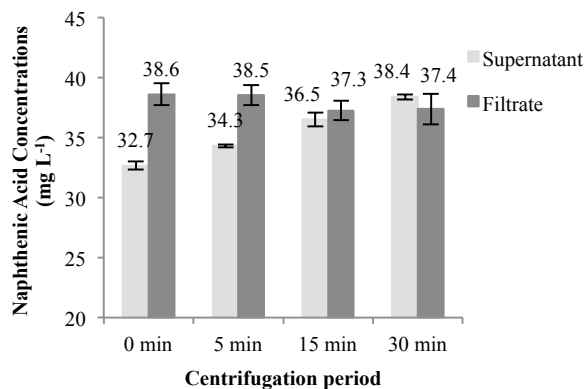
RESULTS AND DISCUSSION

Influence of Suspended Solids

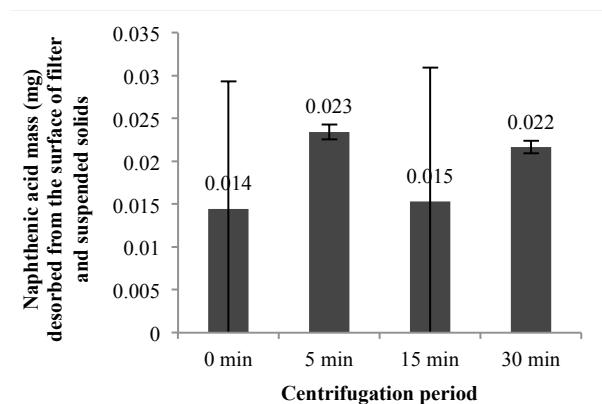
Figure 1 shows NA partitioning in supernatant, filtrate and filter (with solids) after 0min, 5min, 15min, and 30min centrifugation at 3500xg. In Figure 1(a), the concentration of NAs in OSPW supernatant apparently increases with centrifugation time. This might be a result of TSS presence in OSPW, which may interfere with fluorescence spectroscopy and cause falsely lower NA concentration reading.

One-way ANOVA statistical analysis for filtrates after different centrifugation times (0, 5, 15, and 30 min) indicated that there is no significant difference (P-value 0.25). In other words, the centrifugation combined with filtration time did not impact NAs concentration reading. To figure out the contribution of filtration to NA losses, a simple student t-Test (with equal variance validated using F-test) was conducted between filtrate (0 min) and supernatant (30 min). This analysis indicates that there is no significant difference (P-value 0.71) between filtrate from the blank (0min) and supernatant (30 min); or in terms of NA losses, there is not a significant difference between two

methods of filtration and centrifugation. In this experiment a PVDF filter (0.45 μm , Durapore PVDF Membrane, Millipore) was used, however, for other type of filters (depending on material which filter is made) there might be some NA adsorption (losses) on the surface of membrane.



(a)



(b)

Figure 1. Naphthenic acid concentrations, partitioned in 50mL of OSPW sample (a) supernatant (before filtration) and filtrate (filtered supernatant) at different centrifugation times at 3500×g (b) The weight of detected NAs on the surface of suspended solids.

Our observations indicated the small partitioning of NAs on the surface of suspended solids compared with dissolved NAs content. Based on our results, most of NAs in OSPW are present in a soluble form. Figure 1(b), which is NA adsorbed on the filter and suspended solids at different centrifugation times, shows that there is not a clear increasing or decreasing trend in NA content on

the surface of the filter after various centrifugation times. This assumption was verified by running one-way ANOVA statistical analysis among NA content on the filter in different centrifugation times (0, 5, 15, and 30 min). The ANOVA results also implied no significant difference (P-value 0.68) among filters.

Total suspended solids (TSS) in OSPW used in this experiment was $40.53 \pm 3.56 \text{ mg L}^{-1}$ which is lower than those reported in other literatures (Allen 2008) OSPW, used in this experiment, was sampled from the surface of tailings pond, which generally contains smaller total suspended solids concentration, comparing with samples taken from depth.

Container for Storage

Figure 2(a) shows the apparent NA concentrations in OSPW stored in various containers made from different materials after 8 days storage. To minimize the impact of microbial biodegradation on the concentration of NAs, filtered OSPW (0.45 μm) was used. According to this figure, there is no reduction in NA concentration in any bottle, however, in lime soda clear and LDPE bottles a slightly higher concentration was measured.

Regarding the accuracy of fluorescence spectrophotometry method and high standard deviation (error bars) for clear lime-soda, the higher NA concentration might be resulted from the experimental error.

Our results indicate that NA adsorption requires more exposure time to significantly reduce the NA concentration in OSPW sample stored in 60 mL bottles (or 15 mL centrifuge tubes). For future research, it is suggested that storage time should be increased to more than three month. Also at long exposure time, the NA reduction due to natural biodegradation must be considered and autoclaving samples or filter sterilization (0.2 μm membrane) might be necessary.

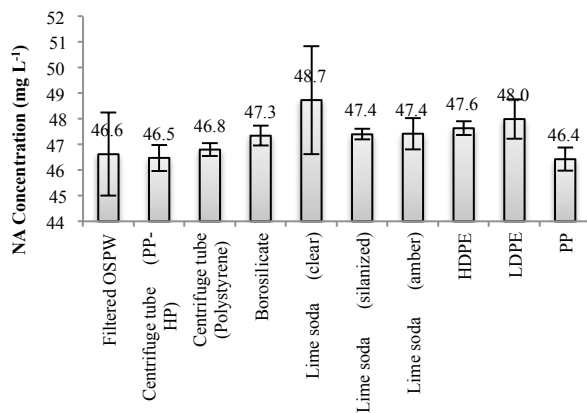
Figure 2(b) illustrates the NAs adsorbed on the inner surface of bottle. Borosilicate glass bottle and all plastic bottles including HDPE, LDPE, and PP had the highest NA adsorbed on the surface of bottles. The minimum adsorption of NAs was observed in lime soda (silanized).

In this experiment, the volume of all the bottles was 60 mL (except for centrifuge tubes that was 15 mL) and the height and shape of bottles were

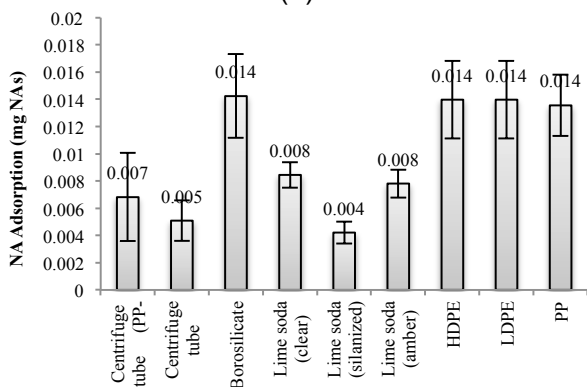
similar except for borosilicate glass (60 mL). Borosilicate glass bottles were taller potentially creating 82 cm² exposure surface with 50 mL OSPW. The exposure surface with 50 mL of OSPW for lime soda glass bottles and plastic bottles were 59 and 55 cm² which are similar. This increase in the exposure surface may contribute to higher mass of NAs observed in figure 2(b) for borosilicate bottle.

Influence of Bottle Cap Liners

One of the important factors that is critical for storage of OSPW is selection of cap liner materials. Cap liner material should have a minimum interaction with liquids stored in bottles.



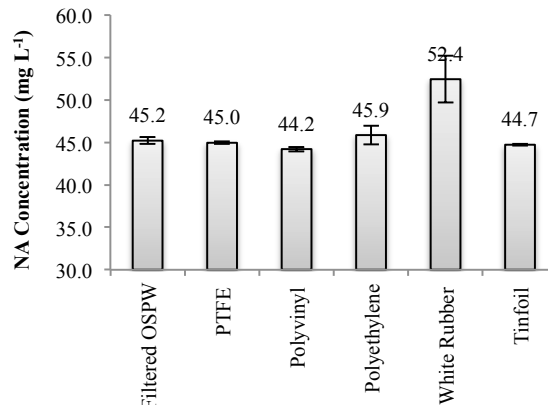
(a)



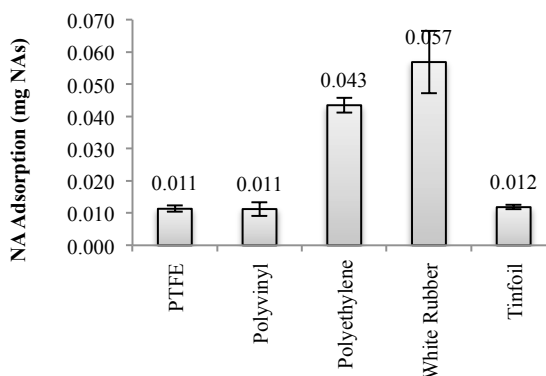
(b)

Figure 2. Partitioning of NAs inside Centrifuge tubes, borosilicate and lime-soda glass bottles, and (HDPE), (LDPE) (PP) plastic bottles. (a) NAs concentration in OSPW sample, (b) mg NAs on the inner surface of bottles (NAs losses).

Figure 3(a) shows that PTFE cap liner, followed by polyvinyl, and tinfoil demonstrated small influence on OSPW within 7 day storage time. However, a higher apparent concentration of NAs in OSPW was observed for white rubber and polyethylene cap liner, which indicate the possibility of leaking of some organic compounds into the OSPW sample from liner materials. Figure 3(b) also verifies the possibility of leakage from white rubber and polyethylene cap liner. Since fluorescence spectroscopy mainly targets the hydrocarbons with aromatic rings, therefore, it can be concluded the leaked compounds from white rubber and polyethylene cap liner might possess an aromatic structure.



(a)



(b)

Figure 3. Cap liner adsorption test. (a) NA concentration in OSPW after 7 day exposure time, (b) NA adsorption on the cap liner.

Storage Conditions

Preservation conditions such as temperature, pH and addition of methanol, may impact NA losses during storage time. According to Figure 4(a), storage at fridge was the best resulting in the NA concentration closest to the original OSPW. Presence of light slightly increased the NAs concentration over the course of 8 days. In this test, the filtered OSPW sample (0.45 μm) was used and therefore the microbial population and consequently microbiological activity was considerably reduced. However, for the storage of non-filtered OSPW, room temperature might impact the NA concentration through microbial biodegradation of NAs (Toor et al. 2013). Also algae growth due to presence of light may cause a false-higher NA concentration in OSPW sample.

It was hypothesized that an addition of methanol may curb the biological activities and result a better preservation condition with the similar NA concentration to original OSPW sample. However, our observations indicated an increase in NA concentration reading from 46.6 ± 1.6 to 53.2 ± 0.3 mg NAs L^{-1} (Figure 4(a)).

At low pH (pH=2.1), the NA molecules turn into non-polar form and become insoluble in water. Over the course of 8 days, the insoluble NAs will aggregate or attach to the surface of glass bottle. In figure 4(b), high mass of NA detected on the surface of glass bottle validates the aggregation and partitioning of NAs at low pH. Since low pH insolubilizes NAs in OSPW and creates non-homogeneous solution, it is not suggested for storage of OSPW if NAs are to be measured in the same solution.

At high pH (pH=11.1), NAs molecules will completely dissociate to the ionized form and fully dissolve in water. Although OSPW at high pH create a homogeneous solution, the high pH and complete dissociation of NAs may impact the intensity detected by fluorescence instrument.

It was reported that the fluorescence intensity decreases with increase in pH (Kavanagh et al. 2009).

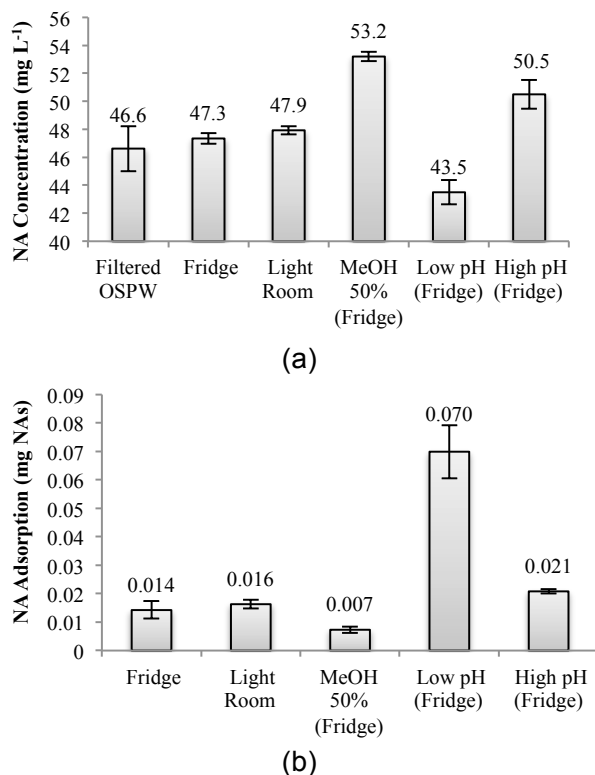


Figure 4. Storage tests: fridge vs. room temperature with presence of light, addition of methanol (50% v/v), low pH (2.1), and high pH (11.1). (a) Concentration of NAs in OSPW samples after 8 days, (b) Adsorbed NAs on the inner surface of borosilicate glass bottles.

The reason for false-higher NA concentration for methanol added sample and high pH sample is unknown at this time; however, using high resolution instruments it is feasible to validate if there has been any change in molecular shapes of NAs after the addition of methanol and increase in pH. We also hypothesize that the addition of methanol or increase in pH may result in separation of dimers, polymers or complete dissolution of micelles over the course of 8 days and this might be responsible for higher intensity on the fluorescence spectroscopy.

Storage in different (plastic) bottles could exacerbate losses and warrants further investigation.

CONCLUSIONS

This investigation was conducted to elucidate the NA losses during sample handling (solid separation, different storage bottles, caps, and conditions) and to determine the best materials and methods to minimize the NA losses. According to our results, there is not a significant difference between centrifugation (using glass tubes) and filtration (using 0.45 µm PVDF Membrane).

In addition, our observations indicated that the best bottle for collection and preservation of OSPW would be lime-soda or borosilicate glass, however, high inner surface of borosilicate glass may contribute to the higher detected adsorbed NAs. HDPE, LDPE, and PP plastic bottles are suspected to have NA adsorption and are not suggested for long term preservation. In addition, polystyrene centrifuge tubes demonstrated slightly better performance for OSPW storage or handling than polypropylene high-performance centrifuge tubes.

Bottle cap liners made of PTFE had the best performance followed by polyvinyl, and tinfoil. Polyethylene and White Rubber might leak unknown chemicals into OSPW which results in apparent false-higher NA concentration. Preservation of OSPW sample at low pH (2.1) resulted in NA insolubilization in OSPW (non-homogeneous solution) with NA molecules visibly separated from water phase and partitioned onto the glass bottle. Storage at high pH (11.1) and addition of methanol caused a higher NA concentration reading after 8 days storage.

Our suggestion for preservation of OSPW is storage in glass bottle in fridge with no change in water chemistry until further research confirms reasons for unexpected results.

All the results and conclusions in this investigation are based on the fluorescence spectroscopy for the measurement of NAs, which mainly targets hydrocarbons with aromatic rings as an indicator for presence of NAs in solution. For future investigation, high resolution instruments for characterization and fingerprinting of NAs are suggested to have a better understanding of partitioning of NAs.

REFERENCES

- Allen, E. W. 2008. Process water treatment in Canada's oil sands industry: I. Target pollutants and treatment objectives. *Journal of Environmental Science*, **7**: 123-138.
- Allen, E. W. 2008. Process water treatment in Canada's oil sands industry: II. A review of emerging technologies. *Journal of Environmental Engineering and Science*, **7(5)**, 499-524.
- Kavanagh, R. J., Burnison, B. K., Frank, R. A., Solomon, K. R. and Van Der Kraak, G. 2009. Detecting oil sands process-affected waters in the Alberta oil sands region using synchronous fluorescence spectroscopy. *Chemosphere*, **76(1)**, 120-126
- Martin, N., Burkus, Z., Mceachern, P., Yu, T. 2014. Naphthenic acids quantification in organic solvents using fluorescence spectroscopy. *Journal of Environmental Science and Health - Part A Toxic/Hazardous Substances and Environmental Engineering*, **49(3)**, 294-306
- Toor, N. S., Han, X., Franz, E., Mackinnon, M. D., Martin, J. W., and Liber, K. 2013. Selective biodegradation of naphthenic acids and a probable link between mixture profiles and aquatic toxicity. *Environmental Toxicology and Chemistry*, **32(10)**, 2207-2216.
- Whitby, C. 2010. Microbial Naphthenic Acid Degradation. *Advances in Applied Microbiology*, **70** 93-125.

The Oil Sands Tailings Research Facility (OSTRF) was established in 2003 as a direct response to the global need for improved tailings management. Through extensive interaction and collaboration with other distinguished research groups, the OSTRF provides the novel research required to develop environmentally superior tailings disposal options. With the flexibility to support concurrent interdisciplinary research projects, the facility attracts the brightest minds in the field and trains early-career, technically competent scientists and engineers—the future leaders, consultants and regulators for the oil sands industry. The OSTRF is pioneering the way to innovative, environmentally conscientious solutions for future generations.

Drs. David C. Sego and G. Ward Wilson, as Co-Principal Investigators of the OSTRF, lead instrumental initiatives to bring together academia, industry and government agencies to find environmentally sustainable solutions for oil sands development. One such initiative is the International Oil Sands Tailings Conference (IOSTC), which is held every two years, and provides a forum for mine waste managers, engineers, regulators and researchers to present new ideas and to discuss the latest developments in the field.

The Fourth International Oil Sands Tailings Conference offers the most recent developments in oil sands tailings and management through invited speakers and select technical presentations. IOSTC'14 will also debut research from the University of Alberta Geotechnical Centre's newest research initiative, the NSERC/COSIA Senior Industrial Research Chair (IRC) in Oil Sands Tailings Geotechnique held by Dr. Ward Wilson. The IRC enables the oil sands industry to combine its efforts with those of leading researchers at the University of Alberta to develop novel technologies and methods to manage oil sands tailings in Alberta. The IRC program will advance the scientific community's fundamental understanding of the behaviour of fluid fine tailings and mature fine tailings through focusing on the following research themes:

- Theme 1: Unsaturated Soil Mechanics for Oil Sands Tailings Deposition
- Theme 2: Consolidation Processes for Mature Fine Tailings
- Theme 3: Assessing and Improving Tailings Deposition
- Theme 4: Tailings Simulation Modelling and Long-term Behaviour of Fine Tailings

For more information about the University of Alberta Geotechnical Centre's current oil sand tailings research projects and initiatives, including the NSERC/COSIA IRC in Oil Sands Tailings Geotechnique, please visit www.ostrf.com or <http://geotechnical.ualberta.ca>.



International Oil Sands Tailings Conference



The UofA
Geotechnical Centre

Proceedings cover photo courtesy of Syncrude Canada Ltd.